Figure front page: Bone marrow biopsy of an essential thrombocythemia patient.
This patient exhibits clusters of hyperploid and large megakaryocytes when stained with trichrome blue. Picture was taken with a 40X objective magnification.
Courtesy of Professor Emeritus Jean-Marie Scheiff.

Université catholique de Louvain
Faculté de Médecine
de Duve Institute
Ludwig Institute for Cancer Research

Thrombopoietin Receptor: Regulation, Dimerization, Oncogenic Activation and Bimodal Signaling

Jean-Philippe Defour

Promoteur: Professor Stefan N. Constantinescu

Thèse présentée en vue de l'obtention du grade de
Docteur en Sciences Biomédicales et Pharmaceutiques.
Orientation: Molecular Hematology and Signal Transduction

-2015-

Ecole doctorale de génétique et d'immunologie

Université catholique de Louvain
Ludwig Institute for Cancer Research
de Duve Institute

Promoter:
Professor Stefan N. Constantinescu (UCL-SIGN, de Duve Institute, Cell Signaling Unit and Ludwig Institute for Cancer Research).

Jury:
Internal members
Professor Thomas Michiels (UCL de Duve Institute – MIPA, Microbial Pathogenesis Unit)

Professor Miikka Vikkula (UCL de Duve Institute, GEHU, Human Molecular Genetics Unit)

Professor Pierre Van der Bruggen (Ludwig Institute for Cancer Research)

Professor Bernard Chatelain (UCL Clinical Biology, Laboratory Hematology, Mont-Godinne Hospital)

Professor Augustin Ferrant (UCL Department of Hematology, St Luc Hospital)

External members
Professor Iris Behrmann
Life Sciences Research Unit, Faculty of Science, Technology and Communication, University of Luxembourg

Professor Steven O. Smith,
Structural Biology, Department of Biochemistry and Cell Biology, Stony Brook University, Stony Brook, NY

This thesis was supported by the FRIA
(Fonds pour la Formation à la Recherche dans l'Industrie et dans l'Agriculture)

I. INTRODUCTION 9
I.1. TRANSMEMBRANE PROTEINS 9
I.1.1. Classification and topology 9
I.1.2. Helical structure 11
I.1.3. Composition 13
I.2. TRYPTOPHAN AND CATION-Π INTERACTIONS 15
I.3. QUALITY CONTROL AND POST-TRANSLATION MODIFICATIONS OF TRANSMEMBRANE PROTEINS 17
I.3.1. General modifications in the secretory pathway 17
I.3.2. ER-associated quality control 18
I.3.3. Golgi-associated quality control 19
I.3.4. Plasma membrane associated quality control and degradation 20
I.4. DIMERIZATION OF TRANSMEMBRANE AND JUXTAMEMBRANE SEQUENCES 21
I.5. COILED-COILS 21
I.6. HEMATOPOIESIS AND CYTOKINE RECEPTORS 22
I.7. MEGAKARYOPOIESIS 24
I.8. PLATELET PHYSIOLOGY 25
I.9. CYTOKINES 25
I.10. CYTOKINE RECEPTORS 25
I.11. JANUS KINASES 27
I.11.1. Murine models of JAK deficiency 27
I.12. SIGNALING PATHWAYS 29
I.12.1. STATs (Signal Transducers and Activators of Transcription) 29
I.12.2. Murine models of STAT deficiency 30
I.12.3. The JAKs/STAT pathway 30
I.12.4. The MAP-kinase pathway 30
I.12.5. The PI3-kinase pathway 31
I.13. THE THROMBOPOIETIN RECEPTOR 31
I.13.1. TpoR structure and domains 31
I.13.2. TpoR artificial activation 33
I.13.3. Activation by Tpo ligand, Eltrombopag and Romiplostim 34
I.13.4. TpoR dimerization and mechanisms of activation 36
I.13.5. TpoR signaling 38
I.13.6. Negative regulation mechanisms 40
I.14. ROLE OF TPOR IN NORMAL HEMATOPOIESIS 43
I.15. *IN VIVO* MODELS 45

I.15.1. Tpo -/- mice *45*
I.15.2. Double Tpo and GCSFR -/- *45*
I.15.3. Tpo +/- mice *45*
I.15.4. TpoR/c-Mpl -/- mice *45*
I.15.5. TpoR/c-Mpl and IL-3R α -/- mice: *45*
I.15.6. TpoR/ c-Mpl floxed mice crossed with PF4cre/PF4cre mice *46*
I.15.7. TpoR (-/-) mice expressing a full-length TpoR transgene under the control of the 2-kb TpoR promoter *46*
I.15.8. c-Mpl/TpoR Δ60 mice: *46*
I.15.9. Mice with retroviral ectopic overexpression of c-Mpl/ TpoR *46*
I.15.10. JAK2 V617F heterozygous knock-in mice *47*
I.15.11. JAK2 V617F Mpl (-/-) mice *47*
I.15.12. JAK2V617F/ STAT1 (-/-) *47*
I.15.13. Chicken: Chicken Tpo and MPl *47*
I.16. MYELOPROLIFERATIVE NEOPLASMS 48
I.17. CYTOLOGICAL PHI- MPN CLASSIFICATION 49
I.17.1. Polycythemia Vera morphology *49*
I.17.2. Essential Thrombocythemia morphology *49*
I.17.3. Primary myelofibrosis morphology *50*
I.18. MOLECULAR MPN CLASSIFICATION 51
I.18.1. Driver mutations in MPNs *51*
I.18.2. Epigenetic mutations and their role in clonal emergence and progression *55*
I.18.3. Mutations involved in the leukemic transformation *56*
I.19. OVERLAP AND DIFFERENCES WITH MYELODYSPLASTIC SYNDROMES 56

II. APPROACHES 58
II.1. PRINCIPLES OF APPROACHES TO STUDY INTERACTIONS AND STRUCTURE OF TRANSMEMBRANE SEQUENCES 58
II.1.1. Toxcat assay *58*
II.1.2. Solid-state deuterium NMR with magic angle spinning *58*
II.1.3. 2D Homonuclear ^{13}C -^{13}C DARR MAS NMR *60*
II.1.4. Polarized attenuated total reflectance Fourier transform infrared spectrometry (ATR- FTIR) *61*
II.1.5. Sedimentation equilibrium analytical ultracentrifugation (AUC) *62*
II.1.6. Gaussia princeps protein-fragment complementation assay *62*
II.1.7. Cys-mediated crosslinking *63*

II.1.8. Co- immunoprecipitation (Co-IP) *63*
II.2. PRINCIPLES OF APPROACHES TO STUDY ACTIVITY 64
II.2.1. Dual Luciferase Assay *64*
II.2.2. Engineering stable cell lines *65*
II.2.3. Bone marrow transplantation experiments in C57Bl6 mice *66*
II.3. PRINCIPLES OF APPROACHES TO STUDY ORIENTATION 67
II.3.1. Coiled coil forced dimers *67*
III. RESULTS 68
III.1. PREAMBLE: ORIENTATION- SPECIFIC SIGNALLING BY THROMBO-POIETIN RECEPTOR DIMERS (EMBO J. 2011) 68
III.1.1. Background *68*
III.1.2. Question and approaches *68*
III.1.3. Authors contribution *69*
III.1.4. Unpublished but related results *90*
III.2. PREAMBLE: TRYPTOPHAN AT THE TRANSMEMBRANE–CYTOSOLIC JUNCTION MODULATES THROMBOPOIETIN RECEPTOR DIMERIZATION AND ACTIVATION (PROC.NATL. ACAD. SCI. USA 2013) 93
III.2.1. Background *93*
III.2.2. Questions *93*
III.2.3. Authors contribution *94*
III.2.4. Unpublished but related results *106*
III.3. PREAMBLE: ONCOGENIC ACTIVATION OF C-MPL/THROMBOPOIETIN RECEPTOR BY 17 MUTATIONS AT W515: IMPLICATIONS FOR MYELOPROLIFERATIVE NEOPLASMS (LEUKEMIA 2015) 113
III.3.1. Background *113*
III.3.2. Questions *114*
III.3.3. Author contribution *114*
III.3.4. Unpublished but related results and discussion *118*
III.4. PREAMBLE: HIS499 REGULATES DIMERIZATION AND PREVENTS ONCOGENIC ACTIVATION BY ASPARAGINE MUTATIONS OF THE HUMAN THROMBOPOIETIN RECEPTOR. (J. BIOL. CHEM. 2016) 129
III.4.1. Background *129*
III.4.2. Questions *129*
III.4.3. Authors contribution *129*
III.4.4. Unpublished but related results and discussion *144*

III.5. PREAMBLE: UNRAVELING TPOR ONCOGENIC MECHANISM: GAINING ORDER FROM LOCAL DISORDER (IN PREPARATION) 145
III.5.1. Background *145*
III.5.2. Questions *145*
III.5.3. Authors contribution *146*
III.5.4. Unraveling TpoR oncogenic mechanism: gaining order from local disorder Oncogenic TpoR activation mechanism unraveled. *146*
III.5.5. Unpublished but related results and discussion *165*
III.6. PREAMBLE ANTIPROLIFERATIVE EFFECT OF TPOR AT HIGH TPO IMPLIES AN IFN-LIKE SIGNALING (IN PREPARATION). 173
III.6.1. Background *173*
III.6.2. ASH abstract related to bimodal signaling *174*
Related results and discussion *176*

IV. DISCUSSION 180
IV.1. DIMERIC STATE OF THE RECEPTOR 180
IV.2. TWO LAYERS OF PROTECTION AGAINST SELF-ACTIVATION IN TPOR 181
IV.3. TRYPTOPHAN SUBSTITUTIONS 182
IV.4. POSITION 516 183
IV.5. INTERFACES 183
IV.5.1. Inactive interfaces *183*
IV.5.2. Active interfaces *185*
IV.6. FROM UNRAVELING TO JAK2 ACTIVATION AND BEYOND 187
IV.6.1. Orientation is not sufficient *187*
IV.6.2. Asymmetric dimer potential or multimeric states *188*
IV.6.3. Coupling orientation to activation or inactivation of TpoR *189*
IV.7. TPOR GENERAL MODEL OF ACTIVATION 190
IV.8. OF MICE AND MEN: PHYSIOLOGICAL MODELS 190
IV.9. ANTIPROLIFERATIVE ROLE OF TPOR 191

V. CONCLUSION 191

VI. PERSPECTIVES 192

VII. APPENDIX 192
VII.1. THROMBOPOIETIN RECEPTOR DOWN-MODULATION BY JAK2 V617F 192
VII.3. COMBINATION TREATMENT FOR MYELOPROLIFERATIVE NEOPLASMS USING JAK AND PAN-CLASS I PI3K INHIBITORS 204

VII.4. DIFFERENTIAL ASSOCIATION OF CALRETICULIN TYPE 1 AND TYPE 2 MUTATIONS WITH MYELOFIBROSIS AND ESSENTIAL THROMBOCYTEMIA: RELEVANCE FOR DISEASE EVOLUTION 218
VII.5. PRESENCE OF ATYPICAL THROMBOPOIETIN RECEPTOR (MPL) MUTATIONS IN TRIPLE NEGATIVE ESSENTIAL THROMBOCYTHEMIA PATIENTS 223
VII.6. THROMBOPOIETIN RECEPTOR ACTIVATION BY MYELOPROLIFERATIVE NEOPLASM ASSOCIATED CALRETICULIN MUTANTS 234
VIII. BIBLIOGRAPHY 246
IX. TABLE OF FIGURE 274
X. TABLE OF TABLE 276

I. INTRODUCTION

I.1. Transmembrane proteins

In the field of single-span transmembrane receptors the relationship between protein sequence and tridimensional structure remains difficult to determine. No crystal structure exists for a full-length single-span receptor or transmembrane protein. Because the protein behavior depends on the lipid environment, molecular approaches and cellular assays must be complemented by biophysical techniques in order to uncover the precise conformations and molecular interactions in native environments. X-ray crystallography of membrane proteins has been difficult due to several factors, such as lipids hindering crystal formation, detergents influencing the stability of proteins, multiple conformational states, and their heterogeneous post-translational modifications. In addition, receptors are usually coupled to intracellular effectors forming complexes that attain their final conformations after coupling and intracellular traffic. For these reasons, we have combined extensive mutagenesis and biological assays with biophysical approaches, in a back-and-forth fashion where biological experiments led to structural studies and those in turn generated hypotheses that were fed back into the functional assays.

I.1.1. Classification and topology

A significant fraction of the proteins coded by the human genome are associated with or embedded in a hydrophobic membrane at the surface of the cell, in vesicles or organelles. Integral membrane proteins are proteins that are stably attached to the membrane. Based on how hydrophobic segments are inserted in the membrane, there are four types of TM proteins: type I, II, III and IV. Single transmembrane proteins are a subset of those integral membrane proteins (IMPs) that are able to cross the membranes and that possess one extracellular domain (ECD), one hydrophobic transmembrane domain (TMD) and one cytosolic intracellular domain (ICD).

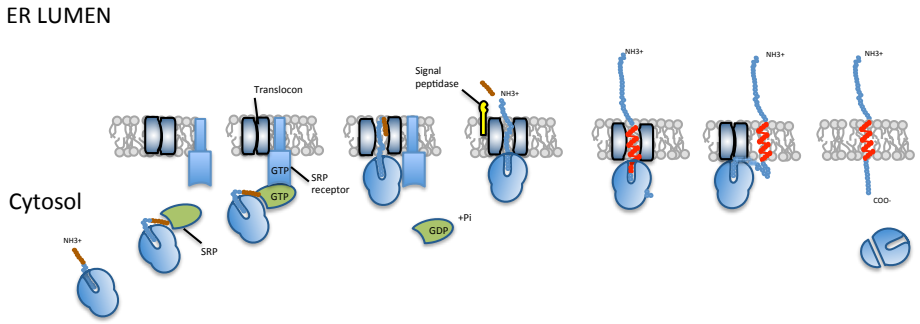


Figure 1 - Type I TM protein translocation in the membrane

Just after translation of the signal sequence by the ribosome, a signal recognition particle (SRP) recognizes the nascent peptide. Then, the SRP/ peptide/ ribosome complex is recognized by the SRP

receptor on the ER membrane. GTP binding to both the SRP and its receptor will tighten the link at the ER membrane. With the ribosome bound at the ER membrane, the nascent peptide will enter the central cavity of the translocon complex, Sec 61. Subsequently, the SRP and SRP receptor hydrolyze their GTP and detach. As the growing peptide passes through the translocon channel and elongates in the ER lumen, a signal peptidase cleaves the N terminal signal peptide. When the so called "stop-transfer-anchor sequence" (corresponding to the TM domain) arrives at the level of the translocon channel, the elongating peptide stops going through the translocon and laterally exits the channel to enter the membrane. The translocon channel closes and then the synthesis continues, with the ribosome still facing the closed translocon and the cytosolic portion of the protein looping into the cytosol until the end of the elongation when the ribosome subunit detaches. Proteins with a cleavable signal sequence will have their amino terminal part in the lumen of the ER[1-3]. Those TM proteins include homodimeric type-1 cytokine receptors, like the thrombopoietin receptor (TpoR). Adapted from Lodish et al. [4]

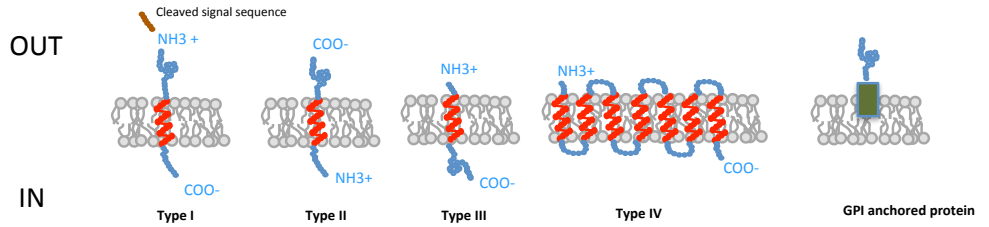


Figure 2 - TM protein classification

Transmembrane protein classification: Type I proteins with a cleavable signal sequence will have their amino terminus in lumen of the ER. This orientation eventually leads to the N-terminus being positioned outside the cell (extracellular domain). Proteins that lack a cleavable signal sequence have a so-called "signal anchor sequence" that possesses both the functions of signal peptide that binds the SRP and anchors the peptide in the membrane. In this case, the orientation of the TMD in the lipids depends on the charge of the 15 residues flanking the signal anchor sequence with the more positive flanking segment facing the cytosol. If the 15 N-terminal residues are more positive than the 15 C-terminal residues, the orientation will be a type II TM protein. These proteins have an inverse topology compared to type I TM proteins. The transferrin receptor is an example of a type-II transmembrane receptor. Type III proteins have the same orientation as type I proteins, but lack the cleavable signal sequence. Type III TM proteins can be exemplified by cytochrome P450. Type IV transmembrane proteins are proteins that possess several TM domains (multipass) and their orientation (N extracellular, C cytosolic) or (N cytosolic, C extracellular) depends on the most N terminal signal anchor sequence; if they start with a hydrophobic sequence they will first insert like type I TM proteins with cleavable or uncleavable signal sequences, while if they start with the hydrophilic sequence they insert with their first TM domain playing the role of the signal anchor, as in type II TM proteins. Then, the next TMs will be inserted alternatively as those in type I and type II TM proteins [3]. If there is an even number of TM segments, the two ends will be on the same side of the membrane, while if there is an odd number of TM helices, the two ends will be on opposite faces. G protein-coupled receptors belong to type-IV TM proteins and have 7 TMDs . In multispan TM proteins transmembrane α helices often interact and can form structures that are more rigid and amenable for X-ray studies, unlike the single-span TM proteins. Adapted from Lodish et al.[4]

Thrombopoeitin receptor
Type 1 receptor

Beta adrenergic receptor
Type 4 receptor

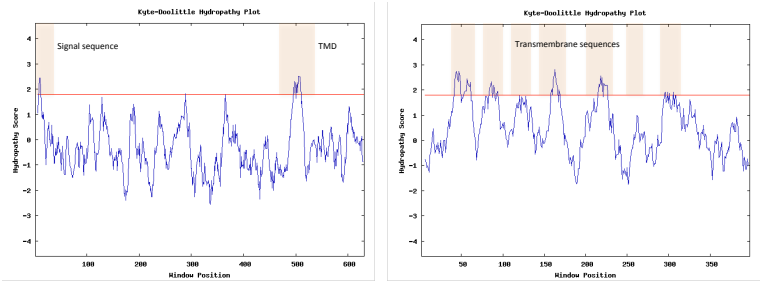


Figure 3 - Hydropathy profile
Hydrophobic TMD segments can be easily detected by making a hydropathy profile.

I.1.2. Helical structure

The vast majority of hydrophobic transmembrane segments are α-helical. One exception is represented by "porins" where the transmembrane segment adopts a ß-barrel structure. The reason for the predominant α-helicity of TMDs is that even for amino acids that contain hydrophobic side chains, the carbonyl backbone and the amide groups are not energetically favorable in this non-polar environment and are forced to make hydrogen bonds that will drive α-helix formation or less frequently ß sheets (for porins), but never both. The reason why α -helices are much more frequent than ß sheets is that they are easily formed by only local hydrogen bonds, while ß sheets require hydrogen bonds between distant linear sequences that assemble as parallel or antiparallel strands. α-helices represent therefore the most common secondary structure found in membrane proteins and are nearly always right-handed (turn segments closer to the observer going up towards the right) due to the fact that Nature uses only left handed amino acids. On the other hand, the crossing angles between helices can be both right and left-handed (helix closer to the observer going up to right or left).

TM proteins can be classified as monotopic if they do not cross the membrane, bitopic if they span the membrane with a single helix, and polytopic (or multispanning) if they contain two or more α-helices that cross the membrane. Helices in bitopic proteins interact only with the lipid environment and with themselves (homomeric interactions) in the case of homo-dimerization/oligomerization. α-helices in polytopic proteins may interact with other α-helices as well. The water-oil transfer energy of a TM α-helix in bitopic proteins is highly favorable -48 kcal/mol and even more favorable than that in polytopic proteins -39 kcal/mol. [5]

Biological membranes are bilayers of phospholipids that resemble a sandwich with the hydrophilic head groups at the exterior (as the bread slices in a sandwich) and the hydrophobic acyl chains as the filling. The acyl chains are more ordered in the vicinity of the polar head groups and more dynamic in the center of the bilayer. The non-polar interior is approximately 25-35 Å thick with the head groups region being an additional 5 to 10 Å.[6]

For common lipids such as POPC (1-palmitoyl-2-oleoyl-sn-glycero-3-phosphocholine) or DPPC (1,2-dipalmitoylphosphatidylcholine), the typical hydrophobic thickness is ~25 Å.[7] The two headgroup layers are often neglected but can, as shown above, be as thick as the hydrophobic region of the bilayer. The composition of the lipids could also vary and be segregated into patches giving additional complexity to the bilayer.

X ray, NMR, and electron microscopy studies use proteins reconstituted in non-native environments (not in cell membrane) such as micelles, bicelles or artificial bilayers. In micelles, the lipid bilayer may not be well modeled because the curvature is stronger; the micelle lipids are more packed and less dynamic at their center than in lipid bilayers.[8] The studies of receptors in bicelles have the advantage of yielding structural information on the full TM sequence in a membrane-like environment. Micelles are mainly used in solution NMR while bicelles can be used in solid state NMR. However, we used in this thesis peptides reconstituted in artificial membranes stacked up as a multilamellar multilayer using no DHPC or detergents.

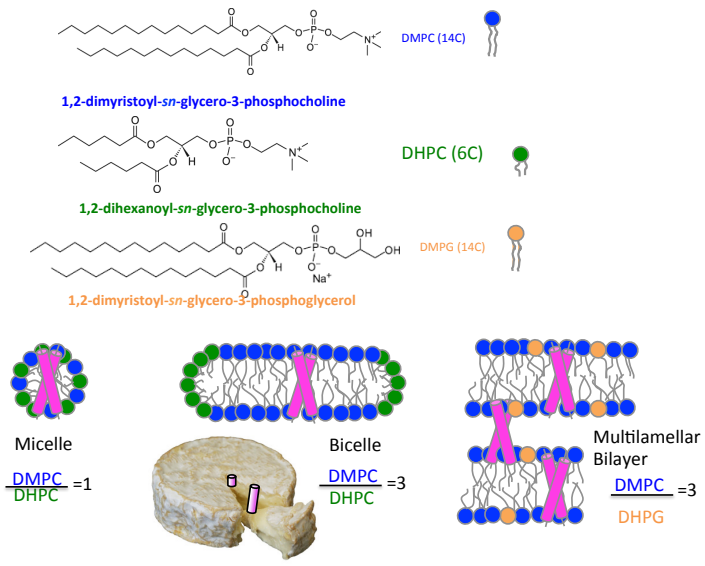


Figure 4 - Micelle and bicelle and bilayers structures
Isotropic bicelles are disc-shaped (cheese) with flat and round bilayer structure formed from mixing long and short chain phospholipids, typically in a 10:3 DMPC /DHPC ratio. Phospholipids segregate with short chain localized on the rim part and long chain on the planar zone of these phospholipid aggregates. These bicelles behave isotropically and have the same magnetic susceptibility and align spontaneously in a magnetic field. Peptides in pink are reconstituted at a 1:60 peptide /lipid ratio for example.

The vertical translation in an α–helix is 1,5 Å per residue and 3,6 residues per turn (100° rotation per residue). So a non-tilted or weakly tilted hydrophobic α-helix takes ~22 amino acids residues or ~6 turns to cross the membrane. The length of TM α-helices should theoretically be comprised between 15 to 30 amino acids. For example, the TMD of vesicular

stomatitis virus G protein (VSVG), which plays the role of a membrane retention signal contains 22 amino acids, and only becomes soluble when truncated to lower than 14 amino acids, showing that short α-helices (15 or 16 amino acid residues) could still maintain membrane crossing/retention. The upper limit is 30 amino acids and corresponds to an α helix with a 48° tilt angle in a 30 Å thick lipid bilayer.

In case of a "positive" mismatch defined as when longer than necessary peptides are introduced in thin membrane bilayers, the system alleviates the mismatch predominantly by tilting the peptide and to a smaller extent by increasing lipid ordering in the immediate vicinity of the peptide. Under "negative" mismatch conditions, where shorter than necessary peptides are introduced in membrane bilayers, alleviation takes place by a combination of local bilayer bending, smaller tilt, and the snorkeling of the positively charged residues of the peptide, which have favorable interactions with specific oxygen atoms of the phospholipid headgroups. All these observations reinforce the general concept of insertion of a hard peptide (with no strong structural changes) into a soft lipid environment.[6,7,9]

I.1.3. Composition

An important aspect of understanding the mechanism of signal transduction by TpoR involves the types of amino acid residues that are present in TMDs of type I IMPs, both in the middle and at the junctions with extracellular and intracellular domains. The composition of the transmembrane helix is correlated with the energetic cost of its constituents to partition into the bilayer. The two Wimley–White whole-residue hydrophobicity scales are very useful and take into account the contribution of the peptide bonds (whole residues). One scale is for the transfer free energy of an unfolded peptide from the water to the bilayer interface, which is a complex and heterogeneous environment and the other from water to octanol, which roughly corresponds to the hydrocarbon core of the bilayer.[10,11]

I.1.3.1. Ionizable amino acids

Not surprisingly, polar and charged residues exhibit the lowest frequency in transmembrane segments, considering the high energetic cost of inserting such amino acids. Whenever present, polar residues represent key residues for the protein activity. An example is the polytopic proton pump bacteriorhodopsin, where protons are transferred from the cytosol to the extracellular space to create a proton gradient that will be subsequently transformed in chemical energy. Protons are transferred from cytosol to Asp 96 carboxylate side chain and then to a Schiff base (that covalently binds retinal to a Lys) and from the Schiff base to Asp 85 carboxylate side chain before being released in the extracellular space.[12] Ionizable amino acids are not supposed to ionize in the membrane and probably make salt bridges to accommodate in the membrane.[13] Lysine and arginine (positively charged residues) are membrane-anchoring residues and are supposed to be located close to the water interface. Their side chains are oriented perpendicular to the acyl chain and their charged residues slightly above the phosphate groups.[14] Charged/polar residues such as Glu, Asn, Gln, and Asp drive the oligomerization of model transmembrane peptides.[15] Examples exist for receptors like the

Neu/Erb-2 (HER2) proto-oncogene where the TMD mutation V664E dimerizes the receptor via strong hydrogen bonding between the two-protonated carboxyl Glu side chains.[16] TpoR can be homodimerized by the introduction of a polar residue (N/D/E/Q) at position S505 in its TMD.[17] The S505N mutation is found in familial forms[18] and rare sporadic case of ET and PMF.[19-21] Another example is represented by the A391E mutation within the TMD of the fibroblast growth factor receptor-3 (FGFR-3) that is associated with Crouzon syndrome (a form of craniosynostosis) and Acanthosis Nigricans (thickened and pigmented skin).[22]

I.1.3.2. Aliphatic amino acids

Isoleucine, leucine, valine, methionine and alanine are the most frequent amino acids in TMDs, with frequencies of 62% in single-span and 52% in multispan TM proteins, respectively. The apparently lower frequency in multispan proteins might be explained by inter-helix neutralization interactions, which explain a higher tolerance for polar and charged residues. Leucine and valine are non-randomly distributed along the helix length with an increased frequency of those amino acids in the middle of the α-helix.[5]

I.1.3.3. Hydroxyl and sulfur-containing amino acids

Cysteine, threonine and serine are the most frequent polar residues. They all can satisfy their polar side chain by making hydrogen bonds to the carbonyl oxygen at position i-4. Cysteine is unique and is the only amino acid with an ascending distribution from the amino terminus to carboxy terminus (extracellular-to-intracellular) in single-span type I proteins. When two or more Cys residues are present in TMDs, they tend to be located close to each other. The reasons for this remain unclear.

Cysteine residues are quite rare in TM proteins. An exception is found in the Cysteine-Rich Transmembrane (CYSTM) protein family, which comprises eukaryotic (including human) small proteins (<150 aa) that possess a unique set of conserved cysteines (5-6 with 3-4 consecutive cysteines) in their TMDs. Their role is not yet clear, but they may be responsible for plasma membrane protection against environmental/toxic/oxygen radical stress by modifying the redox potential of the plasma membrane or using chelation mechanisms.[23]

I.1.3.4. Destabilizing amino acids (Gly and Pro)

Proline and glycine are known to be destabilizing amino acids for helices in soluble proteins, but they appear to be readily tolerated (especially Gly) in TMD helices where the driving force for secondary structure formation is different than in soluble proteins, namely the requirement to satisfy backbone hydrogen bond in the lipid environment. Proline has a descending amino-to-carboxy terminal distribution in type I TMDs proteins and glycine exhibits a somewhat convex distribution, being more prevalent in the center. When several Gly residues are present in a TMD they are found with a peak incidence of 4 residues apart (Gly-x-x-x-Gly) meaning they are located on the same face of the helix and are known to be responsible for grooves in the helix to ensure better packing of interacting helices (knobs into grooves packing). Crick proposed the "knobs-into-holes" model to describe this complementarity of helix dimer.

I.1.3.5. Aromatic amino acids

One of the ubiquitous features of membrane proteins is the predilection of tryptophan and tyrosine residues for both membrane interfaces.[5] In contrast, phenylalanine is distributed randomly.[5] The preference for tryptophan at membrane interfaces is believed to be due to tryptophan's flat rigid shape that restricts access to the hydrocarbon core of the lipids, and to its electronic structure and so called "aromaticity "and "amphipaticity" that favor residing in the complex interface environment. The interfacial location of tryptophan has been described to simply be due to the balance of the hydrophobic effect that tends to drive it out of water, complex electrostatic interactions that favor residing in the hydrated headgroup region, and cohesive repulsion that keeps it out of the hydrocarbon core.[24] It was shown that the Trp indole NH group is adjacent and in close contact with the lipid carbonyl region.[14] Certain authors have shown that antimicrobial peptides rich in tryptophans partition deeply in bilayers suggesting that tryptophans can also penetrate in the hydrocarbon region of the bilayer.[25] Along with Trp and Tyr, other residues, namely Lys, Arg and Leu are often found exposed at the headgroup regions of the membrane, where they exhibit high propensity to face phospholipid headgroups and glycerol backbones.[26] Besides their role in anchoring the TMD to the lipid headgroups, Trp and Tyr can contribute, when placed in the center of the TMD, to TMD-TMD interactions.[27] The complex interactions that tryptophan can be involved in could be as diverse as cation-π, aromatic–aromatic, induced dipole, polar and charge transfer.

I.2. Tryptophan and cation-π interactions

Aromatic residues (phenylalanine, tyrosine, tryptophan) are hydrophobic. But, when compared to classical hydrophobic residues such as valine or leucine, aromatics have much more interaction capabilities including the formation of hydrogen bonds and cation-π interactions.

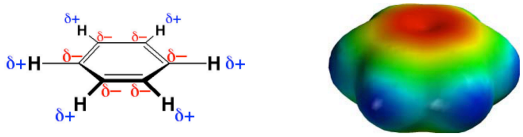


Figure 5 - Aromatic ring electronegativity

The cation-π interaction can be rationalized by the fact that the sp^2 carbon is more electronegative than hydrogen. The 6 C-H bond dipoles around the benzene ring create a charge distribution, which is a build-up of negative charge in the center of the ring and a belt of positive charges around the benzene.

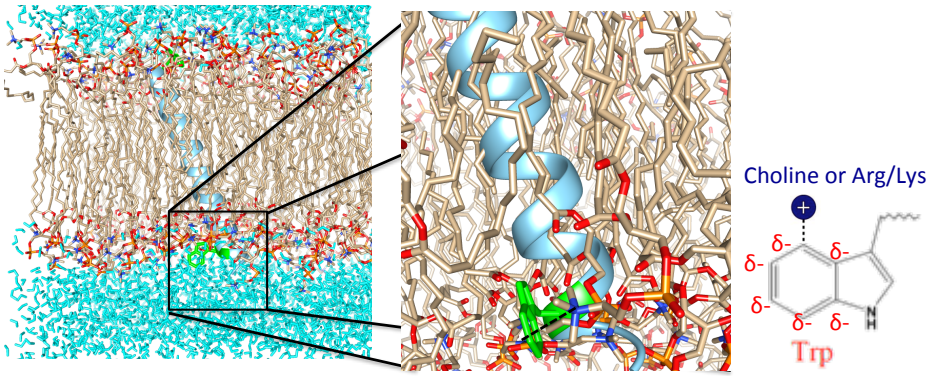


Figure 6 - Cation π interaction
Schematic drawing of a cation-π interaction between tryptophan at the TMD boundary and lipid headgroups.

Cation-π interactions can arise between phenylalanine, tyrosine, tryptophan as the π component and lysine, arginine or choline and ethanolamine as the cationic component. The cation-π interaction with tryptophan is greater than with tyrosine or phenylalanine (Trp> Tyr> Phe) because the indol ring exhibits a greater negative electrostatic potential. In turn, Tyr is more potent than Phe, because the oxygen of tyrosine is a second site of electronegative potential. In the protein data bank, one can find one cation- π interaction for every 77 amino acids. That means that virtually any protein has at least one cation- π interaction. 25% of tryptophans are involved in cation-π interactions. Arginine is the preferred partner over lysine probably because the guanidinium ion of arginine is to some extent hydrophobic.[28] [29] As an example, the SH2 domain of the v-src oncogene recognizes phosphotyrosine by making a cation-π interaction between arginine and lysine and the ring of tyrosine, in addition to hydrogen-bonding interactions with the phosphate.[30]

When an arginine is engaged in a cation-π interaction, it is able to make as many hydrogen bonds as if is not involved in a cation-π interaction, which is in strong contrast with lysine. Lysine cannot participate in any hydrogen bonds anymore when engaged in a cation-π interaction. Cation-π interactions render the entry of the positive arginine easier in the membrane. A very good example is the subset of antimicrobial peptides rich in Arg and in Trp. These peptides have very high activity even at small peptide lengths and their activity depends on membrane insertion.

I.3. Quality control and post-translation modifications of transmembrane proteins

I.3.1. General modifications in the secretory pathway

Transmembrane proteins undergo four main post-translational modifications after their entry in the ER: 1) N-glycosylation, 2) folding of multiple subunits and oligomerization, 3) formation of disulfide bonds and 4) proteolytic cleavage. Those modifications can be regrouped under the term "folding" and require ER chaperones and folding enzymes (Figure 8).

Calreticulin is a major 46-kDa ER chaperone that is a calcium binder, a buffer and a lectin-like chaperone similarly to calnexin, which is a transmembrane protein. Calreticulin deficiency in mice is embryonically lethal.[31] The nucleotide sequences of the mouse and the human gene show greater than 70% identity. The protein contains at least three domains. The "N-terminal" domain binds glycosylated proteins. The middle "P domain" is a proline rich domain critical for the lectin like activity of calreticulin and the "C-domain" is rich in acidic (negative) residues Asp and Glu, which allow calcium binding. Calreticulin sequence begins with an ER targeting cleavable signal sequence and ends by an ER retrieval signal KDEL motif.[32] Of great interest is a class of calreticulin mutants that has recently been discovered to be involved in the oncogenesis process of human myeloproliferative neoplasms. These mutations were located in exon 9 and generate a +1 bp (-1+2) frameshift resulting in a novel positively charged carboxy terminal end and a loss of the KDEL motif.[33,34]

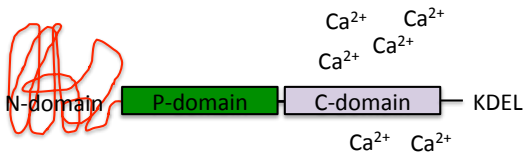


Figure 7 - Calreticulin domains

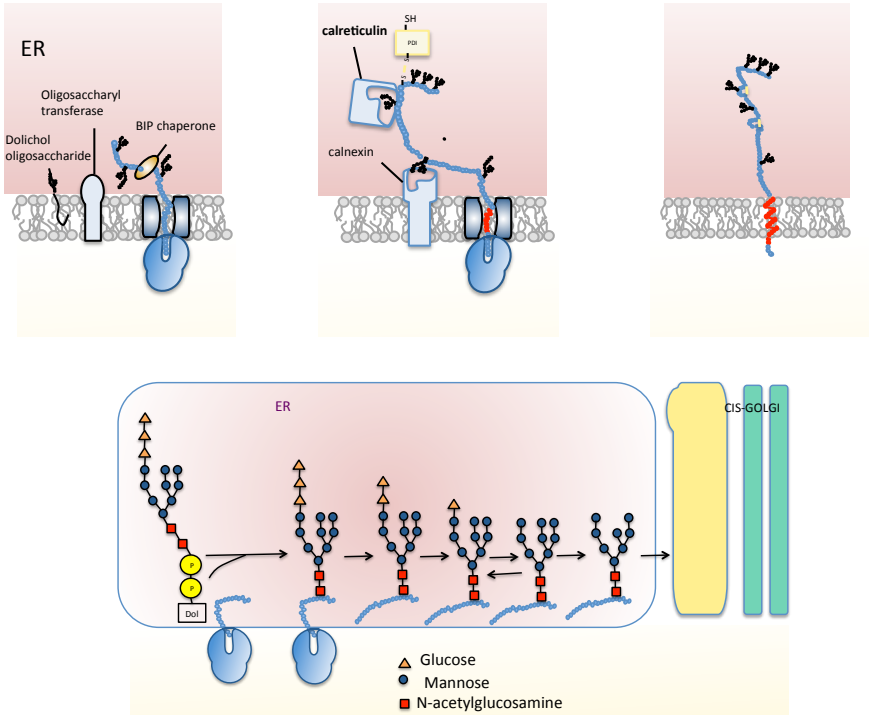


Figure 8 - N glycosylation and chaperones in the ER

N-glycosylation is the main modification of protein within the ER with the transfer, in a nascent peptide, of $Glc_3 Man_9 (GlcNAc)_2$ to asparagine residues situated within consensus N-glycosylation motifs Asn-X-Ser or Asn-X-Thr. Immediately after the transfer to these susceptible asparagines, glucosidase enzymes (glucosidase I and II) remove in a step by step process three glucoses and finally one mannose to give $Man_8 (GlcNAc)_2$. Sometimes a glucose is re-added (reglucosidation process) to the $Man_9 (GlcNAc)_2$ to give $Glu_1-Man_9 (GlcNAc)_2$ by a specific glucosyl transferase (GT) that recognizes the non native (not-folded) peptide. This GT behaves like a sensor of protein conformation.[35] This GT is able to recognize specific sequences surrounding the glycans that could be exposed by folding intermediates.[36] Calreticulin and calnexin are calcium-binding chaperones[37] of the family of lectins (carbohydrate binding protein). They recognize those Glu1-Man9 (GlcNAc)2 and prevent misfolding and aggregation of adjacent segments. Cycles of deglucosylation and reglucosylation repeat until the protein adopts a proper folding. BiP/GRP78 and PDI are also chaperones of the ER lumen. BiP/GRP78 chaperones accelerate and help the folding process. The protein disulfide isomerase (PDI) forms and re-arranges disulfide bonds. The folding machinery is then very sensitive to the ER calcium level.

I.3.2. ER-associated quality control

The endoplasmic reticulum (ER) plays a crucial role in protein folding, secretion, calcium storage and signaling. After their translation, proteins rapidly fold. In general, folding takes place in several compartments such as the ER, the cytosol and the mitochondria with each place being equipped with a specific set of chaperones and folding enzymes. Transmembrane proteins are inserted into the ER membrane from ER bound ribosomes. They attain their native conformation in the ER before reaching the Golgi and other downstream

compartments. The cells possess a quality control (QC) machinery to identify, refold or destroy misfolded proteins.

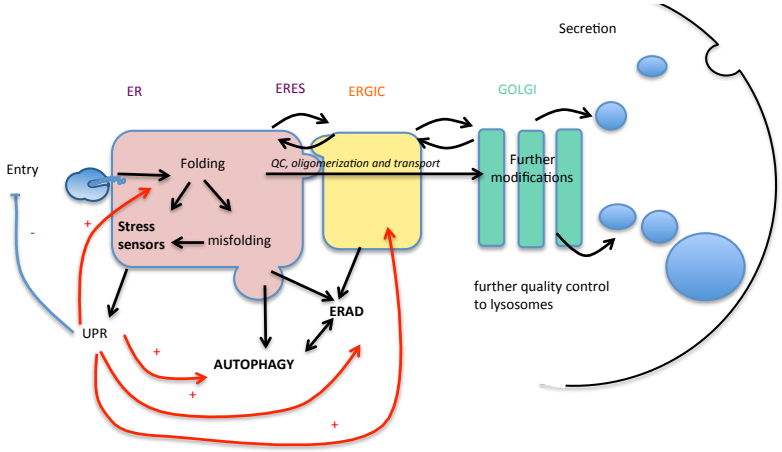


Figure 9 - Endoplasmic reticulum associated degradation

Endoplasmic reticulum associated degradation (ERAD) is a multiple step mechanism consisting of: 1) recognition of the ERAD substrate, 2) retro-translocation of this substrate from the ER to the cytosol, and 3) ubiquitination and degradation by the proteasome.[38] Noteworthy, a few misfolded proteins are able to reach the ERGIC (Endoplasmic Reticulum and Golgi Intermediate Compartment), but are retro-translocated to the ER and eventually degraded. In addition to ERAD, cells can deal with aberrant protein aggregation/misfolding by autophagy. In case of overload in protein processing with accumulation of high levels of aberrant proteins, ER stress is triggered and subsequently activates the unfolded protein response (UPR). The UPR decreases protein production, increases the folding and increases both the ERAD and the autophagy processes. The UPR can also act downstream of the ER.[39] The UPR is modulated by three UPR sensors, namely activating transcription factor-6 (ATF6), inositol-requiring kinase 1 (IRE) and double-stranded RNA-activated protein kinase-like ER kinase (PERK). These are ER transmembrane proteins that transduce the ER stress signal to the nucleus. It is of interest that these sensors are maintained in their inactive state by binding BiP (PERK, IRE, ATF6) and calreticulin (ATF6)[31].Adapted from.[39]

I.3.3. Golgi-associated quality control

A post ER quality control also exists. Certain misfolded proteins can escape the ER and be found in the Golgi. ER chaperones and folding enzymes can follow them beyond the ER. Members of the ER QC machinery such as BiP, calreticulin, glucosidase I and II, GT and PDI possess an ER retrieval KDEL motif.[40] Calnexin instead possesses a KKXX cytosolic retrieval motif (calnexin is a transmembrane protein) and is likely to transit between the ER and Golgi and to be transported back to the ER. Substrates that are misfolded in the Golgi may undergo retrograde ER translocation for ERAD degradation or be targeted directly to the endosomal system for degradation by vacuolar/lysosomal proteases.

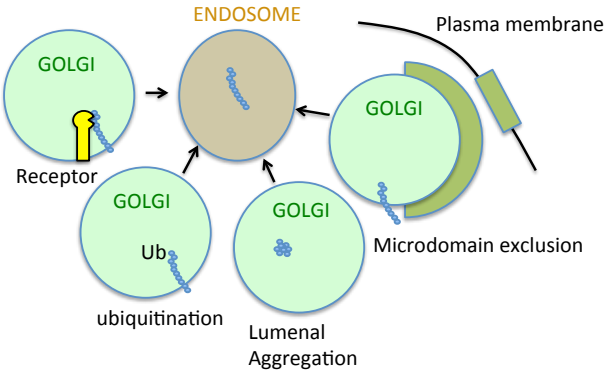


Figure 10 - Degradation pathways in Golgi
A transmembrane protein can be targeted for degradation by ubiquitin ligases (ubiquitinating cytosolic regions), luminal aggregation of the protein itself or failure to properly partition in specific lipid microdomains.[41]

I.3.4. Plasma membrane associated quality control and degradation

Endocytosis involves the capture of TM proteins and their extracellular ligands into cytoplasmic vesicles that are pinched off from the plasma membrane. Endocytosis of TM receptors and their ligands removes them from the surface, where they are able to interact. There are many endocytic pathways and portals such as clathrin-dependent and clathrin-independent pathways. Upon internalization, the TM proteins and their ligands are transported to early endosomes from where they are either recycled to the membrane or degraded.[42]

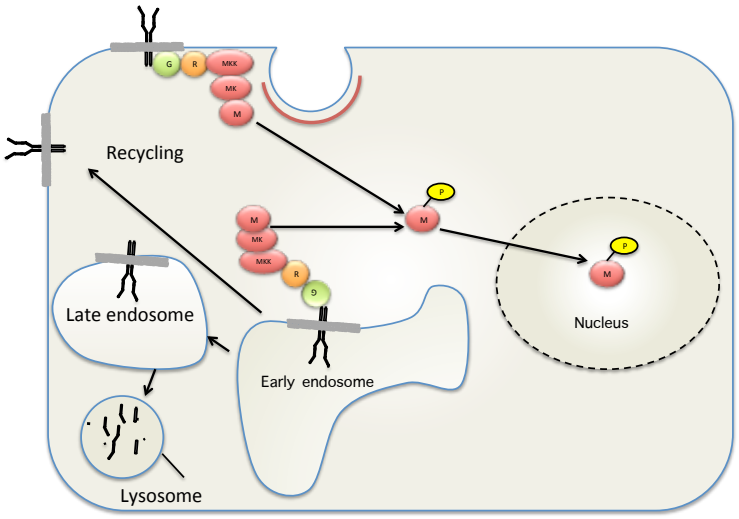


Figure 11 - Plasma membrane associated degradation and recycling
In the case of signal transduction, endocytosis is one of the main regulators of the signal intensity and duration. Conversely, receptor signaling regulates the endocytic machinery. Activation of receptors or downstream effectors often stimulates receptor endocytosis. It is of interest that signaling can also

occur from the endosomal membrane itself and sometimes with higher efficiency.[43] For example, interleukin-4 receptor density sufficient for signaling is only reached inside endosomes.[44,45] Downstream signaling pathways like MAP-kinase are activated by G-CSFR in endosomes.[46] Adapted from.[43]

I.4. Dimerization of transmembrane and juxtamembrane sequences

Dimerization is a general mechanism by which TM proteins and especially growth factors and cytokine receptors trigger their functions. Helix–helix interactions have been shown to drive dimerization in bitopic transmembrane proteins. Examples exist for glycophorin A[47] or T cell receptor.[48] These helix –helix interactions are very specific with the example of native glycophorin A being able to interact only with synthetic peptides corresponding to the TM domain of glycophorin A, but not with synthetic peptides corresponding to the related glycophorin C or IL2-R TM domain.[49]

Helices must closely pack together to form stable dimers. This could be the reason for a high occurrence of glycine and other small amino acids (Ser, Thr, Ala) at i and i+4 at the dimer interface, with motifs such as GxxxG, AxxxG, GxxxA, GxxxS. These small residues are important to remove steric barriers and put the two helix backbones in close proximity allowing inter-helical carbon hydrogen bonds to occur across the helix−helix interface, namely between Cα–H donors and backbone carbonyl oxygen acceptors (Cα–H···O=C bonds).[50,51]

I.5. Coiled-coils

Coiled-coils represent a particular case of oligomerization of helices. They are super secondary structures where two or more α-helices are twisted (coiled) together like the strands of a rope. Linus Pauling and Francis Crick have independently discovered coiled-coils in early fifties.[52] In this special motif, there is a tight packing of the two helices with the side chains of one helix superimposed between the side chains of the other helix in a model known as a knobs-into-holes. The optimal angle for those helix to helix packing corresponds to a 20° left handed coiled coils (LHCC).[53] Helices with left-handed crossing angles are more tightly packed on average than helices with right-handed crossing angles.[53] Keratin, myosin, kinesin or leucine zippers are examples of LHCC that are much more frequent than right-handed coiled coils. The two stranded (dimeric) α- helical coiled coil are characterized by heptad repeats "a,b,c,d,e,f,g", where most "a" and "d" residues are interfacial residues and hydrophobic in nature. Position “e”, “g” can also be considered as interfacial if considering a less restrictive definition of interfacial residue using voronoi polyhedral. LHCC have interfacial residues “a” and “d” each third and fourth residue (axxdxxxaxxd). TMD dimers can adopt such a coiled coil configuration with “a“ and “d position that are enriched with small residues like Gly, Ala or Ser but that rely mainly on Leu, Ala, Val and Ile. The interface can be closely packed in the crossing region and can be loosely packed in the region where the helices deviate. The function of coiled–coils is to drive oligomerization and this is why LHCC are used by a multitude of proteins, including receptors being ideal mediators of helix interaction.

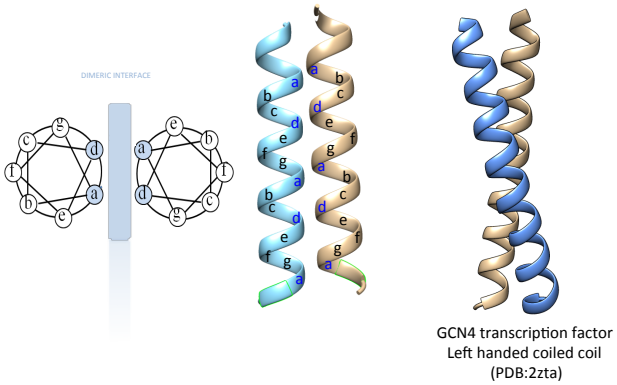


Figure 12 - Left handed coiled-coil
In the heptad nomenclature, the "a" and "d" positions are defined as those residues in the helix–helix interface. Two stranded coiled coils are composed of hydrophobic amino acids in position "a" or "d". Coiled-coils are stabilized by ß branched hydrophobic amino acids in position "a", such as Ile or Val to a higher extent than by non-branched residues like Leu.[54] Ile and Val are found almost three times more frequently at position "a" than at position "d" in the coiled coil domain of myosin.[55] While interacting TM domains can resemble coiled coils, their interfacial positions "a" or "d" are enriched by small residues such as Gly, Ala, Ser (GAS motif).[56]

I.6. Hematopoiesis and cytokine receptors

Blood is a highly regenerative tissue with more than 200 billion red cells, 100 billion platelets and 100 billion leucocytes made everyday. Blood is composed of mature blood cells of the erythroid, megakaryocytic, granulocytic, monocytic or lymphoid lineages that can be classified as "myeloid" or "lymphoid" and as "immune" or "non immune". As most cells are short lived, new blood cells are continuously formed to renew the hematopoietic pool. Those cells are continuously arising from novel clones to sustain a high degree of polyclonality.

Hematopoiesis is the process of making mature and functional blood cells of all lineages. It starts in the embryo and continues throughout adult life. During its ontogeny, hematopoiesis occurs in several and discrete developmental niches. A first wave of hematopoiesis begins in the yolk sac of the early embryo and continues in the aorto-gonado-mesonephros zone (AGM) and in the placenta before moving to the liver and finally switching to the bone marrow where adult hematopoiesis takes place. The definitive hematopoiesis can be depicted as a kind of hierarchized amplification process where mature cells arise from pluripotent long term repopulating hematopoietic stem cells (LT-HSC) that are capable of self-renewal, quiescence and differentiation into more and more committed progenitors of all lineages. We are born with our stem cell pool, which contains around 10^6 stem cells. Recently, Sun and colleagues have suggested that during steady-state hematopoiesis LT-HSC have only a minor contribution to hematopoiesis and that it is rather the long lived MPPs (multipotent progenitor) or the MyPs (myeloid progenitor) that are responsible for the ultra high number of clones.[57] During ontogenesis, the first blood cells do not originate from the LT-HSC. Before the onset of

circulation, a primitive hematopoiesis begins in the yolk sac where primitive nucleated red blood cells and endothelial cells arise from a common hemangioblast progenitor. The formation of early blood cells from the hemangioblast could pass through an intermediate hemogenic endothelial stage at the onset of hematopoiesis.[58] The precise origin of LT-HSC is still conceptual and debatable, with recent observations that indicate LT-HSC emergence from endothelial cells of the aortic region.

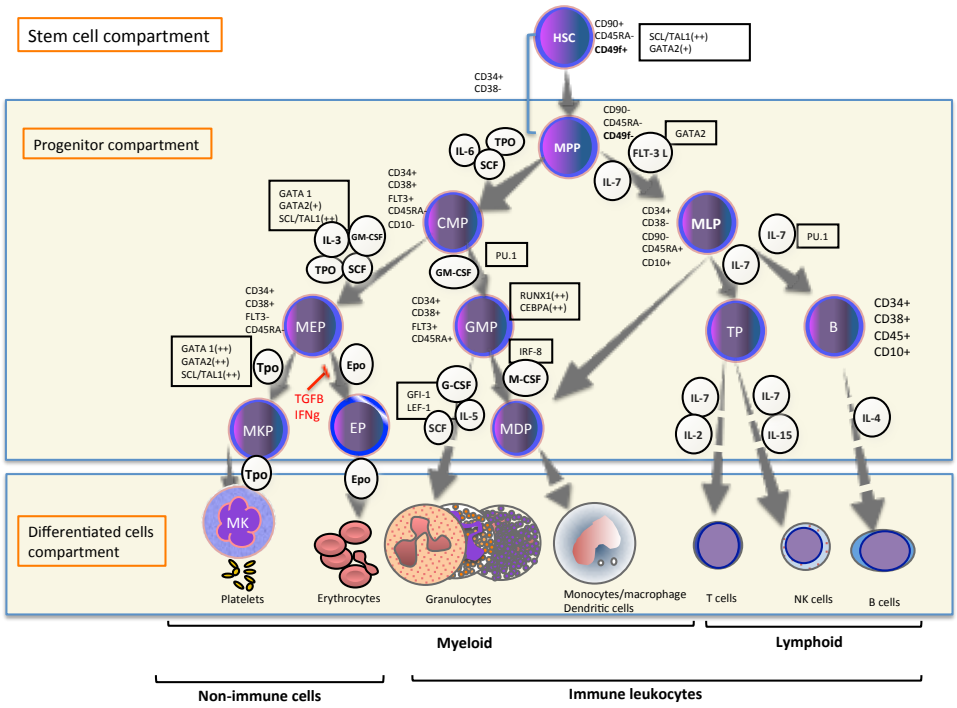


Figure 13 - Hematopoiesis

Players in the hematopoietic cascade include various progenitors, cytokines, and transcription factors, as well as the environment or so called "niche" (not shown).

I.7. Megakaryopoiesis

The megakaryopoiesis is a hematopoietic differentiation process that leads to mature platelet formation.

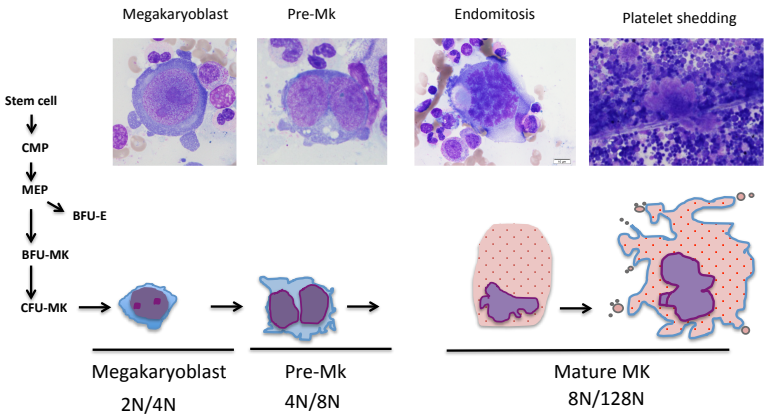


Figure 14 - Megakaryopoiesis

The process begins with the multistep differentiation of a HSC into more differentiated and megakaryocytic committed progenitors called BFU–MKs. Those BFU-MKs continue their maturation into CFU-MKs. Colony assays on collagen for quantitating human and mouse CFU-MKs are difficult because TGF-b and IFNs commonly found in the fetal bovine serum used in colony assays are inhibitors of CFU-MKs. Human CFU-MKs are detected by staining of the cells with an antibody to the GPIIb/IIIa (CD41) while mouse CFU-MKs can be identified by the detection of acetylcholinesterase activity of rodent megakaryocytes.

The CFU-MK engenders the first morphologically distinguishable cell of the megakaryocyte lineage called the megakaryoblast. It takes 5 days for the megakaryoblast (membrane with pseudopods, no granulation, regular nucleus) to give rise, through a pre-megakaryocytes stage (lobated nucleus, rare granules), to mature and polyploid megakaryocytes (multilobated, rich in granules). The ploidization of megakaryocytes results from endomitosis. Endomitosis is a particular case of mitosis where the DNA content is doubling at each step and for which the cytokinesis is replaced by a gap phase. The endomitosis has a cycling pattern with prophase, metaphase, anaphase A, gap phase and prophase again. When the ploidy reaches 16N, the endomitotic cycles stop with megakaryocytes experiencing a senescence-like cell cycle arrest and a terminal differentiation leading to platelets shedding in the circulation.[59]

Due to chemokines and their receptors such as (CXCL12/CXCR4) megakaryocytes are migrating from the osteoblastic niche to the vascular niche of the marrow, where they release platelets in circulation via a process known as proplatelet formation. Proplatelets can be millimeter long and elongate from the megakaryocyte due to microtubules assembly but also microtubules sliding.[60] *The platelet formation is secondary to granules grouping and cytoplasm fragmentations at the proplatelet tip. One megakaryocyte generates 1,000 to 8,000 platelets. Old desialylated platelets bind to the hepatic Ashwell-Morell receptor (AMR) and induce via JAK2/STAT3 the expression of Tpo mRNA.*[61]

I.8. Platelet physiology

Platelets have a mean life span of 8-10 days and are programmed to die by a Bcl–XL/BAK prosurvival/proapoptotic molecular clock.[62]

Some principles about platelets: [63]

- The platelet count mass is quite stable throughout the life of an individual.
- The normal platelet count has great inter-individual variablity.
- Platelet size is inversely correlated with their count.
- The mass of platelets, but not their count, is conserved in an individual.
- MKs respond to a change in platelet mass by varying their number, size and ploidy.

I.9. Cytokines

Cytokines are signaling molecules that play many important roles in growth and differentiation of cells especially of the immune system and blood, but also in the nervous system. Those molecules will induce durable effects on gene expression by activation of transcription factors after binding to their cell surface receptor. Cytokines are relatively small-secreted molecules (160 amino acids) composed of four asymmetric α helices specially arranged, with an up-up-down-down topology. These conserved features are evidence that they are coming from a common ancestor, but these features also play an important role in the way they bind to the extracellular domains (ECDs) of their cognate receptors via two different binding sites and with different affinities. As a consequence, the binding of those cytokines to their receptor is made in a step-by-step manner.[64] Basal hematopoiesis as well as emergency hematopoiesis (in case of blood loss or reactive process) is finely tuned by cytokines and their receptors and the signaling pathways they induce, which can be compared to different melodies played by an orchestra and decoded by the nucleus in signals for survival, proliferation, differentiation or apoptosis. If the cytokines' orchestra is not playing, no blood cells will be made and the marrow will evolve to aplasia. If they are playing too loudly (enhanced or prolonged signaling), too many blood cells will be made and there will be a proliferative neoplasm. Hematopoietic cytokines include interleukins (ILs), colony stimulating factors (CSFs), erythropoietin (Epo) and thrombopoietin (Tpo). Cytokines and their receptors generally play a permissive role on growth and differentiation.[65]

I.10. Cytokine receptors

Cytokine receptors are members of a superfamily of single membrane-spanning receptors devoid of intrinsic kinase activity that all rely on cytosolic Janus kinases (Jaks) bound to their cytosolic domains to transmit their signal. They share similarities including a common tertiary fold and are type I TM proteins as topology. The superfamily is divided in two families, denoted as type-1 and type-2 cytokine receptors that function along the same principles via JAK activation. Type-1 cytokine receptors can form homodimers, heterodimers or oligomers with α, β, γ or gp130 subunits (the α chain being particularly important for cytokine binding) and exhibit several conserved features such as WSXWS motifs and precisely spaced Cys residues in the extracellular domain and conserved Boxes 1 and 2 in the cytosolic domain,

while type-2 cytokine receptors are heterodimeric, lack those conserved features of type-1 receptors, but overall maintain the fold conservation and mechanism of activation of JAKs via oligomerization/heterodimerization. They are composed of two-receptor chains (R1 & R2).

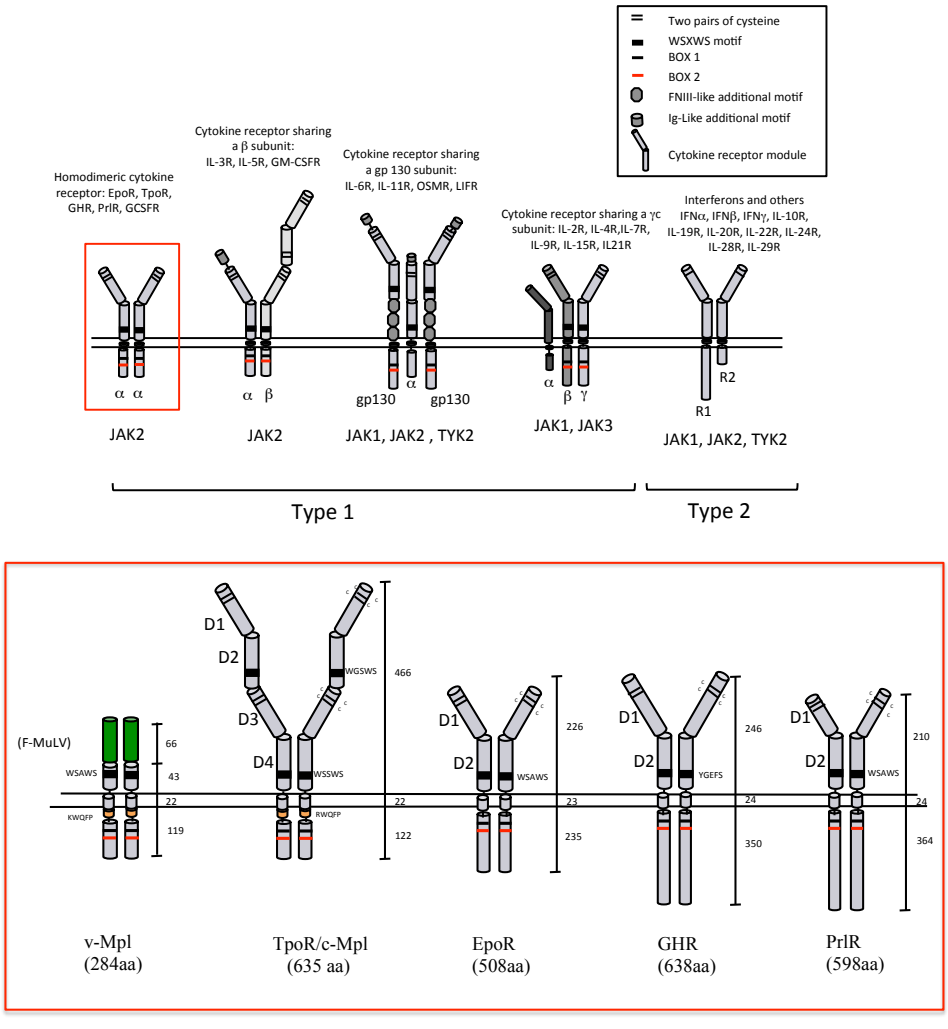


Figure 15 - Cytokine receptor family

Cytokine receptors contain at least one 200-residue extracellular cytokine receptor module (CRM) composed of two fibronectin III-like (FNIII) domains connected by a short linker. Type-1 cytokine receptors can contain additional FNIII-like or Ig-like domains. Each FNIII domain inside the CRM is organized as an antiparallel β-sheet and composed of seven β-strands.[66] *For type-1 cytokine receptors, the CRM possesses two conserved pairs of cysteine in their most N-terminal region and a conserved WSXWS motif at the end of the C-terminal domain. Both contribute to efficient receptor folding and surface expression. Of note, the tryptophan in this WSXWS can barely be replaced by other aromatic*

amino acids (Trp > Phe > Tyr >>> remainder) to ensure a correct folding and proper exit form the ER.[67] Cytokine receptors have a single helical transmembrane domain and share some common properties in their intracellular part, especially for type-1 cytokine receptors, like a proline rich motif (PXXP) called "Box 1" and a motif rich in hydrophobic amino acids followed by several negatively charged residues and ending with one or two positively charged residues called "Box 2". The Box 1 and Box 2 motifs are important for JAK binding. Receptors with intrinsic tyrosine kinase activity, such as PDGFR or EGFR, do not contain those motifs.[68]

The homodimeric receptor family comprises EpoR, TpoR, GHR, G-CSF and PrlR that are made of two identical α-chains and function as homodimers. The IL-3R family comprises IL-3R, IL-5R and GM-CSFR. These are heterodimeric receptor composed of one α-chain and one β-chain. The Il-6R family is composed of IL-6R, IL-11R, OSMR/IL -31, LIFR, and CNTF-R that combine with two gp130 to form a receptor complex. The IL-2R family shares the common γ-chain and is composed of IL-2R, IL-4R, IL-7R, IL-9R, IL-13R, IL-15R, and IL-21R. Despite the fact that they are devoid of any kinase activity and that they rely on JAKs for their signaling, the Box 1 is absent and the Box2 motif is poorly conserved in type-2 cytokine receptors. The two receptor chains (R1 & R2) contain two FNIII-like motifs in their extracellular domain. The R1 chain has a long cytosplasmic tail and the R2 as a short cytoplasmic tail that is enough to bring a member of the JAKS to the complex. The type 2 cytokine receptors include the , so called, type I interferons (IFN-αR and IFN-βR that activate Jak1, Tyk2, STAT1, STAT2 during signal transduction) and type II interferons (IFN-γR) that use Jak1, Jak2, and STAT1 for signaling).[69] The type II interferon family also contains IL-10 related receptor (IL-10R, IL-20R, IL-22R).

I.11. Janus kinases

In the 1990s, different cDNA cloning approach identified the Janus kinases. Their unknown function at the time led to their name "Just Another Kinase", as they were cloned by homology initially by Andrew Wilks at Ludwig Institute for Cancer Research in Melbourne, Australia. More recently, they were renamed Janus Kinases from the Roman God with two faces given that they possess two kinase domains. There are four mammalian JAKs (JAK1, JAK2, JAK3, TYK2) 120-140 kDa related proteins with an amino terminal region of 500 residues and two kinases domains that mediate signaling of approximately 50 cytokines and hormones. JAKs associate with the membrane proximal region of cytokines receptors and are responsible for a range of phosphorylation and signaling events.[70] In the type-1 cytokine receptor superfamily, JAKs associate with with the weakly conserved Box 1 and Box 2 motifs in the cytosolic receptor domains.

I.11.1. Murine models of JAK deficiency

JAK1-/- mice show perinatal lethality due to a defect in neural function and impaired lymphoid development.[71]

JAK2-/- mice die embryonically due to lack of definitive erythropoiesis, whereas normal lymphoid development is observed.[72]

JAK3-/- mice exhibit severe combined immunodeficiency with a low number of T and B lymphocytes.[73]

TYK2-/- mice show defective IFN α/β signaling and unexpectedly show defective IFN γ signaling due to the possible association of IFNγR2 with IFNR1, which might be necessary for full IFN γ signaling. Those mice cannot clear virus and display a reduced T cell response.[74]

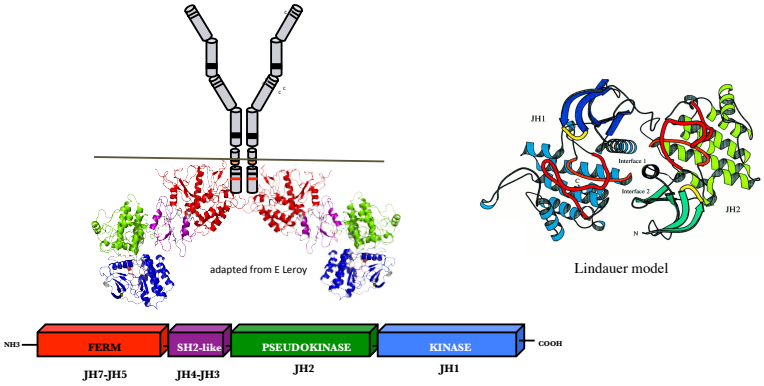


Figure 16 - JAK structure

JAKs are big proteins that contain seven homology domains named Jak Homology domains or JH domains. They contain from the C-terminus to the N-terminus a kinase domain (JH1), a pseudokinase domain (JH2), an SH2 domain (JH3 and part of JH4), and a FERM Band 4.1, ezrin, radixin, moeisin (part of JH4 until JH7). The FERM domain is important for connection with the receptor. Prior to activation, JAK2 kinase is phosphorylated on Ser523 in the SH2 domain, which negatively controls basal JAK2 activity.[75] Upon stimulation, Y1007 and Y1008 in the activation loop are trans-phosphorylated which turns on the kinase activity and allows phosphorylation of other sites.[76] As receptor activation is transient, phosphorylation of the negatively acting residue Y570 in the JH2 domain inhibits JAK2 signaling and terminates the phosphorylation cascade.[77] The pseudokinase domain (JH2) of JAK2 is recognized to inhibit the kinase domain, but there is evidence for both positive and negative roles of JH2 on JH1.

The first clue that there is an inhibitory function of JH2 over JH1 comes from Hopscotch (the fly JAK2) mutation in the Drosophila (Hop tumorous lethal "tuml") and also Hop T42 in JH2 domain which gives a leukemia in flies and a differentiation of hemocytes into lamellocytes giving black melanocytic tumors.[78] On the opposite JH2 mutations in JAK3 lead to a defective IL-2 signaling and to a SCID phenotype indicating this time a positive role.[79] The group of Sandra Pellegrini has also shown that an E775K mutation in the pseudokinase domain of TYK2 kinase acts to increase susceptibility of mice to infection. Deletion of the JH2 domain of JAK2 abrogates cytokine-induced activation but increases basal activity confirming a dual role of the pseudokinase domain of JAK2.[80] The pseudokinase domain of JAK2 was named a pseudokinase because it lacks several catalytic residues. The pseudokinase domain of JAK2 has 1) the catalytic aspartic mutated to an asparagine (N_{673}) in the catalytic loop (orange in the Lindauer model), 2) an alanine (A_{597}) instead of glutamic acid in helix-C, and 3) a $DP_{601}G$ sequence instead of a DFG motif at the beginning of the activation loop (red in the Lindauer model). Finally, a threonine (T_{557}) replaces a glycine in the nucleotide-binding loop (yellow in the Lindauer model). The JH2 domain crystal structure has been obtained and shows a classical kinase conformation.[81] JH2 was shown to bind ATP and to retain catalytic activity phosphorylating Y570 on JH2, itself in trans and Ser 523 of the SH2 –JH2 linker in cis. Noteworthy, in JAK2 V617F Y570 was not phosphorylated due to loss of JH2 function.[82]

I.12. Signaling pathways

I.12.1. STATs (Signal Transducers and Activators of Transcription)

The Signal Transducers and Activators of Transcription (STATs) are latent transcription factors, that were first identified as mediators of interferon- induced signaling (IFN α/β and IFN γ). Later, STATs were shown to be downstream of many ligand induced receptor dimers. STATs contain an N-terminal domain, a DNA binding domain, a linker, an SH2 domain that is involved in STAT dimer formation, and a C-terminal transactivation domain. Seven STATs have been identified in mammals, namely STAT1-6 including STAT5a and STAT5b ranging in size from 90-115kDa. Homo and heteromeric complexes are induced by STATs. STAT1 can form homodimers downstream of IFNγ, or heterodimers with STAT3 in response to gp130 containing receptors (like IL-6). STAT1 can also form a complex with STAT2 and IRF9 (p48) called ISGF3 in response to IFNα/β and sometimes IFNγ.[83] These complexes recognize different DNA regulatory elements. ISGF3 complex recognize IFN-stimulated response element (ISRE) element on DNA regulatory sequence, while STATs heterodimer or homodimers binds palindromic IFN-γ Activation Site (GAS) on promoters and transcriptionally control target genes expression.

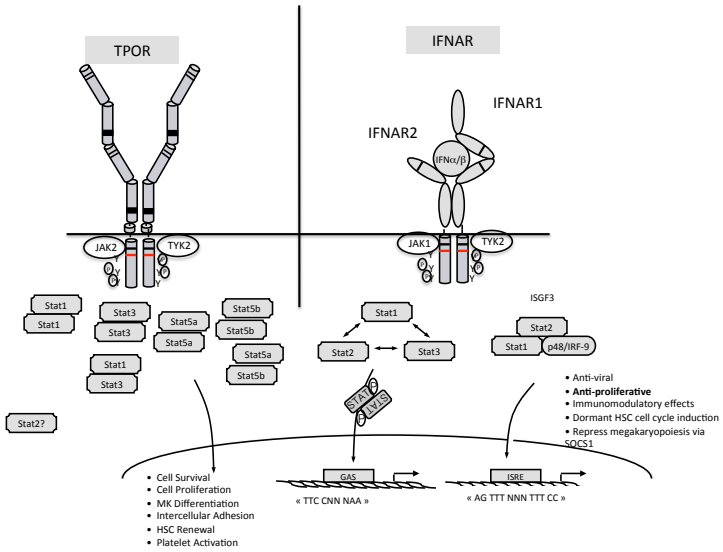


Figure 17 - JAK/STATs pathway for TpoR and IFNaR

The canonical JAK/STAT pathway downstream of TpoR and type I IFN receptor: Various STAT dimers increase the complexity of the signaling compared to the Drosophila situation with only one STAT, STAT92E. Dimers bind to GAS element on reporter while ISGF3 complex binds ISRE.

I.12.2. Murine models of STAT deficiency

STAT1-/- mice show defective innate immunity against microbial pathogens and viruses due to lack of IFN-α and γ.[84]

STAT2-/- mice show immune deficiency such as increase susceptibility to viral infection due to loss of type-1 IFN autocrine and paracrine loops.[85] STAT2 contains an atypical DNA binding domain.

STAT3-/- is embryonically lethal[86] and STAT3-/- T cell specific mice are severely impaired in Il-6 induced proliferation.[87]

STAT4-/- cannot form TH1 cells largely because of IL-12 malfunction.[88]

STAT5a and STAT5b double knockout showed multiple cytokine receptor defects (IL-2, IL-3, GM-CSF, G-CSF.[89]

STAT6-/- mice show that STAT6 is crucial for IL-4 signaling with the same outcome than IL-4 -/- mice that suffer from a defect in TH2 development and IgE-class switching.[90]

I.12.3. The JAKs/STAT pathway

In the canonical model of JAK/STAT signaling, activation of the four Janus Kinases (JAK1-3 and Tyk2) is triggered by ligands, which bind to type-1 cytokine receptors such as GP130, Oncostatin-M receptor (OSM-R), thrombopoietin receptor (TpoR) and erythropoietin receptor (EpoR) or to type-2 cytokine receptors, such as IFN receptors. Generally present on the plasma membrane as either homo- or hetero-dimers, receptor complexes are pre-bound with JAKs before their arrival at the cell surface and, when stimulated by ligand binding, they activate JAKs and trigger them to tyrosine phosphorylate latent STATs. The phosphorylation of the seven human STATs (STAT1-5a, 5b-6) is followed by their dissociation from the receptor, dimerization, exposition of a nuclear localization signal (NLS) and their translocation to the nucleus, where they exert their canonical functions as transcription factors.[91] The JAK/STAT pathway shares a high degree of biochemical and functional conservation over more than 500 million years of evolutionary time between vertebrates and invertebrate systems. The *Drosophila* JAK/STAT cascade is comprised of a transmembrane receptor termed Domeless (Dome), a short negatively acting co-receptor called Latran/Eye Transformer (Lat) and three extracellular ligands of the Unpaired (Upd) family. In addition, a single JAK kinase known as Hopscotch (Hop) and STAT92E act to transduce signaling downstream to the nucleus.[78] But studies in *Drosophila* have also reveal a non canonical mode of action of JAKs when unphosphorylated STATs are localized on heterochromatin in the nucleus associated with heterochromatin protein 1 (HP1). Phosphorylation of STATs by JAKs on heterochromatin can lead to dislodgment of HP1 and STATs and unpacking of heterochromatin to euchromatin due to heterochromatin instability.

I.12.4. The MAP-kinase pathway

Almost all cytokine receptors that couple to JAKs can induce the Ras/Raf/MEK/MAPkinase cascade, to different degrees which will contributes to cell proliferation and differentiation.

Ras is a membrane anchored protein and a member of the GTPase superfamily with an "ON" state GTP bound and an "OFF" state GDP bound. Mutant Ras proteins in cancer are always in the "ON" state.
Grb2 adapter protein binds to both phosphotyrosine on the cytoplasmic tail of the receptor and SOS (son of seveless). SOS has Ras-GDP as a substrate and possesses a guanine nucleotide exchange factor activity that will turn on Ras, by stimulating the release of GDP and exchanbe with GTP. So Ras is bridged to receptor via Grb2 and SOS. Active Ras will then bind to an effector, such as Raf, which releases the inhibition of Raf by the bound 14-3-3 protein, which leads to activation of Raf. GTP to GDP hydrolysis of Ras terminates signaling and releases active Raf. Raf phosphorylates MEK which is a tyrosine and serine /threonine kinase. Then MEK phosphorylates a tyrosine and a serine residue in the activation loop of ERK (a serine /threonine kinase), leading to its activation. ERK dimerizes, phosphorylates p90, enters the nucleus and phosphorylates TCF. By the time, active phospho P90 also enters the nucleus and phosphorylates SRF. The complex of TCF and two SRF bind to SRE enhancer and induces transcription of genes. Adapted from.[92]

I.12.5. The PI3-kinase pathway

Membrane phosphorylated inositol lipids known as phosphoinositides are involved in this pathway. Many cytokine receptors and RTKs recruit the enzyme phosphatidyl inositol-3 kinase (PI3-kinase) to the membrane. This enzyme catalyzes the transformation of PI 4,5 bisphosphate (PIP2) in PI 3,4,5 trisphosphate (PIP3). Akt (also named PKB), as well as PDK1, are recruited to the membrane due to the strong affinity of their pleckstrin homology (PH) domains for PIP3. In this way, they are brought close together at the membrane surface. This proximity allows PDK1 to phosphorylate serine/threonine kinase Akt. Phospho-Akt can directly phosphorylate and inactivate proapoptotic protein Bad. Akt can also phosphorylate serine and threonine of the Forkhead transcription factor FOXO3A. FOXO3A is a pro-transcription factor that is localized in the nucleus. Upon phosphorylation by Akt, FOXO3A binds to a 14-3-3 protein that sequesters it outside of the nucleus preventing its and gene induction roles.[92]

I.13. The thrombopoietin receptor

I.13.1. TpoR structure and domains

TpoR (CD110) is a 635 amino acid type I transmembrane receptor with the N-terminal side facing the extracellular space. TpoR is also named c-Mpl since it is the human homologue of the MyeloProliferative Leukemia virus oncogene (v-Mpl) that induces overgrowth of hematopoietic cells in mice. The v-Mpl is a truncated form of c-Mpl with only a small portion of the ECD but the entire TMD and ICD. It is a member of the type-1 cytokine receptor family.

TpoR gene is located on the human chromosome 1 and on the murine chromosome 4. TpoR /c-MPl was cloned in 1992[93], while its ligand (Tpo) was discovered two years later, as it was

shown that Tpo binds to the extracellular domain of c-Mpl. Moreover, it was shown that the soluble form of the « extracellular domain of c-Mpl » has a dominant negative effect on megakaryopoiesis.[94]

TpoR is an N-glycosylated protein with four N glycosylation sites (Asn_{117}, Asn_{178}, Asn_{298}, Asn_{358}). Structural modeling[95] and calorimetric experiments[96] showed that D1–D2 is responsible for Tpo binding.
TpoR includes 12 exons with exon 1 to 9 coding for the extracellular domain, exon 10 for the transmembrane domain, exon 11 and the beginning of exon 12 coding for the intracellular domain.

Thrombopoetin receptor is a member of the type-1 homodimeric cytokine receptor family that also comprises EpoR, GHR, G-CSFR, PrlR, which are made of two identical α-chains that function as homodimers. The cytoplasmic juxtamembrane domain (JM) of TpoR can be aligned with other cytokine receptor according to the proline rich box 1 with the exception of a unique and conserved amphipathic "RWQFP" motif at its transmembrane cytosolic junction.[97]

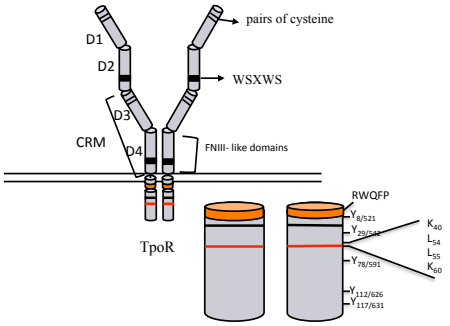


Figure 18 TpoR intracellular domain
TpoR also possess a relatively short intracellular domain starting with the RWQFP motif and that contains Box 1, Box 2 and important tyrosine residues for signal transduction. TpoR intracellular domain contains in fact five tyrosine residues. Three of them are of particular interest. Y78/591 plays a negative role in TpoR signaling. Y112/626 is the main docking site for TpoR signaling. Y117/631 is the second docking site for TpoR signaling. Between the juxtamembrane domain "RWQFP" and Box 1, TpoR contains a hydrophobic motif composed of residues L524, L528, W529 that is important for JAK2 signaling. In the case of EpoR, alanine insertion before the EpoR homologous and α helical L253, I257, W259 motif showed that the orientation of these residues (and not the distance from the bilayer) is crucial for activated JAK2 to signal but not for JAK2 activation itself.[98] TpoR is ubiquitinated after Tpo stimulation on Lys K40 and K60. TpoR KK-RR is not ubiquitinated after Tpo binding. Expression of a mutant where two Leu residues in Box 2 are mutated to alanine, TpoR LL-AA, leads to an enhanced expression on the surface confirming the role of this diLeucine signal in the intenalization of the receptor.

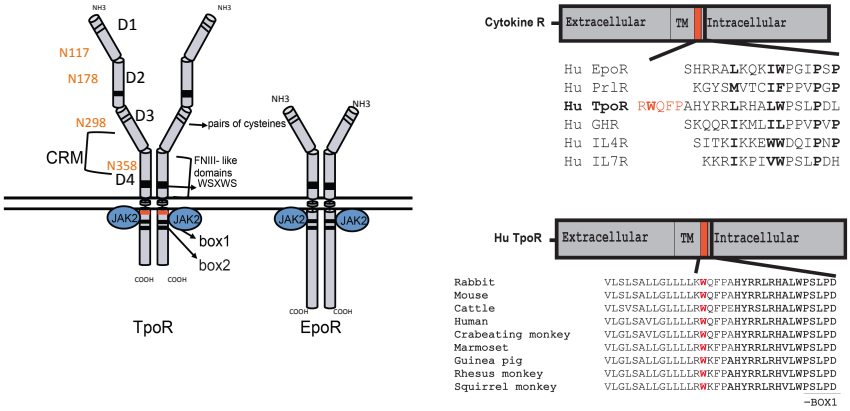


Figure 19 - Structural features of TpoR and comparison to other receptors

The thrombopoietin receptor (TpoR) has several unique features compared to other members of the cytokine receptor family.

The extracellular domain of TpoR is much larger than other homodimeric type-1 cytokine receptors with a duplication of the cytokine receptor module (CRM). The extracellular part of the receptor contains two CRMs, two WSXWS motifs, four pairs of cysteines important for proper folding and four fibronectin-III like domains of approximately 100 residues each, named D1-D2 (distal part) and D3-D4 (membrane proximal part). Deletion of the D1-D2 activates the receptor.[99] Both D1-D2 and D3-D4 are required for cell surface targeting. Deletion of D1-D2 allows the receptor to traffic weakly and to be active, whereas deletion of the D3-D4 prevents cell surface localization (D1–D2 alone having a strong retention effect). Replacing the extracellular domain with the D1-D2 of EpoR (ETT construct) shows a normal traffic.

It is noteworthy, that D1-D2 stop or D1-D2-D3-D4 stop are soluble forms without TM or ICD that can be secreted (Roxana Albu unpublished data).

The extracellular domain contains four N-glycosylation sites (N117, N178, N298, N358). Albu et al have shown that N-glycosylation sites exert important regulatory roles on TpoR cell surface expression. No single site is crucial for TpoR cell surface expression and deletion of three out of four sites reduces but still allows cell surface expression. Sites 1, 2 and 4 have positive effect and site 3 has negative effect on cell surface expression. Asn to Glu mutation of the all four N-glycosylation sites dramatically impaired cell surface expression.[100] The transmembrane domain has a length of 22 amino acids which is a bit shorter than other type I cytokine receptors.

I.13.2. TpoR artificial activation

There are several ways to trigger TpoR activation. First the extracellular domain is duplicated, and deletion of this second (more distal) domain causes constitutive activation while preventing Tpo binding.[99] Second, there are 5 amino acids inserted directly C-terminal to the TM domain, the RWQFP motif that is unique to TpoR and deletion or mutation of this insert causes ligand-independent receptor activation.[97] Besides deletion, there are point mutations that activate the receptor in absence of its ligand mutations. Those mutations include S368C cysteine substitution in the EC domain[101] and clinically relevant mutations described later in the extracellular and intracellular juxtamembrane domains and in the TMD[18,102-104].

The thrombopoietin receptor can also be activated by the truncation of part of its extracellular domain and fusion at its N terminus with a viral sequence leading to v-Mpl.[105]

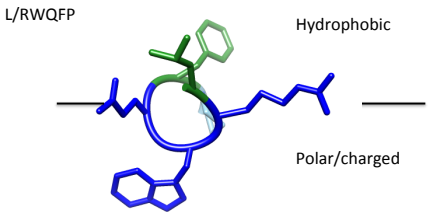


Figure 20 - RWQFP motif
The RWQFP motif is an amphipathic α-helix meaning a stretch of α helix with one side polar and the other hydrophobic.

I.13.3. Activation by Tpo ligand, Eltrombopag and Romiplostim

Tpo binds in a sequential manner to TpoR in a 1:2 stoichiometry. Tpo "site1" first binds to TpoR with a high affinity constant, which is followed by the low affinity binding of Tpo "site2" to TpoR.[96] This mechanism seems to be a more general mechanism that has been also proposed for both EpoR[106] and h-GH Tpo binding is greatly affected by mutations in residues Asp_{235} and Leu_{239} but the nearby WGSWG motif is not important for Tpo binding.

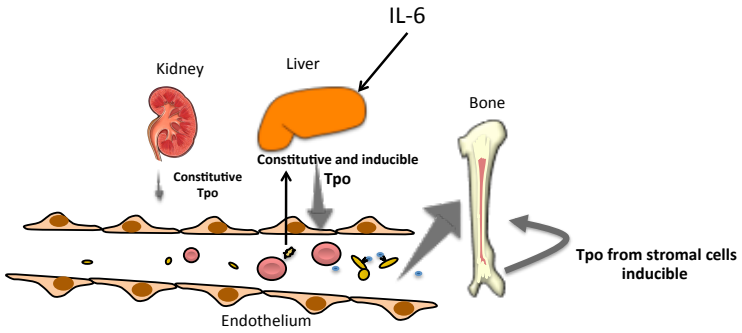


Figure 21 - Tpo physiology and production
Tpo hepatic and renal production has been subject of discussion since 20 years. The production seemed at first glance to be mainly constitutive (with no change in Tpo mRNA levels) in model of induced thrombocytemia.[63,107] IL-6 was later shown to be able to induce hepatic Tpo mRNA production in reactive thrombocytemia.[108] Old desyalated platelets bind to the hepatic endocytic Ashwell Morell Receptor (AMR) and are responsible for the basal hepatic Tpo mRNA production.[61]

Human NDUC, a human homolog of a fungal nuclear migration protein from Aspergillus Nidulans is important for mitotic spindle formation and binds to TpoR on distinct binding sites than Tpo. hNDUC has overlapping biological function with Tpo[109,110]. Two hydrophobic residues, Leu_{228} and Leu_{230} are critical for hNDUC binding as well as the WGSWG motif. hNDUC/Mpl complex traffics through the secretory pathway. Mpl silencing blocks hNDUC secretion.[111]

Concerning drugs, the key concept in treating thrombocytopenia is to treat the underlying cause, which may be using immune regulatory or immunosuppressive therapies such as corticosteroids, immunoglobulins, or even splenectomy if the cause is autoimmune like in ITP. In some case, it could be useful to boost platelet production with the use of TpoR agonist like in myelodysplastic syndrome or in low Tpo condition such like in hepatitis C infection. Recombinant human thrombopoietin cannot be used as a drug due to its immunogenicity.[112] Cross-reactive IgG antibodies, targeting the first 163 aa of endogeneous Tpo and preventing its subsequent binding, are induced in certain patients. Patients with such antibodies do not develop massive bleeding but rather easy bruising and do not respond to prednisone or immunoglobulins.

Romiplostim AMG-531 (Nplate; Amgen) is a peptidyl agonist (60 kDa peptidobody= peptide +antibody) that was discovered by screening peptide libraries that could stimulate Tpo dependent cell lines without producing autoimmune reaction. It is composed of two 14 amino acid peptides (IEGPTLRQWLAARA) with no sequence homology with Tpo linked by the Fc moiety of the heavy chain of an IgG1 antibody. Romiplostim binds at the same distal part than endogenous Tpo.[113,114]

Eltrombopag SB-497115 (Revolade; GlaxoSmith Kline) is non-peptidyl small molecule agonist (442 Da small molecule) and the first orally bioavailable small molecules TpoR agonist. It is a member of the biarylhydrazone class of compounds and binds near the extracellular transmembrane junction of human and chimpanzee TpoR. A specific histidine at position 499 (His499) in the TM domain of Human TpoR and big primates (Chimpanzee) is responsible for this specificity. Eltrombopag essential features include a lipophilic moiety at one end; a linker region composed of heteroatoms in the middle that join a Lewis base at the opposite extremity.[115] This Lewis base binds the positively charged Histidine.
The success of the two compounds to stimulate TpoR and the success of peginesatide to stimulate EPO in chronic kidney disease (EMERALD studies) pave the way for discovering small molecule agonists for good candidates such as GHR and G-CSF.[116] Recently, non-peptidyl small-molecule human G-CSF receptor agonists have been found. Interestingly, A histidine at position 627 in the hGCSFR transmembrane domain is needed for activity of LG7455 similarly to what has been found for Human TpoR agonists such as eltrombopag.[117]

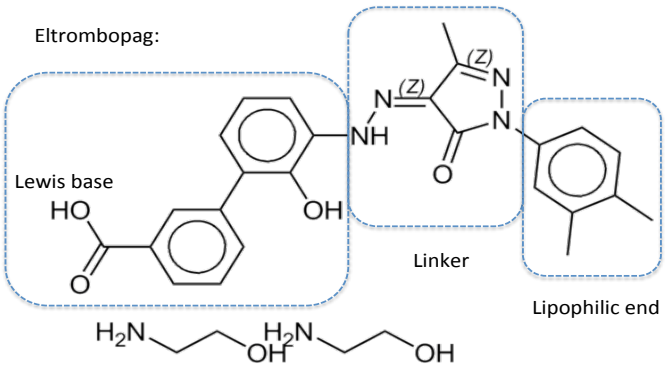


Figure 22 - Eltrombopag structure

Eltrombopag essential features include a lipophilic moiety at one end; a linker region composed of heteroatoms in the middle that join a Lewis base at the opposite extremity.[115] This Lewis base binds the positively charged Histidine.

Eltrombopag is a bisethanolamine salt and the crystalline form should be dissolved in a mixture of ethanolamine and ethanol and warm at 65° to give a red solution. Eltrombopag does not compete with endogeneous Tpo that binds upstream and present additive effect with Tpo.[118]

I.13.4. TpoR dimerization and mechanisms of activation

I.13.4.1. Cytokine receptor dimerization and predimerization

The key evidence to understand TpoR activation mechanism may come from other type-1 cytokine receptors such as EpoR, GHR, PrlR, LIF[119] and IL-6[120]. Those receptors are believed to be ligand independent dimers or in other words preformed dimers. This model of receptor complex formation was first supported by *in vivo* studies of the *Drosophila* receptors Dome and Lat in which ligand independent pre-dimerization is essential for downstream signaling.[121,122] These *in-vivo* studies used a split β-galactosidase (β-gal) complementation assay in which two inactive deletions within the β-gal enzyme (termed Da and Dw) were attached to the intracellular termini of receptors. In this model, β-gal Da and β-gal Dw only generate a functional enzyme following the dimerization of their associated receptors. This approach showed that Dome is dimerized in a ligand-independent, but tissue-specific manner during *Drosophila* embryonic development, suggesting that an unknown process modulates Dome dimerization both spatially and temporally *in vivo*.

Erythropoietin receptor (EpoR), which is the closest to TpoR, is a member of the cytokine superfamily, which contains proteins that are membrane spanning and that transfer a signal after binding growth factor or cytokine protein. EpoR is a single span membrane spanning which possess an extracellular domain, a TMD and an intracellular region. Studies have demonstrated that EpoR is a preformed dimer in absence of EPO. Immunofluorescence copatching assays have shown in chimeric constructs, where domains were swapped with other receptors, that the TMD domain of EpoR is sufficient to maintain the dimeric state of the full-length receptor.[123] Self-assembly of the EpoR transmembrane domain is crucial for efficient

signal transduction. Using the TOXCAT assay, Kubatzky et al, showed that the TMD of EpoR has strong potential to self-interact in bacterial membrane and that disrupting the TMD self interaction potential with a double mutation (LL to GP mutation) prevents an optimal signal transduction. The liganded wild type receptor and the extracellular EpoR R129C active mutant (that brings TM closer due to membrane extracellular domain disulfide bonds) were weaker with this LL-GP mutation.[124] There are also crystallographic evidences that the extracellular domain of the unliganted EpoR is dimeric with a scissor like conformation.[125]

The growth hormone receptor is also a preformed dimer but the mechanism underlying this pre-dimerization remains inconclusive. The TMD does not seem responsible for the preformed dimer but it is rather the dimerization Interface in the ECD that contributes to the predimerization of the GHR.[126]

Comparably the mechanism of PrlR pre-dimerization is still poorly understood, studies using coimmunoprecipitation (Co-IP) and Bioluminescence Resonance Energy Transfer (BRET) experiments revealed the presence of ligand-independent dimers of PrlR. PRL itself did not cause any increase in monomers or dimers of the PRLR.[127] It has been shown that deletion of either the extracellular or the intracellular domain of PRLR does not affect the receptor dimerization, suggesting that the TMD of PRLR is critical for dimerization of PRLR. However, replacement of the extracellular or the intracellular domain of PRLR with the corresponding domain of EpoR abolished the ligand-independent dimerization of PRLR even though the chimeric PrlR retains its TMD.[123] Therefore, unlike EpoR, the preformed dimers of PRLR and GHR may be driven by more complex mechanisms.

I.13.4.2. Cytokine receptor conformational changes

As described above some receptors seem to be already dimeric in absence of ligand. Thus, the dimerization process cannot solely explain the activation mechanism. Dimerization is for sure required for receptor activity but not necessary sufficient condition for activation.
If those receptors exist as preformed dimers in absence of ligand, their activation should be mediated by conformational changes mediated by binding of their ligand.

There are three basic ways for a dimeric receptor to transmit a mechanical signal: rotational of each monomer, increase tilt angle, and translational movement of each monomer.

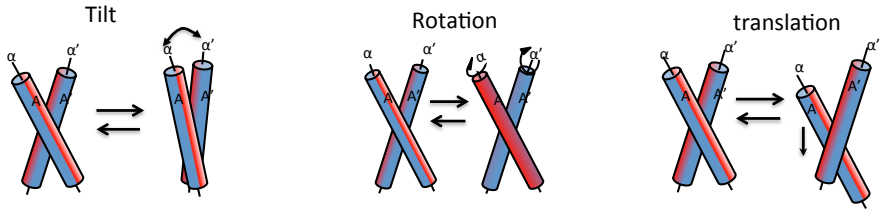


Figure 23 - Tilt, rotation and translation for dimeric transmembrane domains

If we consider again the well-studied EpoR, it can be activated by Epo[128], by small mimetic peptides[129] by monoclonal antibodies directed to the EpoR, by a point mutation R129C in the extracellular domain which covalently stabilize EpoR and activates the receptor[130] or by the spleen focus forming virus (SFFV) gp55-P envelope glycoprotein that can also activate the erythropoietin receptor by specific helix –helix interaction with the TM domain of EpoR when co-expressed in the same cell[131]. So all these modes of activation suggest conformational changes upon the predimeric EpoR. The extracellular domain of the unliganded EpoR is a dimer with a scissor like conformation, but only in high crystallization conditions, while in solution it is monomeric..[125,132] In addition, several studies suggest that a precise orientation of the α helical EpoR TMD continuous with the α helical JM segment is required for EpoR activation.[98] Studies with cysteine scanning mutagenesis (L223C, L226C and I227C) show that certain disulfide-induced orientations in the TMD of EpoR activate the receptor constitutively.[133] Studies with the Put-3 saccharomyces cerevisiae transcription factor dimerization domain coiled-coil fused to the EpoR transmembrane and intracellular domains supports this orientation model.[134,135] Removing one by one amino acid from the TM domain forces the receptor to rotate on its helical axis approximately by 100°. Removing 1-7 amino acids allows one to engineer the seven possible dimeric orientations (cc-TpoR-0 to VI), Seubert et al have shown that only one dimeric TMD orientation corresponding to cc-TpoR-III and VI is active and imparts full activity to the downstream cytosolic domain of EpoR.[136]

The crystal structure of the GhR ECD bound or unbound to GH have been solved. Those structures showed little conformational differences between the liganded or unliganded receptors. The GHR can be activated constitutively by inserting four alanines just after the TMD or just one alanine before Box 1, suggesting that the activation mechanism involves a relative subunit rotation. The discrepancy between the need of +4A in the TMD and +1A only in the JM before Box 1 could come from a twisted or kinked helix.
Molecular dynamics simulations provide evidence at the atomic level that the binding of hGH to the hGHR is associated with a relative rotation 40° counterclockwise of the two subunits.[137] So GH binding initiates signaling by triggering changes in the orientation of the two GHRs.
Recently, Brooks et al. have proposed a mechanism of GHR activation, where the transition of a parallel helix–helix packing to a left handed coiled arrangement in the TMD results in the break apart of the inhibitory pseudokinase domain of one JAK2 from the kinase domain of the other JAK2.

I.13.5. TpoR signaling

The mature form of TpoR is stabilized at the cell surface by the cytosolic kinases by which it signals, JAK2 and TYK2. Those kinases promote both TpoR cell surface localization and an increase in its stability by protection from proteasomal degradation. Proper binding of JAK2 or TYK2 is required for this effect. Inhibiting the JAK /TpoR interaction by alanine mutations in the TpoR intracellular domain encompassing Box1 and Box 2 or by point mutations in the JAKs' FERM domain (JAK2 Y114A and Tyk2 Y102A/F103) affect this increase in cell surface expression.[138]

Activation of TpoR by Tpo leads to a rapid phosphorylation of two JAK family members (JAK2 and TYK2). This activation is dose and time dependent and subsequently induces phosphorylation of STAT1, STAT3 and STAT5.[139] Schulze et al. has found homodimers of STAT1, STAT3, STAT5 and heterodimers of STAT1/STAT3 and STAT5a/STAT5b, but no STAT1/STAT5 or STAT3/STAT5 heterodimers upon Tpo platelet stimulation.[140] JAK2 with its 1132 residues is pretty big compared to the 122 residues of the cytoplasmic part of the TpoR.[141] We have some evidence that JAK2 has a bit more affinity for TpoR than TYK2. TYK2 should bind to TpoR a bit downstream from JAK2 and probably not at the same time. The space along the cytoplasmic tail of the receptor is rather limited.

MAPkinase is involved in the signaling pathway induced by Tpo. Phosphorylation of Erk1 and Erk2 has been demonstrated in Tpo stimulated human megakaryocyte cell line (UT7).[142]
Thrombopoietin activates PI3 kinase pathway and PI3 kinase inhibitors, ie. Wortmannin reduces proliferation of Tpo stimulated cells. The p85 subunit associates with phosphotyrosyne residues of Mpl.[143] In primary the murine megakaryocytic cell line, the p85 subunit of PI3 kinase binds to phosphotyrosine residue in the cytoplasmic tail of the receptor in a complex with src homology 2 protein tyrosine phosphatase (SHP2) and a Gab family adapter protein. p85 conformational changes activate the p110 catalytic subunit of PI3kinase and brings it in close proximity of the cell membrane near its PIP2 substrate.[144]

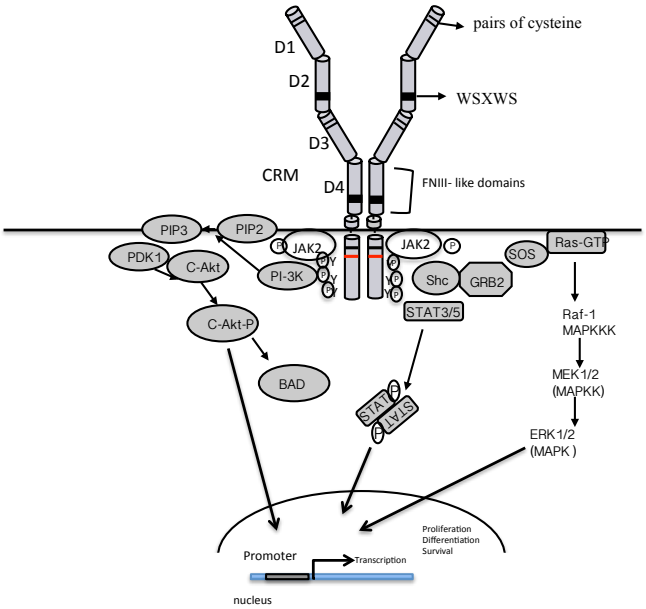


Figure 24 - TpoR signaling adapted from Judith Staerk thesis

I.13.6. Negative regulation mechanisms

In addition to dimerization, receptor stability and turnover also plays a key role in a cells ability to respond to a cytokine signal. A number of negative regulators of the JAK/STAT signaling have also been identified. These include Suppressors of Cytokine Signaling (SOCS)[145], Protein Inhibitors of Activated STATs (PIAS)[146], Protein Tyrosine Phosphatases (PTP, SHP).[147,148] A number of negative regulators have been shown to specifically reduce TpoR induced signaling such as SH2B3 (LNK) adaptor protein through its SH2 domain[149], focal adhesion kinases (FAK) which possesses a FERM domain that could interact with Box1 of TpoR[150], Lyn[151], E3 ubiquitin ligase.[152] These negative regulators act at multiple levels within the signaling pathway and are semi-redundant with one another. Different negative regulators can be recruited at the same site for example on the same phosphotyrosine.[153] The processes that control these regulators and the nature of the scaffolds that bring together both positive and negatively acting pathway components remain largely unknown.

Beside these regulators, the best way to regulate TpoR signaling is to control the expression of TpoR at the cell surface. TpoR contains two specific tyrosine motifs Y8RRL and Y78RRL that are recognized by adaptor protein 2 (AP2), which induces receptor mediated endocytosis to form clathrin-coated vesicles and target the TpoR to lysosomal degradation.[154] A dileucine motif (L54, L55) in the Box2 intracellular domain of TpoR was shown to be important for internalization.[155] TpoR is ubiquitinated on both of its intracytosolic lysine K553 and K573 and target to the proteasome. Mutation to arginine of these specific lysines induces hyperproliferation in cell lines. c-CBl was shown to be at least one of the ligases responsible to the ubiquitination of the TpoR.[156]

I.13.6.1. LNK

Lnk (also called SH2B3) is a member of adaptor protein family that also contains APS and SH2-B. They share a proline-rich amino-terminus, a pleckstrin homology (PH) domain, an SH2 domain, and a conserved tyrosine near the carboxyl-terminus.

Lnk deficient mice are viable but exhibit more lymphoid cells and AGM region developmental defects and display a 3 to 5-fold increase in circulating platelets.[157] Aged Lnk deficient mice develop a CML like phenotype and moreover Lnk deficiency worsens the phenotype in JAK2 V617F mice.[158] Lnk is important for Tpo-mediated megakaryopoiesis and negatively modulates Mpl signaling pathways.[149] Several studies have also shown that Lnk -/- mice have 10 fold more HSC and higher self renewal, which could be explained by higher TpoR signaling.[159,160] Lnk binds to tyrosine 813 of JAK2 and LNK–JAK2 complex is further negatively regulated by 14-3-3 protein. Lnk is induced following JAK2 activation being therefore a part of a negative feedback loop.[161] Patients with JAK2 V617F have an up regulation of Lnk.[162] Recent studies showed that SH2B3 can paradoxically be a positive signal transducer in ovarian cancer, which contrast with findings in hematological malignancies.[163]

I.13.6.2. The CIS/ SOCS proteins

There are 8 members of the CIS / SOCS family (CIS, SOCS1, SOCS2, SOCS3, SOCS4, SOCS5, SOCS6 and SOCS7) that possess a central SH2 domain, an amino terminal domain variable in length and a carboxy 40 amino acids module known as the SOCS box. SOCS gene expression is induced in response to cytokine receptor activation.

CIS (cytokine inducible SH2 containing protein) is a STAT5 target gene[164], whereas SOCS1 is a STAT3 target gene in IL-6 stimulated cells.[165] This suggest that these member act in a classic feedback loop. The SH2 domains determine the target of each SOCS and CIS protein. They can bind directly to JAKs or to phosphotyrosines of activated receptors. CIS, SOCS2 and SOCS 3 bind to phosphotyrosine whereas SOCS 1 and SOCS3 can bind to JAK2 via their SH2 domain thereby inhibiting JAK2 kinase activity.[166] SOCS protein can also target their interaction partner for proteasomal degradation via the proteasomal machinery. The SOCS box interacts with the Elongin B, C complex and recruits Cullin-2 and Rbx-1 as subunits of ubiquitin ligase in the same way than Van Hippel Lindau (VHL) protein with HIF-1.[167] SOCS 1 targets JAK2 for degradation[168], whereas CIS targets EpoR.[169] In addition SOCS proteins can inhibit directly JAKs via their KIR (Kinase Inhibitory Region) domain.[170] SOCS1 and SOCS3 promoter hypermethylation was identified in some JAK2 wild type myeloproliferative neoplasms. Using demethylating agents such as 2-deoxyazacytidine could restore normal mRNA and SOCS proteins levels.[171]
SOCS1, a target gene of IFN-α but not of Tpo, is inhibiting Tpo signaling. This could explain the thrombocytopenia mediated by IFN-α and it is a very good example of receptor crosstalk. Whereas SOCS3 is a target gene of Tpo but not of IFN-α and does not seem to do anything with TPO (unpublished).[172]

Knock out murine models have strengthened the important role of SOCS proteins:
SOCS1-/- mice die from a complex neonatal disease due to a high and toxic interferon γ response.[173]
SOCS2-/- mice develop gigantism probably due to an insufficient control of insulin like growth factor -I (IGF-1) and growth hormone (GH) by SOCS2.[174]
SOCS3-/- is embryonically lethal with placental defect[175] and associated erythrocytosis showing that SOCS3 is important to regulate fetal liver erythropoiesis.[176]
CIS-/- mice are normal in all regards suggesting a redundancy among CIS and others SOCS protein.[176]

I.13.6.3. PIAS Proteins

There are four members (PIAS1, PIAS3, PIASy, PIASx) of Protein Inhibitor of Activating STATs. PIAS1 specifically inhibits STAT1 DNA binding, but not STAT2 or STAT3 [177] PIAS3 selectively binds to phospho-STAT3 and prevents its DNA binding.[146] PIASx inhibits specifically STAT4, but do not prevent its DNA binding and rather acts as a transcriptional

repressor.[178] All PIAS and particularly PIASy protein are also functioning as small ubiquitin like modifier (SUMO) E3 ligase. [179]
PIAS1-/- mice show increase protection against pathogen induce by an enhanced antiviral activity of IFNβ and IFNγ.[180]
PIASy-/- mice have a modest effect on IFN and Wnt signaling suggesting a redundant effect with other PIAS.[181]
PIASx-/- mice show reduced testis weight and suggest a role for normal quantitative spermatogenesis.[182]

I.13.6.4. Phosphatases

Protein tyrosine phosphatases can regulate receptors positively or negatively. They can be receptor-like such as CD45 tyrosine phosphatases, that activate Src family kinases by dephosphorylating regulatory tyrosines[183], or soluble like SHP-1 and SHP-2 that are important for cytokine receptor signaling.

I.13.6.5. SHP1 and SHP2

Src-homology 2-domain phosphatases (SHPs) contain two SH2 domains, a protein phosphatase domain and a C terminal tail. SHP-1 is autoinhibited when the N-terminal SH2 domain protrudes into the protein phosphatase domain. SHP-1, encoded by PTPN6, is expressed at least in the hematopoietic compartment and liver cells and binds to specific tyrosine residues on receptors, dephosphorylates JAK2 or signaling proteins such as STAT3 and terminates signaling. Motheaten mice are SHP-1 deficient mice[184] that suffer from a polycythemia and neutrophile infiltrates in the lung. Sorafenib and analogues, which are promising as systemic treatments in a variety of solid cancers, such as hepatocellular carcinoma, can suppress STAT3 activity by inducing SHP-1 activity.[185]

SHP-2 can also bind to the PDGFR, be phosphorylated and provide docking site for Grb2 linking directly PDGFR to the Grb2 SOS RAS MAPkinase route.[186] But SHP-2 was also incriminated in dephosphorylation of gp130 bound JAKs.[187] In a double knockout model of SHP-1 and SHP-2, mice were severely macrothrombocytopenic and showed impaired megakaryocytes development and proplatelet formation.[188]

I.13.6.6. PTP-1B

PTP-1B recognizes substrates containing the sequence motif [E/D]-pY-pY-[R/K] in which JAK2 (E-Y-Y-R) and TYK2 (E-Y-Y-K) are perfect matches with the motif. PTP-1B interact with both JAK2 and TyK2. Cells deficient in PTP-1B showed hyperphosphorylation of JAK2.[148]

I.13.6.7. PTEN

Phosphatase and tensin homologue deleted on chromosome 10 is a phosphatase that plays a negative role on PI3kinase by mainly dephosphorylating PIP3. Inactivation or deletion of

PTEN leads to accumulation of PIP3 and activation of the PI3 kinase that lead to tumor development.[189]

I.13.6.8. MAP Kinase Phosphatases:

MAPkinases as ERKs are phosphorylated at specific threonine and tyrosine residues within the activation loop specific TxY motif of the kinase domain. MAPkinases can be dephosphorylated by specific kinases at either the serine or the threonine or by dual specificity phosphatases that can dephosphorylate phosphoserine and phosphotyrosine residues within MAP kinases. Those dual specificity phosphatases exemplified by MKP-1 can dephosphorylate at least efficiently ERK, Jun and P38.[190]

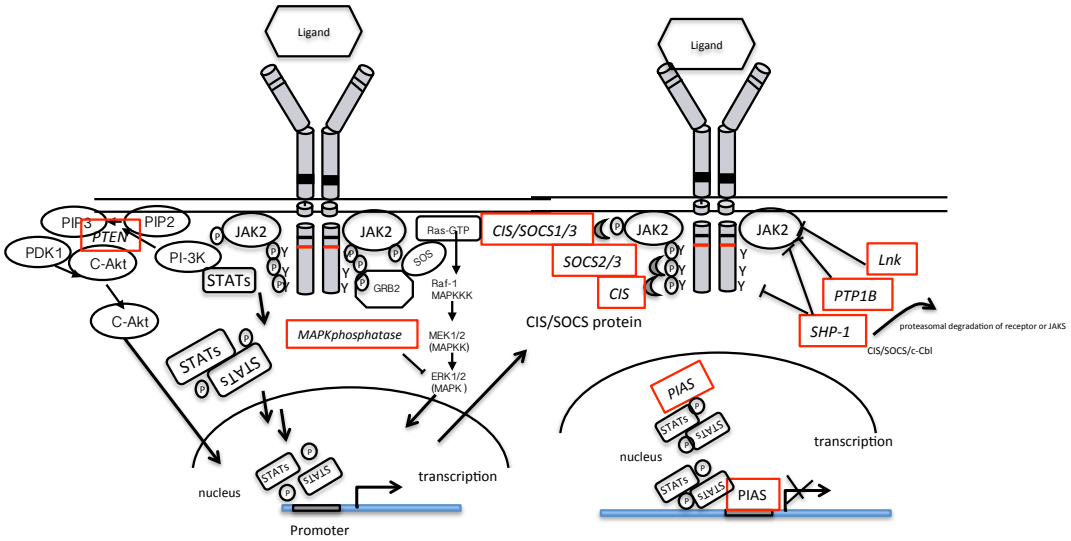


Figure 25 - Negative regulators of cytokine signalisation

I.14. Role of TpoR in normal hematopoiesis

The thrombopoietin receptor (c-Mpl or TpoR) and its ligand Tpo are the main regulators of megakaryocyte differentiation and platelet production. Tpo is a relatively lineage specific cytokine that increases platelet count by increasing marrow megakaryocytes and by shifting their size and ploidy to higher value.[191] The expression of Mpl is restricted to hematopoietic cells of the megakaryocytic lineage and to undifferentiated progenitors such as the MEP, CMP and the hematopoietic stem cell. The role of TpoR has been established by genetically eliminating the c-Mpl receptor. Mice lacking the TpoR or Tpo are severely thrombocytopenic and have less megakaryocytes and their progenitors.[192] In fact, thrombopoietin acts paradoxically at two different step of megakaryocytes differentiation. In the early stages of megakaryopoiesis, it induces a positive proliferative signal and at a latter stage it induces a

negative signal (mimicking a senescence cell cycle arrest) that leads to subsequent platelet production. This Tpo induced cell cycle arrest is mediated via MAPkinase/ERK/Early growth response protein 1 transcription factor (EGR1) pathway and dependent on the p21 cell cycle inhibitor induction. This cell cycle arrest is irreversible and is accompanied by morphological changes such as larger cytoplasm and larger nucleus and markers of senescence such as senescence associated β galactosidase activity (SA β gal), heterochromatin protein 1 foci, but no annexin V staining.[59] TpoR/Mpl is also present in various endothelial cells such as liver endothelial cells and human umbilical cord vein-derived endothelial cells (HUVEC) where Tpo acts as a growth factor and promotes neoangiogenesis.[193,194] TpoR at the platelet surface regulates Tpo level but the TpoR expressed on the endothelial cell does not contribute significantly to Tpo regulation.[195]

Besides its role in megakaryocyte development and platelet production, TpoR also plays an important role in the early hematopoiesis by promoting self-renewal, expansion and maintenance of the HSC pool. Tpo in combination with SCF and IL-3 promotes HSC proliferation *in vitro*. TpoR is present at the HSC level. Progenitors (Lin-Sca1+ containing HSCs) derived from c-mpl knockout mice showed a sevenfold decrease in repopulating activity compared to (Lin-Sca1) from wild-type mice[196]. The role of TpoR on HSC expansion was also confirmed by poor secondary transplant of cells primarily transplant in Tpo-/- mice compare to Tpo+/+ mice.[197] Furthermore, the fraction of HSC containing CD34+CD38- population that expresses lower TpoR levels at the cell surface is also less able to support long-term repopulation after bone marrow transplant.

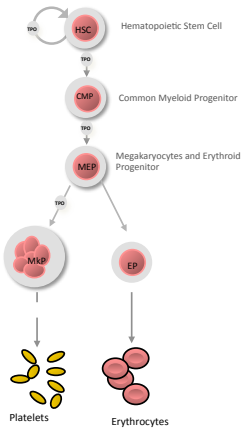


Figure 26 - Tpo dual role in hematopoiesis

An important role of Tpo/TpoR was shown in 2007 for the maintenance of LT-HSCs that are localized on the endosteal surface in the trabecular bone area and kept quiescent by the Tpo producing osteoblastic niche preventing their rapid exhaustion[198,199]. Quiescence was shown by BrdU long-term label retaining and by Pyronin-Y staining that is positive in G1 and negative in G0 quiescent cells.

I.15. *In vivo* models

I.15.1. Tpo -/- mice

They have a reduction of more than 80% of their platelet count, but have a normal level of other lineages. Those mice have a decreased number of megakaryocytes, a lower ploïdy and less CFU-MKs.[192] Those mice display in fact a 60% to 85% reduction in their stem and progenitor cells of all myeloid lineages and present a thrombocytopenia with a normal level of their red cells, granulocytes and monocytes. This discrepancy can be explained by the fact that lineage specific growth factors such as G-CSF can compensate at the post progenitor level.[200] What is also very striking is that these Tpo -/- mice still have residual platelets. The lab of Radek Skoda has suggested that G-CSFR could play a permissive role on megakaryopoiesis. This idea was coming from a chimeric receptor, where the ICD of G-CSFR replaced the ICD of TpoR and that produces platelets.[201]

I.15.2. Double Tpo and GCSFR -/-

Those mice, however, do still have residual platelets. Those double negative mice have however a profound (lower level than GCSFR -/-) reduction in their number of granulocytes confirming the important role of Tpo at the progenitor level.[200] Tpo-/- mice have normal post natal HSC levels, but their HSC number declines within a few weeks after birth due to increase cycling and reduction in their CDKI p57kip2 and p19ink4D[198], confirming the role of Tpo to keep stem cell quiescent.

I.15.3. Tpo +/- mice

Tpo heterozygous mice show a gene dosage effect with half the mRNA produced, a 40% reduction in the number of MKs and a proportional reduction in the platelet count. This proportionality between MKs and platelet decrease suggests that Tpo is not so important in the late stage of platelet production. This suggests that Tpo produced by the liver, the kidney or the osteoblasts is regulated mainly by the platelet mass and seems not to be transcriptionally controlled by a platelet sensing mechanism. On the other hand the receptor on liver cells (AMR) binds old desyalated platelets and might controls basal mRNA production.[61]

I.15.4. TpoR/c-Mpl -/- mice

Those mice develop normally, but exhibit a significant, 10- to 20-fold, reduction in mature megakaryocytes and are severely thrombocytopenic. Those mice exhibit more generalized defect on hematopoiesis with reduced number of progenitors CFU-GM, CFU-GEMM, CFU-MK. With the exception of platelets, normal level of their other mature blood cells are detected.[202]

I.15.5. TpoR/c-Mpl and IL-3R α -/- mice:

Numerous cytokines can have a megakaryopoietic activity such as cytokine signaling through the gp130 chain (IL-6, OSM, IL-11, LIF), SCF, Epo, GM-CSF but among all, IL-3 seems to be the most potent to stimulate CFU-MK or BFU-MK.[203] These double knock-out mice were

created in order to seek for a possible role of IL3 in the residual platelet levels in Mpl deficient mice. But the results demonstrate that IL-3 alone does not contribute to this residual platelet production and that probably other cytokines are responsible for this effect, despite the fact that animals deficient exclusively in these cytokines do not displays any platelet phenotype.[204]

I.15.6. TpoR/ c-Mpl floxed mice crossed with PF4cre/PF4cre mice

Crossing between Mpl fl/fl mice and PF4cre mice have generated Mpl PF4cre/PF4cre mice where Mpl is absent from megakaryocytes and platelets but expressed in the megakaryocyte progenitors. These mice develop a thrombocytosis suggesting that Mpl expression on megakaryocytes and platelets is dispensable for platelet formation, but essential to prevent myeloproliferation.[205]

I.15.7. TpoR (-/-) mice expressing a full-length TpoR transgene under the control of the 2-kb TpoR promoter

The expression of the Mpl transgene driven by a segment of the Mpl promoter, was diminished during late megakaryopoiesis, resulting in a strong thrombocytosis due to a reduce level of TpoR in MKs and platelets. This model reinforces the hypothesis of a strong feedback with TpoR binding and consuming Tpo.[206]

I.15.8. c-Mpl/TpoR Δ60 mice:

Those mice are lacking the last 60 residues of the intracellular domain (at the C-terminal end of the receptor). They have normal platelet and megakaryocyte counts when compared to wild-type mice an their platelets are functionally normal. However, these mice exhibit lower response to exogenous Tpo with lower CFU-MKs *in vitro* and lower phosphorylation of JAK/STATs, MAPkinase, PI3-kinase downstream signaling pathways, resulting in a slower recovery after myelosuppressive therapy. This suggests that both ends of the intracellular domain are important for acute response to Tpo, but that the more distal part of the intracellular domain is dispensable for basal platelet production and basal megakaryocytes differentiation.

I.15.9. Mice with retroviral ectopic overexpression of c-Mpl/ TpoR

Bone marrow cells of 5-FU treated mice retrovirally transduced by a wild type TpoR construct led to expansion of CFU-GEMM, CFU-MK, BFU-E, but not CFU-GM when cultured in clonogenic assay along with Tpo. This is indicating that TpoR overexpression does not restrict cell differentiation of any lineages and does not commit cells preferentially towards megakaryocyte differentiation.[207] In a similar experiment[208], the ectopic overexpression of TpoR leads to a marked erythrocytosis and a reduced megakaryopoiesis. This shows that TpoR can directly contribute to erythropoiesis when ectopically expressed and that these numerous and ectopically expressed cell surface TpoR molecules could deplete Tpo by sequestration.

I.15.10. JAK2 V617F heterozygous knock-in mice

Those mice suffer from marked polycythemia with plethoric extremities, as well as thrombocytosis and granulocytosis. Unlike MPN patients, those heterozygous mice exhibit a PV-like phenotype with evolution around 9 months towards myelofibrosis.[209] JAK2 V617F KI mice exhibit lower LSK cells (which contains LT-HSCs, ST-HSCs and multipotent progenitors) and less repopulating ability.[210] These mice are not fertile and extremely difficult to breed.

I.15.11. JAK2 V617F Mpl (-/-) mice

JAK2 V617F needs a type-1 homodimeric receptor for signaling. Mpl knock-out mice infected with JAK2 V617F have a less severe phenotype with a lower platelet count, less neutrophils, reduced neoplastic stem cell pool and splenomegaly.[211]

I.15.12. JAK2V617F/ STAT1 (-/-)

Those mice that are lacking STAT1 and that are KI for V617F have significantly higher hemoglobin and lower platelets than JAK2V617F/ STAT1 WT mice.[212]

I.15.13. Chicken: Chicken Tpo and MPl

Chicken TpoR was cloned in 2008 as the first non-mammalian Tpo ligand and receptor complex. *In vivo* administration of Tpo in chicken, or retroviral transduction with chicken TpoR plasmid or chicken Tpo plasmid induce erythropoiesis and thrombopoiesis suggesting the presence of a bipotent thrombo-erythropoietic progenitor.[213]

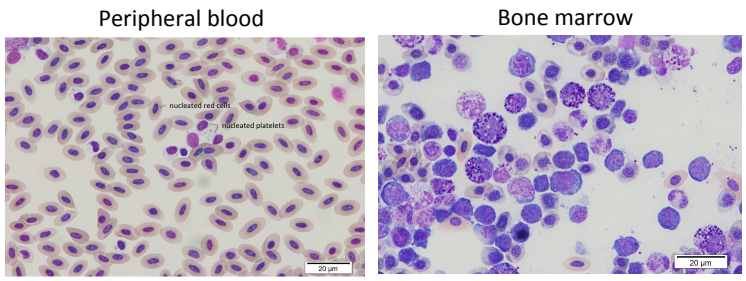


Figure 27 - Comparative blood cytology of chicken

Peripheral blood: Birds have nucleated red cells and platelets that can be differentiated cytologically. Bone marrow: Birds do not have Mks comparable to mouse or human megakaryocytes. Platelet progenitors are not easily identified by May-Grünwald-Giemsa coloration. Granulocyte progenitors have deeply basophilic granules.

I.16. Myeloproliferative neoplasms

Myeloproliferative neoplasms have a chronic clinical course with a median survival updated in 2015 (with treatment) of 14 years for PV and 20 years for ET. Patients have a higher risk of fibrosis or leukemic transformation. Acute leukemic transformation rates at 20 years are expected to be <10% for PV and 5% for ET. Patients are more susceptible to thrombosis and paradoxal bleeding, pruritus and microcirculatory troubles. They can suffer from a splenomegaly.[214] Concerning bleeding, in case of high thrombocytosis >1000 x 10(9)/L, an acquired von Willebrand disease due to the loss of intermediate and large vWF multimers should be ruled out.[215,216] As vWF is a reactive protein, acquired von Willebrand disease is not found in reactive thrombocytosis.[217] Interestingly, platelets in essential thrombocythemia may have some abnormalities with a PFA-100 (platelet function analyzer), with closure time usually significantly elevated. This PFA closure time can be used as a diagnostic marker.[218]

The WHO 2008 (4th edition) regroups under the term "myeloproliferative neoplasm": chronic myelogenous leukemia (CML), chronic neutrophilic leukemia, polycythemia vera, primary myelofribrosis, essential thrombocythemia, chronic eosinophilic leukemia, mastocytosis and the myeloproliferative neoplasm unclassifiable. Some Mpl mutations have been found in disease that are currently in two other WHO groups namely mixed myeloproliferative/myelodysplastic neoplasm and myelodysplastic neoplasm. The WHO 2008 classification of MPN is still very useful but should be soon updated and reviewed mainly because, new mutations, defining new entities, have been described and because WHO does not consider overlapping pathology with concomitant genetic abnormalities. Even if co-occurring driver mutations in MPN are not the rule, finding simultaneous mutations like phi- and phi+ can happen rendering the classification hazardous.

Mutation A	Mutation B	Disease	References
BCR-Abl	JAK2V617F	ET-PMF➔ CML CML➔ET-PMF	219-221
BCR-Abl	Inv 16	CML/CML blast crisis	222-225
JAK2 V617F	CALR EXON9	PMF/ET	226-228
JAK2 V617F	5q-	MDS 5Q- with JAK2 V617F	229
JAK2 V617F	LNK (SH2B3)	In rare MPNs with and without JAK2 V617F	230,231
JAK2 V617F	CBL	In rare MPNs with and without JAK2 V617F	232,233
JAK2 V617F	SOCS	MPNs with and without JAK2 V617F	171,234

JAK2 V617F	TET2	12% of MPNs with and without JAK2 V617F	[235]
JAK2 V617F	ASXL1	Found in ET/PV but more frequent in PMF	[236]
JAK2 V617F	EZH2	Not in ET but in PV and PMF	[157]

Table 1 - Concomitant mutations in MPN

I.17. Cytological Phi- MPN classification

MPN are clonal proliferation of the three hematological lineages due to the transformation of a hematopoietic stem cell or of an early myeloid progenitor. Despite the fact that the three lineages are involved, one generally dominates. Malignant cells in MPN are mainly mature and functional with few morphological characteristics at the exception of the megakaryocytic lineage.

I.17.1. Polycythemia Vera morphology

I.17.1.1. Chronic phase

The main bone marrow feature of Polycythemia Vera is pan-myelosis, which is responsible for bone marrow increased cellularity, with often more striking erythropoiesis and thrombopoiesis than granulopoieisis. The granulopoiesis and the erythropoiesis are morphologically normal, while the megakaryopoiesis shows a high degree of pleiomorphism with some megakaryocytes showing hyperploid nuclei. 20% of patients can display increased reticulin fibrosis, and mild collagen fibrosis. In the peripheral blood, there is an increase in normocytic, normochomic red cells or hypochromic microcytic red cells if an iron deficiency has developed, a mild basophilia and neutrophilia with sometimes immature granulocytes may be seen, as well as a prominent thrombocytosis mimicking an ET phenotype.

I.17.1.2. "Spent phase" and post PV myelofibrosis morphology

Erythropoiesis decreases with progressive bone marrow fibrosis (myelofibrosis) and myeloid metaplasia in spleen and liver. Leuko-erythroblastosis and teardrop cells as well as splenomegaly are detected with myelofibrosis progression due the extramedullary hematopoiesis.

I.17.2. Essential Thrombocythemia morphology

The bone marrow is usually moderately hypercellular. The most striking abnormality is represented by large megakaryocytes, often in clusters with hyperlobated, hyperploid nucleus. There is usually no granulocytic proliferation and rarely we detect excess of erythroid precursors. In the peripheral blood, the main feature is thrombocytosis, with high degree of anisocytosis.

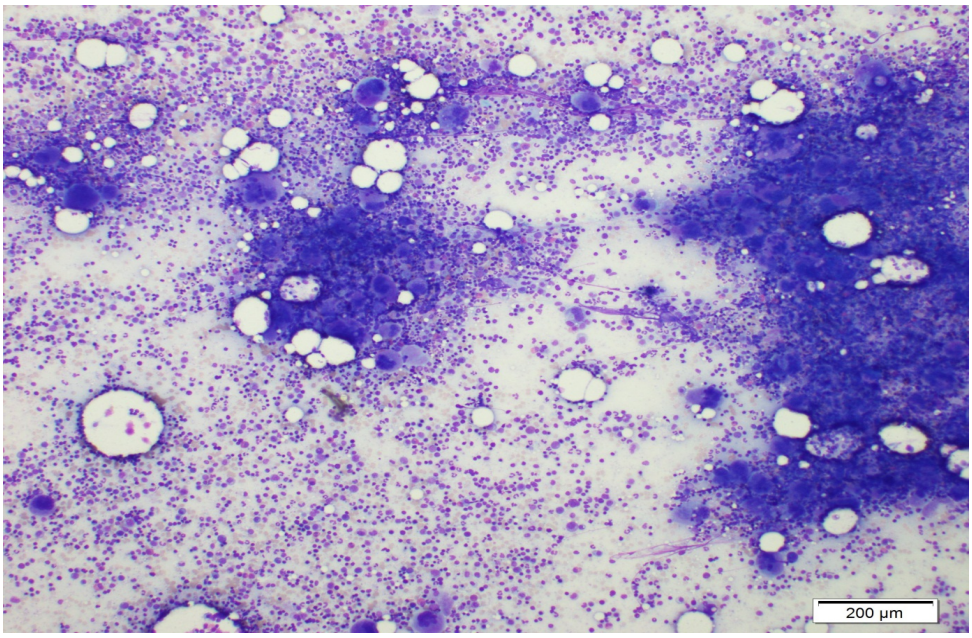


Figure 28 - Bone marrow of an ET patient
Bone marrow of a patient suffering from an Essential Thrombocythemia with a TpoR W515L mutation.

I.17.3. Primary myelofibrosis morphology

I.17.3.1. Prefibrotic stage

At this stage the bone marrow is usually hypercellular with excess of neutrophil granulocytes and megakaryocytes. The megakaryocytes are atypical with cloud, balloon bouquets or even dear antler shapes. Bare megakaryocyte nuclei are also often visualized. Reticulin fibrosis is often negligible at this step.

I.17.3.2. Fibrotic stage

The bone marrow is often hypo or nearly normocellular and rarely focally hypercellular. The biopsy demonstrates a net fibrosis with both reticulin or collagen fibrosis. Atypical megakaryocytes are the most obvious findings. Fibrosis can become diffuse and dense in late stage with osteosclerosis. The peripheral blood film show features of extra medullary hematopoiesis with leuko-erythroblastosis, teardrop shaped red cells.

I.18. Molecular MPN classification

William Dameshek, the founding editor of the journal *Blood* was the first to introduce in 1951 the term "myeloproliferative neoplasms". He postulated that these disorders are closely related and should probably be due to the same hitherto undiscovered stimulus.[237] He was seen as a visionary, when in 2005, JAK2 V617F was discovered.[238] JAK2 was a good candidate because JAK2 inhibitor (AG490) and PI-3 kinase inhibitor (LY294002) seems to reduce endogeneous erythroid colony (EEC) in PV patients[239]. Secondly, an uniparental disomy on JAK2 chromosome 9 due to mitotic homologous recombination was frequent in PV patients.[240] A third argument comes from PV platelets that have impaired TpoR expression and which are stabilized by JAK2 and TYK2.[138] Ten years later, things seem to be more complicated than previously expected. Mutations in epigenetic modifiers have been observed in patients as pre- or post-driver mutation and all suggest a predisposition to acquire new genetic changes and to get a complex clonal architecture. These epigenetic changes are associated with acute or fibrotic transformation and are generally of worse prognosis.

I.18.1. Driver mutations in MPNs

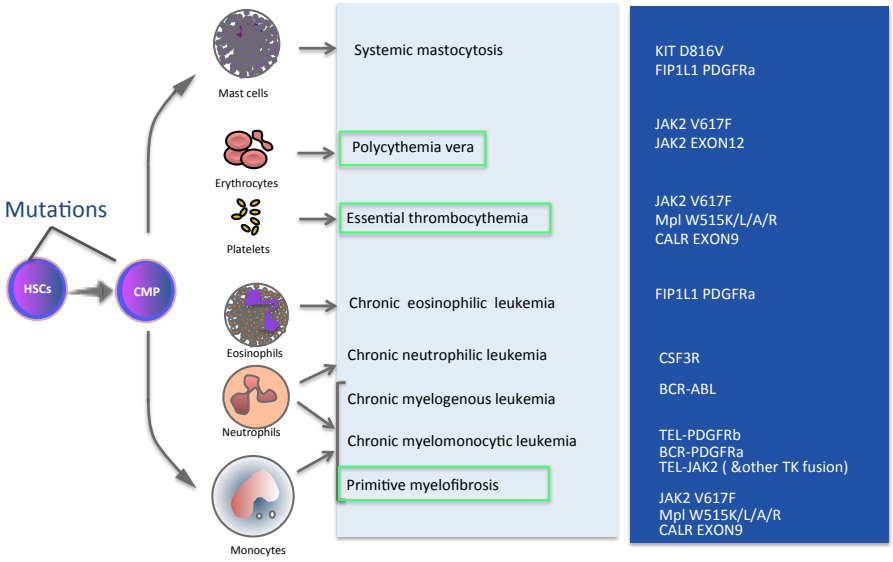


Figure 29 - Driver mutations in MPNs
Various driver mutations have been found for each subset of myeloproliferative neoplasm and some mutations are found in multiple diseases.

I.18.1.1. JAK2 V617F

JAK2 V617F can be found in >98% of Polycythaemia Vera and more than 50% of Essential Thrombocythaemia and Myelofibrosis patients. Homologous mutations in JAK1 (JAK1 V658F) and TYK2 (TYK2 V678F) also activate those kinases[241], while the homologous mutation in JAK3 (JAK3 M592F) is not active.

JAK2 V617F mutation can give multiple phenotypes; the explanations will be discussed later. JAK2 V617F signals via STAT3, STAT5, Erk and PI3kinase and needs to bind via its intact FERM domain[242] to a receptor that allows JAK2 to dimerize[243] like TpoR, EpoR or GCSF-R. V617F can be replaced by Leucine, Valine, Methionine and even better by Tryptophan. V617Y is not activating, probably due to the hydroxyl group[244] JAK2 V617I is obtained by only one base change and is found in association with TpoR in familial thrombocytosis. Thanks to the JH2 x–ray crystal structure[81] it was shown that JAK2 V617F rigidified the helix C through api interaction with F594, F595. We have no current model of how JAK2 V617F activates the receptor but it is not only by removing the pseudokinase inhibition over the kinase domain [141].

The fact that one mutation gives rise to multiple diseases could partially be explained by a relationship between levels of kinase activity and phenotype, thus by the JAK2 allele burden. The allele burden seems to correlate with the phenotype with heterozygous and WT clones being dominant in ET and homozygous clones in PV.[245] Another explanation would be differential association of JAK2 V617F with EpoR, TpoR and G-CSFR based in different affinities to these receptors. Recently, it was shown that the phenotype of the JAK2 V671F KI mice is very weak in a MPL -/- background, highlighting the fact that TpoR could be crucial for the development of the disease.[211] The mutation could also occur in different subsets of HSCs that are biased toward erythroid or megakaryocytic differentiation. More recently, it was shown that a differential JAK/STAT transcriptional activity is responsible for those different phenotypes. JAK2 V617F can activate both STAT5 and STAT1. p-STAT1 was shown to constrain erythropoiesis and favor megakaryopoiesis. Finally, in addition certain JAK2 independent effects like germ-line variations in the genome could be responsible for one phenotype rather than another.

I.18.1.2. JAK2 exon 12 mutations

Less than 3 % of PV patients that do not harbor the JAK2 V617F mutation exhibit mutations around K539 in the exon 12 of JAK2. Those mutations are located in the linker between the SH2 and pseudokinase domains of JAK2. These exon 12 mutants appear to induce preferentially an erythrocytosis phenotype and might activate preferentially EpoR signaling.[246] This mutation was found in 27% of patients with idiopathic pure erythrocytosis, which have erythroid endogeneous colony (EEC) and low Epo in serum.[247] Our experience showed that the penetrance of this mutation in granulocytes is not optimal and that exon 12 sequencing should be performed on EEC.

I.18.1.3. MPL/TpoR activating mutations in MPNs

Several clinically relevant mutations have been identified including extracellular and juxtamembrane T487A mutation found in non-Down's syndrome megakaryoblastic leukemia[248], TM S505N polar mutation[18,104,249] and cytosolic JM W515K/L/A/S/G/R.[21,102,103,250,251] The fact that these mutations are clustered around the TM domain reflects the importance of this region in the regulation of receptor activation.

Judith Staerk was the first to recognize that the RWQFP motif, where the W515 is located, is essential for preventing TpoR activation. Abe and coworkers found the first spontaneous activating Mpl mutation using a muTpoR BaF3 cell selection assay. This mutation was located at the murine W_{515} position (W508S).[252]

Domain	Mutant	Consequence	Reference
EC	K39N	mild Thrombocytosis in African americans (Low TpoR surface expression)	253
	P70L	found in a thrombosis patient, weakly active	Annexe
	P106L	thrombocythemia (Low surface expression)	254
	T119I	found in MPN, weakly active	Annexe
	S204P	found in MPN, , weakly active	Annexe
	S204F	found in MPN, , weakly active in our hand	255
	E230G	found in MPN, , weakly active	Annexe
	Y252H	found in a pediatric ET	256
	V285E	found in MPN, , weakly active	Annexe
	R312W	found in MPN, , weakly active	Annexe
	R321Q	found in MPN, , weakly active	Annexe
JM	T487A	Mpl gain of function, found in AML -M7	248
TM	S505N	Mpl gain of function	18
	V507I	found in 1 MPN	21
	L510P	no gain of function, found in 1 MPN	20
JM	R514K	found in 1 MPN	21
	W515L	Mpl gain of function	103
	W515K	Mpl gain of function	102
	W515R	Mpl gain of function	21
	W515A	Mpl gain of function	250
	W515G	Mpl gain of function	21
	W515S	Mpl gain of function	21
IC	A519V	found in 1 MPN	21
	D545G	found in 1 MPN	21
	D545N	found in 1 MPN	21
	Y591D	found in MPN, weakly active in our hand	Annexe
Domain	**Mutant**	**consequence**	
TM/TM	V501L/S505N	found in one patient	21
	V501A/W515R	found in one patient, in cis	257
TM/JM	V501A/W515L	found in one patient ,in cis	257
	S505C/W515L	found in one patient, in cis	257
	S505N/W515L	found in one patient, same colonie	258
	A506T/ A519T	found in one patient JAK2V617F	20
	G509C/W515L	found in one patient	258
JM/IC	W515L/G540S	found in one patient	21

Domain	Indel	Mutant	Found in	References
TM	gct ctg gtg atc ins	in frame T496-A497 ALVI ins, homo	1 MPN	[21]
	insCTGCTGAGCTGC	in frame LSCRWQFP	1 MPN	[259]
JM	tgg cag ttt cct del /ins aaaact	in frame RKTHAY	1 MPN	[21,259]
IC	AGdel/insT	R525C fs*14	1 MPN	[21]

Table 2 - Mutations in MPL

I.18.1.4. CALR Exon 9 mutations

Robert Kralovics, by carefully analyzing whole genome sequencing data of JAK2 V617F/MPL W515X double negative MPNs, found insertions or deletions in the exon 9 of calreticulin. These all leads to a +1 (-1/+2) bp frameshift with a novel positively charged C-terminal end and a loss of the KDEL retention signal. These mutations were found in 67% of essential thrombocythemia patients and in 88% of those with primary myelofibrosis.[34]

I.18.1.5. Rare mutations in negative regulators of the JAK-STAT pathway

Polymorphisms in genes coding for regulators of the JAK-STAT pathway play a major roles in modulating the output from JAK2 V617F.

I.18.1.5.1. Lnk Mutations

Oh et al. have identified two loss of function mutations in the exon2 LNK regulator with a 5bp deletion and missense mutation leading to a stop codon and loss of the pleckstrin homology (PH) and Src homology 2 (SH2) domains. A second patient had a missense mutation (E208Q) in the PH domain.[230] Lnk mutations target a hot spot in PH homology domain (from E_{208}-D_{234}) and are rare (3%) in chronic phase MPN and more prevalent (13%) in blast crisis. These mutations are not exclusive with other mutations.[260]

I.18.1.5.2. Casitas B-cell lymphoma mutations

While frequent in CMML, mutation in c-CBL (loss of function) have been found in 6% of PMF patients and in AML post MPN but never in ET or PV patient.[261] In a JAK2 V617F patients, The c-CBL clone has been shown to emerge and be responsible for a JAK2 WT AML progression.[262]

I.18.1.5.3. SOCS Mutations

Mutations are infrequently found in SOCS proteins[263] but hypermethylation of promoter CpG islands is much more frequent in both JAK2 V617F positive and negative patients.[171,234]

The role of SOCS protein in the pathogenesis of MPNs remain controversial since it was shown that SOCS3 can down regulate JAK2 exon14 or exon 12 mutations[264] but in the other hand that JAK2 V617F can escape SOCS by phosphorylating the SOCS box.[265]

I.18.1.6. Germ-line JAK mutants

Germ-line JAK2 mutations were found in family with hereditary thrombocytosis. One family harbors a mutation JAK2 R867Q that is located in the kinase domain and another family

harbors a double S755R/R938Q in the pseudokinase and kinase domains. Those mutations confer an autonomous and specific growth of BaF3-Mpl but not of BaF3-EpoR cells. Those mutants have a longer half-life due to better binding to HSP90 that correlate with higher c-MPl/TpoR expression at the cell surface.[266]

I.18.1.6.1. Germ-line mutants that predisposes to MPN

Germ lines mutations in MPNs are uncommon but informative to discover predisposition genetic factors. Those genetic factors could propagate the disease phenotype of randomly acquired phenotypic mutation or even increase the mutagenesis potential. An example is the JAK2 haplotype designated 46/1 or "GGCC" haplotype that increases the risk of developing JAK2 V617F or exon12 mutated MPNs[267] [268] or the SNP found in the second exon of the TERT (telomerase complex reverse transcriptase that maintains telomeres length) gene that is independently and synergistically predisposing to MPNs.[269] Recently, a newly germline copy number variation (CNV) in chromosome 14 through overexpression of 2 out of 6 genes, GSKIP and ATG2B, gives a proliferative advantage to clones that have acquired JAK2, Mpl and CALR. GSKIP mimics activation of the Wnt/B catenin signaling pathway by inhibiting GSK3β and ATG2B plays a role in autophagy.[270]

I.18.2. Epigenetic mutations and their role in clonal emergence and progression

Epigenetic modifiers could influence the phenotype and be responsible for the clonal evolution of the disease.

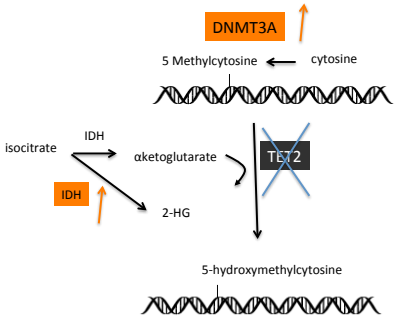


Figure 30 - Epigenetic regulators of DNA methylation

I.18.2.1. TET2 (ten-eleven translocation 2) mutations

TET2 mutants are found in a wide range of neoplasia and are found in 14% of MPNs.[235,271] TET2 is a hydroxylase that is able to hydroxylate methylated cytosine (5mC) in hydroxymethylcytosine (5hmC).[272] TET2 depends on α ketoglutarate for this function. 2HG, an oncometabolite made by IDH1, inhibits TET2.[273] All mutations in MPNs result in a loss of function. They can occur has a pre[235] or post JAK2 V617F event.[274]

I.18.2.2. DNMT3A

DNMT3A is a DNA methyl transferase. Mutations are rare in myeloproliferative neoplasms and rather linked to AML transformation.[275] There is a hot spot at R882 in the catalytic domain that is hypomorphic and could act in a dominant negative way.[276]

I.18.2.3. IDH1

Isocitrate dehydrogenase 1 catalyses normally the transformation of isocitrate to α ketoglutarate. Mutations in IDH1 give a neomorphic activity with the capacity to transform isocitrate to 2 hydroxyglutarate[277] which inhibits TET2.[273] This mutation is rarely found in chronic phase but is found with a 21% frequency in post MPN blast crisis.[278]

I.18.2.4. EZH2

EZH2 is a histone methyl transferase and member of the polycomb repressor 2 complex (PRC2) that methylates histone H3 at Lys27. EZH2 inactivating mutations are associated with 3% PV and 13% myelofibrosis.[279]

I.18.2.5. ASXL1

ASXL1 is a member of the polycomb complex and is capable to deubiquitinate histone H2A. Frameshift and stop mutations in ASXL1 have been found in MPNs with a higher prevalence in PMF (19-40%) than in ET or PV (<7%).[236,280]

I.18.3. Mutations involved in the leukemic transformation

Abnormal translocations involving RUNX1 are found in 30% of AML post MPNs suggesting that RUNX1 could be the most frequent event in transformation.[260] Tp53 mutations are found in 20% frequency in AML post MPN and is also a very important player in leukemic transformation.[262] NRAS/KRAS have also been found in AML–post MPN and in cells of the anterior chronic phase.[262] Ikaros family zinc finger 1 (IKZF1) deletions occur in AML post MPN because it is located on the short arm of chromosome 7 frequently deleted in those AML. IKZF1 deletions are found in mature and immature compartments suggesting that IKZF1 is not responsible for a differentiation block but rather renders progenitors susceptible to transformation.[281] IDH1 is also involved in leukemic transformation and has been discussed previously.

I.19. Overlap and differences with myelodysplastic syndromes

Stong proliferation in lineages always engenders a low level of dysplasia as the marrow iron and vitamin stocks begin to be depleted. Clonal evolution and genomic instability of those leukemic clones can induce a real MDS phenotype with complex caryotype. Evolution of a classical myeloproliferative neoplasm toward a myelodysplastic syndrome is of worse prognosis and could be the forerunner of acute myeloid leukemia transformation.

One can find morphological description of a post ET JAK2V617F positive dysplasia with dysplasia in all three granulocyte lineages with abnormal neutrophils segmentation, degranulation of neutrophils and abnormal granules disposition in eosinophils and basophils. It is noteworthy that basophils are not often recognized as dysplastic due to their rarity and their propensity to degranulate.[282] Moreover, The 2008 WHO classification possesses a chapter dedicated to MPN/MDS phenotype such as atypical CML, CMML and MPN/MDS unclassifiable. Recently, mutations in CSF3R were found in 59% of patient with chronic neutrophilic leukemia and atypical CML. Those mutations segregate in extracellular membrane proximal mutations like T618I and stop codon in the intracellular domain. They claimed that membrane proximal T618I responds better to ruxolutinib (a JAK2 kinase inhibitor) and that truncation mutations respond better to dasatinib.[283] In our experience, we found one patient with a CSF3R stop mutation that has a strong CNL phenotype with important neutrophil dysplasia. This patient evolved in a pure MDS phenotype and was grafted.

II. APPROACHES

II.1. Principles of approaches to study interactions and structure of transmembrane sequences

II.1.1. Toxcat assay

TOXCAT measures transmembrane helix–helix dimerization or oligomerization of transmembrane proteins in natural bacterial membranes.

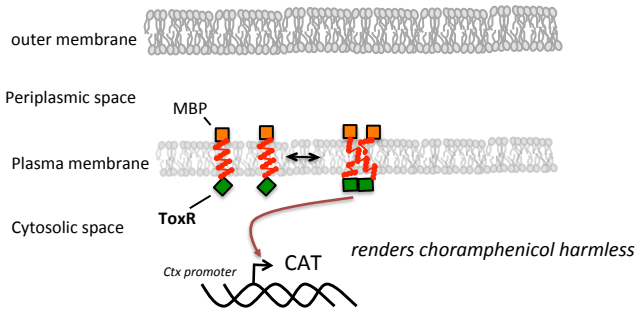


Figure 31 - Toxcat assay

The system uses chimeric constructs made of a maltose binding protein (MBP) that anchors the protein in the inner bacterial membrane of E. Coli, fused to the TM domain of interest, itself fused at its N-terminal part to the DNA binding domain of a ToxR dimerization dependent transcription factor. Upon TM domain dimerization, the ToxR transcription factors drive the production of chloramphenicol acetyl transferase (CAT) gene that renders chloramphenicol harmless for bacteria.[284] The system is based on a type II TM topology and is the method of choice for homodimeric interactions. Disadvantages are that bacterial membranes are thinner than eukaryotic membranes, and so shorter TM sequences are usually tested, and that it is reflecting type II TM topology, although dimeric interactions between type I TM helices can be used and yield dimeric signals as well. In addition, heteromeric interactions cannot be measured if individual helices also homodimerize.

II.1.2. Solid-state deuterium NMR with magic angle spinning

Solid-state NMR is applied to molecules that are not able to rapidly reorient, such as membrane embedded proteins. The lack of mobility results in broad line widths for the NMR resonances. The broad resonances have two consequences: the resolution and sensitivity are both reduced. Magic Angle Spinning (MAS) is a way to mechanically reorient the sample in the magnetic field and can narrow the NMR resonances. The method is based on the fact that many of the contributions to line broadening have an angular dependence ($3\cos 2\theta - 1$) with respect to the magnetic field. At the magic angle ($\theta = 54.7°$), these interactions go to zero. When the MAS spinning frequency is greater than the line broadening interaction, then the lines collapse to their narrow "isotropic" value – similar to what is observed in solution. When MAS spinning frequency is less than the line broadening interaction, then one observes both the isotropic resonance and "spinning" side bands. In this study, our collaborators in the laboratory of Prof. Steven O. Smith obtained solid-state deuterium spectra and ^{13}C spectra. In

the case of ^{13}C spectra, the major line broadening mechanism is the chemical shift anisotropy, which is typically on the order of 10-20 kHz. MAS frequencies of this order can be obtained such that the spectra exhibit only the isotropic resonances (and perhaps 1 or 2 small spinning side bands). In contrast, the major line broadening mechanism in deuterium spectra is the quadrupolar interaction. (Deuterium is a spin = 1 nucleus whereas 1H and ^{13}C are spin = ½ nuclei and do not exhibit a quadrupolar interaction). In the absence of molecular motion, the deuterium line width is on the order of 125 kHz, which is much greater than the highest MAS spinning frequencies that can be obtained generating a high side band pattern. Fortunately, methyl group rotation is hard to suppress unless the sample is cooled to less than ~100K. As a result, methyl rotation results in line widths of ~40 kHz. If only methyl group rotation is observed, then this would be the observed line width. Any additional motion results in narrowing of the line width, while movement constrains increase the side band pattern. As a result, the deuterium nucleus is sensitive to molecular motion.

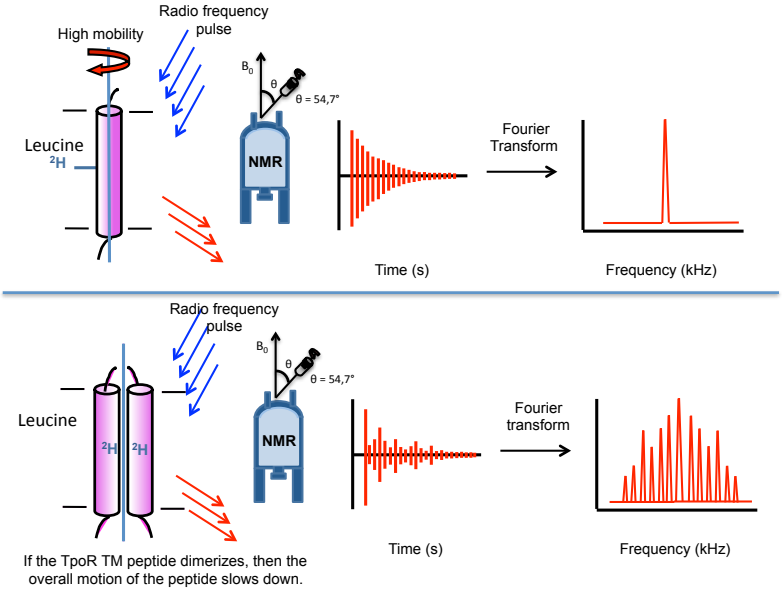


Figure 32 - Deuterium MAS NMR

In our deuterium MAS NMR experiments, the TM peptide is labeled with a single deuterated leucine reconstituted in synthetic membrane, lyophilized and reconstituted in deuterium - depleted water. The sample is placed in a small MAS rotor (4 mm). By spinning the sample at a frequency of 3 kHz at the magic angle, the resolution is greatly increased because the chemical shift anisotropy and the quadrupolar interactions are partially averaged. If the sample is frozen, one observes a spectrum with a center band at the isotropic chemical shift and sets of spinning side bands where the width of the side band pattern spans 40 kHz. The advantage of MAS even at 3 kHz is that the sensitivity is greatly increased because now the NMR signal is concentrated into narrow lines rather than spread across 40 kHz. As the sample is warmed, the proteins in the membrane begin to rotate about their axis and the individual leucine side chains begin to rotate about the side chain single bonds. These motions can narrow the overall side band pattern to less than 40 kHz. The amount of reduction is dependent on the

amount of motion. We take advantage of this by using the line shape to assess whether we have monomer or dimer, and whether the leucines are located in the dimer interface. Both dimerization and placing the leucine side chain in the interface restrict motion and broaden the side band pattern.

II.1.3. 2D Homonuclear ^{13}C -^{13} C DARR MAS NMR

Dipolar Assisted Rotational Resonance (DARR) is useful to find inter-residue contacts. Under MAS, all of the dipolar interactions between ^{13}C are averaged to zero since these interactions are on the order of 1-2 kHz or less (which is much smaller than the MAS frequencies used in our experiments, namely 5 – 12 kHz). The principle of DARR is to reintroduce dipolar interactions between two ^{13}C labeled peptide under MAS using a special RF pulse sequence.[285]

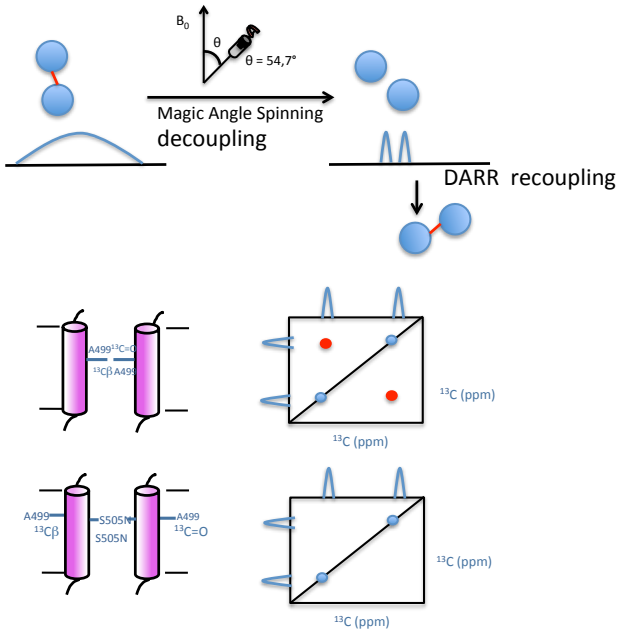


Figure 33 - DARR NMR

DARR is very effective in recoupling the dipolar interactions.[286]
Transmembrane domains are ^{13}C labeled at specific residues and cross peaks in the 2D spectra correspond to resonances that exhibit dipolar interactions. The closer the distance between two ^{13}C nuclei is, the stronger the dipolar interaction and the stronger the observed cross peak. Typically, the distance range for observing cross peaks is ~ 5-6 Å. In a helix dimer, the axial separation is ~10 Å and the backbone-to-backbone separation is ~ 5 Å. Consequently, observing a cross peak between two ^{13}C labels that reside on different peptides can only occur if the peptides are closely associated (e.g. they form dimers) and the ^{13}C labels are in the interface.

II.1.4. Polarized attenuated total reflectance Fourier transform infrared spectrometry (ATR- FTIR)

FTIR can be used to measure the tilt angle of TM peptides.

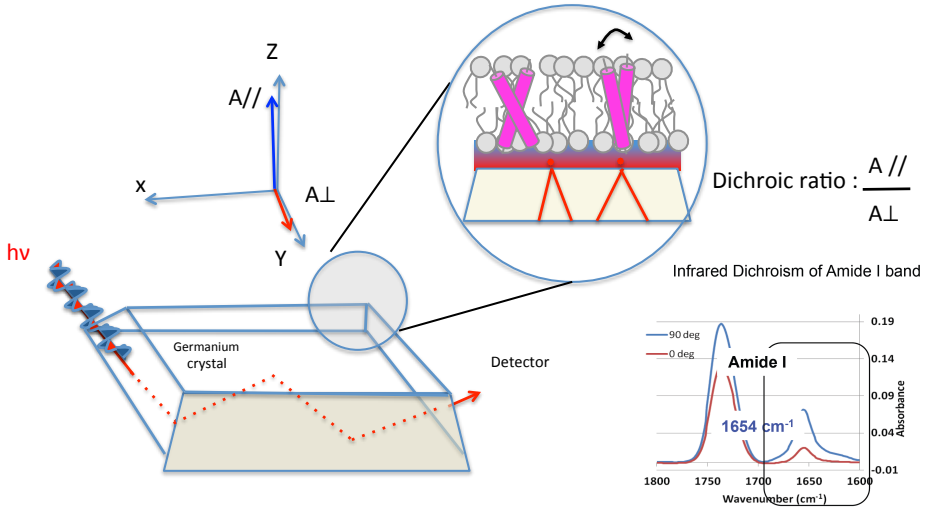


Figure 34 – ATR-FTIR spectroscopy

A polarized infrared beam is directed onto a high refractive index (germanium) crystal, which is optically dense. This internal reflectance creates an evanescent wave that extends beyond the surface of the crystal into the sample that has been layered by a flow of gas (N^2) onto the surface of the crystal. The evanescent waves protrude into the sample and are absorbed or attenuated by it. The interferogram is measured by a detector and transformed by a Fourier transformation to give the spectrum. The peptide bond (RC(O)NHR) exhibits moderately intense vibrations in the IR spectrum. The amide I vibration (which corresponds primarily to the C=O stretching motion) has frequency between 1600 and 1700 cm^{-1}. For a helix, this vibration is at ~1655 cm^{-1}, and the C=O bonds are aligned roughly parallel to the helix axis. IR light is absorbed preferentially when the electric field component of the light oscillates in a direction that aligns with the C=O bond (which for a helix aligns roughly with the helix axis). Consequently, the dichroic ratio (A// /A ⊥) [287] of the amide I band is sensitive to the orientation of the TM helix relative to the plane of membrane. A // is the absorption coefficient of the polarized IR beam parallel to the symmetry axis Z of the membrane bilayer. A⊥ is the absorption coefficient perpendicular to the membrane bilayer. The closer the helix is from the membrane normal, the higher the A// and the dichroic ratio are. Inversely the more the helix is tilted, the lower the dichroic ratio.

II.1.5. Sedimentation equilibrium analytical ultracentrifugation (AUC)

This assay is sensitive to oligomeric states and measures the dimerization in detergent environments using an ultracentrifuge coupled with an optical system.

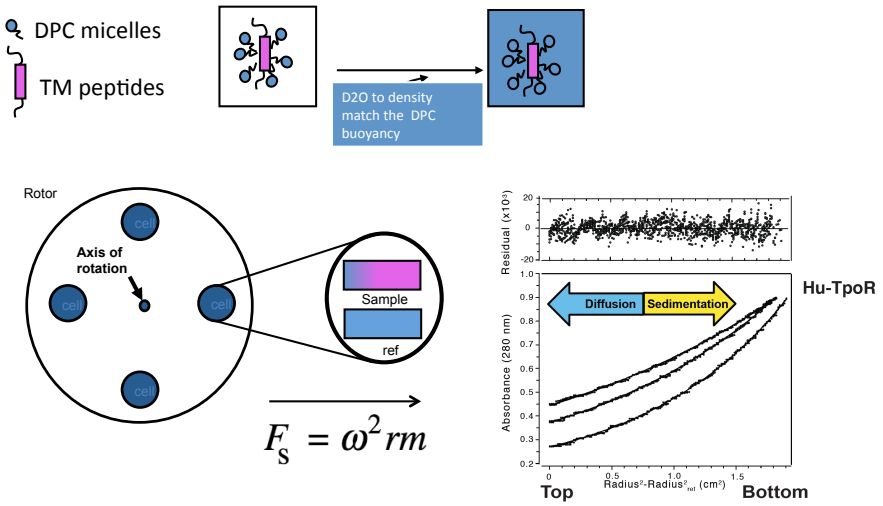


Figure 35 - Analytical ultracentrifugation

Equilibrium between diffusion and forced sedimentation is reached and depends only on the molecular mass and is entirely independent of the shape of the molecule. There is no need to consider the mass of the bound detergent because it is density-matched to account for the buoyancy of the detergent micelles. The resultant multimeric states were obtained by measuring the absorbance at 280 nm (A280). Analysis of the spectra by AUC software, Ultrascan II results in two graphs with at the top the distribution of the residuals (showing how well a model fits to the experimental data) against the radius across the centrifuge cell. The bottom panel is optical density against the radius across the centrifuge cells. Data from three different concentrations are plotted.

II.1.6. *Gaussia princeps* protein-fragment complementation assay

Complementing *Gaussia* princeps luciferase fragments (Gluc1 and Gluc2) are fused in frame to the carboxyl or amino terminus of a test protein. Close proximity of the two fragments induces folding and functional reconstitution of catalytic (luciferase) enzyme activity. This eventually leads to light emitted at 475 nm, which is proportional to dimer strength. This approach has the advantages of reversibility, use for proteins expressed at low physiologic levels and high dynamic range due to the requirement of close proximity for folding, but no affinity between complementing parts.

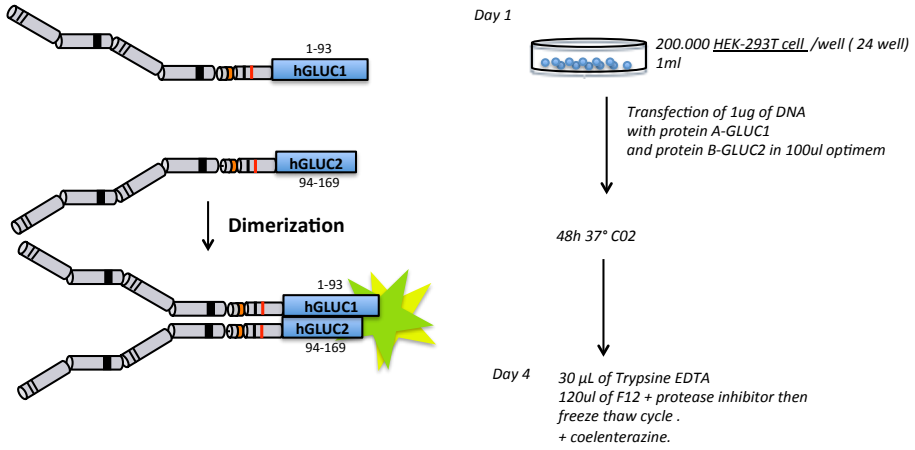


Figure 36 - Gaussia Protein-fragment complementation assay
Recombination of the luciferase fragments results in a positive signal and reveals dimerization.

II.1.7. Cys-mediated crosslinking

This technique allows detection of dimer formation by western blot of receptors engineered to bear a cysteine in the TMD. Those constructs are made on cysteine-free or cysteine-poor TM protein background, so that Cys residues are inserted at reporter positions. Cells expressing such constructs are suspended in a solution of N, N-1, 2-phenylenedimaleimide (o-PDM) and lysed with NP-40 buffer containing 2% of β-mercaptoethanol in order to satisfy excess crosslinker.[133]

II.1.8. Co- immunoprecipitation (Co-IP)

This technique can be used to assess direct and indirect physical association between co-expressed proteins. Those proteins can bear a different tag and are co-immunoprecipitated by specific antibodies coupled to protein G sepharose beads. They are then recovered by centrifugation and analyzed by Western blot. The limitation is represented by the fact that indirect interactions, for example via a bridging or cytoskeleton protein, can also be detected.

II.2. Principles of approaches to study activity

II.2.1. Dual Luciferase Assay

Transcriptional activity of STAT5 and STAT3, MAPKinase or PI3 kinase can be analysed by assaying for firefly luciferase production in cells transiently transfected with luciferase reporters where transcription is dependent on promoters responding to STATs (pGRR5-luc for STAT5/3/1[288], spi-Luc for STAT5[289], pMx-luc[290] for STAT1/STAT2/IRF9 complexes), pSRE-luc construct[291] for MEK-MAPKinase and 6xDBE-Luc reporter[292], which contains six canonical FOXO binding sites and which is inversely correlated with PI3-kinase activation. The pRL-TK vector (Promega, Madison, WI) containing the renilla luciferase gene under control of the constitutive TK promoter is used as an internal control to normalize for transfection efficiency. A luminometer is used to measure sequentially each luciferase signal, with firefly luciferase being measured first by addition of luciferine. Renilla luciferase is next measured after addition of coelenterazine and a quencher.

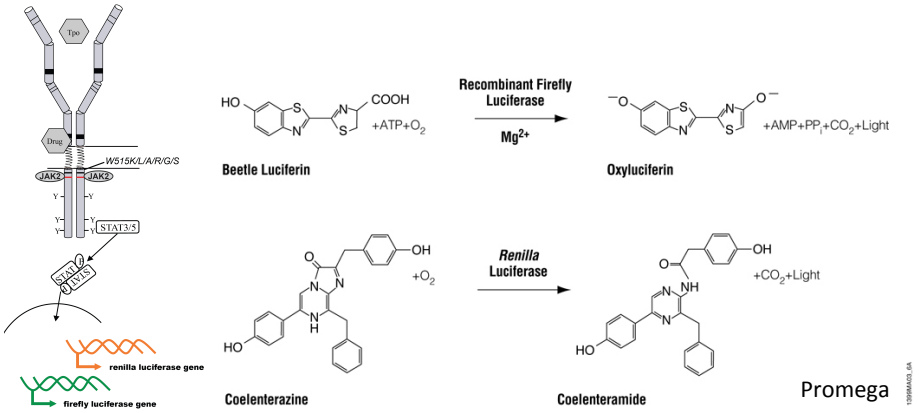


Figure 37 - Dual luciferase assay

Two reporters are used in the dual luciferase assay, the experimental firefly (FF) luciferase reporter, which responds here to JAK/STAT pathway, and a co-transfected renilla (RL) luciferase control reporter driven by a constitutive promoter that provides a baseline signal proportional to transfection levels..The firefly/renilla (FF/RL) ratio normalizes the FF response for experimental variability due to cell viability and transfection efficiency.

II.2.2. Engineering stable cell lines

II.2.2.1. Stable expression

Stable expression in mammalian cells, can be achieved by retroviral transduction using bicistronic retroviral vectors. In such vectors, like pMX-IRES-GFP, there is a simultaneous expression of the transgene, cloned upstream of the IRES (internal ribosome entry site) and of the marker (Green Florescence Protein, CD2, CD4 or others) downstream the IRES. This allows to sort for similar expression levels.[293] High titer of helper free virus are obtained by transfecting BOSC 23 packaging cell line[294] with pCL-ECO packaging vector[295] along with the pMX-HATpoR–IRES-GFP or other constructs. For infection of human primary cells and of mouse primary bone marrow cells we use a packaging system where the vesicular stomatitis virus G protein is used to pseudotype with mouse retroviral components.[238] In this manner packaged viruses can infect all cells, given that the VSV G protein binds to surface phosphatydylserine and that enveloped viruses exposing VSV G are quite stable and can be concentrated by ultracentrifugation. Infection is performed in the presence of polybrene and after infection we employ flow cytometry in order to determined the expression levels of GFP or other bicistronic markers, and also of HA for cell surface localization of receptors such as TpoR, which we engineered to carry an HA epitope tag after the cleavage site of the signal peptidase. For similar total expression we sort for equal marker expression, while for similar cell surface levels we sort for equal cell surface HA.

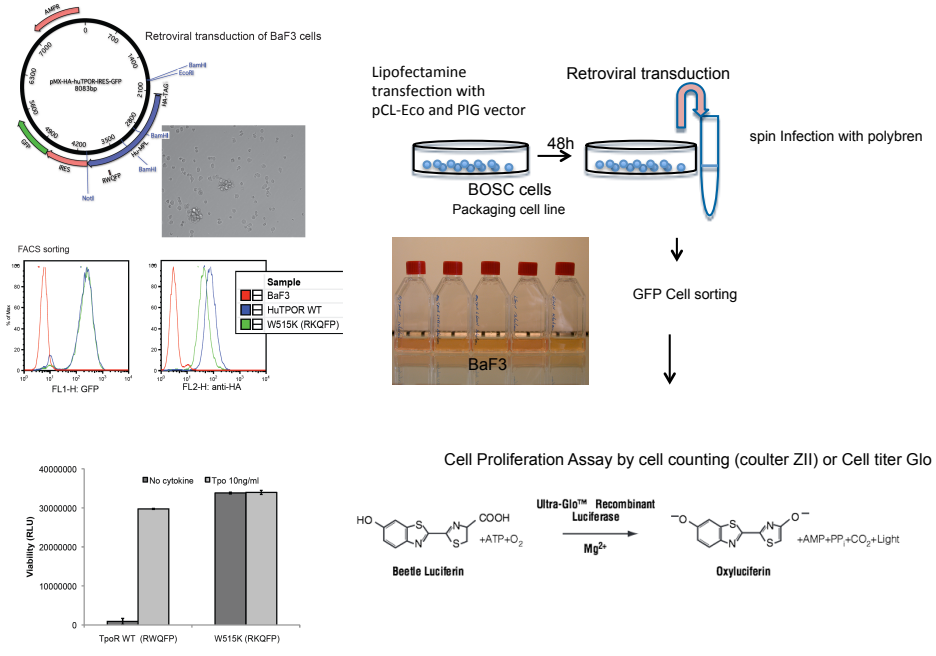


Figure 38 - Growth assay

II.2.2.2. Cell lines

II.2.2.2.1. BaF3 cells

BaF3 cells are mouse pro B cells[296] that are fast growing with a doubling time of approximately 12-18h when grown at 37C° 5% CO2 in RPMI 10% FBS + Wehi (IL-3 containing supernatant of WEHI cells). BaF3 cell maximal density is rapidly reached at 1.5-2. million cells/ml. They are easily transfected, electroporated or even transduced and can be rendered autonomous by expressing activated kinases or mutated cytokine receptors. We measured their growth by either using a Coulter Z™ Beckman coulter or by an ATP-based viability assay Promega.

II.2.2.2.2. γ2A Cells

γ2A cells are JAK2 deficient fibrosarcoma cells derived from 2C4 cells. They have been FACS sorted for non-expression of IFN-γ inducible cell surface marker like HLA class II and I. They were shown to be totally deficient in JAK2 mRNA by northern blot or JAK2 protein by western blot.[297] We grow them in DMEM 10% FBS at 37°C 8%C02.

II.2.2.2.3. WeHI-3 cell line

Those cells are IL-3 producers and are derived from BALB-C mouse B cell lymphoma. They are growth in RPMI 8%FBS + Glutamine 2mM.[298]

II.2.3. Bone marrow transplantation experiments in C57Bl6 mice

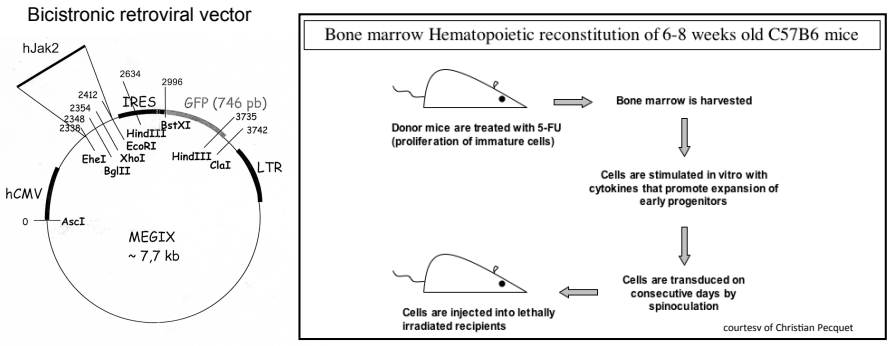


Figure 39 - Bone marrow transplantation protocol

Isolation of bone marrow (male C57B6 mice) and culture of cells in the presence of cytokines (SCF, Flt-3 ligand, Tpo, IL-3 and IL-6)

Day 1: spin infection (300µl concentrated VSV-G pseudo-typed retroviral supernatant)

Day 4: irradiation of female C57B6 mice: 950 Gy and injection of 1x 10^6 cells/mouse intravenously

Assay expression of GFP in peripheral blood two to three weeks after reconstitution

II.3. Principles of approaches to study orientation

II.3.1. Coiled coil forced dimers

The seven possible dimeric orientations of a dimeric receptor (where transmembrane domains form a left-handed crossing) can be engineered by replacing the extracellular domain of TpoR by the coiled-coil dimerization domain of the Put3 transcription factor. One by one deletion of residues at the junction between the coiled-coil (red) and the TMD (green) induce each time a 110° counterclockwise rotation. The stable dimeric orientation of the coiled-coil is transmitted to the downstream TM helix.

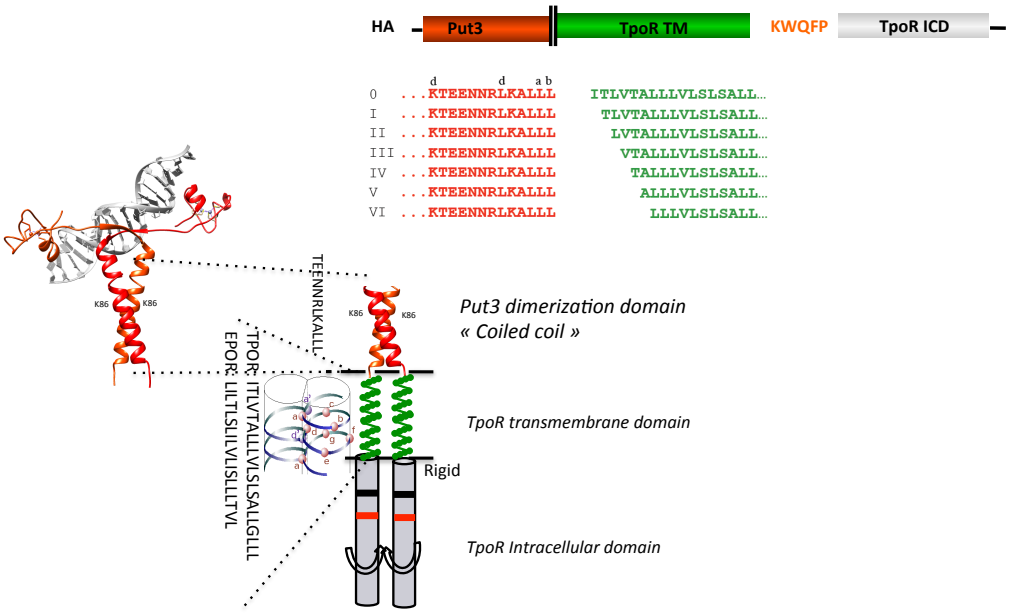


Figure 40 - Coiled coils inducing dimerization

Coiled coils induce distinct dimeric conformations when fused to the TMD-cytosolic part of a receptor.

III. RESULTS

III.1. Preamble: Orientation- specific signalling by thrombopoietin receptor dimers (EMBO J. 2011)

Judith Staerk*, Jean-Philippe Defour*, Christian Pecquet, Emilie Leroy, Hélène Antoine-Poirel, Ian Brett, Miki Itaya, Steven O Smith, William Vainchenker and Stefan N Constantinescu. * First co-authors.

III.1.1. Background

As predimeric states exist in cytokine receptors[119,120,123,126,127 299 125] dimerization is clearly not a sufficient condition to turn on receptor function. The concept of reorientation of preformed dimers is widely acknowledged and can be pictured like turning a car key toward the "start" state. The crossing of transmembrane helices in the TpoR and EpoR dimers adopts a left-handed geometry as shown in NMR experiments performed by our collaborator Prof. Steven O. Smith. In a left-handed transmembrane domain dimer, there are seven possible dimeric interfaces between α-helices that can be generated. Those interfaces are separated by a counterclockwise turn of 110°, engendered by deleting one by one residue at the junction between the dimerizing coiled coil domain (Put-3) and the transmembrane domain. This strategy was previously successfully used for EpoR, which is the closest receptor to TpoR and showed that EpoR possesses a unique inactive dimeric state, one intermediate state with only strong MAP-Kinase signaling and one active conformation requires for red blood cell production.[136] We thought the Put-3 coiled coil was compatible with being an extracellular sequence and allowing traffic of the fusion protein to the cell surface. The strategy was also used previously for type-II transmembrane protein E5 of the papillomavirus that activates EGFR, and where the Put3 coiled coil could function as a cytosolic segment as well.[300]

III.1.2. Question and approaches

The fundamental question that is addressed is whether the TpoR has orientation requirements for signaling and whether the cytosolic juxtamembrane (JM) RWQFP motif regulates Tpo dependent signaling. We engineered specific dimeric orientations using coiled-coil dimerization domain fused at the N-terminal part of the TMD and ICD of TpoR to assess this question. Defining precisely the active and inactive conformation of a receptor is of fundamental interest to better understand receptor physiology but is of practical interest for designing new drugs.

Stable BaF3 and UT-7 cell lines expressing the 7 individual dimeric constructs were tested for Tpo-independent growth. Transcriptional activity of constructs was explored via JAK2 or TYK2 on fibrosarcoma γ2A cells and BaF3 cells with reporters for STAT3, STAT5, PI-3kinase and MAP-Kinase. The rotational dependence mediates by the engineered dimers is of crucial importance and was tested by alanine insertions and by cross-linking experiments. In the context of these 7 constructs, we tested the effect of activating mutations like deletion of the JM amphipathic domain (RWQFP) or W508K (corresponding to human W515K) on

rotational dependence in the context of the cc-TpoR fusion proteins. Mouse bone marrow reconstitutions and CD41 expression of UT7 megakaryocytic cell line, both retrovirally transduced with the seven constructs were realized in view of finding the physiological platelet-producing interface.

III.1.3. Authors contribution

Initially Judith Staerk performed the cloning and initial testing of the constructs in cell lines and mice. Dr Poirel and myself (retrospectively) were responsible for the evaluation of the phenotype in mice. I was responsible for establishing the correspondence between the orientation and the biological *in vivo* effect and in the in-depth testing of signaling downstream each dimer. I have also initiated the testing of the W508K mutants in the context of the coiled coil fusions and compared JAK2 versus TYK2 signaling. I collaborated with Dr Christian Pecquet and PhD student Emilie Leroy and closely interacted with our structural biology collaborator (Prof. Steven O. Smith) and contributed significantly to the writing of the paper and design and flow of Figures.

Christian Pecquet realized immunoprecipitation and immunoblot analysis for signaling experiments as well as receptor recycling studies.

The EMBO Journal (2011), 1–16 | © 2011 European Molecular Biology Organization | All Rights Reserved 0261-4189/11
www.embojournal.org

THE EMBO JOURNAL

Orientation-specific signalling by thrombopoietin receptor dimers

Judith Staerk[1,2,6,7], Jean-Philippe Defour[1,2,6], Christian Pecquet[1,2], Emilie Leroy[1,2], Hélène Antoine-Poirel[3], Ian Brett[4], Miki Itaya[4], Steven O Smith[4], William Vainchenker[5] and Stefan N Constantinescu[1,2,*]

[1]Ludwig Institute for Cancer Research, Brussels, Belgium, [2]de Duve Institute, Université Catholique de Louvain, Brussels, Belgium, [3]Cliniques Universitaires St-Luc, Université Catholique de Louvain, Brussels, Belgium, [4]Center for Structural Biology, Department of Biochemistry and Cell Biology, Stony Brook University, Stony Brook, NY, USA and [5]INSERM, U1009, Université Paris-Sud, Institut Gustave Roussy, Villejuif Cedex, France

Ligand binding to the thrombopoietin receptor is thought to stabilize an active receptor dimer that regulates megakaryocyte differentiation and platelet formation, as well as haematopoietic stem cell renewal. By fusing a dimeric coiled coil in all seven possible orientations to the thrombopoietin receptor transmembrane (TM)–cytoplasmic domains, we show that specific biological effects and *in vivo* phenotypes are imparted by distinct dimeric orientations, which can be visualized by cysteine mutagenesis and crosslinking. Using functional assays and computational searches, we identify one orientation that represents the inactive dimeric state and another similar to a physiologically activated receptor. Several other dimeric orientations are identified that induce proliferation and *in vivo* myeloproliferative and myelodysplastic disorders, indicating the receptor can signal from several dimeric interfaces. The set of dimeric thrombopoietin receptors with different TM orientations may offer new insights into the activation of distinct signalling pathways by a single receptor and suggests that subtle differences in cytokine receptor dimerization provide a new layer of signalling regulation that is relevant for disease.

The EMBO Journal advance online publication, 2 September 2011; doi:10.1038/emboj.2011.315
Subject Categories: signal transduction
Keywords: dimerization; hematopoiesis; JAK2; myeloproliferation; TpoR

*Corresponding author. Ludwig Institute for Cancer Research, Avenue Hippocrate 74, UCL 7459, Brussels 1200, Belgium. Tel.: +32 2 764 7540; Fax: +32 2 764 6566; E-mail: stefan.constantinescu@bru.licr.org
[6]These authors are co-first authors
[7]Present address: Whitehead Institute for Biomedical Research, Cambridge, MA 02142, USA

Received: 4 November 2010; accepted: 4 August 2011

Introduction

The thrombopoietin (Tpo) receptor (TpoR, c-Mpl) is a key regulator of megakaryopoiesis (de Sauvage *et al*, 1994; Kaushansky, 1997), and of haematopoietic stem cell (HSC) renewal (Solar *et al*, 1998) and quiescence (Qian *et al*, 2007; Yoshihara *et al*, 2007). Binding of Tpo induces a conformational change of the receptor (Alexander *et al*, 1995), resulting in activation of the tyrosine kinases JAK2 and TYK2 (Drachman *et al*, 1995, 1999; Miyakawa *et al*, 1995; Watowich *et al*, 1996; Royer *et al*, 2005). Activated Janus kinases (JAKs) in turn phosphorylate tyrosine residues within the TpoR cytosolic domain that function as binding sites for downstream signalling molecules such as STAT3, STAT5 (the signal transducers and activators of transcription 3 and 5) and adaptors triggering phosphatydylinositol-3-kinase (PI-3-kinase) or Mitogen Activated Protein (MAP)-kinase activation (Miyakawa *et al*, 1995, 1996, 2001; Oda *et al*, 1996; Onishi *et al*, 1996; Drachman and Kaushansky, 1997).

Mutations that activate TpoR signalling in the absence of its ligand include single amino-acid substitutions by cysteine or asparagine in the extracellular and transmembrane (TM) domains, respectively (Alexander *et al*, 1995; Onishi *et al*, 1996; Ding *et al*, 2004), as well as mutations in the juxtamembrane (JM) region, on both the extracellular and intracellular sides (Pardanani *et al*, 2006; Pikman *et al*, 2006; Staerk *et al*, 2006; Malinge *et al*, 2008). Furthermore, truncation of part of the extracellular domain and fusion on the amino-terminus with a viral-derived sequence also activates TpoR signalling (Souyri *et al*, 1990). All these mutant receptors trigger cytokine-independent cell proliferation and induce myeloproliferative disorders presumably by ligand-independent dimerization in conformations productive for signalling (Alexander *et al*, 1995; Onishi *et al*, 1996; Ding *et al*, 2009). The precise dimeric interface(s) adopted by these active TpoR mutants remain however unknown.

Among cytokine receptors, TpoR is special as it plays essential roles at different stages of haematopoiesis. To carry out its multiple functions, different ligands and distinct cell types might induce changes in the active dimeric state of the receptor and its interaction with other cellular proteins. It is known that TpoR can respond to at least two ligands, Tpo (Kaushansky, 1997) and a human homologue of a fungal nuclear migration protein (hNUDC) (Chen *et al*, 2010). Very little is known about the dimeric structure of the activated TpoR TM and cytoplasmic domains. Whether the dimeric orientations adopted by ligand-activated TpoR differ in various cell types, megakaryocyte progenitors versus HSCs remains unclear. Different biologic effects of activated TpoR might result from interactions with other receptors or signalling proteins, which may be cell type specific. One hypothesis would posit that TpoR interacts with cell type-specific receptors and signalling proteins through different conformations of the TM and cytoplasmic domains of TpoR. This proposed mechanism for activation is quite different from that of the

©2011 European Molecular Biology Organization

erythropoietin receptor (EpoR), where essentially one dimeric conformation appears to be required for promoting erythroid cell formation (Seubert *et al*, 2003).

To test whether the TpoR requires a specific dimeric conformation for signalling or whether it signals from many different dimeric conformations, we replaced the extracellular domain of the TpoR by a dimeric coiled coil. By engineering the junction of the coiled coil to the TpoR TM domain, we were able to impose the seven possible relative orientations on the TM and cytoplasmic domains of the TpoR. In this approach, we obtain seven individual dimers that adopt different interfaces in the TM and intracellular JM domains, which are due to the register of the coiled coil. The JM cytosolic region of cytokine receptors was suggested to be rigid by both functional assays (Constantinescu *et al*, 2001; Huang *et al*, 2001) and by single particle electron microscopy (Skiniotis *et al*, 2008; Lupardus *et al*, 2011). The different orientations of the TM–JM region are thus likely to be transmitted to the cytosolic domain and influence signalling. Furthermore, in the case of the growth hormone receptor, subunit rotation in a receptor dimer was shown to suffice for activation (Brown *et al*, 2005). To show that the rotation induced by the coiled coil is transmitted, as predicted, to the JM region, we used two approaches, cysteine mutagenesis in combination with crosslinking and alanine insertions at the intracellular boundary.

We tested the biologic effects of the seven possible TpoR dimers in cell lines and *in vivo* in mouse bone marrow reconstitution experiments. This allowed us to use functional blood formation as a read-out in order to identify the precise dimer conformation that most faithfully resembles the effect of Tpo on platelet formation (*cc-TpoR*-I). To our surprise, five other dimeric conformations of the TpoR also led to proliferation of cytokine-dependent cells, with differences in cell morphology and signalling. *In vivo*, these orientations induce different effects, with two being associated with mixed myelodysplastic/myeloproliferative phenotypes, and others with myeloproliferation. We propose the model that different dimeric TpoR interfaces induce different biological outcomes and that different dimeric receptors could possibly favour different myeloproliferative and myelodysplastic disorders. Importantly, we show that this orientation-dependent signalling specificity requires the KWQFP motif in the JM region, which maintains the unliganded TpoR inactive (Staerk *et al*, 2006).

Results

Fusion of the Put3 coiled coil to the TpoR TM and cytosolic domains

The C-terminal 28 amino acids of Put3, a soluble transcriptional activator protein from *Saccharomyces cerevisiae*, associate in a stable left-handed coiled-coil dimer (Swaminathan *et al*, 1997; Walters *et al*, 1997). Fusion of the C-terminal residue of the Put3 sequence to the N-terminal residue of the TM sequence of the TpoR induces dimerization of the TpoR TM domain, which is known to be α-helical through F510 based on polarized infrared spectroscopy of membrane reconstituted peptides corresponding to the TM and JM domains (Supplementary Figure S1). Fusion of the Put3 coiled-coil domain imposes its structure on the α-helical residues downstream in the TM domain and enables us to identify the amino acids that are present in the interface of the active TpoR dimer (Figure 1A and B; Swaminathan *et al*, 1997; Walters *et al*, 1997). Position of heptad repeats characteristic of left-handed coiled coils are denoted *a*–*g* or *a*′–*g*′. The last residue of the Put3 coiled coil is in a *b* position. As a result, the first fused residue of the TpoR TM domain is in a *c* position (Figure 1B). By designing seven different junctions between the coiled coil and the TpoR TM domain, all possible dimeric receptor orientations can be imposed (Mattoon *et al*, 2001; Seubert *et al*, 2003), due to the registry and tight dimerization of the 28 amino acid Put3 coiled coil (Swaminathan *et al*, 1997; Walters *et al*, 1997).

We constructed seven TpoR fusion proteins where the Put3 coiled coil was fused to the TM and cytoplasmic domains of the TpoR, denoted *cc-TpoR*-0–VI. By varying the junction between the Put3 coiled coil and the TpoR TM and cytoplasmic sequences, all seven possible registers could be obtained (Figures 1A, B and 7A). All fusion proteins were expressed at the expected size of 27 kDa in Ba/F3 cells. In order to confirm the orientation of our *cc-TpoR* fusion proteins, we introduced a cysteine residue at position 505 (L505C) for crosslinking studies and eliminated all other cysteine residues by truncation of the cytosolic domain at position 553 in all *cc-TpoRs*. All the truncated fusion proteins were expressed in BOSC cells at the expected size of 12 kDa. Consistent with our hypothesis that only *cc-TpoR*-I, *cc-TpoR*-II and *cc-TpoR*-V should have L505C in the dimeric interface, we only visualized formation of *N*,*N*′-1,2-phenylenedimaleimide (o-PDM) crosslinked dimers for those three receptors (Figure 1C). Indeed, treatment of cells with o-PDM enables formation of intermolecular bonds maintaining stable dimers in denaturing conditions. Crosslinking on live cells, therefore, validates the orientation imposed by the coiled coil up to the outset of the cytosolic JM domain.

Cell surface expression levels of the *cc-TpoR*-0–VI proteins were measured by flow cytometry using an anti-HA tag antibody. Levels of *cc-TpoR* cell surface localization were between 20 and 40%, as compared with the wtTpoR levels, which were taken as 100% for the same level of GFP (Figure 1D).

Proliferation mediated by the cc-TpoR-0–VI fusion proteins

Ba/F3 cells were infected with retroviruses coding for the seven *cc-TpoR* fusion proteins and sorted for equal GFP levels. Cells were washed, grown in the absence of any cytokines and monitored by cell counting at different intervals. Four out of six active conformations induced maximal proliferation, *cc-TpoR*-0, -I, -III and -IV, while two, *cc-TpoR*-V and -VI, were able to promote growth of Ba/F3 cells, but to a lower extent (Figure 2A). *cc-TpoR*-II was inactive.

We next ensured that dimerization of the TpoR TM and cytoplasmic domains mediated by the Put3 coiled-coil fusion was required for the proliferative effects of the *cc-TpoR*-0–VI fusion proteins. We, therefore, substituted the lysine at position 86 within the Put3 amino-acid sequence by a proline (KtP). This mutation has been shown to block dimerization of the Put3 coiled coil (Swaminathan *et al*, 1997). The Put3-KtP substitution disabled cytokine-independent growth mediated by the *cc-TpoR* fusion proteins (Figure 2B), showing that dimerization mediated by the coiled-coil Put3 was crucial for the activity of *cc-TpoR* fusion proteins.

 ©2011 European Molecular Biology Organization

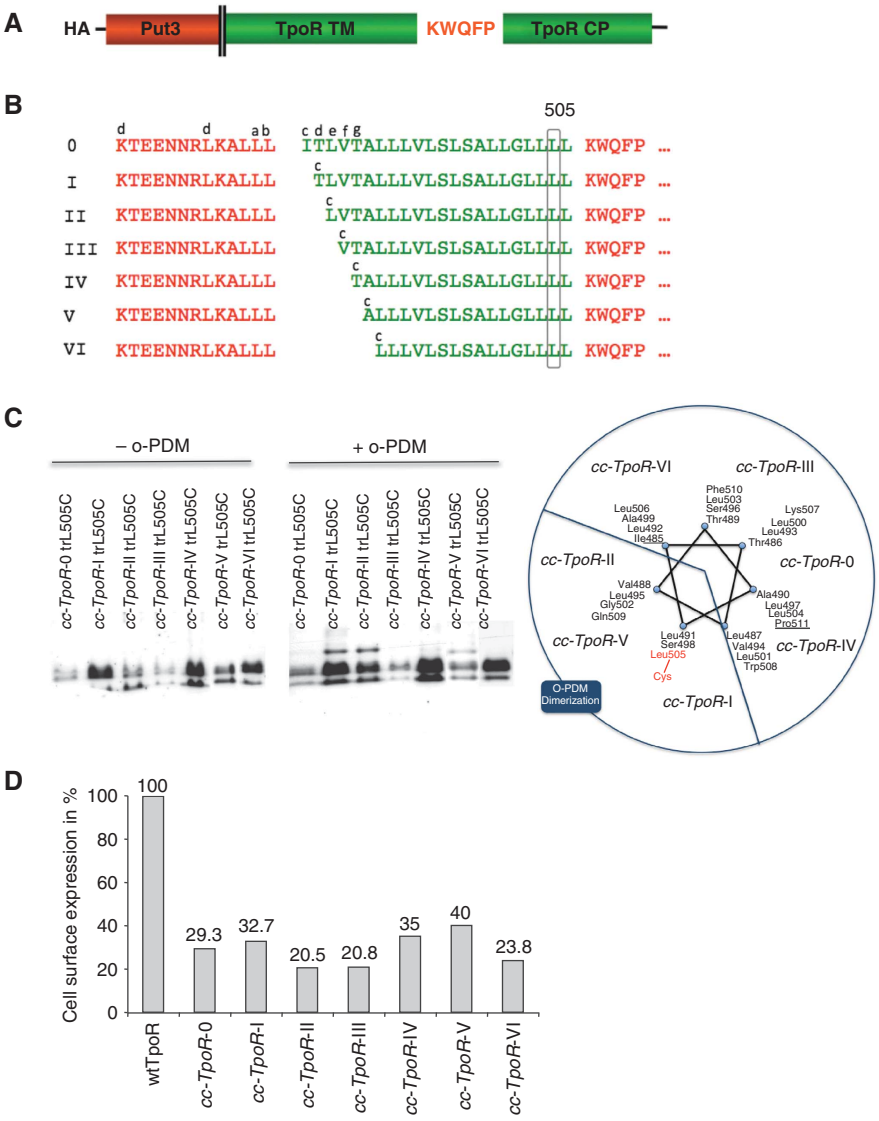


Figure 1 Design, validation and expression of seven fusion proteins that contain the Put3 coiled coil fused in all possible orientations to the TpoR TM–cytoplasmic domains. (**A**) Design of the *cc-TpoR* fusion proteins. The coiled-coil segment of Put3 was fused to the TM and cytoplasmic domains of TpoR. (**B**) By varying the junction between the Put3 coiled coil and the downstream TpoR TM α-helical domain, all seven possible registers could be imposed. All fusion proteins contain an HA tag at their N-terminus. The position of heptad repeats characteristic of coiled coils is denoted *a*–*g* or *a*′–*g*′. The last residue of the Put3 coiled-coil is in a *b* position, while the first fused residue will be in a *c* position. The dimeric interface contains the *a*, *d*, *d*′ and *a*′ positions. (**C**) Crosslinking studies on live cells. *Left panel*: BOSC cells were transiently transfected with cDNA coding for seven truncated coiled-coil TpoR cysteine mutants (L505C). Cells were lysed after crosslinking with *N*,*N*′-1,2-phenylenedimaleimide (+ o-PDM), or in the absence of crosslinking (− o-PDM). Lysates were analysed on 12–14% Bis-Tris Gel followed by immunoblotting with an anti-HA antibody. *Right panel:* Helical representation of the different *cc-TpoR* interfaces and the putative localization of the Cys505 residue. (**D**) HA staining for cell surface expression of the *cc-TpoR* fusion proteins. The wtTpoR cell surface expression was set as 100%. Percent expression of the *cc-TpoR* fusion proteins was related to that of the wtTpoR. Shown is one experiment with data collected for 10 000 cells of three independent determinations; variations were <10%.

Ba/F3 cells expressing the active *cc-TpoR* fusion proteins showed remarkable differences in their morphology. When cells expressed *cc-TpoR*-IV, large clusters were observed (Figure 2C). In contrast, cells that expressed *cc-TpoR*-I or *cc-TpoR*-III did not induce such strong cell-to-cell interactions, although they induced proliferation at similar levels (Figure 2A). Interestingly, *cc-TpoR*-IV induced cell-to-cell adhesion in many cell lines and in primary bone marrow haematopoietic progenitors, both in suspension and in methylcellulose assays (not shown). To examine the ability of the wtTpoR to induce such cell-to-cell interactions, we stimulated wtTpoR expressing Ba/F3 cells (Ba/F3-TpoR) using Tpo concentrations between 5 and 500 ng/ml. Ba/F3-wtTpoR stimulated with extremely high Tpo concentrations (500 ng/ml) formed the same cell clusters (Figure 2C, right panel), as observed with *cc-TpoR*-IV, whereas at lower doses (5 ng/ml) only small clusters could be seen (Figure 2C, left panel). Thus, in the dimeric conformation adopted by *cc-TpoR*-IV, signalling events appear to be similar to those induced by very high Tpo levels via the wtTpoR. Such high levels may be attained in the bone marrow endosteal niches, close to HSC reservoirs.

Our results using the seven *cc-TpoR* fusion proteins suggest that the TpoR can signal from multiple dimeric conforma-

©2011 European Molecular Biology Organization

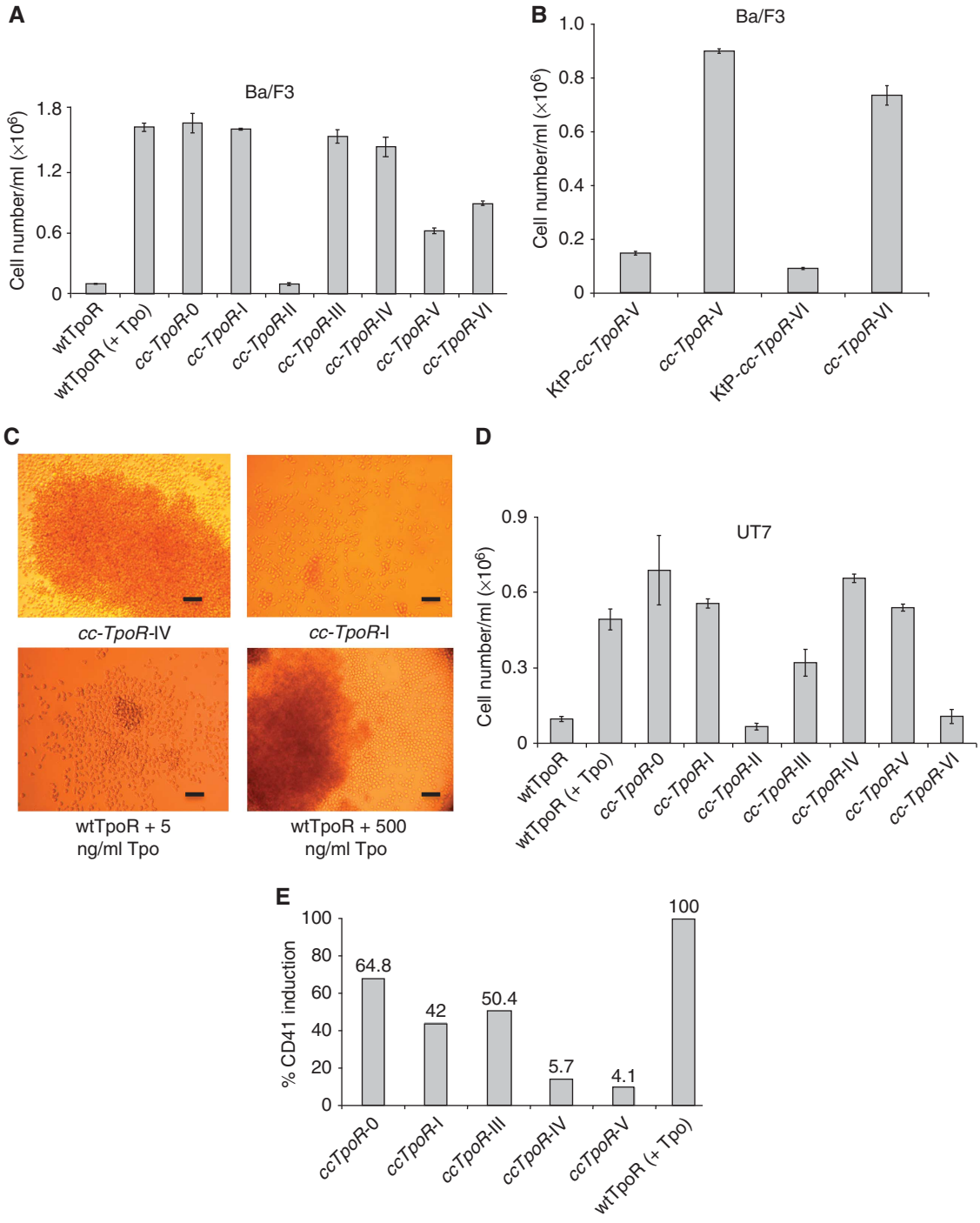


Figure 2 Cell proliferation induced by the seven *cc-TpoR* fusion proteins. (**A**, **B**) Proliferation assays were performed with Ba/F3 cells expressing the wtTpoR or the indicated *cc-TpoR*-0–VI fusion proteins (**A**), or K86P (KtoP) mutants thereof (**B**) at equal GFP levels in the absence of any cytokines or stimulated with 5 ng/ml Tpo as indicated. Cell numbers (averages of triplicates ± s.d.) were counted at day 6. One representative experiment out of four is shown. (**C**) Morphology of Ba/F3 cells expressing *cc-TpoR*-IV or *cc-TpoR*-I. Only *cc-TpoR*-IV induced cell-to-cell adhesion that lead to tight clusters (upper panel). Ba/F3 cells expressing the wtTpoR were stimulated with 5 or 500 ng/ml Tpo. At very high Tpo concentrations, cells formed clusters similar to those induced by *cc-TpoR*-IV (lower panel). Scale bar, 50 μm. (**D**) Proliferation assays were performed with UT7 cells expressing the wtTpoR or the *cc-TpoR*-0–VI fusion proteins at equal infection efficiency (GFP levels) in the absence of any cytokines or stimulated with 5 ng/ml Tpo, as indicated. Cell numbers were counted at day 8 and shown are averages of triplicates ± s.d. (**E**) Induction of CD41 expression of UT7 retrovirally transduced with the seven *cc-TpoR* fusion proteins or with the wtTpoR. Initiation of megakaryocyte differentiation of UT7 cells was assayed by flow cytometry analysis of the induction of cell surface CD41. The induction of CD41 cell surface localization by 5 ng/ml Tpo on cells expressing the wtTpoR was taken as 100%.

tions (except for that of *cc-TpoR*-II, and in certain cells of *cc-TpoR*-VI), but that different orientations induce different effects. We took advantage of the UT7 cell line (Komatsu *et al*, 1991), first to test whether *cc-TpoR* fusion proteins induce similar proliferative effects as in Ba/F3 cells, and second, to explore the abilities of the *cc-TpoR* proteins to

©2011 European Molecular Biology Organization

promote commitment towards the megakaryocyte lineage. UT7 cells are strictly dependent on GM-CSF or Epo for growth (Komatsu *et al*, 1991). We introduced all seven TpoR fusion proteins in parental UT7 cells maintained in GM-CSF, sorted for equivalent GFP expression and then tested proliferation after withdrawal of GM-CSF (Figure 2D). One of these weaker conformations in Ba/F3 cells, *cc-TpoR*-VI, was not able to mediate growth of UT7 cells, similarly to *cc-TpoR*-II, which was inactive in both cell lines (Figure 2A and D). Whereas UT7 cells that expressed *cc-TpoR*-II and -VI did not survive or proliferate in the absence of ligand, UT7 cells expressing *cc-TpoR*-III proliferated to a lower extent compared with the proliferation level in Ba/F3 cells (Figure 2A and D). One explanation for this observation is that *cc-TpoR*-III induces senescence, as it was recently shown for late megakaryocytes and UT7-Mpl cell lines treated with Tpo (Besancenot *et al*, 2010); another possibility is that *cc-TpoR*-III induces higher levels of megakaryocyte commitment.

Stably transfected UT7-TpoR cells respond to Tpo by induction of the expression of the megakaryocyte-specific differentiation antigen CD41 (gpIIb) (Porteu *et al*, 1996), and such cells have been the standard for exploring signals leading to megakaryocyte commitment. We then selected stably transduced UT7 cells for growth factor-independent proliferation. We analysed the expression of the CD41 in these cells and found that *cc-TpoR*-0 and -III, as well as *cc-TpoR*-I, were able to induce CD41 expression, while *cc-TpoR*-IV and -V were very weak inducers of CD41 expression (Figure 2E). On the basis of these data, we predict that one or several of the *cc-TpoR* fusion proteins that induce CD41 expression in UT7 cells might induce *in vivo* physiologic platelet formation.

Transcriptional activity mediated by the cc-TpoR fusion proteins

We examined the transcriptional activity in Ba/F3 and in JAK2-deficient γ2A cells (Kohlhuber *et al*, 1997) expressing the different coiled-coil fusion proteins using the reporter genes for STAT5, STAT3, MAP-kinase, PI-3-kinase, as described in Materials and methods. For all pathways tested, *cc-TpoR*-0, -I and -IV activated signalling via STAT5, STAT3 and MAP-kinase very strongly (Figure 3A and B). As expected, signalling via PI-3-kinase resulted in inhibition of transcriptional activity of the 6xDBE-Luc FoxO reporter, with *cc-TpoR*-0, -I and -IV being strong activators of this pathway (Supplementary Figure S2). Since *cc-TpoR*-I was one of the active orientations not promoting cell-to-cell adhesion, these results rule out the possibility that formation of cell clusters is simply a consequence of the quantitative level of signalling activation and suggests that different dimeric orientations may attract different adaptors or signalling proteins. While in Ba/F3 cells, *cc-TpoR*-III mediates proliferation to the same extent as *cc-TpoR*-0 and -IV, *cc-TpoR*-III induces a slightly lower level of STAT5 and STAT3 activity, when compared with *cc-TpoR*-0, -I, -IV and it only weakly induces MAP-kinase activation (Figure 3A and B). While *cc-TpoR*-III and -V displayed a very weak MAP-kinase activity, *cc-TpoR*-II and -VI failed to induce any detectable MAP-kinase response. Noteworthy cc-*TpoR*-II, -V, and -VI are located on the same face in the helical representation (Figure 1C) and correspond to a low JAK/STAT, low MAP-kinase, and low PI-3-kinase interface (Supplementary Figure S4). On the opposite face, *cc-TpoR*-0, -I, -IV activate very strongly JAK/STAT, MAP-kinase and PI-3-kinase (Figure 1C; Supplementary Figures S2 and S4; Table I).

Orientation-dependent activation of JAK2 and TYK2 signalling

Tpo binding to TpoR leads to activation of two members of the JAK family, JAK2 and TYK2. These kinases exhibit similar potency to promote traffic stability of TpoR at the cell surface (Royer *et al*, 2005). JAK2, however, is much more potent to mediate downstream signalling (Drachman *et al*, 1999; Royer *et al*, 2005). We asked whether differently oriented TpoR dimers would preferentially signal via JAK2 versus TYK2. To this end, we compared STAT5 or STAT3 transcriptional activity of *cc-TpoR* fusion proteins in JAK2-deficient γ2A cells in the presence of JAK2 or TYK2 (Royer *et al*, 2005). As shown in Figure 3B (left panel), *cc-TpoR*-0, -I and -IV induced strong STAT5 signalling in the presence of JAK2. In contrast, in the presence of TYK2 (right panel), *cc-TpoR*-III and cc-*TpoR*-VI induced the highest STAT5 and STAT3 activation. Thus, signalling via JAK2 and TYK2 may be induced via different interfaces (with cc-*TpoR*-VI being specific for TYK2 and cc-*TpoR*-III supporting both JAK2 and TYK2 activations; Table I). Further studies are required to determine whether, in blood progenitors, TpoR could signal via JAK2–TYK2 heterodimers, and whether a dimeric interface, such as that of cc-*TpoR*-III, could actually assemble such JAK2–TYK2 heterodimers.

We then asked whether the differences observed in transcriptional activities of *cc-TpoRs* could also be obtained if rotations were introduced at the end of the TM domain. As a proof of principle, insertions of one or more alanines after the TM domain of *cc-TpoR*s rotate the receptor clockwise. Addition of two alanines to the strongest coiled coil via JAK2 (*cc-TpoR*-IV + 2A) diminished the STAT transcriptional activity, rendering *cc-TpoR-IV* similar to *cc-TpoR*-II, as predicted. Addition of one alanine to the weakest coiled coil via JAK2 (*cc-TpoR*-II + 1A) enhanced the STAT transcriptional activity, to the levels of cc-*TpoR*-I, as predicted (Figure 3C). This rotational effect can also be demonstrated by measuring the signalling downstream TYK2 with cc-*TpoR*-V + 2A being a phenocopy of the powerful cc-*TpoR*-III via TYK2 (Figure 3D). These results indicate that the TM α-helix is a continuum and that rotations at the C-terminus are transmitted to the JM domain in the same manner as those induced by the coiled coil at the N-terminus.

Early downstream signalling and traffic of cc-TpoR fusion proteins

Having determined the biologic activities of *cc-TpoR*s in Ba/F3 cells, and their transcriptional activities, we aimed to determine the immediate signalling events at the receptor cytosolic domain. We immunoprecipitated the receptors and tested the phosphorylation level of the main signalling tyrosine residue, Y626 (Drachman and Kaushansky, 1997), using an antibody specifically recognizing this phosphorylated residue (Pecquet *et al*, 2010). *cc-TpoR*-V, -VI and -II presented very low phosphorylation levels of Y626 compared with *cc-TpoR*-0, -I, -III and -IV (Figure 4A). We validated these results by analysing the activity of some downstream pathways, like STAT1 or STAT3. Indeed, *cc-TpoR*-II shows no activation of these pathways (Figure 4B). *cc-TpoR*-V and -VI

©2011 European Molecular Biology Organization

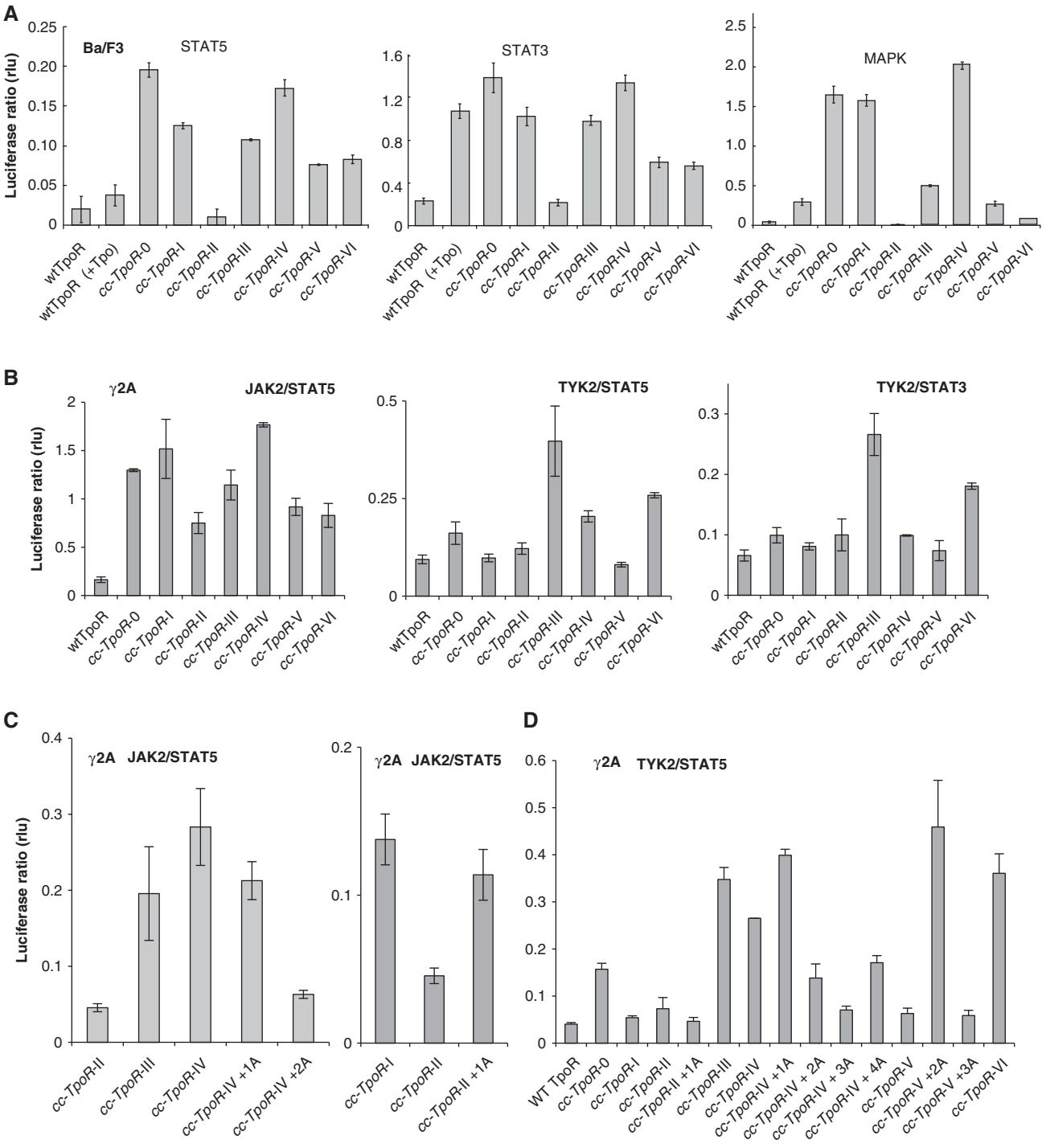


Figure 3 Transcriptional activity mediated by the wild-type (wt) TpoR or *cc-TpoR*-0–VI with and without alanine insertions. (**A**) Ba/F3 cells were selected in Tpo or without cytokines and starved overnight in RPMI/1 mg/ml BSA. To measure the transcriptional activity of STAT5 (left panel), STAT3 (middle) or MAP-kinase (MAPK) (right panel) pLHRE-luc, pGL3bPpr2-luc and pSRE-luc were used, respectively. pRL-TK encoding the renilla luciferase was co-electroporated for normalization of luciferase values. Cells were stimulated with 50 ng/ml Tpo or mock treated, as indicated. The results shown reflect averages of triplicate values ± s.d. Similar results were obtained performing three independent experiments. (**B**) γ2A cells were transfected with cDNAs coding for the *cc-TpoR* fusion proteins, JAK2 (left panel) or TYK2 (right panel), STAT5/STAT3 pGRR5-luc luciferase reporter and pRL-TK. The results represent averages of triplicate values ± s.d. of one representative experiment out of at least three. (**C**, **D**) γ2A cells were co-transfected with pGRR5-luc and pRL-TK luciferase reporter along with cDNAs coding for *cc-TpoR*s in which alanines were inserted at the end of the TM region, as indicated, and for JAK2 (**C**) or TYK2 (**D**).

presented low activation of STAT1 while *cc-TpoR*-0, -I, -III and -IV were fully active (Figure 4B). Thus, the strength of signalling and biologic effects appear to correlate with levels of Y626 phosphorylation.

We next analysed the internalization rate of the fusion proteins as well as their recycling. Cell surface biotinylation followed by cell surface immunoprecipitation enables us to assess the internalization over a certain period of time, but

 ©2011 European Molecular Biology Organization

Table I Summary of biologic effects and signalling of *cc-TpoR* fusion proteins in Ba/F3 cells

	Proliferation	Cell clustering	JAK2/STATs activation	TYK2/STATs activation	MAP-kinase activation	PI-3-K/AKT activation
cc-TpoR-0	+ + +	–	+ + +	–	+ + +	+ +
cc-TpoR-I	+ + +	+	+ + +	–	+ + +	+ +
cc-TpoR-II	–	–	–	–	–	–
cc-TpoR-III	+ + +	–	+ +	+ + +	+	+
cc-TpoR-IV	+ + +	+ + +	+ + +	+	+ + +	+ +
cc-TpoR-V	+	+	+ +	–	+	+
cc-TpoR-VI	+/–	–	+	+ +	–	+

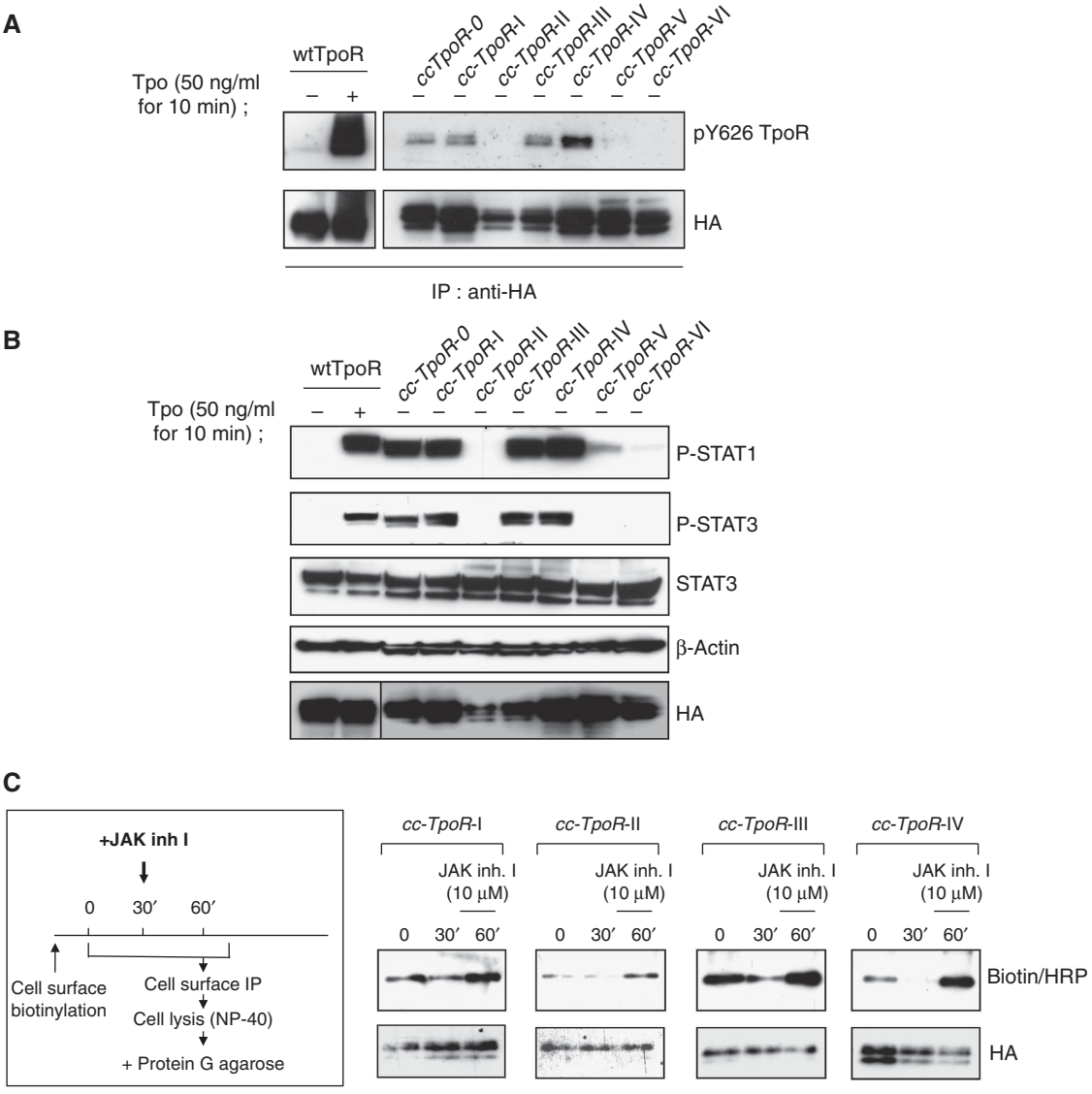


Figure 4 Early signalling and traffic of *cc-TpoR* fusion proteins. (**A**) Immunoprecipitation of the indicated fusion proteins. Induction of phosphorylation of cytosolic Y626 was assessed using an anti-pY626 TpoR antibody. The anti-HA antibody was used to analyse the expression level of the *cc-TpoR* fusion protein. (**B**) Western blot analysis performed on Ba/F3 cells expressing the fusion proteins by using the indicated antibodies. (**C**) Recycling assay on Ba/F3 cells expressing *cc-TpoR*-I, *cc-TpoR*-II, *cc-TpoR*-III or *cc-TpoR*-IV. Cells were subjected to cell surface biotinylation, allowed to internalize the receptor, and then were maintained in culture in presence of JAK inhibitor I, in order to block JAK2 signalling, for the indicated time. Cell surface immunoprecipitation was performed on the cells followed by lysis in NP-40 buffer. Immunoprecipitates were analysed by immunoblot with an anti-biotin/HRP and an anti-HA.

also the recycling. For the latter, we blocked the activity of the receptors with a JAK2 inhibitor, JAK inhibitor I (Thompson *et al*, 2002). All fusion proteins tested (*cc-TpoR*-I, -II, -III or -IV) were internalized after 30 min in Ba/F3 cells, with higher levels of internalization being correlated with signalling strength. Importantly, after treatment with JAK inhibitor I, recycling was observed for the tested fusion proteins, *cc-TpoR*-I, -II, -III or -IV (Figure 4C), suggesting that traffic

©2011 European Molecular Biology Organization

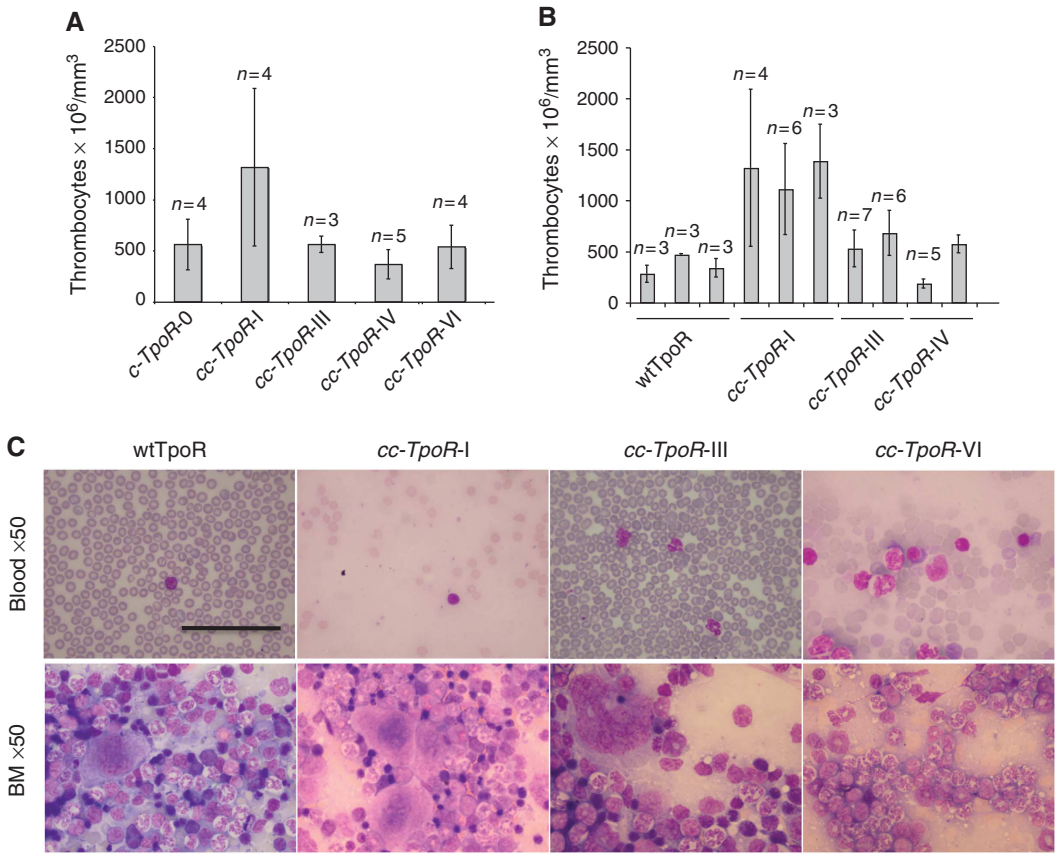


Figure 5 *In vivo* expression of *cc-TpoR* fusion proteins. (**A**, **B**) Mice were reconstituted with bone marrow cells retrovirally transduced with the indicated *cc-TpoR* fusion proteins. Peripheral blood counts were measured 6–8 weeks after reconstitution. (**A**) Platelets counts are the average + s.d. of six mice per construct. (**B**) The peripheral number of platelets is shown for the indicated *cc-TpoR* fusion proteins; *n*, number of mice. Three independent reconstitutions are shown for TpoR wt, *cc-TpoR*-I and *cc-TpoR*-V, and two independent reconstitutions are shown for *cc-TpoR*-III and *cc-TpoR*-IV. (**C**) Peripheral blood was isolated from GFP-positive mice 6 weeks after reconstitution and blood smears were performed. Cover slides were stained using a May-Grunwald stain and analysed for qualitative or quantitative abnormalities in the blood. Bone marrow cytologic examination was performed after May Grunwald staining. The magnification was × 50. Scale bar, 50 μm.

and especially recycling are not the determinants of their different biologic activities.

Expression of different TpoR fusion proteins in bone marrow progenitors induced specific myeloid disorders in bone marrow transplanted mice

We next investigated the *in vivo* effects of the *cc-TpoR*-0–VI fusion proteins. Bone marrow cells from 6- to 8-week-old C57/B6 mice were isolated and infected with retroviruses encoding the wtTpoR or the active *cc-TpoR* fusion proteins. In all, 0.5×10^6 cells were injected intravenously into lethally irradiated mice. Peripheral blood examined 3 weeks after reconstitution by FACS analyses showed that >90% of peripheral blood cells were GFP positive. A high level of platelet formation was induced *in vivo* by *cc-TpoR*-I (Figure 5A and B). Cytology examination on May-Grunwald-Giemsa stained bone marrow showed normal cellularity, with correct maturation of the myeloid lineages and excess of megakaryocytes of small to normal size that did not exhibit phenotypic changes of the myeloproliferative disorders. Interestingly, the *cc-TpoR*-I conformation has S498 (equivalent to S505 in human TpoR) in the interface (Figure 7A), suggesting that this particular orientation might reflect the active wtTpoR interface. Another fusion protein that contains S498 in the interface, *cc-TpoR*-V (Figure 7A), induced a different phenotype with circulating erythroblasts, and dyserythropoietic picture with microcytic red cells overlapping in size with platelets, which gave an artificially high count for platelets. In the marrow, *cc-TpoR*-V induced a picture of dysplasia of the erythroid and granulocytic lineages (not shown). Adopting a different orientation (Figure 7A), *cc-TpoR*-III induced granulocytosis with normal platelet counts, 2% erythroblast peripheral counts with normal red blood cell counts, while in the marrow cytologic examination showed large megakaryocytes with emperipolesis (dysmegakaryopoiesis), dyserythropoiesis and enhanced granulocytopoiesis (Figure 5). *cc-TpoR*-IV is the one orientation that induced strong clustering activity in cell lines and primary bone marrow cells (Figure 2C), which led to variable levels of reconstitution (not shown); this made the analysis difficult. An inducible system would be necessary to avoid factoring in the effects of adhesion during bone marrow reconstitution. Mice reconstituted with *cc-TpoR*-VI (adopting a conformation resembling that of *cc-TpoR*-III; Figure 7A) had a high degree of granulocytosis, at higher levels than *cc-TpoR*-III, with also immature granulocytic precursors in the peripheral blood, high levels of erythroblasts (15%), reticulocytosis and normal platelets. In the marrow, *cc-TpoR*-VI induced a major increase in the granulocytic lineage (very high granuloerythropoietic ratio),

 ©2011 European Molecular Biology Organization

with decreased megakaryocyte numbers and dysmegakaryopoiesis.

No orientation-dependent signalling is induced by the Δ5cc-TpoR fusion proteins

In all of our *cc-TpoR* fusion proteins, the JM KWQFP motif is present at the junction between the TpoR TM and cytosolic domains. This domain, in particular the Trp residue, is required to maintain the unliganded TpoR inactive (Staerk *et al*, 2006). Amino-acid substitutions of W515 result in oncogenic receptors, and are the basis of a fraction of human myeloproliferative neoplasms (MPNs) (Pardanani *et al*, 2006; Pikman *et al*, 2006; Pecquet *et al*, 2010). We, therefore, addressed whether this motif affects signalling by the different dimeric conformations of the TpoR. Ba/F3 or UT7 cells were infected with retroviruses coding for the seven Δ*5cc-TpoR* fusion proteins (Figure 6A) and sorted for equal GFP levels as described above.

Strikingly, when the KWQFP motif was deleted, all seven Δ*5cc-TpoR* fusion proteins promoted maximal proliferation of Ba/F3 or UT7 cells (Figure 6B and C). These results indicate that the KWQFP motif played an important role in orientation-dependent proliferation obtained by the wtTpoR. None of the Δ*5cc-TpoR* fusion proteins could induce formation of cell-to-cell adhesion or cell clusters (Figure 6D, compared with Figure 2C). Furthermore, the inhibitory conformation induced by *cc-TpoR*-II was changed by the deletion of the KWQFP motif and the Δ*5cc-TpoR*-II became active (Figure 6B and C). The specificity of TYK2 activation by only *cc-TpoR*-III and -VI fusion proteins was lost, with all Δ*5cc-TpoR* fusion proteins activating TYK2 (Figure 6E) and JAK2 (not shown) to the same high extent.

Reconstitution of mice with Δ*5cc-TpoR* fusion proteins showed in general a uniform increase in granulocytes and platelets in peripheral blood, without the specific effects seen for the *cc-TpoR* fusion proteins (Figure 6F). For Δ*5cc-TpoR*-I, -III and -VI all three had granulocytosis, while that was not the case for *cc-TpoR*-I. Platelet numbers were increased for Δ*5cc-TpoR*-I, -III, and for the latter this was in direct contrast with *cc-TpoR*-III. Functionally, Δ*5cc-TpoR*-VI resembles the most its *cc-TpoR*-VI counterpart, especially also showing erythroblastosis (10%); however, the platelet numbers increased, which was not the case for *cc-TpoR*-VI. Overall, the differences noted between individual *cc-TpoR* fusion proteins were mostly lost for the Δ*5cc-TpoR* counterparts, with the exception of the erythroblastosis for Δ*5cc-TpoR*-VI.

Introduction of the equivalent of the W515K mutation in the *cc-TpoR* fusion proteins (W508C for the murine TpoR sequence) led to active proteins for all orientations, when signalling was tested via JAK2. This included the inactive *cc-TpoR*-II, which became active upon W508K mutation (Supplementary Figure S3). These results are in agreement with the activating effect induced by deletion of the KWQFP motif.

Computational searches of the TpoR TM dimer interface

The *cc-TpoR* fusion proteins identify several orientations for the TM helices of the TpoR that induce strong receptor activity, as well as orientations that inhibit receptor activity. The choice of Put3 as a fusion partner was dictated by its ability to function as an extracellular domain, and importantly that it forms a left-handed (LHCC) dimeric coiled coil. Structural studies using solid-state NMR spectroscopy on membrane reconstituted peptides that include the TM and JM sequence of the TpoR up to the Box 1 region show that the sequence up to F510 is helical (Staerk *et al*, 2006; Supplementary Figure S1).

The helical wheel diagrams for dimers packing with an LHCC geometry have a spacing of 3.5 residues-per-turn. The heptad repeat is formed by two helical turns. The positions of amino acids relative to the dimer interface are denoted *a*–*g* with the *a* and *d* positions corresponding to those residues that are directly in the dimer interface. The diagrams for the seven Put3 coiled-coil dimers are shown in Figure 7A. In order to evaluate which of these orientations may correspond to low-energy dimer conformations, computational searches were performed using the program CHI (Adams *et al*, 1996; see Materials and methods). For the EpoR TM domain (Seubert *et al*, 2003), using this approach, we were able to identify two stable dimer conformations that corresponded well with active and inactive orientations imposed by the Put3 coiled coil. For the murine TpoR, computational searches were carried out on residues I485–L506 corresponding to the TM domain, and on residues I485–P511 corresponding to the TM domain with the KWQFP motif.

Figure 7B presents the results of a typical computational search on the TpoR TM domain (residues I485–L506) where possible dimer structures are generated by rotating each helix through rotation angles φ1 and φ2 from 0° to 360° with a sampling size of 45° and performing molecular dynamics simulations for each orientation. Favourable orientations are identified by structures that fall into a 'cluster', where a cluster is defined as a minimum of five structures with a root mean square (r.m.s.) deviation of 1 Å or less. An average molecular structure is calculated and the energy is minimized for each cluster. The clusters with the lowest energy are shown for each search.

There are three clusters of structures located along the diagonal of the search plot in Figure 7B. Since symmetric orientations of the TM helices (where $\varphi 1 = \varphi 2$) are induced by the Put3 constructs, these are the clusters of interest that represent the natural tendencies of the TM residues to assume symmetric dimers. The two lowest energy clusters found in the searches correspond to *cc-TpoR*-II and *cc-TpoR*-VI. *cc-TpoR*-II is inactive in both Ba/F3 and UT7 cells. *cc-TpoR*-VI is generated by a 50° counterclockwise rotation from *cc-TpoR*-II. *cc-TpoR*-VI is inactive in UT7 cells and is the least active of the dimers other than *cc-TpoR*-II in Ba/F3 cells. These results suggest that ligand-independent dimerization of the wild-type TpoR via TM domain interactions would result in an inactive receptor. The lowest energy active dimeric orientation that results in cell proliferation in both Ba/F3 and UT7 cells is *cc-TpoR*-V. For this structure, the TM dimer is stabilized by interhelical hydrogen bonding of S498. Higher energy dimer structures are found for the other *cc-TpoR* orientations in the computational searches, including *cc-TpoR*-I.

Computational searches of TM domain along with the five residues KWQFP insert typically yield clusters of *cc-TpoR*-II, *cc-TpoR*-IV and *cc-TpoR*-V. The average molecular structures of the clusters corresponding to the *cc-TpoR*-II and the *cc-TpoR*-V dimers are shown in Figure 7C and D, respectively. In the *cc-TpoR*-II dimer, K507 and W508 are oriented away from the dimer interface. The dimer structure is largely

©2011 European Molecular Biology Organization

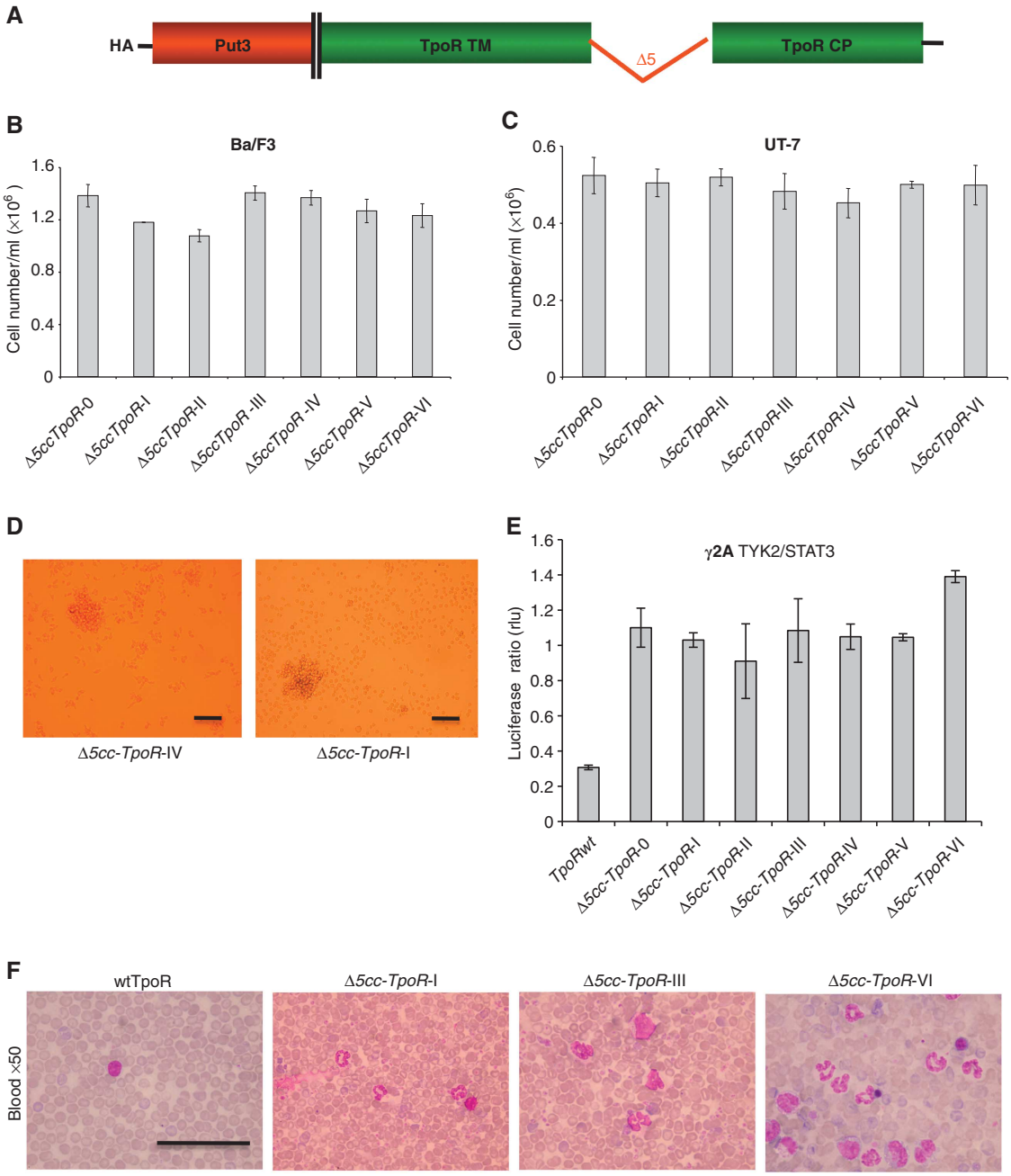


Figure 6 Deletion of the juxtamembrane KWQFP motif eliminates differences in biologic effects between the seven *cc-TpoR* dimers. (**A**) Design of the *cc-TpoR* and Δ*5cc-TpoR* fusion proteins. The coiled-coil segment of Put3 was fused to the TM and cytoplasmic (CP) domains of the wtTpoR or the Δ5TpoR. (**B**, **C**) Proliferation assays were performed with Ba/F3 (**A**) and UT7 (**B**) cells expressing the *cc-TpoR* fusion proteins where the KWQFP motif was deleted (Δ*5cc-TpoR*-0–VI). Cell numbers (averages of triplicates ± s.d.) were counted at day 6 (**A**, **B**). (**D**) Cell morphology of Ba/F3 cells expressing Δ*5cc-TpoR*-IV or Δ*5cc-TpoR*-I. No clusters were induced by Δ*5cc-TpoR*-IV, which lacks the KWQFP motif. For all pictures shown, Ba/F3 cells were plated in 24-well plates and pictures were taken at day 4. (**E**) γ2A cells were transfected with cDNAs coding for the Δ*5cc-TpoR* fusion proteins, and TYK2, STAT3 and STAT5/STAT3 pGRR5-luc luciferase reporter and pRL-TK. The results represent averages of triplicate values ± s.d. of one representative experiment out of at least three. (**F**) Peripheral blood and bone marrow were isolated from mice expressing the indicated Δ*5cc-TpoR* fusion proteins. Coverslides were stained using a May-Grunwald stain and analysed for qualitative or quantitative abnormalities in the blood. Bone marrow was examined by haematoxylin–eosin staining. The magnification was × 50. Scale bar, 50 μm.

stabilized by an interhelical hydrogen bond between the side chain amide of Q509 and the backbone carbonyl of Q509 on the opposing helix. van der Waals interactions between V488, L492, L498, A499, G502 and L506 also contribute to stabilizing this orientation of the TM helices.

One major question we asked was whether the *cc-TpoR*-I conformation (the fully active conformation) could be adopted spontaneously by the TpoR TM domain having the KWQFP JM insert. In our searches with the KWQFP insert, tryptophan at position 508 prevented dimer formation for

©2011 European Molecular Biology Organization

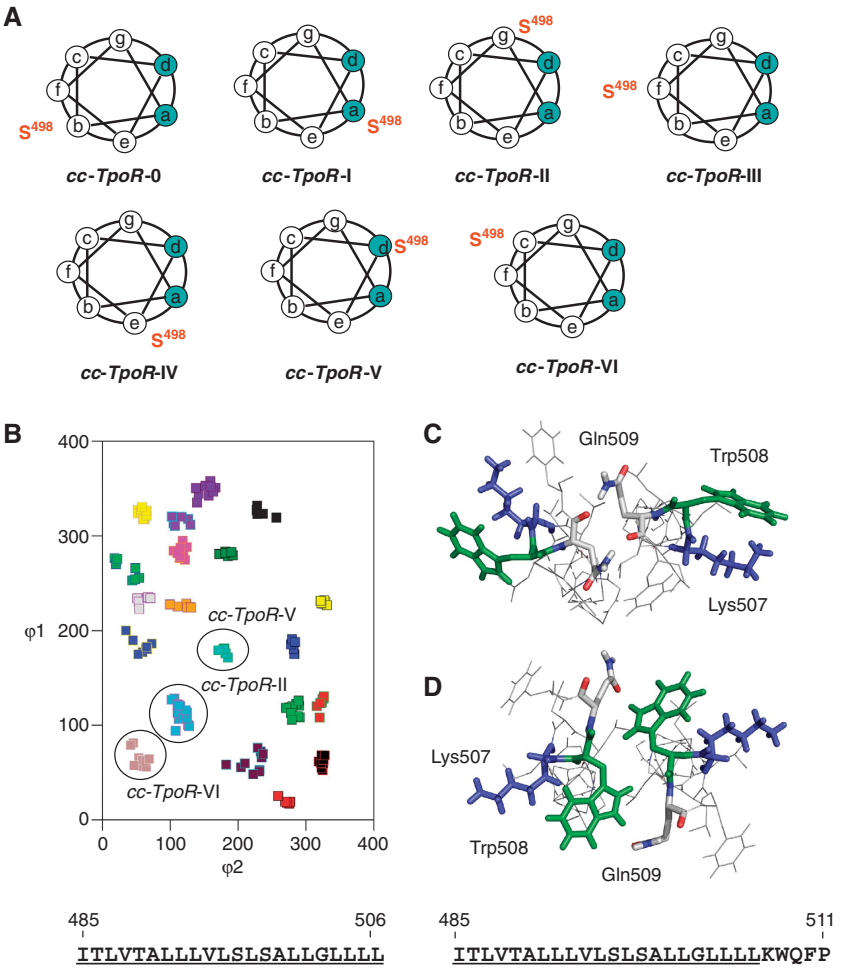


Figure 7 Computational searches of the TpoR transmembrane dimer. (**A**) Helical wheel predictions of the seven dimeric interfaces of the TM domain of the TpoR imposed by the Put3 coiled-coil fusion. Residue S498 of the TM domain is placed in the interface in *cc-TpoR*-I and *cc-TpoR*-V. (**B**) Computational search using the TpoR TM sequence from I485 to L506. The axial separation between the TM helices was set to be 10 Å. Computational searches with axial separations of 9.5–10.5 Å gave similar results. (**C**, **D**) Average molecular structures of the helix dimer corresponding to *cc-TpoR*-II and *cc-TpoR*-V. The helices have left-handed crossing angles and the dimer is viewed down the helix axis from the C-terminal end of the dimer. In *cc-TpoR*-II (**C**), the hydrogen bonding of Q509 stabilizes the helix dimer. The side chain of K509 contacts the aromatic ring of W508 characteristic of a stabilizing cation-π interaction. In *cc-TpoR*-V (**D**), the TM helices have rotated 50° counterclockwise, and hydrogen bonds form between indole NH of W508 and the amide side chain of Q509. The active *cc-TpoR*-I fusion protein adopts a conformation rotated by another 50° from *cc-TpoR*-V, where W508 residues would be predicted to clash.

orientations of TM helices corresponding to *cc-TpoR*-I. One can easily visualize the steric clash of W508 that would occur in *cc-TpoR*-I by rotating the helices in Figure 7D counterclockwise by 50°. A 50° rotation converts the *cc-TpoR*-V structure shown in Figure 7D into *cc-TpoR*-I, with both dimers having S498 in the interface (Figure 7A). This might explain why the KWQFP motif impairs activation of TpoR in the absence of Tpo (Staerk *et al*, 2006), and why adopting this structure needs either coiled-coil fusion or ligand binding to the extracellular domain of the receptor, both events requiring strong conformational changes.

Discussion

Our main observation is that the TpoR can signal from six out of seven possible symmetric dimeric orientations (Table I) leading to cell proliferation and different differentiation outputs, such as different abilities to promote megakaryocyte differentiation, cell-to-cell adhesion and myeloproliferative and myelodysplasia phenotypes *in vivo*. These results are relevant for the mechanisms by which TpoR can function at different stages of differentiation from HSCs to mature platelets in the course of physiologic haematopoiesis. Besides its ligand Tpo, the extracellular domain of TpoR was recently shown to bind a human homologue of a fungal nuclear migration protein (hNUDC) (Chen *et al*, 2010), a novel regulator of haematopoiesis (Miller *et al*, 1999; Gocke *et al*, 2000). It is, thus, conceivable that subtle differences in dimeric conformations are induced by different ligands or by the same ligand in different cell types. On the other hand, our data indicate that signalling by differently oriented TpoR dimers induces *in vivo* myeloproliferative and myelodysplastic disorders. While TpoR has already been discovered to be mutated in Essential Thrombocythemia and Myelofibrosis neoplasms (Pardanani *et al*, 2006; Pikman *et al*, 2006), it is not yet known whether it plays a role in myelodysplasia or mixed myelodysplasia/myeloproliferative disorders. TpoR is one of the three receptors that bind to JAK2 V617F, a mutant

©2011 European Molecular Biology Organization

associated with the vast majority of BCR-ABL-negative MPNs (Vainchenker *et al*, 2008). The basis for the observed orientation-dependent signalling of TpoR is represented by the recently identified JM KWQFP motif, which contains the W515, the very residue that maintains the unliganded TpoR inactive (Staerk *et al*, 2006) and which is mutated to Leu, Lys, Ala residues in MPNs (Pardanani *et al*, 2006; Pikman *et al*, 2006; Pecquet *et al*, 2010).

In addition to the W515 mutations in MPNs, several activating mutations in the TM and JM domains of TpoR signalling have been described in patients or cell lines from leukaemia patients (Onishi *et al*, 1996; Malinge *et al*, 2008). Substitutions of serine at position 498 (mouse) or 505 (human) by asparagine activate TpoR signalling in the absence of the ligand (Onishi *et al*, 1996; Ding *et al*, 2004). This residue is in the interface of *cc-TpoR*-I and *cc-TpoR*-V (Figure 7A); however, the phenotype induced by these two fusion proteins *in vivo* was remarkably different. *cc-TpoR*-I induced high numbers of platelets, without cytological features of myeloproliferation in the marrow, and *cc-TpoR*-V induced a picture of myelodysplasia, with small red blood cells and variable levels of thrombocytosis (Figure 5C). Again, subtle differences in dimeric conformation are translated into important differences in biologic effects.

We investigated the orientation requirements for TpoR-mediated signalling and identified several fusion proteins (*cc-TpoR*-0, -I, and -IV) that induced maximal proliferation of Ba/F3 and UT7 cells, two fusion proteins that supported weaker proliferation and one conformation that was inactive (*cc-TpoR*-II). This situation is different from that of the EpoR where essentially one dimeric orientation is permissive for signalling (Seubert *et al*, 2003). Self-association and packing density of TM sequences were shown to promote signalling by the active EpoR dimeric interface (Kubatzky *et al*, 2001, 2005; Becker *et al*, 2008). That EpoR activation is stringently controlled by dimeric orientation is also supported by the report that only rare anti-EpoR monoclonal antibodies are agonistic (Elliott *et al*, 1996). In contrast, tagged versions of TpoR can be activated by treatment with anti-tag antibodies (Millot *et al*, 2004). While antibodies and other small molecules may activate TpoR signalling in cell lines, our data suggest that careful studies would be necessary in order to establish exactly which biologic function of the TpoR would be induced by agonistic molecules.

Although six out of seven *cc-TpoR* fusion proteins induced cell proliferation, they induced unique effects depending on their dimeric conformation (Figures 2 and 5; Supplementary Figure S4; Table I). *cc-TpoR*-IV induced strong cell-to-cell adhesion (clusters), but was not permissive to induce commitment to the megakaryocyte lineage, as measured by CD41 expression in UT7 cells (Figure 2E). *cc-TpoR*-IV-induced clustering is reminiscent of the effects of high levels of Tpo ligand in TpoR expressing Ba/F3 cells (Figure 2D) or in UT-7-TpoR cells. High local levels of Tpo might exist in niches, such as the osteoblastic niche, where Tpo was reported to maintain quiescence of HSCs (Qian *et al*, 2007; Yoshihara *et al*, 2007). On the other hand, the effect of Tpo was initially described to induce HSC renewal (Alexander *et al*, 1996b) and early haematopoiesis (Solar *et al*, 1998), or to amplify the immediate progenies of HSCs (Abkowitz and Chen, 2007). More recently, we described a senescence-inducing effect of Tpo in late-stage post-mitotic megakaryocytes (Besancenot *et al*, 2010). Such distinct and apparently opposed actions of TpoR might be the result of different dimeric orientations adopted by the receptor in response to various ligand levels, ligand presentation or cell type. Signalling by TpoR was previously shown to require phosphorylation of Y626, which couples the receptor to several signalling pathways, especially to the STAT5/3 and MAP-kinase pathways (Gurney *et al*, 1995; Alexander *et al*, 1996a; Drachman and Kaushansky, 1997; Pecquet *et al*, 2010). The same TpoR cytosolic Y626 residue is absolutely required for induction of myeloproliferative disorder by the TpoR W515A mutant via excessive activation of the STAT3 and MAP-kinase pathways. The strength of signalling by *cc-TpoR* fusion proteins also appears to correlate with levels of phosphorylation of Y626 (Figure 4A). The *in vivo* phenotype induced by *cc-TpoRs* is milder than that of TpoR W515 mutants (Pecquet *et al*, 2010). It will be of interest to determine the precise adaptors associated with phosphorylated Y626, as a function of dimeric orientation (*cc-TpoRs*) or in the case of TpoR W515 mutants.

Transplantation assays in mice with bone marrow cells expressing the active *cc-TpoR* fusion proteins confirmed our hypothesis that different dimeric orientations induce effects that resemble the physiological function of TpoR (*cc-TpoR*-I), or that induce different degrees of myeloproliferative and myelodysplasia disorders (*cc-TpoR*-III, *cc-TpoR*-VI and *cc-TpoR*-V; Figure 5). All seven fusion proteins were equally able to support cell proliferation but lost orientation-specific signalling upon deletion of the KWQFP motif (Δ*5cc-TpoR* fusion proteins). For example, Δ*5cc-TpoR*-II was active after deletion of the KWQFP motif, while *cc-TpoR*-II was not. In addition, Δ*5cc-TpoR*-IV did not induce cell-to-cell adhesion.

These data support our hypothesis that the TpoR could indeed signal through various orientations. One possible explanation for TpoR signalling from multiple dimeric interfaces is the utilization of two JAKs for signal transmission: JAK2 and TYK2. Expression of TYK2 alone, in the absence of JAK2, allows only *cc-TpoR*-III and *cc-TpoR*-VI to activate STAT5 and STAT3 signalling, while expression of JAK2 promotes STAT signalling via multiple interfaces, represented by *cc-TpoR*-0, -I, -III, and -IV (Figure 3). It needs to be further investigated whether the TpoR is signalling *in vivo* via heteromeric JAK2–TYK2 complexes. Of interest, *cc-TpoR*-III and *cc-TpoR*-VI have some common signalling and biologic features: (i) activation of TYK2 signalling in addition to JAK2, (ii) induction of granulocytosis and of different degrees of erythroid and megakaryocytic dysplasia, (iii) lower levels of MAP-kinase activation. A tight control and limitation of the levels of MAP-kinase activation were described to be necessary for normal granulocyte differentiation and maintenance of granulocytic progenitors (Baumann *et al*, 2005; Geest *et al*, 2009).

Coiled coils are symmetric dimers and the models that emerge after the use of coiled-coil fusion proteins have a bias towards symmetric left-handed parallel dimers of α-helices, while membrane proteins may also adopt asymmetric geometries. Further structural studies are required to establish whether the TpoR dimer is symmetric or asymmetric. Cysteine crosslinking (Figure 1C) and alanine insertion mutagenesis (Figure 3C and D) confirmed that the coiled-coil fusion to successive TM residues at the N-terminus of the TM domain enables to dial-in the predicted dimeric

 ©2011 European Molecular Biology Organization

conformations at the outset of the JM cytosolic domain. To gain insight into the dimerization mechanism(s) of the TpoR, we performed computational searches of the TM and JM sequences. In this approach, stable dimer conformations are observed as clusters of structures. A comparison of the computational searches in Figure 7B–D shows that the orientation of the TM helices in *cc-TpoR*-II generates a stable structure. This construct has the only orientation that results in an inactive TpoR dimer. Thus, the natural tendency of the TpoR TM dimer is to adopt the inactive conformation. In this inactive structure, K507 and W508 are oriented as far as possible away from the dimer interface. Rotation of the TM helices in either direction by 50° (leading to *cc-TpoR*-V or *cc-TpoR*-VI) results in partial activity. Functional data indicate that *cc-TpoR*-I represents the closest conformation to the physiologically activated TpoR by Tpo. Although dimeric clusters representing *cc-TpoR*-I are identified by our searches, they are among the higher energy dimer structures (less stable). Thus, this dimeric orientation is unlikely to be adopted spontaneously. Interestingly, in the computational search that includes the KWQFP motif, we could not identify a cluster corresponding to *cc-TpoR*-I. Therefore, it is very likely that the KWQFP motif actively prevents the formation of a dimer corresponding to the *cc-TpoR*-I, and is doing so via a clash between interfacially oriented W508 residues (W515 in the human TpoR). Taken together, functional and computational data indicate that the W508 of the KWQFP motif is crucial for preventing TpoR activation and is required for orientation-specific signalling. Noteworthy, the TM domain of the human TpoR, in the absence of the JM RWQFP motif, was found by bacterial TOXCAT and cysteine cross-linking assays to promote dimerization in three rotationally related orientations, possibly corresponding to inactive, active and partially active states of the receptor (Matthews *et al*, 2011). The proposed interfaces correspond to our coiled coil-induced inactive *cc-TpoR*-II and active orientations.

In conclusion, our data show that several dimeric conformations of the TpoR can support cell proliferation and that specific dimeric orientations imposed by the KWQFP JM motif differ in their signalling output and biologic effects. While one dimeric orientation having S498 in the interface emerges as the best model for the physiologically activated TpoR, and a different one corresponds to the inactive dimer, other orientations induce different degrees of myeloproliferative and myelodysplastic disorders. The system of differently dimerized TpoRs may offer new insights with respect to apportioning a particular signalling pathway to a biologic effect, such as megakaryocytic differentiation or the establishment of myeloid disorders.

Materials and methods

cDNA constructs

The wtTpoR and mutants thereof (TpoR mutants where the KWQFP insert was deleted (Δ5) or mutated (W508K), the *cc-TpoR* fusion proteins (*cc-TpoR*-0-VI) and the *cc-TpoR* fusion proteins where the KWQFP insert was deleted (Δ*5cc-TpoR*-0-VI)) were subcloned in pMX-IRES-GFP and MSCV-IRES-GFP vectors, as described previously (Staerk *et al*, 2006). All TpoRs and *cc-TpoRs* contain an HA tag at the amino-terminus, after the cleavage site of the signal peptidase (Huang *et al*, 2001). For the crosslinking experiment, the seven cysteine-free coiled-coil receptor backbones were created by introducing a stop codon after amino acid 553, and Leu505 was mutated into Cys. To alter the helical register of the seven murine *cc-TpoR* fusion proteins and as a proof of principle, alanines were inserted at the end of the TM region. We also mutated Trp508 (mouse equivalent of Trp515 in the human TpoR) into Lys, introducing in the seven *cc-TpoRs*, the pathological W515K mutation found in MPN patients. All constructs were verified by sequencing.

Crosslinking studies

Six-well plates of human BOSC cells were transfected (Lipofectamine™ 2000, Invitrogen, Carlsbad, CA) with cDNAs encoding the seven cysteine *cc-TpoR* mutants. Cells were harvested 24 h after transfection and checked for GFP expression prior to crosslinking experiments.

Cells were washed with phosphate-buffered saline and resuspended in 1 ml of phosphate-buffered saline containing 1 mM $MgCl_2$ and 0.1 mM $CaCl_2$. Crosslinking was then performed for 10 min at room temperature with a final concentration of the crosslinker *N*,*N*′-1,2-phenylenedimaleimide (o-PDM) dissolved in DMSO of 100 μM. Cells were lysed with 1 × NP-40 lysis buffer containing 2% of β-mercaptoethanol in order to quench excess crosslinker (Kubatzky *et al*, 2005). Lysate samples were analysed by SDS–PAGE using a 4–12% gradient NuPage® NOVEX Bis-Tris Gel (Invitrogen) and then transferred onto nitrocellulose membrane. After blocking with 1% milk PBS, membranes were incubated with a 1:500 diluted mouse anti-HA antibody (HA.11, Covance, Berkeley, CA) followed by a 1:2500 diluted peroxidase-conjugated anti-mouse antibody (GE Healthcare UK Ltd, Buckingham, UK). Detection was then performed using enhanced chemiluminescence.

Generation of cell lines

Ba/F3 and UT7 cell lines were transduced with *cc-TpoR* constructs using ecotropic (Liu *et al*, 2000) or amphotropic viral supernatant, respectively (Chagraoui *et al*, 2002; Staerk *et al*, 2006). Cell populations were sorted for equal GFP expression.

Assay for Tpo-independent growth

Transduced and sorted Ba/F3 cells were expanded in IL-3, washed and subsequently placed in RPMI 10% fetal bovine serum without cytokines or Tpo as indicated. UT7 cells expressing the *cc-TpoR* constructs were washed with α-MEM medium (Invitrogen) to remove GM-CSF and placed in cytokine-free α-MEM medium containing 10% FBS or in α-MEM medium containing 10% FBS and Tpo as specified. Cell numbers were counted at the indicated time points.

Immunoprecipitation and immunoblots

Ba/F3 cells were washed with PBS and starved for 2 h in RMPI with 0.1% BSA. Cells were stimulated with 50 ng/ml rmTpo (R&D) or PBS and lysed in NP-40 buffer as described previously (Staerk *et al*, 2006; Pecquet *et al*, 2010). Immunoprecipitation was performed with anti-HA antibodies (Roche Diagnostics, Indianapolis, IN), incubated with protein G agarose (Invitrogen) overnight. Samples were analysed by western blot using anti-pY626 TpoR (Cell Signaling Technology, Danvers, MA) and anti-HA.

Activation of downstream signalling pathways was analysed using anti-p-STAT1, anti-STAT1, anti-p-STAT3, anti-STAT3, or anti-p-Erk1,2, anti-Erk1,2 (Cell Signaling Technology), anti-β-actin (Sigma, St Louis, MO) and anti-HA antibodies (Roche Diagnostics), as described previously (Pecquet *et al*, 2010).

Receptor-recycling assay and cell surface biotinylation

In all, 3×10^7 Ba/F3 cells expressing the indicated *cc-TpoRs* were incubated with 10 mg/ml EZ link sulfo-NHS-Biotin (Thermo Scientific, Rockford, IL) at 4°C for 2 h. Cells were washed in 100 mM glycine-PBS solution to remove excess biotinylation reagent. After biotinylation, cells were maintained in culture for 30 min and then treated or not with 10 μM JAK inhibitor I (Calbiochem, La Jolla, CA) for additional 30 min. For cell surface immunoprecipitation, cells were incubated with anti-HA antibodies (Roche Diagnostics) for 1 h at 4°C. Cells were then lysed in 1% NP-40 buffer as previously described and lysates were incubated overnight with protein G agarose at 4°C. The beads were washed in lysis buffer and subjected to western blotting by using an anti-biotin/HRP (New England Biolabs, Beverly, MA) and anti-HA antibodies (Roche Diagnostics).

©2011 European Molecular Biology Organization

Dual luciferase assays

Activation of STAT5 and STAT3 was analysed by assaying for luciferase production in cells transfected with pLHRE-Luc (Sotiropoulos *et al*, 1995; Storz *et al*, 1999), pGL3bPpr2 (Eyckerman *et al*, 1999) or pGRR5 constructs (Dumoutier *et al*, 2000). To assess MAPK activation we used the pSRE-luc construct (Treisman, 1995). The PI-3-kinase/Akt pathway negatively affects FoxO activity. PI-3-kinase/Akt activation was, therefore, indirectly measured using a $6\times$ DBE-Luc reporter, which is activated by FoxO family members (Kuiperij *et al*, 2005). The pRL-TK vector (Promega, Madison, WI) containing the renilla luciferase gene under control of the TK promoter was used as internal control. Ba/F3 cells expressing TpoR proteins were starved for 3 h in RPMI/1 mg/ml BSA, Luciferase assays were performed as described (Seubert *et al*, 2003). JAK2-deficient γ2A fibrosarcoma cells (Kohlhuber *et al*, 1997) were transiently transfected with TpoR proteins and signalling proteins as described (Royer *et al*, 2005). Luminescence was recorded in cell lysates 24 h after using a Perkin-Elmer Victor X Light analyzer.

Surface expression of HA-tagged TpoR and HA-tagged cc-TpoR fusion proteins

Surface expression of HA-TpoR and HA-tagged *cc-TpoR* fusion proteins was measured by flow cytometry as described (Huang *et al*, 2001; Pecquet *et al*, 2010).

Bone marrow reconstitutions

Bone marrow was isolated from mice 72 h after 5-fluorouracil injection (Chagraoui *et al*, 2002; Pecquet *et al*, 2010). In all, 1×10^6 bone marrow cells transduced with *cc-TpoRs* or TpoR were injected into lethally irradiated, 6–8-week-old C57Bl6 mice. Reconstitution was assessed by GFP expression in peripheral blood cells using flow cytometry 3 weeks after transplantation. Peripheral blood cell numbers were counted using Melet Schloessing MS9-3. Histopathology analysis and blood smears were performed as described (Pecquet *et al*, 2010).

Computational searches

Low-energy dimer structures of the TM sequence of the TpoR were identified computationally using the program CHI (Adams *et al*, 1996). The program generates canonical helices from the TpoR sequence and constructs a matrix of helix dimers in which each helix is rotated through all possible orientations between 0° and 360° with a sampling size of 45°. For each starting structure, MD simulations with simulated annealing and energy minimization were performed within CHI using the program X-PLOR. The X-PLOR force field uses the TOPH19 and PARAM19 parameters sets with all polar hydrogens included. A non-bonded cutoff of 13 Å is set with a switching function between 10 and 12 Å for the van der Waals and electrostatic terms. Distance constraints are applied between the backbone O_i and N_{i+4} atoms to maintain an α-helical conformation and between the helix directors to maintain a fixed axial separation. Different computational searches were performed for axial distances of 9.5, 10 and 10.5 Å, and for helices starting with left- and right-handed crossing angles. Both the helix rotation and the crossing angles are allowed to vary during the simulations, and the results are plotted as a function of the angles φ1 and φ2, corresponding to rotational orientation of each helix in the dimer. The dimer structures migrate from their initial geometry and cluster into low-energy conformations. All calculations were performed *in vacuo*, approximating the low dielectric environment of the membrane. Separate computational searches were performed for TpoR sequence without (I485–L506) and without (I485–P511) the KWQFP insert.

Supplementary data

Supplementary data are available at *The EMBO Journal* Online (http://www.embojournal.org).

Acknowledgements

We thank Dr Jean-Marie Scheiff for histopathology diagnosis, Céline Mouton for expert technical assistance, André Tonon for expert flow cytometry expertise, Yan Yin and Julie Klein for technical and graphics assistance. This work was supported by grants from *La Ligue Nationale contre le Cancer* (*équipe labellisée* 2010, WV), by NIH grant (GM-46732) to SOS, the *Fondation contre le Cancer*, the de Hovre Foundation, the Salus Sanguinis Foundation, the *Action de Recherche Concertée* MEXP31C1 of the *Université catholique de Louvain*, the PAI Program BCHM61B5, Belgium and the Atlantic Philanthropies, New York, and the FNRS (*Mandat d'impulsion*), Belgium (to SNC). JS was supported by fellowships from Daimler-Benz, Exchange Marie Curie, Télévie and Salus Sanguinis Foundations. J-PD is supported by an FRIA PhD fellowship of the FRS-FNRS Belgium. CP was supported by a postdoctoral fellowship of the de Duve Institute, by the PAI Program BCHM61B5 and by the FRS-FNRS. WV is supported by an interface contract between INSERM and IGR. SNC is a Research Associate of the FNRS.

Author contributions: JS, J-PD and SNC planned and performed experiments, interpreted data and wrote paper; CP, EL and IB performed experiments and interpreted data; SOS and WV planned experiments and interpreted data; MI and SOS performed molecular dynamics simulations; HAP interpreted data.

Conflict of interest

The authors declare that they have no conflict of interest.

References

Abkowitz JL, Chen J (2007) Studies of c-Mpl function distinguish the replication of hematopoietic stem cells from the expansion of differentiating clones. *Blood* **109:** 5186–5190

Adams PD, Engelman DM, Brunger AT (1996) Improved prediction for the structure of the dimeric transmembrane domain of glycophorin A obtained through global searching. *Proteins* **26:** 257–261

Alexander WS, Maurer AB, Novak U, Harrison-Smith M (1996a) Tyrosine-599 of the c-Mpl receptor is required for Shc phosphorylation and the induction of cellular differentiation. *EMBO J* **15:** 6531–6540

Alexander WS, Metcalf D, Dunn AR (1995) Point mutations within a dimer interface homology domain of c-Mpl induce constitutive receptor activity and tumorigenicity. *EMBO J* **14:** 5569–5578

Alexander WS, Roberts AW, Nicola NA, Li R, Metcalf D (1996b) Deficiencies in progenitor cells of multiple hematopoietic lineages and defective megakaryocytopoiesis in mice lacking the thrombopoietic receptor c-Mpl. *Blood* **87:** 2162–2170

Baumann M, Frye T, Naqvi T, Gomez-Cambronero J (2005) Normal neutrophil maturation is associated with selective loss of MAP kinase activation by G-CSF. *Leuk Res* **29:** 73–78

Becker V, Sengupta D, Ketteler R, Ullmann GM, Smith JC, Klingmuller U (2008) Packing density of the erythropoietin receptor transmembrane domain correlates with amplification of biological responses. *Biochemistry* **47:** 11771–11782

Besancenot R, Chaligne R, Tonetti C, Pasquier F, Marty C, Lecluse Y, Vainchenker W, Constantinescu SN, Giraudier S (2010) A senescence-like cell-cycle arrest occurs during megakaryocytic maturation: implications for physiological and pathological megakaryocytic proliferation. *PLoS Biol* **8:** e1000476

Brown RJ, Adams JJ, Pelekanos RA, Wan Y, McKinstry WJ, Palethorpe K, Seeber RM, Monks TA, Eidne KA, Parker MW, Waters MJ (2005) Model for growth hormone receptor activation based on subunit rotation within a receptor dimer. *Nat Struct Mol Biol* **12:** 814–821

Chagraoui H, Komura E, Tulliez M, Giraudier S, Vainchenker W, Wendling F (2002) Prominent role of TGF-beta 1 in thrombopoietin-induced myelofibrosis in mice. *Blood* **100:** 3495–3503

Chen WM, Yu B, Zhang Q, Xu P (2010) Identification of the residues in the extracellular domain of thrombopoietin receptor involved in the binding of thrombopoietin and a nuclear distribution protein (human NUDC). *J Biol Chem* **285:** 26697–26709

Constantinescu SN, Huang LJ, Nam H, Lodish HF (2001) The erythropoietin receptor cytosolic juxtamembrane domain con-

 ©2011 European Molecular Biology Organization

tains an essential, precisely oriented, hydrophobic motif. *Mol Cell* **7:** 377–385

de Sauvage FJ, Hass PE, Spencer SD, Malloy BE, Gurney AL, Spencer SA, Darbonne WC, Henzel WJ, Wong SC, Kuang WJ, Oles KJ, Hultgren B, Solberg Jr LA, Goeddel DV, Eaton DL (1994) Stimulation of megakaryocytopoiesis and thrombopoiesis by the c-Mpl ligand. *Nature* **369:** 533–538

Ding J, Komatsu H, Iida S, Yano H, Kusumoto S, Inagaki A, Mori F, Ri M, Ito A, Wakita A, Ishida T, Nitta M, Ueda R (2009) The Asn505 mutation of the c-MPL gene, which causes familial essential thrombocythemia, induces autonomous homodimerization of the c-Mpl protein due to strong amino acid polarity. *Blood* **114:** 3325–3328

Ding J, Komatsu H, Wakita A, Kato-Uranishi M, Ito M, Satoh A, Tsuboi K, Nitta M, Miyazaki H, Iida S, Ueda R (2004) Familial essential thrombocythemia associated with a dominant-positive activating mutation of the c-MPL gene, which encodes for the receptor for thrombopoietin. *Blood* **103:** 4198–4200

Drachman JG, Griffin JD, Kaushansky K (1995) The c-Mpl ligand (thrombopoietin) stimulates tyrosine phosphorylation of Jak2, Shc, and c-Mpl. *J Biol Chem* **270:** 4979–4982

Drachman JG, Kaushansky K (1997) Dissecting the thrombopoietin receptor: functional elements of the Mpl cytoplasmic domain. *Proc Natl Acad Sci USA* **94:** 2350–2355

Drachman JG, Millett KM, Kaushansky K (1999) Thrombopoietin signal transduction requires functional JAK2, not TYK2. *J Biol Chem* **274:** 13480–13484

Dumoutier L, Van Roost E, Colau D, Renauld JC (2000) Human interleukin-10-related T cell-derived inducible factor: molecular cloning and functional characterization as an hepatocyte-stimulating factor. *Proc Natl Acad Sci USA* **97:** 10144–10149

Elliott S, Lorenzini T, Yanagihara D, Chang D, Elliott G (1996) Activation of the erythropoietin (EPO) receptor by bivalent anti-EPO receptor antibodies. *J Biol Chem* **271:** 24691–24697

Eyckerman S, Waelput W, Verhee A, Broekaert D, Vandekerckhove J, Tavernier J (1999) Analysis of Tyr to Phe and fa/fa leptin receptor mutations in the PC12 cell line. *Eur Cytokine Netw* **10:** 549–556

Geest CR, Buitenhuis M, Groot Koerkamp MJ, Holstege FC, Vellenga E, Coffer PJ (2009) Tight control of MEK-ERK activation is essential in regulating proliferation, survival, and cytokine production of CD34+-derived neutrophil progenitors. *Blood* **114:** 3402–3412

Gocke CD, Reaman GH, Stine C, Zhang MY, Osmani SA, Miller BA (2000) The nuclear migration gene NudC and human hematopoiesis. *Leuk Lymphoma* **39:** 447–454

Gurney AL, Wong SC, Henzel WJ, de Sauvage FJ (1995) Distinct regions of c-Mpl cytoplasmic domain are coupled to the JAK-STAT signal transduction pathway and Shc phosphorylation. *Proc Natl Acad Sci USA* **92:** 5292–5296

Huang LJ, Constantinescu SN, Lodish HF (2001) The N-terminal domain of Janus kinase 2 is required for Golgi processing and cell surface expression of erythropoietin receptor. *Mol Cell* **8:** 1327–1338

Kaushansky K (1997) Thrombopoietin: more than a lineage-specific megakaryocyte growth factor. *Stem Cells* **15** (Suppl 1)**:** 97–102; discussion 102–103

Kohlhuber F, Rogers NC, Watling D, Feng J, Guschin D, Briscoe J, Witthuhn BA, Kotenko SV, Pestka S, Stark GR, Ihle JN, Kerr IM (1997) A JAK1/JAK2 chimera can sustain alpha and gamma interferon responses. *Mol Cell Biol* **17:** 695–706

Komatsu N, Nakauchi H, Miwa A, Ishihara T, Eguchi M, Moroi M, Okada M, Sato Y, Wada H, Yawata Y, Suda T, Miura Y (1991) Establishment and characterization of a human leukemic cell line with megakaryocytic features: dependency on granulocyte-macrophage colony-stimulating factor, interleukin 3, or erythropoietin for growth and survival. *Cancer Res* **51:** 341–348

Kubatzky KF, Liu W, Goldgraben K, Simmerling C, Smith SO, Constantinescu SN (2005) Structural requirements of the extracellular to transmembrane domain junction for erythropoietin receptor function. *J Biol Chem* **280:** 14844–14854

Kubatzky KF, Ruan W, Gurezka R, Cohen J, Ketteler R, Watowich SS, Neumann D, Langosch D, Klingmuller U (2001) Self assembly of the transmembrane domain promotes signal transduction through the erythropoietin receptor. *Curr Biol* **11:** 110–115

Kuiperij HB, van der Horst A, Raaijmakers J, Weijzen S, Medema RH, Bos JL, Burgering BM, Zwartkruis FJ (2005) Activation of FoxO transcription factors contributes to the antiproliferative effect of cAMP. *Oncogene* **24:** 2087–2095

Liu X, Constantinescu SN, Sun Y, Bogan JS, Hirsch D, Weinberg RA, Lodish HF (2000) Generation of mammalian cells stably expressing multiple genes at predetermined levels. *Anal Biochem* **280:** 20–28

Lupardus PJ, Skiniotis G, Rice AJ, Thomas C, Fischer S, Walz T, Garcia KC (2011) Structural snapshots of full-length Jak1, a transmembrane gp130/IL-6/IL-6Ralpha cytokine receptor complex, and the receptor-Jak1 holocomplex. *Structure* **19:** 45–55

Malinge S, Ragu C, Della-Valle V, Pisani D, Constantinescu SN, Perez C, Villeval JL, Reinhardt D, Landman-Parker J, Michaux L, Dastugue N, Baruchel A, Vainchenker W, Bourquin JP, Penard-Lacronique V, Bernard OA (2008) Activating mutations in human acute megakaryoblastic leukemia. *Blood* **112:** 4220–4226

Matthews EE, Thévenin D, Rogers JM, Gotow L, Lira PD, Reiter LA, Brissette WH, Engelman DM (2011) Thrombopoietin receptor activation: transmembrane helix dimerization, rotation and allosteric modulation. *FASEB J* **25:** 2234–2244

Mattoon D, Gupta K, Doyon J, Loll PJ, DiMaio D (2001) Identification of the transmembrane dimer interface of the bovine papillomavirus E5 protein. *Oncogene* **20:** 3824–3834

Miller BA, Zhang MY, Gocke CD, De Souza C, Osmani AH, Lynch C, Davies J, Bell L, Osmani SA (1999) A homolog of the fungal nuclear migration gene nudC is involved in normal and malignant human hematopoiesis. *Exp Hematol* **27:** 742–750

Millot GA, Vainchenker W, Dumenil D, Svinarchuk F (2004) Differential signalling of NH2-terminal flag-labelled thrombopoietin receptor activated by TPO or anti-FLAG antibodies. *Cell Signal* **16:** 355–363

Miyakawa Y, Oda A, Druker BJ, Kato T, Miyazaki H, Handa M, Ikeda Y (1995) Recombinant thrombopoietin induces rapid protein tyrosine phosphorylation of Janus kinase 2 and Shc in human blood platelets. *Blood* **86:** 23–27

Miyakawa Y, Oda A, Druker BJ, Miyazaki H, Handa M, Ohashi H, Ikeda Y (1996) Thrombopoietin induces tyrosine phosphorylation of Stat3 and Stat5 in human blood platelets. *Blood* **87:** 439–446

Miyakawa Y, Rojnuckarin P, Habib T, Kaushansky K (2001) Thrombopoietin induces phosphoinositol 3-kinase activation through SHP2, Gab, and insulin receptor substrate proteins in BAF3 cells and primary murine megakaryocytes. *J Biol Chem* **276:** 2494–2502

Oda A, Miyakawa Y, Druker BJ, Ishida A, Ozaki K, Ohashi H, Wakui M, Handa M, Watanabe K, Okamoto S, Ikeda Y (1996) Crkl is constitutively tyrosine phosphorylated in platelets from chronic myelogenous leukemia patients and inducibly phosphorylated in normal platelets stimulated by thrombopoietin. *Blood* **88:** 4304–4313

Onishi M, Mui AL, Morikawa Y, Cho L, Kinoshita S, Nolan GP, Gorman DM, Miyajima A, Kitamura T (1996) Identification of an oncogenic form of the thrombopoietin receptor MPL using retrovirus-mediated gene transfer. *Blood* **88:** 1399–1406

Pardanani AD, Levine RL, Lasho T, Pikman Y, Mesa RA, Wadleigh M, Steensma DP, Elliott MA, Wolanskyj AP, Hogan WJ, McClure RF, Litzow MR, Gilliland DG, Tefferi A (2006) MPL515 mutations in myeloproliferative and other myeloid disorders: a study of 1182 patients. *Blood* **108:** 3472–3476

Pecquet C, Staerk J, Chaligne R, Goss V, Lee KA, Zhang X, Rush J, Van Hees J, Poirel HA, Scheiff JM, Vainchenker W, Giraudier S, Polakiewicz RD, Constantinescu SN (2010) Induction of myeloproliferative disorder and myelofibrosis by thrombopoietin receptor W515 mutants is mediated by cytosolic tyrosine 112 of the receptor. *Blood* **115:** 1037–1048

Pikman Y, Lee BH, Mercher T, McDowell E, Ebert BL, Gozo M, Cuker A, Wernig G, Moore S, Galinsky I, Deangelo DJ, Clark JJ, Lee SJ, Golub TR, Wadleigh M, Gilliland DG, Levine RL (2006) MPLW515L is a novel somatic activating mutation in myelofibrosis with myeloid metaplasia. *PLoS Med* **3:** e270

Porteu F, Rouyez MC, Cocault L, Benit L, Charon M, Picard F, Gisselbrecht S, Souyri M, Dusanter-Fourt I (1996) Functional regions of the mouse thrombopoietin receptor cytoplasmic domain: evidence for a critical region which is involved in differentiation and can be complemented by erythropoietin. *Mol Cell Biol* **16:** 2473–2482

©2011 European Molecular Biology Organization

Qian H, Buza-Vidas N, Hyland CD, Jensen CT, Antonchuk J, Mansson R, Thoren LA, Ekblom M, Alexander WS, Jacobsen SE (2007) Critical role of thrombopoietin in maintaining adult quiescent hematopoietic stem cells. *Cell Stem Cell* **1:** 671–684

Royer Y, Staerk J, Costuleanu M, Courtoy PJ, Constantinescu SN (2005) Janus kinases affect thrombopoietin receptor cell surface localization and stability. *J Biol Chem* **280:** 27251–27261

Seubert N, Royer Y, Staerk J, Kubatzky KF, Moucadel V, Krishnakumar S, Smith SO, Constantinescu SN (2003) Active and inactive orientations of the transmembrane and cytosolic domains of the erythropoietin receptor dimer. *Mol Cell* **12:** 1239–1250

Skiniotis G, Lupardus PJ, Martick M, Walz T, Garcia KC (2008) Structural organization of a full-length gp130/LIF-R cytokine receptor transmembrane complex. *Mol Cell* **31:** 737–748

Solar GP, Kerr WG, Zeigler FC, Hess D, Donahue C, de Sauvage FJ, Eaton DL (1998) Role of c-mpl in early hematopoiesis. *Blood* **92:** 4–10

Sotiropoulos A, Moutoussamy S, Binart N, Kelly PA, Finidori J (1995) The membrane proximal region of the cytoplasmic domain of the growth hormone receptor is involved in the activation of Stat 3. *FEBS Lett* **369:** 169–172

Souyri M, Vigon I, Penciolelli JF, Heard JM, Tambourin P, Wendling F (1990) A putative truncated cytokine receptor gene transduced by the myeloproliferative leukemia virus immortalizes hematopoietic progenitors. *Cell* **63:** 1137–1147

Staerk J, Lacout C, Smith SO, Vainchenker W, Constantinescu SN (2006) An amphipathic motif at the transmembrane-cytoplasmic junction prevents autonomous activation of the thrombopoietin receptor. *Blood* **107:** 1864–1871

Storz P, Doppler H, Horn-Muller J, Groner B, Pfizenmaier K, Muller G (1999) A cellular reporter assay to monitor insulin receptor kinase activity based on STAT 5-dependent luciferase gene expression. *Anal Biochem* **276:** 97–104

Swaminathan K, Flynn P, Reece RJ, Marmorstein R (1997) Crystal structure of a PUT3-DNA complex reveals a novel mechanism for DNA recognition by a protein containing a Zn2Cys6 binuclear cluster. *Nat Struct Biol* **4:** 751–759

Thompson JE, Cubbon RM, Cummings RT, Wicker LS, Frankshun R, Cunningham BR, Cameron PM, Meinke PT, Liverton N, Weng Y, DeMartino JA (2002) Photochemical preparation of a pyridone containing tetracycle: a Jak protein kinase inhibitor. *Bioorg Med Chem Lett* **12:** 1219–1223

Treisman R (1995) Journey to the surface of the cell: Fos regulation and the SRE. *EMBO J* **14:** 4905–4913

Vainchenker W, Dusa A, Constantinescu SN (2008) JAKs in pathology: role of Janus kinases in hematopoietic malignancies and immunodeficiencies. *Semin Cell Dev Biol* **19:** 385–393

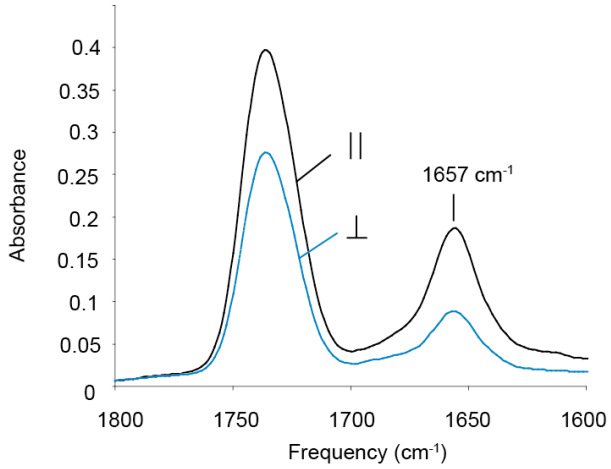
Walters KJ, Dayie KT, Reece RJ, Ptashne M, Wagner G (1997) Structure and mobility of the PUT3 dimer. *Nat Struct Biol* **4:** 744–750

Watowich SS, Wu H, Socolovsky M, Klingmuller U, Constantinescu SN, Lodish HF (1996) Cytokine receptor signal transduction and the control of hematopoietic cell development. *Annu Rev Cell Dev Biol* **12:** 91–128

Yoshihara H, Arai F, Hosokawa K, Hagiwara T, Takubo K, Nakamura Y, Gomei Y, Iwasaki H, Matsuoka S, Miyamoto K, Miyazaki H, Takahashi T, Suda T (2007) Thrombopoietin/MPL signaling regulates hematopoietic stem cell quiescence and interaction with the osteoblastic niche. *Cell Stem Cell* **1:** 685–697

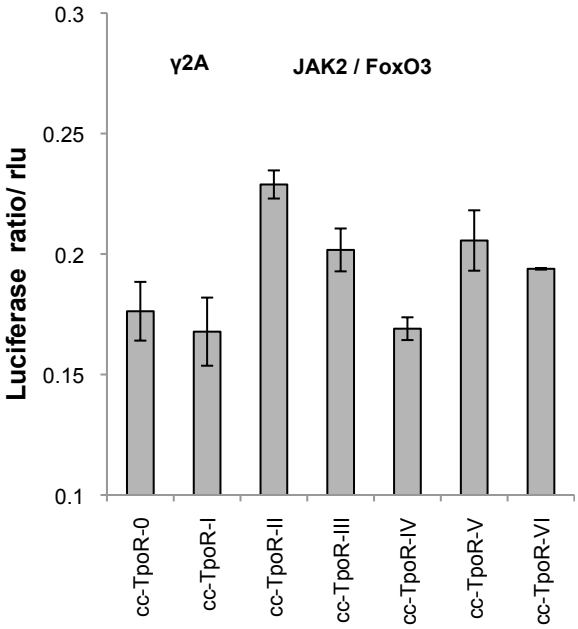
 ©2011 European Molecular Biology Organization

Supplemental Figure 1



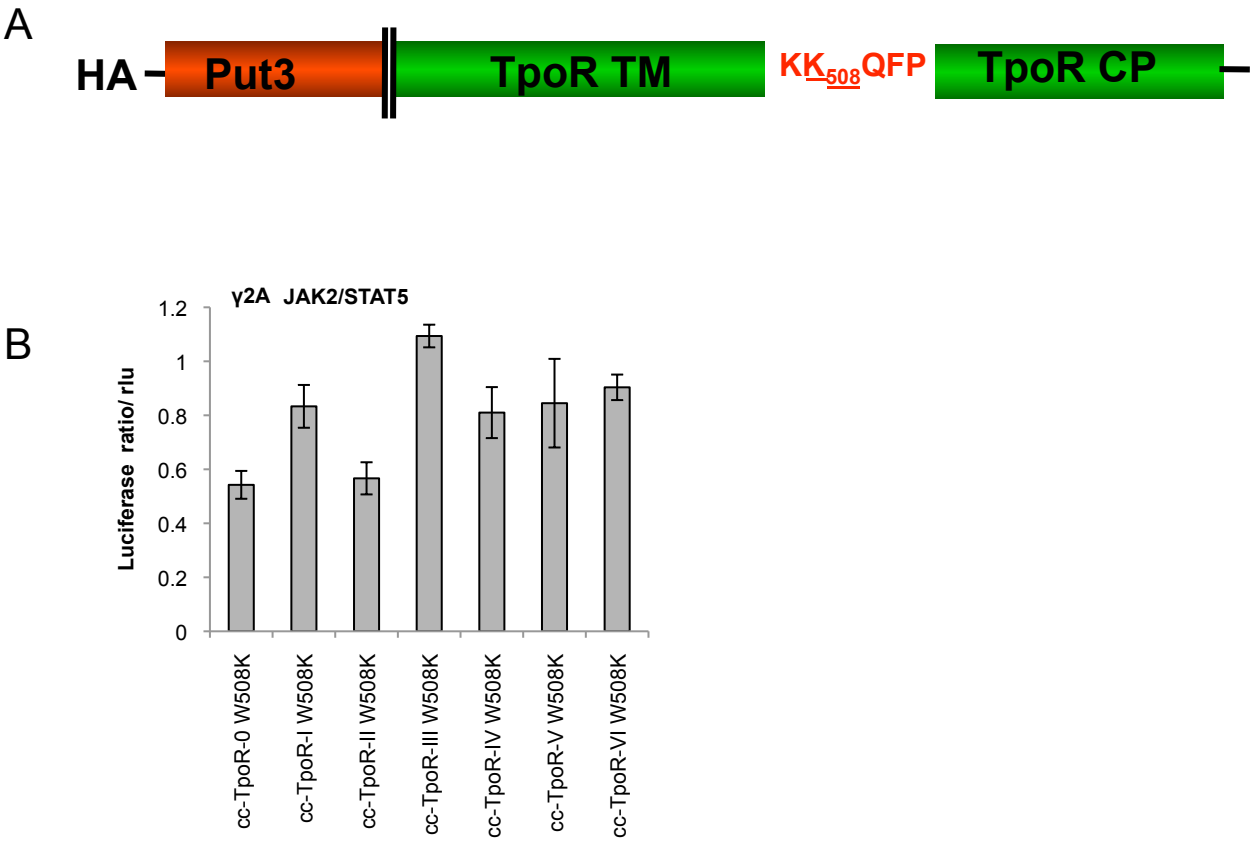
Supplemental Figure 1. Polarized IR spectrum of the TpoR transmembrane domain. Polarized IR spectroscopy can be used to establish the global secondary structure of peptides reconstituted into membrane bilayers. Polarized IR spectra of the mouse TpoR exhibit an amide I vibration at 1,657 cm^{-1}, a frequency characteristic of α-helical structure. The dichroic ratio of the amide I band is sensitive to the orientation of the TM helix relative to the plane of membrane. The observed dichroic ratio of 2.7 corresponds to a helix orientation of 33° relative to the membrane normal. Peptides corresponding to the TM and JM domains of TpoR (amino acids 481-522) were synthesized by solid-phase chemistry. Three arginine residues were added to the N-terminus for solubility, and the C-terminus was amidated. The synthetic peptides were purified by reverse-phase high-performance liquid chromatography (HPLC) on a C4 column with an acetonitrile-water gradient and lyophilized. The purity was confirmed by matrix-assisted laser desorption/ ionization (MALDI) mass spectrometry and HPLC. The reconstitution was carried out by dialysis after co-mixing peptide, lipid (DMPC, DMPG in a 10:3 molar ratio), and detergent (octyl-β-glucoside). The peptide-to-lipid molar ration 1:50. Polarized attenuated total reflection (ATR) FTIR spectra were obtained on a Bruker IFS 66V/S spectrometer.

Supplemental Figure 2



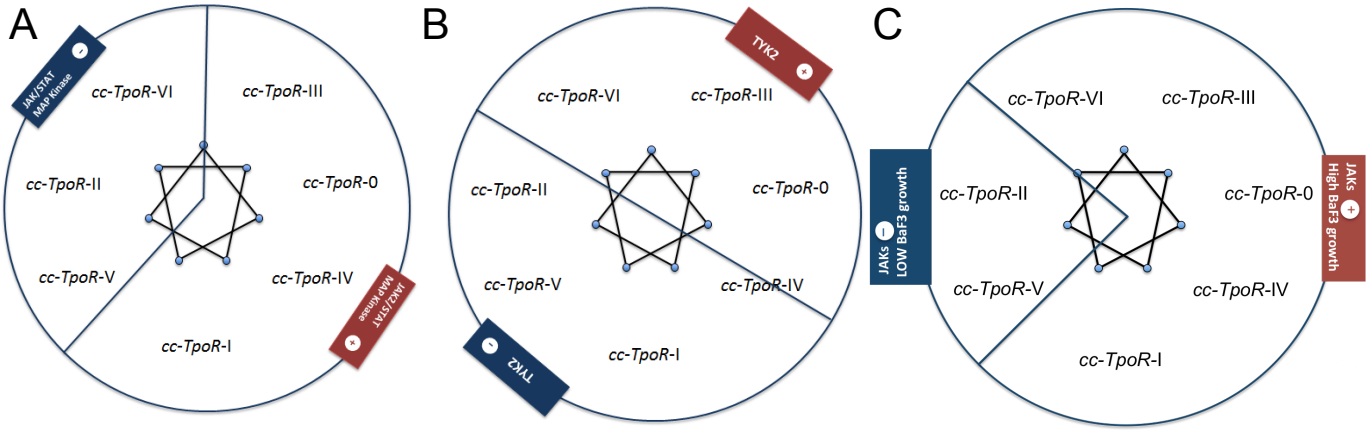
Supplemental Figure 2. Transcriptional activity via FoxO transcription factors was assessed in γ2A cells co-transfected with one of the seven *cc-TpoRs*, pRLTK-luc and with the 6xDBE-Luc reporter, which is known to be activated by FoxO family members. Shown are averages of triplicate values +/- S.D. of one representative experiment out of two independent experiments. PI-3-K/Akt signaling is inversely correlated with 6xDBE-Luc reporter activity.

Supplemental Figure 3



Supplemental Figure 3. (A) The mutation $W_{515}K$ found in ET and PMF patient was introduced at the corresponding W_{508} position in the seven murine *ccTpoR*s. (B) STAT5 transcriptional activity via JAK2 was measured in γ2A cells transiently transfected with reporter plasmids, *cc-TpoRs* W508K and JAK2. The results shown reflect averages of triplicate values +/- S.D. similar results were obtained performing two independent experiments.

Supplemental figure 4



Supplemental Figure 4. Helical wheel representation of *cc-TpoRs* and their weakest (in blue) or strongest (in red) signaling dimeric interfaces for JAK2/STATs, PI-3-kinase and MAP-kinase signaling (A), TYK2/STATs signaling (B). The broad helical face exhibiting high JAK signaling (red) also induces high levels of Ba/F3 proliferation (C). *cc-TpoR*-II adopts a completely inactive interface.

III.1.4. Unpublished but related results

III.1.4.1. Constitutive JAKs do not need a specific receptor orientation to signal

TYK2 V678F is able to signal with an inactive TYK2 TpoR orientation like cc-TpoR-I, suggesting that certain coiled-coils like cc-TpoR-I do not place TYK2 close enough for a proper cross-phosphorylation, but do bind kinases and allow them to signal if they are constitutively active. The same effect can be observed with JAK2 V617F that signal from weak JAK2 (cc-TpoR-I) and strong JAK2 (cc-TpoR-IV) interfaces. Therefore the receptor is merely a scaffold for constitutively active JAKs.

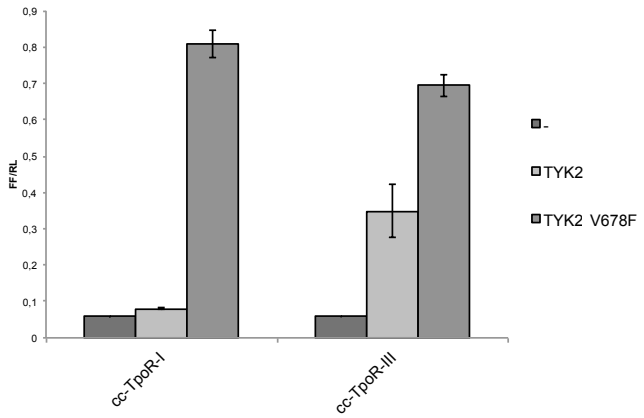


Figure 41 - Luciferase assay of TYK2V678F via coiled coils
Stat3 transcriptional activity via TYK2 or TYK2V678F measured by luciferase shows that active kinases like TYK2 V678F can signal no matter the orientation, while TYK2 can signal via cc-TpoR-III

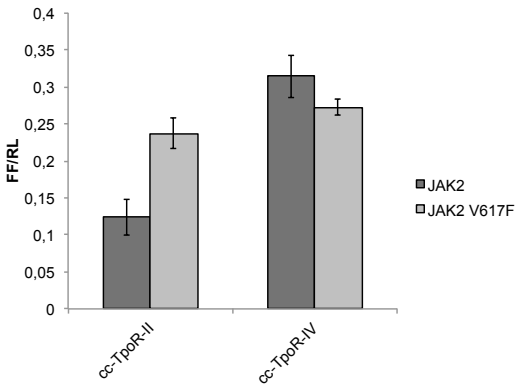


Figure 42 - Luciferase assay of JAK2V617F via coiled coils
STAT3 Transcritpional activity via JAK2 or JAK2 V617F measured by luciferase assay

III.1.4.2. TYK2 on cc-TpoR-III orientation has much less affinity than JAK2

Using empty vector to keep DNA constant and a TYK2 active conformation, we show that TYK2 or TYK2 V678F activity can be easily removed by replacing the empty vector by kinase dead JAK2, where the lysine at residue 882 essential to kinase activity is mutated to an aspartate. These data suggest that TYK2 has less affinity than JAK2 for the receptor.

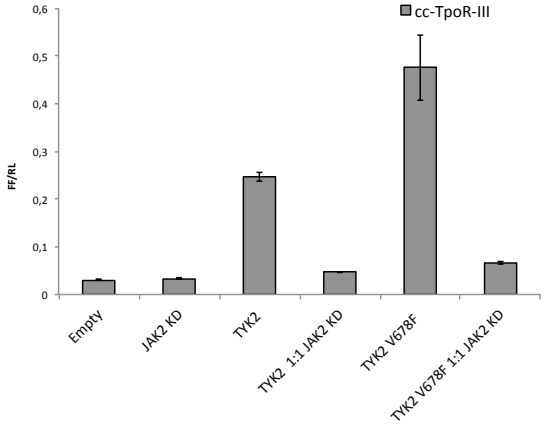


Figure 43 - Luciferase assay competition of TYK2 with JAK2KD

STAT5 Transcriptional activity via cc-TpoR-III measured by luciferase assay: Competition between JAK2 kinase death and TYK2 for cc-TpoR-III.

III.1.4.3. TYK2 using cc-TpoR-I cannot supersede JAK2

JAK2 kinase dead can compete with JAK2 while TYK2 WT cannot.

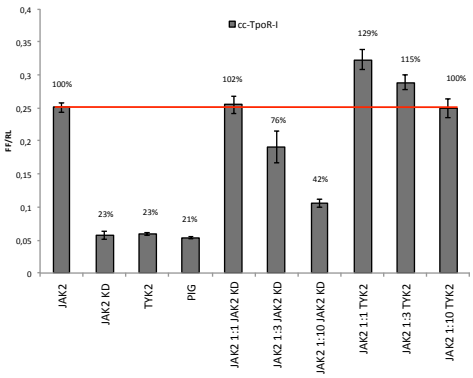


Figure 44 - Luciferase assay: TYK2 does not compete with JAK2

STAT5 trancriptional activity via cc-TpoR-I: TYK2 cannot compete with JAK2 while JAK2 kinase dead does. The increase in transcriptional activity in the presence of an equal amount of TYK2 and JAK2 even suggest the formation of heteromeric complexes.

III.1.4.4. TYK2 competition with JAK2 or JAK2 V617F on a full length receptor

We confirmed this on the full-length receptor; measuring TYK2 competition on JAK2 or JAK2 V617F on a full length Tpo stimulated TpoR. We observe that TYK2 was not able to reduce either JAK2 or JAK2V617F signaling while JAK2 kinase dead mediated a complete inhibition.

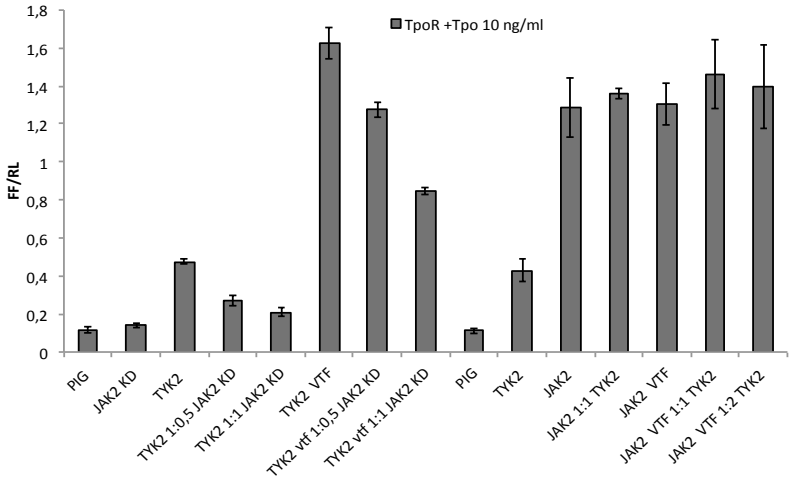


Figure 45 - Luciferase assay: TYK2 does not compete with JAK2 on a full-length receptor
STAT5 transcriptional activity: TYK2 does not compete with JAK2 or JAK2 V617F on a full length TpoR +10 ng/ml of Tpo, unlike JAK2 kinase dead.

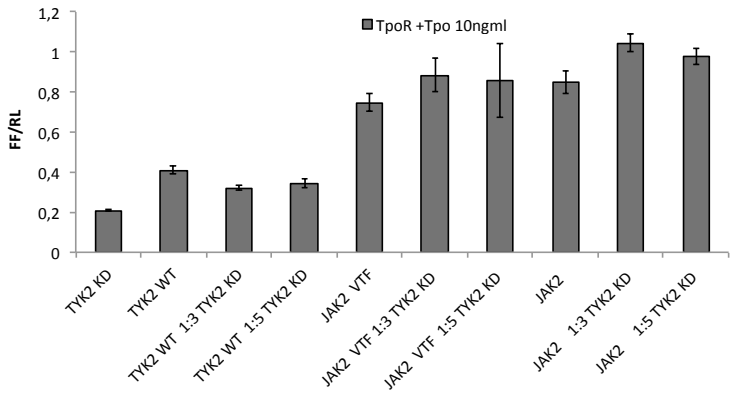


Figure 46 - Luciferase assay: TYK2KD does not compete with JAK on a full-length receptor
pGRR5 STAT3 transcriptional activity: TYK2 kinase dead does not inhibit JAK2 V617F or JAK2 WT signaling.

III.2. Preamble: Tryptophan at the transmembrane–cytosolic junction modulates thrombopoietin receptor dimerization and activation (Proc.Natl. Acad. Sci. USA 2013)

Jean-Philippe Defour*, Miki Itaya*, Vitalina Gryshkov*, Ian C. Brett, Christian Pecquet, Takeshi Sato, Steven O. Smith, and Stefan N. Constantinescu.
*These authors contributed equally to this manuscript.

III.2.1. Background

Cytokine receptors such as EpoR and Growth Hormone receptor are generally primed for activation with the existence of preformed dimers or domains that readily assemble together, and that in the absence of ligand remain inactive. TpoR contains a unique motif, R/KWQFP at its cytosolic juxtamembrane junction, which is not present in any other cytokine receptor family members. This amphipathic motif was shown to prevent autonomous activation of the receptor.[97] The tryptophan residue in this motif (W508 or W515 in the murine and human receptors, respectively) was found to be critical for the inhibitory function, as its mutation to alanine led to constitutive activation in cell lines[97] and a severe myeloproliferative phenotype in mice.[250] Mutations at the W515 position were found soon after in 5-9% of patients with JAK2 V617F negative PMF and ET.[102,103] On larger cohorts like the Primary Thrombocythaemia 1 (PT-1) cohort, W515L/K/A/R mutations were found in 6.4% of ET and 15% of PMF patients that do not harbor a JAK2V617F mutation.[19,257]

III.2.2. Questions

The fundamental question that is addressed in this study concerns the mechanism by which residue W515 prevents autonomous activation of the receptor. By mutagenesis we tried to answer the following questions:

1. Could W515 be involved in the dimerization state of the full-length receptor in the absence of ligand and how does W515 influence the dimerization of the transmembrane domain of TpoR?
2. Does W515 influence orientation and tilt of the transmembrane and juxtamembrane regions of the receptor on the plasma membrane?
3. Could other residues replace the W515 in its physiologic function of maintaining the receptor inactive and secondary site mutations render TpoR W515 mutants wild type for function?

III.2.3. Authors contribution

To answer these questions we performed extensive mutagenesis, transient luciferase assays and engineered stable BaF3 cell lines expressing the receptor mutants. These functional data in γ2A and BaF3 cells represented by STAT5-transcriptional activation, autonomous and ligand-induced proliferation, as well determination of cell surface and total receptor levels, as well as activation of JAK2 and TYK2 were entirely my responsibility. The mutational and functional data that I produced were supported by dimerization data of the full-length receptor using *Gaussia* princeps luciferase complementation assay performed by Dr. Vitalina Gryshkova. Miky Itaya in the laboratory of Prof. Steven O. Smith, SUNY Stony Brook, Long Island, NY examined the dimerization and tilt of the TpoR transmembrane domain flanked by juxtamembrane regions that included the mutations I studied above. Our collaborators used deuterium Magic Angle Spinning NMR, analytical ultracentrifugation and ATR-FTIR spectroscopy.

I was also involved in the research design, in feeding back to our structural collaborators the results of mutagenesis and in the writing of the paper.

Tryptophan at the transmembrane–cytosolic junction modulates thrombopoietin receptor dimerization and activation

Jean-Philippe Defour[a,1], Miki Itaya[b,1], Vitalina Gryshkova[a,1], Ian C. Brett[b], Christian Pecquet[a], Takeshi Sato[c], Steven O. Smith[b,2], and Stefan N. Constantinescu[a,2]

[a]Ludwig Institute for Cancer Research and de Duve Institute, Université catholique de Louvain, 1200 Brussels, Belgium; [b]Department of Biochemistry and Cell Biology, Stony Brook University, Stony Brook, NY 11794-5215; and [c]Institute for Protein Research, Osaka University, Osaka 565-0871, Japan

Edited* by Donald M. Engelman, Yale University, New Haven, CT, and approved December 26, 2012 (received for review July 10, 2012)

Dimerization of single-pass membrane receptors is essential for activation. In the human thrombopoietin receptor (TpoR), a unique amphipathic RWQFP motif separates the transmembrane (TM) and intracellular domains. Using a combination of mutagenesis, spectroscopy, and biochemical assays, we show that W515 of this motif impairs dimerization of the upstream TpoR TM helix. TpoR is unusual in that a specific residue is required for this inhibitory function, which prevents receptor self-activation. Mutations as diverse as W515K and W515L cause oncogenic activation of TpoR and lead to human myeloproliferative neoplasms. Two lines of evidence support a general mechanism in which W515 at the intracellular juxtamembrane boundary inhibits dimerization of the TpoR TM helix by increasing the helix tilt angle relative to the membrane bilayer normal, which prevents the formation of stabilizing TM dimer contacts. First, measurements using polarized infrared spectroscopy show that the isolated TM domain of the active W515K mutant has a helix tilt angle closer to the bilayer normal than that of the wild-type receptor. Second, we identify second-site R514W and Q516W mutations that reverse dimerization and tilt angle changes induced by the W515K and W515L mutations. The second-site mutations prevent constitutive activation of TpoR W515K/L, while preserving ligand-induced signaling. The ability of tryptophan to influence the angle and dimerization of the TM helix in wild-type TpoR and in the second-site revertants is likely associated with its strong preference to be buried in the headgroup region of membrane bilayers.

myeloproliferation | transmembrane domain | JAK2 | NMR spectroscopy | FTIR spectroscopy

The thrombopoietin receptor (TpoR, c-MPL) is a typical single-pass membrane receptor with a large extracellular ligand-binding domain, a single transmembrane (TM) helix, and a cytoplasmic domain that is involved in intracellular signaling (1, 2). In these TM receptors, activation is mediated by ligand-induced dimerization of receptor monomers or structural rearrangement within preformed dimers, which induce changes in the rotational orientation and/or association of the TM and juxtamembrane (JM) regions of the receptor. In many single-pass membrane receptors, receptor activity is regulated through these structural elements (3).

TpoR is unique in that it is expressed in hematopoietic stem cells, where it is essential for maintaining stem cell reservoirs (4–6), and in early myeloid progenitors and megakaryocytes, where it regulates the differentiation and production of platelets (7, 8). In contrast to the TpoR, the erythropoietin receptor (EpoR), a related cytokine receptor, is essentially expressed only in erythroid progenitors, where it regulates red blood cell production.

Tight control of receptor activity is particularly important for the TpoR, because mutations within its TM and JM domains both lead to constitutive activation and myeloproliferative disorders. Within the TM domain, the S505N mutation is associated with familial forms of thrombocytosis (9) and induces stable, active receptor dimers (10, 11). At the intracellular TM–JM boundary, we have described a conserved amphipathic motif (RWQFP) that is specific to the TpoR (12) in which mutations at W515 (W515L/K/A) lead to constitutive receptor activation and are associated with JAK2 V617F-negative myeloproliferative disorders, namely essential thrombocythemia and primary myelofibrosis (13–17).

Biochemical studies and assays for membrane-spanning domain dimerization indicated that the TM domain of TpoR is a dimer and that TpoR can signal from several different helix orientations (18). To establish how the relative rotational orientations of the TM helices influence receptor activation, we have engineered dimers of both the TpoR and EpoR. In the TpoR, we have shown that different in vivo phenotypes are imparted by distinct TM helix orientations (19). We identified one rotational orientation corresponding to an inactive dimeric state, and another orientation corresponding to the activated receptor. Several other orientations induce partial and pathologic signaling. The helix interface identified as inactive using the engineered dimeric coiled coils (19) is identical to the inactive interface identified previously (18). Moreover, the ability of the TpoR to signal through several different dimeric orientations contrasts with the EpoR, where only a single active interface was identified (20).

Here we focus on the role of the JM domain of the TpoR in the regulation of its activity. We address the ability of wild-type TpoR to dimerize in membrane bilayers and discuss how dimerization is controlled by the unique RWQFP motif at the intracellular TM–JM boundary. We describe a unique function for the tryptophan residue within this motif in preventing dimerization of the upstream TM α-helix and productive signaling. We propose a mechanism that explains TpoR activation by mutations at W515, as well as the reversal of constitutive activation by second-site mutations.

Results

Tryptophan Is Absolutely Required at JM Position 515 to Maintain the Unliganded TpoR Inactive. Several specific mutations have been described in the RWQFP insert that lead to myeloproliferative disorders—namely W515 mutations to leucine, lysine, arginine, alanine, and serine (12–17, 21). The diversity of amino acids of both hydrophobic and hydrophilic character that are able to activate the TpoR suggests that Trp515 is unusual and is regulatory as a result of its size and/or aromatic character. We compared

Author contributions: J.-P.D., M.I., V.G., S.O.S., and S.N.C. designed research; J.-P.D., M.I., V.G., I.C.B., C.P., T.S., and S.N.C. performed research; T.S. contributed new reagents/analytic tools; J.-P.D., M.I., V.G., I.C.B., C.P., T.S., S.O.S., and S.N.C. analyzed data; and J.-P.D., S.O.S., and S.N.C. wrote the paper.

The authors declare no conflict of interest.

*This Direct Submission article had a prearranged editor.

[1]J.-P.D., M.I., and V.G. contributed equally to this work.

[2]To whom correspondence may be addressed. E-mail: steven.o.smith@stonybrook.edu or stefan.constantinescu@bru.licr.org.

This article contains supporting information online at www.pnas.org/lookup/suppl/doi:10.1073/pnas.1211560110/-/DCSupplemental.

the influence of mutations at position 515 that have been identified in patients with myeloproliferative neoplasms (MPNs) and then the influence of additional mutations at adjacent positions to test whether Trp515 interacts in concert with Arg514 and Gln516 to stabilize the TpoR in the inactive state.

In the murine (KWQFP) and human (RWQFP) sequences, the first and second residues are conserved as a positively charged amino acid and tryptophan, respectively, suggesting a cation–π interaction (Fig. S1). To address whether an aromatic residue is required at the second position for function, W515 was mutated to phenylalanine or tyrosine. As shown in Fig. 1*A* (*Right*), both tyrosine and phenylalanine lead to constitutive TpoR activation, indicating that aromatic character alone is not sufficient to prevent self-activation. The activity of W515Y and W515F TpoR is significantly higher than wild-type TpoR, although lower than mutations identified in MPN patients (K, L, A, R, or S; Fig. 1 *A* and *B*). The results roughly correlate with the interfacial hydrophobicity scale (22) in which tryptophan has the highest free energy among the amino acids to partition into the headgroup region of the membrane bilayer.

We asked whether residues in the vicinity of W515 impact its inhibitory function. Substitution to lysine of residues 516, 517, and 518 did not induce activation (Fig. S2). Similarly, mutating R514 to A, W, or F did not induce activation. However, all these mutants responded to Tpo addition like the wild-type TpoR.

The data obtained using transient expression in γ-2A cells were confirmed in stably transduced IL-3–dependent Ba/F3 cells (Fig. 2). All mutants of TpoR that exhibited constitutive activation in luciferase assays in γ-2A cells were able to induce IL-3–independent proliferation of Ba/F3 cells after expression at levels similar to that of the wild-type TpoR, which was only activated in the presence of Tpo. Equal levels of expression were confirmed on the basis of equivalent GFP levels by flow cytometry cell sorting (23) and HA-TpoR expression by Western blotting.

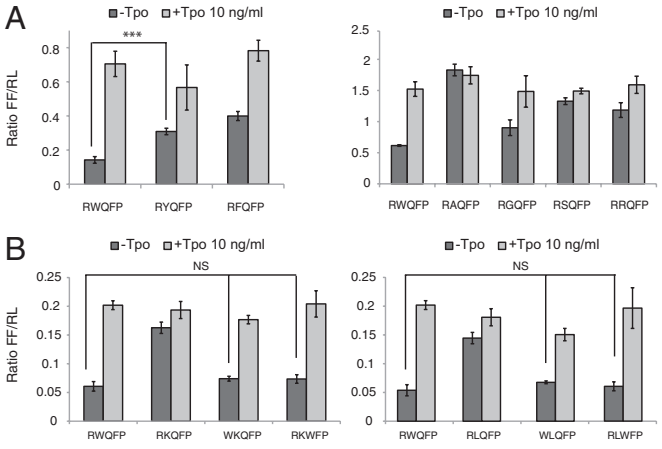


Fig. 1. Mutation of the TpoR W515 residue induces constitutive signaling via JAK2 and STAT5. (*A*) The indicated TpoR W515 mutants, where the W515 residue was replaced by aromatic residues (*Left*) or other residues (*Right*) were expressed in γ-2A cells cotransfected with JAK2 and tested for ligand-dependent and -independent induction of STAT5-dependent transcriptional activity. Two reporters are used in the dual luciferase assay: the experimental firefly (FF) luciferase reporter, which responds to JAK/STAT pathway, and a cotransfected renilla (RL) luciferase control reporter driven by a constitutive promoter that provides a baseline signal proportional to transfection levels. The firefly/renilla (FF/RL) ratio normalizes the FF response for experimental variability due to cell viability and transfection efficiency. (*B*) Constitutive activation of TpoR W515 mutants is reverted by substituting the preceding (R514) or subsequent (Q516) residue by tryptophan. Replacing residue 514 or 516 with a tryptophan residue (R514W or Q516W) reverts TpoR W515K (*Left*) and TpoR W515L (*Right*) to a wild-type TpoR phenotype. Shown in *A* and *B* are averages of three replicates ± SD in one representative experiment out of at least three. NS, nonsignificant; $*P \leq 0.05$; $**P \leq 0.01$; $***P \leq 0.001$, Student *t* test.

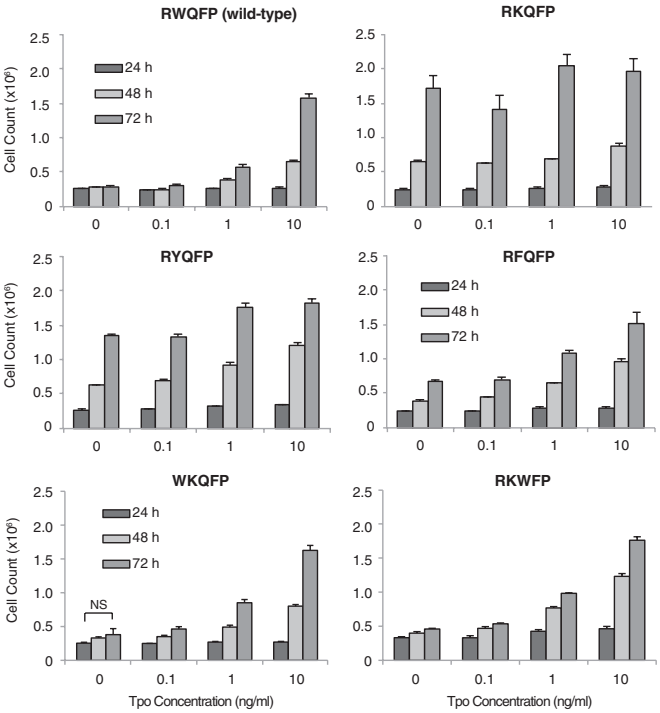


Fig. 2. Dose-dependent effects of Tpo on proliferation of Ba/F3 cells stably expressing TpoR mutants. Constitutive activation of TpoR W515 mutants is reverted by substituting the precedent (514) or subsequent (516) residue by tryptophan. The R514W and Q516W mutations revert the transforming phenotype of TpoR W515K to a wild-type phenotype in Ba/F3 cells stably expressing TpoR mutants. Shown are average of triplicate cell counts at the indicated times ± SD from a representative experiment out of three. $*P \leq 0.05$; $**P \leq 0.01$; $***P \leq 0.001$, Student *t* test.

In addition, we tested STAT-dependent transcriptional signaling of W515 mutants using a luciferase reporter in the JAK2-deficient γ-2A cells (24), in which TYK2 and not JAK2 was coexpressed with the TpoR and luciferase reporters. TpoR W515 mutants did not exhibit constitutive activity in the absence of JAK2 but responded to Tpo like wild-type TpoR. These data indicate that W515 mutants constitutively activate signaling of TpoR via ligand-independent activation of JAK2 (Figs. S3 and S4).

Reversal of Constitutive Activity of TpoR W515 Mutants by Substituting Surrounding Residues to Tryptophan. To further test the hypothesis that tryptophan plays a unique role at the intracellular TM–JM boundary of the TpoR, we engineered R514W or Q516W mutations into the active TpoR W515K and W515L mutants. The idea was that in the context of the active TpoR W515 mutants, a tryptophan residue before or after residue 515 might reverse activation. As shown in Fig. 1*B*, R514W suppressed the constitutive STAT5 activation of TpoR W515K and W515L mutants in γ-2A cells. The doubly mutated receptors behaved as wild-type receptors, in that they responded normally to Tpo. Similarly, the Q516W reversed activation of TpoR W515K and W515L mutants, conferring a wild-type phenotype, with no activation in the absence of Tpo and normal response to Tpo. These data were reproduced upon stable retroviral expression in Ba/F3 cells. Ligand-independent proliferation of Ba/F3 cells induced by the TpoR W515K mutant was prevented by the R514W and Q516W mutations, whereas Tpo-induced proliferation remained intact (Fig. 2). As a control, individual mutations at the rescuing positions, or the WWQFP mutant did not induce constitutive activation and retained response to the Tpo ligand. Overall these data indicate that placing tryptophan in the vicinity of the W515 mutations prevents

receptor self-activation and renders a wild-type phenotype to the TpoR W515 mutant.

Impact of W515 on Dimerization of Full-Length TpoR. To assess the oligomerization status of the TpoR and selected mutants in cell membranes, we used the *Gaussia princeps* luciferase complementation assay (25). This protein fragment complementation assay can be used at levels of expression that are close or similar to those of normal cells (25). Two fragments of *Gaussia princeps* luciferase, Gluc1 and Gluc2, were fused in-frame to the carboxyl terminus of the TpoR after introduction of a short flexible linker and subcloned in pcDNA3.

Fig. 3*A* shows that when the wild-type TpoR-Gluc1 or -Gluc2 constructs were individually transfected in HEK293 cells, no reconstituted luciferase signal could be detected. When the wild-type TpoR-Gluc1 and -Gluc2 constructs were cotransfected, a signal was obtained that reflects a basal level of receptor dimerization. This level is significantly weaker than that of EpoR fused to the same Gluc1 and Gluc2 fragments (~2.5- to 3-fold weaker; Fig. S5), consistent with weaker levels of dimerization previously reported for the TM domain of TpoR (18), compared with EpoR (26–29). We then tested the activating mutations found in the TM (S505N) and JM (W515K) regions of the TpoR. As shown in Fig. 3*A*, both mutations increased the luciferase signal to statistically significant levels ($P < 0.01$ and $P < 0.05$ for the S505N and W515K mutants, respectively). Furthermore, when the double mutant W515K, Q516W was tested, the luciferase signal was not statistically different from that of wild-type TpoR. Taken together these data indicate that the W515K mutation, and as expected the S505N mutation, impact the dimerization status of the full-length receptor. Levels of expression of TpoR mutants are shown in Fig. 3*B*. Fusion of TpoR with the Gluc1 or Gluc2 did not change signaling in the presence of Tpo or activation by the W515K or S505N mutations (Fig. 3*C*).

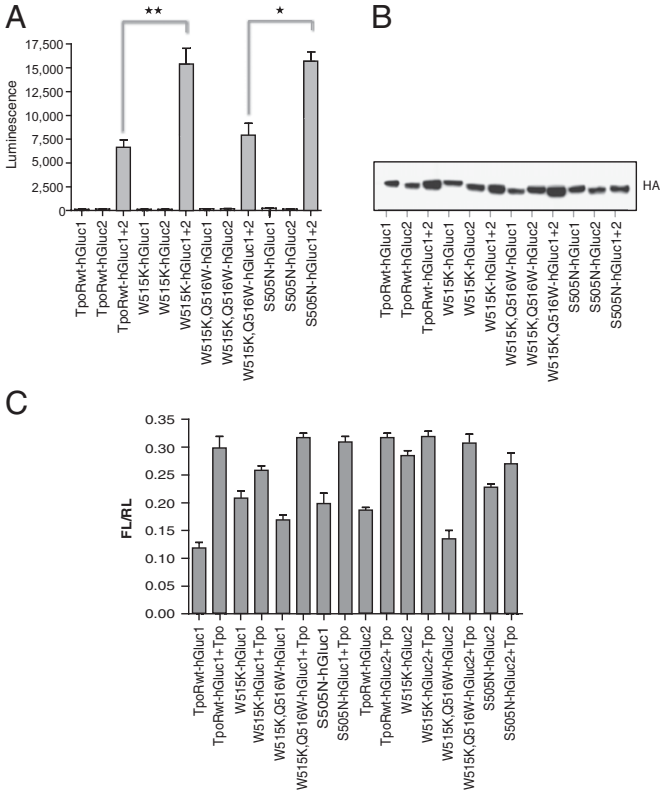


Fig. 3. Detection of TpoR dimers by split-luciferase assay. (*A*) Luciferase assay of HEK293 cell lysates expressing hGluc-tagged TpoR and its mutants (W515K, W515KQ516W, S505N). The average luminescence of triplicate values ± SD is shown for one representative experiment out of at least three. (*B*) Immunoblotting of transfected HEK293 cell lysates by anti-HA antibodies. (*C*) STAT5 transcriptional assays in γ-2A cells transfected with cDNAs coding for hGluc-tagged TpoR, JAK2, and its mutants. *$P < 0.01$; **$P < 0.001$, one-way ANOVA.

Constitutive TpoR Activation Is Associated with TM Helix Dimerization and Modulated by the RWQFP Motif. To address whether dimerization is directly modulated by the RWQFP motif, measurements of dimerization were performed in lipid membrane environments using deuterium magic angle spinning (MAS) NMR spectroscopy and in detergent environments using analytical ultracentrifugation. Deuterium MAS NMR spectroscopy provides a simple approach to compare membrane dimerization of TM peptides (30). The intensities of the side bands in a deuterium MAS spectrum map out the deuterium line shape and are sensitive to molecular motion. Methyl-deuterated leucines facing the lipid have greater rotational freedom and exhibit weaker side band intensities than leucine side chains facing the dimer interface.

Fig. 4*A* shows the deuterium MAS spectrum of the wild-type TpoR TM peptide reconstituted into 1,2-dimyristoyl-sn-glycero-3-phosphocholine (DMPC), 1,2-dimyristoyl-sn-glycero-3-[phospho-rac-(1-glycerol)] (DMPG) bilayers. The spectrum lacks the side band pattern characteristic of constrained deuterated methyl groups. The sharp resonance at zero frequency is from deuterated water in the sample. We interpret the lack of MAS sidebands as resulting from rotational motion of the peptide on the time scale of MAS. Lowering the temperature restricts rotational diffusion of the peptide and results in a spectrum with a distinctive stronger pattern of rotational side bands (Fig. S6).

Fig. 4*B* presents the deuterium NMR spectrum of the TpoR TM domain lacking the five-residue RWQFP motif. The deletion was previously shown to be activating (12) and is similar to the sequence tested by Engelman and coworkers (18) in which the RWQFP was partially deleted. The deletion of the insert restores the pattern of rotational side bands spaced at the MAS frequency of 3 kHz. The width of the side band envelope is characteristic of a TM domain dimer. Fig. 4 *C* and *D* show deuterium MAS spectra of the TpoR TM peptide with the S505N and W515K substitutions. Both mutations are activating. The spectra of both the S505N and W515K mutants exhibit the same pattern of rotational side bands as seen in Fig. 4*B*, indicating that the mutation stabilizes the TM dimer of TpoR.

To test whether inactivation of the TpoR W515K mutant by insertion of tryptophan at positions 514 or 516 influences dimerization, deuterium NMR spectra were obtained of TM peptides containing the R514W, W515K (Fig. 4*E*), and W515K, Q516W (Fig. 4*F*) double mutations. In both of the double mutants, the intensity in the rotational side bands is lost, consistent with greater mobility of L512 due to a shift to monomeric TpoR.

Sedimentation equilibrium analytical ultracentrifugation was also performed to compare the ability of the TM peptides to dimerize in detergent micelles. The wild-type and mutant TpoR TM peptides were reconstituted into DPC micelles at three concentrations (~20 μM, 35 μM, and 50 μM), and data were acquired at three centrifugation speeds (98,784, 129,024 and 185,785 × *g*). Fig. 5*A* presents the sedimentation equilibrium measurements of the wild-type TpoR TM peptide at peptide concentration of 35 μM. The data were analyzed using a single component analysis. Fig. 5*B* presents the M_r of the monomeric peptide and the single component fit to data from all concentrations and rotor speeds. The results roughly match those obtained by deuterium MAS NMR of the TM peptides reconstituted into membrane bilayers. The wild-type TpoR peptide exhibits a M_r close to that of the monomer, whereas the S505N and W515K mutants sediment at an M_r close to that of a dimer. The apparent dimerization of the W515K mutant is reversed in the W515K, Q516W and R514W, W515K double mutants.

Dimerization of the TpoR TM Domain Is Regulated by the TM Helix Tilt Angle. Polarized FTIR spectroscopy of TM peptides was used to assess the extent of helical secondary structure and the angle of

RRRETAWISLVTALHLVLGLSAVLGLLLLRWQFPAHYRRLRHALW

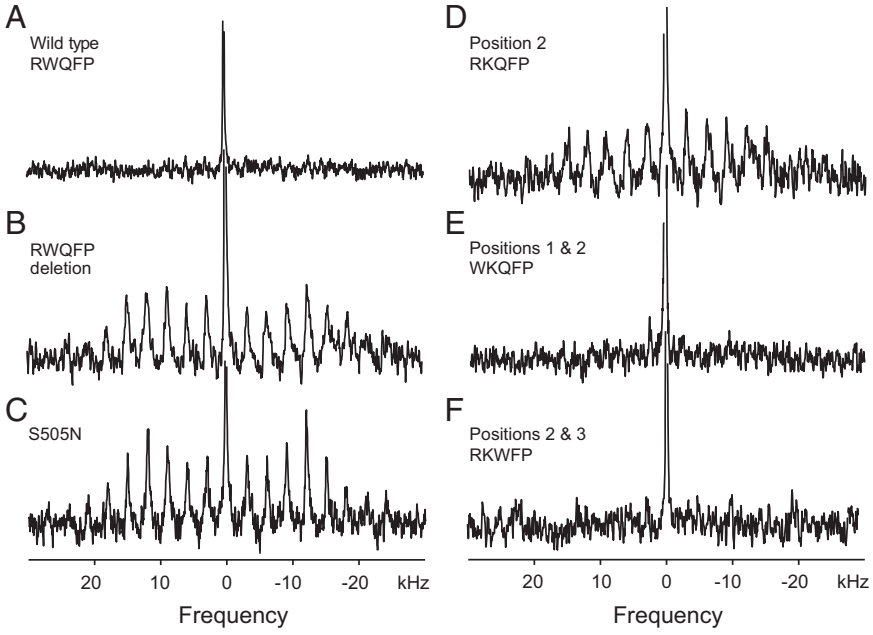


Fig. 4. Deuterium MAS NMR spectra of the TpoR TM domain. Deuterium MAS NMR spectra were obtained of the wild-type Tpo receptor TM peptide (residues 488–529) and of peptides with mutations at S505 and in RWQFP insert: (*A*) wild-type, (*B*) RWQFP deletion mutant, (*C*) S505N, (*D*) W515K, (*E*) R514W, W515K, and (*F*) W515K, Q516W double mutation. The peptides were deuterium labeled at Leu512 and reconstituted into DMPC:DMPG bilayers at a peptide/lipid molar ratio of 1:50. Each experiment was repeated using separate reconstitutions.

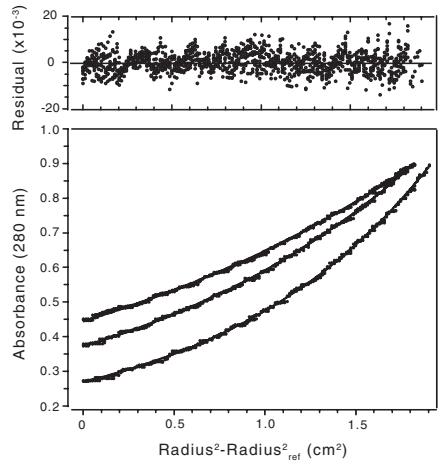
the TM helix relative to the bilayer normal. For the TM domain of the TpoR reconstituted in DMPC bilayers, we typically observe an amide I vibration at 1,657 cm^{-1} (Fig. 6*A*). Fourier deconvolution of the amide I band reveals no significant nonhelical structure. The dichroic ratio of the amide I band is sensitive to the angle of the TM helix relative to the plane of membrane. For the wild-type TpoR TM domain, we observe a dichroic ratio of 2.7 ± 1, which corresponds to a helix angle of ~30° relative to the membrane normal. The W515K mutation results in an increase in the dichroic ratio to 3.0 ± 1 and a helix angle (~23°) closer to the bilayer normal (Fig. 6*B*). In contrast, both the WKQFP and RKWFP sequences lead to lower dichroic ratios (~2.5), consistent with an increase in the helix tilt angle (~38°). We interpret the results from analytical ultracentrifugation, deuterium MAS NMR and IR spectroscopy in terms of a model in which the RWQFP sequence also controls the tilt of the helix in the bilayer, which in turn controls the ability of the helix to dimerize.

Discussion

Our main finding is that W515 in the RWQFP sequence impairs TpoR TM helix dimerization, and by doing so prevents constitutive receptor activation. Mutations (W515K or S505N) that induce TM helix dimerization activate signaling. Second-site mutations (R514W or Q516W), which reverse dimerization of the TM α-helix, prevent signaling. The RWQFP motif seems to regulate a receptor that is primed for activation. NMR and analytical ultracentrifugation measurements of the TpoR TM domain lacking the RWQFP motif demonstrate that the TM sequence alone has an inherent propensity to dimerize and that inclusion of the motif inhibits dimerization.

These observations seem to be associated with several unique functional features of TpoR. First, the receptor is expressed at several distinct stages of hematopoiesis, from stem cells to mature platelets. Second, TpoR functions differently in different cellular contexts, from regulating hematopoietic stem cell quiescence (4–6) to controlling megakaryopoiesis (7, 8), both promoting and inhibiting megakaryocyte proliferation as a function

A



B

	M_r	M_r (fit)
Wild-type: RWQFP	5360	6960
Deletion: RWQFP	4650	12760
S505N	5392	11850
Position 2: RKQFP	5306	10630
Position 1 & 2: WKQFP	5364	8303
Position 2 & 3: RKWFP	5365	7535

Fig. 5. Analytical ultracentrifugation of the TpoR TM domain. (*A*) Sedimentation equilibrium experiments of the wild-type TpoR TM peptide in DPC micelles were analyzed using nonlinear least-squares global curve-fitting. Representative data are shown at rotor speeds of 98,784, 129,024, and 185,785 × *g* using a peptide concentration of 35 μM. Data were collected at 25 °C after 20 h of centrifugation. (*Upper*) Distribution of residuals. (*Lower*) Open circles for experimental data and solid lines for a fit to a single component model. (*B*) Monomer M_rs and M_rs derived from single component fits are shown for wild-type TpoR and its mutants. The experimental M_rs represent the global fit to three concentrations and three rotor speeds.

BIOCHEMISTRY

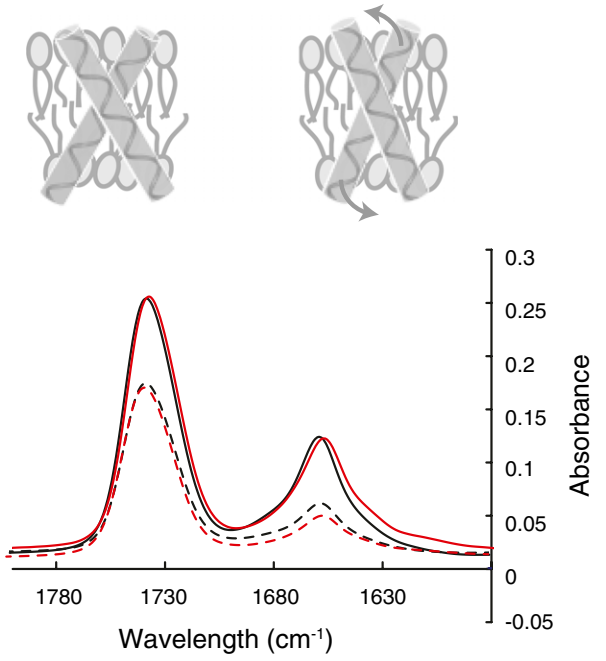


Fig. 6. Polarized FTIR spectra of wild-type and W515K TpoR TM peptides. The wild-type (black) and W515K (red) TpoR spectra were obtained with light polarized parallel (solid line) or perpendicular (dashed line) to the membrane normal. The cartoon illustrates the proposed change in helix tilt angle upon W515K mutation. The IR band at 1,745 cm^{-1} corresponds to the lipid carbonyl vibration, whereas the band at ~1,657 cm^{-1} corresponds to the protein amide I vibration. The dichroic ratios of the amide I band correspond to the average of three separate reconstitutions.

of cellular JAK2 levels (31). Our data indicate that W515 maintains the receptor in the inactive conformation and imparts specific signaling upon ligand activation. In this regard, in our engineered coiled-coil receptor dimers, mutation of W515 to lysine removes the inhibition for the one inactive orientation and abolishes differences in biologic effects induced by several other TpoR dimers (19).

Regulation of dimerization is a critical aspect of all single-pass TM receptors. The isolated TM domains for both the EpoR (26, 27) and TpoR (18) have previously been shown to have a propensity to dimerize, although to different extents; EpoR TM dimerization seems to be comparable to that of the TM domain of glycophorin A (26), whereas TpoR TM dimerization seems to be weaker than glycophorin A (18). Our experiments using the *Gaussia princeps* luciferase assays show that the dimerization of full-length TpoR is weaker than that of EpoR, which is known to be a preformed dimer (32, 33). Our data indicate that mutations that promote TM α-helix dimerization and that induce constitutive activation also impact full-length receptor dimerization.

Our working model for how the RWQFP motif regulates dimerization is that it extends the hydrophobic length of the TM helix, which tilts as the tryptophan side chain partitions into the bilayer. R514 may partition into the membrane owing to favorable cation–π interactions with W515. Solution NMR studies show that the RW region is helical and the TM helix unravels at Phe517-Pro518 (Fig. S7). The increase in the tilt angle reduces the surface contact area between TM helices and disfavors dimerization.

Tryptophan plays a unique role in this mechanism. Tryptophan exhibits a strong preference for the ends of TM helices in single-pass membrane proteins (34) and has the largest free energy for partitioning into the headgroup region of membrane bilayers (22). Model peptide studies have shown that the position of tryptophan and lysine at the ends of TM helices can influence the mismatch between the hydrophobic length of the peptide and the bilayer thickness, which in turn can alter the helix tilt angle (35). In contrast, tryptophan at central positions in single-pass membrane proteins may actually mediate helix association (36).

Ligand binding to the extracellular domain (or the activating S505N mutation) can overcome the favorable membrane interactions of W515 and drive helix dimerization by changing the tilt angle and orientation of the TM helix. The activating W515 mutants remove the stabilizing cation–π interaction and leave the positively charged R514 side chain, as well as the polar Q516, in an unfavorable hydrophobic environment. Arginine and glutamine have unfavorable transfer free energies (22). As a result, the tilt angle of the helix decreases in the W515 mutants as R514 moves out of the membrane. The second site mutations adjacent to W515K and W515L mutations reintroduce a tryptophan at the JM boundary.

On the basis of sequence database searches, the conserved RWQFP sequence seems to be unique at the intracellular end of single-pass membrane receptors. The balance of hydrophilic and hydrophobic amino acids within the motif likely contributes to its ability to partition between membrane and cytosolic environments upon ligand binding. However, a second possible function of the motif may be to guide dimerization of the ligand-activated receptor. Q516 is predicted to be in the interface of the active receptor dimer (18, 19) and has the potential to mediate helix interactions. Thus, this simple five amino acid insert in the TpoR may both hold the TM helix in an inactive conformation in the unliganded receptor and contribute to the rotational dependence of activation in the ligand-bound receptor.

Methods

cDNA Constructs and Cells. The wild-type and mutant human TpoR cDNAs cloned in bicistronic pMX-IRES-GFP contained an HA tag at the amino terminus (2). Human JAK2 and TYK2 cDNAs were cloned in pMX-IRES-CD4 (2). Site-directed mutagenesis was performed with the Stratagene Quick mutagenesis kit or overlapping PCR. All constructs were verified by Sanger sequencing. Ba/F3 cells are IL-3–dependent proB mouse cells that were maintained in RPMI supplemented with 10% (vol/vol) FBS and Walter and Eliza Hall Institute (WEHI) cell supernatant (19) as a source of IL-3. Gamma-2A cells are human fibrosarcoma cells deficient in JAK2 (24).

Retroviral Transduction and Generation of Cell Lines Stably Expressing TpoR Mutants. Ecotropic retroviral supernatants were generated in BOSC cells, and retroviral transduction was performed on Ba/F3 cells (19). Flow cytometry cell sorting was used to isolate pools of cells expressing equivalent levels of GFP (15). Total and cell surface TpoR levels in transduced cells were assessed by Western blotting and flow cytometry with anti-HA antibodies, respectively (15).

Dual Luciferase Transcriptional Assays. Transcriptional activation of STAT5 and STAT3 was analyzed in γ-2A, Ba/F3, and HEK293 cells expressing TpoR or TpoR mutants, as previously described (19), using the STAT5/STAT3 pGRR5 luciferase reporter and pRL-TK driven renilla luciferase. Gamma-2A cells or Ba/F3 cells were transiently transfected using Lipofectamine and electroporation, respectively (2). A Perkin-Elmer Victor X Light analyzer was used for detecting luminescence in cell lysates.

Synthesis and Reconstitution of TpoR TM Helix Peptides. ^{2}H-Labeled amino acids were purchased from Cambridge Isotope Laboratories. Lipids were obtained from Avanti Polar Lipids, as a lyophilized powder and used without further purification. Peptides (45 residues; Fig. 4) corresponding to the TM domain of TpoR were synthesized using solid-phase methods (Keck Facility, Yale University, New Haven, CT). TpoR peptides were purified as previously described for EpoR (37) and reconstituted by detergent dialysis using a 10:3 DMPC/DMPG molar ratio and a ~1:60 peptide/lipid molar ratio. FTIR measurements were made after dialysis. For NMR measurements, the membrane reconstituted peptides were pelleted, lyophilized, rehydrated with deuterium-depleted water (50% ± 5% weight), and incubated at 37 °C for 24 h.

Polarized IR Spectroscopy. Polarized attenuated total reflection FTIR spectra were obtained on a Bruker IFS 66V/S spectrometer. Membranes containing TpoR peptides (~150 μg) were layered on a germanium internal reflection element using a slow flow of nitrogen gas directed at an oblique angle to the IR plate to form an oriented multilamellar lipid–peptide film. One thousand scans were acquired and averaged for each sample at a resolution of 4 cm^{-1}.

Analytical Ultracentrifugation. Sedimentation equilibrium experiments were performed using a Beckman XL-I analytical ultracentrifuge at 25 °C. The solution [15 mM dodecylphosphocholine (DPC), 50 mM Tris·HCl, and 0.1 M NaCl (pH 7.5)] was density matched to account for the buoyancy of DPC micelles by adding 52.5% D_2O (38). Absorbance was measured radially across the cell. Data points were collected in radial increments of 0.001 cm, with each data point representing the average of 10 replicates. Three different peptide concentrations (~20 μM, 35 μM, and 50 μM) and three different speeds (98,784, 129,024, and 185,785 × *g*) were used to ensure the quality of the data. All of the data were analyzed by nonlinear least-squares global curve fitting using the UltraScan II version 9.9 data analysis software. The analysis uses a solvent density ρ of 1.0580 and the partial specific volume for the TpoR peptide of 0.7645 cm^3/g.

Deuterium MAS NMR Spectroscopy. Deuterium NMR spectra were obtained at a ^2H frequency of 55.2 MHz on a Bruker Avance NMR spectrometer using a 4-mm MAS probe and a MAS frequency of 3 kHz. Single pulse excitation was used using a 4- to 7.5-μs 90° pulse, followed by a 4.5-μs delay before data acquisition. The repetition delay was 0.25 s. A total of 600,000–1,500,000 transients were averaged for each spectrum and processed using a 100-Hz exponential line broadening function. Spectra were obtained at 25 °C.

Protein-Fragment Complementation Assay. The cDNA of human wild-type TpoR was inserted between NotI and ClaI restriction sites of pcDNA3.1/Zeo vector upstream of either the hGluc fragment coding amino acids 1–93 (hGluc1) or the fragment coding amino acids 94–169 (hGluc2) of *Gaussia princeps* luciferase (25). Mutants were obtained by QuikChange Site-Directed Mutagenesis (Stratagene). Statistics were calculated using one-way ANOVA using GraphPad. Plasmids for the split luciferase assay coding TpoR and mutants were cotransfected in a ratio of 1:1 (2 μg total DNA per well) in HEK293 cells using Lipofectamine (Invitrogen). Forty-eight hours after transfection, cells were trypsinized, resuspended in 500 μL of cold PBS 1×, pelleted by centrifugation at 4 °C for 1 min, and each pellet was resuspended in 400 μL of DMEM/F-12 (Gibco) containing protease inhibitors. Cell samples were flash-frozen in dry ice for 10 min and thawed in a water bath at 37 °C for 10 min (cycle was repeated twice). After centrifugation (10,000 × *g*, 5 min) the supernatants were collected and aliquoted (100 μL per well) in 96-well white plates (Nunc) to measure the luciferase activity. Native coelenterazine (NanoLight Technology) was reconstituted as a stock solution of 1 mg/mL in methanol and diluted to a final concentration 20 μM in DMEM F12 at room temperature for injection (100 μL). Signal intensities (integrated over 10 s, with an injection delay of 2 s) were read on a Perkin-Elmer Victor X Light analyzer. Aliquots of the supernatants were used also for Western blot determination of TpoR expression levels.

ACKNOWLEDGMENTS. We thank Stephen Michnick (University of Montreal) for the *Gaussia princeps* system and Céline Mouton and Julie Klein for technical and graphics support. Financial support was received from National Institutes of Health Grant GM-46732 (to S.O.S.); a Fonds pour la formation à la Recherche dans l'Industrie et dans l'Agriculture (FRIA) doctoral fellowship (to J.-P.D.); a Delori postdoctoral fellowship (to V.G.); the Fonds de la Recherche Scientifique-Fonds National de la Recherche Scientifique (FRS-FNRS) and Fonds de la Recherche Scientifique Médicale (FRSM) (S.N.C.), Belgium; the Salus Sanguinis Foundation; the Action de Recherche Concertée (ARC) MEXP31C1 and ARC10/15-027 program of the Université catholique de Louvain; the Fondation contre le Cancer; the Belgium Interuniversity Attraction Pole (IAP) Program (S.N.C.); and de Duve Institute and FNRS fellowships (to C.P.).

1. Drachman JG, Griffin JD, Kaushansky K (1995) The c-Mpl ligand (thrombopoietin) stimulates tyrosine phosphorylation of Jak2, Shc, and c-Mpl. *J Biol Chem* 270(10):4979–4982.
2. Royer Y, Staerk J, Costuleanu M, Courtoy PJ, Constantinescu SN (2005) Janus kinases affect thrombopoietin receptor cell surface localization and stability. *J Biol Chem* 280(29):27251–27261.
3. Hubbard SR (2004) Juxtamembrane autoinhibition in receptor tyrosine kinases. *Nat Rev Mol Cell Biol* 5(6):464–471.
4. Solar GP, et al. (1998) Role of c-mpl in early hematopoiesis. *Blood* 92(1):4–10.
5. Yoshihara H, et al. (2007) Thrombopoietin/MPL signaling regulates hematopoietic stem cell quiescence and interaction with the osteoblastic niche. *Cell Stem Cell* 1(6): 685–697.
6. Qian H, et al. (2007) Critical role of thrombopoietin in maintaining adult quiescent hematopoietic stem cells. *Cell Stem Cell* 1(6):671–684.
7. de Sauvage FJ, et al. (1996) Physiological regulation of early and late stages of megakaryocytopoiesis by thrombopoietin. *J Exp Med* 183(2):651–656.
8. Kaushansky K (1997) Thrombopoietin: Understanding and manipulating platelet production. *Annu Rev Med* 48:1–11.
9. Ding J, et al. (2004) Familial essential thrombocythemia associated with a dominant-positive activating mutation of the c-MPL gene, which encodes for the receptor for thrombopoietin. *Blood* 103(11):4198–4200.
10. Onishi M, et al. (1996) Identification of an oncogenic form of the thrombopoietin receptor MPL using retrovirus-mediated gene transfer. *Blood* 88(4):1399–1406.
11. Ding J, et al. (2009) The Asn505 mutation of the c-MPL gene, which causes familial essential thrombocythemia, induces autonomous homodimerization of the c-Mpl protein due to strong amino acid polarity. *Blood* 114(15):3325–3328.
12. Staerk J, et al. (2006) An amphipathic motif at the transmembrane-cytoplasmic junction prevents autonomous activation of the thrombopoietin receptor. *Blood* 107(5): 1864–1871.
13. Pikman Y, et al. (2006) MPLW515L is anovel somatic activating mutation in myelofibrosis with myeloid metaplasia. *PLoS Med* 3(7):1140–1151.
14. Pardanani AD, et al. (2006) MPL515 mutations in myeloproliferative and other myeloid disorders: A study of 1182 patients. *Blood* 108(10):3472–3476.
15. Pecquet C, et al. (2010) Induction of myeloproliferative disorder and myelofibrosis by thrombopoietin receptor W515 mutants is mediated by cytosolic tyrosine 112 of the receptor. *Blood* 115(5):1037–1048.
16. Boyd EM, et al. (2010) Clinical utility of routine MPL exon 10 analysis in the diagnosis of essential thrombocythaemia and primary myelofibrosis. *Br J Haematol* 149(2): 250–257.
17. Beer PA, et al. (2008) MPL mutations in myeloproliferative disorders: Analysis of the PT-1 cohort. *Blood* 112(1):141–149.
18. Matthews EE, et al. (2011) Thrombopoietin receptor activation: Transmembrane helix dimerization, rotation, and allosteric modulation. *FASEB J* 25(7):2234–2244.
19. Staerk J, et al. (2011) Orientation-specific signalling by thrombopoietin receptor dimers. *EMBO J* 30(21):4398–4413.
20. Seubert N, et al. (2003) Active and inactive orientations of the transmembrane and cytosolic domains of the erythropoietin receptor dimer. *Mol Cell* 12(5):1239–1250.
21. Abe M, Suzuki K, Inagaki O, Sassa S, Shikama H (2002) A novel MPL point mutation resulting in thrombopoietin-independent activation. *Leukemia* 16(8):1500–1506.
22. Wimley WC, White SH (1996) Experimentally determined hydrophobicity scale for proteins at membrane interfaces. *Nat Struct Biol* 3(10):842–848.
23. Koffie RM, et al. (2009) Oligomeric amyloid beta associates with postsynaptic densities and correlates with excitatory synapse loss near senile plaques. *Proc Natl Acad Sci USA* 106(10):4012–4017.
24. Kohlhuber F, et al. (1997) A JAK1/JAK2 chimera can sustain alpha and gamma interferon responses. *Mol Cell Biol* 17(2):695–706.
25. Remy I, Michnick SW (2006) A highly sensitive protein-protein interaction assay based on Gaussia luciferase. *Nat Methods* 3(12):977–979.
26. Gurezka R, Laage R, Brosig B, Langosch D (1999) A heptad motif of leucine residues found in membrane proteins can drive self-assembly of artificial transmembrane segments. *J Biol Chem* 274(14):9265–9270.
27. Ebie AZ, Fleming KG (2007) Dimerization of the erythropoietin receptor transmembrane domain in micelles. *J Mol Biol* 366(2):517–524.
28. Ruan WM, Becker V, Klingmüller U, Langosch D (2004) The interface between self-assembling erythropoietin receptor transmembrane segments corresponds to a membrane-spanning leucine zipper. *J Biol Chem* 279(5):3273–3279.
29. Kubatzky KF, et al. (2001) Self assembly of the transmembrane domain promotes signal transduction through the erythropoietin receptor. *Curr Biol* 11(2):110–115.
30. Liu W, Crocker E, Constantinescu SN, Smith SO (2005) Helix packing and orientation in the transmembrane dimer of gp55-P of the spleen focus forming virus. *Biophys J* 89(2):1194–1202.
31. Besancenot R, et al. (2010) A senescence-like cell-cycle arrest occurs during megakaryocytic maturation: Implications for physiological and pathological megakaryocytic proliferation. *PLoS Biol* 8(9):e1000476.
32. Constantinescu SN, et al. (2001) Ligand-independent oligomerization of cell-surface erythropoietin receptor is mediated by the transmembrane domain. *Proc Natl Acad Sci USA* 98(8):4379–4384.
33. Brown RJ, et al. (2005) Model for growth hormone receptor activation based on subunit rotation within a receptor dimer. *Nat Struct Mol Biol* 12(9):814–821.
34. Arkin IT, Brünger AT (1998) Statistical analysis of predicted transmembrane α-helices. *Biochim Biophys Acta* 1429(1):113–128.
35. de Planque MRR, Killian JA (2003) Protein-lipid interactions studied with designed transmembrane peptides: Role of hydrophobic matching and interfacial anchoring. *Mol Membr Biol* 20(4):271–284.
36. Ried CL, Kube S, Kirrbach J, Langosch D (2012) Homotypic interaction and amino acid distribution of unilaterally conserved transmembrane helices. *J Mol Biol* 420(3): 251–257.
37. Itaya M, Brett IC, Smith SO (2012) Synthesis, purification, and characterization of single helix membrane peptides and proteins for NMR spectroscopy. *Methods Mol Biol* 831:333–357.
38. Kochendoerfer GG, et al. (1999) Total chemical synthesis of the integral membrane protein influenza A virus M2: Role of its C-terminal domain in tetramer assembly. *Biochemistry* 38(37):11905–11913.

Supporting Information

Defour et al. 10.1073/pnas.1211560110

SI Substitutions at Positions 514, 516, 517, and 518 Do Not Induce Activation of TpoR

The RWQFP motif is largely conserved in thrombopoietin receptor (TpoR) (Fig. S1), suggesting that each residue in the motif plays a role in the structure or activation mechanism of the receptor. Fig. S2 shows the ability of additional mutations at positions 514, 516, 517, and 518 to constitutively activate the receptor. The mutants were expressed in γ-2A cells cotransfected with JAK2 and tested for ligand-dependent and -independent induction of STAT5-dependent transcriptional activity using the dual luciferase assay.

SI Constitutive Activation of TpoR by W515 Mutants Requires JAK2

In cells, TpoR signals mainly via JAK2 and to a lesser extent via TYK2 (1). We tested signaling of W515 mutants via STATs using the luciferase reporter assay in γ-2A cells, which are deficient in JAK2 but not TYK2 (2). Constitutive activation of STAT5 transcriptional activity is detected in γ-2A cells transfected with JAK2 for both the W515K and W515L mutations. In contrast, the level of ligand-induced and ligand-independent signaling is low in γ-2A cells transfected with TYK2. Data presented in Figs. S3 and S4 indicate that the TpoR W515K mutant is constitutively active only in the presence of JAK2 and not TYK2. Studies performed with engineered TpoR dimers indicate that the W515K mutation seems to induce a dimer interface that is not permissive for activation of TYK2 (Fig. S4). Thus, the dimer induced by the W515K must be distinct from the physiological dimer induced by Tpo.

We next compared signaling by one conformation that is inactive via TYK2 (cc-TpoR-I) in the presence of a constitutive active mutant of TYK2, TYK2 V678F, a mutant homologous to the activating V617F mutation in JAK2 (3). cc-TpoR-I becomes active in the presence of TYK2 V678F (Fig. S4*C*), suggesting that inactive dimeric conformations like cc-TpoR-I fail to trigger TYK2 activation, but once this step accomplished, the receptor dimer could support downstream signaling.

SI Comparison of the Association of TpoR with the Association of EpoR

Erythropoietin receptor (EpoR) and TpoR were fused in frame with Gluc1 and Gluc2 fragments and tested for *Gaussia princeps* luciferase complementation (Fig. S5).

SI Temperature Dependence of Deuterium MAS Side Bands in the TpoR TM Peptides Labeled at Leu512

The loss of NMR intensity in the deuterium magic angle spinning (MAS) spectra of wild-type TpoR transmembrane (TM) peptides suggests that the motion of the peptide interferes with averaging by MAS. To test this idea, the sample temperature was decreased to slow the rotational diffusion of the peptide in the membrane bilayer (Fig. S6).

SI Secondary Structure of the RWQFP Insert by Solution NMR Spectroscopy

Structural studies of TM peptides solubilized in detergent micelles can provide insights into peptide structure. We have undertaken solution NMR measurements of peptides corresponding to the TpoR TM–juxtamembrane (JM) sequence (residues 481–520) to complement our previous solid-state NMR measurements in membrane bilayers (4) and to complement the analytical ultracentrifugation measurements in this study of TpoR peptides solubilized in detergent micelles (Fig. S7). The peptides were expressed as an MBP-His-fusion protein as described by Itaya et al. (5). The MBP and His tags were removed by cleavage with Tobacco Etch Virus (TEV) protease, and the purified protein labeled with ^{13}C and ^{15}N was solubilized in deuterated SDS for NMR experiments.

1. Royer Y, Staerk J, Costuleanu M, Courtoy PJ, Constantinescu SN (2005) Janus kinases affect thrombopoietin receptor cell surface localization and stability. *J Biol Chem* 280(29):27251–27261.
2. Kohlhuber F, et al. (1997) A JAK1/JAK2 chimera can sustain alpha and gamma interferon responses. *Mol Cell Biol* 17(2):695–706.
3. Staerk J, Kallin A, Demoulin JB, Vainchenker W, Constantinescu SN (2005) JAK1 and Tyk2 activation by the homologous polycythemia vera JAK2 V617F mutation: Cross-talk with IGF1 receptor. *J Biol Chem* 280(51):41893–41899.
4. Kubatzky KF, et al. (2005) Structural requirements of the extracellular to transmembrane domain junction for erythropoietin receptor function. *J Biol Chem* 280(15):14844–14854.
5. Itaya M, Brett IC, Smith SO (2012) Synthesis, purification, and characterization of single helix membrane peptides and proteins for NMR spectroscopy. *Methods Mol Biol* 831: 333–357.


```
Rabbit              VLSLSALLGLLLLKWQFPAHYRRLRHALWPSLPDLHRVLGQYLRDTAALSPSKATVT-DS 79
Mouse               VLSLSALLGLLLLKWQFPAHYRRLRHALWPSLPDLHRVLGQYLRDTAALSPSKATVT-DS 550
Cattle              VLSVSALLGLLLLRWQFPEHYRSLRHALWPSLPDLHRVLGQYLRDTAALSPPKAAVS-DV 557
Human               VLGLSAVLGLLLLRWQFPAHYRRLRHALWPSLPDLHRVLGQYLRDTAALSPPKATVS-DT 559
Crabeating monkey   VLGLSAVLGLLLLRWQFPAHYRRLRHALWPSLPDLHRVLGQYLRDTAALSPPKATVS-DT 551
Marmoset            VLGLSALLGLLLLRWKFPAHYRRLRHVLWPSLPDLHRVLGQYLRDTAAPSPPKATVS-DT 565
Guinea pig          VLGLSALLGLLLLRWKFPAHYRRLRHVLWPSLPDLHRVLGQYLRDTAAPSPPKATVS-DT 552
Rhesus monkey       VLGLSALLGLLLLRWKFPAHYRRLRHVLWPSLPDLHRVLGQYLRDTAAPSPPKATVS-DA 552
Squirrel monkey     VLGLSALLGLLLLRWKFPAHYRRLRHVLWPSLPDLHRVLGQYLRDTAAPSPPKATVS-DA 552
                                                    -BOX1-
```

Fig. S1. Alignment of TpoR JM sequences (including W515, red) from different species. Box 1, conserved PxxPxP/x motif required for JAK binding in cytokine receptor type I superfamily.

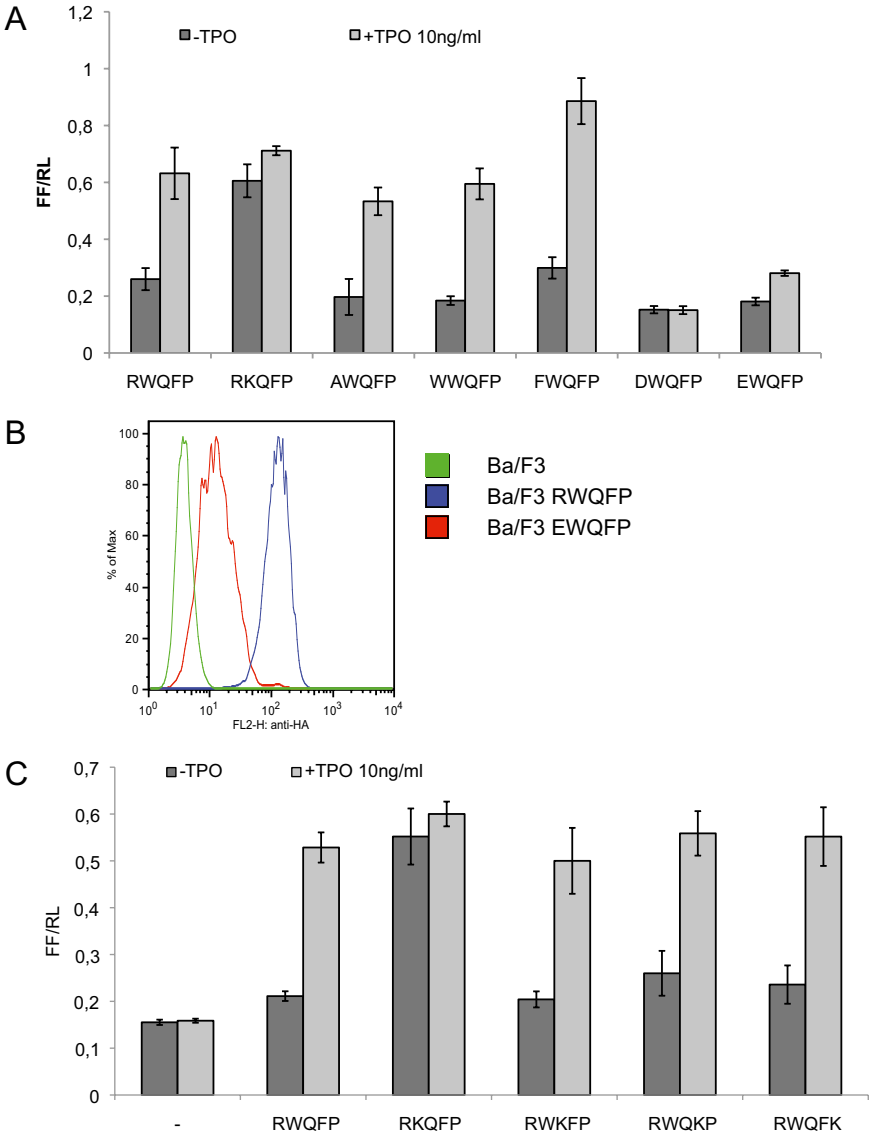


Fig. S2. (*A*) The first residue of the RWQFP motif is conserved as a positively charged arginine or lysine. Mutation of R514 to nonpolar amino acids with either a large (Phe, Trp) or small (Ala) side chain yields receptors that behave like wild-type TpoR (i.e., they do not exhibit constitutive signaling in the absence of Tpo ligand and are fully active in the presence of Tpo ligand). These results demonstrate that a positively charged residue at position 514 is not required for the inhibitory action of W515. Negative charges at position 514 (i.e., R514E) yield receptors that are defective in cell surface localization (*B*), as shown by flow cytometry of cells transduced with equal levels of receptor and stained for HA, the epitope tag placed at the amino terminus of TpoR. Positively charged residues typically define the cytoplasmic boundary of type I membrane proteins (the positive inside rule), and the conservation of Arg or Lys at position 514 may facilitate protein insertion into the endoplasmic reticulum (ER) membrane during synthesis. (*C*) The last three residues of the RWQFP motif are conserved as glutamine or lysine at position 516, phenylalanine at position 517, and proline at position 518. Individual mutations of W515, Q516, F517, and P518 to lysine show that only W515K induces constitutive signaling via JAK2 and STAT5. These results suggest that the occurrence of polar residues at these positions does not influence the ability of W515 to inhibit TpoR activity. With respect to the model proposed for TpoR activation, the presence of charged residues C-terminal to W515 does not influence the ability of the tryptophan side chain to partition into the membrane bilayer and prevent receptor dimerization.

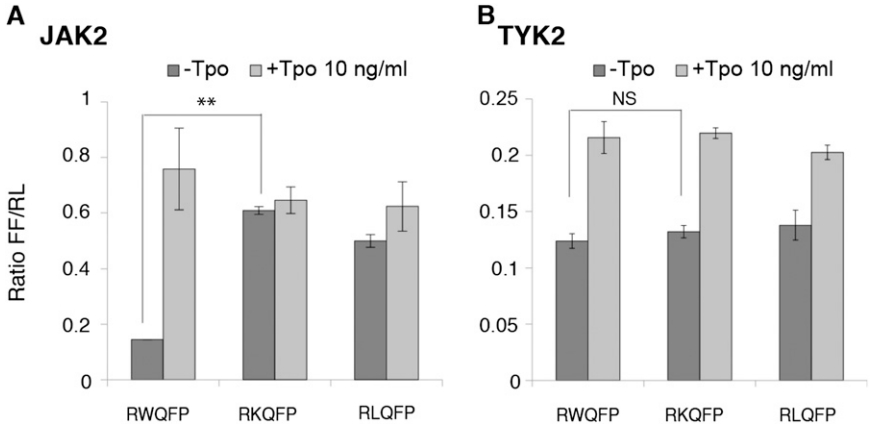


Fig. S3. (*A*) Transient transfection of wild-type TpoR or W515 mutants in γ-2A cells did not induce ligand-independent or -dependent signaling in the absence of JAK2. In contrast, the TpoR W515 mutants were constitutively active by cotransfecting with JAK2. (*B*) Overexpression of TYK2 in γ-2A cells did not allow constitutive activation by TpoR W515 mutants, whereas the Tpo-dependent signaling is still observed. Thus, W515 mutations constitutively activate signaling of TpoR via ligand-independent activation of JAK2.

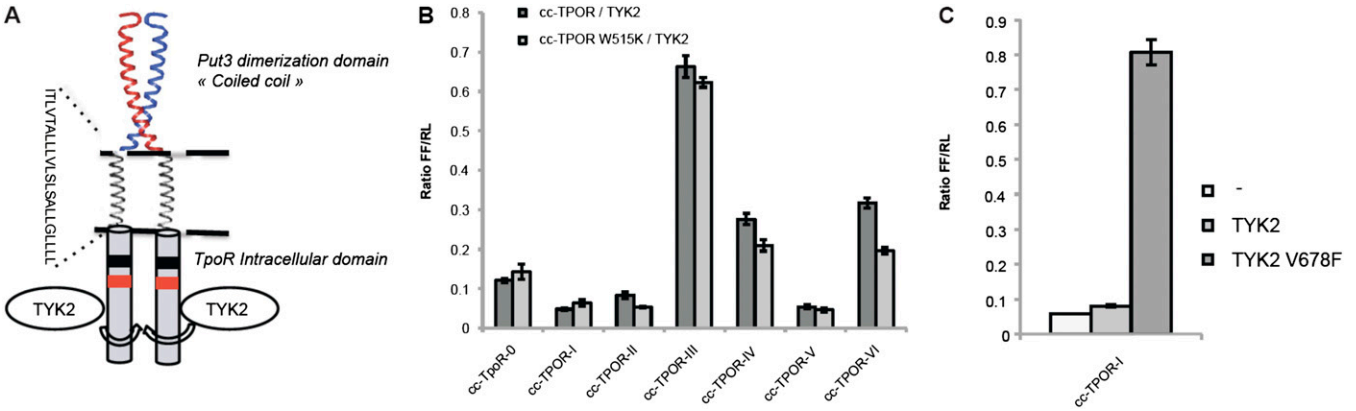


Fig. S4. Introduction of the W515K mutation in engineered coiled-coil TpoR dimers does not change signaling via TYK2. We previously used various engineered coiled-coil TpoR dimers (*cc*-TpoRs) (*A*) that mimic each of seven possible dimer orientations (1). This was accomplished by fusing the Put3 28 amino acid coiled coil with the TM domain of TpoR (cc-TpoR-0) or with progressive deletions of the N-terminal residues of the TpoR TM domain (cc-TpoR-I, II, III, IV, V, and VI). The seven fusion proteins adopt the predicted different dimeric orientations, as shown by cross-linking studies (1). By using these *cc*-TpoR dimers, we found that TYK2 activation can be triggered by only one orientation, represented by cc-TpoR-III and cc-TpoR-VI fusion proteins (1). In contrast, JAK2 could signal in all orientations, except one, cc-TpoR-II (1). Here we show that for TYK2 signaling, introduction of the W515K mutation (human receptor numbering, actually W508K in the mouse TpoR used for the cc-TpoR fusions) does not induce any change from the situation where the wild-type W515 residue is present (*B*, solid bars). Thus, again, the dimeric interface required for TYK2 signaling remains the same after introduction of the W515K mutation, and this is different from the case of JAK2 (1). These differences might be explained by the fact that JAK2 and TYK2 do not bind to the same cytosolic part of the receptor, and TYK2 is believed to bind a lower part of the cytosolic tail, below the Box1 motif (2). One of the dimeric orientations of TpoR that does not support wild type TYK2 signaling, cc-TpoR-I, can support signaling by the constitutive active TYK2 V678F mutant (3), (*C*, solid bars), indicating the defect concerns the activation step and not binding.

1. Staerk J, et al. (2011) Orientation-specific signalling by thrombopoietin receptor dimers. *EMBO J* 30(21):4398–4413.
2. Royer Y, Staerk J, Costuleanu M, Courtoy PJ, Constantinescu SN (2005) Janus kinases affect thrombopoietin receptor cell surface localization and stability. *J Biol Chem* 280(29): 27251–27261.
3. Staerk J, Kallin A, Demoulin J.-B, Vainchenker W, Constantinescu SN (2005) JAK1 and Tyk2 activation by the homologous polycythemia vera JAK2 V617F mutation: Cross talk with IGF1 receptor. *J Biol Chem* 280(51):41893–41899.

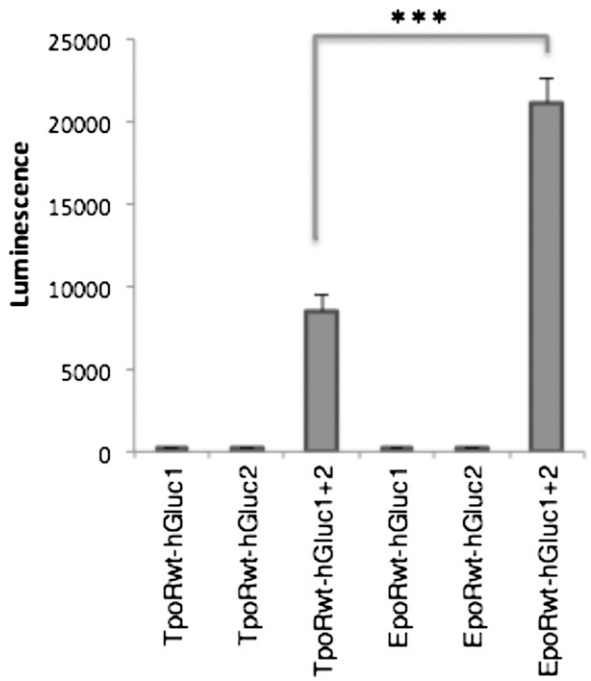


Fig. S5. *Gaussia princeps* luciferase protein fragment complementation assay on HEK293 cells expressing hGluc1 and hGluc2-tagged TpoR and EpoR. Average luminescence of triplicate values ± SD normalized to expression levels of Gluc-tagged proteins by Western blot is shown for one representative experiment out of at least three. ***$P < 0.0001$, ANOVA.

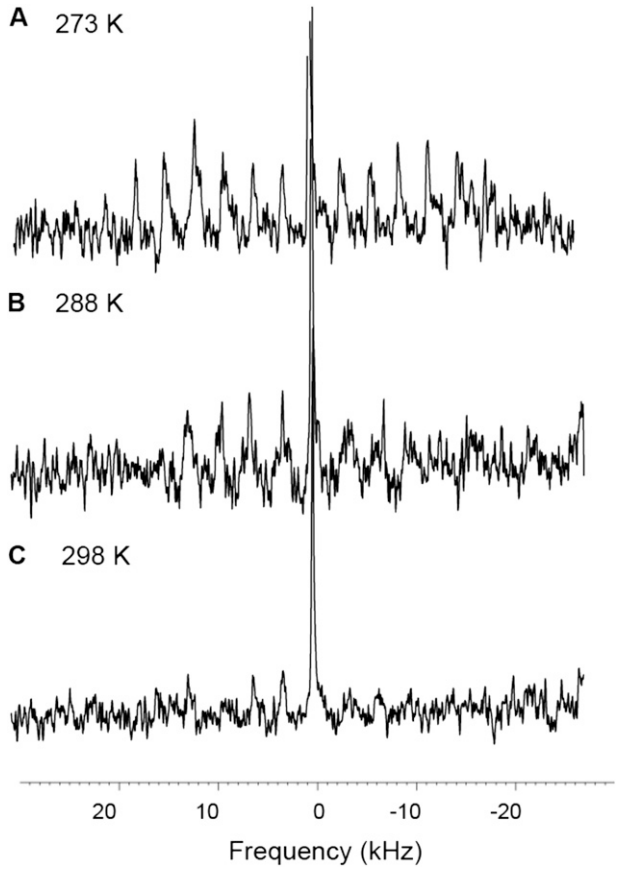


Fig. S6. Temperature dependence of ^{2}H side band pattern in the TpoR TM peptides labeled at Leu512. As the temperature is raised, there is loss of intensity of the deuterium MAS side bands due to increased rotational diffusion of the TM domain of the TpoR. The temperature dependence of the signal intensity is consistent with the suggestion that the frequency of the molecular motion interferes with averaging by MAS. For the W515 mutant peptides, dimerization decreases rotational diffusion, which results in an increase in the side band intensity.

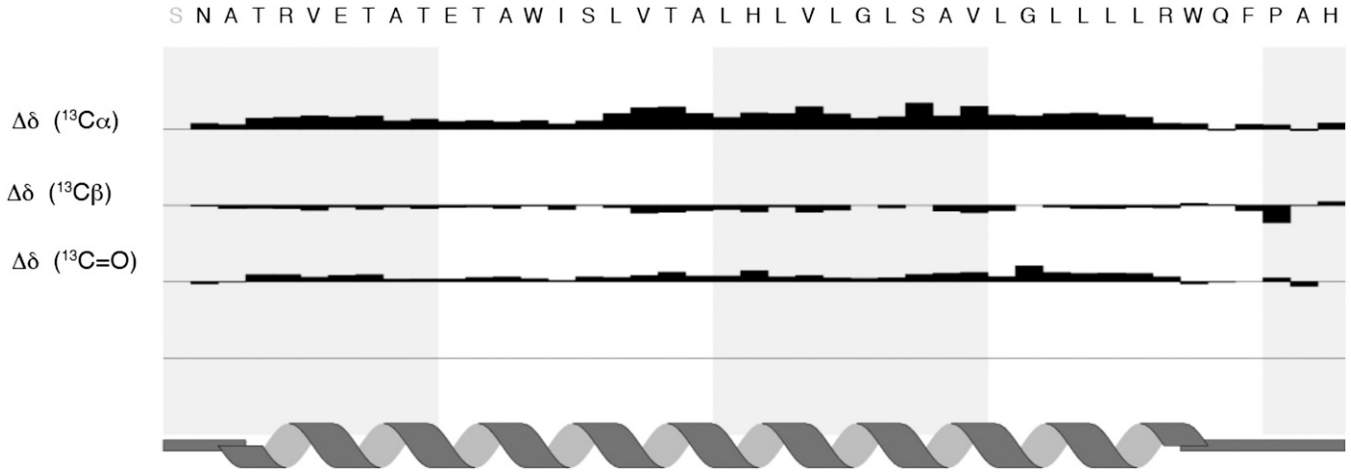


Fig. S7. The TM helix of TpoR TM peptides (residues 481–520) extends through Arg514-Trp515. Solution NMR chemical shift changes characteristic of protein secondary structure are plotted for the TM and JM (RWQFP) region of the TpoR. The output is from the program CCPN (1), which uses the program DANGLE (2) to predict dihedral angle values (and thus, local secondary structure) from the chemical shifts of backbone atoms. The Δδ values for the secondary chemical shifts of the Cα, Cβ, and C′ atoms are measured relative to random coil chemical shifts. Chemical shift deviations from the random coil values provide insight into secondary structure adopted by the peptide, as described by Wishart et al. (3). These deviations from random coil values support the DANGLE-derived data indicating that the residues Arg514-Trp515 are in an α-helical conformation.

1. Vranken WF, et al. (2005) The CCPN data model for NMR spectroscopy: Development of a software pipeline. *Proteins* 59(4):687–696.
2. Cheung MS, Maguire ML, Stevens TJ, Broadhurst RW (2010) DANGLE: A Bayesian inferential method for predicting protein backbone dihedral angles and secondary structure. *J Magn Reson* 202(2):223–233.
3. Wishart DS, Sykes BD (1994) The 13C chemical-shift index: A simple method for the identification of protein secondary structure using 13C chemical-shift data. *J Biomol NMR* 4(2): 171–180.

III.2.4. Unpublished but related results

III.2.4.1. Tryptophan is enriched at the TM-cytosolic edge of type-1 TM proteins

III.2.4.1.1. Single-pass type I

1,226 proteins type I TM proteins were retrieved from the Uniprot database and 1,189 were processed in collaboration with Dr. Ahmed Essaghir The unprocessed proteins either lack a cytoplasmic domain or lack correct annotation of domains. TM domains of single-pass type I proteins are composed of 1.5% tryptophan. Tryptophan has a peak incidence at 8.6% at the end of the postulated TMD (position 0). Thus, Trp is increased **5.7** times at the TM-cytosolic border relative to the mean TM frequency. Aromatic amino acids have almost the same incidence at that position with a tiny increase of Phe and a bit less for tyrosine. As we can observe, positively charged residues are also increased with a peak incidence at +1 (first cytosolic residue) and hydrophobic amino acids start to decrease at position -1 to +1.

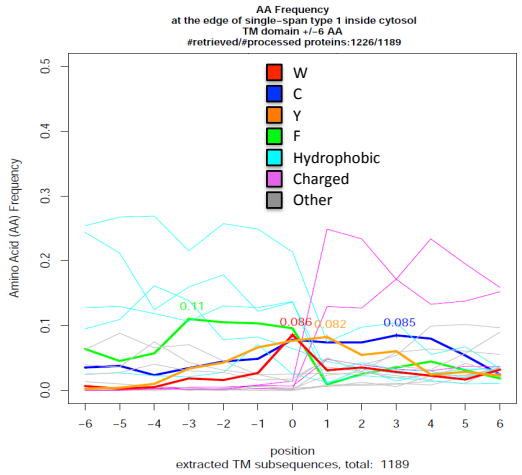


Figure 47 – Amino acid frequency at the edge of single span type I transmembrane domain

III.2.4.1.2. Single-pass type 2

416 proteins were retrieved from the Uniprot database and 397 were processed. Single-pass type II TM domains are composed of tryptophan at a frequency of 2.03 %. Tryptophan has a peak incidence 5% at positions 0 and +2, +3. Phe is more frequent than Trp at position 0 (11%), while tyrosine is less frequent (3%). Trp is **2.5** times increased at the cytosolic border relative to the mean TM frequency.

III.2.4.1.3. Multipass proteins

III.2.4.1.3.1. All multipass TM proteins

2,816 proteins were retrieved from the uniprot database and 1821 were processed. TM domains of multipass proteins are composed of 2.05 % tryptophan. Tryptophan has a peak incidence at position 0 at the cytosolic border of 2.4%. Phe is much more frequent than Trp at position 0 (11%), while tyrosine is also more frequent. In conclusion, for multipass proteins we did not observe a significant increase in Trp at the TM-cytosolic border.

III.2.4.1.3.2. TM proteins with only 2 TMD

132 proteins were processed. Those TM proteins should theoretically be closer to single-pass proteins. We observed a **3.5** fold increase of Trp frequency with a peak at position +1.

III.2.4.1.3.3. Multipass with 3 TMD

48 proteins were analysed. Trp was **4.1** times more frequent at position 0 than elsewhere in the TMD.

III.2.4.1.3.4. More frequent multipass with 7 TMD

On the 862 proteins processed, Trp was not enriched on the cytosolic border of the TMDs of those proteins with a mean frequency of 1,71%. This was also true when each TM domain was analyzed separately, like an individual protein.

Overall, our analysis showed that tryptophan is significantly enriched at the cytosolic borders of the TM domain of type I TM proteins, and to some extent for TM proteins that possess 2 or 3 TMDs, but not for the general class of multispan proteins, and especially not for the 7 TMD proteins. We propose that tryptophan enrichement might occur in order to impair dimer formation and self-activation of type I TMD proteins, such as receptors and adhesion molecules. In contrast, in the abundant 7 TMD proteins, multiple interactions occur between individual helices, and tilt can be imposed by such interactions.

III.2.4.2. Tryptophan at the fourth cytosolic position

RKQWP does not prevent W515K activation. This result could suggest that the inhibitory affect of Trp on receptor activation and dimerization requires its placement in the beginning of the JM motif since mutants WKQFP and RKWFP are effective in reducing constitutive activity of the W515K.

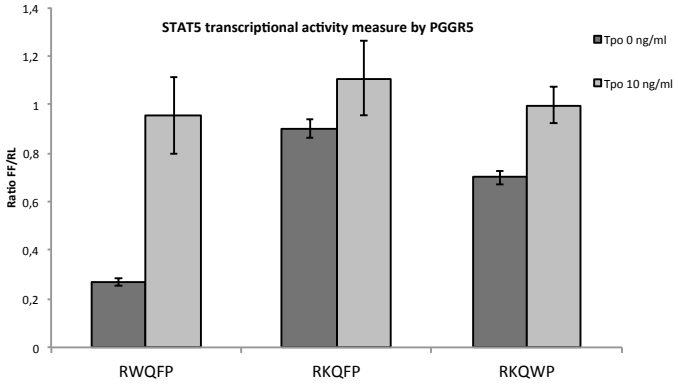


Figure 48 - Luciferase assay: tryptophan at the fourth position in the motif
Figure shows a dual luciferase assay measuring STAT5 transcriptional activity with pGGR5 and JAK2 like in the PNAS paper. RKQWP double mutant activity is not reduced strongly.

III.2.4.3. Tryptophan can prevent self-activation of the receptor even in absence of a charged residue in the motif

As it has been previously shown that the first two residues were critical for preventing TpoR activation with AWQFP, RAQFP and AAQFP being active[97] and as the first residue is conserved as a positively charged residues in nearly all species but the fish, we considered the requirement of an intramolecular cation-π interaction involving W515. As depicted in the western blot and in the following figures, the two mutants AWQFP and WWQFP are not constitutively active and have both a lower basal activity than WT in luciferase assay. Those results demonstrate that the Trp can prevent activation without the need of a positively charged residue in the motif.

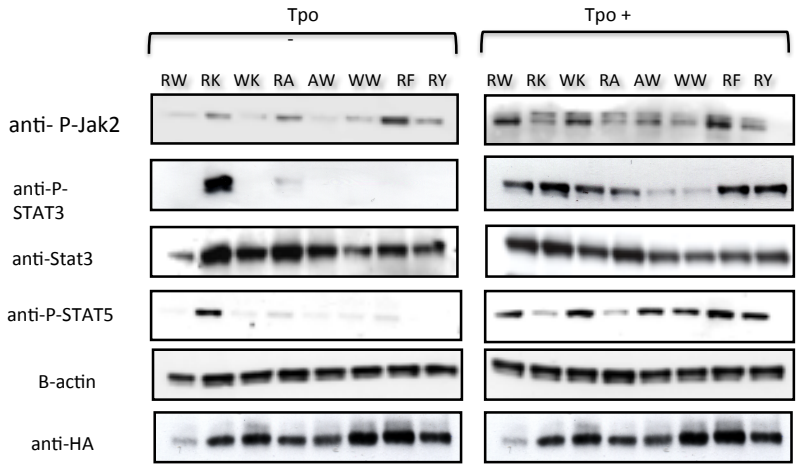


Figure 49 - Western blots results for reversal mutants

Western blot showing the reversal effect mediated by the double mutants W515K R514W (WK) compared to W515K (RK). AWQFP (shown as active in Staerk el al.[97]) behaves like a wild type receptor in human TpoR. (WW) is also inactive which means that an intramolecular cation-π interaction is not required. Notice here that W515F (RFQFP) appears to be more active than W515Y (RYQFP).

III.2.4.4. Reinsertion of a Trp in the murine mutated motif (pMegix vector)

All our PNAS mutants have been made on a human background. Double mutant reversal ability was also confirmed in pMegix vector. This was done with the aim of validating the inhibition of signaling with a murine construct and for future studies in a mouse model with bone marrow reconstitution experiments.

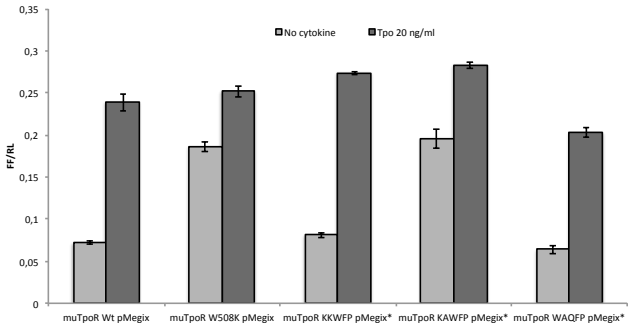


Figure 50 - Luciferase assay of Trp reversal mutants in pMegix
Dual luciferase assay on murine construct: Trp after the W508K or Trp before the W508A are nicely inactivated.

III.2.4.5. The TpoR W515K constitutive activity cannot be inhibited by a tryptophan on the other receptor chain

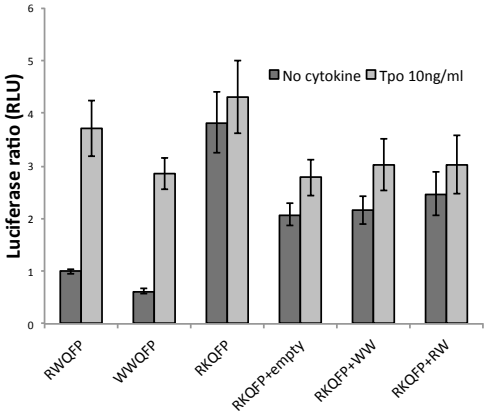


Figure 51 - Luciferase assay: attempt to inhibit W515K via an intermolecular mechanism
Dual luciferase assay of γ2A cells, cotransfected with JAK2 / STAT5 and pGRR5 showing a same level of basal transcriptional activity for W515K (RKQFP) mixed with either WWQFP or TpoR (RWQFP). Notice that WWQFP has lower basal activation level than wild type receptor.

III.2.4.6. Tryptophan reversal effect and the W515A-Q516W (RAWFP) paradigm

Tryptophan reversal effect on W515A mutant was assayed by the dual luciferase reporter assay in γ2A cells and by cell viability in stably transduced BaF3 cells. In the PNAS paper, only the two most frequent mutations W515K and W515L were tested with surrounding tryptophans. JAK2-STAT signaling and cell growth of R514W W515A revertant (WAQFP) were indistinguishable from those of TpoR. Surprisingly, in the case of the double mutants W515A/Q516W, we still observed a strong constitutive activity even if the activity is slightly

reduced. Thus, Q516W can suppress constitutive activity for W515K/L but not W515A mutants.

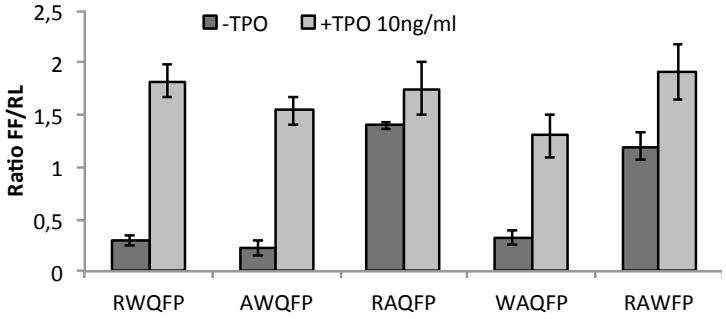


Figure 52 - Luciferase assay: one side Trp reversal of W515A
Dual luciferase assay showing STAT5 induced signaling with W515A RAQFP and reversal with double mutant WAQFP while RAWFP is still active. AWQFP is not active by luciferase.

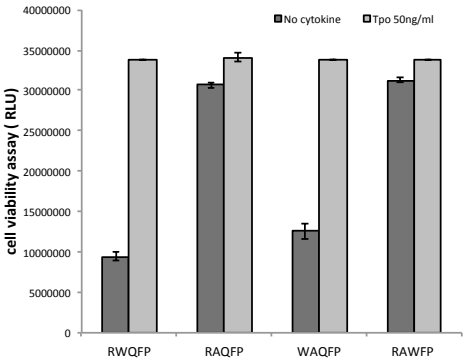


Figure 53 - Cell viability assay: one side Trp reversal of W515A
Cell viability assay showing STAT5 induced signaling with W515A RAQFP and reversal with double mutant WAQFP while RAWFP is still active.

	MW	MW (AUC)	Dichroic ratio	Angle
RWQFP (Wild type)	5360	6960	2,84	29
RKQFP	4306	10630	2,99	24
RAWFP	3989	8558	2,86	28

Table 3 - FTIR data W515K and RAWFP

The RAWFP was confirmed to be dimeric as measured by SE-AUC and possesses a helix tilt close to the wild type TpoR suggesting that the tryptophan is still able to maintain helices tilted and that TM-TM receptor dimerization and helices relative tilt angle are uncoupled. (Results from Miki Itaya and Steven Smith, Stony Brook NY USA)

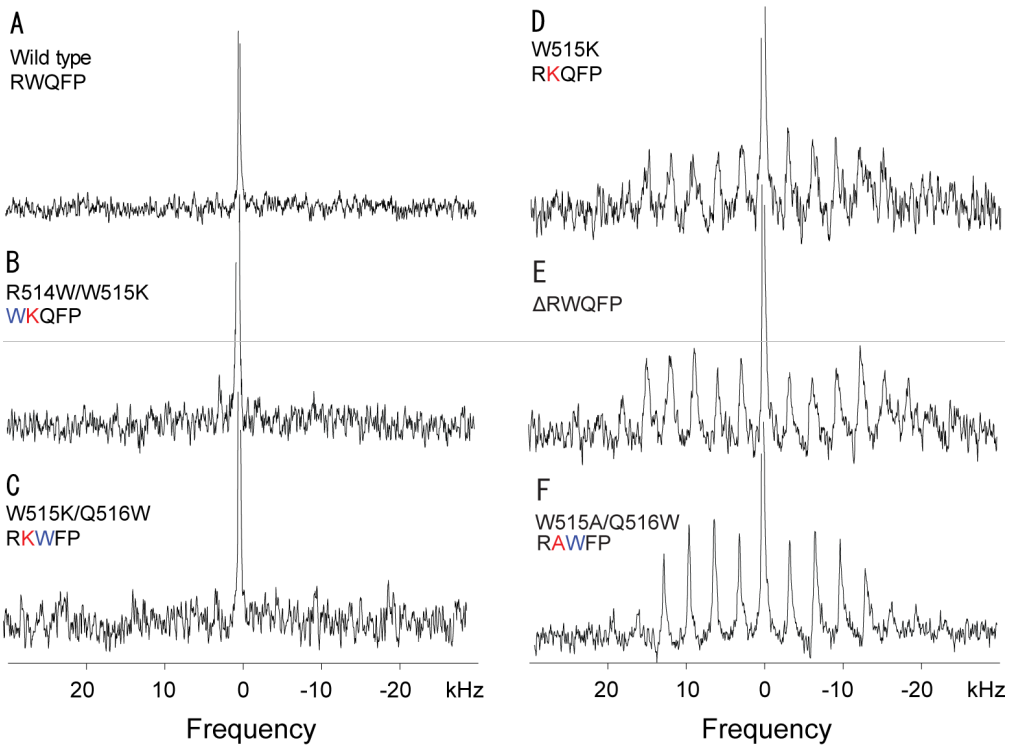


Figure 54 - Deuterium MAS spectra

Mutants on the right including RAWFP show the side band pattern characteristic of a dimer. (Results from Miki Itaya and steven O Smith Stony Brook NY USA)

III.2.4.7. Trp516 reverting effect after small residue at position 515

Our model states that a tryptophan at the beginning of the JM region modulates helix tilt angle and TM-TM interaction. However, the RAWFP, RSWFP and RGWFP double mutant did not fit this model since the Q516W cannot prevent constitutive receptor activation mediated by the W515A/S/G mutants. We hypothesize that not only the presence of tryptophan, but also the size of amino acid adjacent to the tryptophan play a critical role in inhibition of a TM-TM interaction.

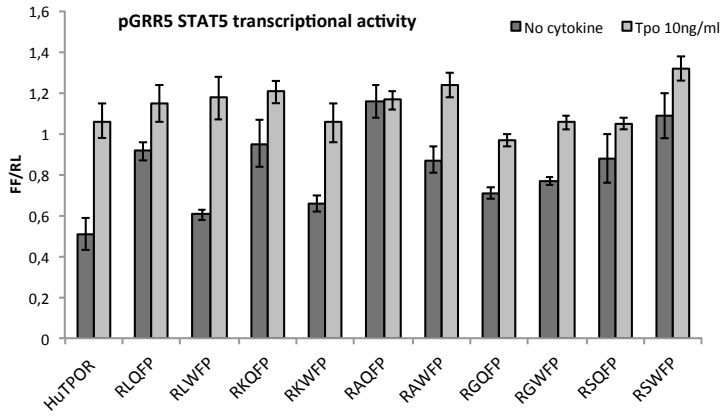


Figure 55 - Luciferase assay: Trp after small residues
Luciferase assay showing the lack of reduction in constitutive activity with small residues placed at position 515. STAT5 transcriptional activity is measured through the pGRR5 reporter (like in our PNAS).

III.3. Preamble: Oncogenic Activation of c-MPL/thrombopoietin Receptor by 17 Mutations at W515: Implications for Myeloproliferative Neoplasms (Leukemia 2015)

Jean-Philippe Defour, Ilyas Chachoua, Christian Pecquet, and Stefan N. Constantinescu
Ludwig Institute for Cancer Research and de Duve Institute, Université catholique de Louvain, Brussels 1200, Belgium

III.3.1. Background

Mutations in c-MPL/thrombopoietin Receptor (TpoR) at position W515 are responsible for 5% of ET and myelofibrosis cases. Our group was the first to describe the W515A activating mutant and the major role that the W515 and the motif play in maintaining TpoR inactive (Staerk et al., Blood 2006). Work from several groups has shown that mutations at W515 are present in ET and myelofibrosis patients and W515L/K/A/R have emerged as the most

prevalent ones. In several sequencing studies other rare mutants or deletions and insertions have been reported.

III.3.2. Questions

Which residues can activate at that position?
Is there any residue that maintains the unliganded receptor as wild type?
Are there residues that are not tolerated at that position?

III.3.3. Author contribution

Here we performed a complete (saturation) mutagenesis at TpoR W515 and also deleted some residues in the RWQFP motif. Ilyas Chachoua assisted with the TpoR cDNAs mutagenesis. I measured the transcriptional activity of γ2A cells co-transfected transiently with one mutant W515 receptor, JAK2, STAT5, pGRR5 "reporter" and pRLTK "normalizer". The cells were lysed after 24 h following transfection and the luciferase activity was measured using Promega dual luciferase reagent. It is noteworthy that the constitutive activity of these mutants can vary with the kind of reporter and the duration of the assay, as demonstrated by Ilyas Chachoua with Spi-luc reporter at 48 and 72h (data not shown). We validated some results by BaF3 cell proliferation assay and by the more definitive *in vivo* mice transplantation assay, thanks to the expertise of Christian Pecquet.

Leukemia (2015), 1–3
© 2015 Macmillan Publishers Limited All rights reserved 0887-6924/15
www.nature.com/leu

LETTER TO THE EDITOR

Oncogenic activation of MPL/thrombopoietin receptor by 17 mutations at W515: implications for myeloproliferative neoplasms

Leukemia advance online publication, 23 October 2015; doi:10.1038/leu.2015.271

Philadelphia negative myeloproliferative neoplasms (MPNs) include polycythemia vera, essential thrombocythemia (ET) and primary myelofibrosis (PMF). Those MPNs are clonal diseases for which the phenotype is almost driven by exon-specific somatic mutations in three genes: *JAK2* exon14, *MPL* exon10 and *CALR* exon9.

MPNs lacking those specific driver mutations are commonly called 'triple negatives', which amount to 15% of ET and PMF and appear to share with phenotypic drivers the ability to activate the JAK/STAT pathway.[1] Beside JAK2 and STATs, MPL/TpoR is a central player in the pathogenesis of MPN being essential for developing a full JAK2 V617F disease in mice.[2] However, the receptor itself can suffer from pathological activating mutations within exon10. Exon10 covers roughly the transmembrane domain (TMD) of TpoR and starts at Trp491 (exoplasmic TMD boundary) to end shortly after Trp515 (cytosolic TMD boundary). Those two tryptophans are predicted to be on the same face of the TMD helix and are capping the TMD helix in the membrane bilayer. Trp515 is found in an amphipathic and helical motif 'RWQFP' that prevents activation of TpoR.[3] Trp515 itself controls dimerization and activation of the receptor.[4] W515S,[5] W515L,[6] W515K,[7] W515A,[8] W515R[9] and W515G[10] were shown to be present in a subset of MPN patients (nearby 4% ET and 8% PMF in large cohorts), or in autonomous cell lines but have never been found in polycythemia vera or other myeloid diseases.[7,11,12] W515L/K mutations are the most prevalent mutations that activate the receptor and recapitulate an ET/PMF phenotype with marked thrombocytosis in murine bone marrow transplant assays.[6,8] Besides missense mutations, rare deletions and insertions around W515 are found in MPN patients.[10,12]

Our goals were: (i) to identify other MPL mutations that should be tested in MPN patients by mutation-specific PCR; and (ii) to determine the amino acid requirements at position 515 to prevent TpoR self-activation.

To these ends, cDNAs coding for HA-TpoR and HA-TpoR mutants were cloned in pMX-IRES-green fluorescent protein (GFP) (for cell line expression) and pMEGIX-IRES-GFP (for bone marrow reconstitution experiments). Vectors were mutated using the QuickChange Site-Directed Mutagenesis Kit (Agilent Technologies, Santa Clara, CA, USA), digested with Dpn-I (NEB) and then used to transform E Coli competent cells. TpoR mutant plasmids were purified for this study using Qiagen kits before being fully sequenced (Qiagen N.V., Venlo, Netherlands). Afterwards, STAT5 transcriptional activity was assessed at 24 h posttransfection by measuring firefly luciferase production in cells transiently transfected using lipofectamine 2000 (Thermo Fisher Scientific, Waltham, MA, USA) by the PGRR5 STATs responsive reporter, JAK2, STAT5 and a pRL-TK internal control. Luciferase ratio were obtained from sequential reads acquire on a Viktor X (Perkin Elmer, Waltham, MA, USA) using DLR reagents (Promega, Madison, WI, USA). Then, to obtain Ba/F3 cell lines stably expressing the TpoR or W515 mutants, retrovirus were produced as described.[3] Infected cells were sorted by fluorescence-activated cell sorting for equivalent GFP levels. The cell proliferation of BaF3 murine pro B cells was measured using a CellTiter-Glo luminescent cell viability assay (Promega). This ATP-based assay was carried out according to the manufacturer's protocol. Cells were first retrovirally infected with virus and plated at 5000 cells/well in RPMI 1640 (Thermo Fisher Scientific)-containing 10% fetal bovine serum for 72 h. Light emission was read with a Viktor X (Perkin Elmer). IL-3 served as an internal control for growth efficiency. For mouse bone marrow transplantation, 10^6 total bone marrow cells retrovirally tranduced with a pMEGIX-TpoR W515C-IRES-GFP retrovirus were injected into 8-weeks-old lethally irradiated C57BL/6 mice as described.[8] Mice were assessed for GFP expression at day 45 and blood was analyzed using a Melet Schloessing MS9-3 cell counter (Melet Schloesing Laboratoires, Osny, France).

In this study, we identify 17 active mutants resulting from substitutions at the Trp515 position. We performed saturation mutagenesis of TpoR Trp515 by mutating position 515 of the full length TpoR to all other 19 amino acids and tested their activity in transcriptional and proliferation assays. Our results show that all polar, charged or hydrophobic residues placed at position W515 activate the TpoR/ JAK2/STAT5 transcriptional cascade in absence of ligand. As previously described,[4] the most conservative aromatic residues show a weaker but significant increase in basal activity confirming the key role of tryptophan at that position. In our hands, only two residues out of 17, namely cysteine (W515C) and proline (W515P) were able to keep the receptor inactive in the absence of Tpo. Although the TpoR W515P mutant shows a defect in responding to Tpo stimulation, W515C can be considered as a fully competent receptor when stimulated by Tpo (Figure 1a, left panel). W515-F517del, where three residues are deleted in the RWQFP motif leads to a '-RXXXPHAY-' motif with a W515P change. This mutant is inactive in the absence of Tpo (Figure 1a, right panel) like the TpoR W515P mutant. In contrast, W515-P518del, where four residues are deleted from the motif leads to '-RXXXXAHAY-' sequence. This mutant is active, with a W515A substitution, like the TpoR W515A mutant (Figure 1a, right panel). Of interest, rare MPN indel TpoR mutants W515-P518delinsAAAA and L513insCTGCTGAGCTGC contains at W515 a lysine or a serine, respectively.[12] Our mutagenesis explains why these mutants are pathogenic as both W515K and W515S are active mutants.

Ba/F3 cells stably expressing the W515C mutant show neither a constitutive growth nor cytokine hypersensitivity (Figure 1b). The growth pattern perfectly matches the one of TpoR wild-type. This is in contrast with the autonomous growth induces by TpoR W515K or by another TMD mutant (S505N) found mainly in familial form of ET.[13]

The W515P also does not allow autonomous Ba/F3 growth, while supporting a full Tpo response (Figure 1c, upper panel). Cell surface localization analysis revealed a mild cell-surface localization defect of W515P, despite a higher level of transcription as

Accepted article preview online 6 October 2015

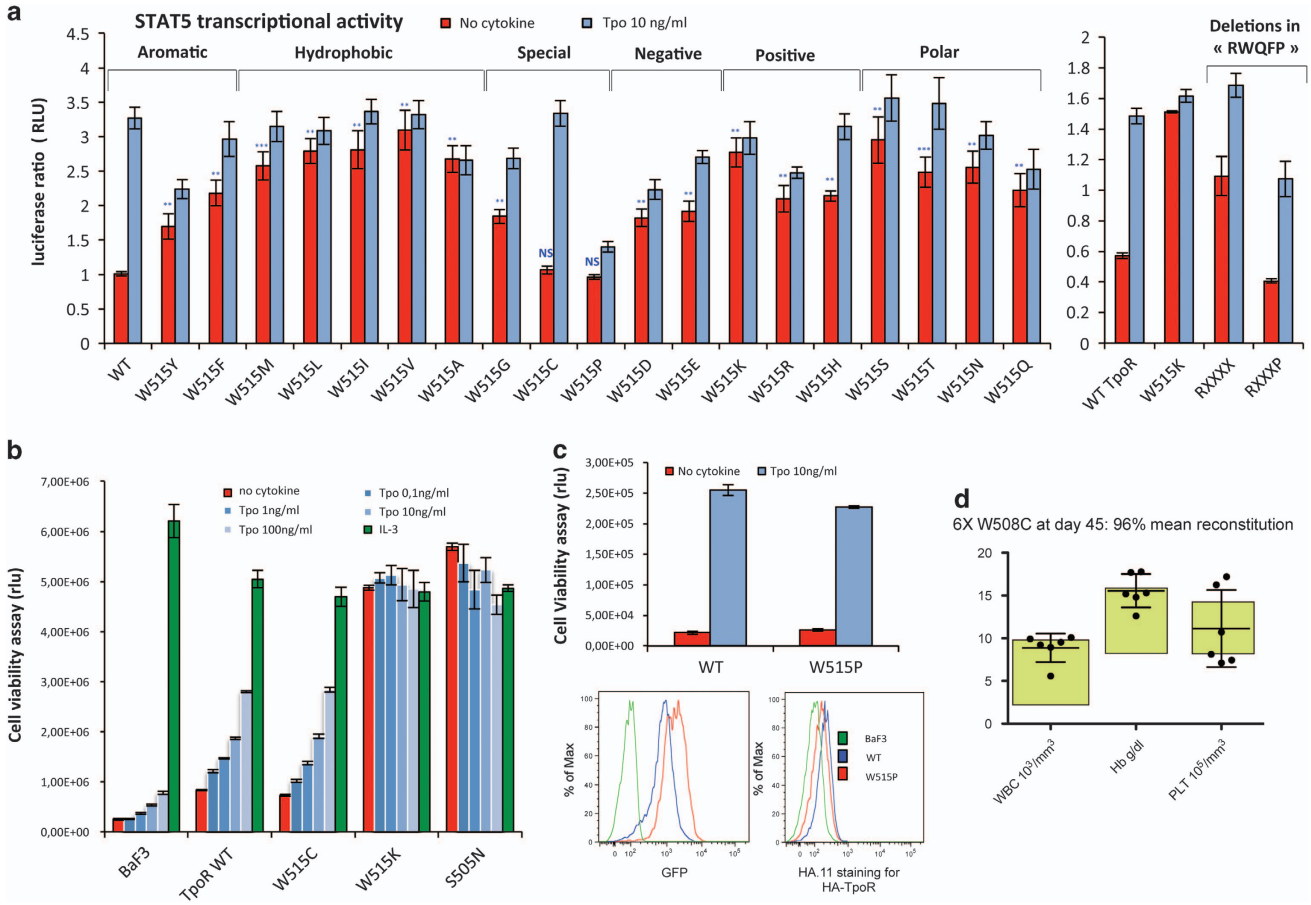


Figure 1. Site-specific W515 saturation mutagenesis (**a**) (left) 17 out of 20 mutations of the TpoR W515 induce constitutive signaling via JAK2 and STAT5. (Right) additional TpoR deletions in the RWQFP juxtamembrane motif (RXXXP or deletion of 3 residues) and (RXXXX or deletion of 4 residues) were tested to mimic W515P or W515A, respectively. The indicated TpoR W515 mutants were expressed in γ-2 A cells cotransfected with JAK2 and tested for Tpo-dependent and -independent induction of STAT5-dependent transcriptional activity. A firefly luciferase reporter (FF), which responds to JAK/STAT1,3,5 pathways was coexpressed with a renilla (RL) luciferase control reporter driven by a constitutive promoter. The luciferase ratio (FF/RL) was used to reduce variability due to cell viability and transfection efficiency. Shown are normalized averages of at least nine replicates ± s.e.m. from three separate experiments. NS, nonsignificant; $*P \leqslant 0.05$; $**P \leqslant 0.01$;$***P \leqslant 0.001$, JMP Pro 11 (SAS Institute, Cary, NC, USA) nonparametric multiple comparison test, Steel test with control. (**b**) Cell proliferation of Ba/F3 cells stably expressing TpoR WT, W515C, W515K and S505N at equivalent expression levels. Proliferation was assessed by CellTiterGlo ATP-based assay (Promega, Sunnyvale, CA, USA) in absence and presence of Tpo. IL-3 in green served as an internal control for growth. (**c**) The TpoR W515P mutant was assayed for cell viability (upper). Cell surface localization of HA-tagged TpoR W515P was measured by flow cytometry (lower). (**d**) Blood parameters were obtained at day 45 by retro-orbital bleeding of six lethally irradiated C57BL/6 mice reconstituted at an average of 96% with the murine TpoR W508C mutant, which is the murine homolog of the human TpoR W515C mutant. Green box represent reference ranges for C57Bl/6 mice.

measured by GFP (Figure 1c, bottom panel). We used bone marrow reconstitution as a stringent test for TpoR W515C activity. Transduction of the TpoR W515C mutant in bone marrow cells and reconstitution were very efficient with near 100% GFP positive cells for each of six mice. Blood counts obtained at day 45 were similar to reference value of normal C57BL/6 with a mean of 8900 WBC/μl, 15.6 g/dl of hemoglobin and a 1 100 000 platelets/μl (Figure 1d). Thus, this mutant is not pathogenic, when we compare with other mutants, like TpoR S505N (not shown) or with TpoR W515L/A mutants.[6,8]

Our data emphasize that seventeen mutations at W515 are potentially oncogenic but only six point mutations have been described to date at this residue in patients. Thus, 11 more mutants could be found in patients, and also deletions or insertions that would place such 11 residues at W515 are predicted to induce oncogenic activation. We showed that tryptophan, cysteine and proline are the only residues maintaining the un-liganded TpoR inactive. W515P prevents full receptor activity probably by disrupting or kinking the helix and interfering with membrane insertion and traffic to the surface. Unlike proline, glycine activates at W515, and glycines are known to be tolerated and mediate interfacial contacts between membrane helices. Surprisingly, cysteine does not activate at W515. Cysteine residues are rare in TM proteins. An exception is found in the cysteine-rich transmembrane (CYSTM) protein family that could protect the membrane from oxygen radical species.[14] It is puzzling that W515A and W515S are active, but W515C is inactive, as these residues all have roughly the same volume. Ser and Cys are both capable of hydrogen bonding. Part of the answer could come from a 1968 paper from Heitmann[15] demonstrating an unexpected hydrophobic nature of the cysteine side chain. Interestingly, a cysteine is found at the equivalent W515 position as in birds (RCTFP motif) or in turtle (RCSFP motif), further supporting the notion that cysteine does not activate TpoR. To validate that

© 2015 Macmillan Publishers Limited

TpoR W515C is not active we used retroviral expression in bone marrow of the murine TpoR W508C and adoptive transplantation. Bone marrow showed a mild increase in cellularity with persistence of adipocytes and without any megakaryocyte hyperplasia or sign of MPN. Mice were sacrificed after 4 month without any evidence of diseases.

This study reports that 17 substitutions at W515 lead to constitutive activation of TpoR. Also, certain delins around W515 that place activating residues at W515 lead to active receptors. We also show that cysteine and proline are the only residues besides tryptophan that do not activate TpoR at position W515. As commercial kits are now only focused on W515K/L and as we are in the beginning of the sequencing era, the region around W515 should be extensively explored in MPN patients.

CONFLICT OF INTEREST

The authors declare no conflict of interest.

ACKNOWLEDGEMENTS

We thank Prof. Steven O. Smith for structural biology insights and Nicolas Dauguet for expert cell sorting. We are grateful for generous support to SNC from the Ludwig Institute for Cancer Research, FRS-FNRS, Salus Sanguinis Foundation, the Action de Recherche Concertée project ARC10/15–027 of the University catholique de Louvain, the Fondation contre le Cancer, the PAI Programs BCHM61B5 and Belgian Medical Genetics Initiative (BeMG), Belgium. JPD and IC were supported by FRIA and Télévie-FRS-FNRS PhD fellowships, Belgium. JPD was also supported by the Cliniques universitaires St Luc, Brussels, Belgium.

J-P Defour, I Chachoua, C Pecquet and SN Constantinescu
Cell Signaling Pole, Signal Transduction and Molecular Hematology, Ludwig Institute for Cancer Research and de Duve Institute, Université catholique de Louvain, Brussels, Belgium
E-mail: stefan.constantinescu@bru.licr.org

REFERENCES

1 Skoda RC, Duek A, Grisouard J. Pathogenesis of myeloproliferative neoplasms. *Exp Hematol* 2015; **43**: 599–608.
2 Sangkhae V, Etheridge SL, Kaushansky K, Hitchcock IS. The thrombopoietin receptor, MPL, is critical for development of a JAK2V617F-induced myeloproliferative neoplasm. *Blood* 2014; **124**: 3956–3963.
3 Staerk J, Lacout C, Sato T, Smith SO, Vainchenker W, Constantinescu SN. An amphipathic motif at the transmembrane-cytoplasmic junction prevents autonomous activation of the thrombopoietin receptor. *Blood* 2006; **107**: 1864–1871.
4 Defour JP, Itaya M, Gryshkova V, Brett IC, Pecquet C, Sato T *et al.* Tryptophan at the transmembrane-cytosolic junction modulates thrombopoietin receptor dimerization and activation. *Proc Natl Acad Sci USA* 2013; **110**: 2540–2545.
5 Abe M, Suzuki K, Inagaki O, Sassa S, Shikama H. A novel MPL point mutation resulting in thrombopoietin-independent activation. *Leukemia* 2002; **16**: 1500–1506.
6 Pikman Y, Lee BH, Mercher T, McDowell E, Ebert BL, Gozo M *et al.* MPLW515L is a novel somatic activating mutation in myelofibrosis with myeloid metaplasia. *PLoS Med* 2006; **3**: e270.
7 Pardanani AD, Levine RL, Lasho T, Pikman Y, Mesa RA, Wadleigh M *et al.* MPL515 mutations in myeloproliferative and other myeloid disorders: a study of 1182 patients. *Blood* 2006; **108**: 3472–3476.
8 Pecquet C, Staerk J, Chaligne R, Goss V, Lee KA, Zhang X *et al.* Induction of myeloproliferative disorder and myelofibrosis by thrombopoietin receptor W515 mutants is mediated by cytosolic tyrosine 112 of the receptor. *Blood* 2010; **115**: 1037–1048.
9 Boyd EM, Bench AJ, Goday-Fernandez A, Anand S, Vaghela KJ, Beer P *et al.* Clinical utility of routine MPL exon 10 analysis in the diagnosis of essential thrombocythaemia and primary myelofibrosis. *Br J Haematol* 2010; **149**: 250–257.
10 Ma W, Zhang X, Wang X, Zhang Z, Yeh CH, Uyeji J *et al.* MPL mutation profile in JAK2 mutation-negative patients with myeloproliferative disorders. *Diagn Mol Pathol* 2011; **20**: 34–39.
11 Beer PA, Campbell PJ, Scott LM, Bench AJ, Erber WN, Bareford D *et al.* MPL mutations in myeloproliferative disorders: analysis of the PT-1 cohort. *Blood* 2008; **112**: 141–149.
12 Pardanani A, Guglielmelli P, Lasho TL, Pancrazzi A, Finke CM, Vannucchi AM *et al.* Primary myelofibrosis with or without mutant MPL: comparison of survival and clinical features involving 603 patients. *Leukemia* 2011; **25**: 1834–1839.
13 Ding J, Komatsu H, Wakita A, Kato-Uranishi M, Ito M, Satoh *et al.* Familial essential thrombocythemia associated with a dominant-positive activating mutation of the c-MPL gene, which encodes for the receptor for thrombopoietin. *Blood* 2004; **103**: 4198–4200.
14 Venancio TM, Aravind L. CYSTM, a novel cysteine-rich transmembrane module with a role in stress tolerance across eukaryotes. *Bioinformatics* 2010; **26**: 149–152.
15 Heitmann P. A model for sulfhydryl groups in proteins. Hydrophobic interactions of the cystein side chain in micelles. *Eur J Biochem* 1968; **3**: 346–350.

© 2015 Macmillan Publishers Limited

III.3.4. Unpublished but related results and discussion

III.3.4.1. W515P and W515C

All the mutations induce a significant increase in the basal level of TpoR activation. This constitutive activity can be further increased by addition of Tpo, suggesting that those receptors are not locked in a fixed conformation, but can still respond to Tpo. W515C and W515P mutants behave as a wild type TpoR.

W515P seems to be less expressed at the cell surface, but the W515P mutant is definitely expressed more than inactive receptor like R102P (found in CAMT patients) in cells transiently electroporated with HA-tagged constructs. W515P could simply be less permissive for physically transmitting the Tpo signal.

We also found that a cysteine at position 515 (W515C) can maintain the TpoR at a low basal activity without any significant difference with the wild type receptor. Interestingly Cys, although comparable to the active residues Ala, Ser and Gly in terms of size or hydrogen bonding abilities, does not activate TpoR when substituted for Trp at position 515. In fact, cysteine side chains have an unexpected hydrophobic nature. This hydrophobic nature of Cys has been revealed in micelles, which strongly depend on hydrophobic interactions for stability. When comparing salt of N-acyl-glycines, N-acyl-DL-serines, and N-acyl-DL-cysteines with the same alkyl length and measuring the critical micelle concentration (CMC), one can observe that the lowest CMC (dilution where micelles disappear) was with N-acyl-cystinates. The lower CMC of the N-acyl-cystinates indicate that the cysteine side chain is involved in the hydrophobic bonding system of the micelle.[301] A low CMC of N-acyl-cystinates corresponds to a higher stability of the micelles. CMC was measured by the absorbance of a mixture of the sodium salts and a dye (rhodamine) followed by subsequent dilution with pure rhodamine. The absorbance of the dye varies if it is in the bulk phase or in the micelle. Last but not least, Cys at position 515 could be post-translationally modified, and in that form act like W515 to inhibit activation. While we cannot exclude this, we believe it to be unlikely. Post-translational modifications at the TMD border cannot be 100% efficient, and any non-modified W515C would generate autonomous cells. In our proliferation assays we can detect 1/10,000 or 1/100,000 cells as autonomously growing. Or, we never detected autonomous growth for BaF3 cells expressing TpoR W515C.

III.3.4.2. Deletion in the RWQFP

Indels around W515 have been discovered in patients. We therefore investigated certain deletions in the RWQFP motif, such as: deletion of Trp at position 515 (Δ515), leading to RQFPA, or deletion of the entire human RWQFP motif (Δ5), resulting in AHYRR. Both are weakly active mutants compared to the clinically relevant mutations (W515L/K/R/A) as measured by luciferase assays in γ2A with STAT5, STAT3 and STAT1 (PGRR5) reporter. Murine Δ5 has been shown to be very active in two independent studies.[97,250] The differences

we observed here with the human Δ5 could be due to a lack of sensitivity of our assay, or by differences in serum composition. The Δ515 mutant is very weak by pGGR5 but seems to be more active with the Spi-luc sensitive STAT5 reporter. Nevertheless, perhaps it is unsurprising that Δ515 is more strongly activating than the deletion of the entire RWQFP motif as it puts a Q at position 515, which is a strongly activating mutant (W515Q).

Deletion of the last four "WQFP" (RΔ4) in the motif leads to RAHYR, which is strongly active like the RAQFP (W515A). Deletion of "WQF" (RΔ3P) results in RPAHY, which is inactive like the RPQFP. These data suggested that the sequence of the residues present at the TM-JM junction is critical. Additionally, the deletion of "WQF" (RΔ3P) reduces Tpo induced response. This effect was also seen with the W515P mutant and with the (Δ4P) where a proline is still present in the initial residues of the novel motif. Deletion of the first four (Δ4P) was active and considerably stronger than the Δ5. The neo motif AHYRR in the Δ5 conserved hydrophobic, aromatic and positive residues.

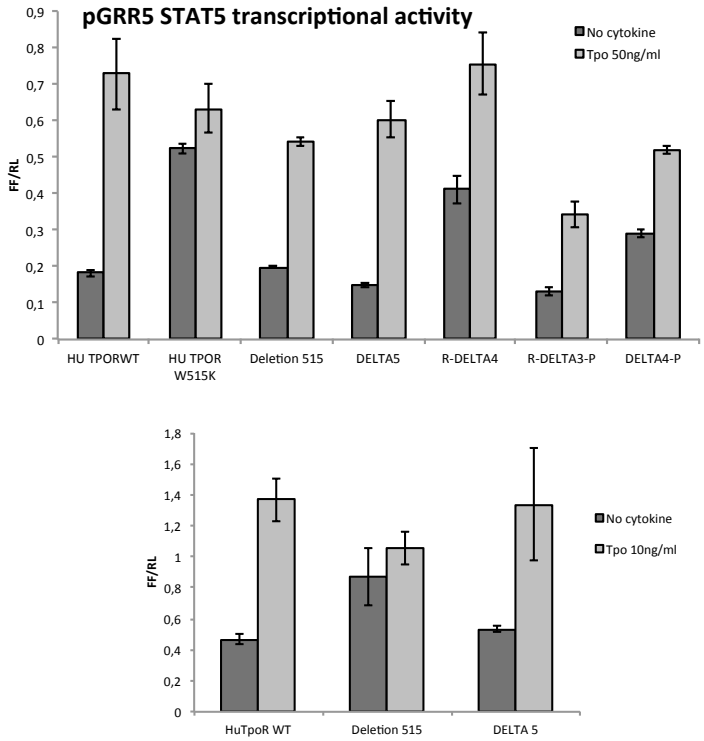


Figure 56 - Luciferase assay of deletions in the motif
Dual Luciferase assay with pGGR5 (top) or Spi-Luc (bottom)

III.3.4.3. Insertion of the KWQFP in murine EpoR

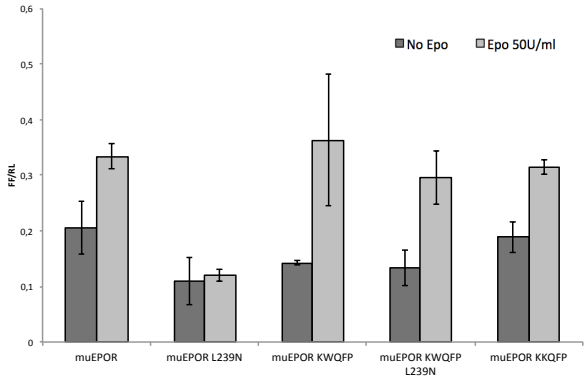
Epo receptor (EpoR) has been extensively studied and exists as a preformed dimer. EpoR activation is stimulated by a structural reorganization of the dimer induced by Epo binding. Introduction of an Asn (L239N) – the EpoR homolog of HuTpoR S505N activating mutation - in the TM of muEpoR is not tolerated for EpoR function. L239N mutation probably either fixes the EpoR in one of its inactive conformation (cc-EpoR-V or I)[136] or prevents proper trafficking to the cell surface, as it is the case for some huTpoR Asn mutants.

EpoR lacks a RWQFP motif and inserting a KWQFP inhibiting motif[97] reduced slightly the basal activity, supporting a minimal inhibitory function on EpoR itself.

However, the KWQFP motif restores the ability of L239N to respond to Epo. One can speculate that the KWQFP allows a greater degree of freedom for further Epo induced rotation or restores normal cell surface localization.

The EpoR mutant containing the KKQFP motif mutation (homologous to HuTpoR W515K) is similar to a wild type EpoR without a KWQFP motif, neutralizing the extremely weak inhibitory function of the RWQFP motif in that assay. However, KKQFP does not constitutively activate the already dimeric EpoR.

```
EpoR+del5   : WSAWSEPASLLTASDLDPLILTLSLILVLISLLLTVLALLKWQFPSHRRTLQQKIWPGIPSP
EpoR+W515K  : WSAWSEPASLLTASDLDPLILTLSLILVLISLLLTVLALLKKQFPSHRRTLQQKIWPGIPSP
S498N+Del5  : WSAWSEPASLLTASDLDPLILTLSLILVLISNLLTVLALLKWQFPSHRRTLQQKIWPGIPSP
muEpoR      : WSAWSEPASLLTASDLDPLILTLSLILVLISNLLTVLALL     SHRRTLQQKIWPGIPSP
```



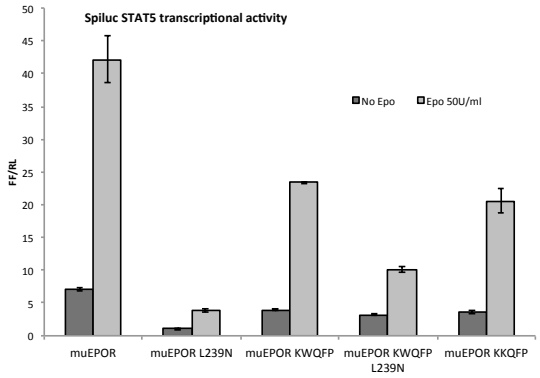


Figure 57 - Luciferase assay of EpoR with Asn and KWQFP motif insertion
Dual Luciferase assay with pGGR5 (top) or Spi-Luc (bottom)

III.3.4.4. The RCTFP or RCSFP motif

When aligning TMD of different species according to Box 1, using Clustal Omega[302] and confirming the TM topology with MEMSAT3[303], we observed that birds and some reptiles have the RCTFP motif instead of the RW_{515}QFP motif. The green sea turtle (*Chelonia Mydas*) possesses a similar motif, RCSFP. The figure below shows that both the RCQFP and the RCTFP motifs can replace the RWQFP in the context of the human receptor and maintain a normal receptor function when compared with human W515K/L/A and murine S498N mutant. RCTFP (the chicken homolog) does not respond to Tpo as well as RCQFP.

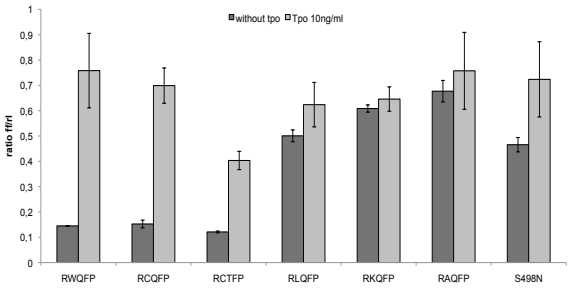


Figure 58 - Luciferase assay of the cystein containing motifs
Dual luciferase assay comparing the avian motif RCTFP and RCQFP in the context of Human TpoR to other W515 and Asn mutants.

III.3.4.5. Mutation at position Q516

Q516 seems to be the second most important position after W515. Glutamine at position 516 is quite conserved, but is a lysine in the marmoset and in the black-capped squirrel monkey and a Ser or a Thr, as mentioned previously, in birds and some reptiles. This position is mainly conserved as Glu, Thr, Ser, Lys or Phe in vertebrates. The importance of this glutamine

might not be immediately obvious, but the following mutagenesis studies suggest that Trp515 mediated inhibition is influenced by position 516.

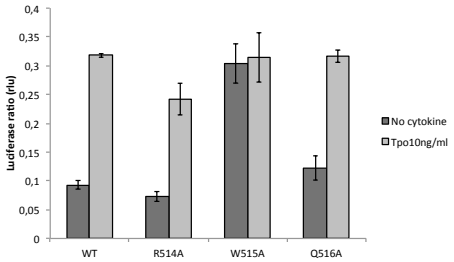


Figure 59 - Luciferase assay of alanine mutation at first, second and third position in the motif
R514 does not activate the receptor but some mutations at position Q516 can weakly activate the TpoR as compared to W515A mutant.

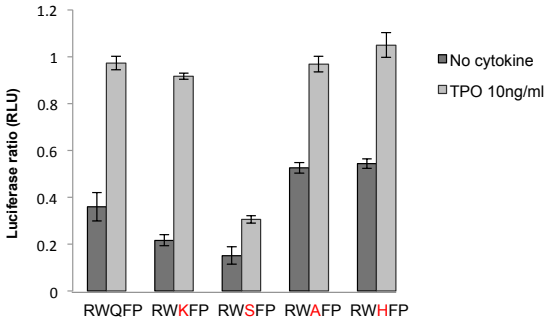


Figure 60 - Luciferase assay of mutations at Q516
Some mutants at Q516 positon are able to weakly activate the receptor, while Serine and Threonine do not allow full Tpo response. RCTFP was shown previously to not fully respond to Tpo. Another Q516 mutant RWSFP also does not respond to Tpo. It appears that residues bearing a hydroxyl group at position 516 do not allow full receptor activity. As discussed previously, a Ser or a Thr are present in birds and turtle at position Q516. Threonine seems to reduce receptor response but does not activate the receptor. We observed also a weak but significant constitutive activity for Q516A and Q516H RWHFP. This suggests that the Q516 position plays a role in maintaining the receptor inactive and these subtle differences can activate the receptor.

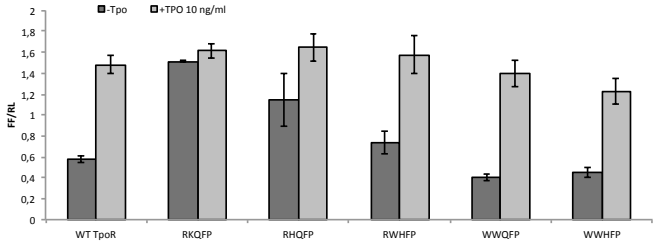


Figure 61 - Luciferase assay of active W515H and Q516H and the requirement of two Trp for efficient control
We can observe that the tandem Trp in the initial positions of the motif maintain the receptor or Q516H in an inactive conformation more effectively than WT.

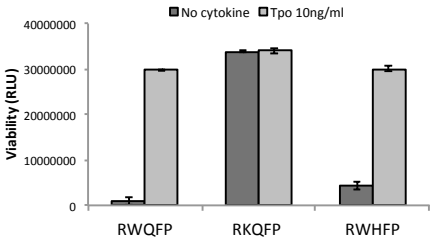


Figure 62 - Cell viability assay showing activity of Q516H
We observe a small autonomous growth for Q516H.

III.3.4.6. The RRFFP (W515R Q516F) or RKFFP (W515K Q516F) motif

W515R/K mutants are found in patients with MPN and are very strongly activating mutations. These two mutants can be restored to wild type levels of basal activity by substituting Q516 with an aromatic residue as shown in our PNAS 2013 paper for RKWFP.[304] This succession of two positive followed by two aromatic residues is found in the opossum motif as RRFFP. This opossum motif RRFFP suggests a kind of cation-π interaction or at least for an amphipathic nature of the motif. Placing a phenylalanine at position Q516 after the W515K/L annihilated the constitutive activity of those two mutants. Notably, this is also the case with the more sensitive spi-luc reporter assay. W515K/R, Q516F double mutation could either allow dimerization in an inactive orientation or maintain the helix as a monomer. In both cases, the suggestion is that this region remains helical. Placing a phenylalanine before the W515K (FKQFP) reduced activation but still weakly activates the receptor and FWQFP is inactive (Fig.S2 PNAS). Overall, these results reinforce the concept of the requirement of aromatic and charged residues within the motif and the role of Q516 in stabilizing the inactive state.

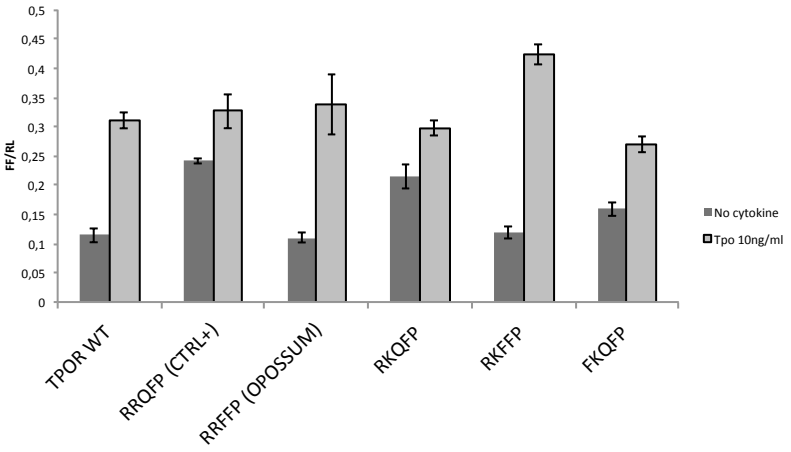


Figure 63 - Luciferase assay via pGGR5: Q516F controls W515R or W515K active mutants

pGRR5 STAT5 transcriptional activity: (positive-positive-aromatic-aromatic) maintain the receptor in an inactive state: validation by opossum TpoR sequence (RRFFP).

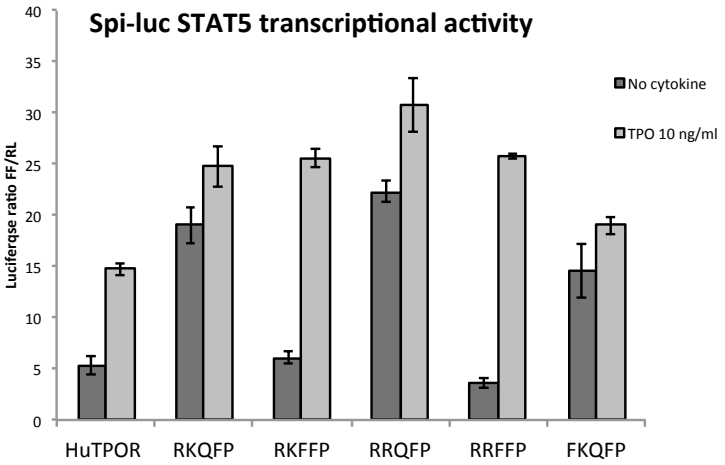


Figure 64 - Luciferase assay via spi-luc: Q516F controls W515R or W515K active mutants
spi-Luc sensitive STAT5 transcriptional reporter: (positive-positive-aromatic-aromatic) maintain an inactive state of the receptor: validation by opossum TpoR sequence (RRFFP).

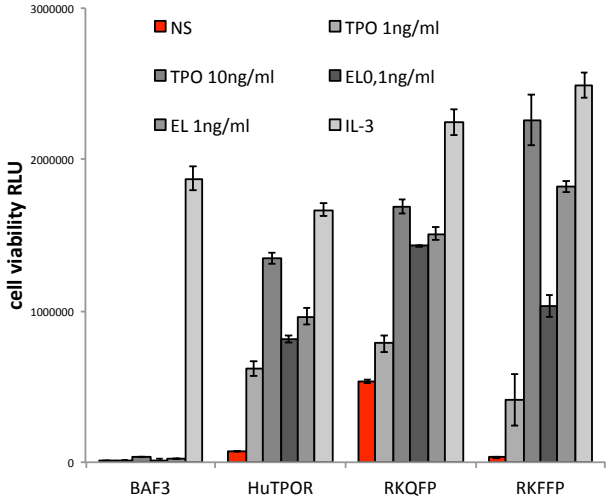


Figure 65 – Cell viability assay: Q516F controls W515K active mutant
Cell viability assay showing that RKFFP is inactive in absence of ligand (red), but can be stimulated more efficiently by Tpo and Eltrombopag (EL), as is also observed in the spi-luc transcriptional activity assay above.

III.3.4.7. Phylogenetic analysis of TpoR

A phylogenetic analysis was realized using Clustal Omega[302] and display using iTOL v2 (interactive tree of life) in an unrooted visual mode.[305] We can observe that TpoR full-length

sequences of 85 different species segregate in five main clusters including mammals (red), marsupials (purple), birds (yellow), fish (blue) and reptiles.

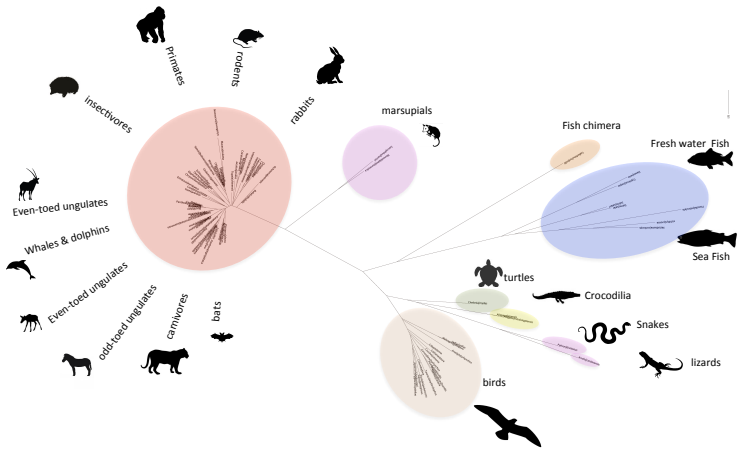


Figure 66 – Evolutionary clusters based on full lenght TpoR sequence

A unique evolutionary cluster includes the marsupials like the opossum with the RRFFP motif and the Tasmanian devil with RRLFP.
The most primitive version of the TpoR is found in the fish chimera (ghost shark), which is the oldest cartilaginous fish alive. The ghost shark genome is a useful reference genome for understanding the origin of mammalian genomes including humans.

Entire sequences of TpoR from 85 species were run with Clustal Omega[302] and a small portion encompassing the extracellular WSXWS motif up to the intracellular Box 1 are shown in the following table. We observe that birds have an insertion of an additional 30 residues at the extracellular JM junction, which is strongly charged and polar. The WSXWS motif and the box1 are very well conserved among all species.

The predicted TMD by MEMSAT3 helix prediction software[306] of some lead species is in bold.

Name	TM sequence alignment
Zebrafish	WSDWSKPVTTNLPLSKEW----------IIFVCIPVALI-------IFATAV-ISFFSRYFRKVKRS---LWPPVPNL
Wild common carp	WSDWSKPLNVLLPLGKEW----------IFIVCIPVALL-------IIASAM-ISFFSRYFRK**V**KKT---**FW**PSVPNL
Salmon	WSDWSPPLTVDTPSDIGA----------LFILCIPLMML-------ILSVVF-LSMFSRYLSK**L**KRY---**LW**PPVPKL
Salmon	WSDWSPRLTVDTPSDIGA----------L-ISCIPLMMI-------VVSVVF-ISMLSRYLSK**L**KQY---**LW**PPVPNL
guppy	WSDWSDVLSGTTTDHTDM----------KLLWCLCVSMP-------IITIFF-ITTVLLYRRK**L**KLL---**FW**PPVPNL
Crocea Clam	WSDWSDVLHDHTPTDRGK----------WLMLCIPALML-------IPAVIL-IYLFPMYLSK**L**KLY---**FW**PPVPNP
Black cod	WSDWSDVLTGETPADAGK----------LLILSIPVALL-------IMAIIV-ISLFPTYLRKLKLY---FWPPVPNL
Chinese alligator	WSAWSEAVVVQAPSE----------AG**WVVPSLAAVPL-----FFTGLLLALRCTFPSA**Y-SS**V**KQK---**LW**PPVPDL
American alligator	WSAWSETVVVQAPSE----------AGWVVPSLAAVPL-----FFTGLLLVLRCTFPSAY-SS**M**KQK---**LW**PPVPDL
Green sea turtle	WSAWSETIVVEAPSGAGMGSKDTGE----------PDAFTAPFS**VPGWIILSLTITL------FFFVGLLGLRCSFPSV**Y-SS**V**KRK---**LW**PPAPDL
Chicken	WSAWSQPVVVDVAAEAGKGREGAEGARGRAEEN----QRAVQNRRS**VAGWVIPSVTVAPL-----IFTGVLLGLRCTF**PSLY-SS**V**KQR---**LW**PPVPDL
Wild turkey	WSAWSQPVVVDVAAEAGKGRAGLR-APGWEEEN----RPAVRNRPSVAGWVIPSVTVAPL-----IFTGVLLGLRCTFPSLY-SS**V**KQR---**LW**PPVPDL
Downy woodpecker	WSAWSKPVVVDAMAD----------TGWIIPSATVVPLL----LFTAVLLGLRCTFPSFY-SN**V**KQK---**IW**PPVPDL
>Cathartes|aura	WSAWSKPVVVDTMADAQRVTGLPRAQ----WWWV-WEGLQCQHSSSDAGWVIPSVTVVPL-----LFTGVLLGLRCTFPSLY----------
American crow	WSAWSKLVVVDAMGDAGKGRGRGGGCGQKSHTADSRRRLQFQRSSSDTGWLIPSVTVVPL-----LFLAMLLGLRCTFPSLY-SN**V**KQK---**LW**PPVPDL
Collared flycatcher	WSAWSKPVVVDAVADVGKGQGRAGGCGQRSHTADR-GRRRFQRSSSDAGWLIPSVTVVPL-----LLSAVLLGLRCTFPSLY-SN**V**KQK---**LW**PPVPDL
Ground tit	WSAWSKPVVVDAMADAGKGQGRAGGWS--SQAADR-RRRRFQRSSSDAGWLIPSVAVVLL-----LFSAVLLGLRCTFPSLY-SN**V**KEK---**LW**PPVPDL
Atlantic canary	WSAWSRPVVVDAMADAGKGQGCCEGLR--GGGV-W-EGLQIRRSSSDAGWLIPSVTVVPL-----LFSAVLLGLRCTFPSLY-SN**V**KQK---**LW**PPVPDL
Red-crested turaco	WSTWSKPVVVDAMADAGKGQGRSIGCSQRSHTAK-GRRPRSQQSSYNAGWLVPSVTVVPL-----LFTGVLLGLRCTFPSLY-SN**M**KQK---**IW**PPVPDL
Anna's hummingbird	WSAWSKPVVVDTMANAGKGRGCSQRSTCLRAEDP-ELGLQSQCSSFDTGWIIPSITVVPL-----LLTGVLLGLRCTFPSLY-SN**V**KQK---**LW**PPVPDL
Common cuckoo	WSAWSKPVVVDAMADAGKGQVGSGGCVQQSCRAK-GR--ICQRSSSDADWIIPSVTVVPL-----VFTGVLLGLRCTFPSLY-SN**V**KQK---**LW**PPVPDL
Rock dove	WSAWSKPVIVDAMADAGKGRDRSDGCCHRSNTAE-GRSLGSQHLSSDAGWIIPSVTVVPL-----LFTGVLLGLRCTFPSLY-SN**M**KQK---**LW**PPVPDL
Peregrine falcon	WSAWSKPVVVDAMADAGKGQGRSGGATRLTAEDX-E-WLQSQRSSPGAGWIIPSVTVVPL-----LFTGVLLGLRCTFPSLY-SN**V**KQK---**LW**PPVPDL
Emperor penguin	WSAWSKPVMVDAMADAGKGQGRSGGCSQRSHTEE-G-DRASQHSSSNAGWIIPSVTVVPL-----LFTGVLLGLRCTFPSLY-SN**V**KQK---**LW**PPIPDL
Adélie penguin	WSAWSKPVMVDAMADAGKGQGRSGGCSQRSHTEE-G-DRASQHSSSNAGWIIPSVTVVPL-----LFTGVLLGLRCTFPSLY-SN**V**KQK---**LW**PPIPDL
python	WSAWSELVCVDVPPGA----------D**SVIMIVA-IALL----LCAGLVLGLGFTCLSNY**SSS**V**KQK---**LW**PPIPDL
Carolina anole lizard	----------TIL**NIG-VLLL----FCTGLLLGVVCIGLPIY-STVK**QK---**IW**PPIPDL
Australian ghostshark	WSSWSDTFTATIPGPMGV----------T**TVA---LITG------SVLLLVIALIMPRLIFPNA**Y-SNVKKK---**LW**PQIPNL
northern white-cheeked gibbon	----------SHSSY**TFAVF----LFVHMMLVPQRL-TQIW-HPL**QH-ER**L**RHA---**LW**PSLPDL
Przewalski's horse	WSAWSDPVRVET-----A----------SETGEG**PAG----------RRR-HAAARFPAHY**-RS**M**RHA---**VW**PSLPDL
Chinese hamster	WSAWSPPARVDT-----G----------SETAWISL**VTALF-LVLCLSVLLGLL-LLKWQFPA**HY-RR**L**RHT---**VW**PSLPDL
black-capped squirrel monkey	WSSWSDSAKVET-----A----------SETAWISLVTALF-LVLGLSALLGLL-LLRWKFPAHY-RR**L**RHV---**LW**PSLPDL
Alpaca	WSPWSDPAWVET-----S----------SETAWISLVTSLL-LVLGLSALLGVL-LLRWQFPEHY-RS**L**RHA---**LW**PSLPDL
Wild Bactrian camel	WSPWSDPSWVET-----S----------SETAWISLVIALL-LVLGLSALLGLL-LLRWQFPERY-RS**L**RHA---**LW**PSLPDL
Bactrian camel	WSPWSDPSWVET-----S----------SETAWISLVIALL-LVLGLSALLGLL-LLRWQFPERY-RS**L**RHA---**LW**PSLPDL
Dromedary	WSPWSDPSWVET-----S----------SETAWISLVIALL-LVLGLSALLGLL-LLRWQFPERY-RS**L**RHA---**LW**PSLPDL
aardvark	WSAWSGPVIVET-----A----------SETAWISLVTALL-LVLGLSVLLGLL-LLRWQFPAHY-RS**L**RHA---**LW**PSLPDL
Cape elephant shrew	WSAWSGLVRVET-----A----------SETAWISLVTALL-LVLGLSALLGLL-LLRWQFPAQY-RS**L**RHA---**LW**PSLPDL
squirrel	WSAWSDPARVET-----A----------SETAWISLVTALL-LLLGVSALLGLL-LLRWQFPARY-RR**L**RHA---**LW**PSLPDL
star-nosed mole	WSAWSDPVRVET-----A----------SETAWISLVTALL-LVLGLSALLGLL-LLRWQFPAYY-RS**L**RHA---**LW**PSLPDL
hedgehog tenrec	WSAWSEPVRVET-----A----------SEMAWISLVTALL-LVLGLSALLGLL-LLRWQFPAHY-RS**L**RHA---**LW**PSLPDL
European hedgehog	WSAWSDPVNVET-----A----------SETAWISLVAALF-LVLSLSTVLGLL-LLRWQFPAHY-RS**L**RHA---**LW**PSLPDL

Cape golden mole	WSAWSDPARVET-----A-------------------------SDTAWISLVTALL-LVLGLSTLLGLL-LLRWQFPAHY-RS**L**RHA---**LW**PSLPDL
Common shrew	WSSWSDPVRVET-----A-------------------------SETAWISLVTALL-LVLGLSAFLGLL-LLRWQFPAHY-RS**L**RHA---**LW**PSLPDL
Chinese tree shrew	WSAWSDPASVET-----A-------------------------SETAWISLVTVLL-LVLGLSAFLGLL-MLRWQFPEHY-RR**L**RHA---**LW**PSLPDL
Mouse	WSAWSPPARVST-----G-------------------------SETAWITLVTALL-LVLSLSALLGLL-LLKWQFPAHY-RR**L**RHA---**LW**PSLPDL
Brown rat	WSAWSPPARVST-----G-------------------------SETAWITLVTALL-LVLSLSALLGLL-LLKWQFPAHY-RR**L**RHA---**LW**PSLPDL
David's myotis bat	WSAWSAPVRVET-----A-------------------------SETGXXXLVTALL-LVLGLTTLLGLL-LLRWQFPAYY-RS**L**RHA---**LW**PSLPDL
Killer whale	WSAWSDPVRVET-----A-------------------------SETAWIFLVTALL-LVLGVSALLGLL-LLRWQFPAHY-RS**L**RRA---**LW**PSVPDL
chinese river dolphin	WSPWSDPVRVET-----A-------------------------SETAWIFLVTALL-LVLGVSALLGLL-LLRWQFPAHY-RS**L**RHV---**LW**PSVPDL
Big brown bat	WSAWSAPVRVET-----A-------------------------SETAWISLVTALL-LVLGLSTLLGLL-LLRWQFPAHY-RS**L**RHA---**LW**PSLPDL
Black flying fox	WSAWSDPVRLET-----A-------------------------SEMAWISLVTALL-LVLGLSALLGLL-LLRWQFLEHY-RS**L**RHA---**LW**PSLPDL
Brandt's bat	WSAWSAPVRVET-----A-------------------------SEVAWISLVTALL-LVLGLSTLLGLL-LLRWQFPAHY-RS**L**RHA---**LW**PSLPDL
Jaculus (rodent)	WSAWSQAARVET-----A-------------------------SETAWISLVTALL-LVLGLSALLSLL-LLRWQFPAHY-RS**L**RHA---**LW**PSLPDL
American pika	WSSWSEPARVET-----A-------------------------SETAWISMVTALL-LVLGLSALLGLL-LLRWQFPAHY-RR**L**RHA---**LW**PSLPDL
Sperm whale	WSAWSDPLRVET-----A-------------------------SETAWIFLVTALL-LVLGVSALLGLL-LLRWQFPAHY-RS**L**RHA---**LW**PSLPDL
Blue whale	WSAWSDPVRVET-----T-------------------------SETAWIFLVTALL-LVLGVSALLGLL-LLRWQFPAHY-RS**L**RHA---**LW**PSLPDL
White rhinoceros	WSAWSDPVRVET-----A-------------------------SETAWISLVTALL-LVLGLSALLGLL-LLRWQFPAHY-RS**L**RHA---**LW**PSLPDL
Plains bison	WSSWSDPVRVET-----A-------------------------SETVWIFLVTALL-LVLSVSALLGLL-LLRWQFPEHY-RS**L**RHA---**LW**PSLPDL
Tibetan antelope	WSSWSDPVRVET-----A-------------------------SETVWIFLVTALL-LVLGVSALLGLL-LLRWQFPEHY-RS**L**RHA---**LW**PSLPDL
Goat	WSPWSDPVRVET-----A-------------------------SETVWIFLVTALL-LVLGVSALLGLL-LLRWQFPEHY-RS**L**RHA---**LW**PSLPDL
Yak	WSSWSDPVRVET-----A-------------------------SETVWIFLVTALL-LVLSVSALLGLL-LLRWQFPEHY-RS**L**RHA---**LW**PSLPDL
Sheep	WSSWSDPVRVET-----A-------------------------SETVWIFLVTALL-LVLGVSALLGLL-LLRWQFPEHY-RS**L**RHA---**LW**PSLPDL
water buffalo	--SALLGLL-LLRWQFPEHY-RS**L**RHA---**LW**PSLPDL
cow	WSSWSDPVRVET-----A-------------------------SETVWIFLVTALL-LVLSVSALLGLL-LLRWQFPEHY-RS**L**RHA---**LW**PSLPDL
Cat	WSAWSDPVSVDT-----A-------------------------SETAWISLVTALL-VVLGLSTLLGLL-LLRWQFPAHY-RS**L**KHA---**LW**PSLPDL
Siberian tiger	WPAWGRGSSLGLQRSDWF-------------------------RPLAWISLVTALL-VVLGLSTLLGLL-LLRWQFPAHY-RS**L**KHA---**LW**PSLPDL
walrus	WSAWSDPVRVET-----T-------------------------SEIAWISLVTALL-VVLGLSALLGLL-LLRWQFPAHY-RS**L**KHA---**LW**PSLPDL
Weddell seal	WSAWSDPVRVET-----T-------------------------SETAWISLVTALL-VVLGLSALLGLL-LLRWQFPAHY-RY**R**PGHSGD**GW**GRRPLN
Ferret	WSAWSEPVRAET-----T-------------------------SDSAWISLVTALL-VVLGLSALLGLL-VLRWQFPAHY-RS**L**KHA---**LW**PSLPDL
Polar bear	--AWISLVTALL-VALGLSALLGLL-LLRWQFPARY-RS**L**KHA---**LW**PSLPDL
Naked mole-rat	WSAWSETEWVET-----A-------------------------SEPAWISLVTVLL-LVLGLSALLGLL-LLRWQFPAHY-RR**L**RHA---**LW**PSLPDL
Damaraland mole-rat	WSAWSETEWVET-----A-------------------------SEPAWISLVTVLL-LVLGLSALLGLL-LLRWQFPEQY-RR**L**RHA---**LW**PSLPDL
guinea pig	WSAWSEPVSVET-----A-------------------------SEPAWISLVTILL-LVLGLSALLGLL-LLRWQFPAHY-RR**L**RHA---**LW**PSLPDL
brush-tailed rat	WSAWSEPARVET-----A-------------------------SEPAWISLVTILL-LVLGLSALLGLL-LLRWQFPAHY-RR**L**RHA---**VW**PSLPDL
thick-tailed bushbabies	WSSWSDPARVET-----A-------------------------SETA**WISLVIALL-LVMGLSSLLGLL-LLRGQFPAHY**-RR**L**RHA---**LW**PSLPDL
rhesus macaque	YSSQSLDHAVIS-----P-------------------------SLTP**WPHCSPTPTALLLHTNSLPWL-----SLLIFS**P-RR**L**RHA---**LW**PSLPDL
Sumatran orangutan	WSSWSDPARVET-----A-------------------------TETA**WISLVTALH-LVLGLRAID----------YPL-Q**R**L**RHA---**LW**PSLPDL
Human	WSSWSDPTRVET-----A-------------------------TETA**WISLVTALH-LVLGLSAVLGLL-LLRWQFP**AHY-RR**L**RHA---**LW**PSLPDL
crab-eating macaque	WSSWSDPARVET-----A-------------------------TETAWISLVTALL-LVLGLSAVLGLL-LLRWQFPAHY-RR**L**RHA---**LW**PSLPDL
green monkey	WSSWSDPARVET-----A-------------------------TETAWISLVTALL-LVLGLSAVLGLL-LLRWQFPAHY-RR**L**RHA---**LW**PSLPEL
golden snub-nosed monkey	WSSWSDPAKVET-----A-------------------------TDTAWISLVTALL-LALGLSAVLGLL-LLRWQFPAHY-RR**L**RHA---**LW**PSLPDL
Tasmanian Devil	WSAWSAPALVEM-----A-------------------------PESG**WVSVVTSAV-LTLGFGGLVGL--VLRRLFPARF**-RA**L**RQT---**LW**PPLPDL
gray short-tailed opossum	WSAWSVPALVEM-----A-------------------------PDSG**WVSVVTSAV-LTLSFGGLVGLCLMLRRFFPA**RF-RA**L**WQT---**LW**PPLPDL

III.3.4.8. RWQFP motif analogs

Possible motif at delta5 position	
AARFP	Przewalski's horse
GFTCL	python
ISFFS	Zebra fish
ISLFP	Black cod
ISMLS	Salmon
ITTVL	guppy
IW-HP	northern white-cheeked gibbon
IYLFP	Crocea Clam
KWQFP	Mus Musculus
LSMFS	Salmon
RCSFP	Green sea turtle
RCTFP	Chicken
RGQFP	Bushbaby
RLIFP	Ghost shark
RRFFP	Opossum
RRLFP	Tasmanian Devil
RWKFP	Marmoset
RWQFL	black flying fox
RWQFP	Human
VCIGL	Carolina anole lizard

Table 4 - Alignment of RWQFP analogs

We notice that the JM motif of those 85 TpoRs is less conserved that might be expected. In the table below, we find 20 different motifs that can be aligned to the Human RWQFP motif.

A striking finding is that the prosimian primate (Otelemur Garnetii) also known as the small-eared galago or garnett's bushbaby posesses a "RGQFP" JM motif corresponding to the activating mutation, W515G found in rare patient and to one of our active receptors (Defour et al, Leukemia 2013). Blood test on this primate (which is sometimes used as a laboratory animal) has shown a higher platelet count when compared to man[307]. The W515G mutation might not be the only reason for thrombocythemia, as mice or elephants with a classic motif for example are also thrombocythemic. The zebrafish with its ISFFS motif contains a hydrophobic followed by a hydrophilic residue, two aromatics and hydrophilic residues that may suggest an amphipathic requirement in the motif. It is noteworthy that the two phenylalanines are conserved in the opossum RRFFP. But if we consider the IYLFP (hydrophobic, aromatic, hydrophobic, aromatic, hydrophobic) of the salt-water crocea clam, the amphipathic requirement is less clear. A RLIFP (a positive followed by hydrophobic and aromatic residues) is found in the Australian ghost-shark primitive cartilaginous fish, which possess the most primitive TpoR, but the entire TM domain sequence is very different.

III.4. Preamble: His499 Regulates Dimerization and Prevents Oncogenic Activation by Asparagine Mutations of the Human Thrombopoietin Receptor. (J. Biol. Chem. 2016)

Emilie Leroy£, Jean-Philippe Defour£, Takeshi Sato, Sharmila Dass, Ian Brett, Miki Itaya, Vitalina Gryshkova, Shwe Myat Marlar, Judith Staerk, Stefan N. Constantinescu and Steven O. Smith. £ Co-first authors

III.4.1. Background

The notion that TpoR signals as a dimer is now generally accepted. In general, introduction of an asparagine residue in transmembrane domains is presumed mediate dimerization of the TM helices by forming symmetrical or asymmetrical hydrogen bonds, provided that the asparagines are placed in or close to the dimeric interface. For example, GCN4 transcriptional activator dimerizes and binds DNA in a left handed coiled-coil conformation due to an asparagine in the "a" position of the heptad repeat, thus facing the interface.[308] Insertion of an asparagine residue at position S505N in the TMD of the TpoR is dimerizing the receptor in an active conformation in absence of ligand in ET patients.[17,18]

III.4.2. Questions

In this study we used asparagine-scanning mutagenesis on both murine and human TpoR transmembrane domains, in order to test whether and how dimeric orientation regulates activation. We introduced asparagine mutations along the TMD of the murine and the human receptor and asked whether such receptors traffic to the cell surface, acquire mature N-glycosylation, form dimers, and induce activation. We were curious to see whether in this system, like in the coiled coil system, a broad interface would be compatible with activation, and whether the murine and the human TpoR exhibit similar requirements for activation.

III.4.3. Authors contribution

Judith Staerk has initiated the mutational work on the mouse TpoR and provided the first results. I have performed the study in the human TpoR and I made the key observation that major differences exist between the mouse and human TpoR asparagine mutants. I also showed that these differences involve major traffic defects for the human TpoR. I also performed in collaboration with Christian Pecquet the *in vivo* experiments testing the effects of the murine mutants in bone marrow transplantation. Emilie Leroy performed mutagenesis at the His499 and obtained functional results on murine and human mutants that contain His or Leu at the position 499, demonstrating that the residue at this position is crucial for the control of the traffic and dimerization of both murine and human TpoRs. Our collaborator in Steven O. Smith lab, Stony Brooks USA, performed polarized IR and solid-state NMR spectroscopy. Vitalina Gryshkova and Shwe Myat Marlar performed *Gaussia* princeps luciferase complementation.

tapraid4/zbc-bc/zbc-bc/zbc00616/zbc3589-16z ZSUBMIT xppws S=5 23/12/15 8:57 4/Color Figure(s) F1–6,9 ARTNO: M115.696534

THE JOURNAL OF BIOLOGICAL CHEMISTRY VOL. 291, NO. ??, pp. 1–xxx, ???? ??, 2016
© 2016 by The American Society for Biochemistry and Molecular Biology, Inc. Published in the U.S.A.

His^{499} Regulates Dimerization and Prevents Oncogenic Activation by Asparagine Mutations of the Human Thrombopoietin Receptor*

Received for publication, October 4, 2015, and in revised form, November 27, 2015 Published, JBC Papers in Press, December 1, 2015, DOI 10.1074/jbc.M115.696534

Emilie Leroy[‡1,2], Jean-Philippe Defour[‡1,3], Takeshi Sato[§], Sharmila Dass[¶], Vitalina Gryshkova[‡4], Shwe Myat Marlar[‡5], Judith Staerk[‖], Stefan N. Constantinescu[‡6], and Steven O. Smith[¶7]

From the [‡]Ludwig Institute for Cancer Research, 1200 Brussels, Belgium de Duve Institute, Université catholique de Louvain, 1200 Brussels, Belgium, [§]Institute for Protein Research, Osaka University, 3-2 Yamadaoka, Suita, Osaka 565-0871, Japan, [¶]Department of Biochemistry and Cell Biology, Stony Brook University, Stony Brook, New York 11794-5215, and [‖]Stem Cell Group, Nordic European Molecular Biology Laboratory Partnership and Center for Molecular Medicine, 0318 Oslo, Norway

AQ: A

Ligand binding to the extracellular domain of the thrombopoietin receptor (TpoR) imparts a specific orientation on the transmembrane (TM) and intracellular domains of the receptors that is required for physiologic activation via receptor dimerization. To map the inactive and active dimeric orientations of the TM helices, we performed asparagine (Asn)-scanning mutagenesis of the TM domains of the murine and human TpoR. Substitution of Asn at only one position (S505N) activated the human receptor, whereas Asn substitutions at several positions activated the murine receptor. Second site mutational studies indicate that His^{499} near the N terminus of the TM domain is responsible for protecting the human receptor from activation by Asn mutations. Structural studies reveal that the sequence preceding His^{499} is helical in the murine receptor but non-helical in peptides corresponding to the TM domain of the inactive human receptor. The activating S505N mutation and the small molecule agonist eltrombopag both induce helix in this region of the TM domain and are associated with dimerization and activation of the human receptor. Thus, His^{499} regulates the activation of human TpoR and provides additional protection against activating mutations, such as oncogenic Asn mutations in the TM domain.

AQ: B

The thrombopoietin (Tpo)[8] or Mpl receptor regulates megakaryocyte development and supports hematopoietic stem cell survival (1). The Tpo receptor (TpoR) shares general homology with other members of the cytokine receptor family, including the erythropoietin and granulocyte colony-stimulating factor receptors (2). These receptors contain a large extracellular domain that binds signaling hormones in a 2:1 ratio of receptor to hormone (3–5) along with a single membrane-spanning helix and an intracellular domain that associates non-covalently with a tyrosine kinase.

AQ: C

AQ: D

The minimal functional region of the intracellular domain stretches from the boundary of the transmembrane (TM) domain and includes three regions with limited sequence homology: a conserved switch region, Box 1, and Box 2. The switch region contains a hydrophobic motif whose orientation is required for signaling (6, 7). Box 1 is characterized by a proline-rich motif (P*XX*P*X*P) that is crucial for cytokine receptors to bind and activate their cognate Janus kinases (8–10). Box 2 is loosely defined as a motif with acidic and hydrophobic residues and is required for maximal cell growth in response to cytokines.

The TpoR has several unique features. First, the extracellular domain is duplicated, and deletion of the membrane-distal domain causes constitutive activation (11). Second, there are 5 amino acids (RWQFP) inserted directly C-terminal to the TM domain whose deletion or mutation causes ligand-independent receptor activation (12). Finally, clinically relevant mutations have been identified that induce constitutive receptor activity in the extracellular juxtamembrane (JM) region (T487A (13)), the TM domain (S505N (14, 15)), and the intracellular RWQFP motif (W515K/L/A (12, 16–19)). The fact that these are clustered in and around the TM domain reflects the importance of this region in the regulation of receptor activation.

It is generally accepted that the active signaling form of cytokine receptors is a dimer, but whether the inactive state is

* This work was supported in part by National Institutes of Health-National Science Foundation Instrumentation Grants S10 RR13889 and DBI-9977553 and National Institutes of Health Grant GM-46732 (to S. O. S.). The authors declare that they have no conflicts of interest with the contents of this article. The content is solely the responsibility of the authors and does not necessarily represent the official views of the National Institutes of Health.

[1] Both authors contributed equally to this work.

[2] Supported by a Fonds pour la formation à la Recherche dans l'Industrie et dans l'Agriculture (FRIA) Ph.D. fellowship.

AQ: GG

[3] Supported by a FRIA Ph.D. fellowship and the Cliniques universitaires St. Luc.

[4] Supported by a de Duve Institute postdoctoral fellowship and a Belspo Interuniversity Attraction Poles fellowship.

AQ: HH

[5] Supported by an Erasmus Mundus Panacea fellowship.

[6] Supported by Ludwig Cancer Research, *Fonds de la Recherche Scientifique*-Fonds National de la Recherche Scientifique, Salus Sanguinis, Fondation contre le cancer, Project Action de Recherche Concertée of the Université catholique de Louvain (Grant ARC10/15-027), and the PAI program Belgian Medical Genetics Initiative. To whom correspondence may be addressed. Tel.: 322-764-7540; Fax: 322-764-6566; E-mail: stefan.constantinescu@bru.licr.org.

AQ: II

[7] To whom correspondence may be addressed. Tel.: 631-632-1210; Fax: 631-632-8575; E-mail: steven.o.smith@stonybrook.edu.

[8] The abbreviations used are: Tpo, thrombopoietin; TpoR, Tpo receptor; EpoR, erythropoietin receptor; ATR, attenuated total reflection; hTpoR, human thrombopoietin receptor; JM, juxtamembrane; mTpoR, murine thrombopoietin receptor; Mpl, myeloproliferative leukemia; TM, transmembrane; EndoH, endoglycosidase H; hGluc, *humanized Gaussia luciferase; MAS,* magic angle spinning; IC, intracellular.

AQ: JJ

dimeric or monomeric is unknown. Several lines of evidence exist to suggest that the erythropoietin receptor (EpoR), one of the most extensively studied cytokine receptors, exists as a preformed dimer, and activation is induced by structural reorganization of the dimer after hormone binding. Crystallographic studies of the EpoR extracellular domain in the presence and absence of ligand suggest that the full-length inactive receptor is dimeric, and hormone binding causes subunit rotation for activation (4, 20). A similar model has been proposed for the structurally related growth hormone receptor (21–23). The first evidence that the TM domain contributes to dimerization of the inactive EpoR came from co-patching measurements using chimeras of the prolactin and erythropoietin receptors in HEK293-derived BOSC cells (24). These studies found the TM domain of the EpoR to be both necessary and sufficient for receptor dimerization in the context of the full-length receptor. This conclusion is supported by biophysical measurements showing that the isolated TM domain of the murine EpoR associates as a dimer (25). However, unlike the TpoR, the TM domain of the EpoR is not a hot spot for activating mutations.

AQ: E

Much less is known about whether the TpoR forms an inactive dimer that changes orientation upon ligand binding. Studies using coiled coil fusions to the TM-cytosolic domain of the murine TpoR showed that one dimeric interface is inactive, one interface mimics the physiologic functions of TpoR, and several orientations induce partial levels of activation *in vitro* and in bone marrow transplantation experiments *in vivo* in mice (26). However, these studies use an artificial receptor where the large, native extracellular domain dimer (preformed or ligand-bound) is replaced with a short, tightly associated coiled coil that forces symmetric dimerization. Biophysical studies on the association of the human TpoR TM domain using cysteine mutagenesis and the TOXCAT reporter assay indicate that the wild-type TM sequence (residues 491–515) associates as a dimer (27). However, we have recently shown that the 5-amino acid (RWQFP) insert at the intracellular TM-JM boundary of the TpoR impairs dimerization of the upstream TpoR TM helix (28). We further showed that mutation of Trp^{515} within this motif leads to dimerization of the TM-JM region of TpoR by changing the orientation of the TM helix relative to the membrane bilayer normal (28). Although the studies on isolated TM-JM regions of TpoR reveal that they have a propensity to dimerize, it remains an open question as to whether the full-length receptor is primarily dimeric or monomeric or exists in a monomer-dimer equilibrium.

In this study, asparagine-scanning mutagenesis of the murine TpoR (mTpoR) and human TpoR (hTpoR) was used to modulate the orientation and dimerization of the TM domain of the receptor. The asparagine mutations provide an alternative to the coiled coil dimerization sequences we have previously used to engineer TpoR dimers (26). Asparagine is able to mediate dimerization of TM helices through strong hydrogen bonding interactions and often does so in a sequence-independent fashion (29–31). Moreover, asparagine-scanning mutagenesis addresses the question of whether the clinically observed S505N mutation in humans is unique or just one of many mutations that lead to constitutive activation. We made use of full-length receptors, truncated receptors, and peptides corresponding to only the TM-JM domain for comparative studies between the murine and human receptors. Together, our results provide the structural basis for why the hTpoR cannot be activated by asparagine mutations that readily activate the mTpoR, suggesting an evolutionary mechanism that results in resistance to oncogenic activation of hTpoR.

Experimental Procedures

cDNA Constructs and Cells—Mouse and human TpoR cDNAs cloned in the pMX-IRES-GFP bicistronic vector contained a hemagglutinin (HA) tag at the N terminus. Site-directed mutagenesis was achieved by the overlapping-extension PCR amplification method. The PCR was performed using 1 μl of PfuTurbo DNA polymerase (2.5 units/μl) following the protocol in the QuikChange XL site-directed mutagenesis kit (Stratagene, Santa Clara, CA) as described (28). Sanger sequencing of the entire coding region was used for each construct.

Cell Proliferation Assay—Pro-B interleukin 3 (IL-3)-dependent Ba/F3 cells were maintained in RPMI 1640 medium and 10% fetal calf serum using WEHI cell supernatant as a source of IL-3. TpoR Asn variants subcloned in the pMX-IRES-GFP were used for packaging ectopic retrovirus in BOSC cells. Cells were infected in medium containing Polybrene with packaged retrovirus, and cell pools expressing similar levels (top 15%) of green fluorescent protein (GFP) coded by the bicistronic retroviral vectors were isolated using flow cytometry cell sorting. Cell surface TpoR was assessed by staining with anti-HA antibodies (Covance, Princeton, NJ; 10 μg/ml) and phycoerythrin-conjugated donkey anti-mouse IgG secondary antibodies (28). The levels of TpoR total protein expression were determined by Western blotting using anti-HA antibodies (Roche Applied Science). For determining the maturation state of the *N*-glycosylated TpoR mutants, we used digestion with endoglycosidase H (EndoH) for 4 h followed by Western blotting with anti-HA antibodies as described (6). Cell proliferation in the presence or absence of cytokines was measured using the CellTiter-Glo luminescent cell viability assay (Promega, Madison, WI).

AQ: F

Dual-Luciferase Transcriptional Assay of STAT Activation—Transcriptional activation of STAT3 and STAT5 downstream TpoR variants was assessed in γ-2A cells (Janus kinase 2-deficient cells reconstituted with Janus kinase 2) using the Dual-Luciferase assay kit (Promega, Madison, WI). The assay measures luciferase luminescence after transient transfection of the pGRR5 reporter containing the firefly luciferase and STAT3/STAT5 binding sites and a control reporter (pRL-TK) containing *Renilla* luciferase. The luminescence ratio of these two luciferases provides a measure of STAT activation (26, 32). Luminescence was detected in cell lysates with a PerkinElmer Life Sciences Victor-X light analyzer.

Split Luciferase Complementation Assay of Receptor Dimerization—TpoR dimerization was measured using a complementation assay in which two halves of *Gaussia princeps* luciferase were attached separately to the C terminus of TpoR. The cDNA of TpoR was inserted between the NotI and ClaI restriction sites of the pcDNA3.1/Zeo vector upstream of either the hGluc fragment coding amino acids 1–93 (hGluc1) or the fragment coding amino acids 94–169 (hGluc2) of *G. princeps*

luciferase (33). BOSC cells plated on 24-well plates were co-transfected with the plasmids (coding hGluc1and hGluc2) using Lipofectamine (Invitrogen). Twenty-four hours after transfection cells were trypsinized and resuspended in 150 μl of DMEM/F-12 without phenol red (Gibco). Cell samples were flash frozen on dry ice for 10 min and thawed in a water bath at 37 °C for 10 min (cycle was repeated twice). After centrifugation (10,000 × *g*, 5 min), the supernatants were collected and aliquoted (100 μl/well) in 96-well white plates (Nunc, Thermo Fisher Scientific) to measure the luciferase activity. Native coelenterazine (NanoLight Technology) was reconstituted as a stock solution (1 mg/ml in methanol) and diluted to a final concentration of 20 μM in DMEM/F-12 at room temperature for injection (100 μl). Signal intensities (integrated over 10 s with an injection delay of 2 s) were read on a Victor-X light analyzer. Aliquots of the supernatants were also used to detect the proteins on Western blots (33).

Membrane Reconstitution of TM-JM Peptides for Biophysical Studies—Peptides (40 residues in length) corresponding to the TM domain and JM regions of hTpoR (TRVETATETAWISLVTALHLVLGLSAVLGLLLLRWQFPAH) and mTpoR (ARVSTGSETAWITLVTALLLVLSLSALLGLLLLKWQFPAH) were synthesized using solid-phase methods. Deuterated (5,5,5-d_3) leucine and deuterium-free water were purchased from Cambridge Isotope Laboratories (Andover, MA). Other amino acids and octyl β-glucoside were obtained from Sigma. The crude peptide (5–15 mg) was purified by reverse-phase HPLC on a C_4 column using gradient elution. Purified TpoR peptides were reconstituted by detergent dialysis using 1,2-dimyristoyl-*sn*-glycero-3-phosphocholine and *1,2-dimyristoyl-sn-glycero-3-phosphoglycerol* (10:3) and a ~1:60 peptide-to-lipid ratio. Lipids were obtained from Avanti Polar Lipids (Alabaster, AL) as lyophilized powders and used without further purification. The lipid, detergent, and peptide were dissolved in organic solvent (*e.g.* hexafluoro-2-propanol or trifluoroethanol). The mixture of lipid, detergent, and peptide in organic solvent was incubated at 37 °C for over 2 h, the solvent was removed by evaporation using a stream of argon gas, and then the sample was placed under vacuum. The dry mixture was rehydrated with phosphate buffer (10 mM phosphate and 50 mM NaCl, pH 7.4) such that the final concentration of octyl β-glucoside was 5–10% (w/v). The rehydrated sample was then stirred slowly for at least 6 h, and the octyl β-glucoside was removed by dialysis using Spectra-Por dialysis tubing (3500 molecular weight cutoff) for 24 h against phosphate buffer at 37 °C. To confirm that the membrane-reconstituted peptides did not aggregate during dialysis, the samples were loaded onto 10–40% (w/v) sucrose gradients and purified. Samples for IR spectroscopy were dialyzed a second time to remove sucrose. The dichroic ratios were compared before and after dialysis. Samples for NMR spectroscopy were pelleted by ultracentrifugation and, if needed, washed twice to remove sucrose. The pelleted samples were lyophilized, rehydrated with deuterium-depleted water (50 ± 5% weight), and incubated at 37 °C for 24 h before loading into NMR rotors.

Polarized IR Spectroscopy—Polarized attenuated total reflection (ATR) Fourier transform infrared (FTIR) spectra were obtained on a Bruker IFS 66V/S spectrometer. Reconstituted hTpoR and mTpoR TM-JM peptides (50–100 μg) were layered onto a germanium internal reflection element using a slow flow of air or argon gas directed at an oblique angle to the ATR plate to form an oriented multilamellar lipid-peptide film. IR spectra were obtained using light having either parallel or perpendicular polarization relative to the surface of the germanium plate. The dichroic ratio (R_{ATR}) is defined as the ratio between the absorption of parallel ($A_{\parallel}$) and perpendicular ($A_{\perp}$) polarized light. The frequency of the amide I vibration is sensitive to the global secondary structure of the protein, and the dichroic ratio of the amide I band provides information on the orientation of TM helices relative to the plane of the membrane (34). A detailed analysis has been described previously (34). 1000 scans were acquired and averaged for each sample at a resolution of 4 cm^{-1}. The calculation of the helix tilt angles from the observed dichroic ratios was based on a value of the transition moment angle (α) of 39.5° and a maximum membrane order parameter (S_{mem}) of 0.85 (34). The use of the values of α and S_{mem} is based on measurements of bacteriorhodopsin, an integral membrane protein with seven transmembrane helices of known structure that forms well ordered, two-dimensional membrane arrays. We do not independently know the disorder of the reconstituted TM helices in our samples. Consequently, we assume that the maximum order obtained is equal to that of bacteriorhodopsin obtained from diffraction measurements (35). This results in a lower estimate for the helix tilt angles reported in Table 1 (*i.e.* greater disorder in our membrane reconstitutions than that found for bacteriorhodopsin would correspond to lower actual tilt angles for an ideal sample with no disorder).

Solid-state NMR Spectroscopy—Deuterium NMR spectra were obtained at a ^2H frequency of 55.2 MHz on a Bruker Avance NMR spectrometer using a 4-mm magic angle spinning (MAS) probe. A MAS frequency of 3 kHz was used to increase the number of spinning side bands. Single pulse excitation was utilized using a 4–7.5-μs 90° pulse followed by a 4.5-μs delay before data acquisition. The repetition delay was 0.25 s. A total of 600,000–1,500,000 transients were averaged for each spectrum and processed using a 100-Hz exponential line broadening function. Spectra were obtained at 25 °C.

Two-dimensional dipolar assisted rotational resonance NMR experiments (36) were performed at a ^{13}C frequency of 125 MHz on a Bruker Avance spectrometer. The MAS spinning rate was set in the range of 9–11 KHz ± 5 Hz. The ramped amplitude cross-polarization contact time was 2 ms. Two-pulse phase-modulated decoupling was used during the evolution, and acquisition periods had a radiofrequency field strength of 80 kHz. Internuclear $^{13}C \ldots {}^{13}C$ distance constraints were obtained from using a mixing time of 600 ms. The sample temperature was maintained at −50 ± 2 °C. All ^{13}C solid-state MAS NMR spectra were externally referenced to the ^{13}C resonance of neat tetramethylsilane at 0 ppm at room temperature. Using tetramethylsilane as the external reference, we calibrated the carbonyl resonance of solid glycine at 176.46 ppm. The chemical shift difference between ^{13}C of *2,2-dimethylsilapentane-5-sulfonic acid* in D_2O relative to neat tetramethylsilane is 2.01 ppm.

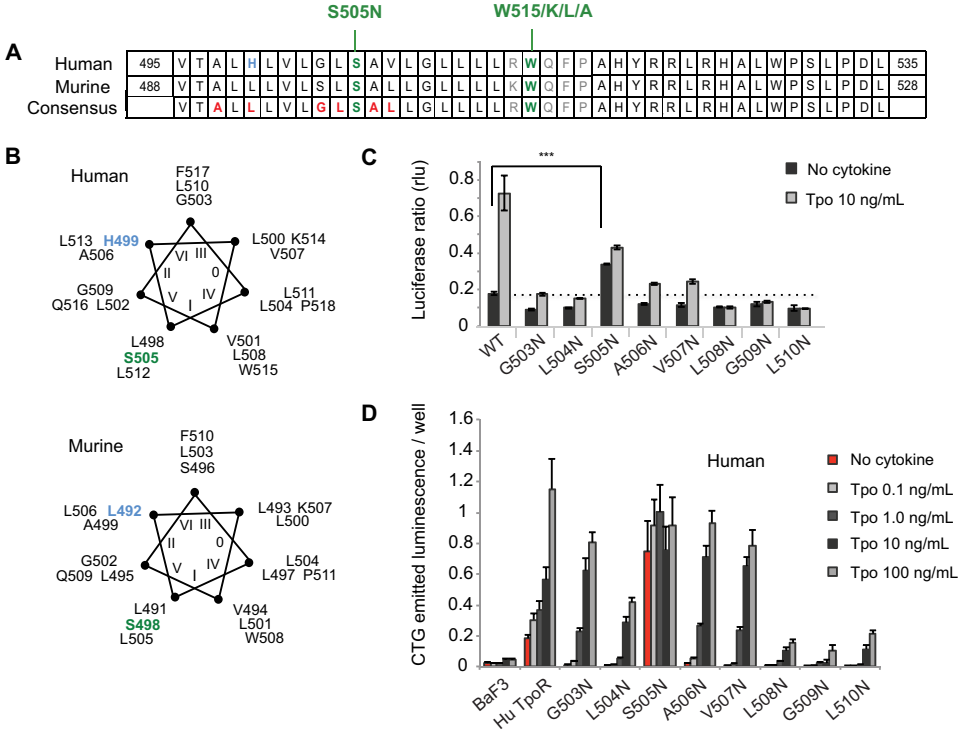


FIGURE 1. **Asparagine substitutions in the transmembrane domain of the human TpoR lead to activation of only one dimeric interface.** *A*, TM sequences of hTpoR (*upper*) and mTpoR (*middle*) showing the position of His^{499} and the intracellular (R/K)WQFP motif. A consensus sequence (*bottom*) of 50 different mammalian TpoRs highlights (*red*) the positions with sequence identity of <90%. Four of these residues bracket Ser^{498} (murine) and Ser^{505} (human), which is highly conserved. *B*, helical wheel diagrams of hTpoR (*left*) and mTpoR (*right*) showing the dimer interfaces that would be predicted for interacting helices in a left-handed coiled coil geometry. *C*, transcriptional activation of hTpoR after substitution of Gly^{503}–Leu^{510} with asparagine. γ2A cells were transiently transfected with Janus kinase 2 and the wild-type TpoR or the different TpoR mutants, and the activity of these receptors was assessed by measuring luciferase luminescence (in relative luciferase units (*rlu*)) in the absence or presence of 50 ng/ml Tpo as indicated. Only the S505N mutation triggers ligand-independent dimerization and signaling. *D*, BaF3 cells stably expressing the hTpoR (*hu TpoR*) variants were grown in the absence of cytokine or in the presence of different concentrations of Tpo as indicated. Only TpoR-S505N induced BaF3 autonomous growth. The presented values are averages of triplicates ±S.D. (*error bars*) for one representative experiment of at least three. ***, $p < 0.001$, one-way analysis of variance.

Results

Asparagine Mutations in the Transmembrane Domain of the Human and Murine TpoR Induce Different Effects—The TM sequences of human and murine receptors are shown in Fig. 1*A* along with a consensus sequence for mammalian TpoRs. Across a wide range of species, the TM domain is relatively well conserved. Ser^{505} and Trp^{515} both have a sequence identity of ~96%. The S505N is associated with familial forms of thrombocytosis, whereas the W515K/L/A mutations are associated with essential thrombocythemia and primary myelofibrosis. There are only a few residues with less than 90% identity (shown in *red*). There are four differences between human and mouse in the TM-JM sequence shown. Based on sequence comparison between TpoRs from 50 species, leucine at positions 492 and 500 in the mouse and glycine and arginine at positions 503 and 514, respectively, in the human are the consensus residues.

Asparagine, the residue that leads to constitutive activation upon mutation at Ser^{505} (human), is able to mediate dimerization of TM helices as left-handed coiled coils. The early studies of leucine zippers involved Asn residues at the "a" position in the heptad repeat characteristic of a left-handed coiled coil (37, 38). The crystal structure of the GCN4 transcription factor shows that the amide side chain of Asn forms an asymmetric hydrogen bond across the dimer interface (38), and dimerization studies showed that this contributes about −2 kcal/mol of binding energy (39).

Helical wheel diagrams illustrate the possible dimer interfaces in hTpoR and mTpoR (Fig. 1, *A* and *B*). Such dimeric interfaces are imposed when the coiled coil domain of Put3 is fused at consecutive positions to the TM domain of mTpoR, thus replacing the extracellular domain (26). There are seven possible symmetric interfaces that might mediate dimerization in the native receptor and that were created by progressive deletion of residues from the N-terminal end of the TM domain after fusion with the Put3 coiled coil (26). These are designated cc-TpoR-0 through cc-TpoR-VI. The cc-TpoR-II interface was found to be inactive, whereas the other interfaces exhibited various degrees of activity.

To investigate whether the full-length TpoR can be activated by asparagine mutations on different TM helix interfaces, TM residues 503–510 were individually substituted with asparagine in the hTpoR, and the receptor activity was monitored using a luciferase assay that reports on STAT5 transcriptional activation (see "Experimental Procedures"). Substitution with Asn only at a single position (S505N) leads to ligand-independent activation of the hTpoR (Fig. 1*C*). This position is the same as that detected in clinical studies showing only a single site (Ser^{505}) where an Asn mutation leads to disease. The results on STAT5 transcriptional activity were confirmed with cell proliferation assays in stable Ba/F3 transduced cells (Fig. 1*D*). For these measurements, each receptor mutant was retrovirally transduced into Ba/F3 cells and sorted using flow cytometry for

tapraid4/zbc-bc/zbc00616/zbc3589-16z ZSUBMIT xppws S=5 23/12/15 8:57 | 4/Color Figure(s) F1–6,9 | ARTNO: M115.696534

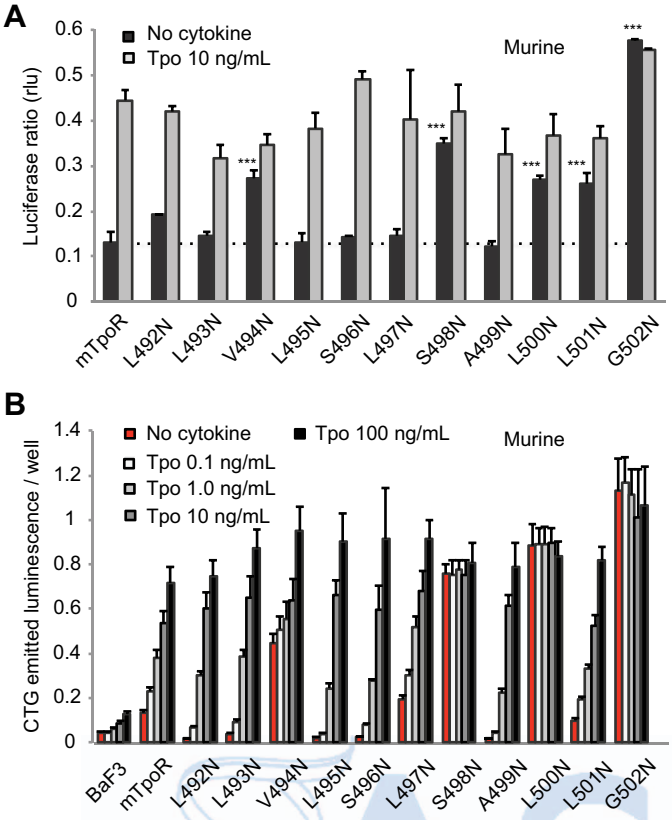


FIGURE 2. **Asparagine substitutions in the transmembrane domain of the murine TpoR lead to activation of several dimeric interfaces.** Leu^{492}–Gly^{502} were substituted with asparagine, and these mutant receptors were assessed for their ability to signal in the absence of cytokine. *A*, γ2A cells were transiently transfected with the constructs, and the transcriptional activation of STAT5 was measured by luciferase luminescence (in relative luciferase units (*rlu*)). V494N, S498N, L500N, L501N, and G502N triggered signaling in the absence of stimulation. *B*, BaF3 cells stably expressing the different constructs were grown, and cell viability was measured in the absence or presence of the different concentrations of Tpo ligand as indicated. V494N, S498N, L500N, and G502N allow proliferation of BaF3 in the absence of cytokine. The values presented are averages of triplicates ±S.D. (*error bars*) for one representative experiment of at least three. ***, $p < 0.001$, one-way analysis of variance between the wild type and each mutant in the absence of cytokine. *CTG*, *CellTiter-Glo*.

AQ: AA
AQ: BB

similar levels of expression. Only the S505N mutant led to cytokine-independent cell proliferation. Importantly, several substitutions (L508N, G509N, and L510N) led to receptors that were unable to traffic to the cell surface and were, as a consequence, inactive when Tpo was added.

Asparagine-scanning measurements of STAT5 transcriptional activation of the mTpoR reveal a very different picture (Fig. 2*A*). In contrast to hTpoR, asparagine substitutions at positions 494, 498, 500, 501, and 502 in mTpoR stabilize active receptors in the absence of ligand. These results were confirmed by cell proliferation assays in Ba/F3 cells for positions 494, 498, 500, and 502 (Fig. 2*B*). Asn substitutions at four different positions of the mTpoR clearly lead to activation, whereas only S505N (equivalent to S498N in the mouse) activates the hTpoR.

Mutation of His^{499} to Leucine Leads to Increased Cell Surface Localization and Signaling by the hTpoR-G509N Mutant—One of the largest sequence differences in the TM and JM regions between the murine and human receptors is at position 499 where histidine in human (His^{499}) is replaced by leucine in mouse (Leu^{492}). This TM residue is unique to TpoR and granulocyte colony-stimulating factor receptor within the family of type I cytokine receptors and only appeared later in species evolution. The histidine in the human receptor has previously been shown to bind eltrombopag, a small molecule agonist of hTpoR, leading to receptor activation (40). In this section, we explore the influence on activation of the H499L and L492H mutants in the context of the human and murine receptors, respectively, and show how these mutations influence the ability of Asn substitutions within the TM domain to activate TpoR. STAT5 activation and cell proliferation were measured using the Dual-Luciferase and cell viability assays, respectively, on the murine (Fig. 3*A*) and human (Fig. 3*B*) receptors with swapped residues (*i.e.* H499L and L492H). Several conclusions can be drawn.

First, mTpoR-G502N (the most strongly activating single Asn mutant) is not active in the context of the mTpoR-G502N/L492H double mutant. Indeed, placement of histidine at position 492 in the mTpoR-G502N mutant abolished the activity of the mutant in the absence and the presence of ligand, yielding the same phenotype as the human receptor with the corresponding G509N substitution.

Second, the mTpoR is not sensitive to eltrombopag, whereas substitution of L492H in the mTpoR imparts sensitivity to eltrombopag as observed previously (40). This confirms that eltrombopag binding requires the presence of histidine in the TM sequence. In contrast, removal of histidine at position 499 in the hTpoR-G509N mutant could restore the activity of this mutant in the presence and absence of ligand. As a control, the human receptor lacking His^{499} could no longer respond to eltrombopag.

Third, the hTpoR-G509N mutant (equivalent to mTpoR-G502N) does not traffic to the plasma membrane. The hTpoR-G509N mutant is retained intracellularly in an EndoH-sensitive form (Fig. 4), indicating that it contains high mannose *N*-glycosylation, characteristic of immature receptor retained in the endoplasmic reticulum, or possibly a receptor that cannot progress past the *cis*-Golgi. In contrast, the double mutation (H499L/G509N) allows the receptor to traffic to the plasma membrane (Fig. 4) and to induce STAT5 activation and autonomous proliferation in Ba/F3 cells (Fig. 3*C*). H499L appears to also rescue activity for additional Asn mutants in the hTpoR. For example, V507N is partially rescued by the H499L mutation and exhibits weak activity (data not shown). Rescued receptors become EndoH-resistant and are localized at the cell surface (Fig. 4). In the background of the mouse TpoR, the L492H mutation inactivates the Asn mutants and impairs their ability to traffic to the cell surface (data not shown).

AQ: Q

Dimerization of hTpoR Causes Straightening of the TM Helix Near His^{499}—The structural basis underlying the mechanism by which His^{499} influences receptor activation and cell surface expression is a challenge to study in full-length Tpo receptors. However, the original studies describing the influence of Asn mutations on TM helix dimerization were undertaken on isolated TM domains that independently fold into helical secondary structure when reconstituted into membrane bilayers (29–31). Indeed, we have previously shown that the activating

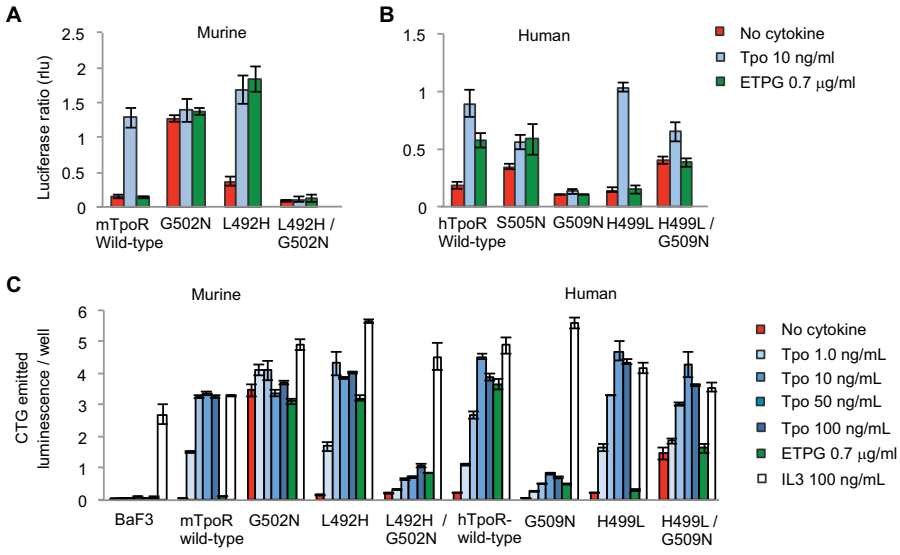


FIGURE 3. **Addition or removal of the TM histidine modifies the activity of the Asn mutants.** *A*, introduction of His instead of Leu at the homologous position in the murine receptor abrogated the activity of the G502N mutant as indicated on the Dual-Luciferase assay performed in transiently transfected γ2A cells. As a control, eltrombopag (*ETPG*) was added and was able to activate the L492H receptor. *B*, substitution of His^{499} by leucine restored the activity of the G509N mutant. Eltrombopag was no longer able to activate the receptor lacking His^{499}. *C*, BaF3 cells stably expressing the TpoR variants were assessed for their ability to grow in the absence of cytokine (*red*) or in the presence of different concentrations of Tpo (gradient of *blue*; 1, 10, 50, and 100 ng/ml) and eltrombopag (*green*; 0.7 μg/ml). Cells were all able to growth in the presence of IL-3 (*white*). The human double mutant G509N/H499L and its murine homolog G502N were able to induce BaF3 autonomous growth in the absence of cytokine. Histograms are averages of triplicates ± S.D. (*error bars*) for one representative experiment of at least three. *CTG*, *CellTiter-Glo; rlu,* relative luciferase units.

AQ: CC

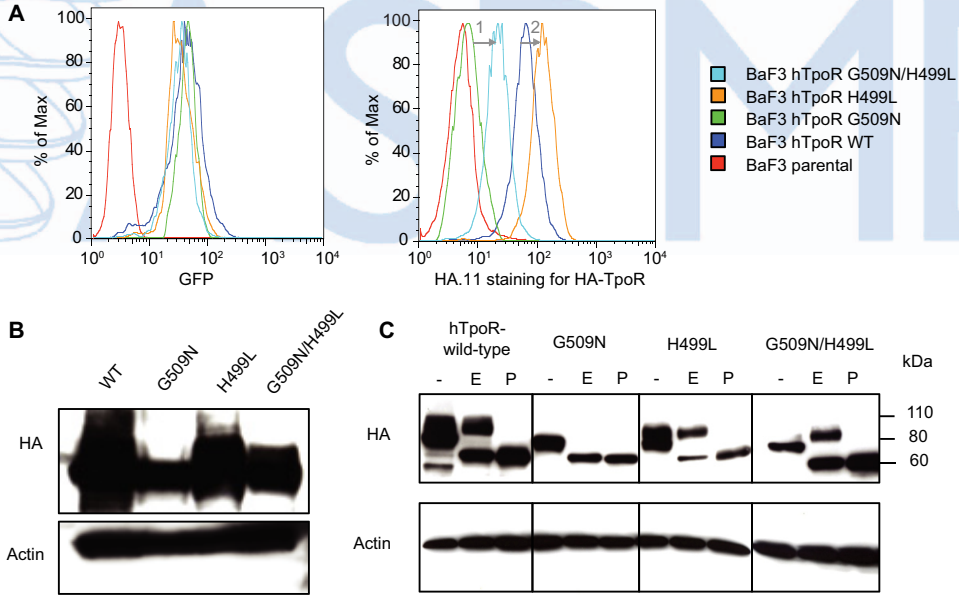


FIGURE 4. **TpoR-G509N is not expressed at the cell surface.** *A*, cell surface expression of HA-tagged TpoR was assessed by FACS using an anti-HA.11 antibody. *B*, BaF3 cells were sorted for the same level of GFP. *C*, the total level of TpoR protein was assessed by Western blotting with Np40 cell extracts using an anti-HA antibody. *D*, EndoH and peptide-*N*-glycosidase F treatment of stable BaF3 cell lines. Sorted BaF3 cells stably expressing the TpoR asparagine variants were treated with EndoH (*E*) or peptide-*N*-glycosidase F (*P*) or not treated (−), and the total level of TpoR protein was assessed using an anti-HA antibody by Western blotting. All the receptors except G509N mutant were resistant to EndoH treatment, revealing that the proteins are mature. The G509N mutant, which was fully degraded by EndoH, is likely immature and does not proceed to the cell surface because of some misfolding that blocks it at the rough endoplasmic reticulum-Golgi transport system. All the receptors depend on *N*-glycosylation for processing as revealed by the peptide-*N*-glycosidase F treatment.

AQ: DD
AQ: EE

S505N and W515K mutations in the context of TM-JM peptides of the human TpoR lead to a change of the tilt angle of the TM helix and induce dimerization, consistent with measurements on the full-length receptor using the split luciferase assay (28). Here, we extend these studies to the G509N and H499L mutants in hTpoR and to the G502N and L492H mutants in mTpoR (Table 1).

Polarized FTIR spectroscopy provides information on the global secondary structure and orientation of membrane-reconstituted TM-JM peptides. Typically, these peptides fold into α-helical secondary structure that gives rise to an amide I vibrational band at ~1655 cm^{-1} in the IR spectrum. The orientation of the TM helix (*i.e.* the helix tilt angle relative to the bilayer normal; see "Experimental Procedures") is probed in polarized

TABLE 1
Orientation, secondary structure, and association of hTpoR-WT, mTpoR-WT, and their mutants

Sequence	Dichroic ratio[a]	Helix tilt angle	Leu 494–Ala[497] structure	Leu[494], Val[4] 95 $^{13}C=O$ shift	Association
		°		*ppm*	
hTpoR-WT	2.7 ± 0.1	35	Extended	172.3, 172.3	Monomer
S505N	3.4 ± 0.1	17	Helix	175.9, 175.9	Dimer
G509N	2.5 ± 0.2	40	Extended	172.3, 172.3	Dimer
H499L	3.2 ± 0.1	23	Helix	176.1, 176.1	Dimer
hTpoR-WT + eltrombopag	3.0 ± 0.1	28	Helix	175.3, 175.3	Dimer
mTpoR-WT	3.3 ± 0.1	20	Helix	176.3, 176.3	Dimer
S498N	3.3 ± 0.1	20	Helix	177.2, 177.2	Dimer
G502N	3.2 ± 0.1	25	Helix	176.6, 176.6	Dimer
L492H	2.6 ± 0.2	38	Extended	173.1, 173.1	Monomer

[a] The error in the dichroic ratio corresponds to the standard deviation in three replicate runs.

IR spectra by measurements of the dichroic ratio (R_{ATR}). Hydrophobic peptides (20–24 residues in length) typically exhibit dichroic ratios of >3.0, corresponding to a maximum helix tilt of ~28°. Lower dichroic ratios indicate something unusual in the TM sequence (or simply reflect poor membrane reconstitutions). Our previous FTIR studies on hTpoR TM-JM peptides revealed dichroic ratios of ≤2.8 (28). In Fig. 5, *A* and *B*, we show using parallel reconstitutions that mTpoR-WT peptides exhibit a striking increase in the dichroic ratio compared with hTpoR-WT, corresponding to a decrease in the helix tilt angle from 35 to 20°. This change in orientation can be mimicked in the hTpoR by the H499L mutation, which exhibits the same dichroic ratio (3.2) within error as the mTpoR (Table 1).

A second mechanism for increasing the dichroic ratio of the hTpoR-WT TM helix is incorporation of the S505N mutation. The hTpoR-S505N dichroic ratio (3.4) is closer to that of mTpoR-WT (3.3) than to that of hTpoR-WT (2.7). We attribute this increase to a shift in the monomer-dimer equilibrium toward dimer in the S505N mutant (28). The mTpoR-S498N and hTpoR-S505N peptides exhibit similar dichroic ratios (3.3 *versus* 3.4), suggesting that they adopt similar active orientations.

We also compared the homologous hTpoR-G509N and mTpoR-G502N mutants. The mTpoR-G502N peptide has a much higher dichroic ratio (3.2) than hTpoR-G509N (2.5), consistent with the higher activity of the full-length mTpoR-G502N mutant. The dichroic ratio of hTpoR-G509N is slightly lower than that of hTpoR-WT (2.7). The presence of two polar residues (His[499] and Asn[509]) appears to alter the orientation of the TM helix in the membrane and may be associated with the poor ability of the G509N mutant to traffic. Similarly, introducing a histidine (at the equivalent His[499] position) in the murine coiled coil constructs induces TpoR protein instability as observed by loss of activity and protein expression at the cell surface (data not shown).

Previous NMR studies on the structure and orientation of the TM helix of hTpoR found that there was a break in helical secondary structure near Ala[497], one turn before His[499] (41). The low dichroic ratio of the amide I band observed in FTIR spectra of wild-type hTpoR would be consistent with this observation. To directly probe the helical secondary structure in this region of the peptide in mTpoR and hTpoR, we made use of intramolecular distance measurements using two-dimensional ^{13}C NMR spectroscopy with MAS (36).

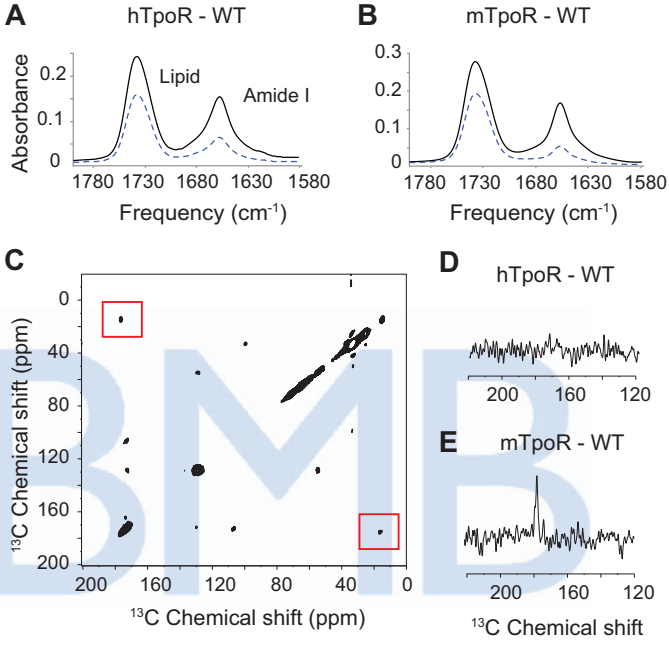


FIGURE 5. **Comparison reveals differences in the secondary structure and orientation of hTpoR and mTpoR TM peptides.** *A* and *B*, polarized IR spectra of hTpoR-WT and mTpoR-WT. *C*, two-dimensional dipolar assisted rotational resonance NMR of mTpoR-WT using TM peptides isotopically labeled at [1-^{13}C]Leu[487], [1-^{13}C]Val[488], and [3-^{13}C]Ala[490]. The cross-peak (*boxed*) between the [3-^{13}C]Ala[490] and the 1-^{13}C resonances of Leu[487] and/or Val[488] is consistent with α-helical secondary structure in this region of the TM-JM peptide. *D*, row through the [3-^{13}C]Ala[497] resonance of hTpoR showing the absence of a cross-peak to either Leu[494] or Val[495], which is consistent with a kink or break in helical secondary structure in this region of the TM-JM peptide. *E*, row through the [3-^{13}C]Ala[490] resonance of mTpoR showing a strong cross-peak to Leu[487] and/or Val[488].

Two-dimensional ^{13}C NMR spectra were obtained on the hTpoR and mTpoR TM sequences isotopically labeled with [1-^{13}C]Leu[494] or [1-^{13}C]Leu[487], [1-^{13}C]Val[495] or [1-^{13}C]Val[488], and [3-^{13}C]Ala[497] or [3-^{13}C]Ala[490]. These positions just precede His[499] and Leu[492] in the hTpoR and mTpoR sequences, respectively. In the two-dimensional NMR spectra, intramolecular cross-peaks are observed between ^{13}C sites with a through space separation of ≤6 Å. For example, in mTpoR, the 3-^{13}C carbon of Ala[490] is in close proximity to the $^{13}C=O$ groups of Leu[487] (4.3 Å) and Val[488] (5.4 Å) in α-helical secondary structure, and cross-peaks between these ^{13}C resonances are observed in the two-dimensional NMR spectrum. Fig. 5*C* shows the full two-dimensional dipolar assisted rotational res-

AQ: R

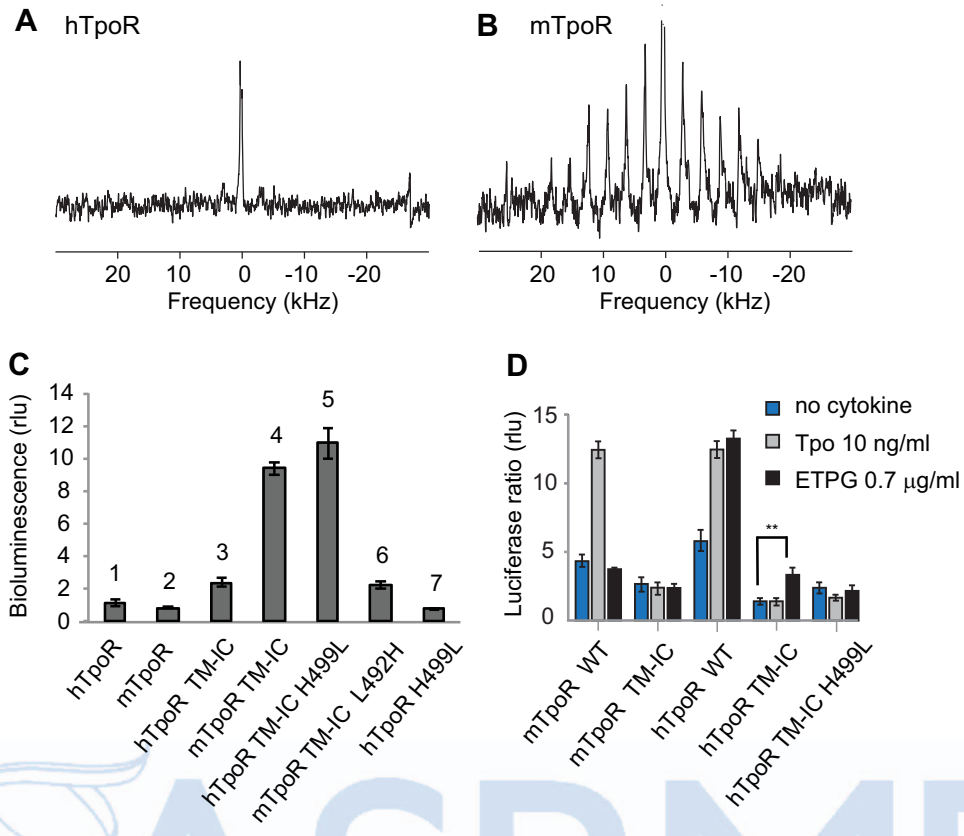


FIGURE 6. **Comparison reveals differences in dimerization of the hTpoR and mTpoR TM peptides.** Deuterium MAS NMR spectra of hTpoR-WT (*A*) and mTpoR-WT (*B*) are shown. The peptides contained deuterated leucine at position 512 (hTpoR) or 505 (mTpoR). *C*, dimerization of full-length hTpoR and mTpoR. Dimerization was detected using the split luciferase assay in cell lysates. hGluc-tagged full-length or TM-IC forms of TpoR as well as mutant hTpoR TM-IC-H499L were co-expressed in BOSC cells, and luciferase activity was measured after cell lysis. *D*, STAT5 transcriptional activity as measured by the split luciferase assay. Histograms are means ± S.D. (*error bars*) of four independent experiments. **, $p < 0.001$, one-way analysis of variance. *ETPG*, eltrombopag; *rlu*, relative luciferase units.

AQ: FF

onance spectrum of mTpoR-WT where a distinct cross-peak is observed between [3-^{13}C]Ala^{490} and either [1-^{13}C]Leu^{487} and/or [1-^{13}C]Val^{488} whose resonances are not resolved. The cross-peak (highlighted in Fig. 5*E*) confirms that this region of mTpoR-WT is α-helical. In contrast, this cross-peak is absent in hTpoR (Fig. 5*D*), revealing that this region does not adopt helical secondary structure.

In addition to the observation of intrahelical cross-peaks in mTpoR, there are distinct changes in chemical shifts of the ^{13}C=O resonances between the hTpoR and mTpoR sequences (Table 1). The ^{13}C=O chemical shifts above ~174 ppm in the mTpoR-WT peptide are consistent with a helical geometry, whereas chemical shifts below ~174 ppm are consistent with unraveling of the helix just N-terminal to His^{499}.

Table 1 summarizes the polarized IR and NMR measurements on hTpoR-WT, mTpoR-WT, and several mutants. There is a general correlation between the dichroic ratio and the presence of helical secondary structure above Leu^{492} (mTpoR) and His^{499} (hTpoR). That is, the TM helices adopt a more parallel orientation (low tilt) when helical structure is observed around Leu^{492} or His^{499}. In the section below, we show that these changes are associated with the ability of the TM helix to dimerize. The comparisons suggest that hTpoR-H499L is structurally similar to mTpoR-WT and that mTpoR-L492H is structurally similar to hTpoR-WT.

The TM Domain of mTpoR Has a Stronger Propensity to Dimerize than hTpoR—In the wild-type and mutant TpoR peptides, dimerization can be estimated from deuterium MAS NMR spectra (28). In these experiments, the peptides are deuterated at Leu^{512} (hTpoR) or Leu^{505} (mTpoR). Comparison of the deuterium MAS NMR spectra of hTpoR-WT and mTpoR-WT reveals a large difference in the MAS spectra (Fig. 6, *A* and *B*). We have previously shown that fast rotational diffusion of the hTpoR monomer results in the loss of the side band pattern and that mutations in the TM and JM regions that lead to dimerization restore the MAS rotational side bands (28). On the basis of the observed side band pattern, we conclude that the monomer-dimer equilibrium in mTpoR-WT is shifted toward dimer compared with hTpoR-WT. The deuterium side band pattern characteristic of dimerization is observed for the activating mutants of hTpoR (S505N and G509N) (Table 1). TM dimerization is also observed for the activating mutants of mTpoR (S498N, G502N, and W508K).

The *G. princeps* luciferase complementation assay (28, 33) was used to assess the dimerization status of the full-length as well as of truncated mouse and human TpoRs containing TM/intracellular (IC) domains. In this assay, two proteins of interest are fused to complementary fragments of *G. princeps* luciferase, denoted hGluc1 and hGluc2. If the proteins interact, luciferase fragments are brought together and fold into their

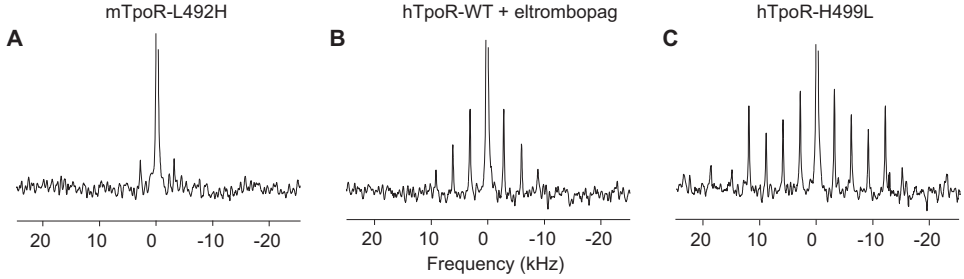


FIGURE 7. **Influence of His^{499} and eltrombopag on TM dimerization.** Deuterium NMR spectra of mTpoR-L492H (*A*), hTpoR-WT with eltrombopag (*B*), and hTpoR-H499L (*C*) are shown. The absence of side bands in the MAS spectra of mTpoR-L492H reflects rapid axial rotation of the peptide in the membrane bilayers. Dimerization induced in the hTpoR-WT peptide by eltrombopag and by the H499L mutation reduces axial diffusion rate and leads to increased intensity in the MAS side bands.

native structure, and the reconstituted luciferase enzyme catalyzes the oxidation of the substrate coelenterazine, which can be detected and quantified using luminescence readers.

The C terminus of murine or human TpoR was fused to complementary fragments of *G. princeps* luciferase (hGluc1 and hGluc2) and transiently co-expressed in BOSC cells where their expression levels were comparable and could be assessed by Western blotting (data not shown). The expression of these constructs individually as expected did not result in reconstitution of luciferase activity (28). The complementation of hGluc-tagged murine and human full-length TpoR was relatively low and appeared to be at similar levels (Fig. 6*C*, conditions 1 and 2), indicating that the level of preformed dimers detected by proximity of cytosolic domains is low. Importantly, removal of the extracellular domain resulted in significantly higher dimerization of the mTpoR (condition 4) but not of the hTpoR (condition 3) whose dimerization remained the same compared with the full-length receptor. Thus, the hTpoR TM-IC segment possesses an additional mechanism to prevent its self-dimerization that could be ascribed to His^{499}. Indeed, substitution of His^{499} to leucine allows dimerization of the TM-IC form of hTpoR (condition 5), whereas substitution of Leu^{492} to histidine in the TM-IC form of the mTpoR dramatically decreased dimerization as assayed by luciferase complementation (condition 6).

The results in Fig. 6*C* for the TM-IC constructs are consistent with the NMR analysis of the TM-JM peptides, namely that His^{499} prevents dimerization of the TM domain of hTpoR in the context of a truncated TpoR lacking the extracellular domain. Using the Dual-Luciferase assay to monitor receptor activity, we show in Fig. 6*D* that the TM-IC constructs of mTpoR are inactive despite increased dimerization. In the hTpoR constructs, truncation of the extracellular domain abolishes Tpo-dependent activity but still allows activation upon the addition of eltrombopag. This activation is not detected in the H499L mutant.

Eltrombopag Induces Dimerization of hTpoR TM Helix Peptides—Comparison of the hTpoR and mTpoR TM-JM peptides shows that the monomer-dimer equilibrium is shifted toward monomer in hTpoR-WT compared with mTpoR-WT (Fig. 6, *A* and *B*). Binding of the small molecule agonist eltrombopag induces receptor activation and requires the presence of His^{499} (40). In the absence of activation, His^{499} was previously shown to cause a kink in the TM helix (41). We asked whether this structure changes in the presence of eltrombopag and whether eltrombopag influences dimerization of the hTpoR TM domains. Comparison of hTpoR-WT peptides without (Fig. 6*A*) and with eltrombopag (Fig. 7*B*) shows a slight increase in the intensity of the deuterium MAS side bands, consistent with a shift toward the peptide dimer. Furthermore, the secondary structure around His^{499} becomes helical in the hTpoR-WT peptide in the presence of eltrombopag (Table 1). Increased dimerization agrees with the studies on the TM-IC constructs containing the full IC domain that exhibit an increase in activity upon eltrombopag binding (Fig. 6*D*). We also asked whether substituting His^{499} with leucine, the corresponding residue in mTpoR, would influence dimerization. Indeed, hTpoR-H499L also becomes more dimeric compared with hTpoR-WT (Fig. 7*C*), consistent with an observed increase in the dichroic ratio from polarized IR measurements (Table 1), whereas the mTpoR-L492H peptide becomes more monomeric compared with mTpoR-WT (Fig. 7*A*). The dimeric interfaces in Fig. 7, *B* and *C*, are predicted to be different between the inactive dimeric and active dimeric states of hTpoR (see below).

Rotational Orientation of TM Helices in Inactive and Active Dimers—Interhelical NMR measurements of specifically labeled 41-residue mTpoR peptides (Glu^{481}–Ser^{524}) allow us to probe the interface that mediates dimerization. In these experiments, two mTpoR peptides with complementary ^{13}C labeling were reconstituted together into 1,2-dimyristoyl-*sn*-glycero-3-phosphocholine/*1,2-dimyristoyl-sn-glycero-3-phosphoglycerol* bilayers at a peptide:lipid molar ratio of 1:60. The positions of the labels were selected on the basis of our previous engineered Put3 constructs that defined the inactive and active interfaces.

To probe the inactive dimer interface, two-dimensional ^{13}C NMR spectra were obtained on mTpoR-WT peptides containing ^{13}C-labeled Ala^{499} and Gly^{502}. One peptide was labeled with [3-^{13}C]Ala^{499} and [1-^{13}C]Gly^{502}, and the other was labeled with [1-^{13}C]Ala^{499} and [2-^{13}C]Gly^{502}. Ala^{499} is predicted to be in the inactive interface, whereas Gly^{502} is at the boundary between inactive and active interfaces. We observe a cross-peak between the diagonal 3-^{13}C and 1-^{13}C resonances of Ala^{499} (Fig. 8*A*) and between the diagonal 2-^{13}C and 1-^{13}C resonances of Gly^{502} (Fig. 8*B*). These ^{13}C-labeled carbons are on different peptides, and the cross-peak intensities are consistent with an interhelical [3-^{13}C]Ala^{499} to ^{13}C=O distance of ~5.4 Å and an interhelical [2-^{13}C]Gly^{502} to C=O distance of ~5.2 Å. An intrahelical cross-peak is also observed between the [2-^{13}C]Gly^{502} resonance and the [1-^{13}C]Ala^{499} resonance. These ^{13}C labels are on the same peptide and are estimated to be ~4.4 Å apart in an

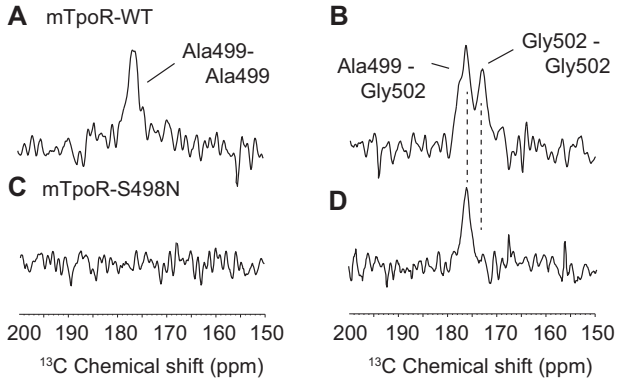


FIGURE 8. **Interhelical NMR measurements of mTpoR peptides (Glu^{481}–Ser^{524}).** *A*, row through the diagonal resonance of the [3-^{13}C]Ala^{499} carbon reveals a cross-peak with the [1-^{13}C]Ala^{499} C=O resonance. In an inactive dimer, the interhelical [3-^{13}C]Ala^{499} to [1-^{13}C]Ala^{499} distance is predicted to be ~5.4 Å. *B*, row through the diagonal resonance of [2-^{13}C]Gly^{502} reveals a cross-peak with the [1-^{13}C]Gly^{502} resonance where the predicted interhelical distance is ~5.2 Å. In this sample, an intrahelical cross-peak is also observed between [2-^{13}C]Gly^{502} and [1-^{13}C]Ala^{499}. *C* and *D*, dipolar assisted rotational resonance NMR experiments were undertaken on mTpoR-S498N using the same labeling strategy as in *A* and *B*. We do not observe Ala^{499}-Ala^{499} or Gly^{502}-Gly^{502} cross-peaks in peptides containing this activating mutation.

α-helical geometry. An intrahelical cross-peak between the [3-^{13}C]Ala^{499} and [1-^{13}C]Gly^{502} resonances was not observed as the distance between ^{13}C sites is >6 Å in an α-helix.

To probe the potential active interface(s), parallel two-dimensional NMR experiments were undertaken on mTpoR-S498N (Fig. 8, *C* and *D*). In contrast to the results above, we do not observe interhelical Ala^{499}-Ala^{499} or Gly^{502}-Gly^{502} cross-peaks in peptides containing this activating mutation, confirming that we lose the inactive interface. The absence of contacts between these residues is consistent with a shift in the dimer interface to either the active cc-TpoR-I or cc-TpoR-V interfaces defined by engineered Put3 dimers, both of which contain Ser^{498} in the interface.

Models of the TM domain of the hTpoR in inactive and active orientations are shown in Fig. 9*A*. The inactive receptor exists in a monomer-dimer equilibrium. The split luciferase measurements of the full-length receptor along with deuterium NMR measurements of the hTpoR-WT TM-JM peptides indicate that the equilibrium is shifted toward monomer. His^{499} induces a break in the TM helix. The side chain of His^{499} is predicted to reside within the headgroup region of phospholipids on the extracellular side of the bilayer. Given the bilayer thickness, this requires the RWQFP motif to partition into the headgroup region of the phospholipids on the intracellular side of the bilayer. The active orientation is modeled as a dimer (Fig. 9*A*, *right*). In the wild-type full-length receptor, ligand binding drives a shift of the receptor dimer to an active orientation with Ser^{505} in the interface. Dimerization is also mediated by hydrogen bonding interactions involving the Asn side chains in the S505N mutant (Fig. 9*A*, *right*). In the TM-JM peptides, dimerization induces helical secondary structure in the region just N-terminal to His^{499} and reduces the overall dichroic ratio (helix tilt angle).

The inactive mTpoR also exists in a monomer-dimer equilibrium (Fig. 9*B*). In the absence of the extracellular domain, the equilibrium shifts toward dimer. The interface mediating the inactive dimer in TM-JM peptides involves packing of Ala^{499} and Gly^{502}. This interface is the same as that found in the engineered Put3 constructs (26). In the wild-type full-length receptor, ligand binding also drives a shift of the receptor dimer to an active orientation with Ser^{498} in the interface. Hydrogen bonding interactions involving Asn side chains stabilize this orientation in the S498N mutant (Fig. 9*B*, *right*).

Discussion

We show that several asparagine mutations in the TM domain of the mTpoR activate signaling, whereas only one asparagine substitution (S505N) does so for the hTpoR. Thus, human TpoR appears to be largely protected from oncogenic activation by Asn mutations. This major difference can be abolished if His^{499} in the hTpoR is substituted by leucine, the homologous residue in the mTpoR. We further show that His^{499} locally influences the structure and orientation of the TM helix, and this change influences the ability of receptors with specific TM asparagine mutations to traffic to the cell surface.

Receptor Dimerization in TpoR Signaling—Dimerization of the cytokine receptors is required for activation. The EpoR (24), prolactin receptor (42), and growth hormone receptor (22, 23) have been found to associate as preformed (inactive) dimers mediated by TM domain interactions. The implication is that there is a change in TM helix interfaces upon ligand binding and that this change is relayed to the intracellular domain to allow receptor activation. AQ: S

Our previous studies indicated that, upon ligand binding or in the constitutively active S505N and W515K mutants, the monomer-dimer equilibrium shifts toward the active dimer (28). We extend these results here using the split luciferase assay to show that both the full-length hTpoR and mTpoR exist at a low level as preformed dimers with the majority of chains detected as monomers. Interestingly, removal of the extracellular domain induces receptor dimerization in the mTpoR but not the hTpoR.

The model that emerges is one where ligand binding triggers a conformational change in the extracellular domain that allows receptor dimerization in an active conformation. Using structural approaches, we are able to mimic the dimerization behavior of the murine and human receptors when the extracellular domain is removed (*i.e.* the TM-JM peptides and the TM-IC constructs are largely monomeric for hTpoR and dimeric for mTpoR). This observation indicates that the extracellular domain blocks the ability of the TM helices to directly interact in the mTpoR. In the hTpoR, there is an additional mechanism that blocks helix association, namely the change in the helix conformation induced by His^{499}. The H499L mutation induces constitutive dimerization of hTpoR in the absence of the extracellular domain in both the TM-IC constructs and the TM-JM peptides. In both the wild-type hTpoR receptor constructs and the TM-JM peptides, the ability of the activating Asn mutations and eltrombopag (for hTpoR) to induce dimerization strongly suggests that helix association is a key element of the activation mechanism.

The comparative studies on dimerization using the split luciferase assay between the full-length WT TpoRs and the cor-

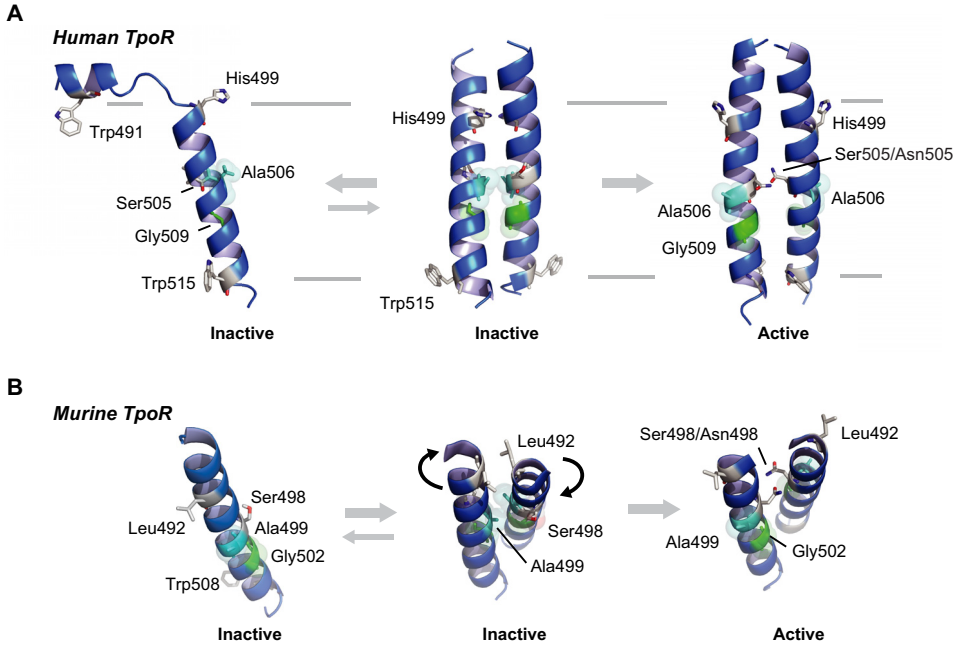


FIGURE 9. **Models of the monomeric and dimeric TM domains of the hTpoR and mTpoR.** *A*, human TpoR. FTIR and NMR measurements on the TM-JM domain of hTpoR show that the wild-type peptide is primarily monomer (*left*) with a break in helical secondary structure in the region N-terminal to His^{499}. In the S505N mutant of the hTpoR TM-JM domain (*right*), an increase in the dichroic ratio of the amide I vibration indicates that the TM helix is oriented closer to the bilayer normal, whereas the NMR measurements indicate that helix is induced in the region N-terminal to His^{499}. In the full-length receptor, we propose that the monomer and inactive dimer (*middle*) are in equilibrium and that either ligand binding or the S505N mutation shifts the equilibrium to the active dimer with either Ser^{505} (WT) or Asn^{505} (mutant) in the dimer interface. *B*, murine TpoR. FTIR and NMR measurements on the TM-JM domain of mTpoR show that the wild-type peptide is primarily dimer (*middle*) in which dimerization is mediated by close packing of Ala^{499} and Gly^{502}. *D*, in the full-length receptor, we propose that the monomer (*right*) and inactive dimer are in equilibrium and that either ligand binding or the S498N mutation shifts the equilibrium to the active dimer with either Ser^{498} (WT) or Asn^{498} (mutant) in the dimer interface. The dimer structures of hTpoR-S505N, mTpoR-WT, and mTpoR-S505N were taken from computational searches using the program CHI (52, 53) as described previously (26). These low energy structures correspond to the average of several structures in the searches that form clusters and best reproduce the experimental data presented here.

responding truncated TM-IC constructs show large differences in receptor dimerization. We have previously compared dimerization for hTpoR-WT and murine EpoR-WT using the split luciferase assay and observed a 2-fold difference in bioluminescence, indicating that both the hTpoR and murine EpoR receptors exist in a monomer-dimer equilibrium with murine EpoR shifted more toward the receptor dimer (28). The subpopulation of preformed dimers may be the relevant form for rapid signaling by TpoR. Although our studies reveal clear differences in dimerization in comparisons of (for *e.g.*) the full-length hTpoR and hTpoR TM-IC-H499L, they open up the question as to how different cell types or membrane environments influence the monomer-dimer equilibrium. For example, there may be differences in the monomer-dimer equilibrium (and hence the level of preformed dimers) between TpoR-expressing cells, namely hematopoietic stem cells and megakaryocyte progenitors, or there may be a shift in equilibrium if the membrane environment changes, such as incorporation of receptors into lipid rafts. The ability of the cell to modulate the monomer-dimer equilibrium would provide an additional control mechanism for receptor activation.

TM Helix Orientation in TpoR Signaling—The orientation of the TM and intracellular domains within dimers of single TM receptors is generally important for activation. In both the EpoR (32) and TpoR (26), we have shown using Put3 coiled coil constructs that receptor activity is dependent on the orientation of the TM helix. For mTpoR, only one dimeric interface (cc-TpoR-II) is inactive. The cc-TpoR-II interface is lined with leucines and an A*XX*G motif and ends with Gln^{509} within the (K/R)WQFP motif, corresponding to Gln^{516} in the hTpoR. The A*XX*G sequence has similarities with the G*XXX*G sequences known to mediate TM dimerization (43, 44). The close packing of the TM helices due to these small side chains places Gln^{509} of mTpoR in a position where it can mediate interhelical hydrogen bonding and stabilize dimerization. We ascribe this inactive interface to the same interface that mediates dimerization of the inactive TM-IC constructs of mTpoR. Moreover, we show with NMR (Fig. 8) that the TM-JM peptides (also lacking a large extracellular domain and hence similar to the TM-IC constructs) dimerize via the same interface as in the inactive cc-TpoR-II construct.

In contrast, several interfaces in the Put3 coiled coil constructs have previously been shown to exhibit various levels of activity (26). cc-TpoR-I induced high numbers of platelets without other cytological features of myeloproliferation in bone marrow, and cc-TpoR-V induced a myeloproliferative phenotype with small red blood cells and variable levels of thrombocytosis (26). Thus, the active helix interfaces identified in the Put3 experiments are consistent with the Asn substitutions reported here, at least for the mTpoR. That is, the cc-TpoR-I and cc-TpoR-V interfaces involve the residues where asparagine mutations lead to the strongest activity (V494N, S498N, L501N, and G502N). In cc-TpoR-V, the dimer interface is mediated by an S*XXX*G sequence, which again allows close helix packing. In our NMR studies, the S498N mutation induces a change in the conformation of the mTpoR peptide

dimer, and we lose the contacts between Ala^{499} and Gly^{502} characteristic of the inactive dimer (Fig. 8). The low energy structure shown in Fig. 9*B* corresponds to cc-TpoR-I in which Asn^{498} forms interhelical hydrogen bonds.

Eltrombopag Drives Dimerization of hTpoR-WT—Eltrombopag is a Food and Drug Administration-approved drug used for the treatment of thrombocytopenia (low platelet numbers). Previous studies have found that eltrombopag can activate hTpoR but not mTpoR (40). Eltrombopag and related small molecule agonists have been found to interact with His^{499} (41). We find that this transmembrane-acting compound increases the dichroic ratio in FTIR measurements, induces helix in the Leu^{494}–Ala^{497} sequence in the TM domain, and leads to receptor dimerization as assayed by deuterium NMR line shapes. The changes in dimerization induced by eltrombopag (Fig. 7*B*) are weaker than those observed for the H499L mutant (Fig. 7*C*). Nevertheless, eltrombopag appears to induce receptor activation in a similar manner as the S505N mutation; namely, both overcome the ability of His^{499} to inhibit TM dimerization.

Multiple Levels of Regulation Involving the TM and JM Regions of TpoR—The wild-type hTpoR has several mechanisms for regulating dimerization of the TM region of the receptor. These involve the extracellular domain, the TM His^{499} residue, and the intracellular RWQFP insert. Removal of the extracellular domain or the H499L mutation alone does not induce dimerization. Both are required in the same construct. Ligand binding within the extracellular domain or mutations of Trp^{515} within the RWQFP insert can both overcome these mechanisms, leading to an active receptor conformation. In the mTpoR, removal of the extracellular domain induces dimerization in an inactive conformation. Dual-Luciferase measurements of receptor activation show that the TM-IC constructs of mTpoR are inactive. Thus, dimerization *per se* does not suffice for activation. Interestingly, the TM-IC constructs differ from the viral Mpl protein of the myeloproliferative leukemia virus by the presence of an extracellular domain of 109 amino acids comprising 43 from the original murine sequence and 66 from the Friend murine leukemia virus. This suggests that the extracellular amino acids in the v-Mpl are able to stabilize the TM-IC portion of the receptor in an active orientation.

Our results reveal that the TM helices in TpoR are not passive elements in ligand-induced dimerization. The TM helices have a stronger propensity to form dimers or higher order oligomers than to remain in a monomeric state. The extracellular, juxtamembrane, and intracellular domains all contribute to modulating TM association. This observation may generally hold for ligand-induced activation of single TM receptors. For example, the TM helices in the *ErbB* family of receptor tyrosine kinases all have a strong propensity to dimerize (45), and removal of the extracellular domain can lead to active dimers (46, 47) or can trigger intramembrane proteolysis (48, 49). In these receptors, the juxtamembrane sequences play an influential role in dimerization and activation (50). Mutation of Val^{664} to Gln in the TM sequence of the *ErbB2-Neu* receptor can induce dimerization and constitutive receptor activation in a manner similar to the S505N mutation in hTpoR (51).

AQ: V

The additional layer of activity control exerted by His^{499} in hTpoR may reflect the central role that this receptor plays in hematopoiesis. TpoR not only regulates megakaryocyte/platelet development but also contributes to the survival of hematopoietic stem cells, which give rise to all other blood cells. The acquisition of histidine at position 499 during evolution protects the hTpoR from the transforming effect of several Asn TM mutations that are activating in the mTpoR.

Author Contributions—S. O. S. and S. N. C. conceived and designed the study, interpreted the data, and wrote the paper. E. L. and J.-P. D. designed and performed experiments (γ2A luciferase assays, Ba/F3 cell retroviral transduction, sorting, cell surface labeling, and proliferation), analyzed the data, prepared the figures, and wrote the paper. J. S. designed and performed experiments (γ2A luciferase assays, Ba/F3 cell retroviral transduction, sorting, cell surface labeling, and proliferation). S. M. M. performed cloning and expression of TpoR constructs. E. L. performed intracellular TpoR metabolism studies. T. S. synthesized and purified the TM peptides. S. D. carried out membrane reconstitutions and FTIR studies. V. G. performed the *Gaussia* luciferase experiments.

Acknowledgments—We are grateful to Dr. Martine Ziliox for assistance with the NMR experiments. We also thank Drs. Ian Brett and Miki Itaya for preliminary experiments that formed the basis for the studies described here, Céline Mouton for expert technical support, and Dr. Nicolas Dauguet for flow cytometry and cell sorting. We gratefully acknowledge the W. M. Keck Foundation for support of the NMR facilities in the Center of Structural Biology at Stony Brook.

References

1. Geddis, A. E., Linden, H. M., and Kaushansky, K. (2002) Thrombopoietin: a pan-hematopoietic cytokine. *Cytokine Growth Factor Rev.* **13,** 61–73
2. Vigon, I., Mornon, J. P., Cocault, L., Mitjavila, M. T., Tambourin, P., Gisselbrecht, S., and Souyri, M. (1992) Molecular-cloning and characterization of Mpl, the human homolog of the v-mpl oncogene—identification of a member of the hematopoietic growth-factor receptor superfamily. *Proc. Natl. Acad. Sci. U.S.A.* **89,** 5640–5644
3. Watowich, S. S., Yoshimura, A., Longmore, G. D., Hilton, D. J., Yoshimura, Y., and Lodish, H. F. (1992) Homodimerization and constitutive activation of the erythropoietin receptor. *Proc. Natl. Acad. Sci. U.S.A.* **89,** 2140–2144
4. Syed, R. S., Reid, S. W., Li, C., Cheetham, J. C., Aoki, K. H., Liu, B., Zhan, H., Osslund, T. D., Chirino, A. J., Zhang, J., Finer-Moore, J., Elliott, S., Sitney, K., Katz, B. A., Matthews, D. J., Wendoloski, J. J., Egrie, J., and Stroud, R. M. (1998) Efficiency of signalling through cytokine receptors depends critically on receptor orientation. *Nature* **395,** 511–516
5. de Vos, A. M., Ultsch, M., and Kossiakoff, A. A. (1992) Human growth-hormone and extracellular domain of its receptor: crystal structure of the complex. *Science* **255,** 306–312
6. Royer, Y., Staerk, J., Costuleanu, M., Courtoy, P. J., and Constantinescu, S. N. (2005) Janus kinases affect thrombopoietin receptor cell surface localization and stability. *J. Biol. Chem.* **280,** 27251–27261
7. Constantinescu, S. N., Huang, L. J., Nam, H., and Lodish, H. F. (2001) The erythropoietin receptor cytosolic juxtamembrane domain contains an essential, precisely oriented, hydrophobic motif. *Mol. Cell* **7,** 377–385
8. Tanner, J. W., Chen, W., Young, R. L., Longmore, G. D., and Shaw, A. S. (1995) The conserved box-1 motif of cytokine receptors is required for association with JAK kinases. *J. Biol. Chem.* **270,** 6523–6530
9. Quelle, F. W., Sato, N., Witthuhn, B. A., Inhorn, R. C., Eder, M., Miyajima, A., Griffin, J. D., and Ihle, J. N. (1994) Jak2 associates with the β_C chain of the receptor far granulocyte-macrophage colony-stimulating factor, and Its activation requires the membrane-proximal region. *Mol. Cell. Biol.* **14,** 4335–4341
10. Tong, W., Sulahian, R., Gross, A. W., Hendon, N., Lodish, H. F., and Huang, L. J. (2006) The membrane-proximal region of the thrombopoietin receptor confers its high surface expression by JAK2-dependent and

-independent mechanisms. *J. Biol. Chem.* **281,** 38930–38940
11. Sabath, D. F., Kaushansky, K., and Broudy, V. C. (1999) Deletion of the extracellular membrane-distal cytokine receptor homology module of Mpl results in constitutive cell growth and loss of thrombopoietin binding. *Blood* **94,** 365–367
12. Staerk, J., Lacout, C., Sato, T., Smith, S. O., Vainchenker, W., and Constantinescu, S. N. (2006) An amphipathic motif at the transmembrane-cytoplasmic junction prevents autonomous activation of the thrombopoietin receptor. *Blood* **107,** 1864–1871
13. Malinge, S., Ragu, C., Della-Valle, V., Pisani, D., Constantinescu, S. N., Perez, C., Villeval, J. L., Reinhardt, D., Landman-Parker, J., Michaux, L., Dastugue, N., Baruchel, A., Vainchenker, W., Bourquin, J. P., Penard-Lacronique, V., and Bernard, O. A. (2008) Activating mutations in human acute megakaryoblastic leukemia. *Blood* **112,** 4220–4226
14. Ding, J., Komatsu, H., Wakita, A., Kato-Uranishi, M., Ito, M., Satoh, A., Tsuboi, K., Nitta, M., Miyazaki, H., Iida, S., and Ueda, R. (2004) Familial essential thrombocythemia associated with a dominant-positive activating mutation of the c-MPL gene, which encodes for the receptor for thrombopoietin. *Blood* **103,** 4198–4200
15. Onishi, M., Mui, A. L., Morikawa, Y., Cho, L., Kinoshita, S., Nolan, G. P., Gorman, D. M., Miyajima, A., and Kitamura, T. (1996) Identification of an oncogenic form of the thrombopoietin receptor MPL using retrovirus-mediated gene transfer. *Blood* **88,** 1399–1406
16. Marty, C., Chaligné, R., Lacout, C., Constantinescu, S. N., Vainchenker, W., and Villeval, J. L. (2009) Ligand-independent thrombopoietin mutant receptor requires cell surface localization for endogenous activity. *J. Biol. Chem.* **284,** 11781–11791
17. Pecquet, C., Staerk, J., Chaligné, R., Goss, V., Lee, K. A., Zhang, X., Rush, J., Van Hees, J., Poirel, H. A., Scheiff, J. M., Vainchenker, W., Giraudier, S., Polakiewicz, R. D., and Constantinescu, S. N. (2010) Induction of myeloproliferative disorder and myelofibrosis by thrombopoietin receptor W515 mutants is mediated by cytosolic tyrosine 112 of the receptor. *Blood* **115,** 1037–1048
18. Pardanani, A. D., Levine, R. L., Lasho, T., Pikman, Y., Mesa, R. A., Wadleigh, M., Steensma, D. P., Elliott, M. A., Wolanskyj, A. P., Hogan, W. J., McClure, R. F., Litzow, M. R., Gilliland, D. G., and Tefferi, A. (2006) MPL515 mutations in myeloproliferative and other myeloid disorders: a study of 1182 patients. *Blood* **108,** 3472–3476
19. Pikman, Y., Lee, B. H., Mercher, T., McDowell, E., Ebert, B. L., Gozo, M., Cuker, A., Wernig, G., Moore, S., Galinsky, I., DeAngelo, D. J., Clark, J. J., Lee, S. J., Golub, T. R., Wadleigh, M., Gilliland, D. G., and Levine, R. L. (2006) MPLW515L is a novel somatic activating mutation in myelofibrosis with myeloid metaplasia. *PLoS Med.* **3,** e270
20. Livnah, O., Stura, E. A., Middleton, S. A., Johnson, D. L., Jolliffe, L. K., and Wilson, I. A. (1999) Crystallographic evidence for preformed dimers of erythropoietin receptor before ligand activation. *Science* **283,** 987–990
21. Brown, R. J., Adams, J. J., Pelekanos, R. A., Wan, Y., McKinstry, W. J., Palethorpe, K., Seeber, R. M., Monks, T. A., Eidne, K. A., Parker, M. W., and Waters, M. J. (2005) Model for growth hormone receptor activation based on subunit rotation within a receptor dimer. *Nat. Struct. Mol. Biol.* **12,** 814–821
22. Brooks, A. J., Chhabra, Y., Abankwa, D., O'Mara, M., Dai, W., Gardon, O., Tunny, K. A., Blucher, K. M., Morton, C. J., Parker, M. W., Sierecki, E., Gambin, Y., Gomez, G. A., Alexandrov, K. K., Doxastakis, M., Mark, A. E., and Waters, M. J. (2014) A new cytokine receptor activation paradigm: activation of JAK2 by the growth hormone receptor. *Cytokine* **70,** 22
23. Brooks, A. J., Dai, W., O'Mara, M. L., Abankwa, D., Chhabra, Y., Pelekanos, R. A., Gardon, O., Tunny, K. A., Blucher, K. M., Morton, C. J., Parker, M. W., Sierecki, E., Gambin, Y., Gomez, G. A., Alexandrov, K., Wilson, I. A., Doxastakis, M., Mark, A. E., and Waters, M. J. (2014) Mechanism of activation of protein kinase JAK2 by the growth hormone receptor. *Science* **344,** 1249783
24. Constantinescu, S. N., Keren, T., Socolovsky, M., Nam, H., Henis, Y. I., and Lodish, H. F. (2001) Ligand-independent oligomerization of cell-surface erythropoietin receptor is mediated by the transmembrane domain. *Proc. Natl. Acad. Sci. U.S.A.* **98,** 4379–4384
25. Ebie, A. Z., and Fleming, K. G. (2007) Dimerization of the erythropoietin receptor transmembrane domain in micelles. *J. Mol. Biol.* **366,** 517–524
26. Staerk, J., Defour, J.-P., Pecquet, C., Leroy, E., Antoine-Poirel, H., Brett, I., Itaya, M., Smith, S. O., Vainchenker, W., and Constantinescu, S. N. (2011) Orientation-specific signalling by thrombopoietin receptor dimers. *EMBO J.* **30,** 4398–4413
27. Matthews, E. E., Thévenin, D., Rogers, J. M., Gotow, L., Lira, P. D., Reiter, L. A., Brissette, W. H., and Engelman, D. M. (2011) Thrombopoietin receptor activation: transmembrane helix dimerization, rotation, and allosteric modulation. *FASEB J.* **25,** 2234–2244
28. Defour, J.-P., Itaya, M., Gryshkova, V., Brett, I. C., Pecquet, C., Sato, T., Smith, S. O., and Constantinescu, S. N. (2013) Tryptophan at the transmembrane-cytosolic junction modulates thrombopoietin receptor dimerization and activation. *Proc. Natl. Acad. Sci. U.S.A.* **110,** 2540–2545
29. Zhou, F. X., Cocco, M. J., Russ, W. P., Brunger, A. T., and Engelman, D. M. (2000) Interhelical hydrogen bonding drives strong interactions in membrane proteins. *Nat. Struct. Biol.* **7,** 154–160
30. Zhou, F. X., Merianos, H. J., Brunger, A. T., and Engelman, D. M. (2001) Polar residues drive association of polyleucine transmembrane helices. *Proc. Natl. Acad. Sci. U.S.A.* **98,** 2250–2255
31. Choma, C., Gratkowski, H., Lear, J. D., and DeGrado, W. F. (2000) Asparagine-mediated self-association of a model transmembrane helix. *Nat. Struct. Biol.* **7,** 161–166
32. Seubert, N., Royer, Y., Staerk, J., Kubatzky, K. F., Moucadel, V., Krishnakumar, S., Smith, S. O., and Constantinescu, S. N. (2003) Active and inactive orientations of the transmembrane and cytosolic domains of the erythropoietin receptor dimer. *Mol. Cell* **12,** 1239–1250
33. Remy, I., and Michnick, S. W. (2006) A highly sensitive protein-protein interaction assay based on *Gaussia* luciferase. *Nat. Methods* **3,** 977–979
34. Liu, W., Crocker, E., Constantinescu, S. N., and Smith, S. O. (2005) Helix packing and orientation in the transmembrane dimer of gp55-P of the spleen focus forming virus. *Biophys. J.* **89,** 1194–1202
35. Rothschild, K. J., and Clark, N. A. (1979) Polarized infrared spectroscopy of oriented purple membrane. *Biophys. J.* **25,** 473–487
36. Takegoshi, K., Nakamura, S., and Terao, T. (2001) ^{13}C-^{1}H dipolar-assisted rotational resonance in magic-angle spinning NMR. *Chem. Phys. Lett.* **344,** 631–637
37. Landschulz, W. H., Johnson, P. F., and McKnight, S. L. (1988) The leucine zipper: a hypothetical structure common to a new class of DNA binding proteins. *Science* **240,** 1759–1764
38. O'Shea, E. K., Klemm, J. D., Kim, P. S., and Alber, T. (1991) X-ray structure of the GCN4 leucine zipper, a two-stranded, parallel coiled coil. *Science* **254,** 539–544
39. Lear, J. D., Gratkowski, H., Adamian, L., Liang, J., and DeGrado, W. F. (2003) Position-dependence of stabilizing polar interactions of asparagine in transmembrane helical bundles. *Biochemistry* **42,** 6400–6407
40. Nakamura, T., Miyakawa, Y., Miyamura, A., Yamane, A., Suzuki, H., Ito, M., Ohnishi, Y., Ishiwata, N., Ikeda, Y., and Tsuruzoe, N. (2006) A novel nonpeptidyl human c-Mpl activator stimulates human megakaryopoiesis and thrombopoiesis. *Blood* **107,** 4300–4307
41. Kim, M. J., Park, S. H., Opella, S. J., Marsilje, T. H., Michellys, P. Y., Seidel, H. M., and Tian, S. S. (2007) NMR structural studies of interactions of a small, nonpeptidyl Tpo mimic with the thrombopoietin receptor extracellular juxtamembrane and transmembrane domains. *J. Biol. Chem.* **282,** 14253–14261
42. Gadd, S. L., and Clevenger, C. V. (2006) Ligand-independent dimerization of the human prolactin receptor isoforms: functional implications. *Mol. Endocrinol.* **20,** 2734–2746
43. MacKenzie, K. R., and Engelman, D. M. (1998) Structure-based prediction of the stability of transmembrane helix-helix interactions: the sequence dependence of glycophorin A dimerization. *Proc. Natl. Acad. Sci. U.S.A.* **95,** 3583–3590
44. Russ, W. P., and Engelman, D. M. (1999) TOXCAT: a measure of transmembrane helix association in a biological membrane. *Proc. Natl. Acad. Sci. U.S.A.* **96,** 863–868
45. Mendrola, J. M., Berger, M. B., King, M. C., and Lemmon, M. A. (2002) The single transmembrane domains of ErbB receptors self-associate in cell membranes. *J. Biol. Chem.* **277,** 4704–4712
46. Downward, J., Yarden, Y., Mayes, E., Scrace, G., Totty, N., Stockwell, P., Ullrich, A., Schlessinger, J., and Waterfield, M. D. (1984) Close similarity

AQ: X

AQ: W

of epidermal growth-factor receptor and V-Erb-B oncogene protein sequences. *Nature* **307,** 521–527
47. Matsushime, H., Wang, L. H., and Shibuya, M. (1986) Human c-ros-1 gene homologous to the v-ros sequence of UR2 sarcoma virus encodes for a transmembrane receptorlike molecule. *Mol. Cell. Biol.* **6,** 3000–3004
48. Lee, H. J., Jung, K. M., Huang, Y. Z., Bennett, L. B., Lee, J. S., Mei, L., and Kim, T. W. (2002) Presenilin-dependent γ-secretase-like intramembrane cleavage of ErbB4. *J. Biol. Chem.* **277,** 6318–6323
49. Vidal, G. A., Naresh, A., Marrero, L., and Jones, F. E. (2005) Presenilin-dependent γ-secretase processing regulates multiple ERBB4/HER4 activities. *J. Biol. Chem.* **280,** 19777–19783
50. Hubbard, S. R. (2004) Juxtamembrane autoinhibition in receptor tyrosine kinases. *Nat. Rev. Mol. Cell Biol.* **5,** 464–471
51. Bargmann, C. I., and Weinberg, R. A. (1988) Oncogenic activation of the *neu*-encoded receptor protein by point mutation and deletion. *EMBO J.* **7,** 2043–2052
52. Arkin, I. T., Adams, P. D., MacKenzie, K. R., Lemmon, M. A., Brünger, A. T., and Engelman, D. M. (1994) Structural organization of the pentameric transmembrane α-helices of phospholamban, a cardiac ion channel. *EMBO J.* **13,** 4757–4764
53. Adams, P. D., Arkin, I. T., Engelman, D. M., and Brünger, A. T. (1995) Computational searching and mutagenesis suggest a structure for the pentameric transmembrane domain of phospholamban. *Nat. Struct. Biol.* **2,** 154–162

ASBMB

III.4.4. Unpublished but related results and discussion

cc-TpoR-II and VI are fusion proteins that adopt weakly activating interfaces for the murine TpoR. To assess the effect of the His499 in the context of the coiled-coil TpoR proteins and to render our system closer to the human TpoR, we introduce the His 492 (His 499 in the human TpoR) in the coiled-coil murine TpoR fusion proteins cc-TpoR-0, cc-TpoR-I, cc-TpoR-II and cc-TpoR-III. The subsequent cc-TpoR-IV, -V, -IV would have His492 very close to the coiled-coil and were not engineered. The weakness of this approach is that we do not know whether the His will also kink the α-helix in the context of the Put3 coiled-coil. However, cc-TpoR-II seems now stronger than cc-TpoR-III. This suggests that His499 in human can change the observed inactive interface. The relative activity changes observed for the 4 coiled-coil proteins tested could be compatible with a 50° CCW rotation, as expected.

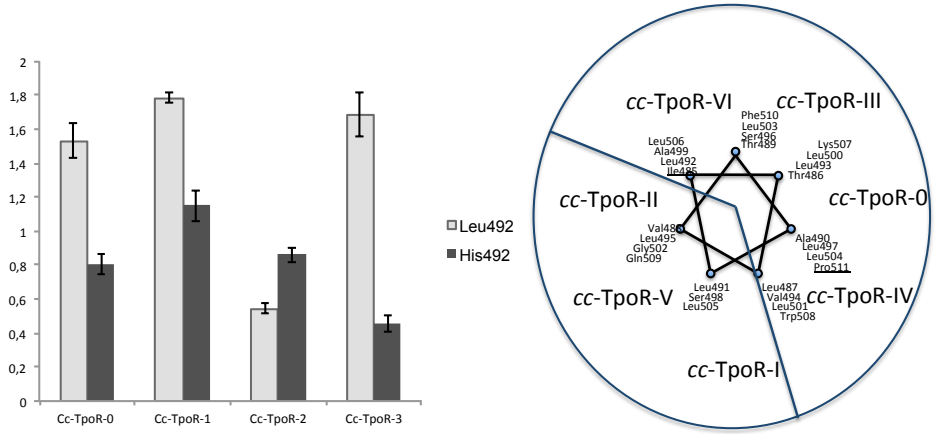


Figure 67 - cc-TpoRs + His 492

The lower maximal response could be explained by a poorer total expression of this His 492.

III.4.4.1. Big apes do have a Histidine at 499, but lack the entire RWQFP motif

Big apes are known to respond to Eltrombopag and possess a histidine at position 499. The TMD alignment according to Box 1 showed an absence of 15 residues including the entire RWQFP motif which interestingly brings the register back to the same interface with approximately 15x100°gets to 4 x 360°. However, we cannot exclude a sequencing or annotation error and we plan to re-sequence TpoR from Big apes.

```
Sumatran orangutan
>Pongo|abelii
WSSWSDPARVETATETAWISLVTALHLVLGLRAV---------------RLRHALWPSLPDL

Human
>Homo|sapiens
WSSWSDPTRVETATETAWISLVTALHLVLGLSAVLGLLLLRWQFPAHYRRLRHALWPSLPDL
```

Figure 68 - big apes alignments

III.5. Preamble: Unraveling TpoR oncogenic mechanism: gaining order from local disorder (In preparation)

Jean-Philippe Defour*, Emilie Leroy*, Sharmila Dass*, Yasmine Ould-Amer*, Ilyas Chachoua, Christian Pecquet, Vitalina Gryshkova, , Steven O. Smith and Stefan N. Constantinescu. *Co-first authors

III.5.1. Background

Polar residues, such as Glu, Asn, Gln, and Asp, drive the oligomerization of model transmembrane peptides.[15] Examples exist for receptors like the Neu/Erb2 (HER2) proto-oncogene (the V664E is exactly in the middle of the TMD)[16], the fibroblast growth factor receptor-3 (FGFR-3) A391E[22] and certainly TpoR that can be homodimerized by the introduction of a polar residue such as Asn at position S505 in TpoR TMD.[17,18] Moreover, the activating S505N mutation is found in both familial forms and rare sporadic case of ET and PMF.[19,21]

III.5.2. Questions

This study addresses three major unanswered questions that emerged from our recent study. One is how several asparagine mutants, placed on apparently different interfaces induce constitutive activation of murine TpoR. The other is why the constitutive active signaling output becomes progressively stronger with descending positions of Asn substitutions towards the cytosolic border of the TMD in one α-helical face. Could we manipulate those dimerization interfaces in order to inhibit constitutive TpoR mutants?

To answer these questions we combined biochemical, Cys cross-linking, cell proliferation, mutagenesis, protein fragment complementation, *in vivo* mouse bone marrow reconstitution and NMR approaches. In the process, we focused on the secondary structure of the R/KWQFP motif containing W508 (W515 in human TpoR), which is mutated in 5-7% of myeloproliferative neoplasms and also assess potentially important differential signalling via JAK2 or TYK2. We tested Ala insertion to rotate active Asn and W508K mutants toward

inactive interfaces or, the other way around, to activate receptors forced in an inactive conformation like the TpoR A499N mutant.

III.5.3. Authors contribution

I have performed the Asn mutagenesis, alanine insertions, luciferase transcriptional assays, saturation mutagenesis at TpoR W515 and BaF3 proliferation assays with the help of Emilie Leroy and of our lab technician Joanne Van Hees. I also performed in collaboration with Dr Christian Pecquet the *in vivo* experiments testing the effects of the murine mutants in bone marrow transplantation. Dr Vitalina Gryshkova performed Split Luciferase Complementation Assay on constructs provided by Emilie Leroy. Emilie Leroy also performed cross-linking studies with Yasmine Ould-Amer. Dr Sharmila Dass has performed solid-state NMR studies on TpoR peptides reconstituted into model membrane bilayer.

III.5.4. Unraveling TpoR oncogenic mechanism: gaining order from local disorder Oncogenic TpoR activation mechanism unraveled.

Jean-Philippe Defour*, Emilie Leroy*, Sharmila Dass*, Yasmine Ould-Amer*, Ilyas Chachoua, Christian Pecquet, Vitalina Gryshkova, , Steven O. Smith and Stefan N. Constantinescu. *Co-first authors

Abstract

Dimerization of the thrombopoietin receptor (TpoR) is necessary for receptor activation and JAK2 downstream signaling. An asparagine TpoR mutant, S505N (S498N in the mouse) is detected in familial and rare sporadic cases of Essential Thrombocythemia and Myelofibrosis. Asparagine substitutions are expected to induce stable dimerization of transmembrane helices in an active orientation. We explored the *in vivo* effects in mouse bone marrow transplantation experiments of the mouse TpoR mutant S498N and of two other asparagine mutants, L494N and G502N inducing a similar dimer interface. The phenotype of myeloproliferation was increased with proximity of the Asn-induced dimerization to the cytosolic leaflet of the membrane, correlating well with progressive signaling via STAT5, STAT3, MAP-kinase and PI-3'-kinase in cell culture assays. Given that the interface of the dimer is the same in these three mutants, we asked whether Asn residues could exert effects on the secondary structure of the region around W508 (equivalent to W515 in the human TpoR), where activating mutations are also detected in ET and MF. Using solid-state NMR we show that increased activity correlated with progressive unraveling of the helical structure around W508 (W515 in the human TpoR). In turn this led to regional flexibility in the TpoR JM region, which eventually is translated by positional changes at the linker between the SH2 and pseudokinase domains of JAK2, which was required for activation. Furthermore, we show that rotation using extra-alanine residues can regulate activity of Asn mutants, and as predicted of the mouse TpoR W508K mutant. Finally, we show that dimerization, unraveling and upstream

rotation all contribute to the necessary two steps of JAK2 activation, proximity of kinase domains, and steric positioning for reciprocal activation.

Introduction

Cytokine receptors regulate key functions in the human body, such as growth and maintenance of cells from the immune system and blood, lactation, after-birth growth and even some protective roles in the nervous system. Their activation induces long-lasting genetic effects by activation of transcription factors via their pre-bound cytosolic Janus kinases. The thrombopoietin receptor (c-Mpl or TpoR) and its ligand Tpo are the main regulators of megakaryocyte differentiation and platelet production.[309] Besides its role in megakaryocytes development and platelet production, TpoR functions in early hematopoiesis by promoting self-renewal, expansion and maintenance of the hematopoietic stem cell pool[196,310,311] (N.E. Fox, 2002).

TpoR is a member of the type-1 cytokine receptor family that also includes the erythropoietin receptor (EpoR), growth hormone receptor (GHR), granulocyte colony stimulating factor receptor (GCSFR) and prolactin receptor (PrlR). These receptors consist of two identical α-chains and function as homodimers. They almost exclusively employ the Janus kinase JAK2, which contains both an activating kinase domain (JH1) and an inhibitory pseudokinase domain (JH2).[75,81,82] Upon activation, Tyr1007 and Tyr1008 in the activation loop are trans-phosphorylated, which turns on the kinase activity and allows phosphorylation of other sites.[76]

EpoR[312], GHR[126] and PrlR[313] are believed to be ligand-independent dimers. Ligand binding induces a conformational change in the receptor that is coupled to a change in the orientation of the intracellular JAK2. The mechanism of this coupling is at the heart of how these receptors transduce cellular signals. For example, Brooks et al. (reference) have proposed a mechanism of GHR activation involving the transition of the dimeric transmembrane domain from a parallel to a left handed coiled coil geometry resulting in the separation of the inhibitory pseudokinase domain of one JAK2 from the kinase domain of the other JAK2. We have previously shown that human TpoR behaves differently than the GHR, since the TM domain does not strongly dimerize in the inactive receptor.[314]

We have previously engineered receptor dimers of TpoR using the dimerization domain of Put3 or by specific Asn substitutions within the TM domain. The engineered Put3 dimers suggest there is one inactive orientation of the TM helices and several orientations that lead to different signaling outputs. More recently, we have explored the use of asparagine scanning mutagenesis to modulate the orientation of the TM helices (Leroy et al., unpublished). The striking observation was that the TM helices in the murine receptor form dimers in various azimuthal orientations, whereas only a single substitution in the human receptor (S505N) results in appreciable activity. The S505N mutation is found in familial forms[18,315] and rare sporadic case of ET and PMF.[21,316,317]

In this manuscript, we take advantage of the Asn and Trp mutations in the context of the murine receptor to more closely understand the role of the rotational orientation and the position of the mutation relative to the intracellular membrane surface in activation. We determine the consequences of progressive dimerization on the structure of the region around the KWQFP motif and on the proximity of Janus kinases during activation, and how that proximity is regulated by dimerization or orientation.

Results and Discussion

Ligand-independent activity in Asn mutations is dependent on both the rotational orientation and the proximity of the mutation to the intracellular membrane surface

Asparagine substitutions induce very different effects in the murine and human Tpo receptors. In the hTpoR, only substitution of Asn at Ser505 results in appreciable ligand independent activity. In contrast, in the murine receptor there are several TM positions that result in activity. Figure 1A plots the constitutive activity of the Asn mutants in mTpoR. The data emphasize the observation that there is primarily a single position around each helical turn that has increased activity. These are at positions V494N, S498N and G502N. In Figure 1C, we measured cell proliferation using the Cell-Titer-Glo luminescent cell viability assay where the growth of BaF3 cells is compared with increasing concentrations of Tpo ligand. The data show that there is increasing cell growth in the order V494N < S498N < G502N.

Val494, Ser498 and Gly502 lie roughly on one face of the mTpoR TM helix (Figure 1B). We have recently shown that the murine receptor forms an inactive dimer mediated by TM helix interactions and that the inactive interface is centered on Ala499 (Leroy *et al.*, unpublished). In contrast to hTpoR, there appear to be several active interfaces for the mTpoR. However, it is important to note that Asn mutants on a specific interface do not generate the same level of activity. For example, Leu495 is two helical turns above Gly502, yet the L495N activity is comparable to that of an inactive receptor. The same increase of activity is observed when comparing L493N and L500N. There is a measureable increase in the L500N receptor, with the Asn mutation closer to the cytoplasmic boundary, compared to L493N, despite the fact that this orientation is 180° from the Gly502-Ser498 active interface.

***In vivo* effects of the TpoR V494N, S498N and G502N mutants**

The results obtained in transient STAT5 luciferase assays and in stably transduced BaF3 cells (Leroy et al. published) were validated by performing bone marrow reconstitution experiments. Bone marrow cells from C57Bl6 mice were transduced with bicistronic retroviruses coding for the V494N, S498N and G502N mTpoR mutants or wild type TpoR and infected cells were used to transplant lethally irradiated C56Bl6 mice. Figure 2A shows that 40 days after reconstitution a gradient of *in vivo* effects could be detected, with strong myeloproliferation for G502N, lower blood counts but still pathologic for S498N and weak increases in platelets for the V494N mutant. Bone marrow histology and spleen histology showed frank fibrosis for the spleens and bone marrow samples of G502N mice (Figure 2B). Furthermore, the weights of

both spleens and liver were higher for G502N than for S498N and at the high limit of normal for V494N (Figure 2C).

Asn mutations near the cytoplasmic boundary induce local changes in secondary structure in the KWQFP motif

The results from Asn substitutions raise the question of how the TM orientation is coupled to receptor activation. To address this mechanism, we take advantage of TM peptides containing the juxtamembrane KWQFP motif. Figure 3 presents solid-state NMR comparing the $^{13}C=O$ chemical shift at position Leu505 in the WT, S498N and G502N constructs using TM peptides. The $^{13}C=O$ chemical shift is sensitive to secondary structure. In helical structure, the Leu505 C=O hydrogen bonds with the NH of Trp508. The observed chemical shift indicates that in the WT sequence, the TM helix extends to at least Trp508. In contrast, in the S498N and G502N mutants, where the Trp508 group is rotated into the interface, the helix unravels. Importantly, there is a larger influence in the G502N mutant compared to the S498N mutant. 499N is missing here.

Alanine insertions increase ligand independent receptor activation with a helical periodicity

The results in Figures 1 and 2 indicate that both the rotational orientation and the membrane proximity influence the activity of the Asn mutations. Figure 3 shows that Asn substitutions induce progressive unraveling of the region around W508, the cytosolic juxtamembrane region of TpoR.

The influence of rotation can be tested with alanine insertions before the KWQFP motif (Figure 4A). Although these substitutions both increase the helix length and change the rotational orientation, the greater influence is likely on helix rotation, which changes by 100° with a single alanine substitution. In contrast, it takes between 3-4 alanine residues to increase the helix length by one helical turn.

In Figure 4B weak ligand independent transcriptional activity is observed with +1 or +2 alanine insertions just N-terminal to the KWQFP motif in the mTpoR. The insertion of +3 and +4 alanines results in slightly less activity. It is noteworthy that Tpo maximal response is progressively lost with Ala insertion probably due to an increase in the hydrophobic length. When +3 and +4 alanines are inserted a stronger helical secondary structure is also likely to be induced, which might be more difficult to disrupt and thus activation by Tpo ends up being weaker. Importantly, the cell surface localization and expression of these constructs is similar.

Figure 4C shows the influence of the alanine insertions on cell viability with a small constitutive activation upon addition of 2A.

The W508K mutant can be inactivated by forcing it into a single inactive conformation

We interpret the activity of the alanine insertions in terms of rotation of Trp508 to the position of Gln509 (+1A) or position of Phe510 (+2A). The explanation is that the large

tryptophan side chain at these positions disrupts the favorable inactive dimer. We have previously described how mutations of Trp508 can be activating (reference). Trp508 is expected to be at the membrane boundary and its mutation may be related to the observation that the Asn mutations closer to the membrane boundary have higher activity. To uncouple the effects of rotational orientation and proximity to the membrane surface, we assessed the effect of alanine insertions in the context of the W508K mutation. Strikingly, the +2 alanine insertion, which is weakly activating in terms of the wild-type receptor, exerted strong inhibition under conditions again where these mutants did not change cell surface and total expression levels (Figure 4B, right panel). The +3 and +4 alanine insertions exerted a weaker inhibitory effect.

To further explore the rotational requirements for activation by W508K, we returned to engineered TpoR constructs in which the TM helices are forced to be dimeric with defined interfaces. By using engineered coiled coil constructs, we previously showed[318] that a single dimeric conformation cc-TpoR-II was not productive for UT-7 TpoR or BaF3 cell growth. Here we tried to inactivate the W508K by forcing it in all possible orientations by fusing a Put-3 dimer to progressively trimmed transmembrane domains (Figure 5). BaF3 cells were retrovirally transduced by those engineered constructs and sorted for same level of expression. cc-TpoR-II W508K was the only conformation that does not permit growth of BaF3 cells. Noteworthy, cc-TpoR-VI is weaker than other active faces but still allows an autonomous BaF3 proliferation. cc-TpoR-VI was described as the human inactive interface using TM peptides by TOXCAT assay and cysteine crosslinking.[319]

Alanine insertions in the region around W508 modulates Asn mutational activity

As a proof of principle, the same 2 Ala insertion that inactivates the W508K mutant was added to the one inactive receptor (A499N) and to the two active receptors (S498N and G502N) (Figure 6). The alanine insertions rotate Asn499 towards the active cc-TpoR-0 interface and rotate the Asn498 and Asn502 towards weakly active interfaces, cc-TpoR-VI and cc-TPoR-III respectively. If the alanine mutations are resulting in rotation of the TM helix, then we predict an increase in activity of the A499N mutant and decrease in activity of the S498N and G502N mutants. These predictions are confirmed in Figure 6.

Influence of TpoR activation on the proximity between JAK2 domains

Our functional assays are based on the activation of the JAK2 kinase domain (also denoted JAK-homology-1 or JH1). We next addressed whether activation is correlated with bringing into proximity of JAK2 JH1 domains, and whether dimers that do not activate JAK2 bring or not JH1 domains into proximity. The question is whether the increased activity observed with Asn substitutions closer to the membrane surface is correlated with the movement of the JAK2 JH1 domains. To answer this question, we employed a protein fragment complementation assay based on *Gaussia* luciferase complementation (Michnick et al., 2006). In this assay two fragments of *Gaussia* luciferase fold and reform a catalytic protein within 1

min when in close proximity (Michnick et al., 2006). The assay permits examination of low levels of proteins and is reversible.

We introduced the two complementing fragments of *Gaussia* luciferase (Gluc1 and Gluc2) at the C-terminus of the JH1 domain, at the C-terminus of the JH2 domain or at the C-terminus of the FERM-SH2 domain (Figure 7). The JAK2 fragments were co-expressed with the wild type TpoR, or with several Asn mutants of the mTpoR (V494N, S498N, A499N or G502N). Of those A499N is an inactive dimer, as shown in Leroy et al. (unpublished) and in Supplemental Figure 1. We show in Figure 7 that the proximity of the FERM-SH2 fragments was progressively decreased with Asn substitutions that were closer to the cytosolic border. The effect appears to be independent of the eventual activation of the JAK2 kinase and signaling, since A499N is inactive. In contrast, the proximity of the JH1 C-terminal ends increased with progressive Asn substitutions towards the cytosolic border, while the C-ends of the JH2 domains were not affected by Asn substitutions.

To avoid effects of kinase activation and internalization experiments in Figure 7 were performed at 20ºC. These results indicated that activation is associated with separation of the C-termini of FERM-SH2 domains, which contact the receptor Box 1- Box 2 regions, and close apposition of JH1 C-termini, but that dimerization in a conformation that is not productive for signaling is also inducing these proximity effects, suggesting that dimerization suffices for these changes, but they are not sufficient for activation. The next step was to explore the role of orientation in this system.

A consensus mechanism of activation involves loosening of restrictions at the intracellular boundary.
The binding of ligands to the type-1 cytokine receptors leads to activation of the Janus kinase bound to intracellular residues in Box 1 and Box 2. Bound JAK2 is required for inactive receptors to traffic to the plasma membranes. Consequently, activation must involve either a change in the relative proximity of the JAK2 kinase domains, a change in their relative orientation, or both.

The results presented highlight the role of orientation in activation. There is a single inactive interface and a broader interface that supports receptor activity. Our results suggest that the JAK2 domains are in close proximity prior to ligand binding but inactive. The combination of the alanine insertion data and NMR data presented here suggests that the change in rotation leads to loss of helical structure at the intracellular TM boundary. We propose that this provides greater flexibility, although unraveling is partial and might preserve certain rigidity.

For the human GHR, which does not contain the unique R/KWQFP insert, it has been shown that activation, promoted by dimerization of TM helices leads to separation of distal cytosolic receptor sequences and release restrictions on the proximity of bound JAK2 (and possibly its relative orientation) upon ligand binding. The structural basis for such a mechanism is not

known. Here we show that in TpoR, several mutations that lead to activation induce partial unraveling of the helix around the JM motif KWQFP, and this is proportional to the proximity to the cytosolic border for the TM Asn substitutions. Given that an Asn mutant that is not active (A499N) separates the FERM-SH2 C-termini, we propose that dimerization controls secondary structure below the membrane, namely unraveling of the JM helix. This is not sufficient for activation, as shown by the A499N mutant where dimerization leads to the separation of the C-termini of the FERM-SH2 domains of JAK2, while promoting proximity of C-termini of JH1 domains. Thus, a second component is necessary for activation, and that is rotation.

To explore the role of rotation we introduced extra alanine residues in the JM region of the mTpoR, before the KWQFP motif. We assessed dimerization of JAK2 fragments for these mutant receptors and the secondary structure around Trp508. Taken together we show that rotation induced by +2 alanine insertion induces weak activation in the wild type TpoR. On the other hand, when W508K mutant was tested, the +2 alanine insertion inhibited its constitutive activity the most, most likely because it decreased dimerization of JAK2 JH1, did not allow separation of FERM-SH2 C-ends, and prevented helix unraveling around 508 (to test). Insertions +3 alanines and +4 alanines were less stringent in preventing unraveling (to test by NMR) and allowed a level of dimerization that was permissive for weak remaining activity of W508K mutant; this +3 alanine and +4 alanine insertions did not block W508K as much as +2 alanine insertion, most likely because of rotational differences adopted of the final mutant (cc-TpoR-II versus cc-TpoR-I and 0 respectively).

Thus, using approaches that allow dimerization and partial helix unraveling without rotation, and rotation without change in secondary structure we conclude that activation of the TpoR requires dimerization, that promotes helix unraveling under the TM domain, which allows the flexibility of distal receptor sequences to allow separation of the C-ends of the FERM-SH2 domains, allowing JH1 ends to come into closer proximity. Thus, our observations that dimerization (at least in certain conformations) lead to progressive loss of helicity and rigidity in the proximal JM cytosolic region (on a finite length) could be the structural basis for the mechanism proposed by M. J. Waters for JAK2 activation, which is based on sliding apart fragments of JAK2, which we also observe. However, all those changes are not sufficient for activation, even with closer proximity of JH1 C-ends, as certain dimers that fullfill these changes remain inactive. In order for the C-ends of JH1, which are found in proximity to initiate productive signaling, a certain orientation (rotation) is required, possibly to bring the kinase loop of one JAK2 into close contact with the activation loop of the other JAK2 kinase. The fact that cc-TpoR-II reorients W508K means unraveling is not sufficient for activation and that orientation matter.

Our data show that proximity and orientation are both required for activation of the TpoR and progressive substitutions in the TM domain with Asn residues closer to the cytosolic domain induces progressive unraveling of the JM helix and separation of FERM-SH2 C-termini. These

effects are coincident with activation only if the register of the helix where the Asn substitutions are introduced are matching the rotational constraints for the JH1 kinase activation. These constraints are not released by the helix loss, as unraveling is not complete, and unraveling *per se* does not suffice for activation. Thus, activation is controlled on two layers: liberation of JAK2 constraints by partial unraveling of JM helices, and precise rotation in order to gauge phosphorylation of activation loop Y1007 by the opposite JAK2. More experiments are needed to determine whether this process is asymmetric with respect to which receptor and JAK2 initiate activation, depending on which receptor subunit unravels first.

One alanine insertion allows receptor activation via TYK2 upon ligand binding

We have previously shown that cc-TpoR-III and cc-TpoR-VI are interfaces that support TYK2 activation by TpoR.[318] Those interfaces are located 250 to 300° CW to the postulated inactive interface cc-TpoR-II. TYK2 has been shown to be important neither for the oncogenic nor the wild type TpoR signaling, but promotes cell surface localization.[138] Adding one alanine is shown in this study to allow a strong TYK2 response after Tpo stimulation. This response was not detected for other alanine insertions probably because none of them can orient the receptor in a TYK2 productive conformation (cc-TpoR-III or -VI) (Figure 8A). If we assume a 100° - 110° CW rotation induced by adding one alanine, Tpo should mediate an additional 150° CW rotation to orient the receptor in a TYK2 fully active conformation, namely cc-TpoR-III. A 150° CW rotation mediated by TpoR ligands has also been proposed by Engelmann to rotate the receptor from a His "in" inactive to a His "out" active conformation.[319] The W508K mutation does not signal constitutively via TYK2 as shown previously in (Supplemental figure 3)[314], probably because in the context of W508K another dimeric interface is adopted (cc-TpoR-IV) where the JH1 domain of TYK2 kinase is not properly facing each other in this oncogenic dimer.

However, we observed that W508K exhibits a Tpo hypersensitivity via TYK2, which is weaker than that of the TpoR +1A mutant. This is similar to the second interface, which can support signaling via TYK2 by TpoR, namely cc-TpoR-VI, suggesting that W508K +1A could adopt a cc-TpoR-III/VI conformation upon ligand binding. However, adding 2 alanines in the W508K context seems to constitutively activate the receptor via TYK2 (This should be confirmed). This is striking that adding 2Ala is inactivating the receptor via JAK2 but paradoxically allows TYK2 to cross phosphorylate and to activate the signaling cascade. This would mean that W508K +2A remains probably partially unraveled and that it places TYK2 JH1 in a good orientation for transphophorylation. As observed in figure 3 with JAK2, Tpo response is also progressively lost via TYK2 when inserting Ala in the W508K probably because Ala insertions stabilize the helix and prevent unraveling.

Methods and Materials

Plasmid Constructs

The TpoR WT, he asparagine substitution mutants and the alanine insertion mutant constructs were subcloned in pMX-IRES-GFP as described previously.[320] All the TpoR constructs contain a Hemagglutinin Tag (HA-Tag) at the NH3-Terminus downstream to the signal peptidase cleavage site (Huang et al., 2001). Mutagenesis was achieved by overlapping extension PCR using the Pfu Turbo® DNA polymerase (Stratagene, La Jolla, CA, USA). For crosslinking experiment, the intracellular domain of the wilt-type TpoR and the TpoR mutants were devoid of cysteine by introduction of a stop codon after amino acid 553 and Leu505 was mutated to a cysteine. For the split luciferase experiment, hGluc fragment coding amino acids 1–93 (hGluc1) or the fragment coding amino acids 94–169 (hGluc2) of *Gaussia princeps* luciferase[321] were inserted 39 amino acids downstream to TpoR Box1 subcloned in pcDNA3.1/Zeo vector. All the constructs were verified by Sanger sequencing (Beckman Coulter, UK).

Dual Luciferase Transcriptional Assay

Transcriptional activity of STAT5 and STAT3 was analyzed in JAK2 deficient γ-2A cells or in TYK2 deficient 11.1 cells co-transfected with the receptors variants, JAK2 WT, STAT5 and spi_Luc (reference?) or pGRR5 (Dumoutier et al., 2000). The pRL-TK vector (Promega, Madison, WI) was used as an internal control. Luminescence was measured in cell lysates 24 hrs after transfection using dual luciferase reporter kit (Promega) on a Perkin-Elmer Victor X Light analyzer.

Split Luciferase Complementation Assay

HEK293 cells plated on 24-well plates were co-transfected with the plasmids (coding hGluc1and hGluc2) using Lipofectamine (Invitrogen). Twenty-four hours after transfection cells were trypsinized and resuspended in 150 μL of DMEM/F-12 without phenol red (Gibco). Cell samples were flash-frozen on dry ice for 10 min and thawed in a water bath at 37°C for 10 min (cycle was repeated twice). After centrifugation (10,000 g, 5 min) the supernatants were collected and aliquoted (100 μL per well) in 96-well white plates (Nunc) to measure the luciferase activity. Signal intensities (integrated over 10 s, with an injection delay of 2 s) were read on a Perkin-Elmer Victor X Light analyzer. Aliquots of the supernatants were used also to detect the proteins on Western blot.[321]

Generation of Cell Lines

BaF3 were transduced with the TpoR constructs using BOSC23 ecotropic viral supernatant. (Liu et al, 2001). Cell populations expressing GFP at a level above 15% were selected by flow cytometry. Cells were grown in IL3 containing RPMI supplemented with 10% FBS.

Surface Expression of HA-tagged Wild Type TpoR and Mutants

Cell surface level of HA-TpoR was determined by flow cytometry using monoclonal anti-HA antibodies (Covance, 10 μg/ml) and PE-conjugated anti-mouse IgG secondary antibody (12.5 μg/ml) (Huang, LJ, 2001).

Cell Viability Assay

The proliferation of BaF3 expressing wild type TpoR or the TpoR mutants was assessed by Cell-Titer-Glo luminescent cell viability assay (Promega). Prior to the experiment, cells were washed three times in PBS. 96 wells-plate were used to plate the cells at 10 000 cells /well in RPMI +10% FBS supplemented or not by different concentrations of recombinant Tpo (R&D Systems). After 72 hours, ATP reacting substrate was added following manufacturer's instructions and luminescence readings were taken using the Perkin-Elmer Victor X Light analyzer.

Bone Marrow Reconstitution

Male C57B6 mice bone marrow was isolated and cultivated in the presence of cytokines (SCF, Flt-3, Tpo, IL-3 and IL-6). Those cells were spin infected with 300 μl concentrated VSV-G pseudo-typed retroviral supernatant obtain as described previously. 10^6 infected cells were then injected intravenously in lethally irradiated female mice. GFP was checked at multiple time point to evaluate chimerism.

Solid-State NMR Spectroscopy

For solid-state NMR studies on TpoR peptides reconstituted into model membrane bilayers, 44 residue peptides corresponding to the TM domain and JM regions of Tpo receptor were synthesized using solid-phase methods:
RRRETAWISLVTALHLVLGLSAVLGLLLWKQFPAHY RRLRHALWPS-NH_2. The peptides include three non-native arginines at the N-terminus for peptide solubility and to terminate both ends of peptide with positive charges. The crude peptide (5–15 mg) was purified by reverse-phase HPLC on a C4 column using gradient elution and reconstituted by detergent dialysis using DMPC and DMPG (10:3) and a ~1: 60 peptide to lipid ratio. Lipids were obtained from Avanti Polar Lipids (Alabaster, AL) as lyophilized powders and used without further purification. Magic angle spinnig NMR experiments were performed at a ^{13}C frequency of 125 MHz on a Bruker AVANCE spectrometer. The MAS spinning rate was set to 9-11 KHz (± 5 Hz). The ramped amplitude cross polarization contact time was 2 ms. Two-pulse phase-modulated decoupling was used during the evolution and acquisition periods with a radio frequency field strength of 80 kHz. The sample temperature was maintained at 198 K (± 2 K).

Figure Legends

Figure1. Activity and relative positions of asn mutants

muTpoR TMD sequence and numbering **(a)**. Wheel diagram shows V494, S498 and G502 positions (blue) on the active interface (left panel). Their relative transcriptional activity was

assessed with the STAT1/3/5 reporter pGRR5 **(b)**. The cell viability of those three mutants was measured by an ATP based assay at various Tpo concentrations **(c)**.

Figure 2. *In vivo* data comparing Asn mutants
Red blood cell, platelets, white blood cells and neutrophils were measured using an MS9 blood cell counter at day 40 **(a)**. Bone marrow/spleen cellularity and fibrosis have been evaluated by a HE and reticulin staining respectively **(b).** Liver and spleens were photographed and weighted **(c).**

Figure 3. Secondary structure changes in the RWQFP insert upon activation
1D ^{13}C MAS NMR spectra are shown of m-TpoR-WT (a), m-TpoR-S498N (b) and m-TpoR-G502N (c) in the region of the ^{13}C=O carbonyl resonances. The m-TpoR peptides labeled with 1-^{13}C Leu505 were reconstituted into DMPC: PG bilayers. A spectrum of unlabeled mTpoR (dashed line) was subtracted to obtain the resonance of the Leu505 13C=O in the lower panels. The ^{13}C=O chemical shift changes from 176.2 ppm in (a) to 174.5 ppm (b) and 173.4 ppm (c).

Figure 4. Effects of Alanine insertions on WT and W508K receptors
One to 5 alanines were inserted before the KWQFP motif or the K<u>K</u>QFP. Each alanine rotates the receptor of 100° clockwise **(a)**. Transcriptional activity via JAK2/STAT5 of these alanines was assessed by luciferase **(b)** or by growth **(c)**.

Figure 5. Cell growth of W508K mutants using coiled-coil
Coiled coil were fused at the TM-IC portion of the receptor and BaF3 cells transduced with those constructs were tested for autonomous growth.

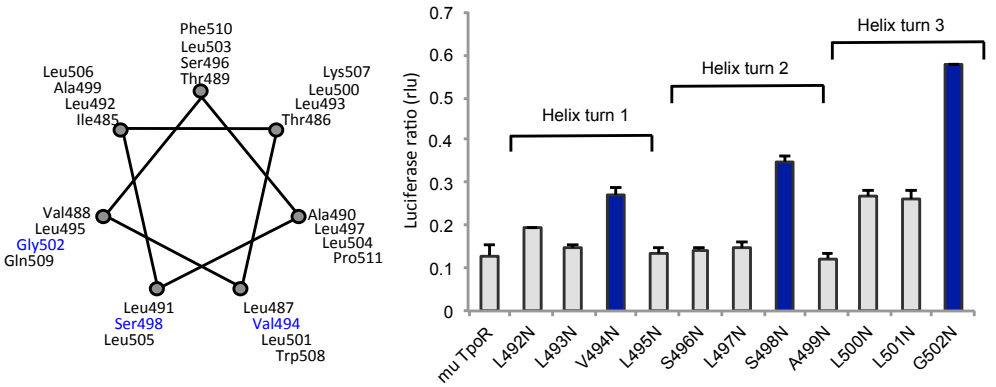
Figure 6. Effects of Alanine insertions on Asn mutants
We add two alanines to A499N inactive (cc-TpoR-II like mutant) and S498N (cc-TpoR-I like mutant) or G502N active mutants (cc-TpoR-V like mutant). These mutants should then be reoriented as cc-TpoR-0 (strong), cc-TpoR-VI (low JAK2 interface) or cc-TpoR-III (low JAK2 interface) upon 2-Ala insertion **(a)**.

Figure 7. Dimerization of JAK2 below the receptor as assayed by *Gaussia* luciferase.
Gluc 1 and Gluc 2 fragments were fused after JH1 **(a**), after JH2 **(b)** or after the FERM-SH2 domain and tested by *Gaussia* complementation assay using coelenterazine as a substrate. Those complementation assays were realized on lysate obtained 24h at 20°C post transfection.

Figure 8. Effect of Alanine insertion on the WT and W508K mutants as measured by a TYK2 specific transcriptional activity assay
Dual luciferase assay has been performed in γ2A JAK2 deficient cell line. Cells were co transfected with STAT5, TYK2, pGRR5 and pRLTK reporters and luciferase signal was read 24h later.

Figure 1

I	T	L	V	T	A	L	L	L	V	L	S	L	S	A	L	L	G	L	L	L	L	R	W	Q	F	P
485	486	487	488	489	490	491	492	493	494	495	496	497	498	499	500	501	502	503	504	505	506	507	508	509	510	511



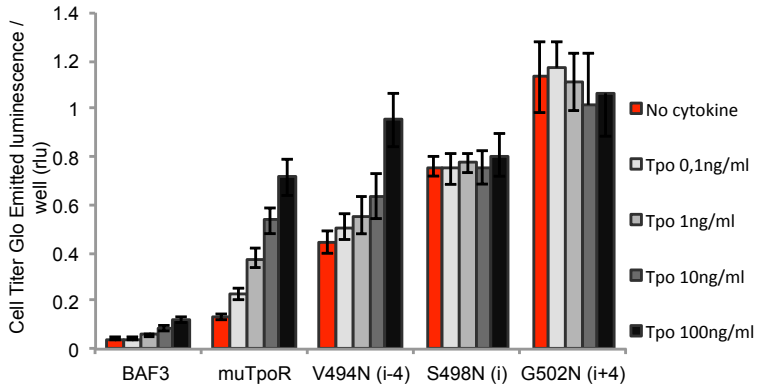
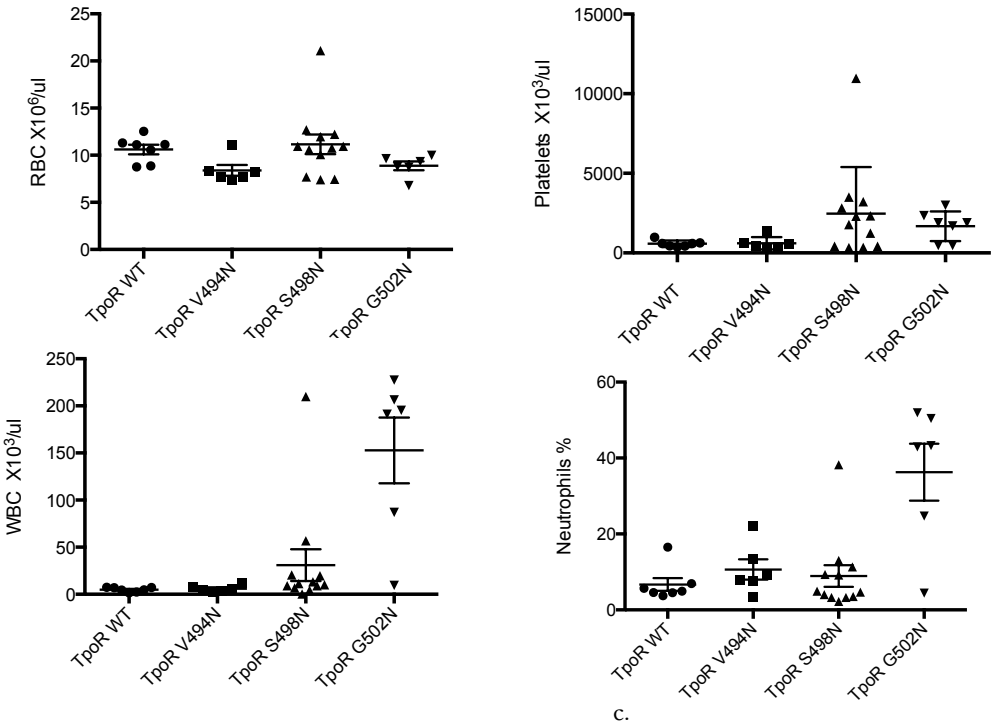


Figure 2

a.


RBC X10^6/ul
25
20
15
10
5
0
TpoR WT
TpoR V494N
TpoR S498N
TpoR G502N
Platelets X10^3/ul
15000
10000
5000
0
TpoR WT
TpoR V494N
TpoR S498N
TpoR G502N
WBC X10^3/ul
250
200
150
100
50
0
TpoR WT
TpoR V494N
TpoR S498N
TpoR G502N
Neutrophils %
60
40
20
0
TpoR WT
TpoR V494N
TpoR S498N
TpoR G502N

b.

c.

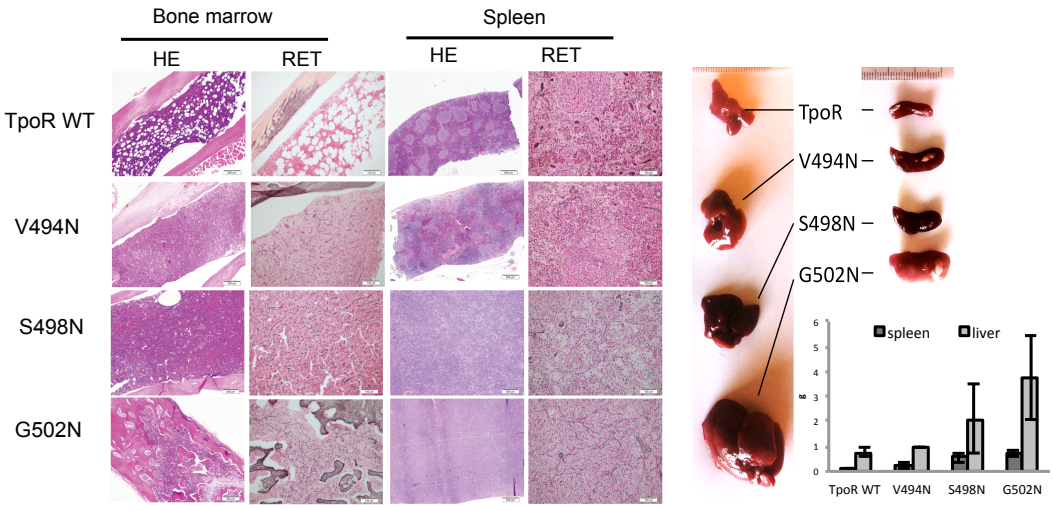

Bone marrow
Spleen
HE
RET
HE
RET
TpoR WT
V494N
S498N
G502N
TpoR
V494N
S498N
G502N
spleen
liver
TpoR WT
V494N
S498N
G502N

Figure 3

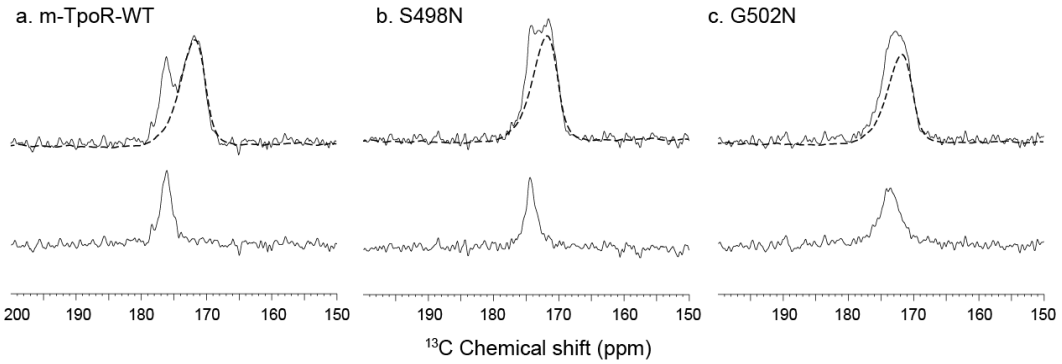
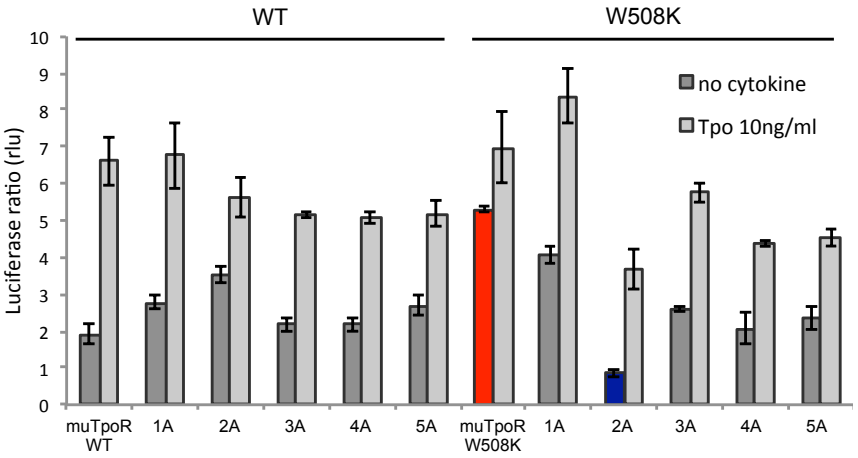

a. m-TpoR-WT
b. S498N
c. G502N
200
190
180
170
160
150
190
180
170
160
150
190
180
170
160
150
13C Chemical shift (ppm)

Figure 4

a.

mTpoR-WT	403-LLLLKWQFP
1A (100°CW)	403-LLLLAKWQFP
2A (200°CW)	403-LLLLAAKWQFP
3A	403-LLLLAAAKWQFP
4A	403-LLLLAAAAKWQFP
5A	403-LLLLAAAAAKWQFP

b.



c.

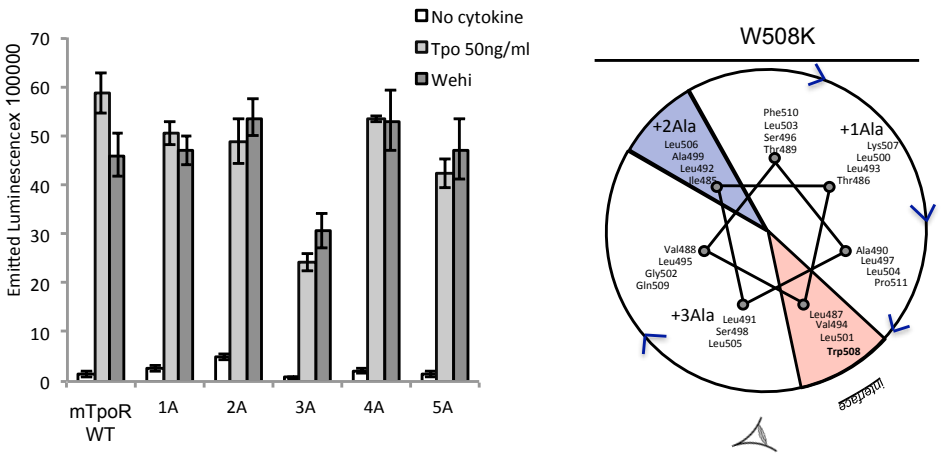


Figure 5

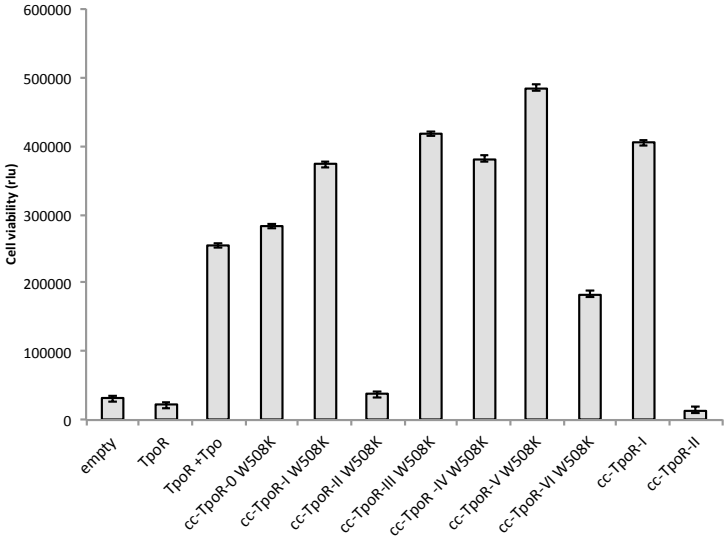


Figure 6

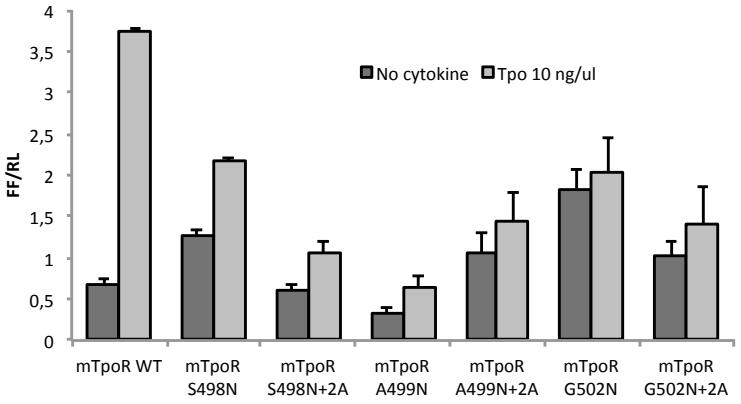
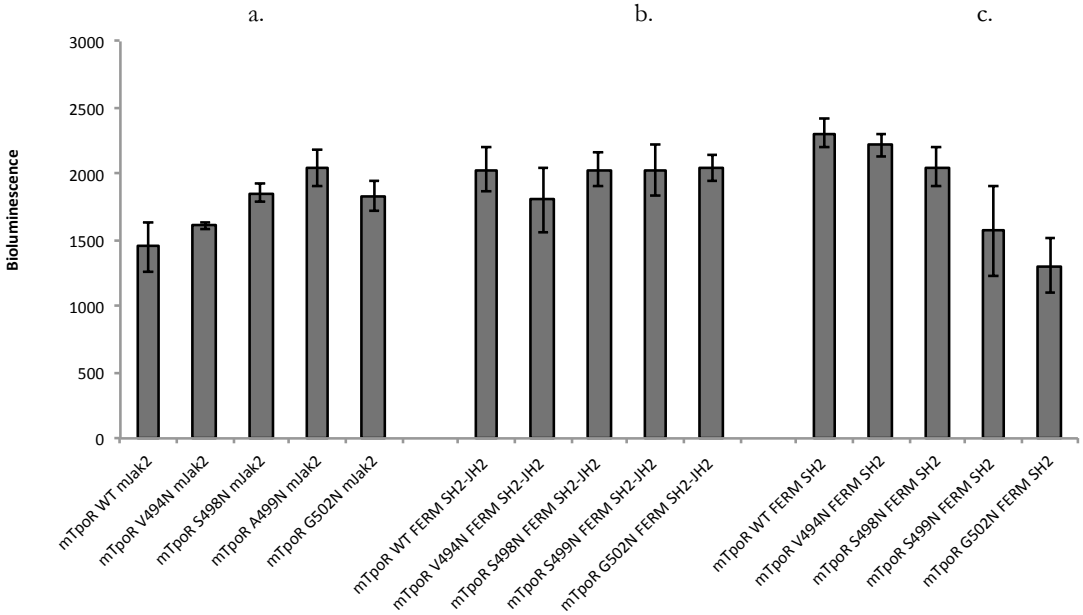


Figure 7


a.
b.
c.
Bioluminescence
3000
2500
2000
1500
1000
500
0
mTpoR WT mJak2
mTpoR V494N mJak2
mTpoR S498N mJak2
mTpoR A499N mJak2
mTpoR G502N mJak2
mTpoR WT FERM SH2-JH2
mTpoR V494N FERM SH2-JH2
mTpoR S498N FERM SH2-JH2
mTpoR S499N FERM SH2-JH2
mTpoR G502N FERM SH2-JH2
mTpoR WT FERM SH2
mTpoR V494N FERM SH2
mTpoR S498N FERM SH2
mTpoR S499N FERM SH2
mTpoR G502N FERM SH2

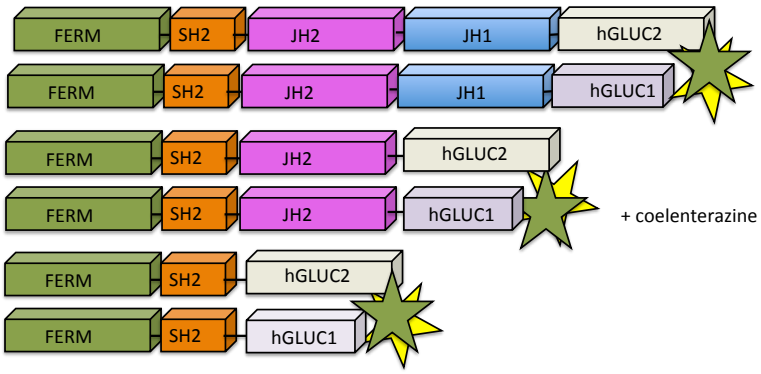
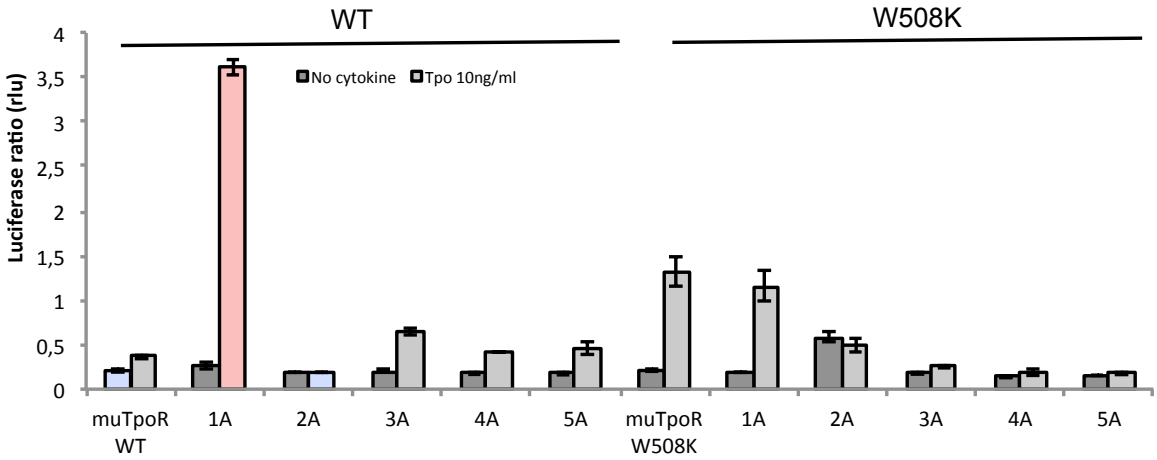
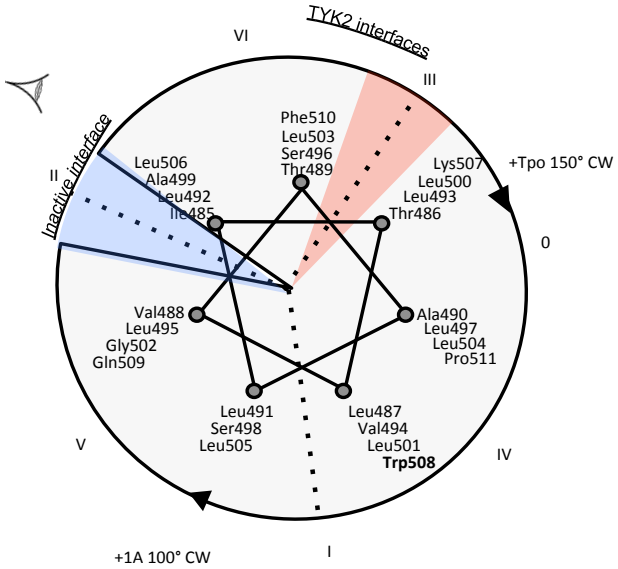

FERM
SH2
JH2
JH1
hGLUC2
FERM
SH2
JH2
JH1
hGLUC1
FERM
SH2
JH2
hGLUC2
FERM
SH2
JH2
hGLUC1
+ coelenterazine
FERM
SH2
hGLUC2
FERM
SH2
hGLUC1

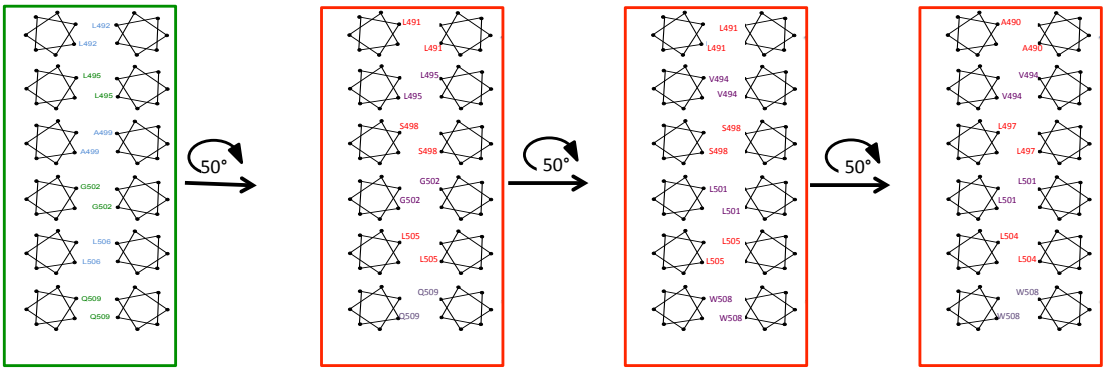
Figure 8

a.


WT
W508K
No cytokine
Tpo 10ng/ml
Luciferase ratio (rlu)
4
3,5
3
2,5
2
1,5
1
0,5
0
muTpoR WT
1A
2A
3A
4A
5A
muTpoR W508K
1A
2A
3A
4A
5A


TYK2 interfaces
VI
III
II
Inactive interface
Phe510
Leu503
Ser496
Thr489
Leu506
Ala499
Leu492
Ile485
Lys507
Leu500
Leu493
Thr486
+Tpo 150° CW
0
Val488
Leu495
Gly502
Gln509
Ala490
Leu497
Leu504
Pro511
Leu491
Ser498
Leu505
Leu487
Val494
Leu501
Trp508
V
IV
+1A 100° CW
I

Supporting Information I



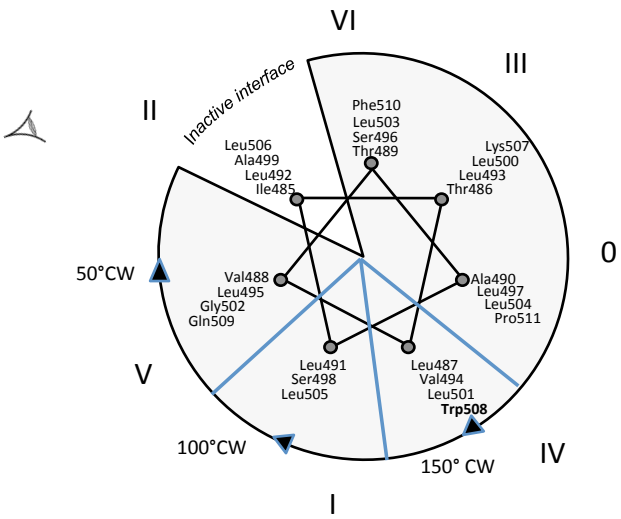
A499 “a”

S498 “d”
G502 “a”

V494 “d”
S498 “a”
W508 “d”

V494 “a”
W508 “a”

muWT	V	T	A	L	L	L	V	L	S	L	S	A	L	L	G	L	L	L	L	K	W	Q	F	P
	488	489	490	491	492	493	494	495	496	497	498	499	500	501	502	503	504	505	506	507	508	509	510	511
	d	e	f	g	a	b	c	d	e	f	g	a	b	c	d	e	f	g	a	b	c	d		
cc-V	V	T	A	L	L	L	V	L	S	L	S	A	L	L	G	L	L	L	L	K	W	Q	F	P
50°CW	a	b	c	d	e	f	g	a	b	c	d	e	f	g	a	b	c	d	e	f	g	a		
cc-I	V	T	A	L	L	L	V	L	S	L	S	A	L	L	G	L	L	L	L	K	W	Q	F	P
100°CW	e	f	g	a	b	c	d	e	f	g	a	b	c	d	e	f	g	a	b	c	d	e		
cc-IV	V	T	A	L	L	L	V	L	S	L	S	A	L	L	G	L	L	L	L	K	W	Q	F	P
150°CW	b	c	d	e	f	g	a	b	c	d	e	f	g	a	b	c	d	e	f	g	a	b		



III.5.5. Unpublished but related results and discussion

III.5.5.1. The activating effect of Asn substitutions is increasing when placed lower in the TMD

This luciferase assay tends to show that the lower we dimerize, the stronger we activate. These asparagines will induce a change in the position of the helix-crossing angle with the biggest difference being a change in the rotation angle. However, this may also be accompanied by a change in helix tilt.

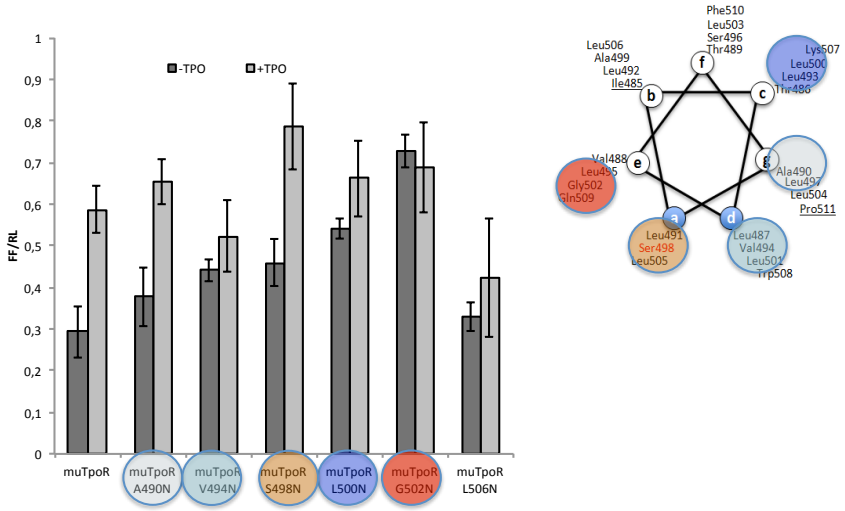


Figure 69 *- Asn activity is increased when going closer to the cytosolic border.*

III.5.5.2. ASN power via PI3 kinase pathway

The FOXO reporter is inversely correlated to PI3 kinase pathway activity. The progressive activity (V494N <S498N <G502N) has been verified.

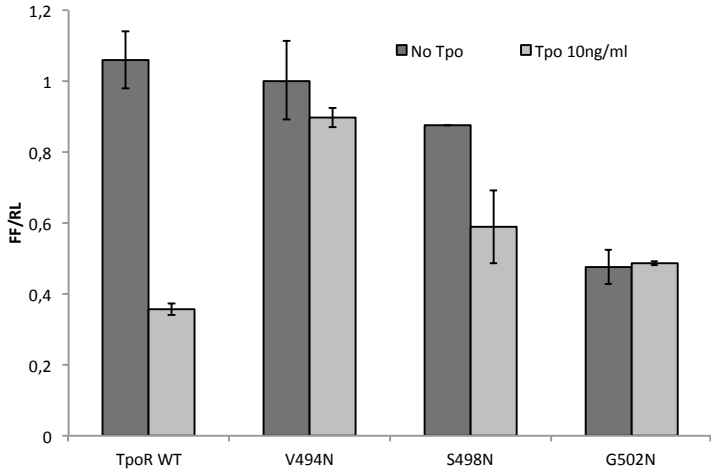


Figure 70 - Luciferase assay: Pi3 kinase activity of Asn mutants
PI3-kinase transcriptional activity at 24h is inversely proportional to 6XDBE-luc FOXO reporter activity.

III.5.5.3. Validation of the L500N in BaF3 and on multiple clones

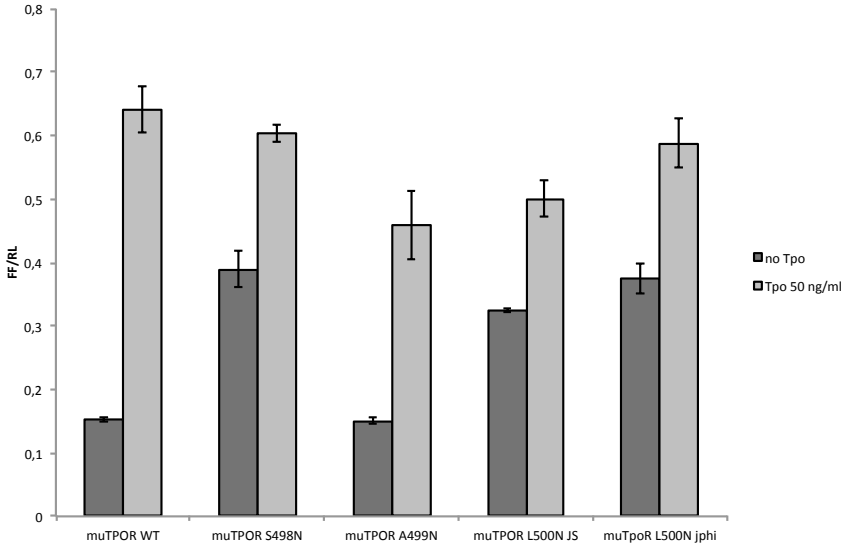


Figure 71 - Luciferase assay: Asn activity of 2 clones of L500N compared to S498N or A499N
Multiple clones of L500N have been shown active.

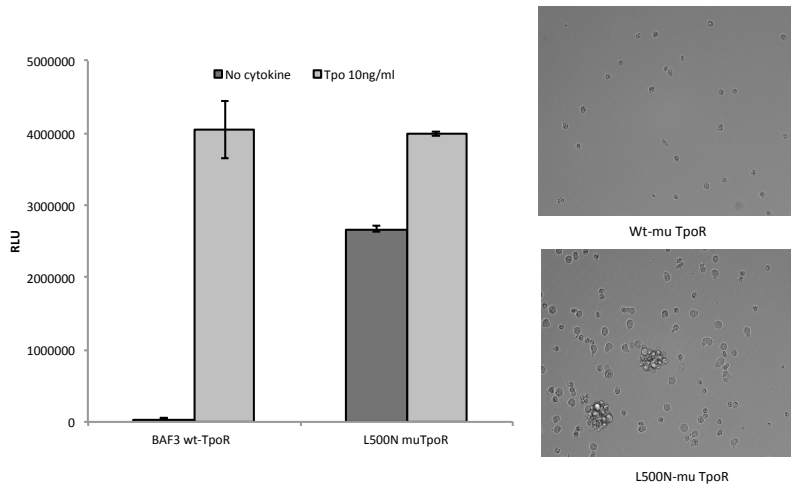


Figure 72 - Cell viability and pictures of BaF3 stably transfected with WT and L500N TpoR
L500N induces BaF3 autonomous growth

TpoR L500N is active and this constitutive activity leads to a classical down regulation of the receptor at the cell surface.

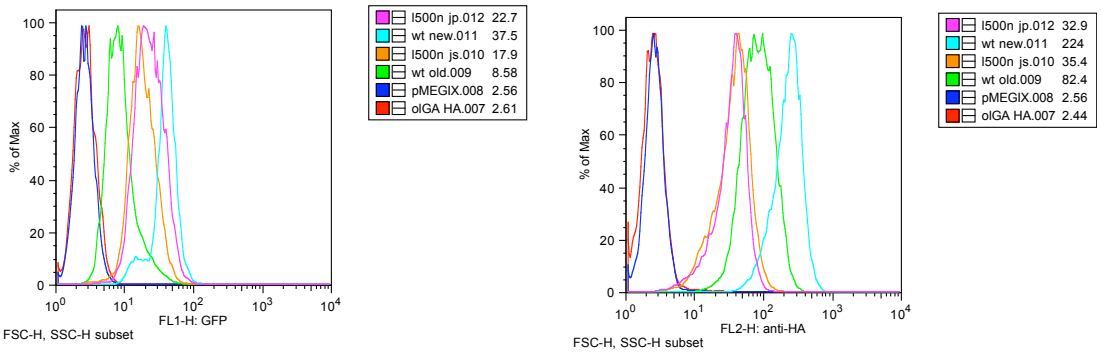


Figure 73 - Cell surface localization of L500N
L500N clone I and clone II and TpoR WT are selected in 1ng/ml Tpo.

The fact that L500N localized on the opposite face of V494N, S498N and G502N is also active is puzzling. The possibility of asymmetric dimer with S498N was proposed to explain the active orientation of L500N. But our experience with coiled coil has shown that muTpoR has multiple active interfaces. Two of them cc-TpoR-III and cc-TpoR-VI are strong TYK2 interface. We would like to test if L500N is a more TYK2 interface and is still properly oriented or rotate to a cc-TpoR-III like interface.

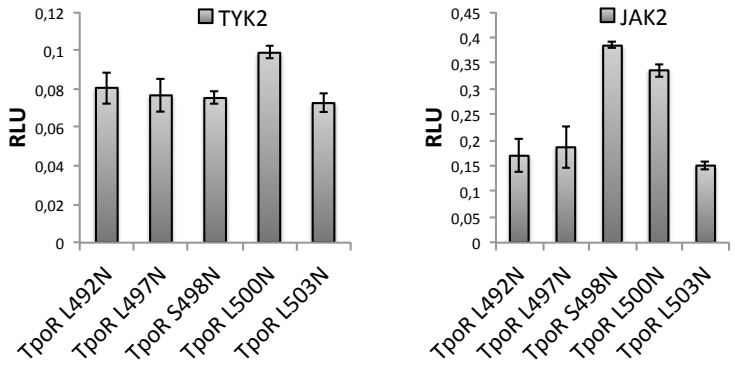


Figure 74 - Luciferase assay via jAK2 and TYK2 of L500N

Dual luciferase assay measuring STAT5 transcriptional activity in γ2A cells via pGGR5 reporter and either JAK2 or TYK2. L500N (=cc-TpoR-III) is the strongest asparagin mutant via TYK2.

III.5.5.4. Adding alanines reduces Tpo response

Adding alanines increase the hydrophobic length of the helix and rotate the receptor by a 100°CW rotation per alanine. We have assayed many times those constructs since +1A and +2A seem to lead to an increase in basal activity. When considering the entire data set, we cannot conclude to any statistically significant increase for one of these mutants.

The increased hydrophobic length of the TpoR TMD leads to a reduction in cell surface expression and to more tilted receptors. Those two reasons could explain the progressive loss in Tpo response.

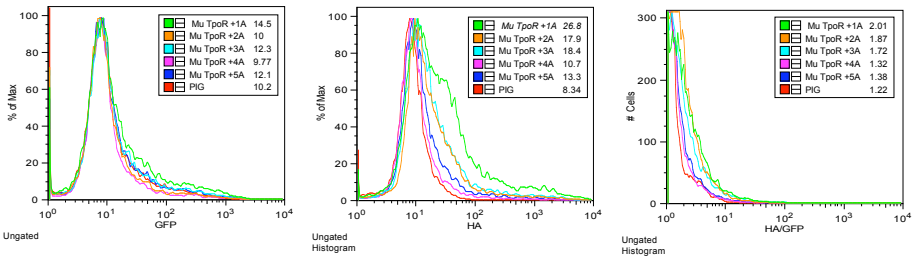


Figure 75 Cell surface localization of TpoR + alanines

We measure the TpoR cell surface expression by flow cytometry. Cells transduced with HA-tagged TpoR-IRES-GFP bicistronic vector were sorted for the same GFP level. We observe a progressive reduction of the HA (PE)/ GFP signal.

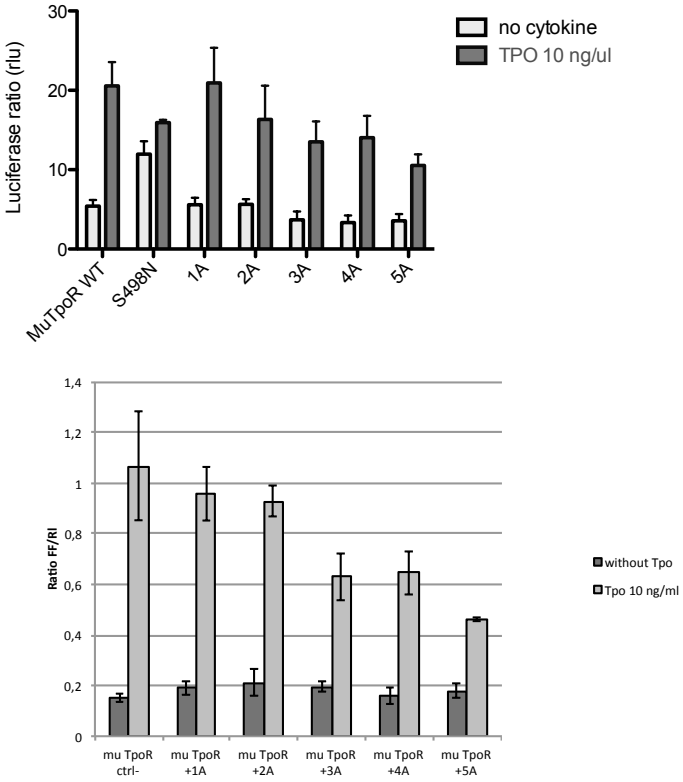


Figure 76 - Luciferase assay: alanines insertions before the KWQFP motif
pGRR5 (top) and Spi-luc (bottom) transcriptional activity of TpoR + Alanines. We observed a progressive decrease in Tpo response. No mutant was as strong as S498N.

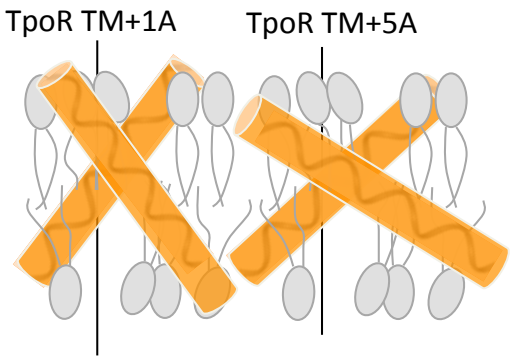


Figure 77- LHCC tilt angle

+1A, +2A, +3A increase the total hydrophobic length of the helix
A LHCC likes to have a tilt angle of about 20°. Increasing this angle may prevent dimerization

III.5.5.5. Combining active human mutants have a synergistic effect

Mutations found in humans (S505N and W515K/L) are located roughly on the same active interface (50° apart). The presence of S505N and W515L mutations on the same ET colonies has been described in Boyd et al.[258] and attributed to the acquisition of a Ser to Asn mutation in the non-W505L mutated chromosome. This clone developed a proliferative advantage over the W515L heterozygous clone. We were interested in the potential antagonistic or synergistic effect of having both mutations in *cis*. As expected both mutations in *cis* in the active interface reinforce the constitutive activity of the mutant leading to a super receptor. Tpo in this super double mutant has no additional effect, as it is the case for single mutant.

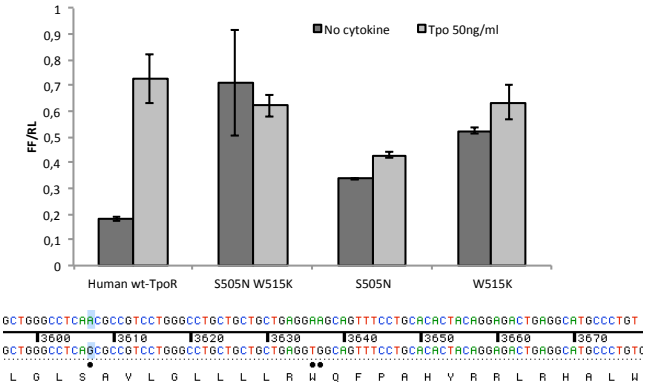


Figure 78 - Luciferase assay: double S505N W515K oncogenic activity
STAT5 transcriptional activity via JAK2 of the double Human mutant compare to single mutant: S505N W515K is stronger than each of them taken separately.
S505N is obtained via a point mutation while W515K requires 2 mutations.

III.5.5.6. Trp 529 is not required for activity of the W515 mutants

W529 is located in a hydrophobic patch just before Box 1 and is oriented exactly in the same interface than W515 if we considere the junction helical. This W529 is extremely conserved in more than 100% of species analyzed. It has been postulated that this Trp could be move towards the membrane upon unraveling. This W529 was shown to be not absolutely required for W515K activation or cytokine stimulation. The double homologous murine mutant $L_{521}W_{522}$ to AA was not properly expressed at the cell surface.

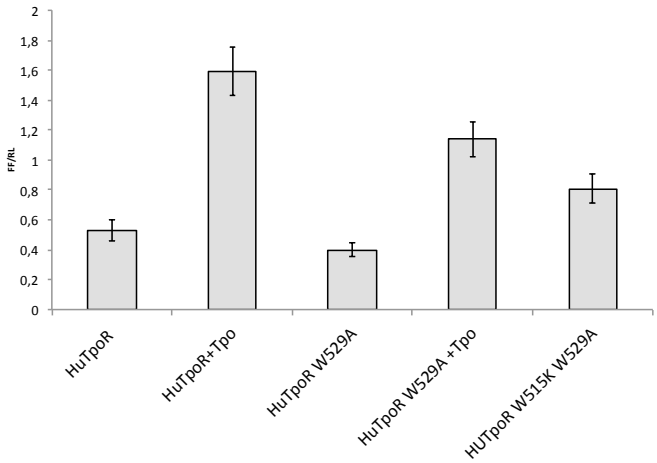


Figure 79 - Luciferase assay: cytosolic W529A

STAT5 transcriptional activity in γ2A cells transfected with pGRR5/JAK2 STAT5 and TpoRs. W529A respond less to Tpo stimulation (probably due to lower surface expression) and is not required for constitutive activity of W515K mutant.

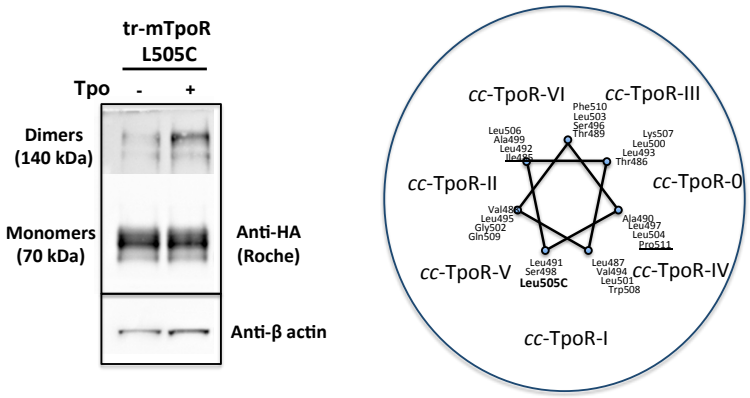


Figure 80 - Crosslinking of tr-mTpoR L505C with Tpo agonist

Tpo dimerizes the receptor in a cc-TpoR-I conformation where truncated murine TpoR (tr-mTpoR) L505C crosslinks

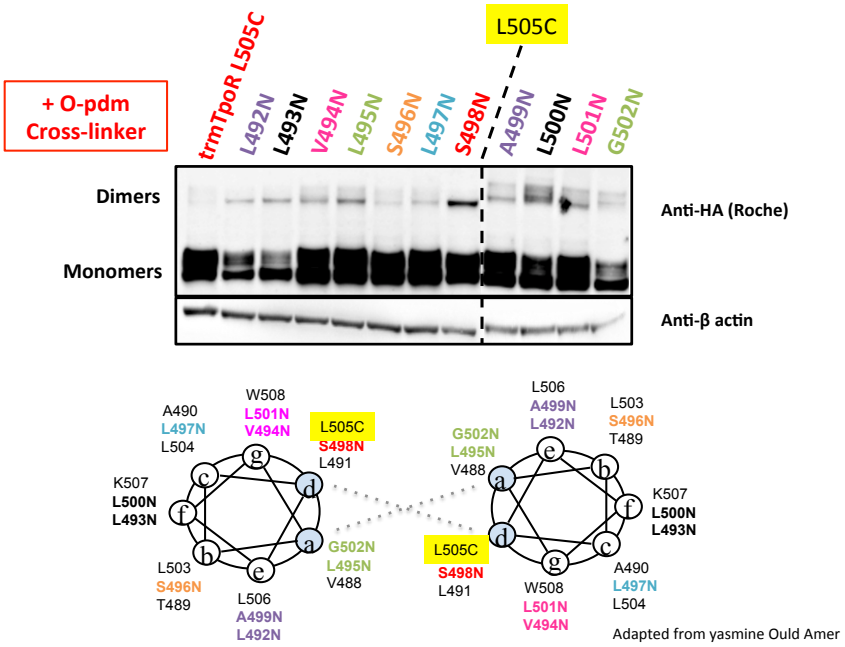


Figure 81 - Crosslinking of tr-mTpoR L505C with Asn mutants.
S498N is dimerizing in the best orientation for L505C crosslinking. The fact that tr-mTpoR L500N L505C strongly crosslinks can be explained by the unraveling theory.

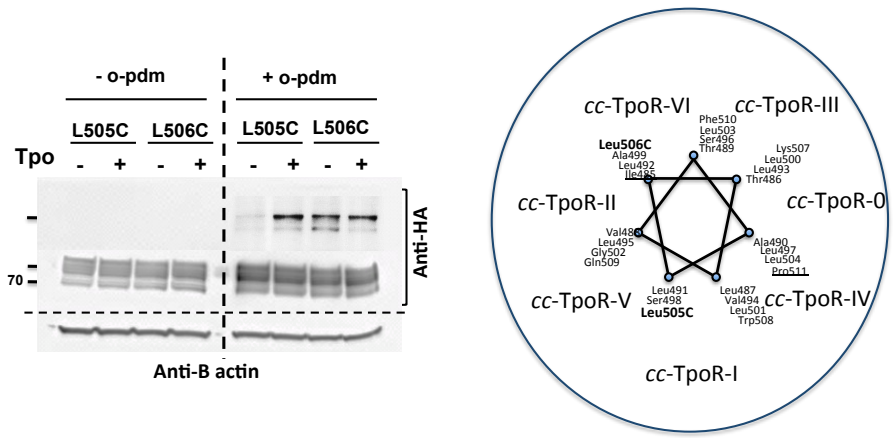


Figure 82 - Crosslinking of tr-mTpoR L505C and L506C with Tpo agonist.
In the presence of o-pdm, tr-mTpoR L506C (located in the inactive interface) crosslinks in the absence of Tpo, while both L505C (active interface) and L506C (inactive interface) tr-mTpoR crosslinks upon Tpo binding supporting the unraveling theory.

III.6. Preamble Antiproliferative effect of TpoR at high TPO implies an IFN-like signaling (in preparation).

III.6.1. Background

TpoR in presence of low doses of Tpo exerts a positive effect on cell viability, proliferation, differentiation of megakaryocyte progenitors like megakaryoblasts and on activation of platelets. On the contrary, high Tpo concentration exerts an antiproliferative effect on BaF3 cells expressing both TpoR and JAK2. Cell titer glo viability assay showed a growth arrest in cell co-expressing JAK2 or TYK2 and TpoR. In absence of JAKs or in cells expressing low JAK2 levels, the receptor density is lower at the cell surface[138] and prevents this antiproliferative signaling.[322] The expression of JAK2 increases during megakaryocyte differentiation, while certain megakaryocytic cell line like UT7 cells express very high levels of JAK2 (>10-fold over Ba/F3 cells).

Results:

The growth inhibition of BaF3/TpoR/JAK2 stimulated during 6h with high Tpo seems to be correlated with an interferon-like signature by microarray with upregulation of hundreds of interferon regulated genes.[323] Using TFactS, we identified that STAT1, STAT3 and other STATs were shown to be potentially involved in the upregulation of genes in the microarray experiment.[324] We confirmed those results by RT-PCR in BaF3 mTpoR/JAK2 cells stimulated with various amount of Tpo. We observed an increase in interferon regulatory factor 7 (IRF-7) and in oligoadenylate synthase-like2 gene (OASL2). We concluded that high level of Tpo induces interferon target genes.

Afterwards, the interferon transcriptional activity was measured with an IFN specific reporter pMx-Luc, which contains the Mx promoter and is responsive to (STAT1/STAT2/IRF9) ISGF3 complex. The pMx-Luc reporter plasmid was electroporated into BaF3 cells. Binding of IFNα to endogeneous interferon cell surface receptors leads to the rapid transcriptional activation of the pMx reporter. Epo binding to EpoR or Tpo in absence of its receptor are not able to induce a type 1 interferon like signal. However, Tpo induces a transcriptional Activity via STAT1/STAT2/IRF9 complex. This interferon signaling induces by Tpo requires the cytosolic Y112 and Y117 residues. Mutations of Y112F and/or Y117F abolish the IFN signal in pMX-Luc dual-luciferase assay and removed the antiproliferative effect of Tpo measured by cell-titer-glo (ATP based viability assay) experiment on BAF3 cells expressing JAK2 and Y-F mutants with the ability of high Tpo concentration to increase more than 10 times the unstimulated level in Y112F-Y117F which contrast with nearly no increase in wild type BaF3 TpoR cells. Using coiled-coil induced TpoR dimeric conformations we show that only ccTpoR-IV (which is highly active) induces phosphorylation of STAT2 followed by induction of transcriptional activity of Mx gene (type I IFN target gene). This conformation of the receptor appears to be reminiscent of that induced by very high Tpo levels (>50-100 ng/ml), and both high Tpo and cc-TpoR-IV induce strong cell-to-cell adhesion possibly reminiscent of the intercellular HSC interactions to the bone marrow niche cells. Noteworthy, Eltrombopag (Tpo non peptidyl agonist) is also able to activate IFN transcriptional activity. We have shown

for the first time, the ability of TpoR to induce a STAT2 phosphorylation in BaF3 TpoR JAK2, in megakaryoblastic UT7 and MO7-e cell lines as well as in CD34+ cells and in platelets from healthy volunteers by western blot. In TpoR delta 60 mice, where TpoR cytosolic tail is truncated and lacks tyrosine residues Y78, Y112 and Y117, We could not observed any phosphorylation of STAT2. IFN transcriptional activity of BaF3/TpoR/JAK2 cells mediates by Tpo cannot be increased by cotransfection of IFNAR1 and IFNAR2 or IL-28R α subunit for IFN lambda. These results confirm that those subunits are not required. The IFN signaling mediates by TPO is a direct effect of TpoR-TpoR activation and is not implicating a cross talk with other receptors. BaF3 cells that have a JAK2V617F mediated down regulation of TpoR escape the antiproliferative effect mediates by Tpo and presents less STAT2 phosphorylation. Finally, Tpo induces an antiviral activity in cells infected with Mengo virus, as shown in collaboration with Prof. Thomas Michiels. We used for this assay γ2A hTpoR hJAK2wt cells: 5000 cells/well were seeded in a 96 well plate (clear flat bottom). After 24h, cells were treated with the indicated doses of Tpo or Intron A. 24 h after cytokine treatment, cells were infected with Mengo virus (encephalomyocarditis virus Mengo strain) for 16-24 hours. At day 3, paraformaldehyde-fixed cells were stained with crystal violet (live cells appear blue).

III.6.2. ASH abstract related to bimodal signaling

820 Thrombopoietin Activates STAT2 Inducing Type I Interferon Effects and Gene Expression: Implications for *in Vivo* Tpo Treatment and for Myeloproliferative Neoplasms
Program: Oral and Poster Abstracts
Type: Oral
Session: 635. Myeloproliferative Syndromes: Basic Science - Transcription Factors and Signaling
Tuesday, December 9, 2014: 8:15 AM
West Building, 3018-3020 (Moscone Center)

Stefan N Constantinescu, MD, PhD, Prof.1*, Jean-Philippe Defour, BPharm,2*, Celine Mouton3*, Isabelle Plo4*, William Vainchenker, MD, PhD5, Jean-Luc Villeval, PhD6*, Thomas Michiels, MD, PhD7*, Judith Staerk8* and Christian Pecquet, PhD2*
1 University of Louvain, Ludwig Institute for Cancer Research, Brussels B1200, Belgium
2 Ludwig Institute for Cancer Research, Brussels, Belgium
3 de Duve Institute, Université catholique de Louvain, Ludwig Institute for Cancer Research, Brussels, Belgium
4 INSERMU1009, Institut Gustave Roussy, Villejuif, France
5 INSERM U1009, Institut Gustave Roussy, Villejuif, France
6 INSERM, Institut Gustave Roussy, Villejuif, France
7 de Duve Institute, University of Louvain, Brussels, Belgium
8 Nordic EMBL Partnership, Center for Molecular Medicine, University of Oslo, Oslo, Norway

Thrombopoietin (Tpo) acts via its cell surface receptor (MPL/TpoR) to promote megakaryocyte progenitor survival, proliferation and differentiation via activation of JAK2, STAT5, STAT3, STAT1, ERK1,2-MAPK-kinase and PI-3'-kinase/Akt. In addition, Tpo signaling in the bone marrow niche is required for maintaining hematopoietic stem cells (HSCs). Recently we showed that in cells expressing high JAK2, such as megakaryocytes or engineered cell lines, Tpo induced an anti-proliferative and pro-senescence physiologic effect. Down-modulation of TpoR in myeloproliferative neoplasms (MPNs) progenitors might confer resistance to such anti-proliferative effects in megakaryocytes, thus contributing to their uncontrolled proliferation.

Here we report that Tpo activates tyrosine phosphorylation and transcriptional activation of STAT2, and of a complex containing STAT2, STAT1 and IRF-9. This is specific for type I interferon (IFN) and is associated with anti-proliferative and antiviral effects. We detected Tpo induced STAT2 activation in platelets of thrombocytopenia patients treated *in vivo* with Tpo or Tpo agonists as well as in human CD34+-derived megakaryocytes. In cell lines reconstituted with MPL/TpoR and JAK2, Tpo behaved like an IFN by protecting cells from subsequent viral infection and inducing IFN-stimulated gene expression. We asked whether Tpo-induced STAT2 activation depended on type I IFN receptors, on TYK2 or on STAT1. Using primary cells from mice where these genes have been knocked-out we show that Tpo indeed activates STAT2 via TpoR itself, and does neither require IFNAR1, IFNAR2 nor TYK2, demonstrating that this effect is direct.

By using cell lines expressing different levels of JAK2 we show that Tpo exerts a bimodal effect. At low JAK2 levels Tpo induces mainly STAT5, STAT3 and STAT1 activation, while at high JAK2 levels (comparable to those in UT7 cells or primary megakaryocytes) Tpo induces STAT2/STAT1/IRF9 activation, in addition to STAT5/STAT3/STAT1 activation. Interestingly, the STAT2 signaling is dominant and induces an anti-proliferative effect, which can be inhibited by shRNA targeting STAT2, or by mutation of distal receptor tyrosines. Moreover, using STAT2-/- mice we show that STAT2 activation by Tpo is relevant for the steady-state levels of platelets, with knock-out mice having significantly higher platelet numbers. Recovery studies after 5-FU injection and examination of HSCs and early progenitors showed that STAT2 acts as a negative regulator of the stimulatory effects of Tpo on myelopoiesis.

We recently identified inactive and active dimeric conformations of TpoR. Here we tested which dimeric receptor conformation activates STAT2 using dimeric fusion proteins where a dimeric coiled coil (Put3) was fused to the transmembrane segment. While cc-TpoR-I was found to recapitulate the classical stimulatory effect of Tpo on STAT5, STAT3 and STAT1 and platelet formation *in vivo*, here we show that STAT2 activation is induced by another dimeric conformation, represented by cc-TpoR-IV, which is the strongest JAK2 activator. cc-TpoR-IV also induces strong cell-to-cell adhesion possibly reminiscent of the intercellular HSC interactions to the bone marrow niche cells. Increasing JAK2 protein levels leads to

stabilization of a Tpo-activated TpoR dimer that assumes a conformation that corresponds to cc-TpoR-IV. Thus, JAK2 levels act on fine-tuning the dimeric conformation of the TpoR dimer, switching it from a classical proliferative cytokine to an IFN-like cytokine, which is anti-proliferative.

The new Tpo-induced signaling pathway we describe is of very high relevance for MPN pathogenesis and treatment with IFN-I. Our data indicate that HSCs and megakaryocytes where TpoR-JAK2 V617F signal would be primed for IFN action, and might explain why IFN-I targets for inhibition the mutated HSCs, eventually decreasing the allele burden. Last but not least, autoimmune and viral-induced thrombocytopenia patients are treated with Tpo mimetics, and we could detect STAT2 activation in certain patients after *in vivo* Tpo treatment. Differences in the ratios of classical versus STAT2 activation might be at the basis of differences in response to Tpo of such patients.

Related results and discussion

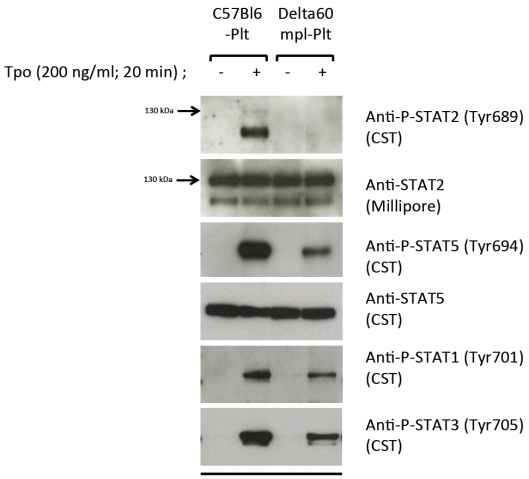


Figure 83 - Tpo induced phosphorylation of STAT2

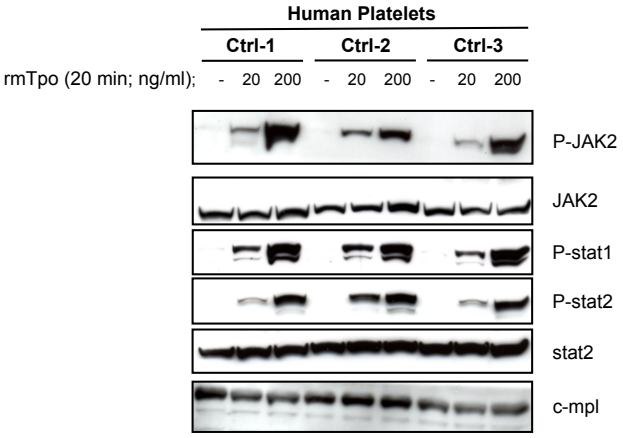


Figure 84 - Tpo induced phosphorylation of STAT2 in platelets of patient

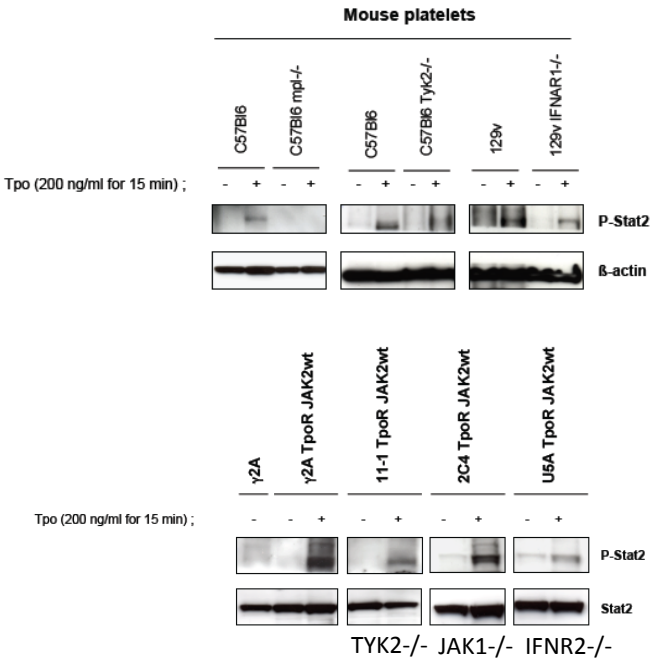


Figure 85 - Activation of STAT2 Is a direct TpoR Induced Effect

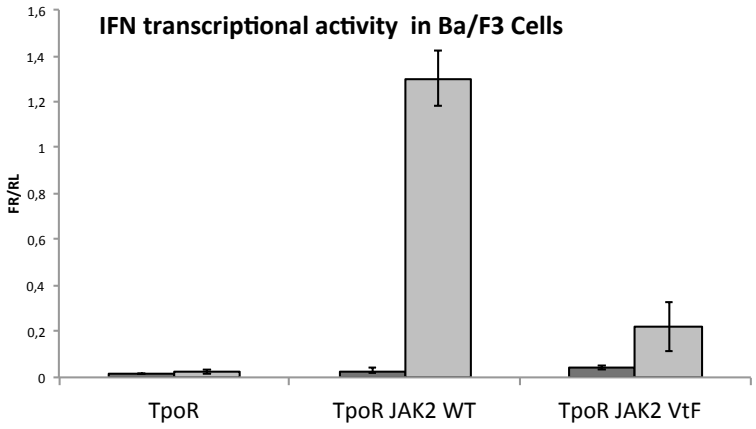


Figure 86 - Tpo induce IFN type I transcriptional activity

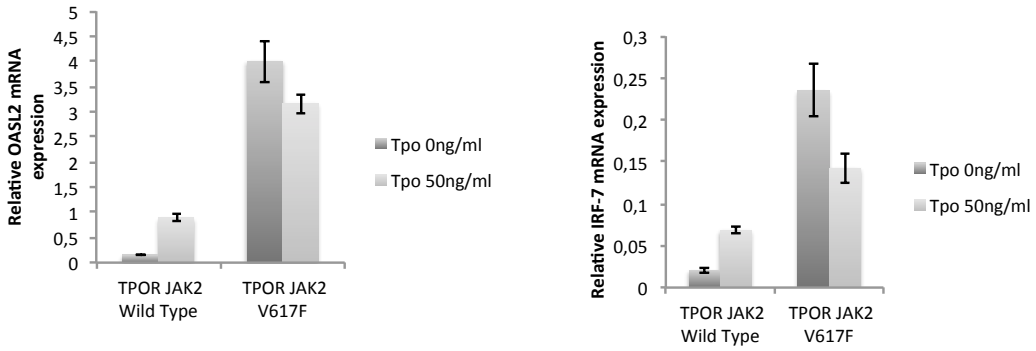


Figure 87 - RT PCR for IFN stimulated gene

High levels of Tpo increase IRF-7 (Interferon regulatory factor 7) and OASL2 (oligoadenylate synthase-like 2 gene) mRNA, two IFN inducible genes, while TpoR JAK2 V617F shows a constitutive activation of these genes.

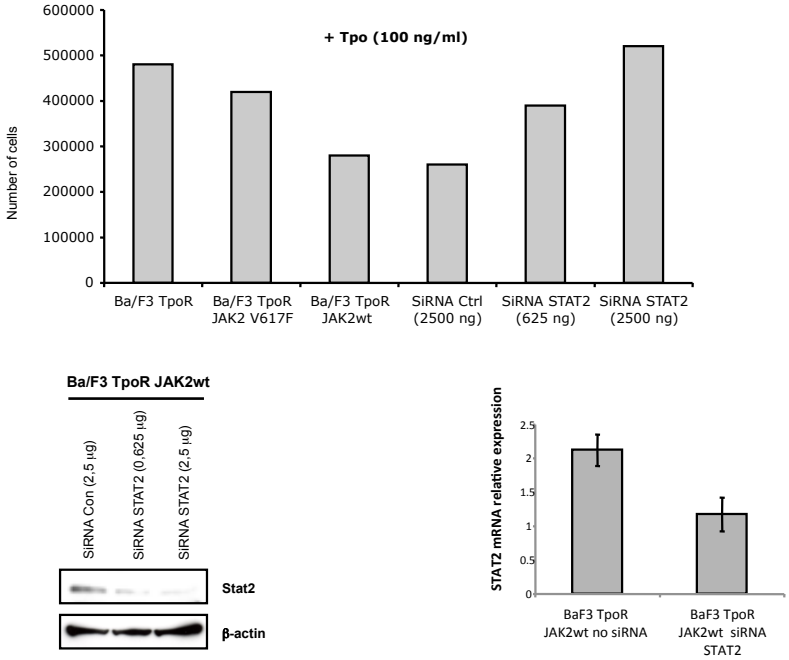


Figure 88 - SiRNA targeting STAT2 prevent the antiproliferative effect of Tpo.

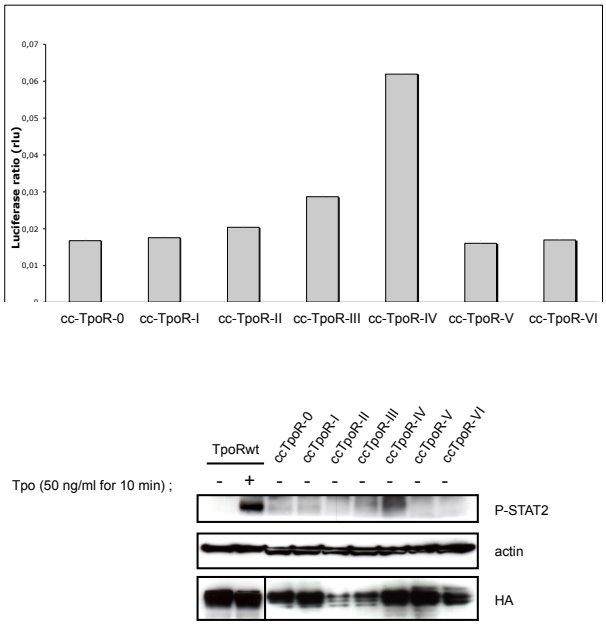


Figure 89 - STAT2 phosphorylation and transcriptional activity is induced by strong cc-TpoR-IV

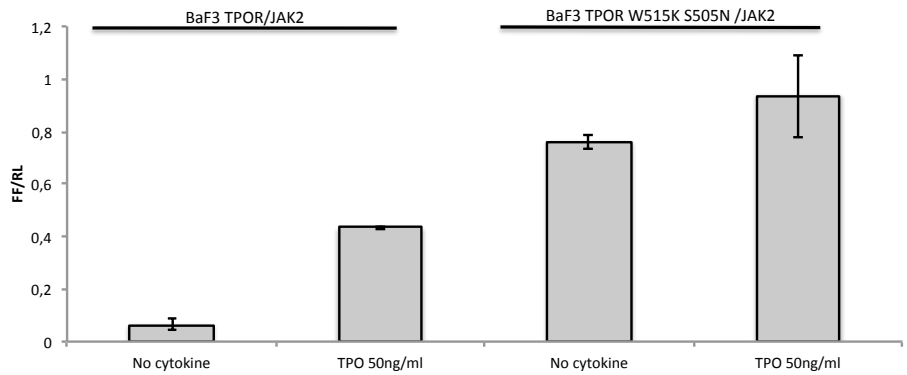


Figure 90- Type-I interferon like transcriptional activity of TpoR and TpoR mutants
The pMx-Luc reporter plasmid was electroporated into BaF3 cells.
The powerfull TpoR mutant S505N W515K leads to constitutive Type I interferon like signaling.

IV. DISCUSSION

IV.1. Dimeric state of the receptor

It is recognised that the TM domain of TpoR transmits the mechanical information from the extracellular space to the intracellular space in an active dimeric conformation. However, it is still not clear whether the full-length receptor is in a dimeric state in the absence of ligand. Unliganded EpoR exists in a predimerized state. TpoR could be monomeric or could be a weak preformed dimer that still requires receptor subunit rotations, or exist in an equilibrium state between these two states. One can expect receptor monomer to be damaging for the cells because of random collisions and potential self-activation of these receptors, and also because ligands need to find rare receptors on cells and activate them (typical surface densities are 500-1,000 receptors/cell surface, yet low occupancy <10% triggers half-maximal responses in general). Evolutionary pressure could have rather favored stable predimeric receptors that are rotated into an active conformation upon ligand binding. However, both human and murine full-length TpoRs seem rather monomeric or weakly monomeric by *Gaussia* assay, when compared to EpoR. This assay measures the proximity of the distal ends of receptors, which might be apart even in a dimer, as suggested for scissors movements of EpoR[124]. On the other hand the same distal ends of TpoR do dimerize strongly when the extracellular domain of murine TpoR is removed, , as also shown by *Gaussia* luciferase assay, suporting the notion that the extracellular receptor domain prevents stable dimerization.

IV.2. Two layers of protection against self-activation in TpoR

It is striking that human TpoR behaves differently and is globally less primed for activation than murine TpoR despite more than 80% identity. His499 was shown in this thesis to be responsible for this discrepancy and can be considered as an evolutionary break and an additional layer of protection to self-dimerization of the human TpoR. His499 and Trp515 are both guardians of the receptor and are responsible for keeping the receptor inactive in absence of ligand. His499 is located in the lipid head group on the extracellular side of the bilayers. His499 outside and Trp515 inside delimit the human TMD. His499 is the target of the small molecule agonist Eltrombopag and is believed to rotate towards the lipids and maintained outside of the interface when binding to Eltrombopag. Notably, a histidine at position 627 in the hGCSFR transmembrane domain is needed for activity of LG7455, similar to what has been found for Eltrombopag (ASH 2011 poster 3391, San Diego). The helix above His499 is unfolded in the inactive state of human TpoR and makes a kink that increases tilt angle. This helix near His499 is re-formed upon activation resulting in more parallel TMD and dimerization.

In the human TpoR context, only one Asn-induced dimer (S505N) can activate the human receptor. Kim et al compared ^{1}H-^{15}N HSQC spectra with or without addition of a small non-peptidyl TpoR agonist (SB394725) and found His499 and Ala506, located in the inactive interface, underwent the stronger chemical shift upon SB394725 addition, but S505 experienced almost no change.[325] Therefore the S505 residue is not rotated or moved by by SB394725. Ser505 could be a kind of pivotal point, fixed with respect to the membrane, when the helix tilts and that could be better tolerated when His is present than other human Asn mutants like G509N, which is not expressed at the cell surface in the presence of the His.

The RWQFP JM motif was previously shown to prevent activation of the TpoR[97] and was shown in this thesis to reduce self-dimerization of the TMD. Moreover, insertion of the RWQFP in EpoR also seems to reduce basal activity. This amphipathic motif is able to achieve this by increasing the tilt angle and by stabilizing the inactive dimeric conformation. The property of this motif is indeed similar to that of antimicrobial peptides that make intramolecular cation-π interaction to accommodate in the lipid interface. In a 3D NMR structure of puroindoline A (puro A) (FPVTWRWWKWWKG-NH2) bound to micelle, all arginines are facing the indol rings, directly correlating with deep penetration in the membrane.[326,327] In the case of cell permeable peptides such as "penetratin", molecular dynamic simulations show that a cation-π interaction between Trp_{48}, Trp_{56} and Arg_{52} shield the peptide from the water phase, while on the other face, positively charged residues contribute to the fast interaction with the negatively charged lipids. The peptide seems to stay parallel or slightly tilted relative to the membrane interface.[328] The ability to participate in cation-π interactions is not the only tryptophan property. Lactoferricin B, which is naturally present in mammalian milk and other body fluids, use tryptophan mainly for its unique property as a

membrane anchor. Inserting a non-natural tryptophan (a so-called "super-tryptophan"), which is more bulky, enhances the antimicrobial effect, suggesting that the size and the three dimensional shape of tryptophan contributes to antimicrobial activity as much as its ability to participate in cation-π interaction.[329] The key residue inside the RWQFP TpoR motif is then obviously Trp515. Trp515 appears to anchor the position and orientation of the TMD in the membrane bilayer. This effect could be due to its strong preference to be buried in the headgroup region of the lipids and make potential cation-π interactions with the positively charged headgroups. We have shown that W515 prevents TM helix dimerization and that mutation like W515K/L induce dimerization and activate signaling. Ligand or S505N can overcome the ability of Trp515 to prevent TpoR self-activation. In the absence of a ligand, TpoR is monomeric or only weakly dimeric because Trp515 prevents upstream TM dimer formation.

IV.3. Tryptophan substitutions

TpoR Trp515 can only be replaced by a cysteine or a proline for the receptor to remain inactive in the absence of ligand. Any of the 17 residues activate at that position, and despite a lesser degree of activation, even closely related aromatic residues trigger constitutive signaling. It is of importance that W515Y is more effective than W515F at inhibiting signal transduction following the (Trp> Tyr> Phe) cation-π scale. The oxygen of tyrosine is a second site of electronegativity, making a more potent cation-π interactor. A previous report showed that mutation of the first residue (RWQFP to AWQFP) was activating. This suggested an intra-molecular cation-π interaction between the Trp515 and the Arg514 to accommodate the positive charge of the Arg. However, R514A was shown to be inactive in this thesis and we propose a minor role for the first position of the **R**WQFP that can be either hydrophobic or positively charged. Negatively charged residues (DWQFP or EWQFP) do not allow traffic and function for the receptor due to electrostatic repulsion with the negatively charged lipids. Double mutants such as WWQFP function better for inhibition than W515 alone, suggesting again that an intramolecular π-cation interaction is not mandatory for good membrane interaction and rather that the two tryptophans can interact in an intermolecular way with the phospholid headgroups. Second site mutations like R514W or Q516W can partially reverse dimerization and prevent self-activation mediated by large residues and most frequent mutations like W515K/L. R514W seems to be more effective than Q516W in reducing basal level since Q516W was not able to restore a low basal activity when placed after small residues like W515A/G/S. Despite a tilt angle of RAWFP equal to the wild-type receptor, the RAWFP motif is active. This means that Trp is playing its role of tilting the receptor but cannot prevent dimerization. Overall, those results have three main implications. Firstly, small molecules (guiding a tryptophan or cysteine like structure) could be used to reinstate a wild type phenotype in the majority of TpoR W515 mutated patients. Secondly, Trp might exert a more general effect between TM and cytosol domains and especially in the first two-positions and influence oligomerization and tilt of type I TM proteins. Lastly, the TMD tilt and the resulting TMD-TMD dimerization can be uncoupled in double mutants bearing a W515A/G/S and

Q516W where receptors are tilted, but still adopting dimer conformation. We hypothesize that small residues might allow a π-π stacking between two tryptophans at 516 (Q516W) that subsequently promote receptor dimerization.

IV.4. Position 516

Position 516, besides its role as a second site to reverse W515 activity, is important in mediating a complete inhibition of the wild type receptor (i.e. Q516A/H mutants are weakly active). These Q516 single mutants are nevertheless marginally active compared to W515 mutants. Q516 is the helix transition point where the helix is disrupted and Q516 is located in the inactive interface (of murine TpoR at least) and might stabilize the inactive interface by making hydrogen bonds. Curiously Q516K is present in some monkeys and could be accommodated at this position by an intramolecular cation-π interaction. We have additionally observed a complete inhibition of the W515K/R (even with our more sensitive spi-luc reporter) by simply mutating Glu516 to Phe. RKFFP and RRFFP are strikingly similar to wild type by growth or by luciferase assay. The positive charges might fit via a cation-π interaction between the indol ring of the Phe and the cationic group of the Arg. The discovery that opossum have a naturally selected RRFFP motif supports this finding.

IV.5. Interfaces

IV.5.1. Inactive interfaces

The TM domain of human or murine TpoR alone are clearly dimeric as demonstrated by TOXCAT assay[319], and by deuterium MAS-NMR in absence of the RWQFP motif [304]. Human and murine TpoR have one unique inactive interface. Besides the His499 in human TpoR, one key difference between murine and human TM domains in the LHCC heptad layout are their postulated inactive interface.[318,319] Considering their suggested inactive interfaces, murine interfacial residues[318] are 50° counterclockwise relative to human inactive interfacial residues.[319]

HuWT inactive	V	T	A	L	H	L	V	L	G	L	S	A	V	L	G	L	L	L	L	R	W	Q	F	P
	495	496	497	498	499	500	501	502	503	504	505	506	507	508	509	510	511	512	513	514	515	516	517	518
	g	a	b	C	**d**	e	f	g	**a**	b	c	**d**	e	f	g	**A**	b	c	**d**	e	f	g		
muWT inactive	V	T	A	L	L	L	V	L	S	L	S	A	L	L	G	L	L	L	L	K	W	Q	F	P
	488	489	490	491	492	493	494	495	496	497	498	499	500	501	502	503	504	505	506	507	508	509	510	511
	d	e	f	G	**a**	b	c	**d**	e	f	g	**a**	b	c	**d**	E	f	g	**a**	b	c	**d**		

Table 5 - Human and murine inactive interface

In other words, the inactive interface of the human TpoR resembles murine cc-TpoR-VI rather than cc-TpoR-II. This cc-TpoR-VI dimeric interface is a low JAK2, strong TYK2 interface in the murine TpoR context. This difference could come from the His499, unique to the human TpoR.

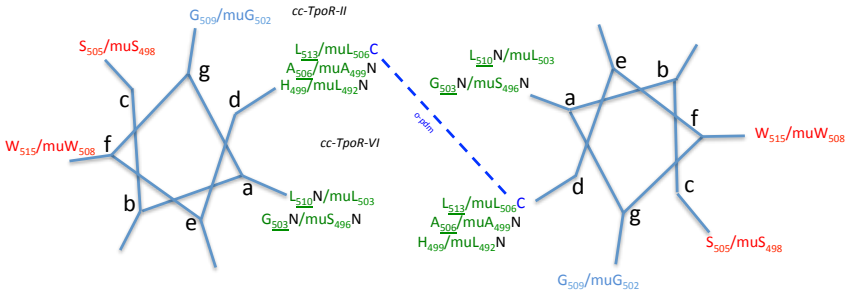


Figure 91 - Coiled coil VI interface
Helical wheel focused on the human inactive interface (corresponding more to cc-TpoR-VI) HxxxGxxAxxxLxxL. Both human and murine residues are annotated. Asn mutants tested in this thesis are in black and cross-linking (blue) study that validate this interface.

cc-TpoR-II corresponds to the inactive interface of the murine TpoR and is a low energy conformation, easily adopted by the receptor TMDs. This interface cannot induce growth of cells or formation of platelets from megakaryocytes *in vivo*. It is also, the lowest (transcriptionally speaking) cc-TpoR fusion protein by luciferase assay.

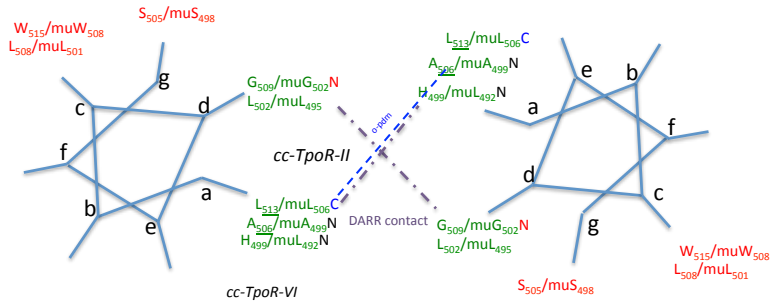


Figure 92 - Coiled coil II interface
Helical wheel focused on the murine inactive interface (cc-TpoR-II). LxxxAxxGxxxL Both Human and murine residues are annotated. Asn mutants (black), cross linking (blue) and DARR (purple) study that validate this interface.

Introduction of His492 in the context of the first four Put3 constructs increases the power of cc-TpoR-II and reduces signaling by cc-TpoR-0, -I, -III. cc-TpoR-I is now the strongest followed dimer by cc-TpoR-0 and cc-TpoR-II. cc-TpoR-III is now lower than cc-TpoR-II. The His492 in this murine dimeric construct may well have a different influence since it might

be forced into a helical geometry, but it shows that cc-TpoR-II in the presence of the His492 is no longer the weakest interface.

IV.5.2. Active interfaces

TOXCAT and cysteine cross-linking studies performed by Matthews et al.[319] (Engelman Lab) have elucidated the human TpoR inactive interface corresponding to H499xxxG503xxA506xxxL510xxL513. The interface mediated by this TM dimer is consistent with a parallel left-handed helical interface with contacts every third or every fourth residue. The human (GxxA) interfacial residues allow tight packing and are conserved as small residues in other species. The human inactive interface possesses a His "in", Trp "out" conformation and corresponds to the unliganded receptor.

The murine inactive interface L495xxxA499xxG502xxxL506 has been determined by our coiled-coil TpoR studies. The murine inactive interface corresponding to cc-TpoR–II possesses Ala499 and Gly502 in their interface (AxxG motif) that allows tight packing. DARR NMR has confirmed intermolecular contacts between those two interfacial residues. This murine interface terminates with Q516 of the RWQFP motif that could stabilize the inactive dimer by hydrogen bonding. Engelman and coworkers[319] have postulated two active interfaces upon Tpo or eltrombopag activation for human TpoR. These two interfaces are that of a low energy dimer by computational searches, namely cluster one and cluster two. Cluster one (L498xxxL502xxN505xxxG509xxL512) resembles the active interface found by making cysteine cross-links in the S505N context. This interface corresponds to ≈100° rotation and has S505 in "d" and W515 not fully rotated in the interface. Cluster II (V501xxL504xxxL508xxL511xxxW515) is a theoretical low energy interface that has W515 fully rotated "in" and His fully rotated "out" of the interface This interface can be obtained by ≈150° CW rotation and corresponds to cc-TpoR-I. Overall, the receptor could potentially be rotated 100°-150° CW to generate either cc-TpoR-V or cc-TpoR-I like configuration with W515 more inside the interface and His more outside.

HuWT	V	T	A	L	H	L	V	L	G	L	S	A	V	L	G	L	L	L	L	R	W	Q	F	P
	495	496	497	498	499	500	501	502	503	504	505	506	507	508	509	510	511	512	513	514	515	516	517	518
	g	a	b	c	**d**	e	f	g	**a**	b	c	**d**	e	f	g	**a**	b	c	**d**	e	f	g		
S505N	V	T	A	L	H	L	V	L	G	L	N	A	V	L	G	L	L	L	L	R	W	Q	F	P
≈100°CW	a	b	c	**d**	e	f	g	**a**	b	c	**d**	e	f	g	**a**	b	c	**d**	e	f	g	a		
His Out	V	T	A	L	H	L	V	L	G	L	S	A	V	L	G	L	L	L	L	R	W	Q	F	P
≈150°CW	e	f	g	**a**	b	c	**d**	e	f	g	**a**	b	c	**d**	e	f	g	**a**	b	c	**d**	e		

Table 6 - Human active interfaces

For murine TpoR, all interfaces except one have been shown to be active.
cc-TpoR-0, cc-TpoR-I, ccTpoR-IV are the strongest JAK2 interfaces and cc-TpoR-III and cc-TpoR-VI are the strongest TYK2 interfaces. Overall, the interfaces that are both strong JAK2 and strong TYK2 activators are the most potent for BaF3 cell growth and correspond to cc-TpoR-0 and IV. At least one active interface (cc-TpoR-I) with S498 and W508 in the interface is a physiological interface and is able to generate platelets. From a rotational point of view, it could be easier to activate muTpoR than HuTpoR.

muWT	V	T	A	L	L	L	V	L	S	L	S	A	L	L	G	L	L	L	L	K	W	Q	F	P
	488	489	490	491	492	493	494	495	496	497	498	499	500	501	502	503	504	505	506	507	508	509	510	511
	d	e	f	g	**a**	b	c	**d**	e	f	G	**a**	b	c	**d**	e	f	g	**a**	b	c	**d**		
cc-V	V	T	A	L	L	L	V	L	S	L	S	A	L	L	G	L	L	L	L	K	W	Q	F	P
50°CW	**a**	b	c	**d**	e	f	g	**a**	b	c	**D**	e	f	g	**a**	b	c	**d**	e	f	g	**a**		
cc-I	V	T	A	L	L	L	V	L	S	L	S	A	L	L	G	L	L	L	L	K	W	Q	F	P
100°CW	e	f	g	a	b	c	**d**	e	f	g	**A**	b	c	**d**	e	f	g	**a**	b	c	**d**	e		
cc-IV	V	T	A	L	L	L	V	L	S	L	S	A	L	L	G	L	L	L	L	K	W	Q	F	P
150°CW	b	c	**d**	e	f	g	**a**	b	c	**d**	E	f	g	**a**	b	c	**d**	e	f	g	**a**	b		

Table 7 - Murine active interfaces

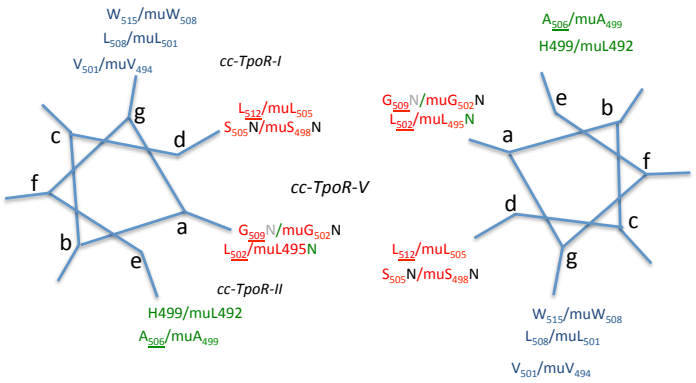


Figure 93 - Coiled coil V interface
cc-TpoR-V : For muTpoR a simple 50° rotation is sufficient to activate by orienting dimers toward cc-TpoR-V with a SxxxG motif in the interface.

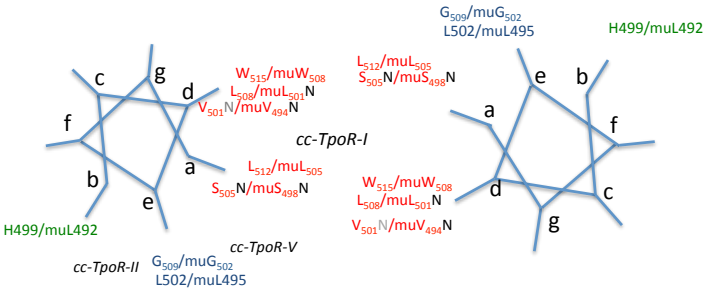


Figure 94 - Coiled coil I interface
cc-TpoR-I : A 100° CW will induce the physiological platelet-producing conformation cc-TpoR-I which has both S498 and W508 in the interface.

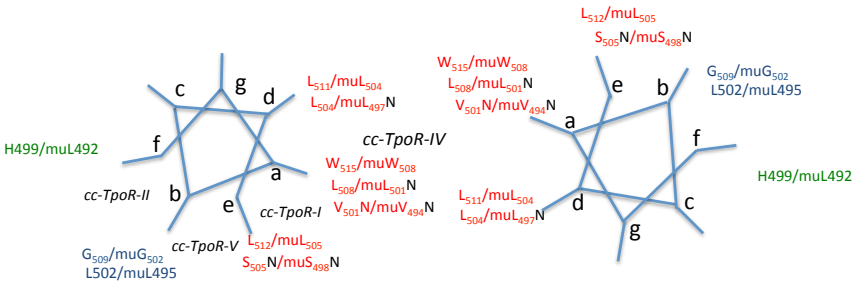


Figure 95 - Coiled coil IV interface
cc-TpoR-IV: The strongest conformation can be obtained by turning cc-TpoR-I by another 50° CW. This means turning 150° CW from the inactive interface. This conformation also has Trp "in" and V494 "in".

IV.6. From unraveling to JAK2 activation and beyond

IV.6.1. Orientation is not sufficient

When we compare the asparagine-induced dimer with the coiled-coils it is striking that the most potently activating murine Asn mutants like G502N do not correspond to the most activating coiled coils. Moreover, other Asn mutants localized on the same interface that G502 like L495N are not active. Unraveling of the α-helix in the cytosolic JM region upon dimerization could be the reason for this discrepancy and a "sine qua non" property for activation. The power of a mutant can therefore be proportional not only to its orientation, but also to its disruptive effect on the RWQFP motif. As shown on the murine schematic, our model is that upon dimerization the receptor is reoriented in one of the active interface. We propose a classical mechanism (that can be applied to the S498/505 and W508/515 mutants) that implies a Leu492/His499 rotation outside and a Trp508/515 rotation inside the TMD interface. The reason why the region around W508 unravels is still unclear. Speculatively, it could be due to steric clash between bulky Trps (for example between tryptophan when they

are rotate into the interface). Another explanation is that the region around W508 is embedded on the membrane and stays helical until activating mutants might pull this region down and it unravels without the protection of the membrane. This unraveling seems to remove constraints on the region between Trp508/515 and Trp522/529 and allows Trp522/529 (preceding Box 1 Pro-rich sequence) to move (data not shown) and to subsequently release intra or intermolecular JH2 constraints that prevent self-activation of the JAKs. In our model, dimerization, unraveling and rotation all contribute to JAK2 reciprocal activation. The correct sequence of all these events is not known, but our model of activation is not inconsistent to the model of Brooks *et al.* for the growth hormone receptor.[299]

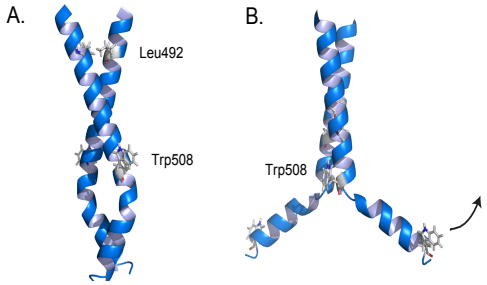


Figure 96 - Model for TpoR and JAK2 activation.

IV.6.2. Asymmetric dimer potential or multimeric states

As a general mechanism of activation for TpoR, we propose that W508 (W515 in human) is rotated in the interface. Most of our experimental data fit with with this hypothesis. However, the unexpectedly high activity of the murine TpoR L500N mutant is not consistent with this model, unless unraveling is taken into account, or asymmetric dimers or oligomeric structures are formed since L500 is on an opposite face. L500N could interact with S498 as an asymmetric dimer. The strong cross-linking of L500N revealed by the reporter L500C position (Figure xxx manuscript xxx) support rotation of W508 into the interface also in this mutant. Symmetric or asymmetric dimers could also allow a trimeric conformation where the active interface is already correctly oriented. These multimeric or asymmetric conformations might be spontaneously formed and trigger receptor activation. However, what is puzzling is that L500N crosslinks with L505C but was shown to be a potent TYK2 active mutant.

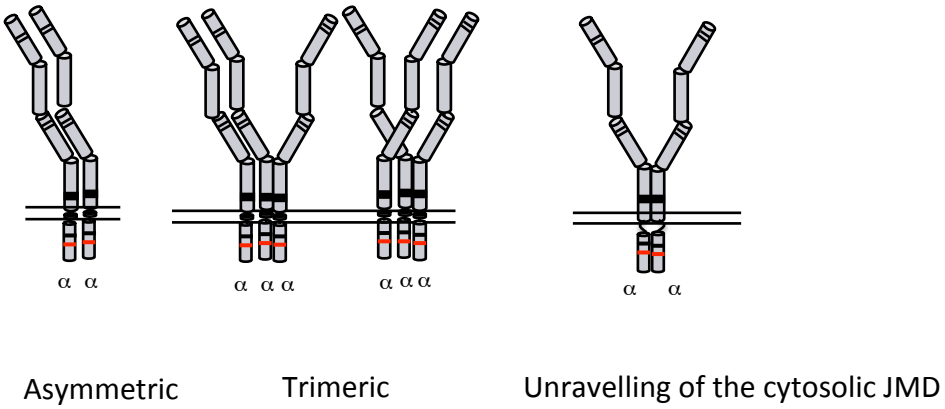


Figure 97 – Hypothesis for crosslinked dimers with tr-mTpoR L500N - L505C
The crosslinking observed could come from asymmetric dimer, trimers or unraveling of the cytosolic JMD

IV.6.3. Coupling orientation to activation or inactivation of TpoR

We have recently observed that the wild type receptor can be primed for activation by the addition of 2 extra-alanines before the KWQFP motif. This mutant is a weakly active mutant by itself that can only be observed in very sensitive luciferase assays with a sensitive reporter and high JAK2/receptor ratio. BaF3 cell growth assays in which cells transfected with +2A are easily selected in the absence of cytokine supports the activity of muTpoR +2A. We deduce that this conformation might orient the receptor in an active conformation that still needs a secondary event to signal. Adding alanines reduces cell surface localization as seen by flow cytometry with our HA tagged receptor. This phenomenon might be provoked by increasing helix length and tilt in the membrane. Interestingly, muTpoR +1A can respond via TYK2 upon Tpo binding. This suggests that Tpo is driving dimerization and gives an additional 150° CW rotation to the +1A to orient the receptor in a TYK2 receptive orientation, namely cc-TpoR-III. This 150° CW rotation is the expected rotation to go from a His499 in (inactive) to a His499 out (active) conformation. We do not really know to what degree Tpo or eltrombopag are able to rotate the receptor and if Tpo or eltrombopag behave the same on already active receptors. None of these ligands were able to reduce activity of our mutants. However, this hypothesis cannot be tested because the mutants (Ala490, Leu497, Leu504) that can be tested are already inactive. It is obvious that adding alanine can activate the inactive A499N mutant. W508K can be rotated to an inactive interface by adding two alanines or by using cc-TpoR-II. This leads to a new concept for MPN treatment that could be rotating the receptor into an inactive orientation. cc-TpoR–II W508K, as cc-TpoR-II, do not induce autonomous growth in BaF3 proliferation assay but generate a puzzlingly and confusingly high luciferase background signal in γ2A as shown in [318]. The problem with cc-TpoRs and the dual luciferase assay comes from the very high basal STAT5 transcriptional activity in γ2A cells

when lipotransfected, which is not present in the BaF3 electroporated using luciferase assay or growth assay. In our classical γ2A protocol, the complete set of signaling partners (including JAK2) are lipotransfected and leads to an abnormally high basal activation when using coiled coils.

We have now evidence that rotating the receptor to the inactive interface using coiled coils or alanine insertions can inactivate constitutively active mutants. This is of interest since diabodies (fusion of VH and VL chain) have been recently shown to induce various modifications in geometry/topology of EpoR dimers. They have also been used as surrogate Epo ligands to tune signaling output.[330] The future development of new tools to rotate the receptor into the inactive interface found in this thesis a proof of concept

IV.7. TpoR general model of activation

There are several aspects that need to be considered for explaining TpoR activation. As a picture is worth a thousand words, here is a drawing.

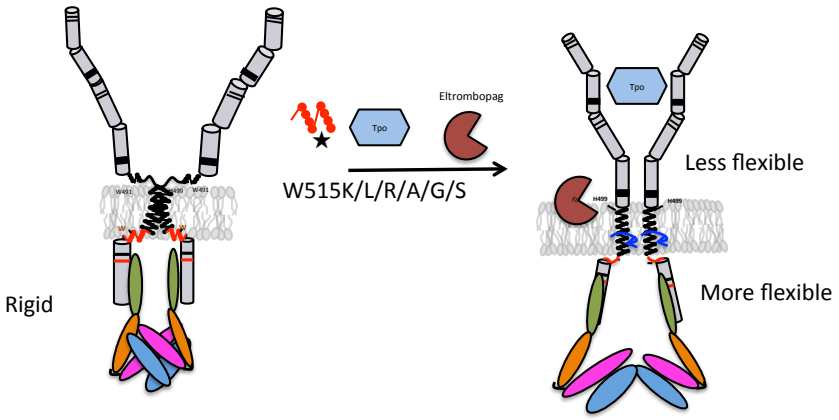


Figure 98 - Our general model of TpoR activation

Prior to ligand binding, the TMD could be stabilized in a LHCC geometry and in a low energy interface (II or VI). Ligand (Tpo) binding, eltrombopag or mutations induce rotation of the transmembrane domains from the inactive to an active interface. In the human TpoR the first event is helix formation around His499, which allows dimerization of TMDs and a change in the helix tilt angle. Upon rotation, unraveling of the region around W515 that is anchored in the membrane occurred and brings more flexibility to the ICD. This leads to closer JH1 domain and JAK activation.

IV.8. Of mice and men: physiological models

Mice have a higher concentration of platelets than humans with a normal platelet count reaching a level of million platelets/ul. Several problematic issues in this thesis emanate from murine data with multiple active interfaces and many more active mutants. The question that then arises is whether our conclusions still hold true in human physiology. We certainly can take lessons from murine TpoR physiology but the Hu TpoR appears in this thesis to reach a

higher level of self-control. In the same vein, even if Tpo from both species can be used interchangeably, small molecule drug development to activate human TpoR has shown a complete inactivity on murine TpoR due to the lack of His499. I would like to emphasize here that extreme caution should be taken to extrapolate data from murine species.

IV.9. Antiproliferative role of TpoR

TpoR plays a dual role in stimulating platelet production and maintaining stem cell quiescent. The antiproliferative effect of Tpo has been shown in this thesis to be mediated by a JAK2/STAT2 pathway. STAT2 activation requires a strong cc-TpoR-IV conformation or the presence of high dose of Tpo (<10 ng/ml). This high dose of Tpo could be reached in the osteoblastic niche near Tpo producing stromal cells.

V. CONCLUSION

Beginning with the discovery of the W515K/L and S505N mutations in patients suffering from MPNs, this thesis tried to uncover the mechanism of TpoR activation by those mutants. Overall, this thesis explains the layers of control that prevent self-activation of a receptor otherwise primed for activation and reinforces the concept of rotational dependence of activation using coiled-coils or alanine insertions. Our current model indicates that a change in helix tilt angle, dimerization, rotation and helix formation and unraveling all contribute to JAK2 reciprocal activation. With the development of new drugs, such as diabodies as surrogate ligands that are able to act on receptor dimerization and rotation, this work is particularly timely. Of interest, we have shown that Tpo can also induce anti-proliferative signals (Pecquet et al., 2012). It will be interesting to determine the precise conformations required for those signals, and how TpoR activates STAT2, which appears to be central for this anti-proliferative activity and for cross talk with type I interferon.

VI. PERSPECTIVES

For a long time we used mouse and human constructs indifferently without appropriate consideration. We now realize that some species specificity could lead to misinterpretation. S505N is the only human active Asn mutant, whereas there are four to five Asn mutants that are able to activate the murine receptor. We have built up a considerable collection of murine plasmids, including the alanine insertions that should be now tested on a human sequence. We do not know whether W515K/L can be inactivated by rotation either in a cc-TpoR-II or a -VI interface. Moreover, we have to test if deleting one leucine before the RWQFP motif of S498N/S505N inactivates the receptor. This should rotate the interface 100° CCW and generate an inactive interface. Further, adding three alanines should inactivate G502N. Adding one alanine should inactivate L500N. Adding two alanines should inactivate V494N, as is the case for W508K. All these constructs are currently being tested with the aim to generate tolls able to conformationally inhibit active mutants of TpoR.

Recently, proof-of-concept experiments have been shown that one can inhibit HER-2 by targeting the TMD with synthetic helices.[331] Therefore, we could also develop transmembrane domain targeting peptides that interact with the TpoR TMD and disrupt homodimers. Moreover, we can take advantage of the knowledge gained on His499 and the fact that preventing helix formation at this position will block receptor dimerization and activation.

VII. Appendix

VII.1. Thrombopoietin receptor down-modulation by JAK2 V617F

From www.bloodjournal.org by guest on January 2, 2016. For personal use only.

Thrombopoietin receptor down-modulation by JAK2 V617F: restoration of receptor levels by inhibitors of pathologic JAK2 signaling and of proteasomes

Christian Pecquet,[1,2] Carmen C. Diaconu,[1,2] Judith Staerk,[1,2] Michael Girardot,[1,2] Caroline Marty,[3] Yohan Royer,[1,2] Jean-Philippe Defour,[1,2] Alexandra Dusa,[1,2] Rodolphe Besancenot,[3] Stephane Giraudier,[3,4] Jean-Luc Villeval,[3] Laurent Knoops,[5] Pierre J. Courtoy,[2] William Vainchenker,[3] and Stefan N. Constantinescu[1,2]

[1]Ludwig Institute for Cancer Research, Brussels, Belgium; [2]de Duve Institute, Université Catholique de Louvain, Brussels, Belgium; [3]Inserm U1009, Institute Gustave Roussy, Villejuif, France; [4]Assistance Publique–Hôpitaux de Paris, Université Paris XII, Laboratoire d'Hématologie, PRB Cellulothèque Hématologie, Hôpital Henri Mondor, Créteil, France; and [5]Cliniques Universitaires St Luc, Université Catholique de Louvain, Brussels, Belgium

The constitutively active JAK2 V617F mutant is the major determinant of human myeloproliferative neoplasms (MPNs). We show that coexpression of murine JAK2 V617F and the murine thrombopoietin (Tpo) receptor (TpoR, c-MPL) in hematopoietic cell lines or heterozygous knock-in of JAK2 V617F in mice leads to down-modulation of TpoR levels. Enhanced TpoR ubiquitinylation, proteasomal degradation, reduced recycling, and maturation are induced by the constitutive JAK2 V617F activity. These effects can be prevented in cell lines by JAK2 and proteasome inhibitors. Restoration of TpoR levels by inhibitors could be detected in platelets from JAK2 inhibitor-treated myelofibrosis patients that express the JAK2 V617F mutant, and in platelets from JAK2 V617F knock-in mice that were treated in vivo with JAK2 or proteasome inhibitors. In addition, we show that Tpo can induce both proliferative and antiproliferative effects via TpoR at low and high JAK2 activation levels, respectively, or on expression of JAK2 V617F. The antiproliferative signaling and receptor down-modulation by JAK2 V617F were dependent on signaling via TpoR cytosolic tyrosine 626. We propose that selection against TpoR antiproliferative signaling occurs by TpoR down-modulation and that restoration of down-modulated TpoR levels could become a biomarker for the treatment of MPNs. (*Blood*. 2012;119(20):4625-4635)

Introduction

The thrombopoietin (Tpo) receptor (c-MPL/TpoR) is crucial for megakaryocyte differentiation, platelet formation, and hematopoietic stem cell homeostasis.[1-6] TpoR signaling relies mainly on Janus kinase 2 (JAK2),[7-11] which also regulates traffic of the erythropoietin receptor (EpoR) and TpoR.[10,12] On Tpo binding to TpoR, JAK2 becomes activated and phosphorylates cytosolic TpoR tyrosine residues, which attract signaling molecules that activate signaling via STAT3/5, MAPK, and PI3K pathways.[7,13-17] After activation, the receptor is internalized and then degraded by the proteasome and lysosome pathways, but also a substantial fraction is recycled back to the cell surface.[10,18-20]

Myeloproliferative neoplasms (MPNs) are malignant conditions arising from hematopoietic stem cells (HSCs) harboring molecular defects that promote excessive and cytokine-independent formation of mature myeloid blood cells. The unique somatic acquired *JAK2* V617F mutation is shared by more than 95% of polycythemia vera and more than 50% of essential thrombocythemia patients.[21-24] The pseudokinase domain V617F mutation constitutively activates signaling,[21] via formation of active complexes with receptors, such as EpoR and TpoR.

A seminal observation was represented by the post-translational down-regulation and impaired maturation of TpoR (c-MPL) in megakaryocytes and platelets of patients with MPNs.[25-27] In contrast, JAK2 strongly enhances maturation and stability of the cell-surface mature form of TpoR.[10] Here we asked whether JAK2 V617F can influence the traffic, maturation, and stability of TpoR, in cell lines, in JAK2 V617F knock-in mice, and in MPN patients that harbor JAK2 V617F.

Methods

cDNA constructs, retroviral transduction

Murine JAK2, murine TpoR, and mutants thereof were cloned into pREX-IRES-CD4 or pMX-IRES-green fluorescent protein (GFP) bicistronic retroviral vectors.[10] TpoR contains an amino-terminal hemagglutinin tag (HA).[12] The human IL9Rα was subcloned into the pREX-IRES-CD2 vector. Mutants were generated using the QuickChange Site-Directed Mutagenesis Kit (Stratagene) and verified by sequencing. Retroviral supernatants were generated in BOSC 23 cells.[28] After retroviral transduction of Ba/F3 cells, top 15% of the populations of cells expressing GFP or/and CD4 were isolated by cell sorting.

Cell proliferation assays

Cell proliferation was measured by the CellTiter 96 Non-Radioactive Cell Proliferation Assay or CellTiter-Glo Luminescent Cell Viability Assay (Promega) and/or using Coulter Z1 cell counter. Cells were plated at 5000 cells/well in RPMI containing 10% FBS. For assessment of autonomous growth, cells were washed and placed in RPMI medium containing 10% FBS. Recombinant murine Tpo was from R&D Systems.

Submitted August 9, 2011; accepted February 3, 2012. Prepublished online as *Blood* First Edition paper, February 29, 2012; DOI 10.1182/blood-2011-08-372524.

There is an Inside *Blood* commentary on this article in this issue.

The online version of this article contains a data supplement.

The publication costs of this article were defrayed in part by page charge payment. Therefore, and solely to indicate this fact, this article is hereby marked "advertisement" in accordance with 18 USC section 1734.

© 2012 by The American Society of Hematology

From www.bloodjournal.org by guest on January 2, 2016. For personal use only.

Surface expression of HA-tagged wild-type TpoR and TpoR mutants

Cell surface HA-TpoR was determined by flow cytometry using monoclonal anti-HA antibodies (Covance; 10 μg/mL) and R-PE–conjugated donkey $F(ab')_2$ anti–mouse IgG secondary antibody (12.5 μg/mL).[12] AG490, JAK inhibitor 1 (Calbiochem), TG101209, and AZD1480 (SynMed Chem), UO126 and PD98054 (MEK inhibitors), SP600125 (JNK inhibitor), SB203580 (p38 inhibitor), the PI3K inhibitor (Ly294002; all from Calbiochem), or the mTOR inhibitor rapamycin (Sigma-Aldrich) were added 20 hours before FACS. Trypan blue exclusion test was performed to monitor toxicity with Invitrogen Countess counter.

Immunoprecipitation and immunoblots

Ba/F3 cells expressing the TpoR and/or JAK2 mutants were lysed and processed for immunoprecipitation with anti-HA antibody (Roche Diagnostics) and Western blotting as described.[28] Western blotting antibodies were directed against: HA (Roche Diagnostics), JAK2 (Upstate Biotechnology), β-actin (Sigma-Aldrich), anti-FLAG M2 (Sigma-Aldrich), anti-MPI (TpoR; Upstate Biotechnology and Genentech), anti–poly/mono-ubiquitin (Enzo Life Sciences).

Cell-surface biotinylation followed by TpoR cell-surface immunoprecipitation, recycling assays

Stably transduced Ba/F3 expressing TpoR with or without JAK2wt or JAK2 V617F were incubated in PBS containing 1.5 mg/mL of sulfo-NHS-biotin (Thermo Scientific) for 30 minutes at room temperature. After cell-surface biotinylation, cells were washed 3 times with PBS containing 100mM glycine and stimulated or not with 25 ng/mL Tpo for different times followed or not by removal of Tpo. For surface immunoprecipitation, cells were incubated with anti-HA antibodies at 4°C for 1 hour, washed, lysed, precipitated with Protein G-Sepharose beads, and analyzed by Western blot with anti–Biotin/HRP (New England Biolabs) and anti-HA.

Ubiquitinylation of cell-surface TpoR

HEK-293 derived BOSC 23 cells were transfected with HA-tagged wild-type or mutant-TpoR and FLAG-tagged Ub using lipofectamine 2000 (Invitrogen). After 48 hours, cells were incubated with bio-Tpo (R&D Systems; 50 ng/mL) for 5 minutes at room temperature and for another 15 minutes at 37°C, then cells were washed with cold PBS, resuspended in lysis buffer and incubated with streptavidin-conjugated magnetic beads (Dynabeads, Invitrogen) for 1 hour at 4°C. Beads were washed and resuspended in 1× Laemmli buffer and supernatants were subjected to Western blotting for detection of HA-TpoR and Flag-Ubiquitin.

Endo-H and proteinase K digestions

Ba/F3 cells expressing different TpoR and JAK2 constructs were processed by immunoprecipitation and Endoglycosidase-H (Endo-H) digestion and assessed by Western blotting, as described.[10,12] Proteinase K (0.5 mg/mL) digestion for 30 minutes at 4°C was performed on live cells on ice in PBS. The cells were lysed in Laemmli buffer after 3 washes in PBS containing 2mM phenylmethylsulfonyl fluoride.

Confocal microscopy

Ba/F3 cells grown on poly–L-lysine–coated coverslips were fixed with 4% paraformaldehyde for 20 minutes, permeabilized with 0.05% saponin (Sigma-Aldrich), and stained at room temperature with anti-HA antibodies followed by goat anti–mouse IgG linked to Alexa-568 (Invitrogen).[10] Preparations were examined with an Axiovert confocal microscope (Carl Zeiss) coupled to MRC 1024 equipment (Bio-Rad) using a Plan-Apochromat 63×/1.4 oil DIC objective. Image acquisitions were made with the Lasersharp 2000 (Bio-Rad) acquisition software.

Mouse bone marrow transfer experiments

Bone marrow cells isolated from mice C57Bl6 mice or from JAK2 V617F knock-in mice[29] were injected (1×10^6) into 6- to 8-week-old C57Bl6 lethally irradiated mice.[21,30,31] Platelets were isolated from peripheral blood of reconstituted mice, and levels of TpoR were assessed by Western blot using an anti-MPL antibody (hamster) kindly provided by Genentech and in parallel by anti–human MPI (TpoR) from Upstate Biotechnology.

Real-time quantitative PCR

Total RNA was isolated with the RNeasy kit (QIAGEN) following the manufacturer's instructions. Quantitative real-time PCR has been performed using the following RT primers: GTG GCA GTT TCC TGC ACA CTA CA (Mpl-E10-S); CAG TGT CCC TAA GGT ACT GGC CTA (Mpl-E11-AS). Quantities of TpoR are normalized to β-actin in each sample. β-Actin was amplified with the following primers: CCT GGC ACC CAG CAC AAT (ActB-S); GGG CCG GAC TCG TCA TAC T (ActB-AS).

Patients

Peripheral blood was obtained from patients with primary myelofibrosis-expressing JAK2 V617F mutant before and after compassionate treatment with ruxolitinib (INCB018424). Approval was obtained from the institutional review board at the Université Catholique de Louvain. Platelets were isolated from peripheral blood and levels of TpoR were assessed by Western blot after lysis in 1% NP40 buffer[28] using an anti–human MPI (TpoR) from Upstate Biotechnology.

Results

JAK2 V617F down-modulates cell surface and total TpoR levels

We first coexpressed in Ba/F3 cells TpoR with either JAK2wt or JAK2 V617F. Ba/F3 cells are IL-3–dependent murine proB cells that can be rendered dependent on several cytokines, provided the specific receptor is expressed. Our previous work indicated that JAK2 strongly enhances cell-surface and total levels of TpoR by enhancing the stability of the mature Endo-H–resistant form of the receptor.[10] Another cytokine receptor, the EpoR, requires JAK2 for cell-surface expression, but the effect of JAK2 is only to enhance the maturation of the receptor (Endo-H–resistant form), without increasing the total receptor levels.[10,12] We then asked whether JAK2 V617F would also modulate traffic of EpoR or TpoR.

Ba/F3 cells maintained in medium supplemented with IL-3 were first transduced with bicistronic retroviruses coding for HA-tagged EpoR or TpoR and GFP and sorted for equal GFP expression levels. Subsequently, cells were transduced with bicistronic retroviruses coding for JAK2 or JAK2 V617F and a truncated human CD4, as a marker, and sorted for equivalent CD4 levels, as described.[10] Levels of exogenously expressed JAK2wt and JAK2 V617F were similar and amounted to 4- to 5-fold higher levels than endogenous JAK2 levels. Figure 1A (top panel left) shows that JAK2 enhanced, as previously described, the cell surface levels of HA-EpoR and HA-TpoR. In the case of the EpoR, expression of JAK2 V617F also enhanced cell-surface levels of the receptor, but to somewhat lower extents than JAK2wt, possibly because of constitutive internalization.

In contrast to the EpoR situation, TpoR was strongly down-modulated by JAK2 V617F coexpression. JAK2 V617F actually down-modulated TpoR to levels lower than those of Ba/F3 TpoR cells (where only endogenous JAK2 levels are present, and at equal GFP expression levels; Figure 1A bottom panel). Down-modulation was less pronounced when cells were selected for proliferation in Tpo-containing medium (Figure 1A bottom panel left), possibly reflecting the requirement for a cytokine (Tpo) for survival and proliferation. Confocal immunofluorescence microscopy images show decreased decoration of the cell surface and intracellular

From www.bloodjournal.org by guest on January 2, 2016. For personal use only.

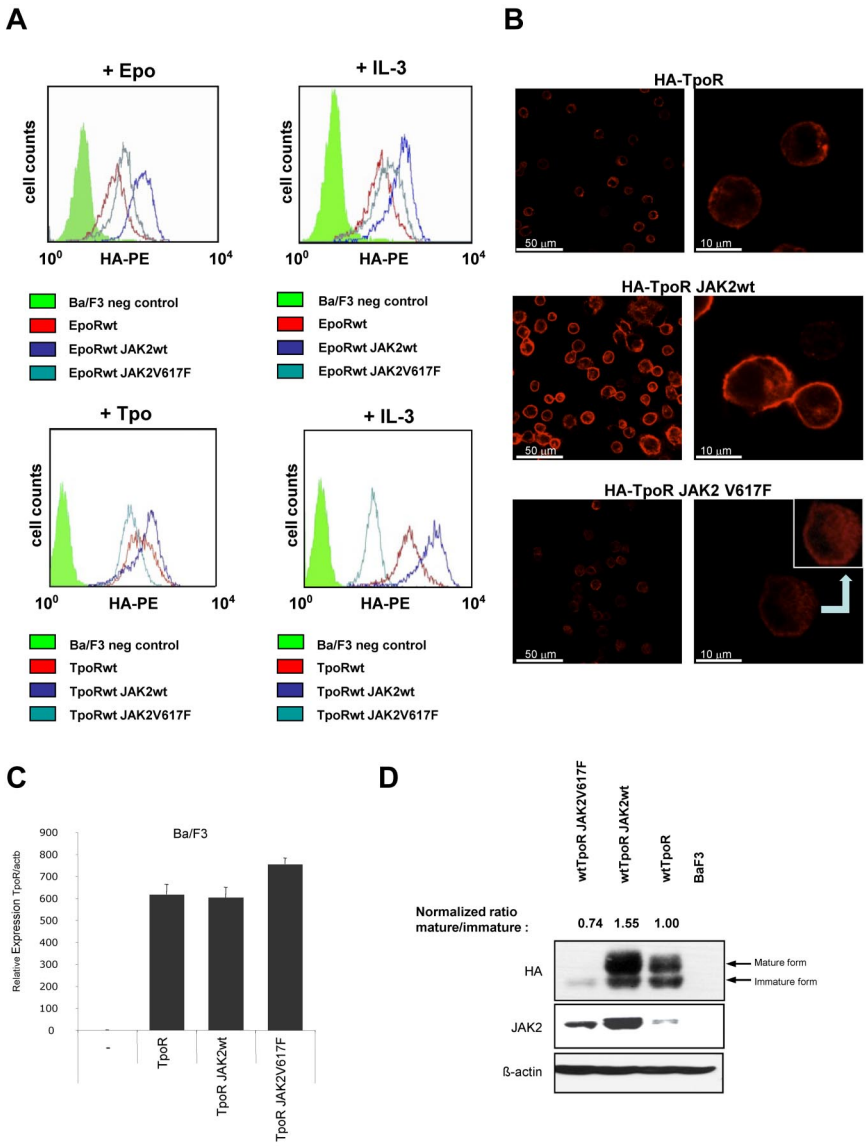


Figure 1. JAK2 V617F expression leads to down-modulation of cell-surface and total TpoR protein. (A) Flow cytometric assessment of cell-surface HA-TpoR levels. Ba/F3 cells retrovirally transduced with the JAK2wt or JAK2 V617F were sorted to equivalent CD4 levels, as a truncated CD4 molecule is also coded by the bicistronic pMX retrovirus. Cells were subsequently transduced with bicistronic pMX viruses coding for TpoR or EpoR and GFP and were sorted for equivalent GFP levels. Shown are Ba/F3 cells maintained in medium supplemented with IL-3, Epo (for EpoR cells), and Tpo (for TpoR cells). Detection of cell-surface HA was performed using monoclonal anti-HA antibodies and R-PE–conjugated donkey $F(ab')_2$ anti–mouse IgG secondary antibody. At least of 10 000 events were analyzed for each flow cytometric measurement. (B) Confocal immunofluorescence analysis of cells expressing the indicated HA-TpoR and JAK2 constructs. Cells were fixed with 4% paraformaldehyde and permeabilized with 0.05% saponin. After quenching of autofluorescence and blocking nonspecific labeling, detection of HA-TpoR was performed with monoclonal anti-HA antibodies and goat anti–mouse IgG linked to Alexa-568 secondary antibody. Bottom right panel: Image with artificially increased luminosity (+40%) and contrast (+40%). (C) Quantitative PCR determining the levels of expression of TpoR mRNA in the indicated cell lines. (D) Western blot analysis with anti-HA antibodies, anti-JAK2, and anti–β-actin antibodies of Ba/F3 cells expressing the indicated TpoR and JAK2 constructs and maintained in medium supplemented with IL-3 (cells shown in panel A bottom right panel, +IL-3). Normalized ratio mature/immature TpoR bands were calculated after dividing the densitometric measurement of the intensities of mature and immature bands (ratio) and normalizing to the ratio in Ba/F3 wtTpoR cells.

vesicles (possibly Golgi vesicles)[10] with anti-HA antibodies (Figure 1B). A punctate perinuclear intracellular staining was characteristic of HA-TpoR in the presence of JAK2 V617F (Figure 1B, and see inset in bottom right panel), suggesting that TpoR traffic was significantly altered by JAK2 V617F. Cells expressing JAK2 V617F did not exhibit down-modulation of endogenous IL-3 receptor α subunit on their surface (supplemental Figure 1, available on the *Blood* Web site; see the Supplemental Materials link at the top of the online article), suggesting that down-modulation of TpoR is not a nonspecific phenomenon.

We then examined whether TpoR mRNA levels were decreased on coexpression of JAK2 V617F. This was not the case, as shown in Figure 1C, whereas total HA-TpoR protein levels were decreased. The upper band of the TpoR doublet, representing the mature Endo-H–resistant form[10] was detected, under conditions of similar GFP expression (Figure 1D). Although JAK2 strongly enhanced the half-life of the mature TpoR form, JAK2 V617F coexpression led to an increase in the immature form and a decrease in the half-life of the mature TpoR form, compared with Ba/F3 TpoR cells or Ba/F3 TpoR JAK2 cells (supplemental Figure 2). In the presence of JAK2wt, we could detect a stabilization of the mature TpoR band that lasted more than 25 hours. In contrast, for Ba/F3 TpoR cells, the half-life of the mature TpoR band was approximately 5 hours. We confirmed the differential sensitivity of the 2 TpoR bands to Endo-H, with the heavier band being resistant and the lighter band being sensitive to Endo-H (supplemental Figure 3A). Thus, coexpression of JAK2 V617F leads to selection for cells that exhibit down-modulation of TpoR and impaired maturation. Furthermore, uniquely the mature form of the receptor was sensitive to proteinase K digestion of live cells (supplemental Figure 3B), indicating the Endo-H–resistant mature form is at the cell surface.

TpoR down-modulation by JAK2 V617F involves an inhibition of receptor recycling

TpoR was reported to be a recycling receptor,[18] with JAK2 and TYK2 enhancing receptor recycling and preventing its degradation.[10] Two mechanisms might contribute to TpoR surface reappearance: (1) recovery of the internalized receptor back to the cell surface (true recycling); or (2) traffic of new mature intracellularly stored TpoR to the cell surface in exchange for internalized receptor. To distinguish between these possibilities, we surface biotinylated Ba/F3 cells that expressed TpoR, TpoR and JAK2, and

From www.bloodjournal.org by guest on January 2, 2016. For personal use only.

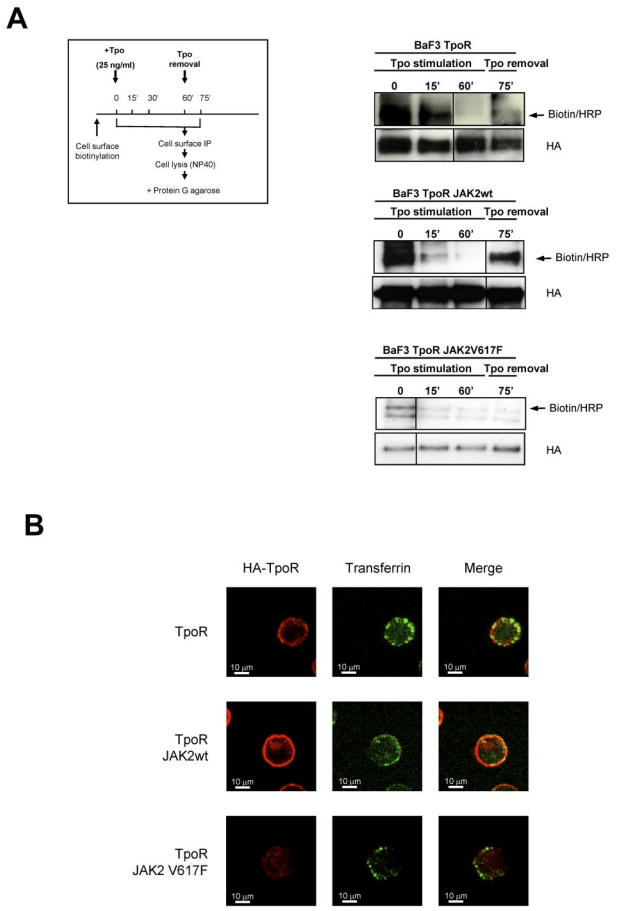


Figure 2. Effects of JAK2wt and JAK2 V617F on TpoR protein processing and recycling. (A) Recycling of biotinylated cell-surface TpoR after ligand addition and removal was assessed after cell-surface biotinylation, as described in "Cell-surface biotinylation followed by TpoR cell-surface immunoprecipitation, recycling assays." After cell-surface biotinylation, cells were treated or not with Tpo for the indicated times; then Tpo was removed for 15 minutes. Cells were surface immunoprecipitated by incubating cells at 4°C with anti-HA for 1 hour. After extensive washing to remove unbound anti-HA, cells were lysed in 1% NP40 buffer. Immune complexes of anti-HA and surface proteins were precipitated by Protein G-Sepharose beads. Samples were denatured by boiling in Laemmli buffer and analyzed by Western blotting with anti-HA or anti-biotin antibodies coupled to HRP to detect biotinylated (cell-surface) proteins. Vertical line(s) have been inserted to indicate a repositioned gel lane. (B) Confocal imaging of the TpoR in the indicated Ba/F3 cells permeabilized with saponin in the presence or absence of an overexpressed JAK2wt or JAK2 V617F. Transferrin/Alexa-488 (left panel) was absorbed, internalized, and recycled by the cells for 25 minutes at 37°C. After paraformaldehyde fixation, staining for the receptor was performed using anti-HA antibody and a secondary antibody labeled with Alexa-568. Ba/F3 cells expressing TpoR alone or with JAK2 show partial colocalization between TpoR and transferrin. In contrast, Ba/F3 TpoR JAK2 V617F shows no colocalization of TpoR with transferrin. TpoR expressed in JAK2 V617F cells exhibits an intracellular distribution and low cell-surface localization.

TpoR and JAK2 V617F. Treatment of cells with Tpo for 15 minutes leads to receptor down-modulation, whereas Tpo treatment for 60 minutes, leads to disappearance of cell-surface TpoR, as assessed by immunoprecipitation with an anti-HA antibody and Western blotting with anti-biotin antibodies coupled with HRP (or anti-biotin–HRP). Tpo was removed, and then we followed the recovery of cell-surface TpoR, especially of biotinylated TpoR, which is diagnostic for internalized receptor, as only cell-surface TpoR had access to biotinylation (Figure 2A). In Ba/F3 TpoR cells, the HA-TpoR band reappeared 15 minutes after Tpo removal; this band was also labeled by biotin, thus establishing that an internalized chain, coming from the biotinylated surface, was actually recycled back to the cell surface. Similarly, recycling could be detected, even to a higher extent in TpoR JAK2 cells, as expected by previous reports showing that JAK2 promotes receptor recycling[10] (Figure 2A middle panel). In contrast, for TpoR JAK2 V617F cells, we could not detect the reappearance of the biotinylated TpoR band (Figure 2A bottom panel). Thus, JAK promotes TpoR recycling, whereas JAK2 V617F impairs and decreases total and mature TpoR levels.

Next, we assessed recycling by confocal microscopy in cells that coexpress TpoR and JAK2 V617F. Normally, TpoR colocalizes with fluorescent transferrin in Ba/F3 cells, a phenomenon that is enhanced by expression of JAK2.[10] Cells are treated with Alexa-488 labeled transferrin for 25 minutes at 37°C to allow transferrin adsorption, internalization, and entry into the recycling compartment. Cells were fixed with 4% paraformaldehyde, permeabilized with 0.05% saponin and HA-TpoR, was detected using antibodies labeled with Alexa-568. As shown in Figure 2B, the colocalization between recycling transferrin (green) and HA-TpoR (red) was evident for Ba/F3 TpoR JAK2 cells (Figure 2B middle panel) and to a lesser extent for Ba/F3 TpoR cells (top panel), as previously reported.[10] In contrast, in Ba/F3 TpoR JAK2 V617F cells, there was no overlap between recycling transferrin and HA-TpoR (Figure 2B bottom panel).

JAK2 V617F-induced TpoR down-modulation is mediated by receptor ubiquitinylation and degradation by the proteasome and lysosome pathways

The mechanisms of Tpo-induced down-modulation of TpoR involve proteasome and lysosome-mediated degradation.[10,19] Because JAK2 V617F exerts an opposite effect to JAK2, mainly to inhibit receptor recycling, we examined the fate of the nonrecycled receptor.

When a combination of lysosome inhibitors (E64, leupeptin, pepstatin A) or NH4Cl was used in steady-state growing cells, we could detect no restoration of cell surface TpoR levels (Figure 3A), whereas Western blotting of the same cell samples showed that lysosome inhibitors weakly increased the levels of the mature TpoR (Figure 3C). In contrast, proteasome inhibitors, such as MG132, epoxomicin, or bortezomib (Velcade), significantly restored cell surface TpoR levels (Figure 3A) and increased total and mature TpoR levels, (Figure 3C). Interestingly, MG132 was stronger than epoxomicin or bortezomib at restoring cell surface levels, although it was weaker in restoring total TpoR protein levels; the basis for this differences remains to be established.

We next tested whether TpoR down-modulation could be reversed by lysosome and proteasome inhibitors in cells where protein synthesis was blocked. We could not detect an effect of lysosome inhibitors on the TpoR half-life in either JAK2 or JAK2 V617F cells, consistent with previous data on cells expressing TpoR and JAK2.[10] Lysosome inhibitors were active in Ba/F3 cells because they enhanced EpoR levels in Ba/F3 EpoR cells (compare second to the fourth lane of top panel of Figure 3B), as expected, because EpoR is degraded by the lysosome and proteasome pathways.[32] Proteasome inhibitors, such as MG132 or epoxomicin, were able to significantly enhance TpoR levels in JAK2 V617F cells treated with cycloheximide. Altogether, these data indicate that proteasome inhibitors can reverse down-modulation of TpoR by JAK2 V617F both in steady-state growing cells and in conditions of protein synthesis inhibition, whereas lysosome inhibitors can only weakly increase newly produced intracellular mature TpoR.

From www.bloodjournal.org by guest on January 2, 2016. For personal use only.

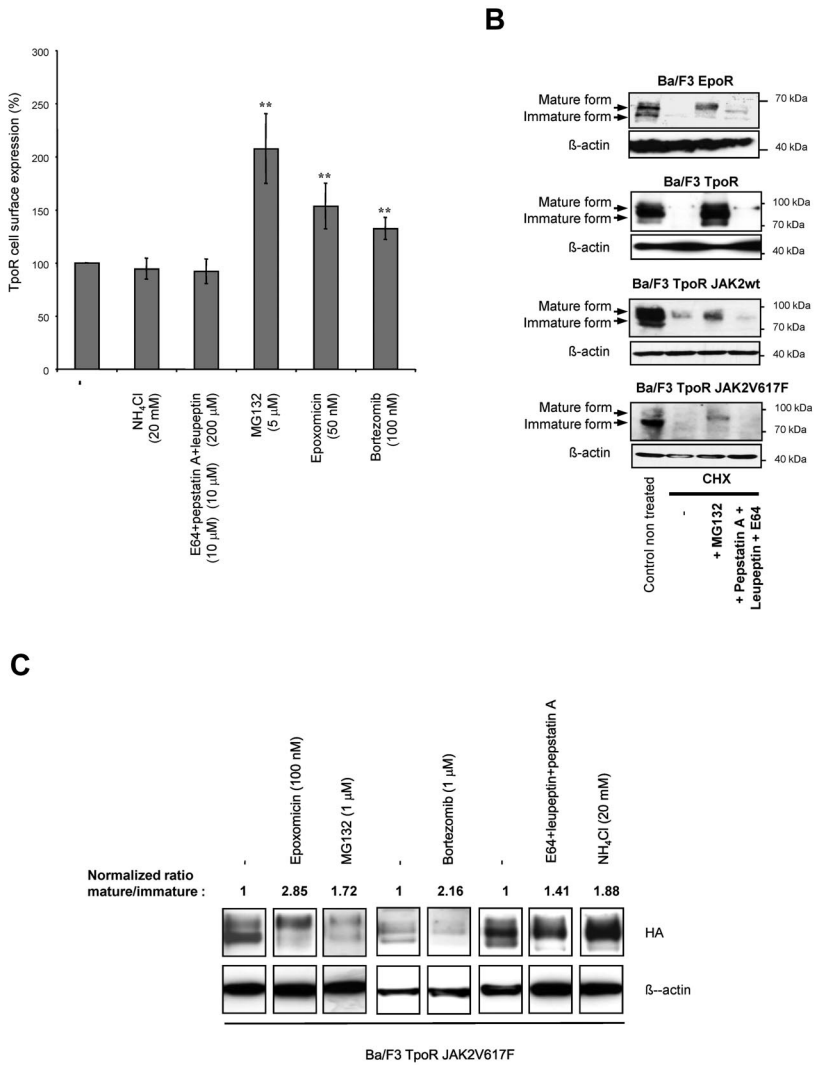


Figure 3. Effects of lysosome and proteasome inhibitors on TpoR cell-surface and total levels in JAK2 V617F cells. (A) Flow cytometric assessment of cell-surface HA-TpoR levels of Ba/F3 TpoR JAK2 V617F treated or not with the indicated inhibitors. Shown are averages of at least 3 independent experiments ± SD. Each experiment reflected analysis of 10 000 cells. **Two-tailed $P < .01$. (B) The indicated Ba/F3 cells were treated with 20 μg/mL cycloheximide for 20 hours or not and simultaneously treated with a combination of lysosome inhibitors (10μM, E64, 10μM pepstatin A, and 200μM leupeptin) or 10μM MG132 proteasome inhibitor. Shown are Western blot analyses for HA-TpoR and β-actin. (C) Western blot analysis with anti-HA antibodies and anti–β-actin antibodies of Ba/F3 TpoR JAK2 V617F cells treated with the indicated inhibitors for 20 hours. The densitometric ratios between the mature and immature TpoR bands were normalized to that of untreated cells.

JAK2 V617F induces constitutive ubiquitinylation of TpoR

Results in Figure 3 led us to ask whether the TpoR is ubiquitinylated when coupled to JAK2 V617F. We subjected Ba/F3 cells coexpressing TpoR with JAK2wt or with JAK2 V617F to immunoprecipitation with anti-HA antibodies and Western blotting with anti–poly/mono-ubiquitin antibodies (Figure 4A). We detected the ubiquitinylated TpoR at molecular weights compatible essentially with poly-ubiquitinylated receptor (120-160 kDa, when TpoR is 90-95 kDa; Figure 4A). Interestingly, whereas levels of receptor were the highest in JAK2 cells, the highest level of ubiquitinylated receptor was detected in JAK2 V617F cells (Figure 4A).

The ubiquitinylation of TpoR was also examined in transiently transfected HEK-derived BOSC cells that were subsequently stimulated with biotinylated Tpo, which also was used to pull down the cell-surface receptor. As shown in Figure 4B, in the presence of both biotinylated Tpo and FLAG-tagged ubiquitin, the receptor was poly-ubiquitinylated (bands at > 160 kDa), and this effect was the strongest when JAK2 V617F was coexpressed. There was a reciprocal relationship between levels of receptor ubiquitinylation and total TpoR protein levels, further establishing that ubiquitinylation promotes receptor degradation.

Next, 2 TpoR mutants were constructed: (1) where both cytosolic domain K544 and K564 residues were mutated to arginine (KKRR) and (2) where only K564 was substituted by arginine (KR; Figure 4C left panel). At the same time, we constructed a receptor that is deficient in internalization, where the di-leucine motif LL (Leu558, Leu559) was mutated to AA (LL to AA).[18] First, we showed that in transiently transfected BOSC cells, the KK to RR mutation inhibits both ubiquitinylation of the receptor and its degradation, indicating that direct ubiquitinylation leads to degradation (Figure 4C right panel). The internalization-defective receptor TpoR LL to AA was also partially resistant to degradation. Second, we tested whether these TpoR mutants were down-modulated when stably expressed in Ba/F3 JAK2 V617F cells. To be comparable with Figure 1A, we tested cells maintained in medium supplemented with IL-3 or with Tpo. A clear protection from down-modulation was detected especially in IL-3 with the lysine mutants, and a weak protection with the internalization mutant (supplemental Table 1). These data support the notion that constitutive ubiquitinylation and degradation of TpoR are major contributors to the down-modulation effect induced by JAK2 V617F.

Down-modulation of TpoR protein levels in platelets from JAK2 V617F knock-in mice and restoration of TpoR levels by in vivo treatment with a proteasome inhibitor

Our results in cell lines predict that mice that express JAK2 V617F should exhibit down-modulation of TpoR protein levels in platelets. We used the JAK2 V617F knock-in model (KI-JAK2 V617F),

From www.bloodjournal.org by guest on January 2, 2016. For personal use only.

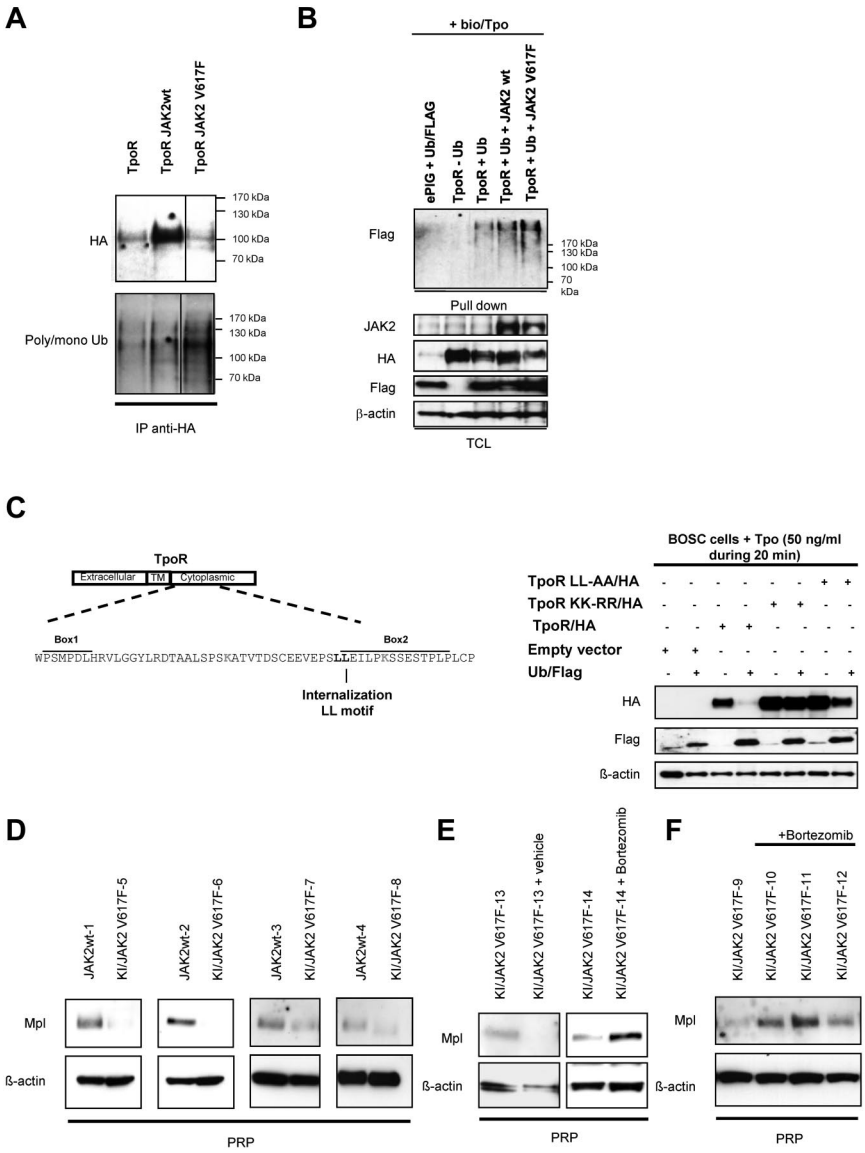


Figure 4. TpoR down-regulation induced by JAK2 V617F is promoted by proteasome degradation through stronger receptor ubiquitinylation in cell lines and in platelets from JAK2 V617F knock-in mice. In vivo proteasome inhibitor treatment restored TpoR levels. (A) The indicated Ba/F3 cell lines were lysed in 1% NP40 buffer, immunoprecipitated with anti-HA, and subjected to Western blotting with anti-HA antibodies or anti–polyubiquitin/monoubiquitin antibodies. Vertical line(s) have been inserted to indicate a repositioned gel lane. (B) HEK293-derived BOSC cells were transfected with the indicated TpoR and JAK2 constructs and with or without Flag-tagged ubiquitin. Two days after transfection, cells were treated with biotinylated Tpo (bio/Tpo) for 5 minutes at room temperature and 15 minutes at 37°C. Cells were lysed in 1% NP40 buffer, incubated streptavidin beads for 1 hour at 4°C. Beads were extensively washed and lysed in Laemmli buffer. Western blot was performed with anti-HA, anti-Flag, and anti–β-actin antibodies. In parallel, total cell lysates of the transfected cells were analyzed by Western blotting. (C) Left panel: Schematic representation of the TpoR cytosolic region that contains the 2 lysine K40 and K60 residues potentially involved in ubiquitinylation and the 2 leucine L54 and L55 residues involved in internalization. Right panel: HEK293-derived BOSC cells were transfected with the indicated TpoR constructs and Flag-tagged ubiquitin or empty vector. Two days after transfection, cells were stimulated with 50 ng/mL Tpo for 20 minutes. Cells were lysed in Laemmli buffer and examined by Western blotting with anti-HA, anti-Flag (for Flag-ubiquitin), or anti–β-actin. (D) Western blot analysis of platelet extracts from the indicated mice with anti-Mpl (TpoR; UBI) and anti–β-actin antibodies. JAK2wt-1 and JAK2wt-2 mice are wild-type C57Bl6 mice, KI/JAK2V617F-6 and -7 are heterozygous JAK2 V617F knock-in mice, JAK2wt-3 and JAK2wt-4 are C57Bl6 mice reconstituted with bone marrow from wild-type mice, whereas KI/JAK2V617F-7 and -8 are mice reconstituted with bone marrow from heterozygous JAK2 V617F knock-in mice. (E) Western blot analysis of paired platelet samples collected before and after drug treatment from the same KI-JAK2 V617F mouse. Mice were treated either with vehicle control (KI-JAK2 V617F-13) or bortezomib (0.5 mg/kg; KI-JAK2 V617F-14) during 2 weeks by intraperitoneal injections. (F) Western blot analysis of platelet extracts from the indicated mice that were reconstituted with bone marrow from JAK2 V617F KI mice. Mice were treated either with vehicle (KI/JAK2 V617F-9) or bortezomib (KI/JAK2 V617F-10, -11, and -12). Mice were treated for 2 weeks (twice per week) with intraperitoneal injections of the proteasome inhibitor bortezomib (0.5 mg/kg).

where an endogenous JAK2 V617F heterozygous state is achieved constitutively.[29] As expected, the KI-JAK2 V617F mice show splenomegaly associated with increased levels of thymocytes, erythrocytes, and leukocytes (supplemental Figure 4A). As shown in Figure 4D for 2 knock-in mice (mice KI/JAK2 V617F-5 and -6), we detected significant lower protein levels of TpoR than in control mice. The same result was obtained when we examined mice reconstituted with bone marrow from JAK2 V6717F heterozygous knock-in mice (mice KI/JAK2V617F-7 and -8; Figure 4D). Two distinct anti-TpoR antibodies were used for Western blotting and the same result was obtained.

We then asked whether in vivo treatment with a proteasome inhibitor could restore the down-modulated TpoR levels. For such an in vivo treatment, we used Velcade (bortezomib), which is an approved drug for several indications and was used in mouse models of Tpo-induced myeloid proliferation and myelofibrosis.[33]

From www.bloodjournal.org by guest on January 2, 2016. For personal use only.

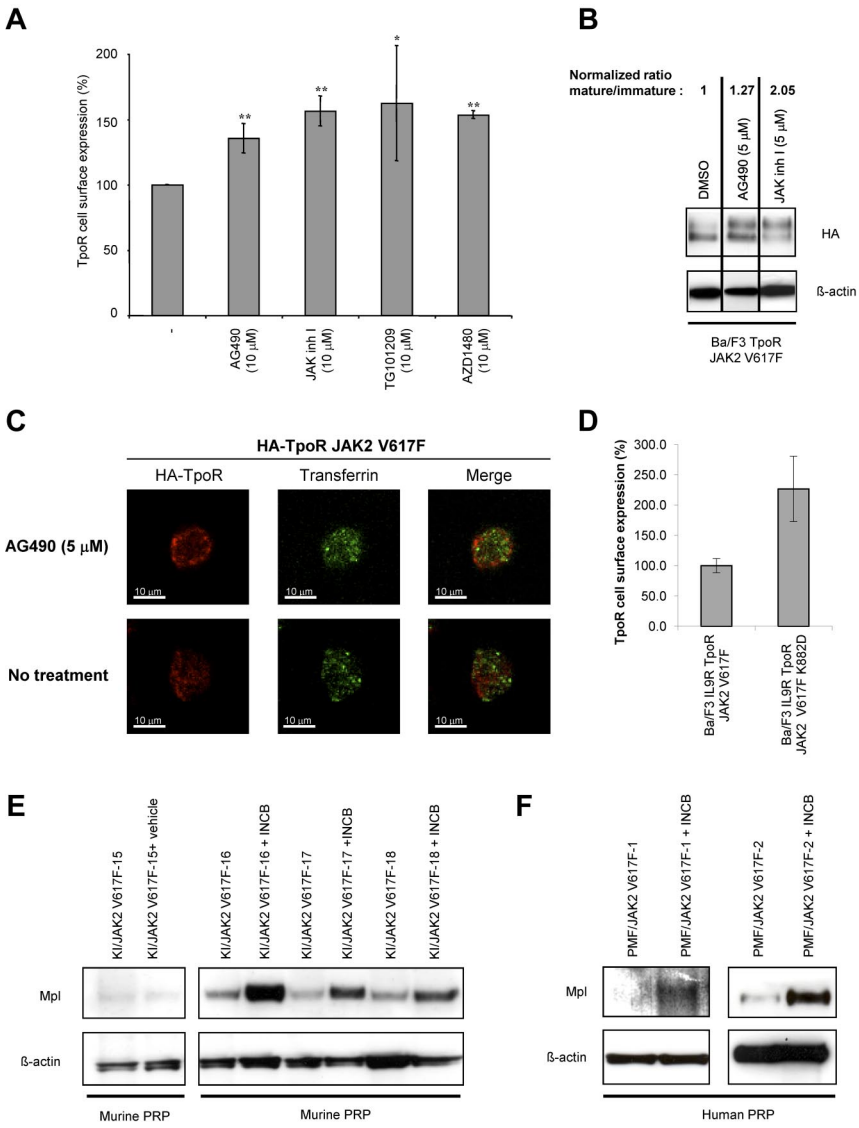


Figure 5. TpoR down-modulation by JAK2 V617F requires kinase activity of JAK2. In vivo JAK2 inhibitor treatment restored TpoR levels in mouse and human cells. (A) Flow cytometric analysis (anti-HA) of the indicated Ba/F3 TpoR JAK2 V617F cells incubated with vehicle control, or the indicated inhibitors for 20 hours. Results are derived from the analysis of at least 10 000 events per replicate. Shown are averages of percentages of TpoR expression of 3 independent experiments ± SD, with TpoR levels in the absence of inhibitors being considered as 100%. *Two-tailed ($P < .05$). **Two-tailed ($P < .01$). Neither compounds induced toxicity, as assessed by Trypan blue exclusion (not shown). (B) Western blot analysis of TpoR total levels of Ba/F3 TpoR JAK2V617F cells treated or not with the indicated inhibitors for 20 hours. The densitometric ratios between the mature and immature TpoR bands were normalized to that of untreated cells. (C) Confocal analysis of HA-TpoR localization on Ba/F3 TpoR JAK2 V617F cells treated or not with AG490 for 20 hours. (D) Flow cytometric analysis (anti-HA for TpoR cell-surface localization) of the indicated Ba/F3 cell lines. Data are mean ± SD values obtained in 3 flow cytometric measurements, each average being obtained for 10 000 events. Differences between JAK2 V617F and JAK2 V617F K882D cells were statistically significant ($P < .01$, Student *t* test). (E) Western blot analysis of paired platelet samples before and after drug treatment from the same KI-JAK2 V617F mouse. Mice were treated either with vehicle (KI-JAK2 V617F-15) or INCB018424 (KI-JAK2 V617F-16, -17, and -18) during 2 weeks (twice a day by gavage). (F) Western blot analysis of platelet extracts from myelofibrosis patients expressing JAK2 V617F (PMF/JAK2V617F-1 and -2). Platelets extracts were obtained before and on ruxolitinib (INCB018424) treatment.

As shown in Figure 4E, paired predrug and postdrug treatment samples were assessed from the same mouse after a 2-week treatment (2 intraperitoneal injections per week) with bortezomib (0.5 mg/kg). Contrary to the mouse treated with vehicle control (KI-JAK2 V617F-13), the bortezomib treatment leads to restoration of TpoR expression (KI-JAK2 V617F-14) without affecting the platelet count in peripheral blood (supplemental Figure 4B). Furthermore, as shown in Figure 4F, levels of platelet TpoR protein were significantly up-regulated by the 2-week bortezomib treatment compared with vehicle-control mouse KI-JAK2 V617F-9. Thus, proteasomal inhibition can be efficient in vivo to counteract the down-modulating effects of JAK2 V617F in the heterozygous knock-in model.

Down-modulation of TpoR by JAK2 V617F depends on JAK2 kinase activity: in vivo treatment with a JAK2 inhibitor restores platelet TpoR protein levels

We tested the effect of ATP-competitive JAK2 inhibitors on TpoR traffic in cells expressing JAK2 V617F. AG490,[34] JAK inhibitor 1,[35] AZD1480,[36] and TG101209[37] were all able to restore cell-surface levels of TpoR in Ba/F3 TpoR JAK2 V617F cells (Figure 5A), although they did not increase TpoR levels in Ba/F3 TpoR or Ba/F3 TpoR JAK2 cells (not shown). This was evident not only by flow cytometric detection of the NH2-terminal HA tag of TpoR (Figure 5A), but also by confocal immunofluorescence on fixed and permeabilized cells (Figure 5C), indicating that the restoration also concerned the intracellular TpoR pools. Indeed, AG490, JAK inhibitor I (Figure 5B), and the other JAK2 inhibitors (not shown) restored the mature band of TpoR.

To further explore this aspect, we created Ba/F3 TpoR cells, where we could express a kinase-dead version of JAK2wt or of JAK2 V617F. To stably express kinase-dead JAK2, we needed to establish Ba/F3 cells that depend on JAKs other than JAK2 for survival and proliferation because a kinase-dead JAK2 inhibits signaling by IL-3 via a dominant negative mechanism. For this purpose, we expressed the IL-9 receptor α (IL9Rα) in Ba/F3 cells. These Ba/F3-IL9R cells can be rendered dependent on IL-9, which activates JAK1 and JAK3 via the transfected IL9Rα and the endogenous γ-chain γc.[38] Subsequently, HA-TpoR and JAK2 or JAK2 V617F or kinase-dead (K882D) of JAK2 V617F were transduced by bicistronic retroviruses. As shown in Figure 5D, levels of cell-surface TpoR were significantly higher in cells expressing the kinase-dead JAK2 V617F, compared with JAK2 V617F cells.

From www.bloodjournal.org by guest on January 2, 2016. For personal use only.

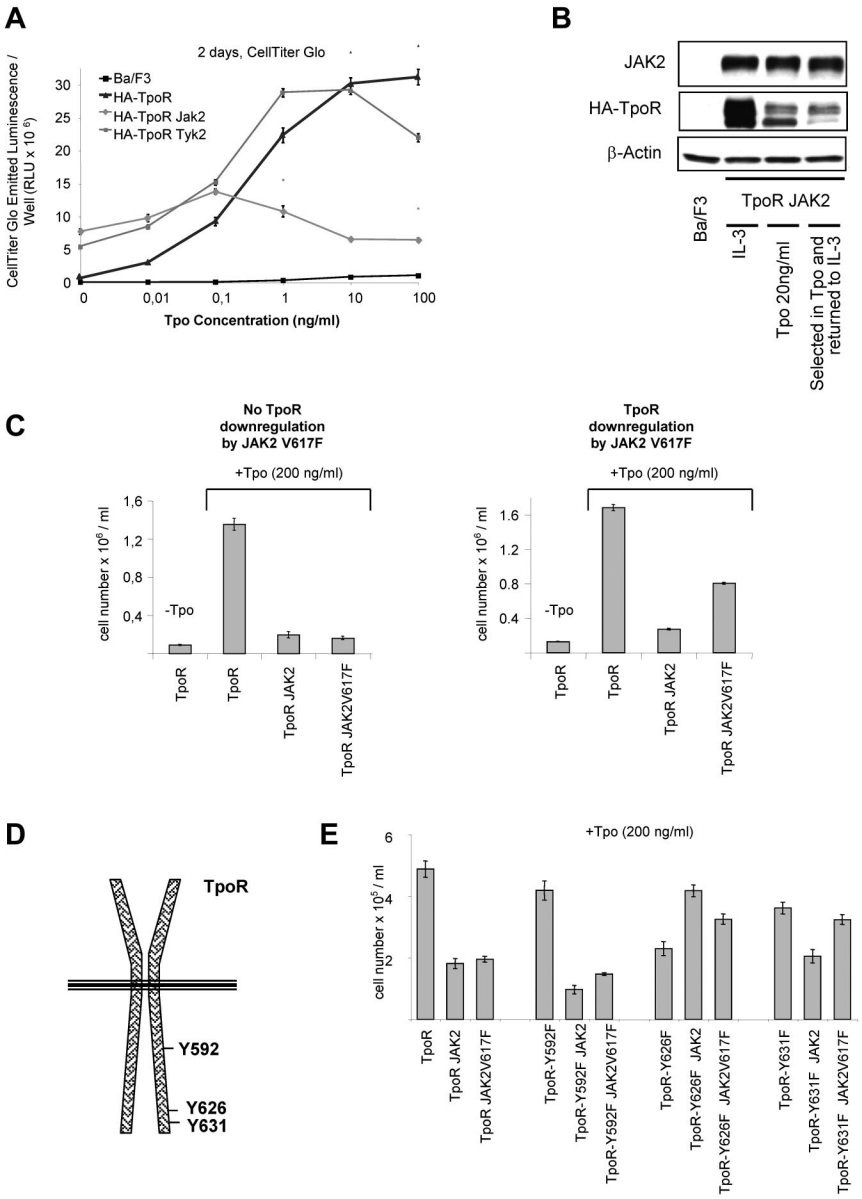


Figure 6. TpoR induces an antiproliferative effect at high ligand concentration. (A) Proliferation assays of the indicated Ba/F3 cells as a function of the concentration of ligand Tpo. Ba/F3 TpoR cells responded to Tpo by proliferation, whereas Ba/F3 TpoR JAK2 cells responded by a stop in cell proliferation at concentrations of Tpo more than 0.5 ng/mL. Ba/F3 TpoR TYK2 cells stopped proliferation at Tpo concentrations more than 10 ng/mL. Cell proliferation was measured by Cell TiterGlo assays 48 hours after seeding. (B) HA-TpoR total levels of Ba/F3 TpoR JAK2wt cells in the indicated conditions were analyzed by Western blot of NP40 buffer extracts using anti-JAK2, anti-HA, and anti–β-actin antibodies. (C) Left panel: The indicated cell lines were obtained by retroviral infection and cell sorting and amplification for a short time, so that down-regulation of TpoR by JAK2 V617F to levels below those of Ba/F3 TpoR cells did not yet occur. Proliferation assays indicate that addition of 200 ng/mL Tpo led to proliferation in Ba/F3 TpoR cells and to a stop in proliferation in cells overexpressing JAK2 or JAK2 V617F and TpoR. Right panel: Proliferation assays performed on the indicated cell lines after longtime amplification so that TpoR down-regulation occurs in presence of JAK2 V617F. Data are mean of triplicates ± SD. Differences between TpoR columns in the +Tpo (200 ng/mL) and all other conditions (TpoR JAK2 and TpoR JAK2 V617F) are statistically significant at $P < .05$ (Student *t* test both on the left and right panels). (D) The location of the 3 main cytosolic tyrosine residues in TpoR cytosolic domain. (E) The indicated Ba/F3 cell lines coexpressing either JAK2 or JAK2 V617F and TpoR variants carrying tyrosine to phenylalanine mutations were analyzed for Tpo (200 ng/mL)-induced proliferation immediately after retroviral transduction, before down-modulation of TpoR occurred in JAK2 V617F cells. (A,C-E) Averages of 3 replicates ± SD of one representative experiment of at least 2 independent experiments. Differences between TpoR and TpoR JAK2 or TpoR JAK2 V617F are statistically significant at $P < .05$ (Student *t* test for the Y626F mutation), and also between all Y592F and Y626F mutants, as well as between TpoR JAK2 V617F and TpoR Y631F JAK2 V617F cells.

We asked whether in vivo treatment with a JAK2 inhibitor could restore the down-modulated TpoR levels in KI-JAK2 V617F mice. INCB018424 is a selective JAK1/2 inhibitor that has been approved as therapy for myelofibrosis.[39] The primary therapeutic benefit in MF is a reduction in splenomegaly with significant improvement in the quality of life without affecting JAK2 V617F allele burden.[40] As shown in Figure 5E, the protein levels of platelet TpoR were significantly higher after 2-week treatment (twice a day by gavage because of short half-life of the compound[41]) with INCB018424 (100 mg/mL) compared with TpoR levels from platelets belonging to the same mouse before treatment (3 KI mice, KI-JAK2 V617F-16, -17, and -18; Figure 5E right panel). Treatment with NaCl or vehicle did not increase TpoR levels in the KI-JAK2 V617F-15 mouse (Figure 5E left panel). The 2-week drug treatment did not change the platelet counts (supplemental Figure 4C).

Next, platelets from patients with myelofibrosis positive for JAK2 V617F mutation were tested before and after ruxolitinib (INCB018424) treatment. The 2 myelofibrosis patients exhibited down-modulated TpoR in platelets before treatment. After JAK2 inhibitor treatment for 6 months, levels of TpoR in platelets were restored as shown by Western blot (PMF/JAK2 V617F-1 and -2; Figure 5F).

Altogether, in vivo data in mice and patients expressing JAK2 V617F mutant clearly demonstrated the capacity of JAK2 inhibition to restore TpoR protein levels in platelets.

TpoR exerts an antiproliferative effect at high levels of signaling via JAK2

We tested the effect of different Tpo concentrations on proliferation by Ba/F3 TpoR, Ba/F3 TpoR JAK2, and Ba/F3 TpoR TYK2 cells. The latter are transduced cells that express JAK2 or TYK2 at approximately 5-fold higher than endogenous JAK levels. These high JAK2 levels remain lower than JAK2 expression levels of UT-7 megakaryocytic leukemia cells, or late megakaryocytes.[42] As expected, Tpo induced a dose-dependent increase in cell proliferation in Ba/F3 TpoR cells (Figure 6A). Unexpectedly, in Ba/F3 TpoR JAK2 cells, Tpo enhanced proliferation at concentrations less than 0.1 ng/mL, but then inhibited, in a dose-dependent

From www.bloodjournal.org by guest on January 2, 2016. For personal use only.

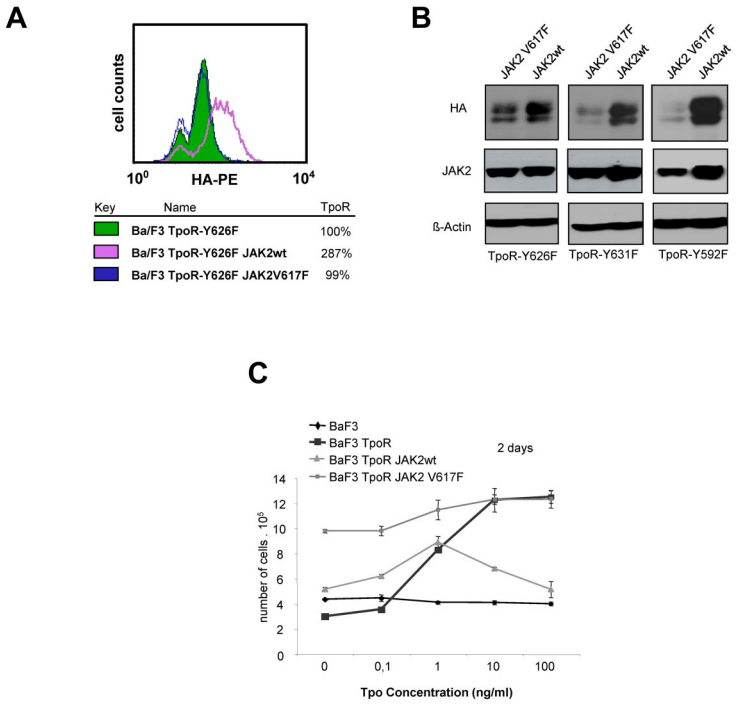


Figure 7. JAK2 V617F-induced TpoR down-modulation is promoted by signaling via TpoR cytosolic Y626 residue. (A) HA-TpoR cell-surface and (B) TpoR total levels were analyzed by flow cytometry and Western blot, respectively, on the indicated cell lines as previously described. (C) Dose-dependence effect of Tpo on the proliferation of the indicated Ba/F3 cell lines. After down-modulation, Ba/F3 TpoR JAK2 V617F cells continue to proliferate both in the presence and absence of Tpo, whereas Ba/F3 TpoR JAK2 cells arrest proliferation in Tpo at concentrations > 1 ng/mL.

manner, cell proliferation (Figure 6A). Interestingly, treatment of he Ba/F3 cell lines with IL-3 did not rescue cell proliferation under conditions where Tpo induced a block in cell growth (supplemental Figure 5B), indicating that Tpo effects are dominant.

These data led us to test the effect of Tpo in cells expressing TpoR and JAK2 V617F either rapidly after infection/cell sorting and before TpoR down-modulation (Figure 6C left panel), or after 6 to 7 days of culture and after TpoR down-modulation (Figure 6C right panel). Tpo (200 ng/mL) exerted its antiproliferative effect on Ba/F3 TpoR JAK2 V617F cells immediately after JAK2 V617F expression. After receptor down-modulation, which occurred after 5 to 7 days of culture, Tpo addition rescued proliferation, albeit not to the full extent (Figure 6C right panel), indicating that receptor down-modulation allows a partial escape from the antiproliferative effects of Tpo.

Selection of Ba/F3 TpoR JAK2 cells in Tpo amplifies cells with down-modulated TpoR that resemble JAK2 V617F cells

Next, we selected Ba/F3 TpoR JAK2 cells in medium supplemented with 20 ng/mL Tpo, which leads to a stop in cell proliferation, and the loss of the majority of cells by apoptosis. Two weeks after initiation of selection, resistant cells emerged that were able to proliferate in 20 ng/mL Tpo. These cells had down-regulated cell-surface and mature TpoR band, compared with the situation in IL-3 (Figure 6B). A further switch of these surviving cells from Tpo back to IL-3 restored the favorable mature-to-immature TpoR ratio but did not increase total levels to the initial ones in IL-3 (Figure 6B). Down-modulation associated with an accumulation of the immature TpoR band, similarly to the situation of JAK2 V617F and TpoR (Figure 1D; supplemental Figure 2).

The antiproliferative effect of TpoR and JAK2 V617F-induced TpoR down-modulation depend on TpoR cytosolic Y626

TpoR contains in its cytosolic domain one negatively acting (Y592) and 2 positively acting (Y626 and Y631) tyrosines (Figure 6D). The antiproliferative effect of Tpo was prevented in JAK2 or JAK2 V617F cells by the Y626F mutation and exacerbated by the Y592F mutation (Figure 6E). The Y631F mutation partially restored proliferation in Tpo of JAK2 V617F cells, but not of JAK2 cells. The same mutation reduced Tpo-induced STAT1 activation in JAK2 V617F but not in JAK2 or parental Ba/F3 cells (supplemental Figure 6).

TpoR Y626F was resistant to down-modulation, as it remained at similar levels at the cell surface and intracellularly after JAK2 V617F expression (Figure 7). Inhibitors of MAPK, PI3K, and mTOR pathways, which are linked to Y626, restore to different extents cell surface or intracellular TpoR levels in JAK2 V617F cells (supplemental Figure 7). The UO126 MEK inhibitor can prevent the antiproliferative effect of Tpo in JAK2 cells while it reduces proliferation in JAK2 V617F cells (supplemental Figure 8), suggesting that, at similar levels of expression for JAK2 and JAK2 V617F, TpoR signaling is qualitatively different in JAK2 V617F cells. Altogether, the extent of down-modulation of TpoR by JAK2 V617F is proportional to the level of signaling by the receptor, especially via Y626.

After down-modulation of TpoR by JAK2 V617F (as in Figure 6C right panel), the antiproliferative effect of Tpo is abolished in JAK2 V617F cells (Figure 7C), thus allowing an escape of these cells from negative effects of Tpo, as described for late megakaryocytes.[42] This effect might be correlated with STAT1 levels of activation, which was linked to essential thrombocythemia and megakaryocyte differentiation.[43]

Discussion

Our major observations are that JAK2 V617F expression leads to down-modulation of cell-surface and total TpoR levels and that small molecule inhibitors of JAK2 kinase activity and of proteasomal-mediated degradation can restore cell-surface and total mature TpoR levels in JAK2 V617F cells. In vivo inhibition of proteasomes or of JAK2 kinase activity restored platelet TpoR

From www.bloodjournal.org by guest on January 2, 2016. For personal use only.

levels in JAK2 V617F knock-in mice. Treatment of myelofibrosis patients that harbor the *JAK2* V617F mutation with JAK2 inhibitor also led to restoration of TpoR platelet levels. Down-modulation of TpoR by JAK2 V617F involves enhanced ubiquitinylation and receptor degradation, in response to the selection pressure induced by an antiproliferative effect of TpoR in complexes with JAK2 V617F.

Tpo was recently shown to promote quiescence of HSCs, especially those in contact with osteoblasts.[5,6,44] High Tpo concentrations were required for these effects in the osteoblastic niche,[6] which is in agreement with our data. We find that, as a function of ligand concentration, JAK2 expression levels, and signaling via positive and negative cytosolic tyrosine residues, TpoR can promote proliferation (at early megakaryocyte levels with lower JAK2 expression) until a certain threshold, above which TpoR signaling induces a stop in proliferation and senescence.[42] At the late megakaryocyte stages, TpoR down-modulation will prevent the negative effects of Tpo, allowing continuous abnormal proliferation of megakaryocytes, which would result in differentiation defects and fibrosis.[30,45,46]

It will be important to determine which E3 ubiquitin ligase is mediating the ubiquitinylation of the 2 TpoR lysine residues in JAK2 V617F cells. TpoR down-modulation was not prevented by dominant negative forms of c-Cbl (not shown), although c-Cbl, which was shown to be one of the ligases involved in Tpo, induced TpoR ubiquitinylation.[20] Our data indicate that lysosomes might weakly contribute to degradation of TpoR in steady-state conditions, as previously shown,[19] but that down-modulation of TpoR by JAK2 V617F resists lysosome inhibitors, whereas proteasome inhibitors restore both total and cell surface TpoR levels in JAK2 V617F cells. Cytosolic domain Y592 opposes TpoR down-modulation in JAK2 V617F cells, whereas it was shown to promote Tpo-induced internalization,[19] suggesting that mechanisms of down-modulation might differ between Tpo-induced and JAK2 V617F-induced TpoR down-modulation. Furthermore, mechanisms other than constitutive activity of JAK2 can also induce low TpoR cell surface levels, as shown, for example, by familial thrombocytosis because of the P106L extracellular mutation, which is associated with high Tpo serum levels.[47] It remains to be determined whether the high Tpo levels associated in certain MPN patients with TpoR down-modulation contribute to thrombocytosis, as was the case in experimental situations of decreased expression of TpoR at late megakaryocyte and platelet levels.[48,49]

Our results provide the molecular bases for the observed down-modulation of TpoR levels in MPN patients, especially those harboring the *JAK2* V617F mutation. Specific for TpoR are antiproliferative effects at high JAK2 activation levels, and receptor recycling; TpoR down-modulation results from selection against these antiproliferative effects, brought about by constitutive ubiquitinylation, inhibition of recycling, and proteasomal degradation. Receptor down-modulation might be a tracer of hyperactivation of TpoR signaling, which could also be achieved in patients who are negative for JAK2 V617F and TpoR W515 mutations, by mutations in other kinases that might also phosphorylate TpoR Y626, such as Lyn,[50] or in phosphatases that would delay receptor dephosphorylation. Selection against the antiproliferative effects of TpoR might be a driving force in establishing the phenotype of MPNs. Restoration of TpoR levels in megakaryocytes and platelets could become a useful biomarker for MPN treatment response after inhibitor treatment.

Acknowledgments

The authors thank André Tonon for expert cell sorting, Patrick Vandersmissen for expert confocal immunofluorescence microscopy, and Céline Mouton for expert technical support. They are grateful for generous support to C.C.D. from the Sectoral Operational Program Human Resources Development (SOP HRD), financed from the European Social Fund and by the Romanian Government (POSDRU/89/1.5/S/64109/ for C.C.D.), for support for S.N.C. from the Fonds de la Recherche Scientifique-Fonds National de le Rescherche Scientifique (FRS-FNRS), Belgium (Mandat d'Impulsion and Fonds de la Recherche Scientifique Médicale), the Salus Sanguinis Foundation, the Action de Recherche Concertée projects MEXP31C1 and ARC10/15-027 of the University Catholique de Louvain, Brussels, the Fondation contre le Cancer, Brussels, the PAI Program BCHM61B5, Belgium and the Atlantic Philanthropies, New York (for S.N.C.), de Duve Institute fellowship and FRS-FNRS fellowships to C.P.

Authorship

Contribution: C.P., C.C.D., J.S., and S.N.C. designed and analyzed research, performed experiments, and wrote the paper; R.B., C.M., J.-L.V., S.G., and A.D. provided essential reagents and analyzed research; L.K. provided patient samples, planned experiments, and analyzed data; P.J.C. and W.V. designed and analyzed research and wrote the paper; and Y.R., J.-P.D. and M.G. performed experiments and analyzed research.

Conflict-of-interest disclosure: The authors declare no competing financial interests.

The current affiliation for C.C.D. is Stefan S. Nicolau Institute of Virology, Bucharest, Romania. The current affiliation for J.S. is Whitehead Institute for Biomedical Research, Cambridge, MA.

Correspondence: Stefan N. Constantinescu, Signal Transduction and Molecular Hematology Laboratory, Ludwig Institute for Cancer Research, Université Catholique de Louvain, de Duve Institute, Avenue Hippocrate 74, UCL 75-4, Brussels B-1200, Belgium; e-mail: stefan.constantinescu@bru.licr.org.

References

1. Wendling F, Maraskovsky E, Debili N, et al. cMpl ligand is a humoral regulator of megakaryocytopoiesis. *Nature.* 1994;369(6481):571-574.
2. de Sauvage FJ, Hass PE, Spencer SD, et al. Stimulation of megakaryocytopoiesis and thrombopoiesis by the c-Mpl ligand. *Nature.* 1994; 369(6481):533-538.
3. Kaushansky K, Lok S, Holly RD, et al. Promotion of megakaryocyte progenitor expansion and differentiation by the c-Mpl ligand thrombopoietin. *Nature.* 1994;369(6481):568-571.
4. Solar GP, Kerr WG, Zeigler FC, et al. Role of c-mpl in early hematopoiesis. *Blood.* 1998;92(1):4-10.
5. Qian H, Buza-Vidas N, Hyland CD, et al. Critical role of thrombopoietin in maintaining adult quiescent hematopoietic stem cells. *Cell Stem Cell.* 2007;1(6):671-684.
6. Yoshihara H, Arai F, Hosokawa K, et al. Thrombopoietin/MPL signaling regulates hematopoietic stem cell quiescence and interaction with the osteoblastic niche. *Cell Stem Cell.* 2007;1(6): 685-697.
7. Miyakawa Y, Oda A, Druker BJ, et al. Recombinant thrombopoietin induces rapid protein tyrosine phosphorylation of Janus kinase 2 and Shc in human blood platelets. *Blood.* 1995;86(1): 23-27.
8. Sattler M, Durstin MA, Frank DA, et al. The thrombopoietin receptor c-MPL activates JAK2 and TYK2 tyrosine kinases. *Exp Hematol.* 1995; 23(9):1040-1048.
9. Drachman JG, Millett KM, Kaushansky K. Thrombopoietin signal transduction requires functional

From www.bloodjournal.org by guest on January 2, 2016. For personal use only.

JAK2, not TYK2. *J Biol Chem.* 1999;274(19):13480-13484.

10. Royer Y, Staerk J, Costuleanu M, Courtoy PJ, Constantinescu SN. Janus kinases affect thrombopoietin receptor cell surface localization and stability. *J Biol Chem.* 2005;280:27251-27261.
11. Alexander WS, Metcalf D, Dunn AR. Point mutations within a dimer interface homology domain of c-Mpl induce constitutive receptor activity and tumorigenicity. *EMBO J.* 1995;14(22):5569-5578.
12. Huang LJ, Constantinescu SN, Lodish HF. The N-terminal domain of Janus kinase 2 is required for Golgi processing and cell surface expression of erythropoietin receptor. *Mol Cell.* 2001;8(6):1327-1338.
13. Gurney AL, Wong SC, Henzel WJ, de Sauvage FJ. Distinct regions of c-Mpl cytoplasmic domain are coupled to the JAK-STAT signal transduction pathway and Shc phosphorylation. *Proc Natl Acad Sci U S A.* 1995;92(12):5292-5296.
14. Drachman JG, Griffin JD, Kaushansky K. The c-Mpl ligand (thrombopoietin) stimulates tyrosine phosphorylation of Jak2, Shc, and c-Mpl. *J Biol Chem.* 1995;270(10):4979-4982.
15. Alexander WS, Maurer AB, Novak U, Harrison-Smith M. Tyrosine-599 of the c-Mpl receptor is required for Shc phosphorylation and the induction of cellular differentiation. *EMBO J.* 1996;15(23):6531-6540.
16. Drachman JG, Kaushansky K. Dissecting the thrombopoietin receptor: functional elements of the Mpl cytoplasmic domain. *Proc Natl Acad Sci U S A.* 1997;94(6):2350-2355.
17. Miyakawa Y, Rojnuckarin P, Habib T, Kaushansky K. Thrombopoietin induces phosphoinositol 3-kinase activation through SHP2, Gab, and insulin receptor substrate proteins in BAF3 cells and primary murine megakaryocytes. *J Biol Chem.* 2001;276(4):2494-2502.
18. Dahlen DD, Broudy VC, Drachman JG. Internalization of the thrombopoietin receptor is regulated by 2 cytoplasmic motifs. *Blood.* 2003;102(1):102-108.
19. Hitchcock IS, Chen MM, King JR, Kaushansky K. YRRL motifs in the cytoplasmic domain of the thrombopoietin receptor regulate receptor internalization and degradation. *Blood.* 2008;112(6):2222-2231.
20. Saur SJ, Sangkhae V, Geddis AE, Kaushansky K, Hitchcock IS. Ubiquitination and degradation of the thrombopoietin receptor c-Mpl. *Blood.* 2010;115(6):1254-1263.
21. James C, Ugo V, Le Couedic JP, et al. A unique clonal JAK2 mutation leading to constitutive signalling causes polycythaemia vera. *Nature.* 2005;434(7037):1144-1148.
22. Baxter EJ, Scott LM, Campbell PJ, et al. Acquired mutation of the tyrosine kinase JAK2 in human myeloproliferative disorders. *Lancet.* 2005;365(9464):1054-1061.
23. Kralovics R, Passamonti F, Buser AS, et al. A gain-of-function mutation of JAK2 in myeloproliferative disorders. *N Engl J Med.* 2005;352(17):1779-1790.
24. Levine RL, Wadleigh M, Cools J, et al. Activating mutation in the tyrosine kinase JAK2 in polycythemia vera, essential thrombocythemia, and myeloid metaplasia with myelofibrosis. *Cancer Cell.* 2005;7(4):387-397.
25. Horikawa Y, Matsumura I, Hashimoto K, et al. Markedly reduced expression of platelet c-mpl receptor in essential thrombocythemia. *Blood.* 1997;90(10):4031-4038.
26. Moliterno AR, Hankins WD, Spivak JL. Impaired expression of the thrombopoietin receptor by platelets from patients with polycythemia vera. *N Engl J Med.* 1998;338(9):572-580.
27. Moliterno AR, Spivak JL. Posttranslational processing of the thrombopoietin receptor is impaired in polycythemia vera. *Blood.* 1999;94(8):2555-2561.
28. Seubert N, Royer Y, Staerk J, et al. Active and inactive orientations of the transmembrane and cytosolic domains of the erythropoietin receptor dimer. *Mol Cell.* 2003;12(5):1239-1250.
29. Marty C, Lacout C, Martin A, et al. Myeloproliferative neoplasm induced by constitutive expression of JAK2V617F in knock-in mice. *Blood.* 2010;116(5):783-787.
30. Chagraoui H, Komura E, Tulliez M, Giraudier S, Vainchenker W, Wendling F. Prominent role of TGF-beta 1 in thrombopoietin-induced myelofibrosis in mice. *Blood.* 2002;100(10):3495-3503.
31. Pecquet C, Staerk J, Chaligne R, et al. Induction of myeloproliferative disorder and myelofibrosis by thrombopoietin receptor W515 mutants is mediated by cytosolic tyrosine 112 of the receptor. *Blood.* 2010;115(5):1037-1048.
32. Walrafen P, Verdier F, Kadri Z, Chretien S, Lacombe C, Mayeux P. Both proteasomes and lysosomes degrade the activated erythropoietin receptor. *Blood.* 2005;105(2):600-608.
33. Wagner-Ballon O, Pisani DF, Gastinne T, et al. Proteasome inhibitor bortezomib impairs both myelofibrosis and osteosclerosis induced by high thrombopoietin levels in mice. *Blood.* 2007;110(1):345-353.
34. Meydan N, Grunberger T, Dadi H, et al. Inhibition of acute lymphoblastic leukaemia by a Jak-2 inhibitor. *Nature.* 1996;379(6566):645-648.
35. Thompson JE, Cubbon RM, Cummings RT, et al. Photochemical preparation of a pyridone containing tetracycle: a Jak protein kinase inhibitor. *Bioorg Med Chem Lett.* 2002;12(8):1219-1223.
36. Hedvat M, Huszar D, Herrmann A, et al. The JAK2 inhibitor AZD1480 potently blocks Stat3 signaling and oncogenesis in solid tumors. *Cancer Cell.* 2009;16(6):487-497.
37. Pardanani A, Hood J, Lasho T, et al. TG101209, a small molecule JAK2-selective kinase inhibitor potently inhibits myeloproliferative disorder-associated JAK2V617F and MPLW515L/K mutations. *Leukemia.* 2007;21(8):1658-1668.
38. Demoulin JB, Renauld JC. Interleukin 9 and its receptor: an overview of structure and function. *Int Rev Immunol.* 1998;16(3):345-364.
39. Verstovsek S, Kantarjian H, Mesa RA, et al. Safety and efficacy of INCB018424, a JAK1 and JAK2 inhibitor, in myelofibrosis. *N Engl J Med.* 2010;363(12):1117-1127.
40. Quintas-Cardama A, Kantarjian H, Cortes J, Verstovsek S. Janus kinase inhibitors for the treatment of myeloproliferative neoplasias and beyond. *Nat Rev Drug Discov.* 2011;10(2):127-140.
41. Shi JG, Chen X, McGee RF, et al. The pharmacokinetics, pharmacodynamics, and safety of orally dosed INCB018424 phosphate in healthy volunteers. *J Clin Pharmacol.* 2011;51(12):1644-1654.
42. Besancenot R, Chaligne R, Tonetti C, et al. A senescence-like cell-cycle arrest occurs during megakaryocytic maturation: implications for physiological and pathological megakaryocytic proliferation. *PLoS Biol.* 2010;8(9):e10000476.
43. Chen E, Beer PA, Godfrey AL, et al. Distinct clinical phenotypes associated with JAK2V617F reflect differential STAT1 signaling. *Cancer Cell.* 2010;18(5):524-535.
44. de Graaf CA, Kauppi M, Baldwin T, et al. Regulation of hematopoietic stem cells by their mature progeny. *Proc Natl Acad Sci U S A.* 2010;107(50):21689-21694.
45. Kaushansky K. The role of the MPL receptor in myeloproliferative disorders. *Leukemia.* 1998;12(suppl 1):S47-S50.
46. Ciurea SO, Merchant D, Mahmud N, et al. Pivotal contributions of megakaryocytes to the biology of idiopathic myelofibrosis. *Blood.* 2007;110(3):986-993.
47. El-Harith el HA, Roesl C, Ballmaier M, et al. Familial thrombocytosis caused by the novel germ-line mutation p.Pro106Leu in the MPL gene. *Br J Haematol.* 2009;144(2):185-194.
48. Lannutti BJ, Epp A, Roy J, Chen J, Josephson NC. Incomplete restoration of Mpl expression in the mpl−/− mouse produces partial correction of the stem cell-repopulating defect and paradoxical thrombocytosis. *Blood.* 2009;113(8):1778-1785.
49. Tiedt R, Coers J, Ziegler S, et al. Pronounced thrombocytosis in transgenic mice expressing reduced levels of Mpl in platelets and terminally differentiated megakaryocytes. *Blood.* 2009;113(8):1768-1777.
50. Lannutti BJ, Drachman JG. Lyn tyrosine kinase regulates thrombopoietin-induced proliferation of hematopoietic cell lines and primary megakaryocytic progenitors. *Blood.* 2004;103(10):3736-3743.

VII.3. Combination treatment for myeloproliferative neoplasms using JAK and pan-class I PI3K inhibitors

Combination treatment for myeloproliferative neoplasms using JAK and pan-class I PI3K inhibitors

Meng Ling Choong [a, #], Christian Pecquet [b, #], Vishal Pendharkar [a], Carmen C. Diaconu [b, c], Jacklyn Wei Yan Yong [a], Shi Jing Tai [a], Si Fang Wang [a], Jean-Philippe Defour [b], Kanda Sangthongpitag [a], Jean-Luc Villeval [d], William Vainchenker [d], Stefan N. Constantinescu [b, *], May Ann Lee [a, *]

[a] *Experimental Therapeutics Centre, Agency for Science Technology and Research, Singapore*
[b] *Ludwig Institute for Cancer Research & de Duve Institute, UniversitéCatholique de Louvain, Brussels, Belgium*
[c] *Stefan S. Nicolau Institute of Virology, Bucharest, Romania*
[d] *INSERM U1009, InstitutGustaveRoussy, Université Paris-Sud, Villejuif Cedex, France*

Received: August 7, 2013; Accepted: September 9, 2013

Abstract

Current JAK2 inhibitors used for myeloproliferative neoplasms (MPN) treatment are not specific enough to selectively suppress aberrant JAK2 signalling and preserve physiological JAK2 signalling. We tested whether combining a JAK2 inhibitor with a series of serine threonine kinase inhibitors, targeting nine signalling pathways and already used in clinical trials, synergized in inhibiting growth of haematopoietic cells expressing mutant and wild-type forms of JAK2 (V617F) or thrombopoietin receptor (W515L). Out of 15 kinase inhibitors, the ZSTK474 phosphatydylinositol-3′-kinase (PI3K) inhibitor molecule showed strong synergic inhibition by Chou and Talalay analysis with JAK2 and JAK2/JAK1 inhibitors. Other pan-class I, but not gamma or delta specific PI3K inhibitors, also synergized with JAK2 inhibitors. Synergy was not observed in Bcr-Abl transformed cells. The best JAK2/JAK1 and PI3K inhibitor combination pair (ruxolitinib and GDC0941) reduces spleen weight in nude mice inoculated with Ba/F3 cells expressing TpoR and JAK2 V617F. It also exerted strong inhibitory effects on erythropoietin-independent erythroid colonies from MPN patients and JAK2 V617F knock-in mice, where at certain doses, a preferential inhibition of JAK2 V617F mutated progenitors was detected. Our data support the use of a combination of JAK2 and pan-class I PI3K inhibitors in the treatment of MPNs.

Keywords: combination treatment • kinases • myeloproliferative neoplasms • JAK2 • PI3K

Introduction

A unique somatic acquired Janus kinase 2 (JAK2) tyrosine kinase mutation at position V617F of the pseudokinase domain is associated with the majority of BCR-ABL-negative MPNs [1–4]. More than 95% of polycythemia vera (PV), and up to 50% of essential thrombocythemia (ET) and primary myelofibrosis (PMF) patients harbour the JAK2 V617F mutation [5, 6]. Activating mutations in one of the JAK2-utilizing receptors in the myeloid lineage, the thrombopoietin receptor (TpoR W515L or TpoR W515K), account for about 5–8% of the JAK2 V617F-negative ET and PMF cases [7–9]. Both JAK2 and TpoR mutations lead to constitutive activation of JAK2 signalling [7, 9, 10]. These discoveries indicated JAK2 as a major target for MPN treatment.

Taken together PV, ET and PMF amount in the United States to a prevalence of ~0.8/1000 [11, 12], which is significantly higher than chronic myeloid leukaemia. Despite the sizable patient population, no Food and Drug Administration (FDA)-approved drug existed until 2012 for MPNs. As of 2009, several JAK2 inhibitors entered active clinical trials for MPNs [13]. In 2012, one JAK2/JAK1 inhibitor, ruxolitinib, was approved by FDA for the treatment of myelofibrosis, following two phase III clinical trials [14, 15].

The key cytokine receptors coupled to JAK2 in the myeloid lineage, such as erythropoietin receptor (EpoR) and TpoR (c-MPL), [6,

#Co-first authors.
*Correspondence to: May Ann LEE,
Cell-Based Assay Development Group,
Experimental Therapeutics Centre, 31 Biopolis Way,
#03-01 Nanos Building, Singapore 138669, Singapore.
Tel.: +65-64070339
Fax: +65-64788768
E-mail: malee@etc.a-star.edu.sg
Stefan N. CONSTANTINESCU,
Ludwig Institute for Cancer Research,
Avenue Hippocrate 74, UCL 75-4, Brussels B1200, Belgium.
Tel.: 3227647540
Fax: 322-7646566
E-mail: stefan.constantinescu@bru.licr.org

doi: 10.1111/jcmm.12156

© 2013 The Authors.
Journal of Cellular and Molecular Medicine published by John Wiley & Sons Ltd and Foundation for Cellular and Molecular Medicine.
This is an open access article under the terms of the Creative Commons Attribution License, which permits use, distribution and reproduction in any medium, provided the original work is properly cited.

16] are known to trigger activation of phosphatidylinositol-3′-kinase (PI3K) [17–19]. JAK2 V617F was shown to activate PI3K, which is required for transformation [1, 20]. The biology of the cytokine receptor-JAK/signal transducers and activators of transcription (STAT) pathway activation is complicated by interactions with other signalling pathways, themselves also promoting PI3K activation. The receptor tyrosine kinase/RAS/mitogen-activated protein kinase (RTK/RAS/MAPK) pathway was found to interact with the JAK/STAT pathway at multiple levels [21, 22]. JAKs may phosphorylate insulin receptor substrate (IRS) and p85, which results in the activation of the PI3K pathway [23, 24]. Input integration from many signalling pathways needs to be considered for treatment of constitutive JAK2 activation-related neoplasms.

All JAK2 inhibitors currently in development are type I competitive ATP-pocket binders/inhibitors of the JH1 kinase domain. The JAK2 V617F mutation occurs in the pseudokinase domain located away from the kinase domain ATP-binding pocket. As such, they are not expected to be specific for JAK2 mutant. JAK2 inhibitors used in the clinics reduce spleen size and diminish constitutional symptoms [14, 15]. However, the inhibitors are not able to rapidly reverse marrow fibrosis, decrease allele burden or peripheral blasts in myelofibrosis [14, 15]. These and other challenges facing JAK inhibitor treatment in myelofibrosis [25] could be explained either by insufficient dosing because of anaemia and thrombocytopenia resulting from inhibition of wild-type (WT) JAK2, by addiction to one pathway downstream of JAK2 that needs very low levels of residual JAK activation, by continuous signalling from other JAKs in heteromeric complexes with the inhibited JAK2 [26], or by other genetic events that might drive MPN in addition from JAK pathway. On the other hand, recent data obtained after long-term observation (24–48 months) do show that long-term therapy with ruxolitinib retarded advancement of marrow fibrosis, and worsening of marrow fibrosis was significantly more prevalent in the best available therapy arm [27]. Evidence has also been reported for a survival advantage of myelofibrosis patients after treatment with ruxolitinib, such as the 3-year data of the COMFORT-II trial [28] or the 2-year data of the COMFORT-I trial [29].

We postulate that MPNs can be more efficiently treated if we target the constitutive JAK2 signalling with a combination of a JAK2 inhibitor with another kinase inhibitor targeting a pathway downstream of the aberrant JAK2 signalling. This should increase targeting specificity, reduce the required doses, and minimize potential side effects of the drugs. To test this hypothesis, we have constructed cell line models of MPN haematopoietic progenitors. These cells are used in a cellular screen by using a JAK2 inhibitor in combination with a panel of kinase inhibitors to identify synergic pairs, which will then be tested in primary cells and explored further by using *in vivo* systems.

Materials and methods

Cell lines

Mouse pro-B Ba/F3 cells were first transduced with green fluorescent protein (GFP)-containing bicistronic viruses coding for human WT JAK2 or human JAK2 V617F (cloned into pMX-IRES-GFP) or Bcr-Abl (cloned into MSCV-IRES-GFP) as described previously [10]. Populations of cells expressing GFP were isolated by fluorescence-activated cell sorting. Cells stably expressing human JAK2 or JAK2 V617F were subsequently infected with pMX-IRES-GFP retroviruses coding for human WT TpoR, while parental cells were transduced with human TpoR W515L mutant. TpoR was engineered to contain an amino-terminal haemagglutinin (HA) tag [30]. Infected cells were sorted for equal HA cell surface expression.

Ba/F3 cells stably expressing TpoR JAK2 WT or JAK2 WT are interleukin-3 (IL3)-dependent for proliferation. IL3 (R&D Systems, Minneapolis, MN, USA) is used at 0.01 μg/ml. Ba/F3 cells expressing JAK2 V617F, TpoR-JAK2 V617F, TpoR W515L or Bcr-Abl are IL3-independent, proliferate to similar extents and exhibit similar levels of STAT5 activation, as measured by luciferase assays with STAT5-dependent luciferase reporters [31] and anti-phospho-Y694 STAT5 western blotting [32]. Activation of signalling proteins was determined by Western blot with phospho-specific antibodies, as described [9].

Drug compounds

The JAK2/JAK1 inhibitor ruxolitinib (also known as INC424 or INCB018424) (Albany Molecular Research Inc., Albany, NY, USA) and the JAK2 inhibitor TG101348 (SYNthesis Med Chem, San Diego, CA, USA) were used. All compounds were dissolved in 100% dimethyl sulfoxide (Sigma-Aldrich, St. Louis, MO, USA) to prepare 20 mM stocks except for NVP-BEZ235, which was dissolved to prepare 10 mM stock. The identity of compounds used in this study is shown in Figure 1. All compounds were synthesized by SynMedChem except AZD6244 and XL147 (Selleck Chemicals, Houstan, TX, USA), Rapamycin and Temsirolimus (Tocris Bioscience, Bristol, UK), LY294002 from Sigma-Aldrich and SB1518 and CC401 from AMRI (Albany Molecular Research Inc.).

Design of an 8 × 8 drug combination study and cell viability assay

Combination studies were performed as described [33]. Constant ratio combination was used where the two combination drugs were used at their equipotent ratio (*i.e.* at the ratio of their IC_{50}s which was pre-determined individually from dose–response studies). An 8 × 8 Latin Square design was constructed with eight different constant molar ratios between the two drugs. Each column was a serial dilution of the two drugs so that eight dose–response curves could be plotted for combination index (CI) calculations (Fig. 1B). The experiments were carried out in quadruplicate in a 384-well plate (Greiner Bio-One, Frickenhausen, Germany) for each pair of drug combination. Volumes of 25 μl of compound mixture and 25 μl of cells (5,000 cells/well) were added to each well. IL3 (0.01 μg/ml) was added to the TpoR JAK2 WT and JAK2 WT cells. Cells were incubated at 37°C for 18 h and then lysed, and ATP levels were measured with a luciferase assay kit (Cell Titer-Glo, Promega, Madison, WI, USA).

Drug synergism calculation

Combination index was obtained by using the CalcuSyn software version 2.1 (BioSoft, Ferguson, MO, USA). CI values of 0.9–1.1 are considered additive, values of 0.8 and below show moderate-to-strong synergism, while values above 1.2 are moderate-to-strong antagonism

© 2013 The Authors.
Journal of Cellular and Molecular Medicine published by John Wiley & Sons Ltd and Foundation for Cellular and Molecular Medicine.

for the drug pair tested [34]. CIs were calculated only when the goodness of fit of the dose–response curves to the median-effect plot has a correlation coefficient of $r \geq 0.9$ for the cell-based assays.

The JAK2 mutant Ba/F3 tumour mouse model

1×10^7 Ba/F3 TpoR JAK2 V617F cells were inoculated intravenously into 7- to 10-week-old female nude mice *via* tail vein injection. Mice were randomly divided into 5–10 per group. Two protocols were used, namely, progression of tumour (leukaemia) burden in mice inoculated with Ba/F3 TpoR JAK2 V617F cells (Fig. S1, Protocol 1); and effect of JAK2 and PI3K inhibitions on reduction in spleen weight (Fig. S1, Protocol 2).

A Vet ABC Hematology Analyzer (Scil, Gurnee, IL, USA) was used for blood counting. Spleen and liver were weighed. Percentages of GFP-positive cells in marrow and peripheral blood mononuclear cells were determined by flow cytometry.

Colony assays (CFU-E and BFU-E) using bone marrow from JAK2 V617F knock-in and littermate JAK2 wild-type mice

Colony assays (CFU-E and BFU-E) were performed on bone marrow from heterozygous JAK2 V617F or littermate JAK2 WT mice or from mice reconstituted with haematopoietic marrow cells from JAK2 V617F knock-in mice [35], after lethal irradiation, as previously described [32].

$1.5–2 \times 10^5$ cells were plated in cytokine-depleted methylcellulose medium (M3234) supplemented or not with the indicated cytokines (10 U/ml Epo alone or 5 ng/ml SCF+3 ng/ml IL3 with or without 3 U/ml Epo). Day+2 Epo-independent CFU-E formation was assessed in the presence of ruxolitinib or GDC0941 alone or in combination at several concentrations (0.1–5 μM for ruxolitinib and 1–10 μM for GDC0941) or with vehicle control.

To investigate preference of the combination for JAK2 V617F mutated progenitors, nucleated bone marrow JAK2 V617F and JAK2 WT cells were mixed in a 1:1 ratio (7.5×10^4 cells each) and plated on M3234 methylcellulose medium complemented or not with 3 U/ml Epo, 5 ng/ml SCF and 3 ng/ml IL3. Individual BFU-E colonies were harvested at day 6 and collected in 5 μL water before colony denaturation at 95°C during 10 min. Samples were then genotyped for JAK2 V617F and actin by PCR with the following primers: PR-V617F-for TGT CTT ACT AAA GCC CAG GTG ATG G, PR-V617F-rev GCT CCA GGG TTA CAC GAG TC. PR-actin-for, GGC TGT ATT CCC CTC CAT CG, PR-actin-rev TGG GGG TAC TTC AGG GTC AGG.

Colony-forming assays on primary human cells

Peripheral blood from two PV patients (JAK2 V617F allele burdens of 49% and 57%) was used to perform BFU-E and CFU-E colony assay. PBMC were collected and plated on methylcellulose medium (H4236 from Stem Cell Technologies, Vancouver, BC, Canada) supplemented or not with 10 U/ml Epo (Eprex: Erythropoietin (Epoetin alfa), Janssen-Cilag, Beerse, Belgium) in triplicate (500,000 cells/plate). Colony formation was assessed at days 7 and 16 for CFU-E and BFU-E colonies, respectively, in presence of drugs alone (0.1 μM ruxolitinib or 1 μM GDC0941), in combination or with vehicle as control.

Results

Strong synergy between JAK and PI3K inhibitors in cell-based assays

Cell lines used in the synergy study are shown in Figure 1A. A summary of CI values (Fig. 1B) for ruxolitinib with the various kinase inhibitors targeting nine signalling pathways in Ba/F3 cells expressing TpoR JAK2 V617F is shown in Figure 1C. Both JAK inhibitors ruxolitinib and TG101348 showed strong drug synergism with PI3K inhibitor ZSTK474 (CI ≤0.5 in more than 50% of the entries in the 8 × 8 Latin Square) in inhibiting the growth of all cell lines, except Bcr-Abl cells, which indicates specificity for cytokine receptor/JAK2 pathway (Fig. 2 for results with ruxolitinib, not shown for results with TG101348). The effective dose ratio ranges for TG101348-ZSTK474 combination are narrower than those observed with the ruxolitinib combination.

Subsequently, other PI3K inhibitors were analysed in the combination study. A summary of CI values for ruxolitinib with the PI3K inhibitors in Ba/F3 cells expressing TpoR JAK2 V617F is shown in Figure 1D. Three PI3K inhibitors, NVP-BEZ235, GDC0941 and TGX221 were also found to strongly synergize (CI ≤0.5 in more than 50% of the entries in the 8 × 8 Latin Square) with ruxolitinib or TG101348 (Fig. 3 for results of GDC0941 with ruxolitinib, Fig. S2 for selected PI3K inhibitors with ruxolitinib, results for PI3K inhibitors with TG101348 are not shown). Other tested PI3K inhibitors, especially those specific for the gamma or delta PI3K, were not found to synergize well with the JAK inhibitors.

The synergy between JAK and PI3K inhibitors occurs best when the concentration ratio set based on individual IC50s is in favour of JAK inhibitor over the PI3K inhibitor. This observation implies that the PI3K signalling is secondary to the JAK2 signalling in our cell models. Inhibition of the JAK2 signalling is crucial to sensitize cells to the PI3K inhibitors for specific targeting of the JAK2 or TpoR mutant cells.

Downstream of PI3K is the mTOR pathway, which is considered a major mediator of PI3K signalling. We next tested if the compound Ku-0063794, a specific mTOR inhibitor, will synergize with the JAK1/JAK2 inhibitor ruxolitinib. Ku-0063794 and its derivative, AZD8055, are currently in Phase I/II trial for advance solid tumours, lymphoma and endometrial carcinoma [36]. Ku-0063794 strongly synergized with ruxolitinib only in cells stably expressing JAK2 V617F, but not also TpoR (Fig. S3). It remains unclear why JAK2 signalling through TpoR interaction is not targeted effectively by the JAK2-mTOR inhibitors combination, and requires a PI3K inhibitor (Fig. 1C). Nevertheless, a recent study reported that another mTOR inhibitor, everolimus, as a single agent, was effective in a phase 1/2 study of patients with myelofibrosis, supporting the notion that deregulated signalling *via* this pathway is pathogenic in MPNs [37].

Target specificity of the JAK and PI3K inhibitors

The IC_{50} for cell viability for both JAK inhibitors, ruxolitinib and TG101348, was in the single digit micro molar range. Compared with the JAK2 V617F and TpoR W515L cells, IC_{50} for cell viability was

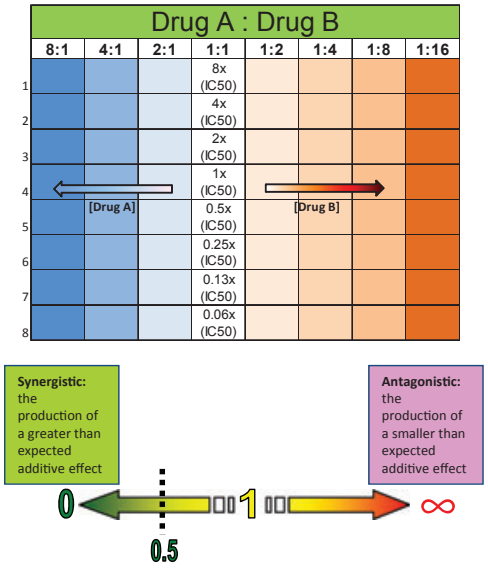
© 2013 The Authors.

Journal of Cellular and Molecular Medicine published by John Wiley & Sons Ltd and Foundation for Cellular and Molecular Medicine.

A

Ba/F3 cells:
- JAK2 WT
- JAK2 V617F
- TpoR JAK2 WT
- TpoR JAK2 V617F
- TpoR W515L
- Bcr-Abl

B



C

No.	Compound	Class	CI values at ED50
1	AT-7519	CDK inhibitor	1.2
2	SNS-032	CDK inhibitor	2.6
3	AZD6244	MEK/ERK inhibitor	0.6
4	PD0325901	MEK/ERK inhibitor	0.6
5	CC-401	JNK inhibitor	3.0
6	VX-702	P38 MAPK inhibitor	1.3
7	SB203580	P38 MAPK inhibitor	1.1
8	SB202190	P38 MAPK inhibitor	5.6
9	PLX4720	Raf inhibitor	1.4
10	Rho-15	ROCK inhibitor	1.0
11	AMG-Tie2-1	Tie inhibitor	8.5
12	Temsirolimus	mTOR inhibitor	0.8
13	Rapamycin	mTOR inhibitor	0.9
14	Ku-0063794	mTOR inhibitor	0.6
15	ZSTK474	Pan PI3K inhibitor	0.2

D

No.	Compound	Target	CI values at ED50
1	AS252424	PI3Kγ	0.7
2	TGX221	PI3Kβ	0.6
3	TG100115	PI3Kγ/δ	1.0
4	IC87114	PI3Kδ	1.0
5	GDC0941	Pan PI3K	0.3
6	LY294002	PIM-1, mTOR, PI3Kγ	0.4
7	NVP-BEZ235	Pan PI3K, mTOR	0.1
8	XL147 (SAR245408)	Pan PI3K	1.1

Fig. 1 Cell lines and small molecules used in combination for detection of synergy with JAK2 inhibitors in inhibiting proliferation of model myeloproliferative neoplasm cells. (**A**) Ba/F3 cell lines used for inhibitor screens. Ba/F3 parental and Ba/F3 TpoR JAK2 wild-type (WT) cells were maintained in medium supplemented with IL3, while Ba/F3 JAK2 V617F, TpoR V617F, TpoR W515L and Bcr-Abl were maintained in medium without cytokines. (**B**) A schematic representation of an 8 × 8 constant ratio design for combination treatment. The two combination drugs were used at their equipotent concentration ratio (IC_{50} of drug A to IC_{50} of drug B is 1:1) in the centre column. The concentration ratio of drug A to drug B is progressively increased towards the left, while the concentration ratio of drug B to drug A is progressively increased towards the right. Each column in the design is a dose–response curve with constant concentration ratio between drug A and drug B. Although usually C.I. <0.8 is considered significant, we selected for combinations showing C.I. <0.5. (**C**) Combination study using JAK2/JAK1 inhibitor ruxolitinib with various kinase inhibitors at equipotent concentration ratio on TpoR JAK2 V617F cells. (**D**) Combination study using JAK2/JAK1 inhibitor ruxolitinib with several other PI3K inhibitors at equipotent concentration ratio on TpoR JAK2 V617F cells.

higher with Bcr-Abl transfected cells, but not with JAK2 WT cells (Table 1). The IC values we obtain for Ba/F3 JAK2 V617F cells are comparable to those previously reported [38]. We have also observed inhibition of phosphorylation in STAT3, STAT5 and p44/42 (ERK1/2) with ruxolitinib treatment for both WT and mutant JAK2 transfected cells (Fig. S4). This confirms that JAK2 inhibitors are not able to distinguish between WT and mutant JAK2.

On the other hand, the engineered Ba/F3 cells were not very responsive to PI3K inhibitors alone, in the absence of JAK2 inhibitors. IC_{50} for cell viability was in the double to triple digit micro molar range with NVP-BEZ235 being more potent than other PI3K inhibitors tested (Table 1), possibly because this compound targets both PI3K and mTOR. TGX221 is a class I PI3Kβ-specific inhibitor, whereas ZSTK474, GDC0941 and NVP-BEZ235 are pan-class I PI3K inhibitors. It is unclear at present why the pan PI3K inhibitors have a wide range of IC_{50} values and why only certain pan PI3K inhibitors demonstrated synergism with the JAK2 inhibitors in inhibiting Ba/F3 cell growth. All four PI3K inhibitors seemed to be selective for cells expressing JAK2 V617F and TpoR W515L, while cells expressing WT JAK2 or Bcr-Abl were more resistant towards the PI3K inhibitors (Fig. S2).

© 2013 The Authors.
Journal of Cellular and Molecular Medicine published by John Wiley & Sons Ltd and Foundation for Cellular and Molecular Medicine.

A TpoR JAK2 WT

Drug (Ratio)	Combination index at	
	ED50	ED75
ZSTK474/Ruxolitinib (1:8)	0.1	0.1
ZSTK474/Ruxolitinib (1:4)	0.1	0.2
ZSTK474/Ruxolitinib (1:2)	0.1	0.2
ZSTK474/Ruxolitinib (1:1)	0.2	0.2
ZSTK474/Ruxolitinib (2:1)	0.2	0.2
ZSTK474/Ruxolitinib (4:1)	0.3	0.2
ZSTK474/Ruxolitinib (8:1)	0.4	0.3
ZSTK474/Ruxolitinib (16:1)	0.5	0.4

B TpoR JAK2 V617F

Drug (Ratio)	Combination index at	
	ED50	ED75
ZSTK474/Ruxolitinib (1:8)	0.0	0.0
ZSTK474/Ruxolitinib (1:4)	0.2	0.1
ZSTK474/Ruxolitinib (1:2)	0.1	0.1
ZSTK474/Ruxolitinib (1:1)	0.2	0.1
ZSTK474/Ruxolitinib (2:1)	0.2	0.1
ZSTK474/Ruxolitinib (4:1)	0.2	0.1
ZSTK474/Ruxolitinib (8:1)	0.2	0.1
ZSTK474/Ruxolitinib (16:1)	0.3	0.2

C TpoR W515L

Drug (Ratio)	Combination index at	
	ED50	ED75
ZSTK474/Ruxolitinib (1:8)	0.2	0.2
ZSTK474/Ruxolitinib (1:4)	0.2	0.2
ZSTK474/Ruxolitinib (1:2)	0.3	0.2
ZSTK474/Ruxolitinib (1:1)	0.2	0.2
ZSTK474/Ruxolitinib (2:1)	0.3	0.2
ZSTK474/Ruxolitinib (4:1)	0.3	0.3
ZSTK474/Ruxolitinib (8:1)	0.3	0.3
ZSTK474/Ruxolitinib (16:1)	0.4	0.5

D Bcr-abl

Drug (Ratio)	Combination index at	
	ED50	ED75
ZSTK474/Ruxolitinib (1:8)	>10	>10
ZSTK474/Ruxolitinib (1:4)	>10	>10
ZSTK474/Ruxolitinib (1:2)	1.6	>10
ZSTK474/Ruxolitinib (1:1)	6.0	>10
ZSTK474/Ruxolitinib (2:1)	3.2	>10
ZSTK474/Ruxolitinib (4:1)	1.8	>10
ZSTK474/Ruxolitinib (8:1)	3.3	>10
ZSTK474/Ruxolitinib (16:1)	4.3	>10

E JAK2 WT

Drug (Ratio)	Combination index at	
	ED50	ED75
ZSTK474/Ruxolitinib (1:8)	0.5	0.4
ZSTK474/Ruxolitinib (1:4)	0.3	0.3
ZSTK474/Ruxolitinib (1:2)	0.3	0.3
ZSTK474/Ruxolitinib (1:1)	0.2	0.2
ZSTK474/Ruxolitinib (2:1)	0.1	0.1
ZSTK474/Ruxolitinib (4:1)	0.2	0.1
ZSTK474/Ruxolitinib (8:1)	0.1	0.1
ZSTK474/Ruxolitinib (16:1)	0.1	0.1

F JAK2 V617F

Drug (Ratio)	Combination index at	
	ED50	ED75
ZSTK474/Ruxolitinib (1:8)	0.1	0.1
ZSTK474/Ruxolitinib (1:4)	0.1	0.1
ZSTK474/Ruxolitinib (1:2)	0.1	0.0
ZSTK474/Ruxolitinib (1:1)	0.3	0.1
ZSTK474/Ruxolitinib (2:1)	0.3	0.0
ZSTK474/Ruxolitinib (4:1)	0.3	0.0
ZSTK474/Ruxolitinib (8:1)	0.1	0.0
ZSTK474/Ruxolitinib (16:1)	0.2	0.0

Fig. 2 Combination study using JAK2/JAK1 inhibitor ruxolitinib with ZSTK474 in the Ba/F3 cell model. (**A**) Ba/F3 TpoR JAK2 wild-type (WT) cells; (**B**) Ba/F3 TpoR JAK2 V617F cells; (**C**) Ba/F3 TpoR W515L cells; (**D**) Ba/F3 Bcr-Abl cells; (**D** and **E**) Ba/F3 JAK2 WT cells; (**F**) Ba/F3 JAK2 V617F cells.

Effect of inhibitors on signalling pathways

We examined the effect of JAK2 and PI3K inhibitors alone and in combination on our model Ba/F3 cell lines. As expected, phosphorylation at Y1007 of JAK2 was stabilized by ruxolitinib because of the type I mechanism of inhibition, where molecules bind to active state kinases, block catalytic activity, while maintaining open conformation of activation loop continues to be phosphorylated by other kinases [39]. We observed inhibition by NVP-BEZ235 of p70 S6 kinase and S6 ribosomal protein phosphorylation (both are downstream effectors of PI3K signalling) when JAK2 or JAK2 V617F cells were co-expressed with TpoR (Fig. 4) or not (Fig. S4A). The effect of NVP-BEZ235 was less pronounced in the cell line expressing the active mutant TpoR W515L (Fig. S4B). Ruxolitinib inhibited the STAT activation (STAT5

© 2013 The Authors.

Journal of Cellular and Molecular Medicine published by John Wiley & Sons Ltd and Foundation for Cellular and Molecular Medicine.

A TpoR JAK2 WT

Drug (Ratio)	Combination index at	
	ED50	ED75
GDC0941/Ruxolitinib (1:8)	0.2	0.3
GDC0941/Ruxolitinib (1:4)	0.3	0.6
GDC0941/Ruxolitinib (1:2)	0.3	0.3
GDC0941/Ruxolitinib (1:1)	0.3	0.3
GDC0941/Ruxolitinib (2:1)	0.3	0.3
GDC0941/Ruxolitinib (4:1)	0.3	0.2
GDC0941/Ruxolitinib (8:1)	0.3	0.2
GDC0941/Ruxolitinib (16:1)	0.4	0.3

B TpoR JAK2 V617F

Drug (Ratio)	Combination index at	
	ED50	ED75
GDC0941/Ruxolitinib (1:8)	0.3	0.5
GDC0941/Ruxolitinib (1:4)	0.2	0.6
GDC0941/Ruxolitinib (1:2)	0.4	0.5
GDC0941/Ruxolitinib (1:1)	0.5	0.4
GDC0941/Ruxolitinib (2:1)	0.6	0.5
GDC0941/Ruxolitinib (4:1)	0.4	0.4
GDC0941/Ruxolitinib (8:1)	0.4	0.5
GDC0941/Ruxolitinib (16:1)	0.8	0.6

C TpoR W515L

Drug (Ratio)	Combination index at	
	ED50	ED75
GDC0941/Ruxolitinib (1:8)	0.4	0.4
GDC0941/Ruxolitinib (1:4)	0.4	0.4
GDC0941/Ruxolitinib (1:2)	0.4	0.5
GDC0941/Ruxolitinib (1:1)	0.6	0.5
GDC0941/Ruxolitinib (2:1)	0.5	0.3
GDC0941/Ruxolitinib (4:1)	0.3	0.3
GDC0941/Ruxolitinib (8:1)	0.4	0.3
GDC0941/Ruxolitinib (16:1)	0.6	0.3

D Bcr-abl

Drug (Ratio)	Combination index at	
	ED50	ED75
GDC0941/Ruxolitinib (1:8)	4.3	>10
GDC0941/Ruxolitinib (1:4)	2.9	>10
GDC0941/Ruxolitinib (1:2)	8.8	>10
GDC0941/Ruxolitinib (1:1)	1.8	2.5
GDC0941/Ruxolitinib (2:1)	1.8	1.2
GDC0941/Ruxolitinib (4:1)	1.9	4.5
GDC0941/Ruxolitinib (8:1)	1.6	2.6
GDC0941/Ruxolitinib (16:1)	1.8	3.6

E JAK2 WT

Drug (Ratio)	Combination index at	
	ED50	ED75
GDC0941/Ruxolitinib (1:8)	0.2	0.2
GDC0941/Ruxolitinib (1:4)	0.2	0.2
GDC0941/Ruxolitinib (1:2)	0.2	0.2
GDC0941/Ruxolitinib (1:1)	0.4	0.3
GDC0941/Ruxolitinib (2:1)	0.2	0.2
GDC0941/Ruxolitinib (4:1)	0.2	0.2
GDC0941/Ruxolitinib (8:1)	0.3	0.4
GDC0941/Ruxolitinib (16:1)	0.3	0.4

F JAK2 V617F

Drug (Ratio)	Combination index at	
	ED50	ED75
GDC0941/Ruxolitinib (1:8)	0.1	0.2
GDC0941/Ruxolitinib (1:4)	0.1	0.2
GDC0941/Ruxolitinib (1:2)	0.2	0.2
GDC0941/Ruxolitinib (1:1)	0.3	0.2
GDC0941/Ruxolitinib (2:1)	0.4	0.3
GDC0941/Ruxolitinib (4:1)	0.5	0.4
GDC0941/Ruxolitinib (8:1)	0.4	0.4
GDC0941/Ruxolitinib (16:1)	0.5	0.4

Fig. 3 Combination study using the JAK2/JAK1 inhibitor ruxolitinib with GDC0941in the Ba/F3 cell model. Results shown are for eight dose ratios and at two effective doses (ED50 and ED75). (**A**) Ba/F3 TpoR JAK2 wild-type (WT) cells; (**B**) Ba/F3 TpoR JAK2 V617F cells; (**C**) Ba/F3 TpoR W515L cells; (**D**) Ba/F3 Bcr-Abl cells; (**D** and **E**) Ba/F3 JAK2 WT cells; (**F**) Ba/F3 JAK2 V617F cells.

and STAT3), as expected. In contrast, ruxolitinib did not inhibit STAT5 and STAT3 phosphorylation in Ba/F3 cells expressing Bcr-Abl (Fig. S4C). Interestingly, NVP-BEZ235 weakly inhibited STAT5 activation in TpoR expressing cells, but not in JAK2 or JAK2 V617F cells (Fig. 4, Fig. S4A and B).

In combination, JAK2 and PI3K inhibitors blocked both STAT and downstream PI3K targets p70 S6 kinase and S6 ribosomal protein (Fig. 4 and Fig. S4). Akt phosphorylation at S473 (mTORC2 site) was only marginally inhibited by NVP-BEZ235 in TpoR cells, and was not inhibited in JAK2 or JAK2 V617F cells, with almost no effect by the combination. The combination appears to weakly diminish activation of ERK1/2, but not of p38 MAP-kinase (Fig. 4, Fig. S4A). Overall, strong effects were seen with the drug combination on the JAK/STAT and certain PI3K downstream pathways (p70 S6 kinase). These data

© 2013 The Authors.
Journal of Cellular and Molecular Medicine published by John Wiley & Sons Ltd and Foundation for Cellular and Molecular Medicine.

Table 1 The 50% inhibitory concentrations with their corresponding 95% confidence intervals in parenthesis of the JAK2 and PI3K inhibitors

		IC50 (μM) (95% Confidence Interval)					
		TpoR JAK2 WT	TpoR JAK2 V617F	TpoR W515L	Bcr-abl	JAK2 TW	JAK2 V617F
JAK2 inhibitors	INC424	4.2 (2.4–7.2)	1.6 (1.1–2.4)	0.1 (0.07–0.13)	45.3 (29.9–68.7)	1.0 (0.6–1.7)	0.4 (0.2–0.6)
	TG101348	1.4 (1.3–1.5)	0.8 (0.7–0.9)	0.8 (0.7–1.0)	2.7 (2.2–3.3)	1.8 (1.5–2.3)	0.6 (0.6–0.7)
PI3K inhibitors	ZSTK474	225.2 (170.7–297.2)	80.5 (56.9–113.9)	64.3 (47.1–87.8)	125.9 (76.7–206.4)	250.5 (173.6–361.6)	116.5 (99.7–136.2)
	NVP-BEZ235	36.8 (23.9–56.6)	3.5 (2.7–4.6)	1.8 (1.4–2.5)	>200	7.5 (4.5–12.7)	0.04 (0.02–0.06)
	GDC0941	192.3 (127.6–289.7)	17.9 (13.8–23.1)	43.7 (28.3–67.6)	147.2 (61.5–352.2)	185.1 (165.6–206.8)	25.8 (10.7–61.8)
	TGX221	76.1 (67.4–86.0)	49.4 (44.7–54.5)	50.0 (45.9–54.6)	75.9 (66.3–86.9)	28.3 (15.1–53.2)	20.39 (11.9–34.9)

suggest that the synergic inhibition is because of the PI3K- p70 S6 kinase arm and less so because of inhibition of the PI3K-Akt arm. Interestingly, an Akt inhibitor, MK-2206 was shown also to synergize with ruxolitinib in cell lines, MPN primary cells and a retroviral reconstitution model of TpoR W515L mutant [40]. In aggregate, inhibition of both arms of the PI3K pathway may prove very effective in MPNs, along with JAK2.

Effect of JAK2 and PI3K inhibitors on spleen weight in the Ba/F3 TpoR JAK2 V617F mouse model

Female BALB/c nude mice injected with Ba/F3 TpoR JAK2 V617F cells were studied for overall survival and enlargement of spleen (Fig. 5). Tissue samples were collected from mice killed on day 8 and day 14. Spleen weight increased after 8 days of cell implantation, while increase of liver weight was observed by day 14 (Fig. S5A). A progressive increase of Ba/F3 TpoR JAK2 V617F cells in the systemic blood circulation and spleen was observed from day 8 to day 14 (Fig. S5B). An increase of Ba/F3 TpoR JAK2 V617F cells in the bone marrow was observed on day 8 (results not shown). Platelet and red blood cell numbers decreased when compared with the control groups, most likely because of replacement by proliferating Ba/F3 transformed cells (Fig. S5C).

The mice inoculated with Ba/F3 TpoR JAK2 V617F cells were either treated with vehicle alone, GDC0941 alone, ruxolitinib alone or a combination of GDC0941 and ruxolitinib (Fig. S1, see Protocol 2). An evaluation of *in vivo* drug–drug interactions between ruxolitinib and GDC0941 is documented in Table S1. GDC0941 was chosen over NVP-BEZ235 for this study because of solubility issue with NVP-BEZ235 in our oral formulation.

All mice in the treated groups with the compound combination at 50 mg/kg body weight had no overt sign of clinical distress except for enlarged organs. At day 12 post-inoculation, spleen weights of mice treated with the compound combination were ~70% less than the spleen weights of mice treated with vehicle alone, and ~60% less than the spleen weights of mice treated with GDC0941 alone or ruxolitinib alone at 50 mg/kg body weight. Combination treatment extended survival when compared with vehicle control and to individual treatments (Fig. 5A). The increase in size and weight of spleen was also significantly delayed ($P < 0.001$) in mice receiving the combination treatment (Fig. 5B).

Effect of JAK2 and PI3K inhibitors on colony assays from JAK2 V617F knock-in mice and MPN patient cells

We performed colony-forming unit (CFU) assays to assess effect of drugs combination on formation of colonies from bone marrow of mice that were knock-in for JAK2 V617F in their haematopoietic system following bone marrow transplantation with JAK2 V617F knock-in bone marrow [32, 35]. As shown in Figure 6A, CFU-Es were observed

© 2013 The Authors.

Journal of Cellular and Molecular Medicine published by John Wiley & Sons Ltd and Foundation for Cellular and Molecular Medicine.

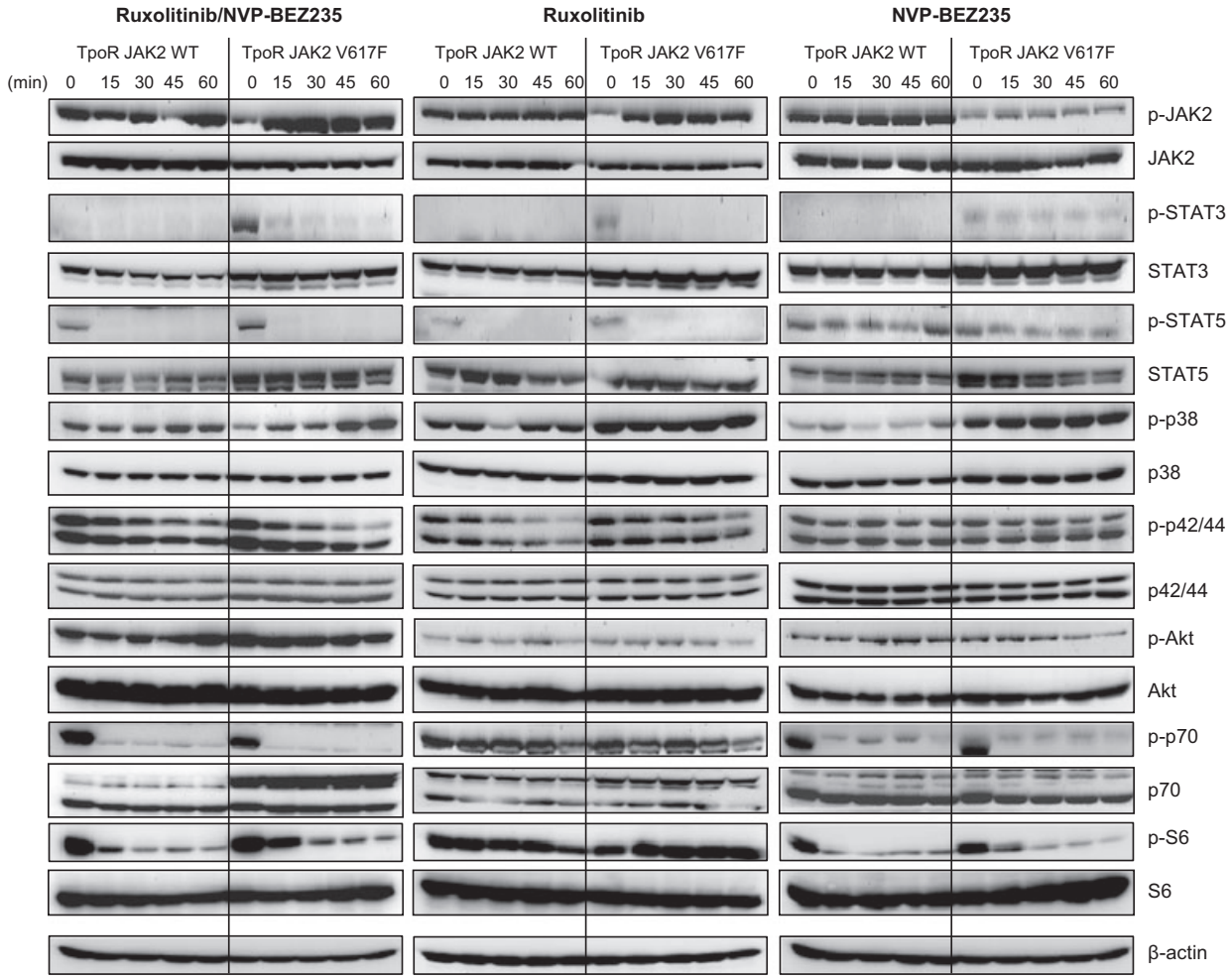


Fig. 4 Effect of the JAK2/JAK1 inhibitor ruxolitinib and PI3K inhibitor NVP-BEZ236 alone or in combination on signalling in Ba/F3 TpoR cells over-expressing JAK2 wild-type (WT) or JAK2 V617F. Cells expressing TpoR JAK2 V617F were autonomous for growth, while Ba/F3 TpoR JAK2 WT cells were grown in medium supplemented with IL3. Cells were treated for the indicated intervals with 1 μM ruxolitinib and 10 μM NVP-BEZ235 alone or in combination and western blotting was performed with the phospho-specific antibodies (phospho-JAK2 (Tyr1007/1008), phospho-STAT3 (Tyr705), phospho-STAT5 (Tyr694), phospho-p70 S6 kinase (Thr389), phospho-S6 ribosomal protein (Ser235/236), phospho-AKT (Ser473), phospho-p38 MAP-kinase (Thr180/Tyr182), phospho-p44/42 ERK1/2 (Thr202/Tyr204), with antibodies to actin (as loading control) and with antibodies detecting the signalling proteins themselves.

at day 2 in the absence of Epo, indicating the capacity of those colonies to growth independently of cytokines (EEC). Both ruxolitinib and GDC0941 used individually were able to inhibit EEC formation at 5 and 10 μM, respectively (Fig. 6A). Furthermore, combination of those drugs at the same concentration drastically blocks EEC formation.

A similar synergy induced by the combination of the two inhibitors could be detected on patient derived day 7 Epo-independent CFU-E (Fig. S6A) and day 16 BFU-E (Fig. S6B).

We aimed to assess whether this synergic effect showed any preference for JAK2 V617F colonies, especially at concentrations of ruxolitinib inhibitor that are lower than those utilized in the clinic, given their known toxicities. We chose (lower) concentrations that fit with the IC50 data obtained from our Ba/F3 TpoR JAK2 V617F cells for the combination (Table S1), or to the IC50 data obtained for individual ruxolitinib treatment of the Ba/F3 JAK2 V617F and Ba/F3 TpoR W515L cells (Table 1), namely 0.1 μM ruxolitinib and 1 μM GDC0941 and 0.3 μM ruxolitinib and 3 μM GDC0941. These concentrations are also fitting well with pharmacokinetics measurements in mice injected with 50 mg/kg body ruxolitinib and with a recent study that examined synergy between an Akt inhibitor and ruxolitinib [40]. We then tested whether there was any preference for inhibition of JAK2 V617F *versus* JAK2 WT CFU-Es by the ruxolitinib and GDC0941 combination.

To this end, we performed two types of experiments. In the first, we compared the effects of the combination on CFU-E formation from

© 2013 The Authors.
Journal of Cellular and Molecular Medicine published by John Wiley & Sons Ltd and Foundation for Cellular and Molecular Medicine.

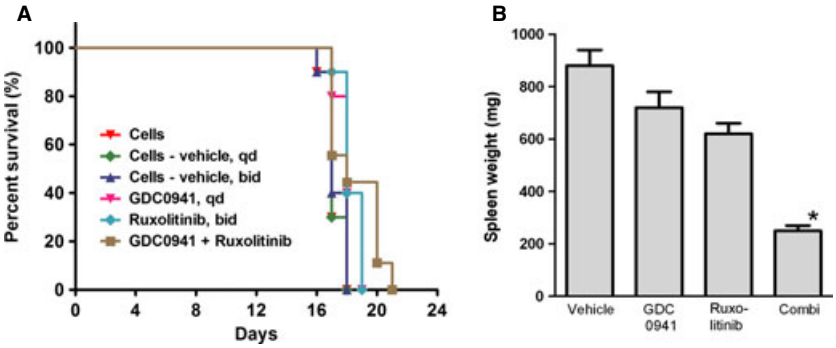


Fig. 5 Effect of JAK and PI3K inhibitions on survival (**A**) and spleen weight (**B**) in the JAK2 mutation-driven leukaemia mouse model. Ba/F3 TpoR JAK2 V617F cells (1×10^7) were intravenously inoculated into 8- to 10-week-old female nude mice. After 3 days, mice were treated with either vehicle, GDC0941 alone at 50 mg/kg body weight, ruxolitinib alone at 50 mg/kg body weight, or a combination of both compounds for 12 days. Combination treatment increased survival by 2 days compared with single compound treatment. Combination treatment also reduced spleen weight significantly compared with vehicle-treated mice, or mice treated with GDC0941 alone, or ruxolitinib alone (*$P < 0.001$ for each comparison). qd: every day, bid: twice a day.

JAK2 V617F heterozygous knock-in and littermate JAK2 WT bone marrow cells. In Figure 6B, we show that there is a statistically significant preference for inhibiting the JAK2 V617F CFU-Es. In the second type of experiments, we mixed 1:1 WT and JAK2 V617F knock-in bone marrow cells and BFU-Es were counted in two conditions, with cytokines and with cytokines and combination of inhibitors (Fig. 6C), and then individual colonies were picked and genotyped for JAK2 V617F and reference actin (Fig. 6D). Results showed a preference for inhibition of the mutated colonies. In one such experiment, of 11 colonies derived from three independent plates not treated with inhibitor, six BFU-Es were JAK2 V617F, while in the presence of the inhibitor combination, all 16 colonies were negative for JAK2 V617F. These results show that preference of the combination for the JAK2 V617F colonies can be observed.

Discussion

The Chou-Talalay method of determining CI values has rigorous mathematical proof and extensive validation [41] and is more accurate than descriptive drug combination studies [42–44]. Progressively smaller CI values are an estimation of progressively stronger synergism. The accepted cut-off value for synergism is ≤0.8 [34]. Here, we used a cut-off value of ≤0.5 to ensure that only very strong synergistic drug-pairs are selected.

TGX221 (PI3Kβ inhibitor) is in research phase, while ZSTK474, NVP-BEZ235 and GDC0941 (all pan PI3K inhibitors) are in clinical trials. A comprehensive study [45] showed that ZSTK474 and GDC0941 have highly similar inhibition profiles and specificity for class I PI3K, while NVP-BEZ235 is different, being able to inhibit both PI3K and mTOR. Other isoform specific PI3K inhibitors (against γ and δ isoforms) analysed in this study were not found to synergize with the JAK2 inhibitors. Our findings support earlier studies that PI3Kα and PI3Kβ isoforms play an important role in tumourigenesis [46, 47], while PI3Kδ and PI3Kγ are involved in other diseases [48, 49]. Furthermore, the NVP-BEZ235 was found by Fiskus *et al.* to synergize with JAK2 inhibition in inhibiting growth of cultured and primary MPN cells [50]. In our study, we show that these effects can be detected in primary JAK2 V617F knock-in and patient cells, and in an *in vivo* tumourigenic system based on JAK2 V617F expression. Our finding is that cells expressing constitutively active JAK2 mutants are dependent on the PI3K pathway for their survival. Possible dose-reduction of ruxolitinib by combined use of a pan type I PI3K inhibitor may result in the reduction of adverse events of ruxolitinib, and this may represent a major benefit of the combination therapy.

Although MEK/ERK/p38 and JNK pathways are activated downstream of cytokine receptors [5, 6], none of the MAP-kinase inhibitors strongly synergized (CI <0.5) with JAK2 inhibitors in our assays. However, the two MEK/ERK dual inhibitors that we tested, AZD6244 and PD0325901 did synergize with a CI of 0.6 (Fig. 1C), which qualifies as a weak synergy by the Chou-Talalay method, suggesting that the MEK/ERK pathway does contribute to the cytokine-independent growth of MPN cells. In previous studies, we have shown that severe MPN and myelofibrosis are induced by TpoR W515A mutant *via* the cytosolic TpoR tyrosine (Y626) that connects to the shc-ras-MEK-ERK1/2 pathway [9], and that the same tyrosine residue was required for down-modulation of TpoR in JAK2 V617F by excessive ERK1/2 and STAT3 activation, again linked to severe MPN [32]. Finally, the ERK1/2 pathway is involved in the antiproliferative and senescence effects induced by Tpo *via* TpoR in cells that physiologically express high JAK2 levels, such as late megakaryocytes [32, 51]. Altogether excessive MAP-kinase ERK1/2 and STAT3 activation might be linked to myelofibrosis, and contribute to cytokine-independent growth, while the PI3K appears to be the major pathway linked to proliferation. These results strengthen the existing evidence of molecular crosstalk between the JAK/STAT and the PI3K pathways in various tissues [52–54] and supported the importance of a combination treatment targeting both JAK2 and the PI3K signalling. Mechanistically, it has been shown that activated mutant forms of STAT5 interact with the regulatory subunit p85 of PI3K, *via* the adaptor Gab2 [55]. Further studies will be required to assess the precise mechanism by which inhibiting

© 2013 The Authors.

Journal of Cellular and Molecular Medicine published by John Wiley & Sons Ltd and Foundation for Cellular and Molecular Medicine.

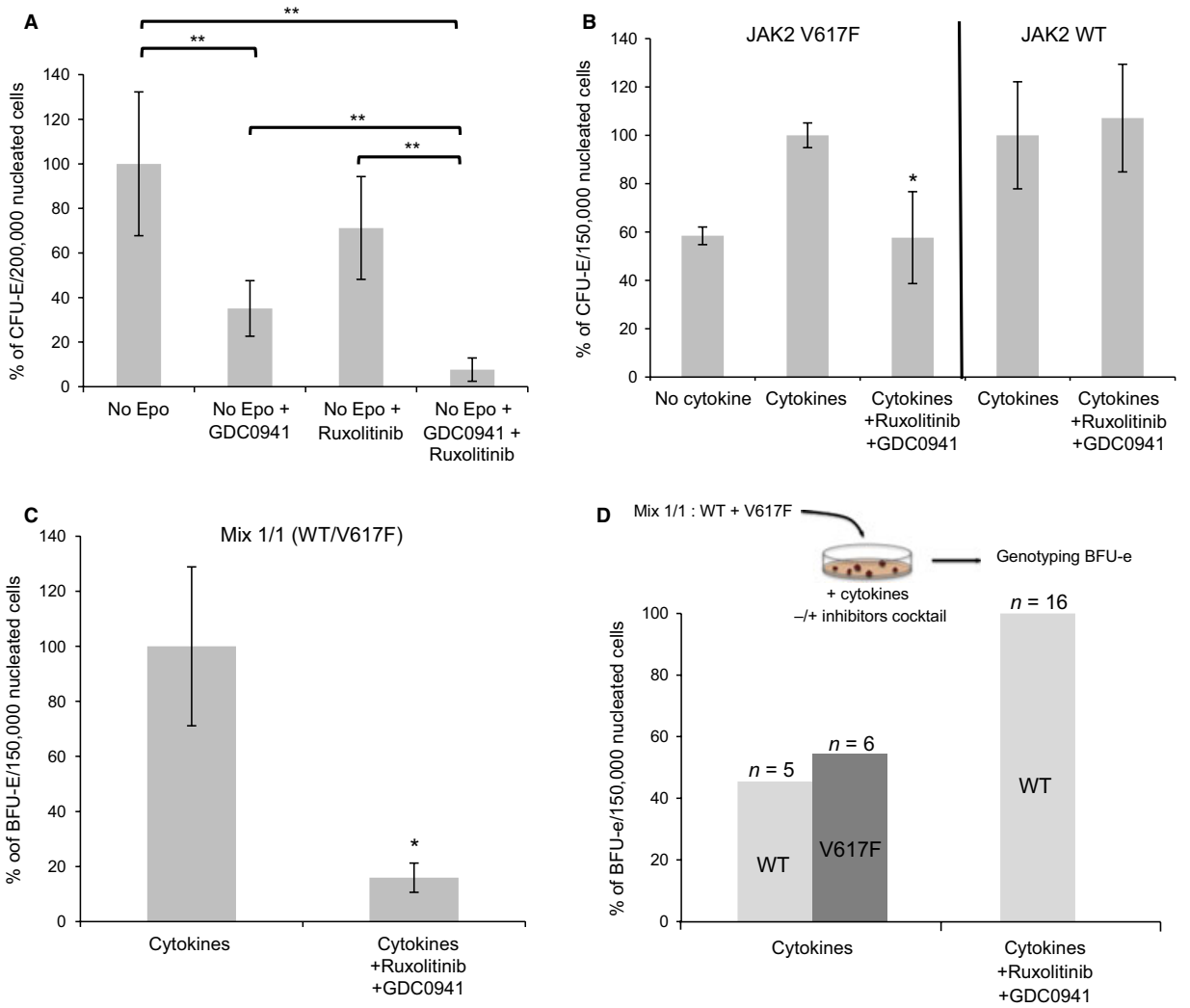


Fig. 6 Effect of JAK and PI3K inhibitors on colony formation from heterozygous JAK2 V617F knock-in bone marrow cells and mixtures of knock-in and wild-type (WT) mice. (**A**) Effect of ruxolitinib (5 μM) and GDC 0942 (10 μM) or combination thereof on Epo-independent CFU-E (2% foetal serum, no cytokines) from bone marrow of reconstituted heterozygous JAK2 V617F knock-in mice. The number of colonies was normalized to those in the untreated controls in the absence of Epo (936 ± 302 EEC/200,000 bone marrow nucleated heterozygous JAK2 V617F knock-in cells). Shown are averages of two mice, each performed in duplicate (average of six points) ±SD. $^{**}P < 0.01$ unpaired Student's test with unequal variance. (**B**) Comparison between generation of CFU-E colonies between bone marrow cells from JAK2 V617F knock-in mice and JAK2 WT littermate mice. Cells were plated in methylcellulose in the presence of cytokines (3 U/ml Epo, 5 ng/ml SCF, 3 ng/ml IL3) alone or with the combination of 0.1 μM ruxolitinib and 1 μM GDC 0941. The number of colonies was normalized to those in the untreated controls in presence of cytokines, which was 1099 ± 56/150,000 bone marrow nucleated heterozygous JAK2 V617F cells and 837 ± 185/150,000 bone marrow nucleated WT JAK2 cells. Shown are averages of triplicates ±SD of one representative experiment out of two. $^{*}P < 0.05$ unpaired Student's test with unequal variance. (**C**) Bone marrow cells from JAK2 V617F knock-in mice and WT littermate mice were mixed in a 1:1 ratio (75,000 cells each) and BFU-E formation was determined in the absence or presence of the combination of 0.1 μM ruxolitinib and 1 μM GDC 0941 in the presence of cytokines (3 U/ml Epo, 5 ng/ml SCF, 3 ng/ml IL3). The number of colonies was normalized to those in the untreated controls in the presence of cytokines, which was 339 ± 98 BFU-E colonies/150,000 nucleated cells. Shown are averages of triplicates ±SD of one representative experiment out of two. $^{*}P < 0.05$ unpaired Student's test with unequal variance. (**D**) Preferential inhibition of JAK2 V617F knock-in BFU-E compared with WT BFU-E by the combination of 0.1 μM ruxolitinib and 1 μM GDC 0941. 1:1 mixed JAK2 V617F knock-in and WT cells were plated in methylcellulose in the presence of cytokines (3 U/ml Epo, 5 ng/ml SCF, 3 ng/ml IL3) alone or with the combination of inhibitors. BFU-E colonies were harvested at day 6 from three plates for each condition and genotyped for JAK2 V617F. Three plates were used for each condition. Genotyping was performed on 4, 2 and 5 BFU-Es for the condition 'cytokines' and 4, 6 and 6 for the condition 'cytokines + inhibitor' combination. Values represent% of BFU-Es genotyped as JAK2 V617F-positive or JAK2 WT-positive per 150,000 nucleated mixed cells. Shown are the results of one representative experiment out of two.

© 2013 The Authors.
Journal of Cellular and Molecular Medicine published by John Wiley & Sons Ltd and Foundation for Cellular and Molecular Medicine.

PI3K synergizes with JAK2 in blocking MPN cell proliferation. Importantly, we could observe the synergic action of JAK2 and PI3K inhibitors also in cells cultivated in defined medium in the absence of serum, which indicates that PI3K activation is largely derived from JAK2 activation.

Our results showed that Ba/F3 TpoR JAK2 V617F cells can propagate *in vivo* in nude mice leading to accumulation of GFP-positive cells and anaemia, thrombocytopenia, splenomegaly and hepatomegaly. This was also reported with Ba/F3 JAK2 V617F cells [56]. Splenomegaly was most prominent during early development of this oncogenic model with spleen weight as a good indicator of disease progression. We demonstrated that simultaneous inhibition of JAK2 and PI3K signalling pathways led to significantly delayed splenomegaly in mice inoculated with Ba/F3 TpoR JAK2 V617F cells.

Furthermore, combining JAK2 and PI3K inhibitors inhibited Epo-independent CFU-E and BFU-E colony formation from primary cells from JAK2 V617F-positive MPN patients and JAK2 V617F knock-in mice. The Ruxolitinib-GDC0941 combination, used at certain doses, exerted preferential inhibitory effects on JAK2 V617F knock-in CFU-E and BFU-E. These data suggest that careful dosing can achieve specificity for the mutated progenitors.

Our pre-clinical studies indicate that the ruxolitinib and GDC0941 combination is safe and effective when administered orally. Clinical trials with JAK2/JAK1 or JAK2 inhibitors indicate that these drugs are uniformly active based on reduction in patient spleen size and improvement in constitutional symptoms, but they induce varying toxicity profiles [15, 57–59]. Our findings suggest that we may be able to administer these drugs at lower concentrations when adding PI3K inhibitors. Our study gives the first evidence of synergistic effects of JAK2 inhibitors with PI3K inhibitors and provides a framework for combination trials using compounds in these two classes in patients with MPNs.

Acknowledgements

We are grateful for support to S.N.C. from the F.R.S.-F.N.R.S., Belgium, the Salus Sanguinis Foundation, the Action de Recherche Concertée of the University catholique de Louvain, Brussels, the Fondation contre le Cancer, Brussels, the PAI Program, Belgium and the Atlantic Philanthropies, New York, for support to CCD from the Sectorial Operational Program Human Resources Development POSDRU/89/1.5/S/64109, and F.R.S.- F.N.R.S./F.R.I.A. fellowships to CP and JPD, respectively. The work was supported by the Agency for Science Technology and Research (A*STAR), Singapore and the Ludwig Institute for Cancer Research.

Conflicts of interest

The authors confirm that there are no conflicts of interest.

Supporting information

Additional Supporting Information may be found in the online version of this article:

Figure S1. Protocols for *in vivo* tumour model of Ba/F3 TpoR JAK2 V617F cells in nude mice.

Figure S2. Combination study with ruxolitinib and PI3K inhibitors.

Figure S3. Combination study with ruxolitinib and Ku0063794 (mTOR inhibitor).

Figure S4. Effects of JAK and PI3K inhibitors on signalling *via* the JAK2, STAT3/STAT5, PI3K, mTOR and MAPK/ERK1/2 in the Ba/F3 JAK2 WT and BaF3 JAK2 V617F (A), Ba/F3 TpoR wt and TpoR-W515L (B) or Ba/F3 Bcr-Abl (C) cell lines.

Figure S5. Effects of inoculating Ba/F3 TpoR JAK2 V617F cells into BALB/c mice.

Figure S6. Effects of the combination of JAK and PI3K inhibitors on Epo-independent CFU-Es (EECs) and Epo-independent BFU-Es from PV patients.

Table S1. Pharmacokinetic profile of ruxolitinib and GDC0941 when administered in combination to nude mice injected with Ba/F3 TpoR JAK2 V617F cells.

References

1. **James C, Ugo V, Le Couedic JP, *et al.*** A unique clonal JAK2 mutation leading to constitutive signalling causes polycythaemia vera. *Nature*. 2005; 434: 1144–8.
2. **Kralovics R, Passamonti F, Buser AS, *et al.*** A gain-of-function mutation of JAK2 in myeloproliferative disorders. *N Engl J Med*. 2005; 352: 1779–90.
3. **Levine RL, Wadleigh M, Cools J, *et al.*** Activating mutation in the tyrosine kinase JAK2 in polycythemia vera, essential thrombocythemia, and myeloid metaplasia with myelofibrosis. *Cancer Cell*. 2005; 7: 387–97.
4. **Baxter EJ, Scott LM, Campbell PJ, *et al.*** Acquired mutation of the tyrosine kinase JAK2 in human myeloproliferative disorders. *Lancet*. 2005; 365: 1054–61.
5. **Levine RL, Pardanani A, Tefferi A, *et al.*** Role of JAK2 in the pathogenesis and therapy of myeloproliferative disorders. *Nat Rev Cancer*. 2007; 7: 673–83.
6. **Vainchenker W, Dusa A, Constantinescu SN.** JAKs in pathology: role of Janus kinases in hematopoietic malignancies and immunodeficiencies. *Semin Cell Dev Biol*. 2008; 19: 385–93.
7. **Pikman Y, Lee BH, Mercher T, *et al.*** MPLW515L is a novel somatic activating mutation in myelofibrosis with myeloid metaplasia. *PLoS Med*. 2006; 3: e270.
8. **Pardanani AD, Levine RL, Lasho T, *et al.*** MPL515 mutations in myeloproliferative and

© 2013 The Authors.

Journal of Cellular and Molecular Medicine published by John Wiley & Sons Ltd and Foundation for Cellular and Molecular Medicine.

other myeloid disorders: a study of 1182 patients. *Blood*. 2006; 108: 3472–6.

9. **Pecquet C, Staerk J, Chaligne R, *et al.*** Induction of myeloproliferative disorder and myelofibrosis by thrombopoietin receptor W515 mutants is mediated by cytosolic tyrosine 112 of the receptor. *Blood*. 2010; 115: 1037–48.
10. **Staerk J, Lacout C, Sato T, *et al.*** An amphipathic motif at the transmembrane-cytoplasmic junction prevents autonomous activation of the thrombopoietin receptor. *Blood*. 2006; 107: 1864–71.
11. **Ma X, Vanasse G, Cartmel B, *et al.*** Prevalence of polycythemia vera and essential thrombocythemia. *Am J Hematol*. 2008; 83: 359–62.
12. **Mesa RA, Silverstein MN, Jacobsen SJ, *et al.*** Population-based incidence and survival figures in essential thrombocythemia and agnogenic myeloid metaplasia: an Olmsted County Study, 1976–1995. *Am J Hematol*. 1999; 61: 10–5.
13. **Mesa RA.** New drugs for the treatment of myelofibrosis. *Curr Hematol Malig Rep*. 2010; 5: 15–21.
14. **Verstovsek S, Mesa RA, Gotlib J, *et al.*** A double-blind, placebo-controlled trial of ruxolitinib for myelofibrosis. *N Engl J Med*. 2012; 366: 799–807.
15. **Harrison C, Kiladjian JJ, Al-Ali HK, *et al.*** JAK inhibition with ruxolitinib *versus* best available therapy for myelofibrosis. *N Engl J Med*. 2012; 366: 787–98.
16. **Lu X, Huang LJ, Lodish HF.** Dimerization by a cytokine receptor is necessary for constitutive activation of JAK2V617F. *J Biol Chem*. 2008; 283: 5258–66.
17. **Damen JE, Cutler RL, Jiao H, *et al.*** Phosphorylation of tyrosine 503 in the erythropoietin receptor (EpR) is essential for binding the P85 subunit of phosphatidylinositol (PI) 3-kinase and for EpR-associated PI 3-kinase activity. *J Biol Chem*. 1995; 270: 23402–8.
18. **Klingmuller U, Wu H, Hsiao JG, *et al.*** Identification of a novel pathway important for proliferation and differentiation of primary erythroid progenitors. *Proc Natl Acad Sci USA*. 1997; 94: 3016–21.
19. **Miyakawa Y, Rojnuckarin P, Habib T, *et al.*** Thrombopoietin induces phosphoinositol 3-kinase activation through SHP2, Gab, and insulin receptor substrate proteins in BAF3 cells and primary murine megakaryocytes. *J Biol Chem*. 2001; 276: 2494–502.
20. **Kamishimoto J, Tago K, Kasahara T, *et al.*** Akt activation through the phosphorylation of erythropoietin receptor at tyrosine 479 is required for myeloproliferative disorder-associated JAK2 V617F mutant-induced cellular transformation. *Cell Signal*. 2011; 23: 849–56.
21. **Rane SG, Reddy EP.** Janus kinases: components of multiple signaling pathways. *Oncogene*. 2000; 19: 5662–79.
22. **Heinrich PC, Behrmann I, Haan S, *et al.*** Principles of interleukin (IL)-6-type cytokine signalling and its regulation. *Biochem J*. 2003; 374: 1–20.
23. **Foster FM, Traer CJ, Abraham SM, *et al.*** The phosphoinositide (PI) 3-kinase family. *J Cell Sci*. 2003; 116: 3037–40.
24. **Vanhaesebroeck B, Guillermet-Guibert J, Graupera M, *et al.*** The emerging mechanisms of isoform-specific PI3K signalling. *Nat Rev Mol Cell Biol*. 2010; 11: 329–41.
25. **Tefferi A.** Challenges facing JAK inhibitor therapy for myeloproliferative neoplasms. *N Engl J Med*. 2012; 366: 844–6.
26. **Koppikar P, Bhagwat N, Kilpivaara O, *et al.*** Heterodimeric JAK-STAT activation as a mechanism of persistence to JAK2 inhibitor therapy. *Nature*. 2012; 489: 155–9.
27. **Kvasnicka H, Thiele J, Bueso-Ramos C, *et al.*** Long-term intervention effects on bone marrow morphology in myelofibrosis: patients treated with ruxolitinib and best available therapy. *Haematologica*. 2013; 98 (Suppl): Abstract S591.
28. **Vannucchi AM, Kiladjian J-J, Cervantes F, *et al.*** Long-term outcomes from a phase 3 study comparing ruxolitinib with best available therapy (BAT) for the treatment of myelofibrosis (MF): a 3-year update of COMFORT-II. *Haematologica*. 2013; 98: Abstract S1111.
29. **Verstovsek S, Mesa RA, Gotlib J, *et al.*** Long-term outcome of ruxolitinib treatment in patients with myelofibrosis: durable reductions in spleen volume, improvements in quality of life, and overall survival advantage in COMFORT-I. *Blood (ASH Annual Meeting Abstracts)*. 2012; 120: Abstract 800.
30. **Huang LJ, Constantinescu SN, Lodish HF.** The N-terminal domain of Janus kinase 2 is required for Golgi processing and cell surface expression of erythropoietin receptor. *Mol Cell*. 2001; 8: 1327–38.
31. **Seubert N, Royer Y, Staerk J, *et al.*** Active and inactive orientations of the transmembrane and cytosolic domains of the erythropoietin receptor dimer. *Mol Cell*. 2003; 12: 1239–50.
32. **Pecquet C, Diaconu CC, Staerk J, *et al.*** Thrombopoietin receptor down-modulation by JAK2 V617F: restoration of receptor levels by inhibitors of pathologic JAK2 signaling and of proteasomes. *Blood*. 2012; 119: 4625–35.
33. **Chou TC, Talalay P.** Analysis of combined drug effects: a new look at a very old problem. *Trends Pharmacol Sci*. 1983; 4: 450–4.
34. **Chou TC, Talalay P.** Quantitative analysis of dose-effect relationships: the combined effects of multiple drugs or enzyme inhibitors. *Adv Enzyme Regul*. 1984; 22: 27–55.
35. **Marty C, Lacout C, Martin A, *et al.*** Myeloproliferative neoplasm induced by constitutive expression of JAK2V617F in knock-in mice. *Blood*. 2010; 116: 783–7.
36. **Garcia-Martinez JM, Moran J, Clarke RG, *et al.*** Ku-0063794 is a specific inhibitor of the mammalian target of rapamycin (mTOR). *Biochem J*. 2009; 421: 29–42.
37. **Guglielmelli P, Barosi G, Rambaldi A, *et al.*** Safety and efficacy of everolimus, a mTOR inhibitor, as single agent in a phase 1/2 study in patients with myelofibrosis. *Blood*. 2011; 118: 2069–76.
38. **Quintas-Cardama A, Vaddi K, Liu P, *et al.*** Preclinical characterization of the selective JAK1/2 inhibitor INCB018424: therapeutic implications for the treatment of myeloproliferative neoplasms. *Blood*. 2010; 115: 3109–17.
39. **Andraos R, Qian Z, Bonenfant D, *et al.*** Modulation of activation-loop phosphorylation by JAK inhibitors is binding mode dependent. *Cancer Discov*. 2012; 2: 512–23.
40. **Khan I, Huang Z, Wen Q, *et al.*** AKT is a therapeutic target in myeloproliferative neoplasms. *Leukemia*. 2013; 27: 1882–90.
41. **Chou TC.** Drug combination studies and their synergy quantification using the Chou-Talalay method. *Cancer Res*. 2010; 70: 440–6.
42. **Harrington KJ, Hingorani M, Tanay MA, *et al.*** Phase I/II study of oncolytic HSV GM-CSF in combination with radiotherapy and cisplatin in untreated stage III/IV squamous cell cancer of the head and neck. *Clin Cancer Res*. 2010; 16: 4005–15.
43. **Mihu CN, Kassis C, Ramos ER, *et al.*** Does combination of lipid formulation of amphotericin B and echinocandins improve outcome of invasive aspergillosis in hematological malignancy patients? *Cancer*. 2010; 116: 5290–6.
44. **Chen Y, Alvarez EA, Azzam D, *et al.*** Combined Src and ER blockade impairs human breast cancer proliferation *in vitro* and *in vivo*. *Breast Cancer Res Treat*. 2011; 128: 69–78.
45. **Kong D, Dan S, Yamazaki K, *et al.*** Inhibition profiles of phosphatidylinositol 3-kinase inhibitors against PI3K superfamily and human cancer cell line panel JFCR39. *Eur J Cancer*. 2010; 46: 1111–21.
46. **Levine DA, Bogomolniy F, Yee CJ, *et al.*** Frequent mutation of the PIK3CA gene in

© 2013 The Authors.
Journal of Cellular and Molecular Medicine published by John Wiley & Sons Ltd and Foundation for Cellular and Molecular Medicine.

ovarian and breast cancers. *Clin Cancer Res*. 2005; 11: 2875–8.

47. **Jia S, Liu Z, Zhang S, *et al.*** Essential roles of PI(3)K-p110beta in cell growth, metabolism and tumorigenesis. *Nature*. 2008; 454: 776–9.
48. **Sasaki T, Irie-Sasaki J, Jones RG, *et al.*** Function of PI3K gamma in thymocyte development, T cell activation, and neutrophil migration. *Science*. 2000; 287: 1040–6.
49. **Sadhu C, Masinovsky B, Dick K, *et al.*** Essential role of phosphoinositide 3-kinase delta in neutrophil directional movement. *J Immunol*. 2003; 170: 2647–54.
50. **Fiskus W, Verstovsek S, Manshouri T, *et al.*** Dual PI3K/AKT/mTOR inhibitor BEZ235 synergistically enhances the activity of JAK2 inhibitor against cultured and primary human myeloproliferative neoplasm cells. *Mol Cancer Ther*. 2013; 12: 577–88.
51. **Besancenot R, Chaligne R, Tonetti C, *et al.*** A senescence-like cell-cycle arrest occurs during megakaryocytic maturation: implications for physiological and pathological megakaryocytic proliferation. *PLoS Biol*. 2010; 8: e1000476.
52. **Nguyen MH, Ho JM, Beattie BK, *et al.*** TEL-JAK2 mediates constitutive activation of the phosphatidylinositol 3′-kinase/protein kinase B signaling pathway. *J Biol Chem*. 2001; 276: 32704–13.
53. **Carvalho CR, Carvalheira JB, Lima MH, *et al.*** Novel signal transduction pathway for luteinizing hormone and its interaction with insulin: activation of Janus kinase/signal transducer and activator of transcription and phosphoinositol 3-kinase/Akt pathways. *Endocrinology*. 2003; 144: 638–47.
54. **Gross ER, Hsu AK, Gross GJ.** The JAK/STAT pathway is essential for opioid-induced cardioprotection: JAK2 as a mediator of STAT3, Akt, and GSK-3 beta. *Am J Physiol Heart Circ Physiol*. 2006; 291: H827–34.
55. **Harir N, Pecquet C, Kerenyi M, *et al.*** Constitutive activation of Stat5 promotes its cytoplasmic localization and association with PI3-kinase in myeloid leukemias. *Blood*. 2007; 109: 1678–86.
56. **Abe M, Funakoshi-Tago M, Tago K, *et al.*** The polycythemia vera-associated Jak2 V617F mutant induces tumorigenesis in nude mice. *Int Immunopharmacol*. 2009; 9: 870–7.
57. **Verstovsek S, Kantarjian H, Mesa RA, *et al.*** Safety and efficacy of INCB018424, a JAK1 and JAK2 inhibitor, in myelofibrosis. *N Engl J Med*. 2010; 363: 1117–27.
58. **Pardanani A, Gotlib JR, Jamieson C, *et al.*** Safety and efficacy of TG101348, a selective JAK2 inhibitor, in myelofibrosis. *J Clin Oncol*. 2011; 29: 789–96.
59. **Vertovsek S, Kantarjian HM, Estrov Z, *et al.*** Long term outcomes of 107 patients with myelofibrosis receiving JAK1/JAK2 inhibitor ruxolitinib: survival advantage in comparison to matched historical controls. *Blood*. 2012; 120: 1202–9.

© 2013 The Authors.

Journal of Cellular and Molecular Medicine published by John Wiley & Sons Ltd and Foundation for Cellular and Molecular Medicine.

VII.4. Differential association of calreticulin type 1 and type 2 mutations with myelofibrosis and essential thrombocytemia: relevance for disease evolution

REFERENCES

1 O'Donnell MR, Tallman MS, Abboud CN, Altman JK, Appelbaum FR, Arber DA *et al.* Acute myeloid leukemia, version 2. *J Natl Compr Canc Netw* 2013; **11**: 1047–1055.
2 Mattison R, Luger S, Lazarus H. New strategies for the evaluation of the nadir bone marrow following induction in acute myeloid leukemia. *Curr Opin Hematol* 2013; **20**: 93–99.
3 Hussein K, Jahagirdar B, Gupta P, Burns L, Larsen K, Weisdorf D. Day 14 bone marrow biopsy in predicting complete remission and survival in acute myeloid leukemia. *Am J Hematol* 2008; **83**: 446–450.
4 Morris TA, DeCastro CM, Diehl LF, Gockerman JP, Lagoo AS, Li Z *et al.* Re-induction therapy decisions based on day 14 bone marrow biopsy in acute myeloid leukemia. *Leuk Res* 2013; **37**: 28–31.
5 Yanada M, Borthakur G, Ravandi F, Bueso-Ramos C, Kantarjian H, Estey E. Kinetics of bone marrow blasts during induction and achievement of complete remission in acute myeloid leukemia. *Haematologica* 2008; **93**: 1263–1265.
6 Slovak ML, Kopecky KJ, Cassileth PA, Harrington DH, Theil KS, Mohamed A *et al.* Karyotypic analysis predicts outcome of preremission and postremission therapy in adult acute myeloid leukemia: a Southwest Oncology Group/Eastern Cooperative Group study. *Blood* 2000; **96**: 4075–4083.
7 Othus M, Sudipto M, Sekeres M, Godwin J, Anderson J, Petersdorf S *et al.* Prediction of CR on reinduction in patients with newly diagnosed acute myeloid leukemia given intensive induction regimens; a report from SWOG and Cleveland Clinic. *Blood 2013* **122**: 3924 (ASH Abstract 2013).
8 Vainstein V, Buckley SA, Shukron O, Estey EH, Abkowitz JL, Wood BL *et al.* Rapid rate of peripheral blood blast clearance accurately predicts complete remission in acute myeloid leukemia. *Leukemia* 2014; **28**: 713–716.

Differential association of calreticulin type 1 and type 2 mutations with myelofibrosis and essential thrombocytemia: relevance for disease evolution

Leukemia (2015) **29,** 249–252; doi:10.1038/leu.2014.270

Recent advances in myeloproliferative neoplasms (MPNs) have highlighted the prevalence of mutations in the calreticulin gene (*CALR*),[1,2] bringing a major new actor in these disorders. Numerous studies have highly contributed to understanding of the role of *JAK2* and *MPL* in the pathogenesis of MPN development and progression.[3–5] In contrast to *JAK2* mutations that are associated in a causative manner with polycythemia vera,[6] myelofibrosis (MF) or essential thrombocytemia (ET),[7] *CALR* mutations are only associated with ET and MF. Indeed, *CALR* mutations were reported in 25% of ET and in 35% of MF patients who were non-mutated for *JAK2* and *MPL*. All recurrent *CALR* mutations that have been observed lead to a frame-shift generating a common 36 amino-acid C-terminal end and loss of the KDEL motif.[1,2,8–11] Among these mutations, two variants are largely predominant: type 1, a 52-bp deletion (p.L367fs*46) and type 2, a 5-bp insertion (p.K385fs*47). They account for 85% of the *CALR* mutations in ET and primary myelofibrosis (PMF).[1,2] There is strong evidence that the clinical features of *CALR* and *JAK2*-mutated ET and PMF are different and represent two facets of these disorders, although they both activate the JAK/STAT signaling pathway. It remains possible that the different *CALR* mutants exert different signaling activities. Thus, it would be important to characterize the potential differences between the different *CALR* mutations and also the phenotype of MPN devoid of *JAK2*, *MPL* and *CALR* mutations, now called triple-negative MPNs to understand whether they represent a homogeneous population.

A total of 572 MPN patients negative for *JAK2* and *MPL* mutations were collected according to sex, age at diagnosis and main clinical characteristics from several French and Belgian hospitals under the auspices of French Intergroup of Myeloproliferative disorders. The mutational status of *CALR* was determined using previously described high-resolution sizing of fluorescent dye-labeled PCR amplification of exon 9, with Sanger sequencing controls.[1] Beyond its contribution to mutant detection, high-resolution sizing also allows to estimate the allelic burden. Laboratory data and clinical parameters were obtained at diagnosis. The GraphPad Prism statistical package (GraphPad Software, Inc., La Jolla, CA, USA) was used to perform statistical analysis on these data, as described in Supplementary Information.

The median age at diagnosis of the entire patient series was 59 years (range, 7–92); 241 were males (43.1%). In our series, 396 patients were diagnosed as ET (including potential unidentified prefibrotic stage of myelofibrosis), 108 as MF (including PMF and post-ET MF) and 68 as mixed myelodysplastic syndrome (MDS)/MPN. We identified mutations localized in exon 9 of *CALR* in 368 patients (63.3%). The remaining 204 patients were designated as triple negative.

The global distribution of *CALR* mutations in our series was similar to previous studies[1,2] with 206 type 1 mutations (56%), 119 type 2 mutations (32%) and 43 other mutations (12%) representing 17 different CALR variants (Figure 1a). Importantly, nine were previously described but eight represented new variants (Figure 1b). Notably one of them, p.Glu378Cysfs*36, shortened the consensus C-terminal end to 33 amino acids only. In contrast to the rather low numbers of *JAK2* and *MPL* mutation variants, the growing number of *CALR* genomic variants identified implies that these mutants might not be completely biologically equivalent, despite the common loss of the KDEL motif and the acquisition of a new functional domain. Differences in the sequence of the C-terminal domain could indeed reach up to 25 amino acids, which is predicted to change the properties of the protein.

Our striking result is the distribution of CALR mutation type according to the MPN type. In MF there is an overrepresentation of type 1 CALR mutation (70%) and an underrepresentation of type 2 CALR mutation (13%) as compared with patients with ET that have a distribution of *CALR* mutations comparable to the global series of patients (Figure 1a; $P = 0.0002$). In MPNs, it has been highlighted that different allelic burdens of JAK2V617F and MPLW515K/L are associated with different phenotypes.[4,5] In our series, a higher allelic burden of CALR mutation was found in MF ($P < 0.0001$; Table 1). Even if it affects a small number of patients, it is to be noted that a high allelic burden (over 60%) was more frequent in MF (5/35 = 14.3%) than in ET (6/158 = 3.8%; $P = 0.0256$). This highly suggests the presence of rare homozygous mutations as described by Klampfl.[1] However, and contrary to that study, we observed a high allelic burden mainly

Accepted article preview online 12 September 2014; advance online publication, 14 October 2014

© 2015 Macmillan Publishers Limited

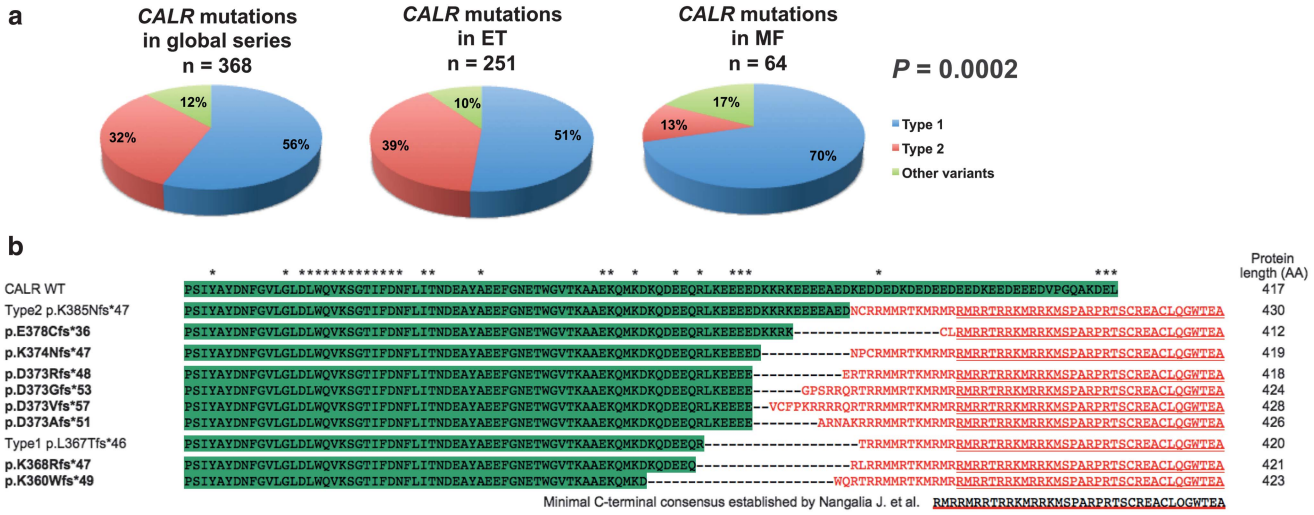


Figure 1. (**a**) Distribution of *CALR* mutations according to their type in *CALR*-mutated MPNs in the global series, ET and MF. (**b**) Alignment of CALR C-terminal domain in wild-type and mutant proteins. Mutation denomination is indicated on the left (new variants in bold). Green highlighted sequences represent the remaining wild-type amino acids in mutant proteins. Red sequences represent the C-terminal amino acids present in mutants (33 common to all mutants are underlined). A star indicates amino acids that are conserved from *Caenorhabditis elegans* to *Homo sapiens* according to clustalIW 2.0 alignment.

for type 1 mutations because no patient with type 2 mutation in ET and only one in MF, had an allelic burden over 60%. On the opposite, patients with a low allelic burden (under 25%) were only observed in ET (19/158 = 11.9%). Taken together these results suggest a link between CALR mutation allelic burden and disease phenotype as it was demonstrated for *JAK2* mutation.

To go further in the characterization of patients with type 1 or type 2 mutations, we sorted clinical characteristics of patients according to their diagnosis, presence or absence of *CALR* mutations and type of mutations (Table 1). These comparisons underscore a quite homogeneous MF group. Patients were mostly men (61%; $P = 0.0009$), the median age at diagnosis was 62.5 with several specific abnormalities including a low hemoglobin concentration (10.1 g/dl; $P < 0.0001$) and a low platelet count (median at 237×10^9/l; $P < 0.0001$). These results are in line with a recently published series.[12,13] It is to note, however, that MF patients with type 2 mutation may represent a particular entity characterized by a higher median platelet count as highlighted by an absence of patients with platelet count under 100×10^9/l. Owing to their rarity it is difficult to have full features of these patients that should be better characterized in future larger series.

Compared with MF, in ET patients the clinical presentation was more heterogeneous. A global overview indicated that they were mostly women (>61%; $P < 0.0001$), the median age at diagnosis was 57; $P = 0.0179$) with a median platelet count of 724×10^9/l ($P < 0.0001$). In *CALR*-mutated patients, however, there were no sex prevalence and a more important thrombocytosis (785×10^9/l; $P < 0.0001$). The type of CALR mutation impacted also age and platelet count. Indeed, patients with type 1 mutation were diagnosed at a median age of 61 with a median platelet count of 731×10^9/l, whereas those with type 2 mutations were diagnosed younger (median of 52.5 years) with a median platelet count over 870×10^9/l ($P = 0.04$).

An important other contribution of our series concerns the clinical parameters of the 204 triple-negative patients. A majority of triple-negative ETs were women (76.9%; $P < 0.0001$). This bias, which was not retrieved in *CALR*-mutated patients, was even more important for young triple-negative ET patients (< 50 years old) that were almost exclusively women (27/28 = 96.4%; $P < 0.0001$). This clearly suggests that the prevalence of women in ET is mostly owing to triple-negative cases. In MF, triple-negative patients presented a low hemoglobin concentration (8.85 g/dl; $P = 0.0255$) and a low leukocyte count (1.995×10^9/l; $P = 0.0002$). A striking characteristic was their platelet count that was significantly lower than their group mates (563.5 vs 785×10^9/l in ET and 108.5 vs 389×10^9/l in MF; $P < 0.0001$). This lower platelet count may suggest that in the general population, putative asymptomatic triple-negative ET male patients could be retrieved, which would only be diagnosed at more advanced age with a symptomatic MF.

Taken together, our results underline the differences between the two most frequent types of CALR mutation and show that *CALR*-mutated patients should not be considered as a single entity. A recent study suggests a better prognosis for patients with *CALR* type 1 mutation.[12] On the contrary, our results suggest that type 1 is associated with a shorter survival in MF (hazards ratio: 36.35, 95% confidence interval: 4.069–324.7; Supplementary Figure 1). However, these results remain to be confirmed in future larger series. In particular, it would be important to determine whether differences in survival between series could be explained by the presence or absence of mutation in epigenetic modifiers or spliceosome components (giving unfavorable prognosis) in the case of type 2 mutations. Indeed, as this mutation was described as weaker,[1] it could associates to a higher degree with epigenetic mutations in order to induce a MF phenotype, and thus the type 2 mutation *per se* might not be responsible for the prognosis. Of note, in ET patients, the type 2 CALR mutation was more frequent than type 1 in young patients and type 2 patients were less frequent than expected in MF. These data strongly suggest a less potent transforming capacity of type 2 variant, as it was initially hypothesized.[1] Taken together these findings suggest an association of type 2 CALR mutation with a true ET phenotype. As some of our ET patients could correspond to a prefibrotic stage of MF, and those patients are eventually MF patients with the MF mutational profiles (70% type 1 CALR mutation), the difference highlighted by our series of patients could be even more biased toward an increased proportion of type 2 CALR mutation in ET. However, longitudinal studies are needed to fully characterize ET patients with type 2 CALR mutation, which would clearly impact

© 2015 Macmillan Publishers Limited

© 2015 Macmillan Publishers Limited

Table 1. Clinical and laboratory features of 581 patients negative for *JAK2* and *MPL* mutations

		All patients (n = *572*)	*ET* (n = *396*)					*MF* (n = *108*)					*P-value global*	*ET vs MF*	*ET CALR+ vs ET CALR−*	*ET CALR type 1 vs ET CALR type 2*	*MF CALR+ vs MF CALR−*	*MF CALR type 1 vs MF CALR type 2*
				ET CALR− (n = *145*)	*ET CALR+* (n = *251*)				*MF CALR−* (n = *44*)	*MF CALR+* (n = *64*)								
						ET CALR type 1 (n = *129*)	*ET CALR type 2* (n = *98*)				*MF CALR type 1* (n = *45*)	*MF CALR type 2* (n = *8*)						
Allelic burden	*N* = 234	0.44 (0.09–1)	0.43 (0.09–0.79)	—	0.43 (0.09–0.79)	0.43 (0.09–0.79)	0.39 (0.19–0.54)	0.50 (0.29–1)	—	0.50 (0.29–1)	0.50 (0.29–1)	0.51 (0.36–0.81)	**< 0.0001**	**< 0.0001**		0.2907		0.8224
Allelic burden, > 0.6, *n* (%)		12 (5.1)	6 (3.8)	—	6 (3.8)	4 (5.1)	0 (0)	5 (14.3)	—	5 (14.3)	3 (12)	1 (25)	**0.0086**	**0.0256**				
Allelic burden, < 0.25, *n* (%)		23 (9.8)	19 (11.9)	—	19 (11.9)	10 (12.7)	4 (12.1)	0 (0)	—	0 (0)	0 (0)	0 (0)						
Age in years, median (range)	*N* = 416	59 (7–92)	57 (7–90)	50 (9–89)	57 (7–90)	61 (7–87)	52.5 (15–90)	62.5 (27–89)	60 (31–88)	63 (27–89)	63 (27–84)	55.5 (38–80)	**0.015**	**0.0179**	**0.0242**	0.0672	0.8456	0.3191
Age < 50 years, *n* (%)		128 (30.8)	102 (36.7)	28 (49.1)	74 (33.9)	30 (26.3)	36 (43.9)	16 (19)	5 (16.7)	11 (20.4)	6 (16.2)	3 (37.5)	**< 0.0001**	**0.0022**	**0.0449**	**0.0062**	0.7775	0.3262
Males (%)	*N* = 559	241 (43.1)	148 (38.2)	31 (23.1)	116 (46.4)	66 (51.2)	42 (43.3)	64 (61)	23 (59)	40 (62.5)	27 (60)	3 (42.9)	**< 0.0001**	**< 0.0001**	**< 0.0001**	0.2822	0.8353	0.4385
Males < 50 years, *n* (%)		53 (41.4)	41 (40.2)	1 (3.6)	40 (54.1)	18 (60)	19 (52.8)	9 (56.3)	1 (20)	8 (72.7)	5 (83.3)	1 (50)	**< 0.0001**	0.2803	**< 0.0001**	0.6233	0.1058	0.4643
Hemoglobin, g /dl, median (range)	*N* = 280	12.5 (2.9–20.6)	12.9 (7.3–20.6)	12.7 (7.3–15.7)	13.15 (9.3–20.6)	13.2 (9.3–20.6)	13 (9.6–16.1)	10.1 (2.9–15.9)	8.85 (2.9–15.7)	10.4 (6.7–15.9)	10.55 (6.7–15.9)	12 (9.6–13.1)	**< 0.0001**	**< 0.0001**	0.2301	0.6413	**0.0255**	0.2132
Leukocytes, $\times 10^9$/l, median (range)	*N* = 265	6.81 (0–35.5)	7 (0–17.28)	6.93 (0–17.28)	7.1 (1.06–15.9)	7.345 (1.06–13.8)	7.325 (1.54–15.9)	5.2 (0.18–35.5)	1.995 (0.18–25.72)	6.655 (0.6–35.5)	6.25 (0.6–35.5)	4.645 (2.27–9.22)	**< 0.0001**	**0.0027**	0.1605	0.9707	**0.0002**	0.6835
Platelets, $\times 10^9$/l, median (range)	*N* = 337	684 (8–3152)	724 (198–2500)	563.5 (198–1659)	785 (315–2500)	731 (315–2500)	865 (411–1775)	237 (10–3152)	108.5 (10–2623)	389 (40–3152)	389 (40–3152)	683 (211–826)	**< 0.0001**	**< 0.0001**	**< 0.0001**	**0.04**	**< 0.0001**	0.1675
Hemoglobin < 10 g/dl, *n* (%)		38 (13.6)	10 (4.6)	6 (7.6)	4 (2.9)	2 (2.5)	2 (4.1)	20 (42.6)	9 (64.3)	11 (33.3)	5 (22.7)	1 (25)	**< 0.0001**	**< 0.0001**	**0.1753**	0.6368	**0.0617**	1.0000
Leukocytes > 10×10^9/l, n (%)		39 (15.1)	25 (12.5)	11 (14.1)	14 (11.7)	7 (10.1)	5 (12.2)	12 (24)	3 (16.7)	9 (28.1)	9 (42.9)	5 (125)	0.3188	0.0769	0.8328	0.7798	0.4973	0.5494
Platelets, > 450×10^9/l, *n* (%)		257 (79.1)	234 (90.3)	70 (79.5)	162 (95.9)	87 (94.6)	58 (96.7)	19 (35.8)	2 (11.1)	17 (48.6)	11 (47.8)	3 (60)	**< 0.0001**	**< 0.0001**	**< 0.0001**	0.4737	**0.0077**	1.0000
Platelets, < 100×10^9/l, *n* (%)		17 (5)	0 (0)	0 (0)	0 (0)	0 (0)	0 (0)	12 (15,2)	9 (11,4)	3 (3,8)	3 (8,6)	0 (0)	ns					
Follow-up, months, median (range)	*N* = 415	69 (0–528)	72 (2–360)	84 (3–348)	72 (2–360)	72 (2–348)	72 (2–360)	60 (4–528)	48 (4–132)	90 (12–528)	84 (12–528)	54 (12–300)	ns					

Abreviations: CALR, calreticulin; ET, essential thrombocytemia; MF, myelofibrosis; ns, nonsignificant. Significant *P*-values < 0.05 are indicated in bold.

the clinical management of *CALR*-mutated patients according to the mutation type.

Future studies will be important to determine the quantitative or qualitative differences in signaling between type 1 and type 2 *CALR* mutations, which could be the basis for these phenotypic differences. In addition, according to a recent publication, triple-negative ET are also associated to a JAK/STAT signature.[14] Therefore it will be important to find the rare signaling mutations responsible for these disorders.

CONFLICT OF INTEREST

The authors declare no conflict of interest.

ACKNOWLEDGEMENTS

We thank F Fava, C Legrand, I Teyssandier, F Lorre, R Tang and Laboratoire Commun de Biologie et Génétique Moléculaires, AP-HP, hôpital Saint-Antoine, Drs D Carp, J Dewulf, S Frederic, L Heuberger, I Leduc, F Lefrere, E Legac, E Ronez, J Roussi, C Salanoubat, J-L Vaerman, M Van Butsel, MD Venon, Professor D Latinne and Professor O Legrand for molecular and clinical biology support. This work was supported by grants from la Ligue contre le Cancer (XC, IP, ES WV and OB, équipe labellisée 2012), from the Agence Nationale de la Recherche (IP, WV ANR Thrombocytosis and GERMPN) and the Laurette Fugain association (WV). XC and OB are supported respectively by grants from the University Paris Diderot and from the ANR. We are grateful for generous support to S.N.C. from the F.R.S.-F.N.R.S., Belgium, the Salus Sanguinis Foundation, the Action de Recherche Concertée ARC10/15-027, the Fondation contre le Cancer, Brussels, and the PAI Program Belgian Medical Genetics Initiative Project P7/43 (BeMG) IAP, Belgium.

X Cabagnols[1,2,3], JP Defour[4,5,6], V Ugo[7,8,9], JC Ianotto[7], P Mossuz[10], J Mondet[10], F Girodon[11,12], JH Alexandre[11], O Mansier[13], JF Viallard[14], E Lippert[13], A Murati[15], MJ Mozziconacci[15], P Saussoy[6], MC Vekemans[16], L Knoops[5], F Pasquier[1,2,3], V Ribrag[1,2,3], E Solary[1,2,3], I Plo[1,2,3], SN Constantinescu[4,5], N Casadevall[1,2,17], W Vainchenker[1,2,3], C Marzac[17,18,19,20] and O Bluteau[1,2,3,20]

[1]UMR 1009 INSERM, Laboratory of Excellence GR-Ex, Villejuif, France;
[2]Gustave Roussy, UMR 1009, Villejuif, France;
[3]Université Paris-Sud, UMR 1009, Villejuif, France;
[4]Ludwig Institute for Cancer Research, Brussels, Belgium;
[5]de Duve Institute, Université catholique de Louvain, Brussels, Belgium;
[6]Department of Clinical Biology, Cliniques universitaires St Luc, Brussels, Belgium;
[7]CHU de Brest, Laboratoire d'Hématologie, Brest, France;
[8]Université de Brest, Faculté de Médecine, Université Européenne de Bretagne, Brest, France;
[9]INSERM U1078, Brest, France;
[10]UMR 5525 CNRS- équipe TheRex, Université Joseph Fourier-Grenoble-1 Grenoble, France;
[11]Laboratoire d'Hématologie, CHU de Dijon, Dijon, France;
[12]INSERM U866, Faculté de Médecine, Dijon, France;
[13]Laboratoire d'Hématologie, CHU de Bordeaux et Laboratoire Hématopoïèse Leucémique et Cibles Thérapeutiques, INSERM U1035, Université de Bordeaux, Bordeaux, France;
[14]Service de Médecine Interne et Maladies Infectieuses, Hôpital Haut-Lévêque, CHU de Bordeaux, Bordeaux, France;
[15]Département de Biopathologie et d'Oncologie Moléculaire, Institut Paoli-Calmettes, Marseille, France;
[16]Department of Hematology, Cliniques universitaires St Luc, Brussels, Belgium;
[17]AP-HP, Hôpital Saint-Antoine, Laboratoire d'Hématologie, Paris, France;
[18]Sorbonne Universités, UPMC Univ Paris 06, GRC n°07, Groupe de Recherche Clinique sur les Myéloprolifératives Aiguës et Chroniques MyPAC, Paris, France and
[19]INSERM, UMR_S 938, CDR Saint-Antoine, Paris, France
E-mail: christophe.marzac@sat.aphp.fr
[20]These authors contributed equally to this work.

REFERENCES

1 Klampfl T, Gisslinger H, Harutyunyan AS, Nivarthi H, Rumi E, Milosevic JD *et al.* Somatic mutations of calreticulin in myeloproliferative neoplasms. *N Engl J Med* 2013; **369**: 2379–2390.
2 Nangalia J, Massie CE, Baxter EJ, Nice FL, Gundem G, Wedge DC *et al.* Somatic CALR mutations in myeloproliferative neoplasms with nonmutated JAK2. *N Engl J Med* 2013; **369**: 2391–2405.
3 Levine RL, Gilliland DG. Myeloproliferative disorders. *Blood* 2008; **112**: 2190–2198.
4 Campbell PJ, Scott LM, Buck G, Wheatley K, East CL, Marsden JT *et al.* Definition of subtypes of essential thrombocythaemia and relation to polycythaemia vera based on JAK2 V617F mutation status: a prospective study. *Lancet* 2005; **366**: 1945–1953.
5 Beer PA, Campbell PJ, Scott LM, Bench AJ, Erber WN, Bareford D *et al.* MPL mutations in myeloproliferative disorders: analysis of the PT-1 cohort. *Blood* 2008; **112**: 141–149.
6 James C, Ugo V, Le Couedic JP, Staerk J, Delhommeau F, Lacout C *et al.* A unique clonal JAK2 mutation leading to constitutive signalling causes polycythaemia vera. *Nature* 2005; **434**: 1144–1148.
7 Baxter EJ, Scott LM, Campbell PJ, East C, Fourouclas N, Swanton S *et al.* Acquired mutation of the tyrosine kinase JAK2 in human myeloproliferative disorders. *Lancet* 2005; **365**: 1054–1061.
8 Chi J, Nicolaou KA, Nicolaidou V. Calreticulin gene exon 9 frameshift mutations in patients with thrombocytosis. *Leukemia* 2013; **28**: 1152–1154.
9 Lundberg P, Karow A, Nienhold R, Looser R, Hao-Shen H, Nissen I *et al.* Clonal evolution and clinical correlates of somatic mutations in myeloproliferative neoplasms. *Blood* 2014; **123**: 2220–2228.
10 Maffioli M, Genoni A, Caramazza D, Mora B, Bussini A, Merli M *et al.* Looking for CALR mutations in familial myeloproliferative neoplasms. *Leukemia* 2014; **28**: 1357–1360.
11 Rumi E, Harutyunyan AS, Pietra D, Milosevic JD, Casetti IC, Bellini M *et al.* CALR exon 9 mutations are somatically acquired events in familial cases of essential thrombocythemia or primary myelofibrosis. *Blood* 2014; **123**: 2416–2419.
12 Tefferi A, Lasho TL, Finke CM, Knudson RA, Ketterling R, Hanson CH *et al.* CALR vs JAK2 vs MPL-mutated or triple-negative myelofibrosis: clinical, cytogenetic and molecular comparisons. *Leukemia* 2014; **28**: 1472–1477.
13 Tefferi A, Wassie EA, Guglielmelli P, Gangat N, Belachew AA, Lasho TL *et al.* Type 1 vs type 2 calreticulin mutations in essential thrombocythemia: a collaborative study of 1027 patients. *Am J Hematol* 2014; **89**: E121–E124.
14 Rampal R, Al-Shahrour F, Abdel-Wahab O, Patel J, Brunel JP, Mermel CH *et al.* Integrated genomic analysis illustrates the central role of JAK-STAT pathway activation in myeloproliferative neoplasm pathogenesis. *Blood* 2014; **123**: e123–e133.

Supplementary Information accompanies this paper on the Leukemia website (http://www.nature.com/leu)

© 2015

VII.5. Presence of atypical thrombopoietin receptor (MPL) mutations in triple negative Essential Thrombocythemia Patients

Proof Only

MYELOID NEOPLASIA

Q:A1

Presence of atypical thrombopoietin receptor (MPL) mutations in triple-negative essential thrombocythemia patients

Xénia Cabagnols,[1-3,*] Fabrizia Favale,[1-3,*] Florence Pasquier,[1-3,*] Kahia Messaoudi,[1-3] Jean Philippe Defour,[4,5] Jean Christophe Ianotto,[6] Christophe Marzac,[7] Jean Pierre Le Couédic,[1-3] Nathalie Droin,[1-3] Ilyas Chachoua,[4,5] Remi Favier,[1-3] M'boyba Khadija Diop,[1-3] Valérie Ugo,[8] Nicole Casadevall,[1-3,7] Najet Debili,[1-3] Hana Raslova,[1-3] Christine Bellanne-Chantelot,[1-3,9] Stefan N. Constantinescu,[4,5] Olivier Bluteau,[1-3] Isabelle Plo,[1-3,†]
Q:1 and William Vainchenker[1-3,10,†]
Q:2
Q:3 [1]INSERM, Unité Mixte de Recherche (UMR) 1170, Gustave Roussy, Villejuif, France; [2]Université Paris-Sud, UMR1170, Gustave Roussy, Villejuif, France;
Q:4 [3]Gustave Roussy, Villejuif, France; [4]de Duve Institute, Université Catholique de Louvain, Brussels, Belgium; [5]Ludwig Institute for Cancer Research, Brussels, Belgium; [6]Service d'Hématologie, Centre Hospitalier Universitaire (CHU) Brest, Brest, France; [7]Laboratoire d'Hématologie, Hôpital Saint Antoine, Assistance Publique-Hôpitaux de Paris, Paris, France; [8]Laboratoire d'Hématologie, CHU Brest, Brest, France; [9]Département de Génétique, Hôpital Pitié-Salpêtrière, Université Pierre et Marie Curie, Assistance Publique-Hôpitaux de Paris, Paris, France; and [10]Consultation d'Hématologie-Immunologie, Hôpital Saint Louis, Assistance Publique-Hôpitaux de Paris, Paris, France

Key Points

- Enrichment of atypical MPL mutations in essential thrombocythemia.
- *MPLS204P* and *MPLY591N* mutants are weak gain-of-function mutants.

Q:5

Mutations in signaling molecules of the cytokine receptor axis play a central role in myeloproliferative neoplasm (MPN) pathogenesis. Polycythemia vera is mainly related to *JAK2* mutations, whereas a wider mutational spectrum is detected in essential thrombocythemia (ET) with mutations in *JAK2*, the thrombopoietin (TPO) receptor (*MPL*), and the calreticulin (*CALR*) genes. Here, we studied the mutational profile of 17 ET patients negative for *JAK2V617F*, *MPLW515K/L*, and *CALR* mutations, using whole-exome sequencing and next-generation sequencing (NGS) targeted on *JAK2* and *MPL*. We found several signaling mutations including *JAK2V617F* at very low allele frequency, 1 homozygous *SH2B3* mutation, 1 *MPLS505N*, 1 *MPLW515R*, and 2 *MPLS204*P mutations. In the remaining patients, 4 presented a clonal and 7 a polyclonal hematopoiesis, suggesting that certain triple-negative ETs are not MPNs.
Q:6 **NGS on 26 additional triple-negative ETs detected only 1 *MPLY591N* mutation. Functional studies on MPLS204P and MPLY591N**
Q:7 **revealed that they are weak gain-of-function mutants increasing MPL signaling and conferring either TPO hypersensitivity or independence to expressing cells, but with a low efficiency. Further studies should be performed to precisely determine the frequency of *MPLS204* and *MPLY591* mutants in a bigger cohort of MPN. (*Blood*. 2015;00(00):1-10)**

Introduction

According to the World Health Organization (WHO) classification, essential thrombocythemia (ET), polycythemia vera, and primary myelofibrosis (PMF) belong to the classical non-BCR-ABL1 myeloproliferative neoplasms (MPNs).[1,2] All of the non-BCR-ABL1 MPNs
Q:8 are associated with persistent and hyperactivation of the Janus kinase 2 (JAK2)/signal transducer and activator of transcription (STAT) signaling pathway, but ET and PMF are heterogeneous disorders. *JAK2V617F* is the predominant mutation found in 50% to 60% of the
Q:9 ET cases.[3] Other signaling molecules are mutated in ET including MPL and SH2B3 (LNK). The most prevalent *MPL* mutations in ET and PMF occur on tryptophan 515, an amino acid that maintains MPL in an inactive form in the absence of cytokine. The most frequent mutations are the substitution of W515 to L and K found in 3% to 5% of ETs and PMFs. Of note, it is the loss of tryptophan, but not the acquisition of a particular residue, that induces constitutive activation of MPL,[4] leading to the MPN phenotype. Less frequently, the S505N mutation located in the exon 10 coding for the transmembrane domain induces a dimerization of the transmembrane helix in an active conformation.[5] This last mutation has been initially found not only in some hereditary thrombocytosis,[6] but it has also been detected in rare sporadic ETs and PMFs.[7,8] In addition, other MPL mutants have already been described, more particularly in the extracellular domain of MPL in very rare ETs and PMFs, but without providing evidence for a gain-of-function.[8-12] *SH2B3* loss-of-function mutations are present in $<1\%$ of ET and PMF, but may not be sufficient to induce a MPN.[13,14]

Recurrent mutations in the exon 9 of calreticulin (*CALR*) have been recently found in around 25% of ETs and PMFs. They all induce a frameshift leading to a new C-terminus peptide composed of at least 35 aa with loss of the endoplasmic reticulum (ER) retention signal, KDEL.[15,16] Whereas wild-type (WT) CALR is essentially involved in the quality control of proteins and in calcium storage in the ER,[17] the CALR mutants are able to activate the JAK2/STAT pathway via an

Submitted July 31, 2015; accepted September 24, 2015. Prepublished online as *Blood* First Edition paper, October 8, 2015; DOI 10.1182/blood-2015-07-661983.

*X.C., F.F., and F.P. contributed equally.

†I.P. and W.V. contributed equally.

The online version of this article contains a data supplement.

The publication costs of this article were defrayed in part by page charge payment. Therefore, and solely to indicate this fact, this article is hereby marked "advertisement" in accordance with 18 USC section 1734.

© 2015 by The American Society of Hematology

Proof Only

Proof Only

unknown mechanism like the other MPN driver mutations.[15] The same signaling mutations are found in ETs and PMFs, underscoring they have a close pathogenesis requiring MK hyperplasia although they are clinically different diseases.[15,16]

Presently, the ETs and PMFs, which are negative for *JAK2V617F*, *CALR*, and *MPL* mutations are called "triple-negative" MPNs.[1] However, the entire sequence of MPL is not usually examined in patients. Depending on the particular clinical centers, there is a wide variety of MPL mutations that are screened (MPLW515K/L or all substitutions of W515 or mutations on exon 10 including MPLS505N). Usually, only MPLW515K/L are searched by allele-specific polymerase chain reaction (PCR). Whereas the triple-negative PMF have a poor prognosis,[18,19] triple-negative ETs have a good prognosis. However, it is presently unknown whether these triple-negative MPNs are a homogeneous entity.

In this study, we have investigated, using whole-exome sequencing (WES), the mutational profile of 17 triple-negative ET patients previously identified as negative for *JAK2*, *MPL*, and *CALR* mutations. This group was heterogeneous with 7 cases that did not display any clonal mutations. In the other cases, there was enrichment in *SH2B3* and atypical *MPL* mutations located in the exons 10 and 4 (*MPLS204P*). NGS targeted on *MPL* and *JAK2* exons in 5 of these patients and 26 additional patients led to the discovery of a second MPLS204P mutation not seen in WES and another atypical *MPL* mutation (MPLY591N). Sensitive functional studies revealed that both were low gain-of-function mutants. Our results demonstrate that some clonal noncanonical *MPL* gain-of-function mutations are associated with triple-negative ETs.

Material and methods

Patient cohort

Blood samples were obtained from Saint Louis Hospital and Saint Antoine Hospital (Paris, France) and Brest Centre Hospitalier Universitaire (CHU) and approved by the local ethics committees. Written informed consent was in accordance with the Declaration of Helsinki. For most of the patients, the diagnosis was performed according to the WHO recommendation including a bone marrow biopsy.[20,21] *MPLW515K/L* and *JAK2V617F* genotyping were performed by allele-specific quantitative PCR.[22,23] The mutational status of *CALR* was determined using previously described high-resolution sizing of fluorescent dye-labeled PCR amplification of exon 9 and Sanger sequencing for validation.[24] Plasma thrombopoietin (TPO) levels were measured by enzyme-linked immunosorbent assay (ELISA) according to the manufacturer's instructions (R&D Systems).

CGH arrays

Comparative genomic hybridization (CGH) arrays from granulocytes were conducted on human CGH 2x400K (G4448A) by hybridization of sample vs normal-matched commercial reference and a hierarchical clustering was performed.[25]

Whole-exome sequencing

WES was performed on genomic DNA (1 μg) from paired samples (granulocytes vs T cells) The final libraries were indexed, pooled, and sequenced on an Illumina HiSeq-2000 sequencer. Only nonsynonymous and splice-site mutations were further pursued. A special analysis using BWA ALN for mapping and GATK HaplotyCaller allowed us to detect insertions and deletions. Candidate mutations observed in the exon sequencing were validated using Sanger sequencing.[15,16,26]

MPL and JAK2 gene sequencing

Ion AmpliSeq custom panel primer pools for *MPL* and *JAK2* were used (10 ng of genomic DNA per primer pool) to perform multiplex PCR but the protocol to generate libraries was modified by adding paired-end adaptors (NEXTflex; Bio Scientific) to sequence in an Illumina MiSeq flow cell using the onboard cluster method, as paired-end sequencing (2 × 250 bp reads) (Illumina). The entire *MPL* and *JAK2* exons were sequenced to reach a 1000× depth. Minimum variant frequency was set at 1%. Sanger sequencing of the $CD3^+$ DNA assessed the somatic status of the mutation.

Cell lines and cell culture

The cytokine-dependent (granulocyte macrophage colony-stimulating factor [GM-CSF]) human UT7 cell line was cultured in α medium 10% stromal vascular fraction (SVF) and 5 ng/mL GM-CSF. This UT7 cell line did not express MPL and did not respond to TPO. Interleukin-3 (IL-3)-dependent murine pro-B Ba/F3 cells were cultured in Dulbecco medium with 10% SVF and 5% WEHI.

DNA manipulations, production of retroviruses

The 1531T>A (Y591N), 610T>C (S204P) point mutations were introduced into the MEGIX-human MPL-IRES-GFP plasmid by the site-directed mutagenesis method using the PfuUltra high-fidelity DNA polymerase (Stratagene; Agilent Technologies). Vesicular stomatitis virus glycoprotein pseudotyped viral particles were produced into 293EBNA cells as previously described.[27]

Flow cytometry

Cells were labeled with a monoclonal anti-hemagglutinin (HA) antibody conjugated to phycoerythrin (PE) or an isotype control. Allophycocyanin-Annexin V staining was performed according to the manufacturer's recommendations (Becton Dickinson). For cell cycle analysis, cells were treated with lysis buffer (sodium acetate with Triton X-100), RNAse, and labeled with propidium iodide for 30 minutes. Cells were analyzed on a LSR2 flow cytometer (Becton Dickinson). Data were analyzed with Flow Jo software.

Confocal microscopy

Cells (100 000) were plated on polylysine slides, fixed with 4% paraformaldehyde for 10 minutes, permeabilized with 0.2% Triton. Primary monoclonal antibodies against GM130 and CALR (Abcam) and HA (Covance; Eurogenec) were incubated in bovine serum albumin 0.2% solution for 1 hour followed by secondary goat anti-mouse (Alexa 546) or anti-rabbit (Alexa 633) antibodies (Life Technologies). 4,6 Diamidino-2-phenylindole was used to label nuclei. Cells were analyzed using a confocal Leica microscope.

Western blotting

Signaling studies were performed on UT7 and Ba/F3 cell lines by western blot analysis of JAK2 (Tyr 1007/1008), STAT1 (Tyr 701), STAT3 (Tyr 705), STAT5 (Tyr 694), extracellular signal-regulated kinase 1/2 (ERK1/2; Thr 202/Tyr 204), and AKT (Thr 308) and of these different pan proteins (Cell Signaling Technology [Ozyme]). HSC70 (Stressgen) or β-actin (Sigma) serves as loading control.

STAT5 reporter assay

γ2A JAK2-deficient cells[28] were transfected with complementary DNA (cDNA) coding for MPL or MPL mutants, STAT5, JAK2, Spi-Luc (STAT5 transcriptional reporter), and pRL-TK.[29,30] After 5 hours, the cells were stimulated with 10 ng/mL human TPO. Cells were lysed from 24 hours to 48 hours later and the luciferase activity was measured, as described.[4]

Cell proliferation

Thirty thousand cells per mL were seeded in a 96-well plate with TPO or GM-CSF at various concentrations. Cell proliferation was quantified 3 days later using a WST-1 assay (Takara [Ozyme]).[31] Experiments were done in triplicate. Dose-response curves to TPO were expressed as a percentage of viability of the maximal response.

Colony formation assay

Twenty cells per well were sorted in a 96-well plate. For each condition, we filled 1 plate with GM-CSF at 5 ng/mL and 8 plates without cytokine. After 3 days,

Proof Only

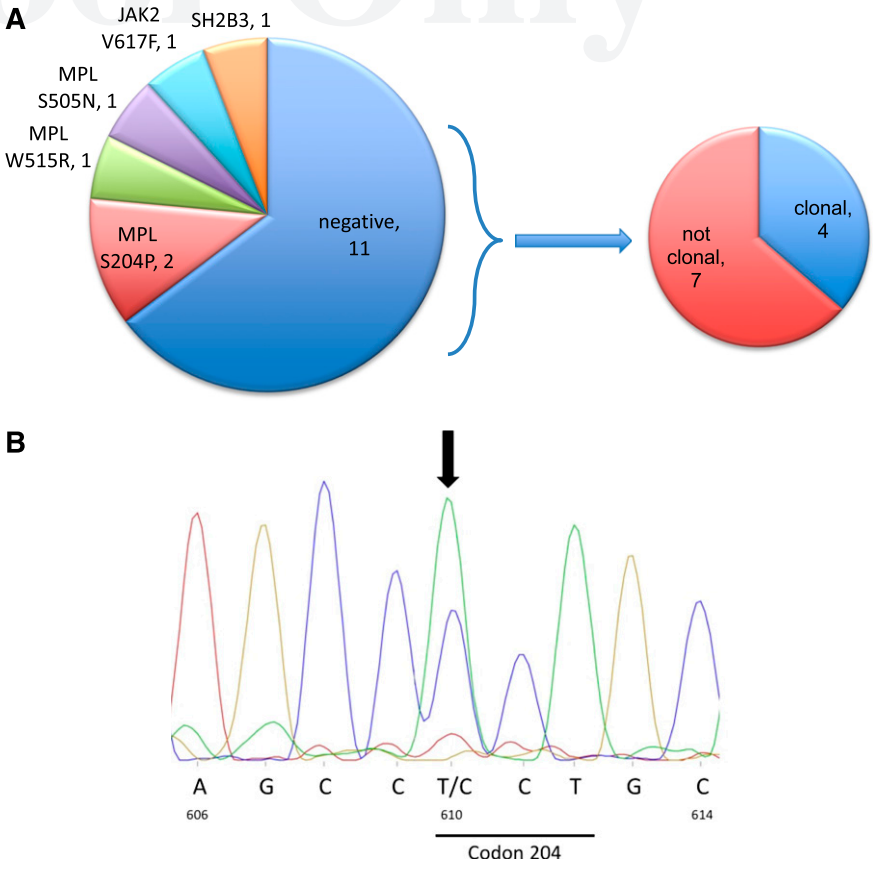


Figure 1. Genomic analysis. (A) A schematic representation of the signaling mutations in the 17 patients and of the type of hematopoiesis in triple-negative ETs. We consider as polyclonal ETs the patients that exhibit no mutation (driver or passenger) in WES. (B) Sanger sequencing of MPLS204P. Nucleotides and amino acid numbers are indicated.

5 ng/mL GM-CSF or 10 ng/mL TPO were added to perform rescue experiments in half of the plates grown without cytokine. Colony formation was counted at day 8. Each experiment was repeated 3 times, but the TPO addition was performed in only 1 experiment.

Results

WES and overview of genetic alterations

We studied 17 patients diagnosed as triple-negative ETs namely negative for any *JAK2V617F*, *MPLW515K/L*, and *CALR* exon 9 mutations. We performed WES on paired granulocyte and T-cell samples that were considered as the tumoral and control cells, respectively. The sequencing coverage mean was 110× and 75% of the target sequences could be analyzed with a coverage above 15×. All candidate mutations with a $P < .05$ generated by the bioinformatics analysis were verified by Sanger sequencing.

Sanger sequencing confirmed 22 missense, 4 nonsense and 2 splice mutations, and 3 frame-shifting indels, leading to a total of 31 mutations of 80 candidates. The mutation rate per sample was low (1.82), even in comparison with other myeloid malignancies (supplemental Table 1, see supplemental Data available at the *Blood* Web site). Furthermore, CGH arrays performed on 5 samples were normal.

In a first analysis, 3 patients displayed previously described *MPL* mutations, including 2 in exon 10 (*MPLW515R* and *MPLS505N*) and Q:14 1 in exon 4 (*MPLS204P*) (Figure 1B). A homozygous nonsense mutation in the *SH2B3* gene was identified in 1 patient. The unexpected identification of known *MPL* mutations led us to perform deep resequencing of all *MPL* and *JAK2* exons, resulting in the detection of *JAK2V617F* in 1 patient and again a *MPLS204P* mutation in another patient (Figure 1; supplemental Table 2). These mutations were not Q:15 seen in WES because of low allelic burden for the *JAK2* mutation (<5%) and low depth of coverage at this position for the *MPLS204P*.

No signaling mutations were identified in the remaining 11 ET patients (Figure 1A). We divided them into clonal and nonclonal disorders, as performed in several previous studies.[32-35] Four of them showed a clonal hematopoiesis in granulocytes based on the presence of nonrecurrent mutations of unknown function. Seven patients had no detectable clonal mutations, suggesting the presence of a polyclonal hematopoiesis in granulocytes. Neither *CALR* exon 9 mutations nor *JAK2V617F* could be detected in their platelets (data not shown).

It is noteworthy that the 2 *MPLS204P*-positive samples were associated with other mutations: 1 displayed 3 other mutations, including another driver mutation *ASXL1*, and the second presented 5 mutations different from known MPN driver mutations, but with a mutation of the RNA helicase *HELZ*, which may play a role in oncogenesis (Table 1). The patient identified with an acquired Q:16 *MPLS505N* mutation (absent in T cells) also exhibited a mutation in *SRSF2* with a higher variant allele frequency (VAF), suggesting that *MPLS505N* was a secondary event (Table 1). Of interest, this case presented some myelodysplatic features detected by pathology associated with a slight increase in blast count in a bone marrow aspirate. This patient was reclassified as a myelodysplastic syndrome (MDS) with a thrombocytosis rather than as a true ET patient. Finally, there was a case exhibiting both homozygous nonsense *SH2B3* and *SF3B1* mutations (Table 1) without any noticeable increase in ring sideroblasts or sign of MDS at bone marrow aspiration, thus eliminating a RARS-T. Q:17

Taken together, these data indicated that atypical *MPL* mutations seem to be recurrent in the so-called triple-negative ET. Next-generation sequencing (NGS) targeted on *MPL* and on *JAK2* was

Proof Only

Table 1. Mutational profile in granulocytes from 10 ET patients by exome sequencing

Sample	Mutations					
3	SCNN1G (21.34)					
12	SHOC2 (22.22)	CASC5 (25.0)				
14	MPL S204P (19.26)*	ASXL1 (20.97)	EDA (41.18)			
21	KPNA1 (28.21)	VPS13D (39.29)	EEA1 (39.79)	SF3B1 (54.55)*	SH2B3 (98.33)*	
24	FUBP1 (23.88)	PPP1R37 (30.77)	COMP (36.14)	ADCY5 (36.67)	HELZ (37.25)	MPL S204P (47.74)*
25	ATXN7L1 (21.95)					
32	LYZL2 (30.77)					
91	MPL S505N (23.02)*	DDI1 (24.18)	IMPG2 (24.24)	PPP2R5A (43.75)	SRSF2 (44.35)*	APOL4 (86.52)
92	JAK2 V617F (11.77)*	ALDH3A2 (28.12)				
98	MPL W515R (23.94)*					

The percentage of VAF is indicated in parentheses.
*■■■■■■.

performed on 31 patients including 5 ETs studied in WES and 26 additional less well-characterized ETs. Another mutation of *MPL* with a VAF of 9.28% was detected. This missense *MPL* mutation (c.1351T>A) leads to the substitution of a tyrosine by asparagine in the cytosolic domain (Y591N). We also detected a missense mutation in *JAK2* (N1108S) with a VAF of 50% in both the granulocytes and the T cells. Sequencing of hair DNA confirmed it was a germ-line mutation (supplemental Figure 1). The c.3323A>G has been reported as a rare polymorphism (0.36%). However, the 3-dimensional modeling of JAK2N1108S predicts that it may provide a slight gain-of-function based on a higher propensity of formation of a tighter hydrogen bond between S1108 and N1085, which is linked to the active state of JAK2 kinase domain (supplemental Figure 2).

Q:18

Functional analysis of the MPLS204P mutant

In 1 of the 2 *MPLS204P*-positive patients, we examined the TPO level that was in the normal range (12 pg/mL; normal, <30 pg/mL) and comparable to other ETs (range, 8.25-96.1 pg/mL). To study cell-surface localization of MPL, we transduced the human factor-dependent UT7 cell line with the HA-tagged MPLWT- and MPLS204P-expressing retrovirus (internal ribosomal entry site [IRES]-green fluorescent protein [GFP]). At similar GFP levels, the mean fluorescence intensity of HA labeling was comparable for both receptors using flow cytometry (Figure 2A). Expression of MPLS204P at the cell surface was further confirmed by western blotting. A 85-kDa endoglycosidase H (EndoH)-resistant band corresponding to the mature form of MPL was detected

Q:19

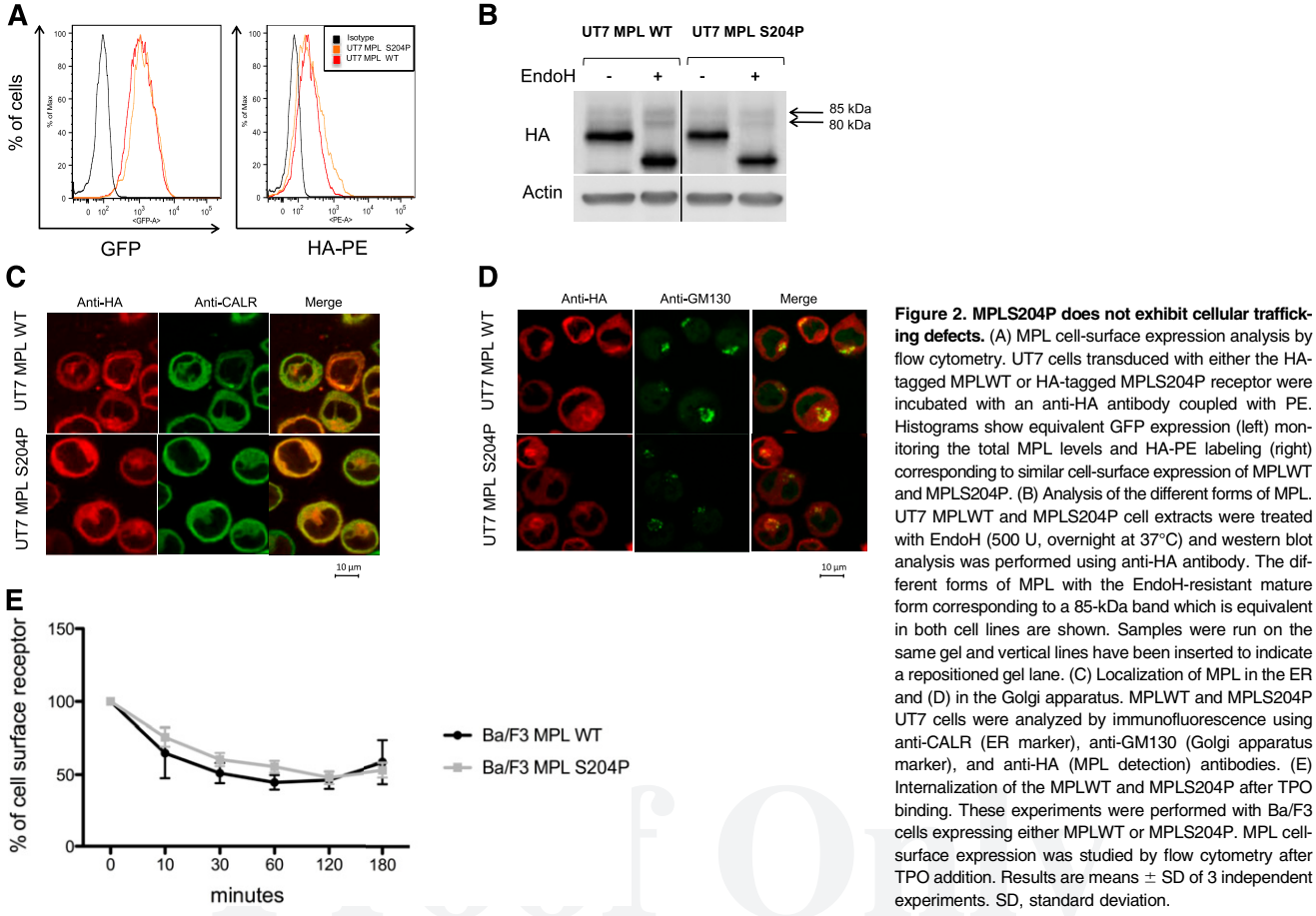


Figure 2. MPLS204P does not exhibit cellular trafficking defects. (A) MPL cell-surface expression analysis by flow cytometry. UT7 cells transduced with either the HA-tagged MPLWT or HA-tagged MPLS204P receptor were incubated with an anti-HA antibody coupled with PE. Histograms show equivalent GFP expression (left) monitoring the total MPL levels and HA-PE labeling (right) corresponding to similar cell-surface expression of MPLWT and MPLS204P. (B) Analysis of the different forms of MPL. UT7 MPLWT and MPLS204P cell extracts were treated with EndoH (500 U, overnight at 37°C) and western blot analysis was performed using anti-HA antibody. The different forms of MPL with the EndoH-resistant mature form corresponding to a 85-kDa band which is equivalent in both cell lines are shown. Samples were run on the same gel and vertical lines have been inserted to indicate a repositioned gel lane. (C) Localization of MPL in the ER and (D) in the Golgi apparatus. MPLWT and MPLS204P UT7 cells were analyzed by immunofluorescence using anti-CALR (ER marker), anti-GM130 (Golgi apparatus marker), and anti-HA (MPL detection) antibodies. (E) Internalization of the MPLWT and MPLS204P after TPO binding. These experiments were performed with Ba/F3 cells expressing either MPLWT or MPLS204P. MPL cell-surface expression was studied by flow cytometry after TPO addition. Results are means ± SD of 3 independent experiments. SD, standard deviation.

Q:28

Proof Only

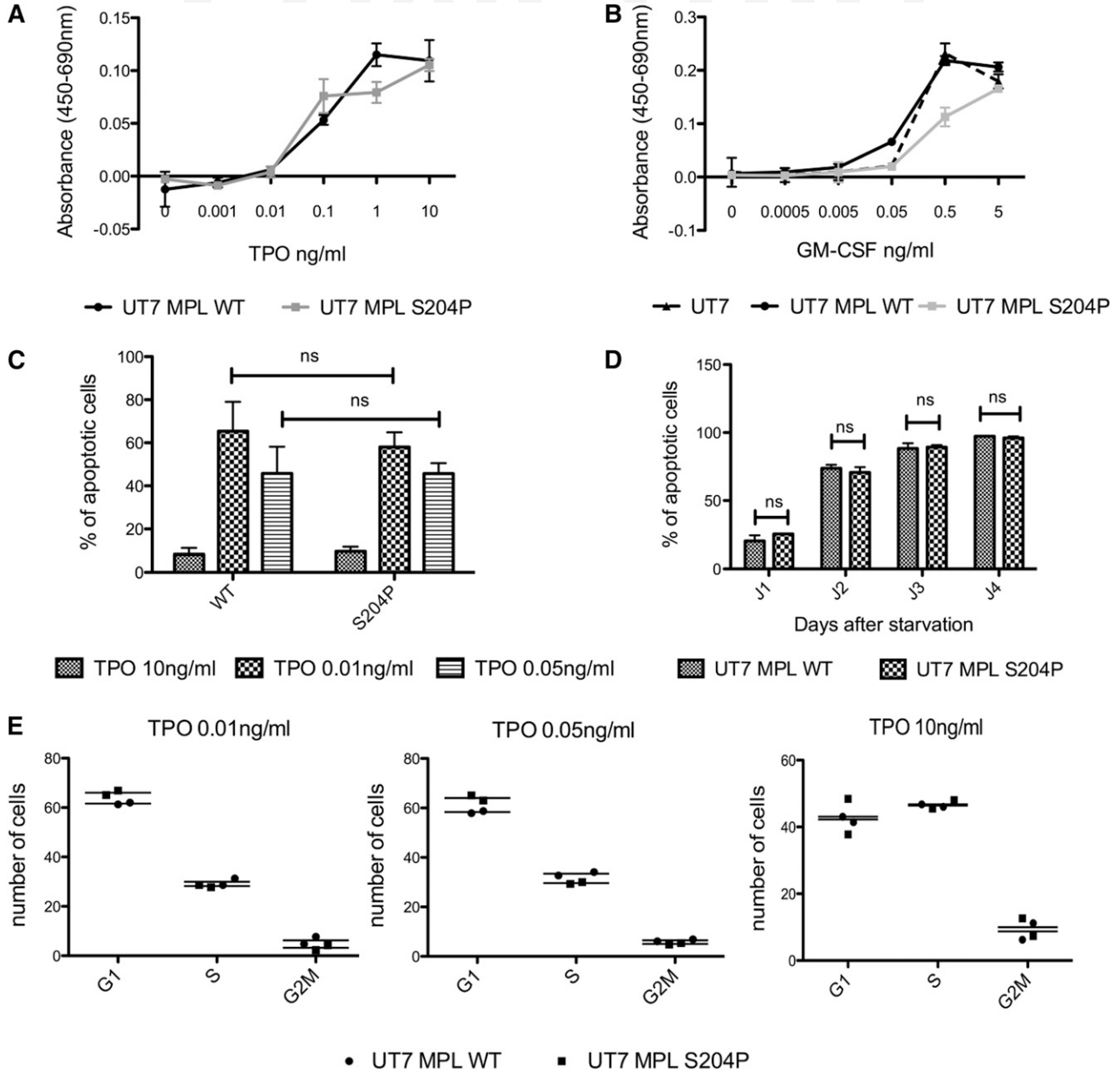


Figure 3. MPLS204P does not present proliferative advantage in bulky cultures. (A-B) Cell proliferation induced by TPO of MPLWT and MPLS204P UT7 cells. Cells were cultured in the presence of various concentrations of TPO (A) or GM-CSF (B) for 72 hours. Viable cells were quantified by WST-1 proliferation assay. Dose-response curves are means ± SEM (n = 3 in triplicate). (C-D) Apoptosis analysis in MPLWT and MPLS204P UT7 cells. (C) Cells were cultured for 2 days with various concentration of TPO (0.01, 0.05, and 10 ng/mL) and the percentage of apoptotic cells (Annexin V positive) was analyzed by flow cytometry using the Annexin V assay. (D) Cells were cultured for 24 hours with TPO (10 ng/mL) followed by overnight deprivation. The percentage of apoptotic cells (Annexin V-positive) was analyzed at different times after TPO removal (1, 2, 3, and 4 days). (E) Cell-cycle analysis of MPLWT and MPLS204P UT7 cells. Cells were cultured for 2 days with various concentrations of TPO (0.01, 0.05, and 10 ng/mL) and the percentage of cells in G1, S, and G2 phases were determined after propidium iodide labeling, by flow cytometry analysis. SEM, standard error of the mean.

Q:29

for MPLWT and MPLS204P (Figure 2B). The subcellular localization of the 2 receptors was examined by confocal microscopy. They had a similar localization in the ER (anti-CALR antibody) and Golgi (anti-GM130 antibody) compartments (Figure 2C-D). Finally, we studied the internalization of the receptors after TPO addition using the Ba/F3 cell line. No difference was observed between the MPLWT and MPLS204P (Figure 2E). Taken together, these results suggest that the thrombocytosis was not related to a defect in cell-surface localization of MPLS204P, which would have induced a loss of TPO clearance activity.

We studied the effects of MPLS204P on cell proliferation. MPLS204P did not induce cytokine-independent growth nor render cells hypersensitive to TPO or GM-CSF hypersensitivity (Figure 3A-B). In addition, we could not find any difference in apoptosis in the presence (Figure 3C) or absence (Figure 3D) of TPO or in cell cycle at different TPO doses (Figure 3E). No constitutive activation in STAT3, STAT5, and AKT was observed in UT7 cells expressing MPLS204P (Figure 4A). These results suggest that MPLS204P is a weak gain-of-function mutant. We further used a more sensitive technique to ask whether the MPLS204P was able to support TPO-independent JAK/STAT signaling like MPLW515K.[4] We used a luciferase reporter assay for STAT5 activation induced via MPL in the JAK2-deficient γ2A cells.[4] Expression of MPLS204P supported TPO-independent JAK2/STAT5 signaling, albeit to lower levels than MPLW515K (Figure 4B). Of interest,

Proof Only

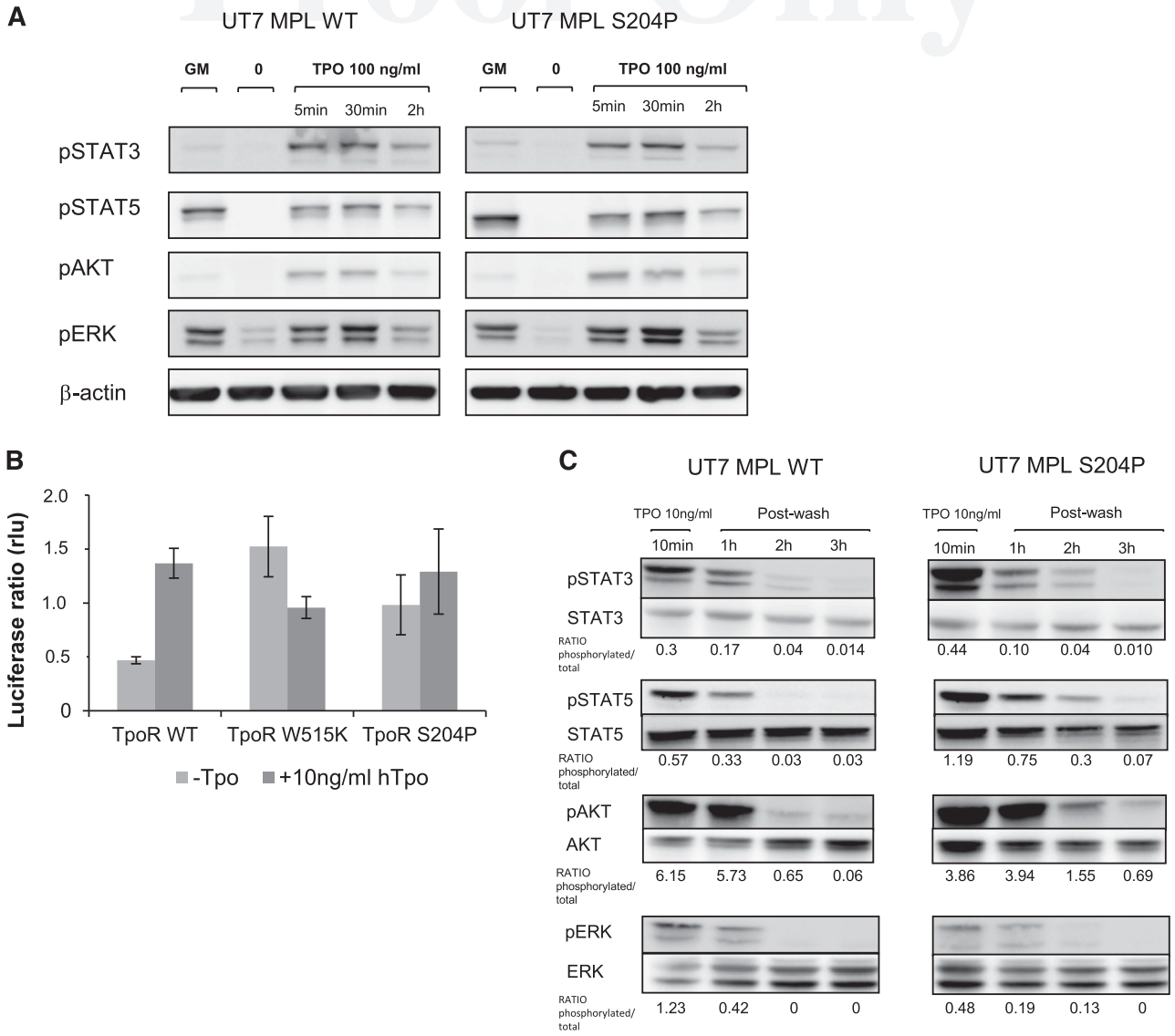


Figure 4. MPLS204P is a weak gain-of-function mutant. (A) Signaling studies induced by high TPO concentration in MPLWT and MPLS204P UT7 cells. After cytokine deprivation, cells were stimulated with TPO (100 ng/mL for 5 minutes, 30 minutes, or 2 hours). The phosphorylation status of STAT3, STAT5, AKT, and ERK1/2 was examined by western blotting and results were compared with cells stimulated by GM-CSF (5 ng/mL). (B) STAT5 transcriptional activity in γ2A JAK2-deficient cells expressing MPLWT or MPLS204P. Cells were transfected with cDNAs coding for MPLWT or MPLS204P, JAK2, STAT5, and with Firefly STAT5 luciferase reporter spi-Luc and pRL-TK vectors coding for renilla luciferase. Luminescence was measured after 48 hours' transfection. Shown are average units ± SEM of 1 representative experiment performed in triplicate of 3. (C) Persistent signaling in UT7 MPLS204P. UT7 MPLWT and UT7 MPLS204P were stimulated by TPO (10 ng/mL) for 10 minutes and subsequently washed. A 3-hour time course was performed followed with western blotting, as in previous figures. MPLWT and MPLS204P samples were run on the same gel. P-STAT5/STAT5 or P-ERK/ERK ratios are indicated after quantification by image J software.

although MPLW515K-induced JAK2/STAT5 activation was evident at 24 to 30 hours after transfection, a longer period was necessary for MPLS204P (>40 hours). This indicates that the MPLS204P mutant signals are weaker than those induced by MPLW515K.

Finally, we tested whether MPLS204P could induce prolonged signaling in UT7 cells. Cells were stimulated with 10 ng/mL TPO, subsequently washed, and then cultured without cytokine for 3 hours. A sustained phosphorylation of STAT5 and AKT was observed for the mutant cells (Figure 4C). To demonstrate that this weak constitutive activity exerts some biological consequence, a limiting dilution of MPLWT and MPLS204P UT7 cells (20 cells per well in a 96-well plate) were grown without cytokine for 1 week (Figure 5A). Autonomous growth numbered as colonies was observed with UT7 MPLS204P (5%-10%), but not with UT7 MPLWT, except in rare wells, suggesting that around 0.25% of UT7 cells became cytokine-independent due to MPLS204P. Furthermore, after 3 days of culture without cytokines, we added GM-CSF or TPO for rescue, and observed a twofold to fourfold increased cloning efficiency for UT7 MPLS204P compared with MPLWT (Figure 5B-C).

Altogether, these results demonstrate that MPLS204P is a gain-of-function mutant.

Functional analysis of the MPLY591N mutant

We conducted the functional analysis of another MPL mutant identified by NGS using Ba/F3 cells lines. Flow cytometry analysis showed that MPLY591N was addressed more efficiently (1.63- ± 0.07-fold) to the cell-surface membrane compared with MPLWT at similar GFP levels (Figure 6A), indicating either an increased trafficking of MPL mutant to cell surface or a decreased internalization. We measured the impact of

this mutant on cellular proliferation in response to TPO. MPLY591N conferred a fourfold to fivefold hypersensitivity to TPO compared with Q:20 MPLWT (50% inhibitory concentration of 0.10 ng/mL for WT and 0.02 ng/mL for Y591N), but without spontaneous growth in the absence of cytokine (Figure 6B).

We next verified the effect of the MPLY591N mutant on signaling in Ba/F3 cells by western blot analysis. Noticeably, these cells expressed similar levels of exogenous MPL. Interestingly, a constitutive phosphorylation of STAT3, STAT5, and ERK was observed in MPLY591N mutant cells compared with MPLWT cells. The TPO dose-dependent increase in the phosphorylation of these molecules was higher in presence of MPLY591N than MPLWT. No difference was observed on AKT or STAT1 phosphorylation (Figure 6C).

Altogether, these results show that MPLY591N is also a weak gain-of-function mutation that leads to TPO hypersensitivity without independent growth and to a partial spontaneous activation of signaling pathways.

Discussion

The goal of this work was to characterize the mutational genomic profile of triple-negative ETs using WES. Among the 17 triple-negative ETs, we considered that 7 had a polyclonal hematopoiesis in granulocytes as no mutation was detected by WES. This molecular approach has clear limitation because it cannot detect mutations in noncoding sequences and gene fusion and even more cannot detect mutations in coding sequences at low VAF. In this work, we defined clonal hematopoiesis as the presence of any somatic mutation either in a known driver of hematopoietic malignancies or in another gene (passenger mutation),[32-35] but without using X chromosome inactivation assays except in 2 cases where results were concordant. It has been calculated that each normal Q:21 HSC accumulates 0.13 mutation per year in coding sequences.[36] Thus, it was expected that in the case of clonal hematopoiesis in patients older Q:22 than 50 years of age, several mutations would be found. However, the technique has a sensitivity of around 10% for VAF. Thus, it seems likely that these "polyclonal" triple-negative thrombocytosis cases can be MPNs with a low VAF in granulocytes similar to *JAK2V617F* ET in which VAF is much higher in platelet RNA than in granulocyte DNA.[37] Therefore, it will be important in the future to directly perform WES or whole-genome sequencing on megakaryocytes or to sequence platelet RNA. Alternatively, some of these disorders can be other diseases than MPNs, more particularly hereditary thrombocytosis. In the companion article, germ-line gain-of-function mutations in *JAK2* and *MPL* were found in triple-negative ETs.[38] Hereditary thrombocytosis may arise without other familial cases if the patient is the founder. In 1 case, we detected a germ-line mutation in *JAK2* (N1108S) that appears in in silico modeling as a possible gain-of-function mutation, suggesting a hereditary thrombocytosis. However, this mutation has also been described as a rare polymorphism. Thus, we cannot exclude that rare JAK2 or MPL variants, which may be present in the general population, can induce a MPN disease in certain individuals.

The enrichment in previously described rare signaling mutations[9] was striking in triple-negative ETs. One was a homozygous nonsense mutation in *SH2B3*. Heterozygous *SH2B3* mutations were reported in MPNs and it is discussed whether by themselves they could give rise to a MPN.[14] In some cases, they are associated with *JAK2V617F*.[39] Here, the mutation is homozygous and because mice totally deficient in Sh2b3 develop a myeloproliferative disorder,[40] we can suggest that this homozygous mutation leading to an absence of LNK was really the driver of the MPN. Interestingly, a *SF3B1* mutation was associated with this homozygous *SH2B3* mutation, but the phenotype of the disease was an ET.

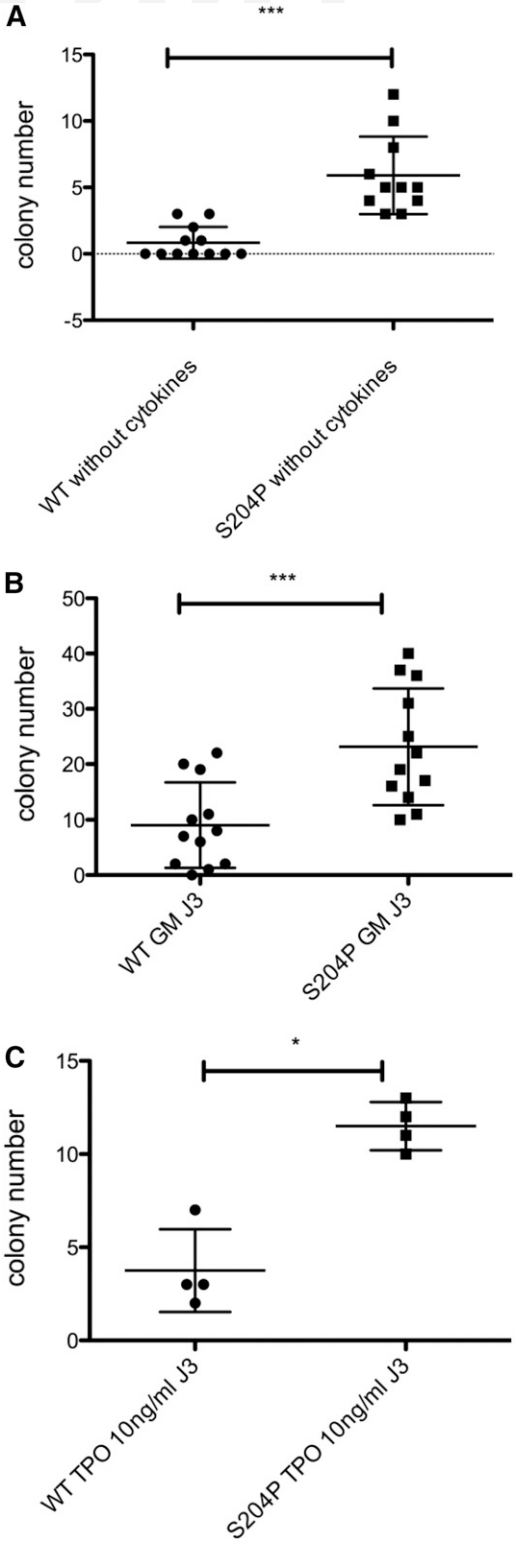


Figure 5. UT7 MPL S204P cells are less cytokine-dependent than UT7 MPL WT. (A) Growth of UT7 MPLS204P and UT7 MPLWT at limiting dilution without cytokines. Cells (20 per well) were cultured without cytokines in a 96-well plate. Colony growth was counted 1 week later. (B) Rescue experiments by GM-CSF. Cells (20 per well) were cultured without cytokines in a 96-well plate. After 3 days, GM-CSF (5 ng/mL) was added and colonies were counted 1 week later. (C) Rescue experiments by TPO. Cells (20 per well) were cultured without cytokines in a 96-well plate. After 3 days, TPO (10 ng/mL) was added and colonies were counted 1 week later. Results represent the means ± SD of the number of colonies/96-well plate. Each point corresponds to the number of clone in 1 plate.

Proof Only

Proof Only

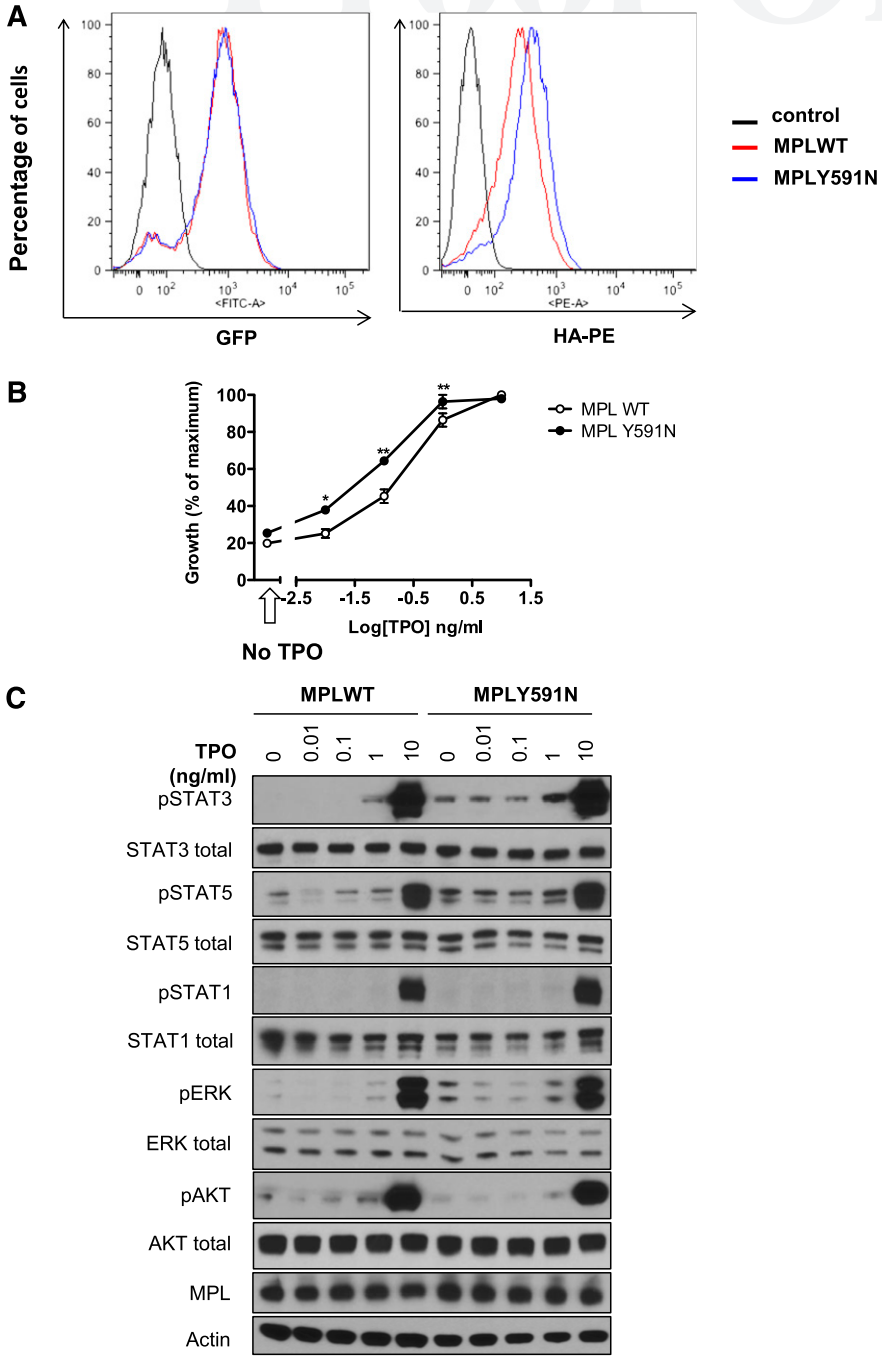


Figure 6. Analysis of the MPLY591N mutant. (A) MPL cell-surface localization in Ba/F3 cells. Ba/F3 cells expressing the bicistronic retroviral pMEGIX-IRES-GFP vector encoding HA-tagged MPLWT or MPLY591N and GFP were maintained in IL3-supplemented medium. Flow cytometry analysis was assessed and histograms show equivalent GFP expression (left) monitoring the total MPL levels and HA-PE labeling (right) corresponding to cell-surface expression of MPLWT and MPLY591N. (B) Sensitivity to TPO of Ba/F3 cells. Ba/F3-MPLWT or MPLY591N cells were cultured for 72 hours either in absence of cytokine (black arrow, x-axis) or in presence of increasing doses of TPO (0.01, 0.1, 1, and 10 ng/mL). Viable cells were quantified by WST-1 proliferation assay. Dose-response curves are means expressed in percentages of maximum growth value ± SEM (n = 3 in triplicate). Two-tailed *t* test; *< .05; **$P < .01$. (C) Signaling studies in Ba/F3-MPL cells. Ba/F3-MPLWT or MPLY591N cells were serum- and cytokine-starved for 6 hours prior to a 15-minute stimulation without or with TPO (0.01, 0.1, 1, and 10 ng/mL) as indicated. Cells were lysed and the phosphorylation status of STAT1, STAT3, STAT5, AKT, and ERK1/2 was examined by western blotting with the respective anti-phospho-specific antibodies, as indicated. MPL expression was also verified. Expression of β-actin in the samples was used as loading control and was consistent with expression of total AKT, ERK1/2, and the individual STAT isoforms. Blots shown were reproduced in 3 independent experiments.

Four mutations in *MPL* were found in the first series of patients, including *MPLS505N* and *MPLW515R* located in exon 10 that are not commonly screened. The latter were somatic mutations in our study although they can also be identified as germ-line mutations in hereditary thrombocytosis.[6,41]

In 2 other patients, we detected an acquired *MPLS204P* mutation. This mutation has been previously described in a myelofibrosis, and a S204F mutation was described in another myelofibrosis case.[10,12] In the companion article, S204P and S204F mutations were detected in 2 triple-negative patients.[38] It is interesting to note that mouse MPL residue 204 is a proline instead of a serine in human MPL, thus the S204P mutation restores the mouse MPL sequence into the human MPL. Moreover, the germ-line mutation K39N (MPL Baltimore) present in a heterozygous form in 7% of an African-American population also restores a mouse sequence and is associated with a thrombocytosis.[42] It is tempting to assume that differences between the human and mouse MPL sequences may contribute to the high platelet count in mice associated with an elevated plasma TPO level in comparison with the situation in humans. In the case of the K39N, there is evidence that the membrane expression level of the MPL mutant is lower than MPLWT and this can explain a thrombocytosis phenotype due to decreased TPO clearance activity of MPL, which is in great part related to the expression level of MPL on the surface of mature megakaryocyte and platelets.[42] This has been well demonstrated in 3 murine models.[43-45] Here, we clearly demonstrate that the thrombocytosis induced by MPLS204P is not due to a defect in cell trafficking of the receptor. In contrast, MPLS204P is a weak gain-of-function mutant in signaling, inducing constitutive STAT activation using sensitive approaches and

Proof Only

an increased and more prolonged ligand-induced STAT phosphorylation than MPLWT. Using limiting dilution techniques, it was possible to demonstrate that MPLS204P could induce cytokine-independent growth with low efficiency in around 1 of 400 UT7 cells. Furthermore, UT7 MPLS204P cells were more resistant than UT7 MPLWT cells to 3-day cytokine deprivation. The 2 cases with MPLS204P were associated with several other mutations: 1 with *ASXL1*, the second with a mutation in an RNA helicase implicated in proliferation. Thus, we suspect that these mutants with very low oncogenic potential would need to be associated to other drivers to give rise to a MPN.

Finally, we detected a MPLY591N mutant in 1 patient. MPLY591D has been previously described in a polycythemia vera patient in association with a heterozygous *JAK2V617F* mutation[10] as reported in the companion article. Here, we detected the MPLY591N in the absence of a *JAK2* mutation. This mutation was assumed to be a gain-of-function for 2 reasons. Previously, it was shown that this tyrosine also called 78 (intracellular tyrosine) is phosphorylated on the MPLW515A and that the double-mutant MPLW515A/Y591F induced a much more severe MPN in the mouse than the single MPLW515A mutant.[46] Furthermore, this tyrosine is also phosphorylated after TPO binding, and negatively regulates MPL signaling by promoting its internalization degradation as well as ERK signaling.[46-48] Asparagine is a polar residue in contrast to the negative charge represented by tyrosine phosphorylation and, thus, the Y591N mutation resembles a Y591 loss-of-function, like Y591F, but possibly weaker because unlike phenylalanine, asparagine is polar. When the Y591N mutant was expressed in Ba/F3 cells it induced a slight TPO hypersensitivity, which was associated with constitutive activation of STAT3 and ERK. In the *MPLY591N*-positive patient, we did not perform WES to assess whether other driver mutations were present, as for *MPLS204P*. However, this mutant was detected in a case of ET occurring in a familial form of MPN where we have recently identified the predisposition locus consisting of a 700-kb duplication involving 6 genes. The overexpression of 2 of them, *ATG2B* and *GSKIP*, induces TPO hypersensitivity and cooperates with *JAK2*, *MPL*, and *CALR* mutations to give an ET.[25] Thus, the predisposition locus could be the initiating event and the low gain-of-function MPLY591N could be sufficient to induce an overt ET.

Altogether, this study has shown that in a fraction of the so-called triple-negative ETs a significant proportion of patients have mutations in signaling molecules, more particularly in *MPL*. This group of patients appears heterogeneous including some with a polyclonal hematopoiesis as previously shown in pediatric ETs.[49] Further studies using WES and RNA sequencing will be required to better understand the pathogenesis of these ETs.

Acknowledgments

The authors thank E. Leroy for modeling JAK2N1108S and the bioinformatic platform of Gustave Roussy for analyzing the NGS experiments. The authors are grateful to P. Rameau for cell sorting experiments.

Support to S.N.C. is acknowledged from Ludwig Institute, Salus Sanguinis, Fondation Contre le Cancer, Fonds National de la Recherche Scientifique, Inter-University Attraction Pole and Action de Recherche Concertée Projects, Belgium. This work was supported by grants from the Agence Nationale pour la Recherche (Thrombocytosis [W.V.]), the Ligue Nationale contre le Cancer (Équipe Labellisée), the Fondation Laurette Fugain (W.V., I.P.), Agence Nationale pour la Recherche-Jeune Chercheur (I.P.), a specific grant from Gustave Roussy (Taxe d'Apprentissage) and from the INSERM. I.C. was supported by a FRIA fellowship. X.C. was supported by the University Paris-Diderot, F.F. by the INSERM (Poste d'Accueil), and F.P. by the Fondation Pour la Recherche Contre le Cancer. Q:23

Authorship

Contribution: W.V. and I.P. designed and performed research, analyzed data, prepared figures, and wrote the paper; X.C. performed and interpreted pangenomic analysis, prepared figures, and wrote the paper; F.F. and F.P. performed functional analysis, prepared figures, and wrote the paper; K.M. performed functional analysis and prepared figures; J.P.D. and I.C. performed luciferase assays; J.C.I., V.U., and N.C. were involved in the clinical part; R.F. performed the TPO ELISA assays; C.M. performed the CALR sizing and provided genotyped samples; J.P.L.C. and N.D. performed the WES; M.K.D. Q:24 did bioinformatics study of exome data; O.B. collected samples, performed the targeted NGS approach, and prepared figures; N.D., H.R., and S.N.C. gave experimental/intellectual input and corrected the manuscript; C.B.-C. provided samples, interpreted the NGS, and gave experimental/intellectual input; and all authors contributed to editing.

Conflict-of-interest disclosure: The authors declare no competing financial interests.

Correspondence: William Vainchenker, UMR U1170, Gustave Roussy, 114 rue Edouard Vaillant, 94805 Villejuif, France; e-mail: verpre@igr.fr. Q:25

References

1. Tefferi A, Thiele J, Vannucchi AM, Barbui T. An overview on CALR and CSF3R mutations and a proposal for revision of WHO diagnostic criteria for myeloproliferative neoplasms. *Leukemia.* 2014;28(7):1407-1413.
2. Wadleigh M, Tefferi A. Classification and diagnosis of myeloproliferative neoplasms according to the 2008 World Health Organization criteria. *Int J Hematol.* 2010;91(2):174-179.
3. Vainchenker W, Dusa A, Constantinescu SN. JAKs in pathology: role of Janus kinases in hematopoietic malignancies and immunodeficiencies. *Semin Cell Dev Biol.* 2008; 19(4):385-393.
4. Defour JP, Itaya M, Gryshkova V, et al. Tryptophan at the transmembrane-cytosolic junction modulates thrombopoietin receptor dimerization and activation. *Proc Natl Acad Sci USA.* 2013;110(7):2540-2545.
5. Ding J, Komatsu H, Iida S, et al. The Asn505 mutation of the c-MPL gene, which causes familial essential thrombocythemia, induces autonomous homodimerization of the c-Mpl protein due to strong amino acid polarity. *Blood.* 2009;114(15): 3325-3328.
6. Ding J, Komatsu H, Wakita A, et al. Familial essential thrombocythemia associated with a dominant-positive activating mutation of the c-MPL gene, which encodes for the receptor for thrombopoietin. *Blood.* 2004;103(11): 4198-4200.
7. Beer PA, Campbell PJ, Scott LM, et al. MPL mutations in myeloproliferative disorders: analysis of the PT-1 cohort. *Blood.* 2008;112(1):141-149.
8. Chaligné R, Tonetti C, Besancenot R, et al. New mutations of MPL in primitive myelofibrosis: only the MPL W515 mutations promote a G1/S-phase transition. *Leukemia.* 2008;22(8):1557-1566.
9. He X, Chen Z, Jiang Y, Qiu X, Zhao X. Different mutations of the human c-mpl gene indicate distinct haematopoietic diseases. *J Hematol Oncol.* 2013;6:11.
10. Kawamata N, Ogawa S, Yamamoto G, et al. Genetic profiling of myeloproliferative disorders by single-nucleotide polymorphism oligonucleotide microarray. *Exp Hematol.* 2008;36(11): 1471-1479.
11. Lambert MP, Jiang J, Batra V, Wu C, Tong W. A novel mutation in MPL (Y252H) results in increased thrombopoietin sensitivity in essential thrombocythemia. *Am J Hematol.* 2012;87(5): 532-534.
12. Williams DM, Kim AH, Rogers O, Spivak JL, Moliterno AR. Phenotypic variations and new mutations in JAK2 V617F-negative polycythemia vera, erythrocytosis, and idiopathic myelofibrosis. *Exp Hematol.* 2007;35(11):1641-1646.

Proof Only

Proof Only

13. Koren-Michowitz M, Gery S, Tabayashi T, et al. SH2B3 (LNK) mutations from myeloproliferative neoplasms patients have mild loss of function against wild type JAK2 and JAK2 V617F. *Br J Haematol.* 2013;161(6):811-820.
14. Oh ST, Simonds EF, Jones C, et al. Novel mutations in the inhibitory adaptor protein LNK drive JAK-STAT signaling in patients with myeloproliferative neoplasms. *Blood.* 2010; 116(6):988-992.
15. Klampfl T, Gisslinger H, Harutyunyan AS, et al. Somatic mutations of calreticulin in myeloproliferative neoplasms. *N Engl J Med.* 2013;369(25):2379-2390.
16. Nangalia J, Massie CE, Baxter EJ, et al. Somatic CALR mutations in myeloproliferative neoplasms with nonmutated JAK2. *N Engl J Med.* 2013; 369(25):2391-2405.
17. Wang WA, Groenendyk J, Michalak M. Calreticulin signaling in health and disease. *Int J Biochem Cell Biol.* 2012;44(6):842-846.
18. Tefferi A, Guglielmelli P, Larson DR, et al. Long-term survival and blast transformation in molecularly annotated essential thrombocythemia, polycythemia vera, and myelofibrosis. *Blood.* 2014;124(16):2507-2513.
19. Tefferi A, Lasho TL, Finke CM, et al. CALR vs JAK2 vs MPL-mutated or triple-negative myelofibrosis: clinical, cytogenetic and molecular comparisons. *Leukemia.* 2014;28(7):1472-1477.
20. Cervantes F, Barosi G. Myelofibrosis with myeloid metaplasia: diagnosis, prognostic factors, and staging. *Semin Oncol.* 2005;32(4):395-402.
21. Barosi G, Ambrosetti A, Finelli C, et al. The Italian Consensus Conference on Diagnostic Criteria for Myelofibrosis with Myeloid Metaplasia. *Br J Haematol.* 1999;104(4):730-737.
22. James C, Ugo V, Le Couédic JP, et al. A unique clonal JAK2 mutation leading to constitutive signalling causes polycythaemia vera. *Nature.* 2005;434(7037):1144-1148.
23. Chaligné R, James C, Tonetti C, et al. Evidence for MPL W515L/K mutations in hematopoietic stem cells in primitive myelofibrosis. *Blood.* 2007; 110(10):3735-3743.
24. Cabagnols X, Defour JP, Ugo V, et al. Differential association of calreticulin type 1 and type 2 mutations with myelofibrosis and essential thrombocytemia: relevance for disease evolution. *Leukemia.* 2015;29(1):249-252.
25. Saliba J, Saint-Martin C, Di Stefano A, et al. Germline duplication of ATG2B and GSKIP predisposes to familial myeloid malignancies. *Nat Genet.* 2015;47(10):1131-1140.
26. Damm F, Mylonas E, Cosson A, et al. Acquired initiating mutations in early hematopoietic cells of CLL patients. *Cancer Discov.* 2014;4(9): 1088-1101.
27. Plo I, Nakatake M, Malivert L, et al. JAK2 stimulates homologous recombination and genetic instability: potential implication in the heterogeneity of myeloproliferative disorders. *Blood.* 2008;112(4):1402-1412.
28. Kohlhuber F, Rogers NC, Watling D, et al. A JAK1/JAK2 chimera can sustain alpha and gamma interferon responses. *Mol Cell Biol.* 1997; 17(2):695-706.
29. Saharinen P, Silvennoinen O. The pseudokinase domain is required for suppression of basal activity of Jak2 and Jak3 tyrosine kinases and for cytokine-inducible activation of signal transduction. *J Biol Chem.* 2002;277(49): 47954-47963.
30. Sliva D, Wood TJ, Schindler C, Lobie PE, Norstedt G. Growth hormone specifically regulates serine protease inhibitor gene transcription via gamma-activated sequence-like DNA elements. *J Biol Chem.* 1994;269(42): 26208-26214.
31. Marty C, Saint-Martin C, Pecquet C, et al. Germline JAK2 mutations in the kinase domain are responsible for hereditary thrombocytosis and are resistant to JAK2 and HSP90 inhibitors. *Blood.* 2014;123(9):1372-1383.
32. Xie M, Lu C, Wang J, et al. Age-related mutations associated with clonal hematopoietic expansion and malignancies. *Nat Med.* 2014;20(12): 1472-1478.
33. McKerrell T, Park N, Moreno T, et al; Understanding Society Scientific Group. Leukemia-associated somatic mutations drive distinct patterns of age-related clonal hemopoiesis. *Cell Reports.* 2015;10(8): 1239-1245.
34. Genovese G, Kähler AK, Handsaker RE, et al. Clonal hematopoiesis and blood-cancer risk inferred from blood DNA sequence. *N Engl J Med.* 2014;371(26):2477-2487.
35. Jaiswal S, Fontanillas P, Flannick J, et al. Age-related clonal hematopoiesis associated with adverse outcomes. *N Engl J Med.* 2014;371(26): 2488-2498.
36. Klco JM, Spencer DH, Miller CA, et al. Functional heterogeneity of genetically defined subclones in acute myeloid leukemia. *Cancer Cell.* 2014;25(3): 379-392.
37. Moliterno AR, Williams DM, Rogers O, Spivak JL. Molecular mimicry in the chronic myeloproliferative disorders: reciprocity between quantitative JAK2 V617F and Mpl expression. *Blood.* 2006;108(12):3913-3915.
38. Milosevic Feenstra JD, Nivarthi H, Gisslinger H, et al. Whole-exome sequencing identifies novel MPL and JAK2 mutations in triple-negative myeloproliferative neoplasms. *Blood.* **Q:26**
39. Pardanani A, Lasho T, Finke C, Oh ST, Gotlib J, Tefferi A. LNK mutation studies in blast-phase myeloproliferative neoplasms, and in chronic-phase disease with TET2, IDH, JAK2 or MPL mutations. *Leukemia.* 2010;24(10):1713-1718.
40. Velazquez L, Cheng AM, Fleming HE, et al. Cytokine signaling and hematopoietic homeostasis are disrupted in Lnk-deficient mice. *J Exp Med.* 2002;195(12):1599-1611.
41. Vilaine M, Gourain V, Cleyrat C, et al. Germline MPLW515R mutation in a family with isolated thrombocytosis. In: Proceedings from the 54th Annual Meeting of the American Society of Hematology; December 8, 2012; Atlanta, GA. Abstract 1764.
42. Moliterno AR, Williams DM, Gutierrez-Alamillo LI, Salvatori R, Ingersoll RG, Spivak JL. Mpl Baltimore: a thrombopoietin receptor polymorphism associated with thrombocytosis. *Proc Natl Acad Sci USA.* 2004;101(31): 11444-11447.
43. Lannutti BJ, Epp A, Roy J, Chen J, Josephson NC. Incomplete restoration of Mpl expression in the mpl-/- mouse produces partial correction of the stem cell-repopulating defect and paradoxical thrombocytosis. *Blood.* 2009;113(8):1778-1785.
44. Meyer SC, Keller MD, Woods BA, et al. Genetic studies reveal an unexpected negative regulatory role for Jak2 in thrombopoiesis. *Blood.* 2014; 124(14):2280-2284.
45. Ng AP, Kauppi M, Metcalf D, et al. Mpl expression on megakaryocytes and platelets is dispensable for thrombopoiesis but essential to prevent myeloproliferation. *Proc Natl Acad Sci USA.* 2014; 111(16):5884-5889.
46. Pecquet C, Staerk J, Chaligné R, et al. Induction of myeloproliferative disorder and myelofibrosis by thrombopoietin receptor W515 mutants is mediated by cytosolic tyrosine 112 of the receptor. *Blood.* 2010;115(5):1037-1048.
47. Drachman JG, Kaushansky K. Dissecting the thrombopoietin receptor: functional elements of the Mpl cytoplasmic domain. *Proc Natl Acad Sci USA.* 1997;94(6):2350-2355.
48. Sangkhae V, Saur SJ, Kaushansky A, Kaushansky K, Hitchcock IS. Phosphorylated c-Mpl tyrosine 591 regulates thrombopoietin-induced signaling. *Exp Hematol.* 2014;42(6): 477-486.
49. Karow A, Nienhold R, Lundberg P, et al. Mutational profile of childhood myeloproliferative neoplasms [published online ahead of print July 30, 2015]. *Leukemia.* **Q:27**

Proof Only

VII.6. Thrombopoietin receptor activation by myeloproliferative neoplasm associated calreticulin mutants

Proof Only

MYELOID NEOPLASIA

Q:A1

Thrombopoietin receptor activation by myeloproliferative neoplasm associated calreticulin mutants

Ilyas Chachoua,[1,2,*] Christian Pecquet,[1,2,*] Mira El-Khoury,[3-5,*] Harini Nivarthi,[6] Roxana-Irina Albu,[1,2] Caroline Marty,[3-5] Vitalina Gryshkova,[1,2] Jean-Philippe Defour,[1,2] Gaëlle Vertenoeil,[1,2] Anna Ngo,[7] Ann Koay,[7] Hana Raslova,[3-5] Pierre J. Courtoy,[2] Meng Ling Choong,[7] Isabelle Plo,[3-5] William Vainchenker,[3-5] Robert Kralovics,[6] and Q:1 Stefan N. Constantinescu[1,2]

[1]Ludwig Institute for Cancer Research Brussels, Brussels, Belgium; [2]Université Catholique de Louvain and de Duve Institute, Brussels, Belgium; [3]INSERM, UMR1170, Institut Gustave Roussy, Villejuif, France; [4]Paris-Saclay, UMR1170, Institut Gustave Roussy, Villejuif, France; [5]Gustave Roussy, UMR1170, Villejuif, France; [6]CeMM Research Center for Molecular Medicine of the Austrian Academy of Sciences, Vienna, Austria; and [7]Experimental Therapeutics Center, Singapore

Key Points

- Calreticulin mutants responsible for myeloproliferative neoplasms specifically activate the thrombopoietin receptor and in turn JAK2.
- Activation of the thrombopoietin receptor requires the glycan binding site and a novel C-terminal tail of the mutant calreticulin.

Mutations in the calreticulin gene *(CALR)* represented by deletions and insertions in exon 9 inducing a −1/+2 frameshift are associated with a significant fraction of myeloproliferative neoplasms (MPNs). The mechanisms by which CALR mutants induce MPN are unknown. Here, we show by transcriptional, proliferation, biochemical, and primary cell assays that the pathogenic CALR mutants specifically activate the thrombopoietin receptor (TpoR/MPL). No activation is detected with a battery of type I and II cytokine receptors, except granulocyte colony-stimulating factor receptor, which supported only transient and weak activation. CALR mutants induce ligand-independent activation of JAK2/STAT/phosphatydylinositol-3′-kinase (PI-3K) and mitogen-activated protein (MAP) kinase pathways via TpoR, and autonomous growth in Ba/F3 cells. In these transformed cells, no synergy is observed between JAK2 and PI3-K inhibitors in inhibiting cytokine-independent proliferation, thus showing that a major difference from JAK2V617F cells with such synergy is strong. TpoR activation was dependent on its extracellular domain and its *N*-glycosylation, especially at N117. The glycan binding site and the novel C-terminal tail of the mutant CALR proteins were required for TpoR activation. A soluble form of TpoR was able to prevent activation of full-length TpoR provided that it was *N*-glycosylated. By confocal microscopy and subcellular fractionation, CALR mutants exhibit different intracellular localization from that of wild-type CALR. Finally, knocking down either *MPL/TpoR* or *JAK2* in megakaryocytic progenitors from patients carrying *CALR* mutations inhibited cytokine-independent megakaryocytic colony formation. Taken together, our study provides a novel signaling paradigm, whereby a mutated chaperone constitutively activates cytokine receptor signaling. (*Blood*. 2016;00(00):1-11)

Introduction

Myeloproliferative neoplasms (MPNs) are clonal disorders that affect hematopoietic stem cells (HSCs) and lead to a pathologic expansion of the myeloid lineage, mainly platelets in essential thrombocythemia (ET), red blood cells in polycythemia vera (PV), or platelets with collagen fiber formation in primary myelofibrosis (PMF).[1] The hallmark of these disorders is the constitutive activation of the JAK-STAT pathway.[2,3] The first and most recurrent mutation was described in JAK2 (JAK2 V617F), and was found in PV, ET, and PMF patients. Activating thrombopoietin receptor (TpoR/MPL) mutations (W515K/R/L/A) are found in ET and PMF patients.[4] Recently, mutations were described in the gene encoding the endoplasmic reticulum (ER) resident chaperone, CALR.[5,6] These mutations affect the exon 9 and lead to the loss of its ER retention signal, KDEL, and the generation of a positively charged and Met-rich C-terminal sequence. CALR mutants have been identified in ET and PMF patients, being correlated with a marked thrombocytosis and pathologic megakaryocyte features. Furthermore, expression of the 2 most prevalent CALR mutants type I (52 bp deletion) and type II (5 bp insertion) in a retroviral mouse model led to an ET phenotype[7] (and companion manuscript[8]). Interestingly, for type I CALR mutant, this ET phenotype evolved to myelofibrosis, in agreement with recent clinical observations.[9,10]

In the present study, we show that CALR mutants acquire the ability to activate TpoR, explaining the phenotype of the disease centered on megakaryocytes. We detail the requirements for this interaction and show that pathologic signaling via the JAK-STAT/PI3-K pathways appears different from that induced by JAK2V617F.

Submitted November 16, 2015; accepted December 7, 2015. Prepublished online as *Blood* First Edition paper, December 14, 2015; DOI 10.1182/blood-2015-11-681932.

*These authors contributed equally to this study.

The online version of this article contains a data supplement.

The publication costs of this article were defrayed in part by page charge payment. Therefore, and solely to indicate this fact, this article is hereby marked “advertisement” in accordance with 18 USC section 1734.

© 2016 by The American Society of Hematology

Proof Only

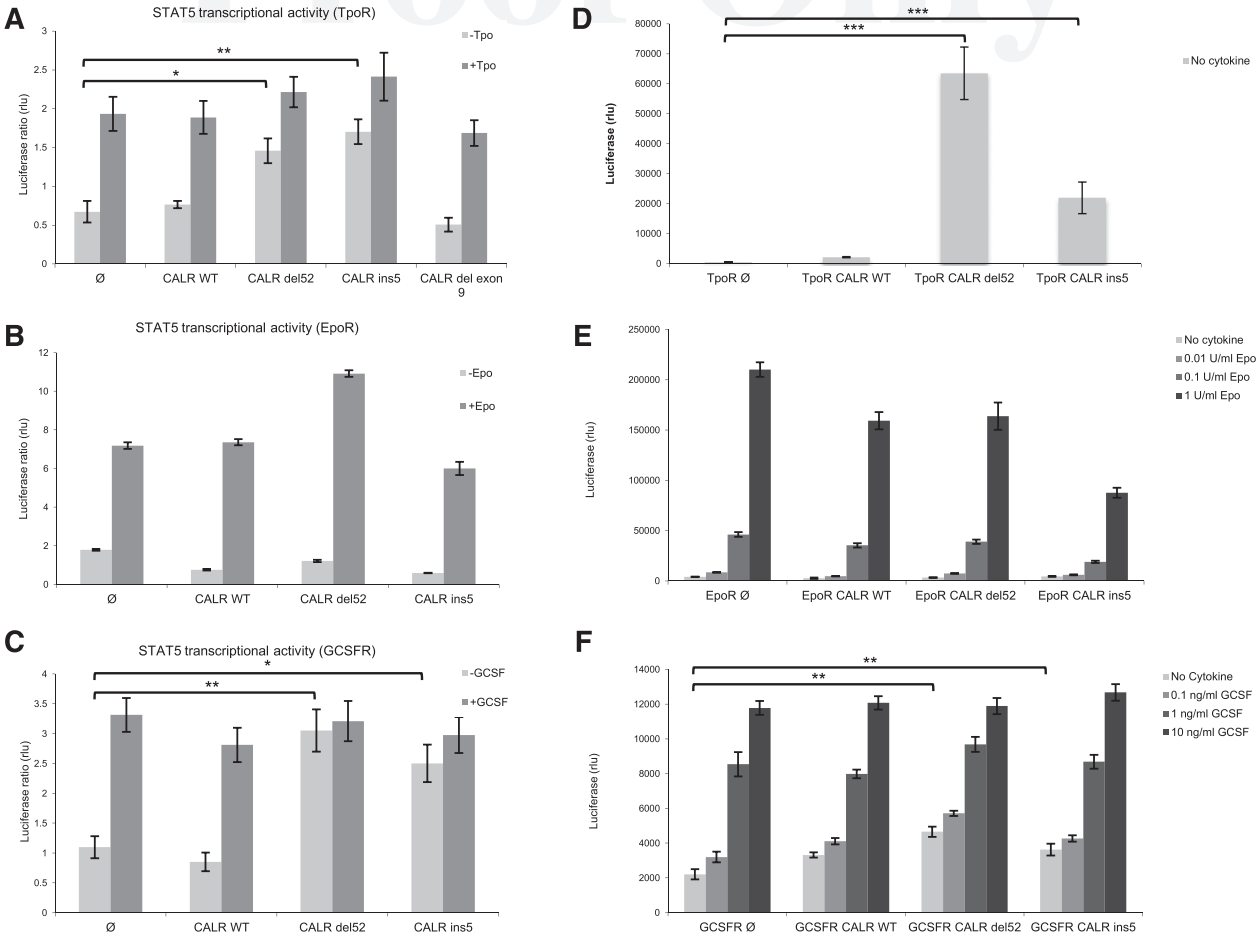


Figure 1. CALR mutants specifically activate TpoR, leading to cell transformation. γ2A cells were transfected with JAK2, STAT5, and CALR wild-type (wt) or the indicated mutants in the presence of TpoR (A), EpoR (B), and GCSFR (C). Luciferase assay was performed using the firefly reporter, Spi-Luc/STAT5 (STAT5-luc) and pRL-TK renilla luciferase for normalization. Ba/F3 cells stably transduced with CALR constructs together with TpoR (D), EpoR (E), or GCSFR (F) were cultured for 3 days, in the absence of cytokines. Positive controls of Epo and GCSF treatment are shown for Ba/F3 EpoR and GCSFR cells, respectively. Relative viability was measured using CellTiter-Glo technology. Statistical analysis (jmp pro11) was performed by the nonparametric multiple comparisons Steel test with a control group; $*P < .05$, $**P < .01$, $***P < .001$.

Materials and methods

DNA manipulations, production of retroviruses

The CALR wild-type, del52, ins5, and Δex9 sequences were cloned into pMSCV retroviral plasmids with mCherry. cDNAs coding for HA-tagged cytokine receptors TpoR (and mutants), EpoR, GCSFR, and all other receptors and JAK proteins were cloned in pMX-IRES-GFP as described.[11] TpoRbox1dead-GFP was previously described,[12] and soluble TpoR was generated by adding a stop codon at W491. The TpoR Asn mutants were as described.[13] Viral infections were performed as previously described.[11] shRNA against *JAK2* and *MPL/TpoR* cloned into PRRLsin-PGK-eGFP-WPRE lentiviral vector (Généthon, Evry, France) were used as previously described.[14-16]

Cell lines

The murine Ba/F3 cells were grown and infected as described.[11] Ba/F3-TpoR, EpoR, and G-CSFR cell lines expressing the various CALR mutants were generated after viral infection and sorted for equal (GFP or mCherry) expression level (FACSAria III; BD Biosciences). γ-2A (γ2A) cells are JAK2-deficient fibrosarcoma cells[17] were used for transcriptional studies.[11]

Q:2

calr$^{-/-}$ murine embryonic fibroblast cells (MEFs) were kindly provided by Dr. Marek Michalak, University of Alberta, Edmonton, Canada.[18]

Transcriptional assays

Dual luciferase assay was performed in γ2A cells transfected with cDNAs coding for STAT5, JAK2, and the respective cytokine receptor and CALR wild-type, mutants, or empty vector[11]; pRL-TK was used as an internal control (Promega, Madison, WI). Reporters used were Spi-Luc,[19] pGRR5, pSRE, and pFOXO (6xDBE).[11] Stimulations were with the appropriate cytokine (10 ng/mL rhTpo [Milteneyi Biotec], 10 U/mL rhEpo [Eprex; Hospital pharmacy], 10 ng/mL rhGCSF [Milteneyi Biotec]).

Growth assays

5000 cells per well were seeded in 96-well plates in medium with the indicated doses of cytokine and assayed at day 3, by the CellTiter-Glo luminescent Cell Viability Assay reagent (Promega). To determine long-term cytokine independence of transduced Ba/F3, cells were plated at a density of 250 000/mL, and live cells were evaluated after 10 days of culture by cell counting using a Coulter counter.

Cell surface immunoprecipitation

Ba/F3 cells were incubated with anti-HA antibodies (Roche Diagnostics, Indianapolis, IN) for 1 hour at 4°C, and washed 3 times and lysed in NP40 buffer with 100 μM phenylmethylsulfonyl fluoride, 100 μM orthovanadate, and a cocktail of protease inhibitor. The lysate was incubated with protein G agarose

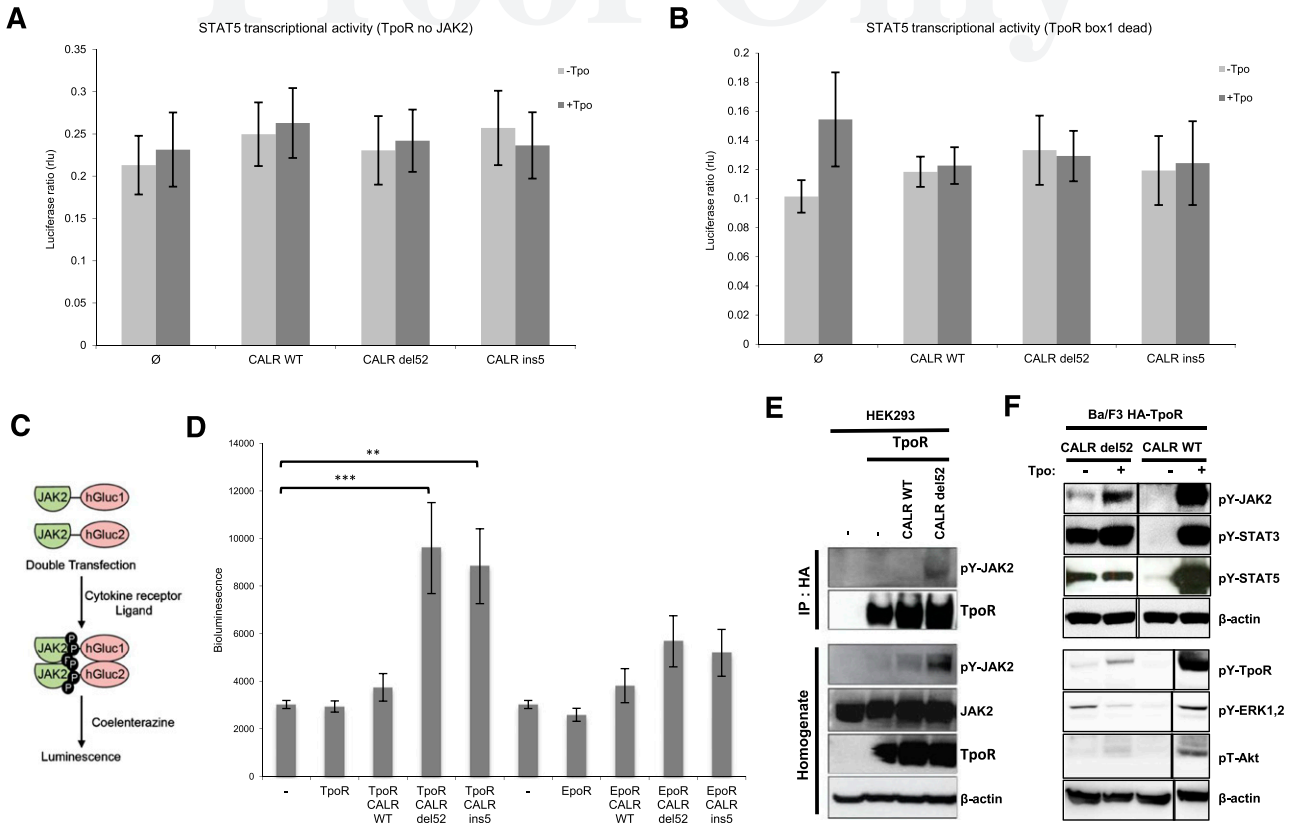


Figure 2. Constitutive signaling of TpoR induced by CALR mutants is JAK2-dependent. JAK2 requirement for STAT5 transcriptional activation was tested by luciferase assay in JAK2-deficient cell, γ2A, transfected with CALR wild-type or mutants, STAT5, and TpoR. (A) CALR mutants were unable to induce STAT5 activation downstream of TpoR in the absence of JAK2. (B) This observation was confirmed by luciferase assay with the TpoR box 1 dead mutant deficient in JAK2 binding. (C) Schematic representation of *Gaussia princeps* luciferase complementation assay used to test JAK2 dimerization in HEK293-derived BOSC cells. (D) Close proximity between the C-terminal kinase domains of JAK2 activation is induced by CALR del52 and ins5 only in the presence of TpoR. Values shown represent the average of 3 pooled independent experiments, each performed with 3 biological replicates ± standard error of the mean (SEM). Statistical analysis (jmp pro11) was performed by the nonparametric multiple comparisons Steel test with a control group; $*P < .05$, $**P < .01$, $***P < .001$. (E) Immunoprecipitation using anti-HA antibody from lysates of HEK293 cells transiently transfected with respective CALR (wild-type or del52) and HA-TpoR constructs, followed by western blotting with the indicated antibodies. Phosphorylated form of JAK2 interacted with TpoR only in the presence of CALR del52 but not wild-type. (F) JAK2 (Y1007/1008), STAT3 (Y705), STAT5 (Y694), TpoR (Y626), ERK1/2, (T202/Y204) and Akt (T308) activation by CALR del52 in Ba/F3 cells in the absence of Tpo. The condition +Tpo for CALR wild-type probed with pY-TpoR, pY-ERK1/2, pT-AKT, and β-actin was run in the same gel, but before CALR del52 minus Tpo. It had been displaced for symmetry.

(Invitrogen, Carlsbad, CA) overnight at 4°C. The beads were washed and subjected to western blotting with the indicated antibodies.

Coimmunoprecipitation

NP40 extracts from Hek293 cells were transiently transfected with TpoR and CALR wild-type or del52 by calcium phosphate and incubated with anti-HA antibodies (Roche) overnight at 4°C. Protein G agarose (Invitrogen) beads were added and incubated for 2 hours at 4°C. The beads were washed and subjected to western blotting with the indicated antibodies.

Antibodies

Phospho-specific antibodies were from Cell Signaling Technologies, as described,[11] and anti-CALR antibodies were from Millipore. β-actin (Sigma) was used as loading control. Antibodies detecting HA were from Roche.

Endo-H digestion

Endo-H (endoglycosidase H) digestion was performed as previously described on NP40 extracts from Ba/F3 cell lines.[12]

Patients

This study was conducted in accordance with the Declaration of Helsinki. $CD34^+$ cells from the peripheral blood of ET patients, with different CALR mutants identified by fragment sizing and Sanger sequencing, were purified by cell sorting and were transduced for lentiviral delivery of *MPL* and *JAK2* short hairpin RNAs. Two days later, sorted cells were evaluated on a serum-free fibrin clot assay to quantify megakaryocyte colonies in the presence of stem cell factor alone or with Tpo.[20] Effect of short hairpin RNAs on *MPL/TpoR* and *JAK2* mRNA levels was measured by quantitative real-time polymerase chain reaction in the plated cells.

Split-luciferase (*Gaussia princeps*) complementation assay

The cDNA of murine wild-type *JAK2* was inserted between NotI and ClaI restriction sites of pcDNA3.1/Zeo vector upstream of either the hGluc fragment coding amino acids 1-93 (hGluc1) or the fragment coding amino acids 94-169 (hGluc2) of *Gaussia princeps* luciferase as described.[21]

BOSC 23 cells were transfected and processed as described.[22]

Confocal microscopy

$calr^{-/-}$ MEFs grown overnight on coverslips were fixed with 4% paraformaldehyde for 15 minutes, were permeabilized, and were blocked with 0.5% Triton X-100 in phosphate-buffered saline containing 100 μg/mL of goat γ-globulin (Jackson Immunoresearch Laboratories [Bio Connect], Huissen, the Netherlands) for 1 hour at room temperature. Rabbit anti-CALR (Millipore [Merck Chemicals], Overijse, BE) and mouse anti-Calnexin (Abcam, Cambridge, UK) were incubated overnight at 4°C followed by goat anti-mouse IgG coupled to Alexa 568 or goat anti-rabbit IgG linked to Alexa 488 (Invitrogen/Life Technologies, Gent, Belgium). Slides were examined by confocal microscopy

Proof Only

Table 1. Combination study using JAK2/JAK1 inhibitor ruxolitinib with a series of serine threonine kinase inhibitors in Ba/F3 cells expressing TpoR and the indicated CALR mutants

				Ba/F3 TpoR (+Tpo)				Ba/F3 TpoR CALR WT (+Tpo)				Ba/F3 TpoR CALR del52 (+Tpo)				Ba/F3 TpoR CALR del52 (no Tpo)				Ba/F3 TpoR CALR ins5 (+ Tpo)				Ba/F3 TpoR CALR ins5 (no Tpo)			
				Combination with ruxolitinib				Combination with ruxolitinib				Combination with ruxolitinib				Combination with ruxolitinib				Combination with ruxolitinib				Combination with ruxolitinib			
				CI at				CI at				CI at				CI at				CI at				CI at			
No.	Inhibitor	Compound	IC50 (μM)	ED50	ED75	ED90	ED95	ED50	ED75	ED90	ED95	ED50	ED75	ED90	ED95	ED50	ED75	ED90	ED95	ED50	ED75	ED90	ED95	ED50	ED75	ED90	ED95
1	JAK2	Ruxolitinib	1.34																								
2	Smoothen	Erismodegib	>40	0.89	0.90	0.91	0.91	0.55	0.61	0.68	0.73	1.01	0.92	0.84	0.79	0.93	0.89	0.86	0.84	0.74	0.74	0.76	0.77	1.17	1.09	1.02	0.98
3	Bcr-abl	Imatinib	16.51	1.47	1.04	0.77	0.64	0.98	0.88	0.80	0.76	0.64	0.65	0.67	0.68	0.86	0.92	0.99	1.05	0.68	0.68	0.67	0.67	0.93	0.93	0.93	0.93
4	mTOR	Rapamycin	16.80	1.27	1.17	1.12	1.12	0.71	0.70	0.69	0.69	0.51	0.55	0.60	0.63	0.74	0.76	0.80	0.82	0.61	0.74	0.90	1.04	0.63	0.67	0.72	0.75
5	mTOR	Temsirolimus	16.31	1.12	1.08	1.09	1.12	0.67	0.69	0.72	0.75	0.56	0.57	0.59	0.60	0.57	0.57	0.57	0.57	0.54	0.66	0.81	0.93	0.66	0.65	0.70	0.73
6	ROCK1	Rho15	>40	1.67	1.49	1.34	1.25	1.14	1.09	1.05	1.02	0.75	0.79	0.83	0.85	0.99	0.96	0.93	0.91	0.64	0.65	0.65	0.65	1.04	1.00	0.97	0.95
7	JNK	CC401	22.88	1.37	1.11	0.91	0.79	0.48	0.48	0.49	0.50	0.54	0.53	0.53	0.52	0.71	0.74	0.78	0.80	0.59	0.57	0.56	0.55	0.84	0.85	0.85	0.85
8	Tie-2	AMG-Tie-2	9.57	2.32	1.48	0.96	0.72	1.43	1.07	0.82	0.69	0.82	0.73	0.68	0.66	1.18	1.08	1.00	0.95	1.06	1.01	1.00	1.01	1.17	1.05	0.95	0.90
9	p38 MAPK	SB202190	19.85	0.85	0.81	0.80	0.80	1.38	1.14	0.94	0.83	1.26	1.28	1.32	1.35	0.99	1.08	1.17	1.23	1.06	1.00	0.95	0.92	0.83	0.91	1.01	1.08
10	p38 MAPK	SB203580	39.08	1.21	1.07	0.96	0.89	1.09	0.98	0.88	0.82	0.74	0.76	0.78	0.80	0.89	0.82	0.76	0.72	0.75	0.70	0.66	0.63	0.94	0.92	0.90	0.89
11	p38 MAPK	VX702	>40	1.18	1.09	1.01	0.95	0.86	0.78	0.72	0.68	0.76	0.74	0.73	0.72	1.13	1.01	0.90	0.83	0.81	0.80	0.79	0.78	0.74	0.73	0.73	0.73
12	CDK	AT7519	6.60	1.11	1.05	0.99	0.95	1.81	1.30	0.93	0.74	1.05	0.97	0.89	0.84	1.38	1.24	1.13	1.06	0.74	0.77	0.79	0.81	0.94	0.91	0.89	0.87
13	B-RAF	PLX4720	>40	1.47	1.33	1.20	1.13	1.43	1.23	1.07	0.98	1.07	1.18	1.31	1.40	1.25	1.33	1.42	1.48	0.83	0.94	1.06	1.15	1.00	1.03	1.05	1.07
14	CDK	SNS032	0.46	1.01	1.41	2.03	2.64	1.51	1.44	1.37	1.34	0.41	0.72	1.31	2.02	1.33	1.68	2.30	2.96	0.67	1.81	4.88	9.63	0.80	0.85	0.90	0.93
15	MEK/ERK	AS703026	4.70	0.44	0.35	0.45	0.53	0.53	0.47	0.49	0.53	0.39	0.40	0.41	0.42	0.60	0.52	0.46	0.42	0.48	0.48	0.50	0.52	0.52	0.48	0.50	0.51
16	MEK/ERK	RDEA119	4.40	0.39	0.41	0.49	0.57	0.31	0.33	0.42	0.51	0.80	0.74	0.70	0.67	0.64	0.55	0.48	0.45	0.52	0.42	0.40	0.39	0.62	0.54	0.55	0.57
17	MEK/ERK	CI1040	7.41	0.49	0.46	0.45	0.45	0.39	0.42	0.45	0.47	0.73	0.68	0.64	0.61	0.76	0.69	0.67	0.66	0.47	0.44	0.42	0.41	0.50	0.53	0.57	0.60
18	MEK/ERK	Sorafenib	5.31	1.22	1.08	0.98	0.93	0.95	0.91	0.88	0.87	1.54	1.34	1.16	1.05	1.22	1.22	1.24	1.26	1.35	1.23	1.12	1.05	1.35	1.31	1.27	1.24
19	PI3K	ZSTK474	1.26	0.33	0.39	0.49	0.57	0.46	0.51	0.56	0.61	0.58	0.59	0.61	0.63	0.67	0.68	0.68	0.69	0.59	0.62	0.68	0.72	0.52	0.59	0.69	0.76
20	PI3K	BEZ235	0.19	0.02	0.06	0.14	0.28	0.58	0.54	0.51	0.49	0.87	0.68	0.55	0.49	0.77	0.66	0.59	0.56	0.87	0.74	0.70	0.69	1.00	0.82	0.71	0.65
21	PI3K	Buparlisib	3.07	0.56	0.45	0.36	0.32	0.67	0.52	0.41	0.35	0.57	0.54	0.51	0.49	0.73	0.67	0.61	0.58	0.65	0.61	0.57	0.54	0.82	0.83	0.83	0.84
22	PI3K	GDC0941	12.00	0.77	0.83	0.91	0.97	0.85	0.83	0.81	0.80	0.68	0.62	0.60	0.60	0.89	0.93	1.01	1.08	0.57	0.54	0.56	0.58	0.90	0.84	0.85	0.87
23	HDAC	Panobinostat	0.03	1.22	1.14	1.07	1.02	0.84	0.92	1.01	1.07	1.10	1.13	1.16	1.19	1.33	1.64	2.06	2.42	1.20	1.24	1.28	1.31	1.07	1.25	1.47	1.64

CI, combination index.

Combination index values of 0.9-1.1 are considered additive, values of 0.8 and below show moderate to strong synergism, and values >1.2 are moderate to strong antagonism for the drug pair tested. Compounds showing no inhibition are in yellow. For synergic combinations, the darkness of green correlates with increased synergy.

using a confocal server spinning disc Zeiss platform equipped with a 100× objective.

Cell fractionation

calr$^{-/-}$ MEF cells (5×10^7) stably expressing TpoR and CALR wild-type or del52 were harvested in 2 mL of homogenization medium (0.25 M sucrose, 1 mM ethylenediaminetetraacetic acid, 3 mM imadazole, pH 7) and homogenized on ice with a tight dounce homogenizer (6 strokes).[23]

After removal of nuclei and cell debris at 7700 *g*xmin, subcellular particles sedimenting at 7×10^6 *g*xmin were layered on top of preformed sucrose density gradients and equilibrated for 105×10^6 *g*xmin. Twelve fractions were collected from the bottom and analyzed for density and by western blotting. Fractionation of the 2 cell lines was performed strictly in parallel. Representative data are from 2 experiments.

Inhibitor assays

Ruxolitinib, erismodegib, buparlisib, and panobinostat (SelleckChem); rapamycin and temsirolimus (Tocris); and the other 17 compounds (SynMedChem) were dissolved in 100% dimethylsulfoxide (Sigma) to prepare 20 mM stocks except for NVP-BEZ235, which was dissolved to prepare 10 mM stock. Combination studies were performed[24] in the presence or absence of Tpo (40 ng/mL).Cell viability was determined by CellTiter-Glo (Promega). Combination index (CI) was calculated using the CompuSyn software version 1.0 (ComboSyn Inc). CI values of ≤0.8 show moderate to strong synergism.[25] CIs were calculated as described.[24]

Results

CALR mutants specifically activate TpoR

CALR is an ER-resident chaperone implicated in the folding of newly synthetized proteins through binding to their *N*-glycosylated sites.[26] We hypothesized that the CALR mutants associated with MPN might bind to and activate cytokine receptors, which are highly *N*-glycosylated[12,13,27] and because MPNs are known to be driven either by indirect (JAK2V617F) or direct (TpoR W515L/A/K and S505N) cytokine receptor activation.[2] To test this hypothesis, we measured STAT5 transcriptional activity in γ2A cells transiently transfected with CALR wild-type or mutants along with a cytokine receptor, such as TpoR, EpoR, and GCSFR, or a battery of type I and II cytokine receptors. As shown in Figure 1B, CALR mutants do not induce constitutive STAT5 activation via EpoR. In contrast, they specifically induce STAT5 constitutive activation downstream of TpoR and GCSFR (Figure 1A,C). TpoR-dependent STAT5 activation was induced by the 2 most common MPN-associated mutants of CALR, type I (del52) and type II (ins5), but not by an artificial mutant lacking the entire exon 9 (Δex9). These results were confirmed using a pan STAT1/3/5 luciferase reporter (pGRR5), but the activation via GCSFR was shown to be weaker (data not shown). In supplemental Figure 1A-E, we show that no STAT5 activation by CALR mutants could be detected via IL-2R, IL-9R, growth hormone receptor, Leptin receptor (LepR), and type I interferon receptors.

We further validated our data by stable transduction of Ba/F3 cells with TpoR, EpoR, or GCSFR along with wild-type CALR or mutants (Figure 1D-F). Because Ba/F3 cells are IL3-dependent requiring cytokines for their growth, we tested the capacity of CALR mutants to induce autonomous growth. We measured short-term growth of the stable Ba/F3 cell lines by using Cell Titer Glo assay after 3 days of IL-3 removal (Figure 1D-F). Long-term autonomous growth was also studied after 10 days of culture in the absence of cytokine. Although EpoR did not induce increased short- and long-term autonomous proliferation in *CALR*-mutated cells, interestingly, GCSFR supported a mild increase in short-term growth in *CALR*-mutated cells, but no long-term cytokine-independent proliferation was obtained after repeated

Proof Only

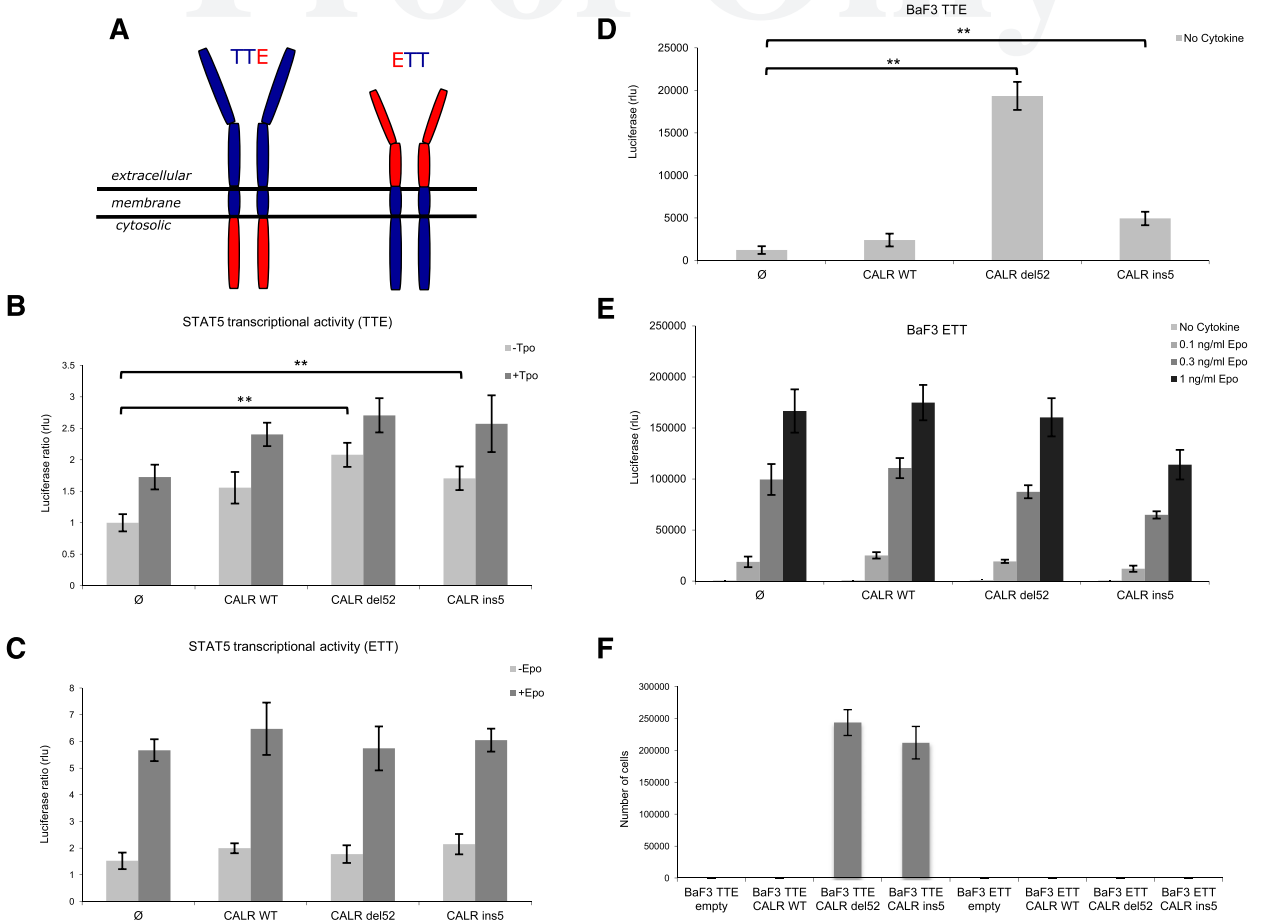


Figure 3. The extracellular domain of TpoR, but not of EpoR, is indispensable for CALR mutants activity. (A) Schematic representation of engineered chimeric receptors. On the left, chimeric receptor TTE is composed of the extracellular and transmembrane domains of TpoR (in blue) fused to the cytosolic domain of EpoR (in red). On the right, chimeric receptor ETT is composed by the extracellular domain of EpoR (in red) fused to the transmembrane and cytosolic domains of TpoR (in blue). STAT5 transcriptional activity was measured by luciferase assay in γ2A cells transiently transfected with JAK2 and CALR wild-type or mutants in the presence of the chimeric receptor TTE (B) or ETT (C). Only the chimeric receptor presenting the extracellular domain of TpoR (TTE) is able to support constitutive activity induced by CALR mutants. Ba/F3 cells stably transduced with CALR constructs together with TTE (D) or ETT (E) were cultured for 3 days without cytokine to measure short-term autonomous growth using CellTiter-Glo technology. ETT cells were also tested for response to Epo, as positive control. (F) Long-term proliferation (day 10) of Ba/F3 expressing the indicated chimeric receptors and CALR variants. Values shown represent the average of 3 pooled independent experiments, each performed with 3 biological replicates ± SEM. Statistical analysis (jmp pro11) was performed by the nonparametric multiple comparisons Steel test with a control group; $*P < .05$, $**P < .01$, $***P < .001$.

attempts. Although CALR mutants did not induce autonomous growth in Ba/F3 cells expressing EpoR and GCSFR, cells did respond to their cytokines (Figure 1E-F). Only TpoR maintained long-term cytokine-independent cell growth in the presence of both CALR mutants (Figure 1D-F), as described in the companion paper.[8]

Altogether, these results suggest that CALR mutants induce strong and specific signaling via TpoR, leading to increased proliferation and autonomous growth.

JAK2 is required for TpoR activation by CALR mutants

JAK2 is required for signaling by TpoR, as well as for its traffic and stability.[12,28,29] To test whether JAK2 is required for TpoR activation by CALR mutants, we performed STAT5 transcriptional assays in the human JAK2-deficient γ2A cells in the absence of JAK2 or using a TpoR receptor mutant that does not bind JAK2. CALR mutants could not induce TpoR activation in the absence of JAK2 (Figure 2A). Furthermore, a TpoR box 1 dead mutant, which is deficient in JAK2 binding,[12] was not able to activate JAK-STAT pathway in the presence of CALR mutants, indicating that the interaction between TpoR and JAK2 is crucial for signaling by CALR mutants (Figure 2B). In addition, we evaluated dimerization of the JAK2 C-terminal kinase domains by *Gaussia luciferase* complementation assay[21,22] (Figure 2C). We show that, in transiently transfected HEK293 cells, CALR mutants induce dimerization of JAK2 C-terminal domains in the presence of TpoR, but not of EpoR (Figure 2D). This was accompanied by the phosphorylation of the JAK2 activation loop at Y1007 residue (Figure 2E). We also show by coimmunoprecipitation assay that TpoR is associated with phosphorylated JAK2 only when coexpressed with CALR del52 (Figure 2E). Furthermore, constitutive STAT3 and 5 activation was observed in Ba/F3 TpoR expressing CALR mutants by western blotting, along with detectable MAPK ERK1/2, and PI-3K signaling (Figure 2F). Constitutive activation of MAPK and PI3-K pathways was also seen by luciferase assay with pSRE and 6xDBE (supplemental Figure 2A, C). Interestingly, CALR mutant[30] found in the MARIMO cell line and exhibiting the same −2/+1 frameshift was also capable of activating STAT5 and MAPK (supplemental Figure 2A-B).

Absence of synergy between JAK2 and PI3-K inhibitors in the case of hematopoietic cell lines coexpressing TpoR and CALR mutants

We then studied which signaling pathways induced by CALR mutants were involved in autonomous proliferation of Ba/F3 TpoR cells by

Proof Only

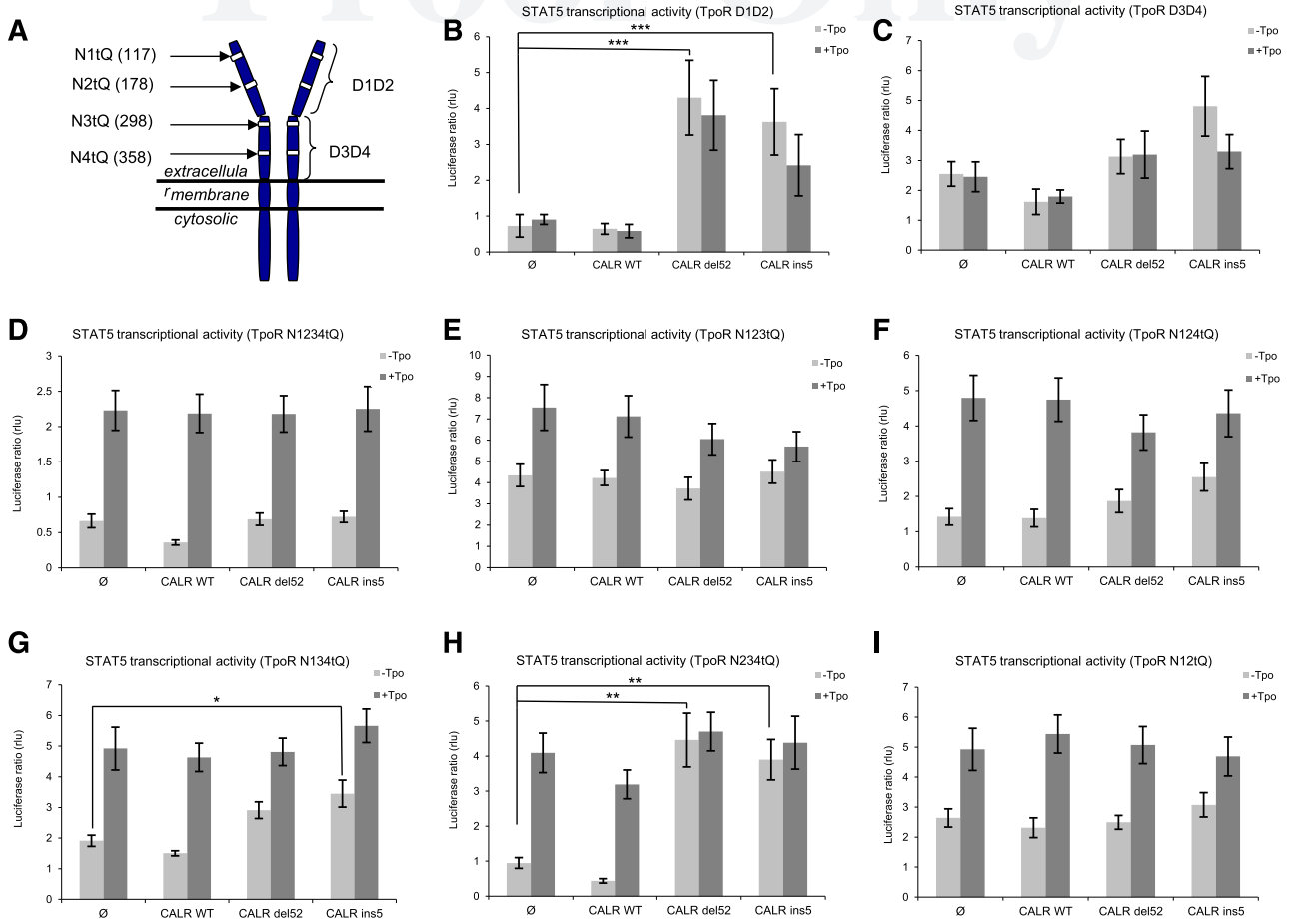


Figure 4. The membrane-distal part of extracellular domain of TpoR (D1D2) and its associated *N*-glycosylation sites control CALR mutant activity. (A) Schematic representation of TpoR with its extracellular subdomains and the *N*-glycosylation sites that have been mutated into Q. The more distal subdomains of extracellular domain of TpoR, namely D1D2, contain 2 *N*-glycosylated sites annotated N1 (N117) and N2 (N178). The proximal subdomains D3D4 contain two *N*-glycosylated sites annotated N3 (N298) and N4 (N358). STAT5 transcriptional activity was assessed by luciferase assay in γ2A cells transiently expressing STAT5, JAK2, CALR wild-type, or mutants together with the following TpoR mutants: TpoR D1D2 (B), TpoR D3D4 (C), TpoR N1234tQ (D), TpoR N123tQ (E), TpoR N124tQ (F), TpoR N134tQ (G), TpoR N234tQ (H), and TpoR N12tQ (I). Mutant TpoR missing D1D2, rather than D3D4, is unable to support CALR mutant activity (B). Contrary to TpoR N3tQ and N4tQ, TpoR N1tQ and N2tQ abrogated completely or partially TpoR constitutive activation induced by CALR mutants, respectively. Values shown represent the average of 3 pooled independent experiments, each performed with 3 biological replicates ± SEM. Statistical analysis (jmp pro11) was performed by the nonparametric multiple comparisons Steel test with a control group; **P* < .05, ***P* < .01, ****P* < .001.

using different inhibitors. After 2 days of treatment, cells expressing mutated CALR (del52 and ins5) show increasing sensitivity toward ruxolitinib, when compared with wild-type CALR (supplemental Table 1). This is consistent with reports showing that JAK-STAT pathway inhibition by ruxolitinib and fedratinib inhibits constitutive signaling induced by CALR mutants.[31-33]

Then we tested whether ruxolitinib could synergize with the PI3-K inhibitors GDC-421, ZSTK474, and BEZ235 (also an mTOR inhibitor), as previously shown for JAK2V617F,[24] and with a series of serine threonine kinase inhibitors to block growth of CALR mutants-expressing Ba/F3 TpoR cells (Table 1). In the absence of Tpo, using the Chou-Talalay method, no synergy was detected between JAK2 and PI3-K inhibitors. For del52 CALR mutant specifically, synergy was detected between JAK2 inhibitor and the mTOR inhibitor temsirolimus. Conversely, synergy between JAK2 and MEK-ERK inhibitors could be detected in CALR-mutants cells. Synergy was restored in the presence of Tpo, as described.[24] These data indicate that signaling by CALR mutants depends mainly on JAK2 and MAP-kinase pathways, in contrast to JAK2V617F, which is heavily dependent on JAK2 and PI3-K.[24,34,35]

The extracellular domain and the *N*-glycosylation sites of TpoR are indispensable for TpoR activation by CALR mutants

To uncover the mechanism of TpoR activation by CALR mutants, we generated chimeric constructs in which the extracellular and cytosolic domains of TpoR and EpoR were reciprocally fused together (Figure 3A). Only the chimeric receptor that contained the extracellular domain of TpoR (TTE) supported constitutive STAT5 activation by both CALR mutants in transient transfection luciferase assays (Figure 3B-C). In addition, the TTE receptor was also able to support short- and long-term cell proliferation of Ba/F3 cells (Figure 3D,F), whereas ETT did not (Figure 3E-F). Although ETT did not support constitutive growth induced by CALR mutants, this receptor still responded to Epo (Figure 3E). Thus, the extracellular domain of TpoR is absolutely required for activation by CALR mutants.

The TpoR extracellular domain is composed of 4 subdomains (D1, D2, D3, and D4) (Figure 4A). We generated constructs expressing TpoR with only D1D2 (TpoR D1D2) or D3D4 (TpoR D3D4). Only the more membrane-distal region of TpoR (TpoR D1D2) supported constitutive activation by CALR mutants (Figure 4B-C).

Proof Only

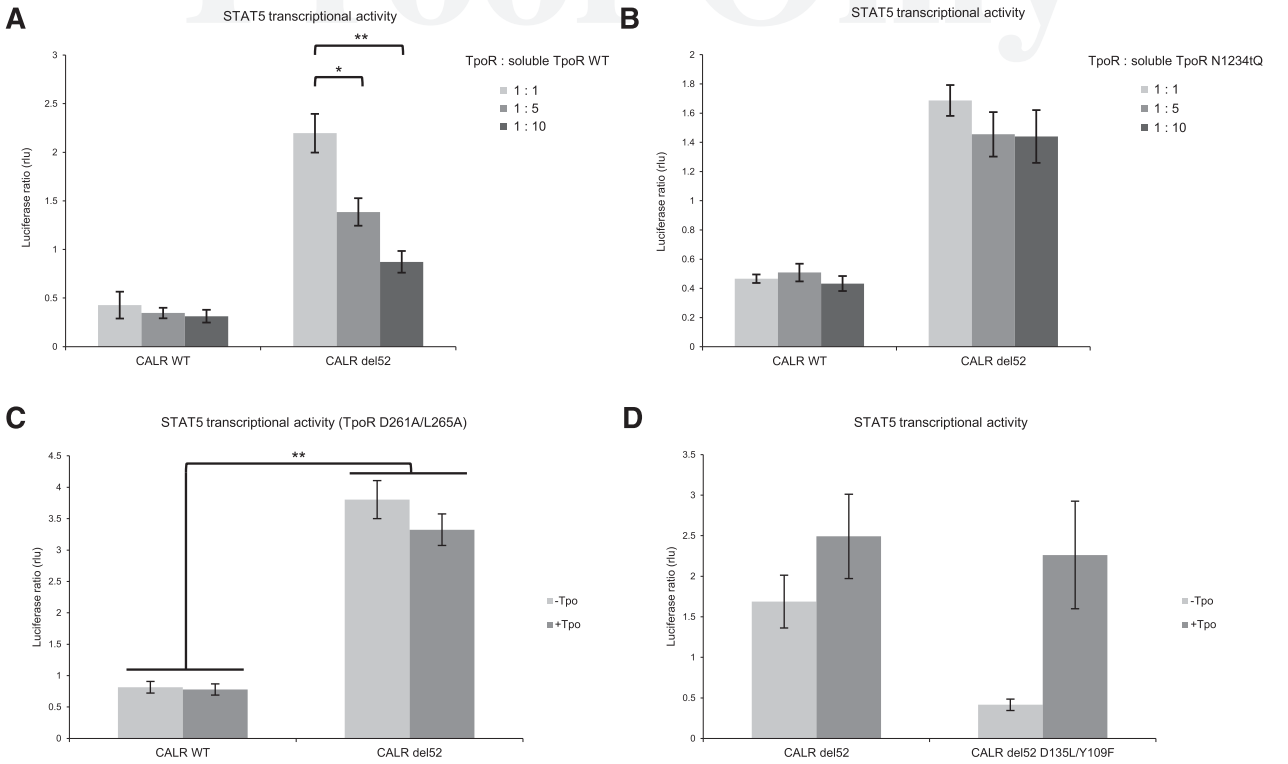


Figure 5. TpoR constitutive activation induced by CALR mutants is abrogated by the TpoR soluble form and requires the glycan binding site of CALR. (A) The soluble extracellular domain of TpoR acts as a competitive inhibitor of TpoR activation by the CALR mutants as shown by luciferase assay (STAT5 transcriptional activity). This inhibitory effect is lost when all the *N*-glycosylated asparagine residues of the soluble TpoR are mutated to glutamine (soluble TpoR-NtQ) (B). (C) The γ2A luciferase assay showed that the TpoR -D261A/L265A mutant, unable to bind Tpo, is activated by CALR del52. CALR del52 mutant unable to bind *N*-glycosylation modifications (CALR del52 D135L/Y109F) do not induce TpoR -dependent STAT5 activation (D). Values shown represent the average of 3 pooled independent experiments, each performed with 3 biological replicates ± SEM. Statistical analysis was performed by the nonparametric multiple comparisons Steel test with a control group; $*P < .05$, $**P < .01$.

We generated mutations in the extracellular domain of TpoR, where all the 4, 3, or 2 asparagine (Asn) residues were mutated to glutamine (Gln) (Figure 4A).[13] The TpoR mutant devoid of all 4 *N*-glycosylation sites (TpoR N1234tQ) failed to support STAT5 activation in the presence of CALR mutants (Figure 4D). When individual Asn residues were restored in TpoR N1234tQ background, N117 (N1, the most *N*-terminal) residue was shown to be the most activating (Figure 4H), N298 and N358 were not activating, and N178 supported weak activation only by CALR ins5 (Figure 4E-G). Consistent with these results, a TpoR mutant lacking both N117 and N178 (N12tQ) is completely unable to support activation by both CALR mutants (Figure 4I). These results show that 2 Asn residues (N117 and N178) present in D1D2 are key players for TpoR activation by CALR mutants.

Next, we showed that the soluble extracellular domain of TpoR (stop codon at W491 upstream of the TpoR transmembrane domain) acts as a competitor to the full-length TpoR and blocks STAT5 activation by CALR mutants (Figure 5A). Importantly, a soluble extracellular domain where all the 4 Asn sites were mutated to Gln failed to exert inhibition (Figure 5B). However, CALR del52 mutant could still induce activation of the Tpo-binding–deficient TpoR mutant (D261A/L265A)[36] (Figure 5C).

Altogether these results show that activation of TpoR by CALR mutants is dependent on TpoR *N*-glycosylation sites, but independent of the TPO binding site.

The glycan binding site of CALR del52 mutant is required for TpoR activation

Because the *N*-glycosylation sites of TpoR are required for its activation by CALR mutants, we mutated the glycan binding site (Y109F/D135L)[37] in CALR del 52 and could show that it does not activate TpoR in the absence of Tpo (Figure 5D). This supports the notion that the interaction between CALR mutant and TpoR requires CALR glycan binding site and the TpoR *N*-glycosylated sites for TpoR activation

CALR mutants show differential stability, localization, and TpoR maturation

To study CALR mutants in a cell background devoid of wild-type CALR, we used MEFs derived from $calr^{-/-}$ mice. $calr^{-/-}$ MEFs were transduced with viruses coding for TpoR and CALR wild-type or mutants and sorted for equivalent levels of GFP (for TpoR) and mCherry (for CALR). We assessed by confocal microscopy and western blotting the level of CALR expression and its stability. In contrast to wild-type CALR, the CALR mutants were unstable and this was accompanied with less CALR mutant protein expression (Figure 6A).

Also, we showed that CALR mutants induce tyrosine phosphorylation and nuclear translocation of STAT3, indicating that wild-type CALR was not required for JAK-STAT activation by CALR mutants (supplemental Figure 3A).

To define the subcellular localization of wild-type and mutant CALR, postnuclear fractions were prepared by sedimentation of homogenates that were partitioned on sucrose density gradients (Figure 6B). The distribution of all markers tested as well as the density of each fraction are shown in supplemental Figure 4. The sedimentable ER-marker, GRP78, equilibrates with CALR wild-type (fraction #5), but not with CALR del52 (fraction #7), suggesting the dissociation of CALR mutant from ER (Figure 6B). High-resolution confocal microscopy was performed in $calr^{-/-}$ MEFs to avoid the interference of the endogenous CALR. CALR wild type and mutants exhibited

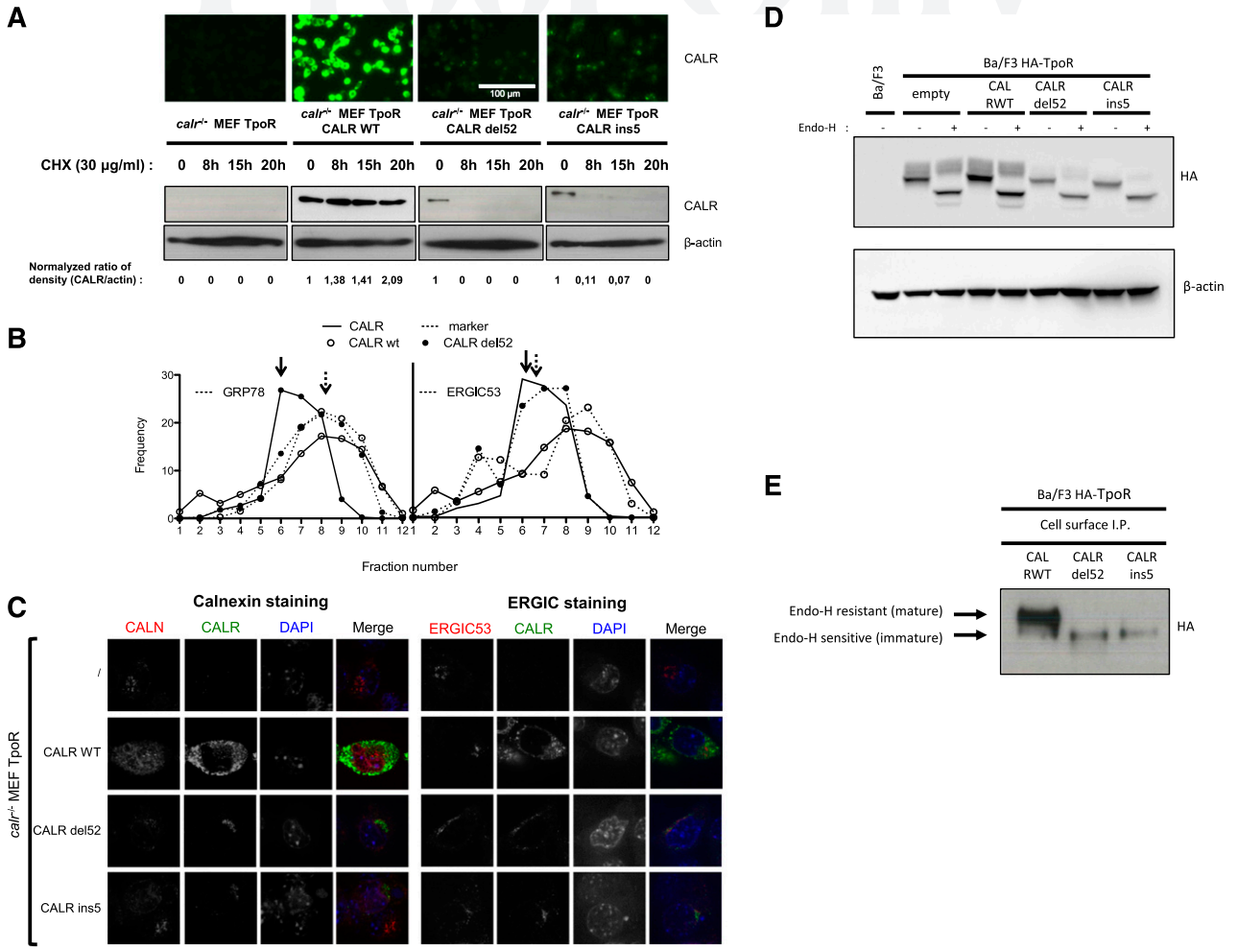


Figure 6. CALR mutants modify TpoR stability, maturation, and trafficking. (A) The expression of CALR in *calr*$^{-/-}$ MEFs transduced with retroviral constructs expressing TpoR and CALR wild-type or mutants was assessed by immunofluorescence (top panel) and by western blotting after cycloheximide (30 µg/mL) treatment (bottom panel). (B) Maturation state of TpoR in Ba/F3-TpoR cells in the presence of CALR wild-type or mutants was assessed by western blotting upon endoglycosidase H treatment or not. (B) Subcellular fractionation of CALR wild-type and mutant del52 proteins in *calr*$^{-/-}$ MEF TpoR cells. The distribution patterns of CALR and GRP78 were shown in the diagram and the blots. (C) Confocal immunofluorescence microscopy was performed in previously described *calr*$^{-/-}$ MEF cell lines and stained with anti-CALN (Calnexin), anti-CALR, and 4,6 diamidino-2-phenylindole. (D) Maturation state of TpoR in Ba/F3-TpoR cells in the presence of wild-type or mutant CALR was assessed by western blotting upon endoglycosidase H treatment or not. (E) Western blot analysis of immunoprecipitated *N*-terminal HA-tagged TpoR present on cell surface, in Ba/F3-TpoR cells expressing wild-type or mutant CALR. All data are normalized, C being the amount per volume of subfraction, and Ci the corresponding value in the pooled subfractions.

different intracellular localizations, ER *vs* vesicle (ER to Golgi), respectively (Figure 6C and supplemental Figure 3B). Wild-type CALR colocalized with the ER marker calnexin (Figure 6C, left panel). This was not the case for del52 or ins5 mutant (Figure 6C, right panel), which colocalized with ERGIC53 (ER to Golgi intermediate compartment) (supplemental Figure 2C) and partially with or adjacent to GM130 (Golgi marker) (supplemental Figure 3B).

We observed maturation defects of TpoR in the Ba/F3-TpoR cells expressing CALR mutants by western blotting, with the majority of TpoR remaining EndoH-sensitive (immature, high mannose form). In contrast, the CALR wild-type promotes EndoH-resistant mature form of TpoR (Figure 6D). Surface immunoprecipitation of TpoR in Ba/F3 TpoR–expressing cells showed that CALR mutants are associated only with the immature form of TpoR (Figure 6E).

Spontaneous megakaryocytic progenitor growth in *CALR*-mutated ET patients requires TpoR and JAK2

To confirm the involvement of the TpoR/JAK2 axis in the human disease, we performed in vitro studies using primary cells from *CALR*-mutated ET patients carrying either *CALR ins5* or *del52* mutations. As previously reported, we detected spontaneous (Tpo-independent) growth of megakaryocyte progenitors in such patients.[38] CD34^{+} cells were transduced with lentiviruses expressing either short hairpin RNAs targeting *TpoR/MPL* or *JAK2* or a scrambled sequence, and GFP as a reporter marker. Downregulation of *TpoR/MPL* or of *JAK2* gene expression (Figure 7A) led to a significant inhibition of Tpo-independent colonies (~50% reduction) associated in both types of CALR mutants (Figure 7B). Our data thus confirm that TpoR and JAK2 are absolutely required for the phenotype induced by CALR mutants in primary megakaryocyte progenitors from patients.

Discussion

This study uncovers a novel signaling mechanism in which a cytokine receptor is activated by a mutant chaperone protein leading to a phenotype linked to the lineage-restricted TpoR. We demonstrate that the 2 most common MPN-associated *CALR* mutants induce constitutive,

Proof Only

ligand-independent activation of TpoR, in several systems and with different read-outs. The interaction between CALR mutants and TpoR directly leads to close dimerization of JAK2 kinase domain and its activation. These observations are in accordance with the results of bone marrow transplantation studies[7] and companion study,[8] where CALR mutants induced an ET phenotype, as well as with TpoR being essential for the megakaryocytic lineage, which is affected in ET and PMF patients. No other receptor tested could support activation of JAK-STAT pathway by CALR mutants, except GCSFR, where activation did not lead to long-term proliferation. It remains to be determined whether the weak GCSFR effects contribute to the phenotype or penetrance in the granulocytic lineage.

We show that the extracellular domain of TpoR is crucial for activation by CALR mutants, but Tpo-binding site is not. Further studies are required for determining the structural details of exactly how CALR mutants interact with the TpoR extracellular domain. TpoR *N*-linked sugars and CALR glycan-binding domain and the novel tail are required. Interestingly, unlike most of the cytokine receptors (including the closely related EpoR),[39] TpoR has been shown to be able to signal from several dimeric interfaces.[11,40] Because CALR can bind to *N*-glycosylated residues of several proteins,[26] the specificity of TpoR activation cannot be attributed only to the interaction of CALR mutant to the receptor; rather the CALR mutant might stabilize one of the many active interfaces of TpoR,[11,40] resulting in constitutive activation of the receptor. del52 and ins5 CALR mutants might stabilize 2 related, but not identical, active dimeric interfaces of TpoR, leading to differences in the phenotype, as suggested.[41,42] This hypothesis would also explain why *CALR* mutants are not seen in other cancers driven by *N*-glycosylated mutated receptors (eg, EGFR, EPOR, KIT, FLT3D).[6] Furthermore, binding of CALR mutant to TpoR and its activation do not require Tpo-binding.

Recently, the pathogenic effects of CALR mutants were shown to depend on the length of the stretch of negatively-charged residues that are retained before the frameshift.[10] Type 1–like mutations resemble del52 CALR, where most of the stretches are deleted; this leads to high cytosolic calcium levels in megakaryocytes, presumably caused by the absence of calcium storage capacity in the ER.[10] Another type 1 mutant, del61 CALR, reported in the MARIMO cell line,[30] derived from an ET patient who was treated with Busulfan,[43] also activates TpoR (supplemental Figure 2A-B). Mutants that preserve stretches of negatively-charged residues like ins5 do not show calcium defects.[10] Further studies are required to determine whether the higher signaling we note in the case of del52 CALR is linked to its effects on calcium.

The interaction between TpoR and CALR is not only important in cell lines as Ba/F3 but also in the pathogenesis of the disease. We could show that Tpo-independent growth of megakaryocytic progenitors, which is a hallmark of CALR-mutated MPNs, is inhibited when TpoR or JAK2 are downregulated by shRNAs. This is in agreement with the observation that patients with CALR-mutated PMF may respond to ruxolitinib[31] and with the results of the retroviral CALR mouse model[7] described in the companion paper, where the thrombocytosis was dependent of the presence of TpoR.[8]

We observed a differential localization of CALR mutants compared with the wild-type. Our preliminary data indicate that activation already occurs intracellularly for the JAK-STAT pathway, but because we detect immature TpoR on the cell surface along with CALR mutant, it is possible that both intracellular and cell surface forms are required for transformation.

Contrary to JAK2V617F-transformed hematopoietic cells, there was no synergy between JAK2 and PI3-K inhibitors in inhibiting CALR mutant cells. Interestingly, a certain degree of synergy can be detected between JAK2 and MAP-kinase inhibitors. These differences might relate to the precise mechanisms of activation of TpoR by JAK2V617F vs CALR mutants. We suggest that combining JAK2 and PI3-K inhibitors might not be effective in CALR-mutated MPNs. Overall, our results are in agreement with CALR mutants activating the JAK-STAT pathway with signatures that overlap,[44] but they are not identical with those of JAK2V617F.[45]

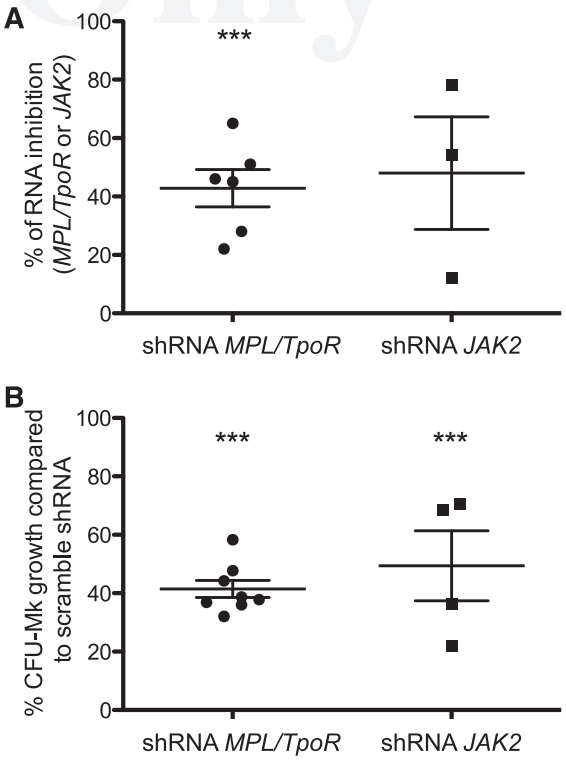


Figure 7. TpoR and JAK2 are required in CALR mutant–induced spontaneous growth of megakaryocytic progenitors in patients. $CD34^+$ cells from patients carrying *CALR*del52 or *CALR*ins5 mutations were purified. (A) The percentages of inhibition of *MPL/TpoR* and *JAK2* mRNA expression level by quantitative real-time polymerase chain reaction in $CD34^+$ progenitors transduced with lentivirus expressing either sort hairpin RNAs (shRNA) targeting *MPL/TpoR* or *JAK2*, sorted on GFP, and cultured for 2 additional days. (B) The percentages of Tpo-dependent or -independent growth of megakaryocyte colonies derived from CFU-Mk (colony-forming unit megakaryocyte) in the presence of shRNA directed against *MPL/TpoR* or *JAK2* compared with scramble sequence. Results are means ± SEM. Student *t* test: $^{***}P < .0001$.

In conclusion, this work demonstrates that CALR mutants specifically activate TpoR in a Tpo-independent manner and bring forward a new and unexpected oncogenic mechanism: cytokine receptor activation by a mutated chaperone.

Acknowledgments

The authors thank Nicolas Dauguet for expert cell sorting, Dr. M. Shwe for the CALR mutant N-glycan deficient. cDNAs for IL-2Rbeta, IL-9R and STAT1 were kindly provided by Dr. J.-C. Renauld, Ludwig Cancer Research, Brussels. Chimeric EpoR-TpoR constructs were from Dr. J. Staerk.

This work is supported by Institut National du Cancer (PLBIO2015), Agence Nationale de la Recherche, Programme Jeunes Chercheuses et Jeunes Chercheurs (ANR-13-JVSV1-GERMPN-01), and Institut National de la Santé et de la Recherche Médicale (INSERM) (I.P.); a grant from la Ligue Nationale contre le Cancer (équipe labellisée HR 2013, 2016) (H.R., I.P., W.V., C.M., M.E.); the Ludwig Institute for Cancer Research, FRS-FNRS, Salus

Proof Only

Sanguinis Foundation, the Action de Recherche Concertée project ARC10/15–027 of the Université catholique de Louvain, the Fondation contre le Cancer, the PAI Programs BCHM61B5, and Belgian Medical Genetics Initiative (S.N.C.); FRIA, Télévie, and FNRS-Aspirant fellowships (J.P.D., I.C., G.V.); Cliniques universitaires St-Luc, Brussels (J.P.D.); and a Belspo postdoctoral fellowship (V.G.).

Authorship

Contribution: I.C., C.P., and M.E.K. designed, performed, and interpreted experiments and corrected the paper; R.I.A., C.M., V.G., J.P.D., and G.V. performed experiments and interpreted results; A.N., A.K., and M.L.C. designed, performed, and interpreted drug inhibition studies; P.C. gave key input, designed fractionation and confocal microscopy experiments, interpreted experiments, and wrote a section; H.R. designed and interpreted experiments; and I.P., W.V., R.K., and S.N.C. designed and interpreted experiments and wrote the paper.

Conflict-of-interest disclosure: The authors declare no competing financial interests.

Correspondence: Stefan N. Constantinescu, Ludwig Institute for Cancer Research and de Duve Institute, Université catholique de Louvain, Avenue Hippocrate 74, UCL 75-4, Brussels B-1200, Belgium; e-mail: Stefan.Constantinescu@bru.licr.org.

References

1. Vardiman JW, Thiele J, Arber DA, et al. The 2008 revision of the World Health Organization (WHO) classification of myeloid neoplasms and acute leukemia: rationale and important changes. *Blood.* 2009;114(5):937-951.
2. Vainchenker W, Constantinescu SN. JAK/STAT signaling in hematological malignancies. *Oncogene.* 2013;32(21):2601-2613.
3. Cazzola M, Kralovics R. From Janus kinase 2 to calreticulin: the clinically relevant genomic landscape of myeloproliferative neoplasms. *Blood.* 2014;123(24):3714-3719.
4. Vainchenker W, Delhommeau F, Constantinescu SN, Bernard OA. New mutations and pathogenesis of myeloproliferative neoplasms. *Blood.* 2011;118(7):1723-1735.
5. Klampfl T, Gisslinger H, Harutyunyan AS, et al. Somatic mutations of calreticulin in myeloproliferative neoplasms. *N Engl J Med.* 2013;369(25):2379-2390.
6. Nangalia J, Massie CE, Baxter EJ, et al. Somatic CALR mutations in myeloproliferative neoplasms with nonmutated JAK2. *N Engl J Med.* 2013; 369(25):2391-2405.
7. Marty C, Harini N, Pecquet C, et al. Calr mutants retroviral mouse models lead to a myeloproliferative neoplasm mimicking an essential thrombocythemia progressing to a myelofibrosis [abstract]. *Blood.* 2014;124(21). Abstract 157.
8. Marty C, Pecquet C, Nivarthi H, et al. Expression of calreticulin mutants in mice induce a MPL-dependent thrombocytosis progressing to myelofibrosis for the type I mutant. *Blood.* 2015. pii: blood-2015-11-679571, In press.
9. Cabagnols X, Defour JP, Ugo V, et al. Differential association of calreticulin type 1 and type 2 mutations with myelofibrosis and essential thrombocytemia: relevance for disease evolution. *Leukemia.* 2015;29(1):249-252.
10. Pietra D, Rumi E, Ferretti VV, et al. Differential clinical effects of different mutation subtypes in CALR-mutant myeloproliferative neoplasms [published online ahead of print October 9, 2015]. *Leukemia.* 2015. doi: 10.1038/leu.2015.277.
11. Staerk J, Defour JP, Pecquet C, et al. Orientation-specific signalling by thrombopoietin receptor dimers. *EMBO J.* 2011;30(21):4398-4413.
12. Royer Y, Staerk J, Costuleanu M, Courtoy PJ, Constantinescu SN. Janus kinases affect thrombopoietin receptor cell surface localization and stability. *J Biol Chem.* 2005;280(29): 27251-27261.
13. Albu RI, Constantinescu SN. Extracellular domain N-glycosylation controls human thrombopoietin receptor cell surface levels. *Front Endocrinol (Lausanne).* 2011;2:71.
14. Besancenot R, Chaligné R, Tonetti C, et al. A senescence-like cell-cycle arrest occurs during megakaryocytic maturation: implications for physiological and pathological megakaryocytic proliferation. *PLoS Biol.* 2010;8(9):e1000476.
15. Pang SF, Li XK, Zhang Q, Yang F, Xu P. Interference RNA (RNAi)-based silencing of endogenous thrombopoietin receptor (Mpl) in Dami cells resulted in decreased hNUDC-mediated megakaryocyte proliferation and differentiation. *Exp Cell Res.* 2009;315(20): 3563-3573.
16. da Costa Reis Monte-Mór B, Plo I, da Cunha AF, et al. Constitutive JunB expression, associated with the JAK2 V617F mutation, stimulates proliferation of the erythroid lineage. *Leukemia.* 2009;23(1):144-152.
17. Kohlhuber F, Rogers NC, Watling D, et al. A JAK1/JAK2 chimera can sustain alpha and gamma interferon responses. *Mol Cell Biol.* 1997; 17(2):695-706.
18. Mesaeli N, Nakamura K, Zvaritch E, et al. Calreticulin is essential for cardiac development. *J Cell Biol.* 1999;144(5):857-868.
19. Wood TJ, Sliva D, Lobie PE, et al. Specificity of transcription enhancement via the STAT responsive element in the serine protease inhibitor 2.1 promoter. *Mol Cell Endocrinol.* 1997; 130(1-2):69-81.
20. Debili N, Coulombel L, Croisille L, et al. Characterization of a bipotent erythro-megakaryocytic progenitor in human bone marrow. *Blood.* 1996;88(4):1284-1296.
21. Remy I, Michnick SW. A highly sensitive protein-protein interaction assay based on Gaussia luciferase. *Nat Methods.* 2006;3(12):977-979.
22. Defour JP, Itaya M, Gryshkova V, et al. Tryptophan at the transmembrane-cytosolic junction modulates thrombopoietin receptor dimerization and activation. *Proc Natl Acad Sci USA.* 2013;110(7):2540-2545.
23. Courtoy PJ. Analytical subcellular fractionation of endosomal compartments in rat hepatocytes. *Subcell Biochem.* 1993;19:29-68.
24. Choong ML, Pecquet C, Pendharkar V, et al. Combination treatment for myeloproliferative neoplasms using JAK and pan-class I PI3K inhibitors. *J Cell Mol Med.* 2013;17(11): 1397-1409.
25. Chou TC. Theoretical basis, experimental design, and computerized simulation of synergism and antagonism in drug combination studies. *Pharmacol Rev.* 2006;58(3):621-681.
26. Michalak M, Groenendyk J, Szabo E, Gold LI, Opas M. Calreticulin, a multi-process calcium-buffering chaperone of the endoplasmic reticulum. *Biochem J.* 2009;417(3):651-666.
27. Huang LJ, Constantinescu SN, Lodish HF. The N-terminal domain of Janus kinase 2 is required for Golgi processing and cell surface expression of erythropoietin receptor. *Mol Cell.* 2001;8(6): 1327-1338.
28. Tong W, Sulahian R, Gross AW, Hendon N, Lodish HF, Huang LJ. The membrane-proximal region of the thrombopoietin receptor confers its high surface expression by JAK2-dependent and -independent mechanisms. *J Biol Chem.* 2006; 281(50):38930-38940.
29. Drachman JG, Millett KM, Kaushansky K. Thrombopoietin signal transduction requires functional JAK2, not TYK2. *J Biol Chem.* 1999; 274(19):13480-13484.
30. Kollmann K, Nangalia J, Warsch W, et al. MARIMO cells harbor a CALR mutation but are not dependent on JAK2/STAT5 signaling. *Leukemia.* 2015;29(2):494-497.
31. Guglielmelli P, Rotunno G, Bogani C, et al. Ruxolitinib is an effective treatment for CALR-positive patients with myelofibrosis. *Br J Haematol.* 2015; doi: 10.1111/bjh.13644.:In press.
32. Patel KP, Newberry KJ, Luthra R, et al. Correlation of mutation profile and response in patients with myelofibrosis treated with ruxolitinib. *Blood.* 2015;126(6):790-797.
33. Passamonti F, Caramazza D, Maffioli M. JAK inhibitor in CALR-mutant myelofibrosis. *N Engl J Med.* 2014;370(12):1168-1169.
34. Bartalucci N, Tozzi L, Bogani C, et al. Co-targeting the PI3K/mTOR and JAK2 signalling pathways produces synergistic activity against myeloproliferative neoplasms. *J Cell Mol Med.* 2013;17(11):1385-1396.
35. Bartalucci N, Guglielmelli P, Vannucchi AM. Rationale for targeting the PI3K/Akt/mTOR pathway in myeloproliferative neoplasms. *Clin Lymphoma Myeloma Leuk.* 2013;13(Suppl 2): S307-S309.
36. Chen WM, Yu B, Zhang Q, Xu P. Identification of the residues in the extracellular domain of thrombopoietin receptor involved in the binding of thrombopoietin and a nuclear distribution protein (human NUDC). *J Biol Chem.* 2010;285(34): 26697-26709.
37. Kapoor M, Ellgaard L, Gopalakrishnapai J, et al. Mutational analysis provides molecular insight into the carbohydrate-binding region of calreticulin: pivotal roles of tyrosine-109 and aspartate-135 in carbohydrate recognition. *Biochemistry.* 2004;43(1):97-106.
38. Mondet J, Park JH, Menard A, et al. Endogenous megakaryocytic colonies underline association between megakaryocytes and calreticulin mutations in essential thrombocythemia. *Haematologica.* 2015;100(5):e176-e178.

Proof Only

Proof Only

39. Seubert N, Royer Y, Staerk J, et al. Active and inactive orientations of the transmembrane and cytosolic domains of the erythropoietin receptor dimer. *Mol Cell.* 2003;12(5): 1239-1250.

40. Matthews EE, Thévenin D, Rogers JM, et al. Thrombopoietin receptor activation: transmembrane helix dimerization, rotation, and allosteric modulation. *FASEB J.* 2011;25(7): 2234-2244.

41. Tefferi A, Lasho TL, Finke C, et al. Type 1 vs type 2 calreticulin mutations in primary myelofibrosis: differences in phenotype and prognostic impact. *Leukemia.* 2014;28(7): 1568-1570.

42. Tefferi A, Wassie EA, Guglielmelli P, et al. Type 1 versus Type 2 calreticulin mutations in essential thrombocythemia: a collaborative study of 1027 patients. *Am J Hematol.* 2014; 89(8):E121-E124.

43. Yoshida H, Kondo M, Ichihashi T, et al. A novel myeloid cell line, Marimo, derived from therapy-related acute myeloid leukemia during treatment of essential thrombocythemia: consistent chromosomal abnormalities and temporary C-MYC gene amplification. *Cancer Genet Cytogenet.* 1998;100(1):21-24.

44. Rampal R, Al-Shahrour F, Abdel-Wahab O, et al. Integrated genomic analysis illustrates the central role of JAK-STAT pathway activation in myeloproliferative neoplasm pathogenesis. *Blood.* 2014;123(22):e123-e133.

45. Lau WW, Hannah R, Green AR, Göttgens B. The JAK-STAT signaling pathway is differentially activated in CALR-positive compared with JAK2V617F-positive ET patients. *Blood.* 2015; 125(10):1679-1681.

Proof Only

VIII. BIBLIOGRAPHY

1. Mothes W, Heinrich SU, Graf R, et al. Molecular mechanism of membrane protein integration into the endoplasmic reticulum. *Cell* 1997; **89**(4): 523-33.
2. Do H, Falcone D, Lin J, Andrews DW, Johnson AE. The cotranslational integration of membrane proteins into the phospholipid bilayer is a multistep process. *Cell* 1996; **85**(3): 369-78.
3. Hartmann E, Rapoport TA, Lodish HF. Predicting the orientation of eukaryotic membrane-spanning proteins. *Proc Natl Acad Sci U S A* 1989; **86**(15): 5786-90.
4. Lodish. Molecular Cell Biology. 7th ed. New York; 2013.
5. Arkin IT, Brunger AT. Statistical analysis of predicted transmembrane alpha-helices. *Biochim Biophys Acta* 1998; **1429**(1): 113-28.
6. Pesko GAR, D . Protein structure and function: Oxford University press; 2009.
7. Kandasamy SK, Larson RG. Molecular dynamics simulations of model trans-membrane peptides in lipid bilayers: a systematic investigation of hydrophobic mismatch. *Biophys J* 2006; **90**(7): 2326-43.
8. Matthews EE, Zoonens M, Engelman DM. Dynamic helix interactions in transmembrane signaling. *Cell* 2006; **127**(3): 447-50.
9. Jensen MO, Mouritsen OG. Lipids do influence protein function-the hydrophobic matching hypothesis revisited. *Biochim Biophys Acta* 2004; **1666**(1-2): 205-26.
10. Wimley WC, White SH. Experimentally determined hydrophobicity scale for proteins at membrane interfaces. *Nat Struct Biol* 1996; **3**(10): 842-8.
11. Wimley WC, Creamer TP, White SH. Solvation energies of amino acid side chains and backbone in a family of host-guest pentapeptides. *Biochemistry* 1996; **35**(16): 5109-24.
12. Henderson R, Baldwin JM, Ceska TA, Zemlin F, Beckmann E, Downing KH. Model for the structure of bacteriorhodopsin based on high-resolution electron cryo-microscopy. *J Mol Biol* 1990; **213**(4): 899-929.

13. Engelman DM, Steitz TA, Goldman A. Identifying nonpolar transbilayer helices in amino acid sequences of membrane proteins. *Annu Rev Biophys Biophys Chem* 1986; **15**: 321-53.
14. de Planque MR, Kruijtzer JA, Liskamp RM, et al. Different membrane anchoring positions of tryptophan and lysine in synthetic transmembrane alpha-helical peptides. *J Biol Chem* 1999; **274**(30): 20839-46.
15. Gratkowski H, Lear JD, DeGrado WF. Polar side chains drive the association of model transmembrane peptides. *Proc Natl Acad Sci U S A* 2001; **98**(3): 880-5.
16. Smith SO, Smith CS, Bormann BJ. Strong hydrogen bonding interactions involving a buried glutamic acid in the transmembrane sequence of the neu/erbB-2 receptor. *Nat Struct Biol* 1996; **3**(3): 252-8.
17. Ding J, Komatsu H, Iida S, et al. The Asn505 mutation of the c-MPL gene, which causes familial essential thrombocythemia, induces autonomous homodimerization of the c-Mpl protein due to strong amino acid polarity. *Blood* 2009; **114**(15): 3325-8.
18. Ding J, Komatsu H, Wakita A, et al. Familial essential thrombocythemia associated with a dominant-positive activating mutation of the c-MPL gene, which encodes for the receptor for thrombopoietin. *Blood* 2004; **103**(11): 4198-200.
19. Beer PA, Campbell PJ, Scott LM, et al. MPL mutations in myeloproliferative disorders: analysis of the PT-1 cohort. *Blood* 2008; **112**(1): 141-9.
20. Chaligne R, Tonetti C, Besancenot R, et al. New mutations of MPL in primitive myelofibrosis: only the MPL W515 mutations promote a G1/S-phase transition. *Leukemia* 2008; **22**(8): 1557-66.
21. Ma W, Zhang X, Wang X, et al. MPL mutation profile in JAK2 mutation-negative patients with myeloproliferative disorders. *Diagn Mol Pathol* 2011; **20**(1): 34-9.
22. Wilkes D, Rutland P, Pulleyn LJ, et al. A recurrent mutation, ala391glu, in the transmembrane region of FGFR3 causes Crouzon syndrome and acanthosis nigricans. *J Med Genet* 1996; **33**(9): 744-8.
23. Venancio TM, Aravind L. CYSTM, a novel cysteine-rich transmembrane module with a role in stress tolerance across eukaryotes. *Bioinformatics* 2010; **26**(2): 149-52.
24. Yau WM, Wimley WC, Gawrisch K, White SH. The preference of tryptophan for membrane interfaces. *Biochemistry* 1998; **37**(42): 14713-8.

25. Ladokhin AS, Selsted ME, White SH. Bilayer interactions of indolicidin, a small antimicrobial peptide rich in tryptophan, proline, and basic amino acids. *Biophys J* 1997; **72**(2 Pt 1): 794-805.
26. Adamian L, Nanda V, DeGrado WF, Liang J. Empirical lipid propensities of amino acid residues in multispan alpha helical membrane proteins. *Proteins* 2005; **59**(3): 496-509.
27. Ried CL, Kube S, Kirrbach J, Langosch D. Homotypic interaction and amino acid distribution of unilaterally conserved transmembrane helices. *J Mol Biol* 2012; **420**(3): 251-7.
28. Dougherty DA. Cation-pi interactions involving aromatic amino acids. *J Nutr* 2007; **137**(6 Suppl 1): 1504S-8S; discussion 16S-17S.
29. Dougherty DA. Cation-pi interactions in chemistry and biology: a new view of benzene, Phe, Tyr, and Trp. *Science* 1996; **271**(5246): 163-8.
30. Waksman G, Kominos D, Robertson SC, et al. Crystal structure of the phosphotyrosine recognition domain SH2 of v-src complexed with tyrosine-phosphorylated peptides. *Nature* 1992; **358**(6388): 646-53.
31. Coe H, Michalak M. Calcium binding chaperones of the endoplasmic reticulum. *Gen Physiol Biophys* 2009; **28 Spec No Focus**: F96-F103.
32. Michalak M, Corbett EF, Mesaeli N, Nakamura K, Opas M. Calreticulin: one protein, one gene, many functions. *Biochem J* 1999; **344 Pt 2**: 281-92.
33. Nangalia J, Massie CE, Baxter EJ, et al. Somatic CALR mutations in myeloproliferative neoplasms with nonmutated JAK2. *N Engl J Med* 2013; **369**(25): 2391-405.
34. Klampfl T, Gisslinger H, Harutyunyan AS, et al. Somatic mutations of calreticulin in myeloproliferative neoplasms. *N Engl J Med* 2013; **369**(25): 2379-90.
35. Parodi AJ. Protein glucosylation and its role in protein folding. *Annu Rev Biochem* 2000; **69**: 69-93.
36. Taylor SC, Thibault P, Tessier DC, Bergeron JJ, Thomas DY. Glycopeptide specificity of the secretory protein folding sensor UDP-glucose glycoprotein:glucosyltransferase. *EMBO Rep* 2003; **4**(4): 405-11.
37. Michalak M, Robert Parker JM, Opas M. Ca2+ signaling and calcium binding chaperones of the endoplasmic reticulum. *Cell Calcium* 2002; **32**(5-6): 269-78.

38. Ahner A, Brodsky JL. Checkpoints in ER-associated degradation: excuse me, which way to the proteasome? *Trends Cell Biol* 2004; **14**(9): 474-8.
39. Anelli T, Sitia R. Protein quality control in the early secretory pathway. *EMBO J* 2008; **27**(2): 315-27.
40. Zuber C, Fan JY, Guhl B, et al. Immunolocalization of UDP-glucose:glycoprotein glucosyltransferase indicates involvement of pre-Golgi intermediates in protein quality control. *Proc Natl Acad Sci U S A* 2001; **98**(19): 10710-5.
41. Arvan P, Zhao X, Ramos-Castaneda J, Chang A. Secretory pathway quality control operating in Golgi, plasmalemmal, and endosomal systems. *Traffic* 2002; **3**(11): 771-80.
42. Doherty GJ, McMahon HT. Mechanisms of endocytosis. *Annu Rev Biochem* 2009; **78**: 857-902.
43. Sorkin A, von Zastrow M. Endocytosis and signalling: intertwining molecular networks. *Nat Rev Mol Cell Biol* 2009; **10**(9): 609-22.
44. Gandhi H, Worch R, Kurgonaite K, et al. Dynamics and interaction of interleukin-4 receptor subunits in living cells. *Biophys J* 2014; **107**(11): 2515-27.
45. Constantinescu SN. Gathering support for critical mass: interleukin 4 receptor signaling requires clustering in endosomes. *Biophys J* 2014; **107**(11): 2479-80.
46. Palande K, Meenhuis A, Jevdjovic T, Touw IP. Scratching the surface: signaling and routing dynamics of the CSF3 receptor. *Front Biosci (Landmark Ed)* 2013; **18**: 91-105.
47. Engelman DM, Adair BD, Brunger A, et al. Dimerization of glycophorin A transmembrane helices: mutagenesis and modeling. *Soc Gen Physiol Ser* 1993; **48**: 11-21.
48. Manolios N, Bonifacino JS, Klausner RD. Transmembrane helical interactions and the assembly of the T cell receptor complex. *Science* 1990; **249**(4966): 274-7.
49. Bormann BJ, Knowles WJ, Marchesi VT. Synthetic peptides mimic the assembly of transmembrane glycoproteins. *J Biol Chem* 1989; **264**(7): 4033-7.
50. Senes A, Ubarretxena-Belandia I, Engelman DM. The Calpha ---H...O hydrogen bond: a determinant of stability and specificity in transmembrane helix interactions. *Proc Natl Acad Sci U S A* 2001; **98**(16): 9056-61.

51. Mueller BK, Subramaniam S, Senes A. A frequent, GxxxG-mediated, transmembrane association motif is optimized for the formation of interhelical Calpha-H hydrogen bonds. *Proc Natl Acad Sci U S A* 2014; **111**(10): E888-95.
52. Crick FH. Is alpha-keratin a coiled coil? *Nature* 1952; **170**(4334): 882-3.
53. Eilers M, Patel AB, Liu W, Smith SO. Comparison of helix interactions in membrane and soluble alpha-bundle proteins. *Biophys J* 2002; **82**(5): 2720-36.
54. Zhu BY, Zhou NE, Kay CM, Hodges RS. Packing and hydrophobicity effects on protein folding and stability: effects of beta-branched amino acids, valine and isoleucine, on the formation and stability of two-stranded alpha-helical coiled coils/leucine zippers. *Protein Sci* 1993; **2**(3): 383-94.
55. McLachlan AD, Karn J. Periodic features in the amino acid sequence of nematode myosin rod. *J Mol Biol* 1983; **164**(4): 605-26.
56. Walters RF, DeGrado WF. Helix-packing motifs in membrane proteins. *Proc Natl Acad Sci U S A* 2006; **103**(37): 13658-63.
57. Sun J, Ramos A, Chapman B, et al. Clonal dynamics of native haematopoiesis. *Nature* 2014; **514**(7522): 322-7.
58. Costa G, Kouskoff V, Lacaud G. Origin of blood cells and HSC production in the embryo. *Trends Immunol* 2012; **33**(5): 215-23.
59. Besancenot R, Chaligne R, Tonetti C, et al. A senescence-like cell-cycle arrest occurs during megakaryocytic maturation: implications for physiological and pathological megakaryocytic proliferation. *PLoS Biol* 2010; **8**(9).
60. Patel SR, Richardson JL, Schulze H, et al. Differential roles of microtubule assembly and sliding in proplatelet formation by megakaryocytes. *Blood* 2005; **106**(13): 4076-85.
61. Grozovsky R, Begonja AJ, Liu K, et al. The Ashwell-Morell receptor regulates hepatic thrombopoietin production via JAK2-STAT3 signaling. *Nat Med* 2015; **21**(1): 47-54.
62. Mason KD, Carpinelli MR, Fletcher JI, et al. Programmed anuclear cell death delimits platelet life span. *Cell* 2007; **128**(6): 1173-86.
63. Kuter DJ. The physiology of platelet production. *Stem Cells* 1996; **14 Suppl 1**: 88-101.
64. Kossiakoff AA. The structural basis for biological signaling, regulation, and specificity in the growth hormone-prolactin system of hormones and receptors. *Adv Protein Chem* 2004; **68**: 147-69.

65. Robb L. Cytokine receptors and hematopoietic differentiation. *Oncogene* 2007; **26**(47): 6715-23.
66. de Vos AM, Ultsch M, Kossiakoff AA. Human growth hormone and extracellular domain of its receptor: crystal structure of the complex. *Science* 1992; **255**(5042): 306-12.
67. Hilton DJ, Watowich SS, Katz L, Lodish HF. Saturation mutagenesis of the WSXWS motif of the erythropoietin receptor. *J Biol Chem* 1996; **271**(9): 4699-708.
68. Murakami M, Narazaki M, Hibi M, et al. Critical cytoplasmic region of the interleukin 6 signal transducer gp130 is conserved in the cytokine receptor family. *Proc Natl Acad Sci U S A* 1991; **88**(24): 11349-53.
69. Kotenko SV, Izotova LS, Pollack BP, et al. Other kinases can substitute for Jak2 in signal transduction by interferon-gamma. *J Biol Chem* 1996; **271**(29): 17174-82.
70. Ward AC, Touw I, Yoshimura A. The Jak-Stat pathway in normal and perturbed hematopoiesis. *Blood* 2000; **95**(1): 19-29.
71. Rodig SJ, Meraz MA, White JM, et al. Disruption of the Jak1 gene demonstrates obligatory and nonredundant roles of the Jaks in cytokine-induced biologic responses. *Cell* 1998; **93**(3): 373-83.
72. Neubauer H, Cumano A, Muller M, Wu H, Huffstadt U, Pfeffer K. Jak2 deficiency defines an essential developmental checkpoint in definitive hematopoiesis. *Cell* 1998; **93**(3): 397-409.
73. Nosaka T, van Deursen JM, Tripp RA, et al. Defective lymphoid development in mice lacking Jak3. *Science* 1995; **270**(5237): 800-2.
74. Karaghiosoff M, Neubauer H, Lassnig C, et al. Partial impairment of cytokine responses in Tyk2-deficient mice. *Immunity* 2000; **13**(4): 549-60.
75. Ishida-Takahashi R, Rosario F, Gong Y, et al. Phosphorylation of Jak2 on Ser(523) inhibits Jak2-dependent leptin receptor signaling. *Mol Cell Biol* 2006; **26**(11): 4063-73.
76. Feng J, Witthuhn BA, Matsuda T, Kohlhuber F, Kerr IM, Ihle JN. Activation of Jak2 catalytic activity requires phosphorylation of Y1007 in the kinase activation loop. *Mol Cell Biol* 1997; **17**(5): 2497-501.
77. Feener EP, Rosario F, Dunn SL, Stancheva Z, Myers MG, Jr. Tyrosine phosphorylation of Jak2 in the JH2 domain inhibits cytokine signaling. *Mol Cell Biol* 2004; **24**(11): 4968-78.
78. Zeidler MPBN. The Drosophila JAK-STAT pathway. *JAK-STAT* 2013; **2/3**(e25353).

79. Candotti F, Oakes SA, Johnston JA, et al. Structural and functional basis for JAK3-deficient severe combined immunodeficiency. *Blood* 1997; **90**(10): 3996-4003.
80. Saharinen P, Silvennoinen O. The pseudokinase domain is required for suppression of basal activity of Jak2 and Jak3 tyrosine kinases and for cytokine-inducible activation of signal transduction. *J Biol Chem* 2002; **277**(49): 47954-63.
81. Bandaranayake RM, Ungureanu D, Shan Y, Shaw DE, Silvennoinen O, Hubbard SR. Crystal structures of the JAK2 pseudokinase domain and the pathogenic mutant V617F. *Nat Struct Mol Biol* 2012; **19**(8): 754-9.
82. Ungureanu D, Wu J, Pekkala T, et al. The pseudokinase domain of JAK2 is a dual-specificity protein kinase that negatively regulates cytokine signaling. *Nat Struct Mol Biol* 2011; **18**(9): 971-6.
83. Chatterjee-Kishore M, van den Akker F, Stark GR. Association of STATs with relatives and friends. *Trends Cell Biol* 2000; **10**(3): 106-11.
84. Meraz MA, White JM, Sheehan KC, et al. Targeted disruption of the Stat1 gene in mice reveals unexpected physiologic specificity in the JAK-STAT signaling pathway. *Cell* 1996; **84**(3): 431-42.
85. Park C, Li S, Cha E, Schindler C. Immune response in Stat2 knockout mice. *Immunity* 2000; **13**(6): 795-804.
86. Takeda K, Noguchi K, Shi W, et al. Targeted disruption of the mouse Stat3 gene leads to early embryonic lethality. *Proc Natl Acad Sci U S A* 1997; **94**(8): 3801-4.
87. Takeda K, Kaisho T, Yoshida N, Takeda J, Kishimoto T, Akira S. Stat3 activation is responsible for IL-6-dependent T cell proliferation through preventing apoptosis: generation and characterization of T cell-specific Stat3-deficient mice. *J Immunol* 1998; **161**(9): 4652-60.
88. Kaplan MH, Sun YL, Hoey T, Grusby MJ. Impaired IL-12 responses and enhanced development of Th2 cells in Stat4-deficient mice. *Nature* 1996; **382**(6587): 174-7.
89. Teglund S, McKay C, Schuetz E, et al. Stat5a and Stat5b proteins have essential and nonessential, or redundant, roles in cytokine responses. *Cell* 1998; **93**(5): 841-50.
90. Takeda K, Tanaka T, Shi W, et al. Essential role of Stat6 in IL-4 signalling. *Nature* 1996; **380**(6575): 627-30.
91. Li WX. Canonical and non-canonical JAK-STAT signaling. *Trends Cell Biol* 2008; **18**(11): 545-51.

92. Lodish HF. Molecular cell biology. sixth edition ed: W H freeman and company; 2008.
93. Vigon I, Mornon JP, Cocault L, et al. Molecular cloning and characterization of MPL, the human homolog of the v-mpl oncogene: identification of a member of the hematopoietic growth factor receptor superfamily. *Proc Natl Acad Sci U S A* 1992; **89**(12): 5640-4.
94. Bartley TD, Bogenberger J, Hunt P, et al. Identification and cloning of a megakaryocyte growth and development factor that is a ligand for the cytokine receptor Mpl. *Cell* 1994; **77**(7): 1117-24.
95. Deane CM, Kroemer RT, Richards WG. A structural model of the human thrombopoietin receptor complex. *J Mol Graph Model* 1997; **15**(3): 170-8, 85-8.
96. Feese MD, Tamada T, Kato Y, et al. Structure of the receptor-binding domain of human thrombopoietin determined by complexation with a neutralizing antibody fragment. *Proc Natl Acad Sci U S A* 2004; **101**(7): 1816-21.
97. Staerk J, Lacout C, Sato T, Smith SO, Vainchenker W, Constantinescu SN. An amphipathic motif at the transmembrane-cytoplasmic junction prevents autonomous activation of the thrombopoietin receptor. *Blood* 2006; **107**(5): 1864-71.
98. Constantinescu SN, Huang LJ, Nam H, Lodish HF. The erythropoietin receptor cytosolic juxtamembrane domain contains an essential, precisely oriented, hydrophobic motif. *Mol Cell* 2001; **7**(2): 377-85.
99. Sabath DF, Kaushansky K, Broudy VC. Deletion of the extracellular membrane-distal cytokine receptor homology module of Mpl results in constitutive cell growth and loss of thrombopoietin binding. *Blood* 1999; **94**(1): 365-7.
100. Albu RI, Constantinescu SN. Extracellular domain N-glycosylation controls human thrombopoietin receptor cell surface levels. *Front Endocrinol (Lausanne)* 2011; **2**: 71.
101. Alexander WS, Metcalf D, Dunn AR. Point mutations within a dimer interface homology domain of c-Mpl induce constitutive receptor activity and tumorigenicity. *EMBO J* 1995; **14**(22): 5569-78.
102. Pardanani AD, Levine RL, Lasho T, et al. MPL515 mutations in myeloproliferative and other myeloid disorders: a study of 1182 patients. *Blood* 2006; **108**(10): 3472-6.

103. Pikman Y, Lee BH, Mercher T, et al. MPLW515L is a novel somatic activating mutation in myelofibrosis with myeloid metaplasia. *PLoS Med* 2006; **3**(7): e270.
104. Onishi M, Mui AL, Morikawa Y, et al. Identification of an oncogenic form of the thrombopoietin receptor MPL using retrovirus-mediated gene transfer. *Blood* 1996; **88**(4): 1399-406.
105. Souyri M, Vigon I, Penciolelli JF, Heard JM, Tambourin P, Wendling F. A putative truncated cytokine receptor gene transduced by the myeloproliferative leukemia virus immortalizes hematopoietic progenitors. *Cell* 1990; **63**(6): 1137-47.
106. Matthews DJ, Topping RS, Cass RT, Giebel LB. A sequential dimerization mechanism for erythropoietin receptor activation. *Proc Natl Acad Sci U S A* 1996; **93**(18): 9471-6.
107. Sungaran R, Markovic B, Chong BH. Localization and regulation of thrombopoietin mRNA expression in human kidney, liver, bone marrow, and spleen using in situ hybridization. *Blood* 1997; **89**(1): 101-7.
108. Wolber EM, Fandrey J, Frackowski U, Jelkmann W. Hepatic thrombopoietin mRNA is increased in acute inflammation. *Thromb Haemost* 2001; **86**(6): 1421-4.
109. Chen WM, Yu B, Zhang Q, Xu P. Identification of the residues in the extracellular domain of thrombopoietin receptor involved in the binding of thrombopoietin and a nuclear distribution protein (human NUDC). *J Biol Chem* 2010; **285**(34): 26697-709.
110. Tang YS, Zhang YP, Xu P. hNUDC promotes the cell proliferation and differentiation in a leukemic cell line via activation of the thrombopoietin receptor (Mpl). *Leukemia* 2008; **22**(5): 1018-25.
111. Zheng YB, Xiao YY, Tan P, Zhang Q, Xu P. Live-cell visualization of intracellular interaction between a nuclear migration protein (hNUDC) and the thrombopoietin receptor (Mpl). *PLoS One* 2012; **7**(12): e51849.
112. Li J, Yang C, Xia Y, et al. Thrombocytopenia caused by the development of antibodies to thrombopoietin. *Blood* 2001; **98**(12): 3241-8.
113. Cohn CS, Bussel JB. Romiplostim: a second-generation thrombopoietin agonist. *Drugs Today (Barc)* 2009; **45**(3): 175-88.
114. Bussel JB, Kuter DJ, George JN, et al. AMG 531, a thrombopoiesis-stimulating protein, for chronic ITP. *N Engl J Med* 2006; **355**(16): 1672-81.

115. Tarasova A, Haylock D, Winkler D. Principal signalling complexes in haematopoiesis: structural aspects and mimetic discovery. *Cytokine Growth Factor Rev* 2011; **22**(4): 231-53.
116. Perugini M, Varelias A, Sadlon T, D'Andrea RJ. Hematopoietic growth factor mimetics: from concept to clinic. *Cytokine Growth Factor Rev* 2009; **20**(1): 87-94.
117. Marschke KB. Discovery of Non-Peptidyl Small-Molecule Human GCSF Receptor Agonists
for the Potential Treatment of Neutropenia. *53 rd ASH poster* 2011; **3391**.
118. Erickson-Miller CL, Delorme E, Tian SS, et al. Preclinical activity of eltrombopag (SB-497115), an oral, nonpeptide thrombopoietin receptor agonist. *Stem Cells* 2009; **27**(2): 424-30.
119. Tenhumberg S, Schuster B, Zhu L, et al. gp130 dimerization in the absence of ligand: preformed cytokine receptor complexes. *Biochem Biophys Res Commun* 2006; **346**(3): 649-57.
120. Schutt A, Zacharias M, Schneider N, et al. gp130 activation is regulated by D2-D3 interdomain connectivity. *Biochem J* 2013; **450**(3): 487-96.
121. Makki R, Meister M, Pennetier D, et al. A short receptor downregulates JAK/STAT signalling to control the Drosophila cellular immune response. *PLoS Biol* 2010; **8**(8): e1000441.
122. Brown S, Hu N, Hombria JC. Novel level of signalling control in the JAK/STAT pathway revealed by in situ visualisation of protein-protein interaction during Drosophila development. *Development* 2003; **130**(14): 3077-84.
123. Constantinescu SN, Keren T, Socolovsky M, Nam H, Henis YI, Lodish HF. Ligand-independent oligomerization of cell-surface erythropoietin receptor is mediated by the transmembrane domain. *Proc Natl Acad Sci U S A* 2001; **98**(8): 4379-84.
124. Kubatzky KF, Ruan W, Gurezka R, et al. Self assembly of the transmembrane domain promotes signal transduction through the erythropoietin receptor. *Curr Biol* 2001; **11**(2): 110-5.
125. Livnah O, Stura EA, Middleton SA, Johnson DL, Jolliffe LK, Wilson IA. Crystallographic evidence for preformed dimers of erythropoietin receptor before ligand activation. *Science* 1999; **283**(5404): 987-90.
126. Yang N, Wang X, Jiang J, Frank SJ. Role of the growth hormone (GH) receptor transmembrane domain in receptor predimerization and GH-induced activation. *Mol Endocrinol* 2007; **21**(7): 1642-55.

127. Qazi AM, Tsai-Morris CH, Dufau ML. Ligand-independent homo- and heterodimerization of human prolactin receptor variants: inhibitory action of the short forms by heterodimerization. *Mol Endocrinol* 2006; **20**(8): 1912-23.
128. Watowich SS, Hilton DJ, Lodish HF. Activation and inhibition of erythropoietin receptor function: role of receptor dimerization. *Mol Cell Biol* 1994; **14**(6): 3535-49.
129. Wrighton NC, Farrell FX, Chang R, et al. Small peptides as potent mimetics of the protein hormone erythropoietin. *Science* 1996; **273**(5274): 458-64.
130. Yoshimura A, Longmore G, Lodish HF. Point mutation in the exoplasmic domain of the erythropoietin receptor resulting in hormone-independent activation and tumorigenicity. *Nature* 1990; **348**(6302): 647-9.
131. Constantinescu SN, Liu X, Beyer W, et al. Activation of the erythropoietin receptor by the gp55-P viral envelope protein is determined by a single amino acid in its transmembrane domain. *EMBO J* 1999; **18**(12): 3334-47.
132. Remy I, Wilson IA, Michnick SW. Erythropoietin receptor activation by a ligand-induced conformation change. *Science* 1999; **283**(5404): 990-3.
133. Kubatzky KF, Liu W, Goldgraben K, Simmerling C, Smith SO, Constantinescu SN. Structural requirements of the extracellular to transmembrane domain junction for erythropoietin receptor function. *J Biol Chem* 2005; **280**(15): 14844-54.
134. Swaminathan K, Flynn P, Reece RJ, Marmorstein R. Crystal structure of a PUT3-DNA complex reveals a novel mechanism for DNA recognition by a protein containing a Zn2Cys6 binuclear cluster. *Nat Struct Biol* 1997; **4**(9): 751-9.
135. Walters KJ, Dayie KT, Reece RJ, Ptashne M, Wagner G. Structure and mobility of the PUT3 dimer. *Nat Struct Biol* 1997; **4**(9): 744-50.
136. Seubert N, Royer Y, Staerk J, et al. Active and inactive orientations of the transmembrane and cytosolic domains of the erythropoietin receptor dimer. *Mol Cell* 2003; **12**(5): 1239-50.
137. Poger D, Mark AE. Turning the growth hormone receptor on: evidence that hormone binding induces subunit rotation. *Proteins* 2010; **78**(5): 1163-74.

138. Royer Y, Staerk J, Costuleanu M, Courtoy PJ, Constantinescu SN. Janus kinases affect thrombopoietin receptor cell surface localization and stability. *J Biol Chem* 2005; **280**(29): 27251-61.
139. Sattler M, Durstin MA, Frank DA, et al. The thrombopoietin receptor c-MPL activates JAK2 and TYK2 tyrosine kinases. *Exp Hematol* 1995; **23**(9): 1040-8.
140. Schulze H, Ballmaier M, Welte K, Germeshausen M. Thrombopoietin induces the generation of distinct Stat1, Stat3, Stat5a and Stat5b homo- and heterodimeric complexes with different kinetics in human platelets. *Exp Hematol* 2000; **28**(3): 294-304.
141. Constantinescu SN, Leroy E, Gryshkova V, Pecquet C, Dusa A. Activating Janus kinase pseudokinase domain mutations in myeloproliferative and other blood cancers. *Biochem Soc Trans* 2013; **41**(4): 1048-54.
142. Yamada M, Komatsu N, Okada K, Kato T, Miyazaki H, Miura Y. Thrombopoietin induces tyrosine phosphorylation and activation of mitogen-activated protein kinases in a human thrombopoietin-dependent cell line. *Biochem Biophys Res Commun* 1995; **217**(1): 230-7.
143. Sattler M, Salgia R, Durstin MA, Prasad KV, Griffin JD. Thrombopoietin induces activation of the phosphatidylinositol-3' kinase pathway and formation of a complex containing p85PI3K and the protooncoprotein p120CBL. *J Cell Physiol* 1997; **171**(1): 28-33.
144. Miyakawa Y, Rojnuckarin P, Habib T, Kaushansky K. Thrombopoietin induces phosphoinositol 3-kinase activation through SHP2, Gab, and insulin receptor substrate proteins in BAF3 cells and primary murine megakaryocytes. *J Biol Chem* 2001; **276**(4): 2494-502.
145. Tamiya T, Kashiwagi I, Takahashi R, Yasukawa H, Yoshimura A. Suppressors of cytokine signaling (SOCS) proteins and JAK/STAT pathways: regulation of T-cell inflammation by SOCS1 and SOCS3. *Arterioscler Thromb Vasc Biol* 2011; **31**(5): 980-5.
146. Chung CD, Liao J, Liu B, et al. Specific inhibition of Stat3 signal transduction by PIAS3. *Science* 1997; **278**(5344): 1803-5.
147. Aoki N, Matsuda T. A cytosolic protein-tyrosine phosphatase PTP1B specifically dephosphorylates and deactivates prolactin-activated STAT5a and STAT5b. *J Biol Chem* 2000; **275**(50): 39718-26.
148. Myers MP, Andersen JN, Cheng A, et al. TYK2 and JAK2 are substrates of protein-tyrosine phosphatase 1B. *J Biol Chem* 2001; **276**(51): 47771-4.

149. Tong W, Zhang J, Lodish HF. Lnk inhibits erythropoiesis and Epo-dependent JAK2 activation and downstream signaling pathways. *Blood* 2005; **105**(12): 4604-12.
150. Hitchcock IS, Fox NE, Prevost N, Sear K, Shattil SJ, Kaushansky K. Roles of focal adhesion kinase (FAK) in megakaryopoiesis and platelet function: studies using a megakaryocyte lineage specific FAK knockout. *Blood* 2008; **111**(2): 596-604.
151. Lannutti BJ, Minear J, Blake N, Drachman JG. Increased megakaryocytopoiesis in Lyn-deficient mice. *Oncogene* 2006; **25**(23): 3316-24.
152. Tong W. A means to an end: ubiquitination of Mpl. *Blood* 2010; **115**(6): 1111-2.
153. Lehmann U, Schmitz J, Weissenbach M, et al. SHP2 and SOCS3 contribute to Tyr-759-dependent attenuation of interleukin-6 signaling through gp130. *J Biol Chem* 2003; **278**(1): 661-71.
154. Hitchcock IS, Chen MM, King JR, Kaushansky K. YRRL motifs in the cytoplasmic domain of the thrombopoietin receptor regulate receptor internalization and degradation. *Blood* 2008; **112**(6): 2222-31.
155. Dahlen DD, Broudy VC, Drachman JG. Internalization of the thrombopoietin receptor is regulated by 2 cytoplasmic motifs. *Blood* 2003; **102**(1): 102-8.
156. Saur SJ, Sangkhae V, Geddis AE, Kaushansky K, Hitchcock IS. Ubiquitination and degradation of the thrombopoietin receptor c-Mpl. *Blood* 2010; **115**(6): 1254-63.
157. Velazquez L, Cheng AM, Fleming HE, et al. Cytokine signaling and hematopoietic homeostasis are disrupted in Lnk-deficient mice. *J Exp Med* 2002; **195**(12): 1599-611.
158. Bersenev A, Wu C, Balcerek J, et al. Lnk constrains myeloproliferative diseases in mice. *J Clin Invest* 2010; **120**(6): 2058-69.
159. Ema H, Sudo K, Seita J, et al. Quantification of self-renewal capacity in single hematopoietic stem cells from normal and Lnk-deficient mice. *Dev Cell* 2005; **8**(6): 907-14.
160. Takizawa H, Kubo-Akashi C, Nobuhisa I, et al. Enhanced engraftment of hematopoietic stem/progenitor cells by the transient inhibition of an adaptor protein, Lnk. *Blood* 2006; **107**(7): 2968-75.
161. Gery S, Koeffler HP. Role of the adaptor protein LNK in normal and malignant hematopoiesis. *Oncogene* 2013; **32**(26): 3111-8.

162. Baran-Marszak F, Magdoud H, Desterke C, et al. Expression level and differential JAK2-V617F-binding of the adaptor protein Lnk regulates JAK2-mediated signals in myeloproliferative neoplasms. *Blood* 2010; **116**(26): 5961-71.
163. Ding LW, Sun QY, Lin DC, et al. LNK (SH2B3): paradoxical effects in ovarian cancer. *Oncogene* 2014.
164. Matsumoto A, Masuhara M, Mitsui K, et al. CIS, a cytokine inducible SH2 protein, is a target of the JAK-STAT5 pathway and modulates STAT5 activation. *Blood* 1997; **89**(9): 3148-54.
165. Starr R, Willson TA, Viney EM, et al. A family of cytokine-inducible inhibitors of signalling. *Nature* 1997; **387**(6636): 917-21.
166. Yoshimura A, Ohkubo T, Kiguchi T, et al. A novel cytokine-inducible gene CIS encodes an SH2-containing protein that binds to tyrosine-phosphorylated interleukin 3 and erythropoietin receptors. *EMBO J* 1995; **14**(12): 2816-26.
167. Kamizono S, Hanada T, Yasukawa H, et al. The SOCS box of SOCS-1 accelerates ubiquitin-dependent proteolysis of TEL-JAK2. *J Biol Chem* 2001; **276**(16): 12530-8.
168. Ungureanu D, Saharinen P, Junttila I, Hilton DJ, Silvennoinen O. Regulation of Jak2 through the ubiquitin-proteasome pathway involves phosphorylation of Jak2 on Y1007 and interaction with SOCS-1. *Mol Cell Biol* 2002; **22**(10): 3316-26.
169. Verdier F, Chretien S, Muller O, et al. Proteasomes regulate erythropoietin receptor and signal transducer and activator of transcription 5 (STAT5) activation. Possible involvement of the ubiquitinated Cis protein. *J Biol Chem* 1998; **273**(43): 28185-90.
170. Yasukawa H, Misawa H, Sakamoto H, et al. The JAK-binding protein JAB inhibits Janus tyrosine kinase activity through binding in the activation loop. *EMBO J* 1999; **18**(5): 1309-20.
171. Teofili L, Martini M, Cenci T, et al. Epigenetic alteration of SOCS family members is a possible pathogenetic mechanism in JAK2 wild type myeloproliferative diseases. *Int J Cancer* 2008; **123**(7): 1586-92.
172. Wang Q, Miyakawa Y, Fox N, Kaushansky K. Interferon-alpha directly represses megakaryopoiesis by inhibiting thrombopoietin-induced signaling through induction of SOCS-1. *Blood* 2000; **96**(6): 2093-9.
173. Alexander WS, Starr R, Fenner JE, et al. SOCS1 is a critical inhibitor of interferon gamma signaling and prevents the potentially fatal neonatal actions of this cytokine. *Cell* 1999; **98**(5): 597-608.

174. Metcalf D, Greenhalgh CJ, Viney E, et al. Gigantism in mice lacking suppressor of cytokine signalling-2. *Nature* 2000; **405**(6790): 1069-73.
175. Roberts AW, Robb L, Rakar S, et al. Placental defects and embryonic lethality in mice lacking suppressor of cytokine signaling 3. *Proc Natl Acad Sci U S A* 2001; **98**(16): 9324-9.
176. Marine JC, McKay C, Wang D, et al. SOCS3 is essential in the regulation of fetal liver erythropoiesis. *Cell* 1999; **98**(5): 617-27.
177. Liu B, Liao J, Rao X, et al. Inhibition of Stat1-mediated gene activation by PIAS1. *Proc Natl Acad Sci U S A* 1998; **95**(18): 10626-31.
178. Arora T, Liu B, He H, et al. PIASx is a transcriptional co-repressor of signal transducer and activator of transcription 4. *J Biol Chem* 2003; **278**(24): 21327-30.
179. Schmidt D, Muller S. PIAS/SUMO: new partners in transcriptional regulation. *Cell Mol Life Sci* 2003; **60**(12): 2561-74.
180. Liu B, Mink S, Wong KA, et al. PIAS1 selectively inhibits interferon-inducible genes and is important in innate immunity. *Nat Immunol* 2004; **5**(9): 891-8.
181. Roth W, Sustmann C, Kieslinger M, et al. PIASy-deficient mice display modest defects in IFN and Wnt signaling. *J Immunol* 2004; **173**(10): 6189-99.
182. Santti H, Mikkonen L, Anand A, et al. Disruption of the murine PIASx gene results in reduced testis weight. *J Mol Endocrinol* 2005; **34**(3): 645-54.
183. Burns CM, Sakaguchi K, Appella E, Ashwell JD. CD45 regulation of tyrosine phosphorylation and enzyme activity of src family kinases. *J Biol Chem* 1994; **269**(18): 13594-600.
184. Shultz LD, Rajan TV, Greiner DL. Severe defects in immunity and hematopoiesis caused by SHP-1 protein-tyrosine-phosphatase deficiency. *Trends Biotechnol* 1997; **15**(8): 302-7.
185. Kharitonenkov A, Schnekenburger J, Chen Z, et al. Adapter function of protein-tyrosine phosphatase 1D in insulin receptor/insulin receptor substrate-1 interaction. *J Biol Chem* 1995; **270**(49): 29189-93.
186. Bennett AM, Tang TL, Sugimoto S, Walsh CT, Neel BG. Protein-tyrosine-phosphatase SHPTP2 couples platelet-derived growth factor receptor beta to Ras. *Proc Natl Acad Sci U S A* 1994; **91**(15): 7335-9.
187. Kim H, Hawley TS, Hawley RG, Baumann H. Protein tyrosine phosphatase 2 (SHP-2) moderates signaling by gp130 but is not required for the induction of acute-phase plasma protein genes in hepatic cells. *Mol Cell Biol* 1998; **18**(3): 1525-33.

188. Mazharian A, Mori J, Wang YJ, et al. Megakaryocyte-specific deletion of the protein-tyrosine phosphatases Shp1 and Shp2 causes abnormal megakaryocyte development, platelet production, and function. *Blood* 2013; **121**(20): 4205-20.
189. Myers MP, Pass I, Batty IH, et al. The lipid phosphatase activity of PTEN is critical for its tumor supressor function. *Proc Natl Acad Sci U S A* 1998; **95**(23): 13513-8.
190. Camps M, Nichols A, Arkinstall S. Dual specificity phosphatases: a gene family for control of MAP kinase function. *FASEB J* 2000; **14**(1): 6-16.
191. Kaushansky K, Lok S, Holly RD, et al. Promotion of megakaryocyte progenitor expansion and differentiation by the c-Mpl ligand thrombopoietin. *Nature* 1994; **369**(6481): 568-71.
192. de Sauvage FJ, Carver-Moore K, Luoh SM, et al. Physiological regulation of early and late stages of megakaryocytopoiesis by thrombopoietin. *J Exp Med* 1996; **183**(2): 651-6.
193. Brizzi MF, Battaglia E, Montrucchio G, et al. Thrombopoietin stimulates endothelial cell motility and neoangiogenesis by a platelet-activating factor-dependent mechanism. *Circ Res* 1999; **84**(7): 785-96.
194. Cardier JE, Dempsey J. Thrombopoietin and its receptor, c-mpl, are constitutively expressed by mouse liver endothelial cells: evidence of thrombopoietin as a growth factor for liver endothelial cells. *Blood* 1998; **91**(3): 923-9.
195. Geddis AE, Fox NE, Kaushansky K. The Mpl receptor expressed on endothelial cells does not contribute significantly to the regulation of circulating thrombopoietin levels. *Exp Hematol* 2006; **34**(1): 82-6.
196. Solar GP, Kerr WG, Zeigler FC, et al. Role of c-mpl in early hematopoiesis. *Blood* 1998; **92**(1): 4-10.
197. Fox N, Priestley G, Papayannopoulou T, Kaushansky K. Thrombopoietin expands hematopoietic stem cells after transplantation. *J Clin Invest* 2002; **110**(3): 389-94.
198. Qian H, Buza-Vidas N, Hyland CD, et al. Critical role of thrombopoietin in maintaining adult quiescent hematopoietic stem cells. *Cell Stem Cell* 2007; **1**(6): 671-84.
199. Yoshihara H, Arai F, Hosokawa K, et al. Thrombopoietin/MPL signaling regulates hematopoietic stem cell quiescence and interaction with the osteoblastic niche. *Cell Stem Cell* 2007; **1**(6): 685-97.
200. Kaushansky K, Fox N, Lin NL, Liles WC. Lineage-specific growth factors can compensate for stem and progenitor cell deficiencies at the

postprogenitor cell level: an analysis of doubly TPO- and G-CSF receptor-deficient mice. *Blood* 2002; **99**(10): 3573-8.
201. Stoffel R, Ziegler S, Ghilardi N, Ledermann B, de Sauvage FJ, Skoda RC. Permissive role of thrombopoietin and granulocyte colony-stimulating factor receptors in hematopoietic cell fate decisions in vivo. *Proc Natl Acad Sci U S A* 1999; **96**(2): 698-702.
202. Alexander WS, Roberts AW, Maurer AB, Nicola NA, Dunn AR, Metcalf D. Studies of the c-Mpl thrombopoietin receptor through gene disruption and activation. *Stem Cells* 1996; **14 Suppl 1**: 124-32.
203. Gordon MS, Hoffman R. Growth factors affecting human thrombocytopoiesis: potential agents for the treatment of thrombocytopenia. *Blood* 1992; **80**(2): 302-7.
204. Chen Q, Solar G, Eaton DL, de Sauvage FJ. IL-3 does not contribute to platelet production in c-Mpl-deficient mice. *Stem Cells* 1998; **16 Suppl 2**: 31-6.
205. Ng AP, Kauppi M, Metcalf D, et al. Mpl expression on megakaryocytes and platelets is dispensable for thrombopoiesis but essential to prevent myeloproliferation. *Proc Natl Acad Sci U S A* 2014; **111**(16): 5884-9.
206. Tiedt R, Coers J, Ziegler S, et al. Pronounced thrombocytosis in transgenic mice expressing reduced levels of Mpl in platelets and terminally differentiated megakaryocytes. *Blood* 2009; **113**(8): 1768-77.
207. Goncalves F, Lacout C, Villeval JL, Wendling F, Vainchenker W, Dumenil D. Thrombopoietin does not induce lineage-restricted commitment of Mpl-R expressing pluripotent progenitors but permits their complete erythroid and megakaryocytic differentiation. *Blood* 1997; **89**(10): 3544-53.
208. Yan XQ, Lacey DL, Saris C, et al. Ectopic overexpression of c-mpl by retroviral-mediated gene transfer suppressed megakaryopoiesis but enhanced erythropoiesis in mice. *Exp Hematol* 1999; **27**(9): 1409-17.
209. Marty C, Lacout C, Martin A, et al. Myeloproliferative neoplasm induced by constitutive expression of JAK2V617F in knock-in mice. *Blood* 2010; **116**(5): 783-7.
210. Li J, Spensberger D, Ahn JS, et al. JAK2 V617F impairs hematopoietic stem cell function in a conditional knock-in mouse model of JAK2 V617F-positive essential thrombocythemia. *Blood* 2010; **116**(9): 1528-38.

211. Sangkhae V, Etheridge SL, Kaushansky K, Hitchcock IS. The thrombopoietin receptor, MPL, is critical for development of a JAK2V617F-induced myeloproliferative neoplasm. *Blood* 2014; **124**(26): 3956-63.
212. Duek A, Lundberg P, Shimizu T, et al. Loss of Stat1 decreases megakaryopoiesis and favors erythropoiesis in a JAK2-V617F-driven mouse model of MPNs. *Blood* 2014; **123**(25): 3943-50.
213. Bartunek P, Karafiat V, Bartunkova J, et al. Impact of chicken thrombopoietin and its receptor c-Mpl on hematopoietic cell development. *Exp Hematol* 2008; **36**(4): 495-505.
214. Tefferi A, Barbui T. Polycythemia vera and essential thrombocythemia: 2015 update on diagnosis, risk-stratification and management. *Am J Hematol* 2015; **90**(2): 162-73.
215. Michiels JJ. Acquired von Willebrand disease due to increasing platelet count can readily explain the paradox of thrombosis and bleeding in thrombocythemia. *Clin Appl Thromb Hemost* 1999; **5**(3): 147-51.
216. van Genderen PJ, Budde U, Michiels JJ, van Strik R, van Vliet HH. The reduction of large von Willebrand factor multimers in plasma in essential thrombocythaemia is related to the platelet count. *Br J Haematol* 1996; **93**(4): 962-5.
217. Budde U, van Genderen PJ. Acquired von Willebrand disease in patients with high platelet counts. *Semin Thromb Hemost* 1997; **23**(5): 425-31.
218. Cesar JM, de Miguel D, Garcia Avello A, Burgaleta C. Platelet dysfunction in primary thrombocythemia using the platelet function analyzer, PFA-100. *Am J Clin Pathol* 2005; **123**(5): 772-7.
219. Bornhauser M, Mohr B, Oelschlaegel U, et al. Concurrent JAK2(V617F) mutation and BCR-ABL translocation within committed myeloid progenitors in myelofibrosis. *Leukemia* 2007; **21**(8): 1824-6.
220. Hummel JM, Kletecka MC, Sanks JK, et al. Concomitant BCR-ABL1 translocation and JAK2(V617F) mutation in three patients with myeloproliferative neoplasms. *Diagn Mol Pathol* 2012; **21**(3): 176-83.
221. Curtin NJ, Campbell PJ, Green AR. The Philadelphia translocation and pre-existing myeloproliferative disorders. *Br J Haematol* 2005; **128**(5): 734-6.
222. Wu Y, Slovak ML, Snyder DS, Arber DA. Coexistence of inversion 16 and the Philadelphia chromosome in acute and chronic myeloid

leukemias : report of six cases and review of literature. *Am J Clin Pathol* 2006; **125**(2): 260-6.
223. Dai HP, Xue YQ, Wu LL, et al. p210 BCR/ABL1 as a secondary change in a patient with acute myelomonocytic leukemia (M4Eo) with inv(16). *Int J Hematol* 2012; **96**(6): 814-7.
224. Ninomiya S, Kanemura N, Tsurumi H, et al. Coexistence of inversion 16 and the Philadelphia chromosome comprising P190 BCR/ABL in chronic myeloid leukemia blast crisis. *Int J Hematol* 2011; **93**(6): 806-10.
225. Han E, Lee H, Kim M, et al. Characteristics of hematologic malignancies with coexisting t(9;22) and inv(16) chromosomal abnormalities. *Blood Res* 2014; **49**(1): 22-8.
226. Lundberg P, Karow A, Nienhold R, et al. Clonal evolution and clinical correlates of somatic mutations in myeloproliferative neoplasms. *Blood* 2014; **123**(14): 2220-8.
227. Tefferi A, Lasho TL, Finke CM, et al. CALR vs JAK2 vs MPL-mutated or triple-negative myelofibrosis: clinical, cytogenetic and molecular comparisons. *Leukemia* 2014; **28**(7): 1472-7.
228. McGaffin G, Harper K, Stirling D, McLintock L. JAK2 V617F and CALR mutations are not mutually exclusive; findings from retrospective analysis of a small patient cohort. *Br J Haematol* 2014; **167**(2): 276-8.
229. Ingram W, Lea NC, Cervera J, et al. The JAK2 V617F mutation identifies a subgroup of MDS patients with isolated deletion 5q and a proliferative bone marrow. *Leukemia* 2006; **20**(7): 1319-21.
230. Oh ST, Simonds EF, Jones C, et al. Novel mutations in the inhibitory adaptor protein LNK drive JAK-STAT signaling in patients with myeloproliferative neoplasms. *Blood* 2010; **116**(6): 988-92.
231. Hurtado C, Erquiaga I, Aranaz P, et al. LNK can also be mutated outside PH and SH2 domains in myeloproliferative neoplasms with and without V617FJAK2 mutation. *Leuk Res* 2011; **35**(11): 1537-9.
232. Aranaz P, Hurtado C, Erquiaga I, et al. CBL mutations in myeloproliferative neoplasms are also found in the gene's proline-rich domain and in patients with the V617FJAK2. *Haematologica* 2012; **97**(8): 1234-41.
233. Schnittger S, Bacher U, Alpermann T, et al. Use of CBL exon 8 and 9 mutations in diagnosis of myeloproliferative neoplasms and myelodysplastic/myeloproliferative disorders: an analysis of 636 cases. *Haematologica* 2012; **97**(12): 1890-4.

234. Jost E, do ON, Dahl E, et al. Epigenetic alterations complement mutation of JAK2 tyrosine kinase in patients with BCR/ABL-negative myeloproliferative disorders. *Leukemia* 2007; **21**(3): 505-10.
235. Delhommeau F, Dupont S, Della Valle V, et al. Mutation in TET2 in myeloid cancers. *N Engl J Med* 2009; **360**(22): 2289-301.
236. Carbuccia N, Murati A, Trouplin V, et al. Mutations of ASXL1 gene in myeloproliferative neoplasms. *Leukemia* 2009; **23**(11): 2183-6.
237. Dameshek W. Some speculations on the myeloproliferative syndromes. *Blood* 1951; **6**(4): 372-5.
238. James C, Ugo V, Le Couedic JP, et al. A unique clonal JAK2 mutation leading to constitutive signalling causes polycythaemia vera. *Nature* 2005; **434**(7037): 1144-8.
239. Ugo V, Marzac C, Teyssandier I, et al. Multiple signaling pathways are involved in erythropoietin-independent differentiation of erythroid progenitors in polycythemia vera. *Exp Hematol* 2004; **32**(2): 179-87.
240. Kralovics R, Guan Y, Prchal JT. Acquired uniparental disomy of chromosome 9p is a frequent stem cell defect in polycythemia vera. *Exp Hematol* 2002; **30**(3): 229-36.
241. Staerk J, Kallin A, Demoulin JB, Vainchenker W, Constantinescu SN. JAK1 and Tyk2 activation by the homologous polycythemia vera JAK2 V617F mutation: cross-talk with IGF1 receptor. *J Biol Chem* 2005; **280**(51): 41893-9.
242. Wernig G, Gonneville JR, Crowley BJ, et al. The Jak2V617F oncogene associated with myeloproliferative diseases requires a functional FERM domain for transformation and for expression of the Myc and Pim proto-oncogenes. *Blood* 2008; **111**(7): 3751-9.
243. Lu X, Huang LJ, Lodish HF. Dimerization by a cytokine receptor is necessary for constitutive activation of JAK2V617F. *J Biol Chem* 2008; **283**(9): 5258-66.
244. Dusa A, Staerk J, Elliott J, et al. Substitution of pseudokinase domain residue Val-617 by large non-polar amino acids causes activation of JAK2. *J Biol Chem* 2008; **283**(19): 12941-8.
245. Moliterno AR, Williams DM, Rogers O, Isaacs MA, Spivak JL. Phenotypic variability within the JAK2 V617F-positive MPD: roles of progenitor cell and neutrophil allele burdens. *Exp Hematol* 2008; **36**(11): 1480-6.
246. Scott LM, Beer PA, Bench AJ, Erber WN, Green AR. Prevalance of JAK2 V617F and exon 12 mutations in polycythaemia vera. *Br J Haematol* 2007; **139**(3): 511-2.

247. Percy MJ, Scott LM, Erber WN, et al. The frequency of JAK2 exon 12 mutations in idiopathic erythrocytosis patients with low serum erythropoietin levels. *Haematologica* 2007; **92**(12): 1607-14.
248. Malinge S, Ragu C, Della-Valle V, et al. Activating mutations in human acute megakaryoblastic leukemia. *Blood* 2008; **112**(10): 4220-6.
249. Liu K, Martini M, Rocca B, et al. Evidence for a founder effect of the MPL-S505N mutation in eight Italian pedigrees with hereditary thrombocythemia. *Haematologica* 2009; **94**(10): 1368-74.
250. Pecquet C, Staerk J, Chaligne R, et al. Induction of myeloproliferative disorder and myelofibrosis by thrombopoietin receptor W515 mutants is mediated by cytosolic tyrosine 112 of the receptor. *Blood* 2010; **115**(5): 1037-48.
251. Marty C, Chaligne R, Lacout C, Constantinescu SN, Vainchenker W, Villeval JL. Ligand-independent thrombopoietin mutant receptor requires cell surface localization for endogenous activity. *J Biol Chem* 2009; **284**(18): 11781-91.
252. Abe M, Suzuki K, Inagaki O, Sassa S, Shikama H. A novel MPL point mutation resulting in thrombopoietin-independent activation. *Leukemia* 2002; **16**(8): 1500-6.
253. Moliterno AR, Williams DM, Gutierrez-Alamillo LI, Salvatori R, Ingersoll RG, Spivak JL. Mpl Baltimore: a thrombopoietin receptor polymorphism associated with thrombocytosis. *Proc Natl Acad Sci U S A* 2004; **101**(31): 11444-7.
254. Stockklausner C, Klotter AC, Dickemann N, et al. The thrombopoietin receptor P106L mutation functionally separates receptor signaling activity from thrombopoietin homeostasis. *Blood* 2014.
255. Kawamata N, Ogawa S, Yamamoto G, et al. Genetic profiling of myeloproliferative disorders by single-nucleotide polymorphism oligonucleotide microarray. *Exp Hematol* 2008; **36**(11): 1471-9.
256. Lambert MP, Jiang J, Batra V, Wu C, Tong W. A novel mutation in MPL (Y252H) results in increased thrombopoietin sensitivity in essential thrombocythemia. *Am J Hematol* 2012; **87**(5): 532-4.
257. Pietra D, Brisci A, Rumi E, et al. Deep sequencing reveals double mutations in cis of MPL exon 10 in myeloproliferative neoplasms. *Haematologica* 2011; **96**(4): 607-11.
258. Boyd EM, Bench AJ, Goday-Fernandez A, et al. Clinical utility of routine MPL exon 10 analysis in the diagnosis of essential

thrombocythaemia and primary myelofibrosis. *Br J Haematol* 2010; **149**(2): 250-7.
259. Pardanani A, Guglielmelli P, Lasho TL, et al. Primary myelofibrosis with or without mutant MPL: comparison of survival and clinical features involving 603 patients. *Leukemia* 2011; **25**(12): 1834-9.
260. Pardanani A, Lasho T, Finke C, Oh ST, Gotlib J, Tefferi A. LNK mutation studies in blast-phase myeloproliferative neoplasms, and in chronic-phase disease with TET2, IDH, JAK2 or MPL mutations. *Leukemia* 2010; **24**(10): 1713-8.
261. Grand FH, Hidalgo-Curtis CE, Ernst T, et al. Frequent CBL mutations associated with 11q acquired uniparental disomy in myeloproliferative neoplasms. *Blood* 2009; **113**(24): 6182-92.
262. Beer PA, Delhommeau F, LeCouedic JP, et al. Two routes to leukemic transformation after a JAK2 mutation-positive myeloproliferative neoplasm. *Blood* 2010; **115**(14): 2891-900.
263. Suessmuth Y, Elliott J, Percy MJ, et al. A new polycythaemia vera-associated SOCS3 SH2 mutant (SOCS3F136L) cannot regulate erythropoietin responses. *Br J Haematol* 2009; **147**(4): 450-8.
264. Haan S, Wuller S, Kaczor J, et al. SOCS-mediated downregulation of mutant Jak2 (V617F, T875N and K539L) counteracts cytokine-independent signaling. *Oncogene* 2009; **28**(34): 3069-80.
265. Hookham MB, Elliott J, Suessmuth Y, et al. The myeloproliferative disorder-associated JAK2 V617F mutant escapes negative regulation by suppressor of cytokine signaling 3. *Blood* 2007; **109**(11): 4924-9.
266. Marty C, Saint-Martin C, Pecquet C, et al. Germ-line JAK2 mutations in the kinase domain are responsible for hereditary thrombocytosis and are resistant to JAK2 and HSP90 inhibitors. *Blood* 2014; **123**(9): 1372-83.
267. Jones AV, Chase A, Silver RT, et al. JAK2 haplotype is a major risk factor for the development of myeloproliferative neoplasms. *Nat Genet* 2009; **41**(4): 446-9.
268. Olcaydu D, Harutyunyan A, Jager R, et al. A common JAK2 haplotype confers susceptibility to myeloproliferative neoplasms. *Nat Genet* 2009; **41**(4): 450-4.
269. Jager R, Harutyunyan AS, Rumi E, et al. Common germline variation at the TERT locus contributes to familial clustering of myeloproliferative neoplasms. *Am J Hematol* 2014; **89**(12): 1107-10.

270. Saliba J, Saint-Martin C, Di Stefano A, et al. Germline duplication of ATG2B and GSKIP predisposes to familial myeloid malignancies. *Nat Genet* 2015.
271. Tefferi A, Pardanani A, Lim KH, et al. TET2 mutations and their clinical correlates in polycythemia vera, essential thrombocythemia and myelofibrosis. *Leukemia* 2009; **23**(5): 905-11.
272. Ito S, D'Alessio AC, Taranova OV, Hong K, Sowers LC, Zhang Y. Role of Tet proteins in 5mC to 5hmC conversion, ES-cell self-renewal and inner cell mass specification. *Nature* 2010; **466**(7310): 1129-33.
273. Xu W, Yang H, Liu Y, et al. Oncometabolite 2-hydroxyglutarate is a competitive inhibitor of alpha-ketoglutarate-dependent dioxygenases. *Cancer Cell* 2011; **19**(1): 17-30.
274. Schaub FX, Looser R, Li S, et al. Clonal analysis of TET2 and JAK2 mutations suggests that TET2 can be a late event in the progression of myeloproliferative neoplasms. *Blood* 2010; **115**(10): 2003-7.
275. Brecqueville M, Cervera N, Gelsi-Boyer V, et al. Rare mutations in DNMT3A in myeloproliferative neoplasms and myelodysplastic syndromes. *Blood Cancer J* 2011; **1**(5): e18.
276. Kim SJ, Zhao H, Hardikar S, Singh AK, Goodell MA, Chen T. A DNMT3A mutation common in AML exhibits dominant-negative effects in murine ES cells. *Blood* 2013; **122**(25): 4086-9.
277. Yen KE, Bittinger MA, Su SM, Fantin VR. Cancer-associated IDH mutations: biomarker and therapeutic opportunities. *Oncogene* 2010; **29**(49): 6409-17.
278. Pardanani A, Lasho TL, Finke CM, Mai M, McClure RF, Tefferi A. IDH1 and IDH2 mutation analysis in chronic- and blast-phase myeloproliferative neoplasms. *Leukemia* 2010; **24**(6): 1146-51.
279. Ernst T, Chase AJ, Score J, et al. Inactivating mutations of the histone methyltransferase gene EZH2 in myeloid disorders. *Nat Genet* 2010; **42**(8): 722-6.
280. Tefferi A. Novel mutations and their functional and clinical relevance in myeloproliferative neoplasms: JAK2, MPL, TET2, ASXL1, CBL, IDH and IKZF1. *Leukemia* 2010; **24**(6): 1128-38.
281. Jager R, Gisslinger H, Passamonti F, et al. Deletions of the transcription factor Ikaros in myeloproliferative neoplasms. *Leukemia* 2010; **24**(7): 1290-8.
282. Bain B. Dysplasia of all granulocyte lineages in myelodysplastic evolution of essential thrombocythemia. *Am J Hematol* 2013; (88): 426.

283. Maxson JE, Gotlib J, Pollyea DA, et al. Oncogenic CSF3R mutations in chronic neutrophilic leukemia and atypical CML. *N Engl J Med* 2013; **368**(19): 1781-90.
284. Russ WP, Engelman DM. TOXCAT: a measure of transmembrane helix association in a biological membrane. *Proc Natl Acad Sci U S A* 1999; **96**(3): 863-8.
285. Takegoshi K, Terao T. 13C-1H dipolar recoupling under very fast magic-angle spinning using virtual pulses. *Solid State Nucl Magn Reson* 1999; **13**(4): 203-12.
286. Crocker E, Patel AB, Eilers M, et al. Dipolar assisted rotational resonance NMR of tryptophan and tyrosine in rhodopsin. *J Biomol NMR* 2004; **29**(1): 11-20.
287. Bolterauer CH, H. Calculation of IR dichroic values and order parameters from molecular dynamics simulations and their application to structure determination of lipid bilayers. *Eur Biophys J* 1996; **24**: 322-34.
288. Dumoutier L, Van Roost E, Colau D, Renauld JC. Human interleukin-10-related T cell-derived inducible factor: molecular cloning and functional characterization as an hepatocyte-stimulating factor. *Proc Natl Acad Sci U S A* 2000; **97**(18): 10144-9.
289. Kotaja N, Aittomaki S, Silvennoinen O, Palvimo JJ, Janne OA. ARIP3 (androgen receptor-interacting protein 3) and other PIAS (protein inhibitor of activated STAT) proteins differ in their ability to modulate steroid receptor-dependent transcriptional activation. *Mol Endocrinol* 2000; **14**(12): 1986-2000.
290. Canosi U, Mascia M, Gazza L, et al. A highly precise reporter gene bioassay for type I interferon. *J Immunol Methods* 1996; **199**(1): 69-76.
291. Kuiperij HB, van der Horst A, Raaijmakers J, et al. Activation of FoxO transcription factors contributes to the antiproliferative effect of cAMP. *Oncogene* 2005; **24**(12): 2087-95.
292. Furuyama T, Nakazawa T, Nakano I, Mori N. Identification of the differential distribution patterns of mRNAs and consensus binding sequences for mouse DAF-16 homologues. *Biochem J* 2000; **349**(Pt 2): 629-34.
293. Royer Y, Menu C, Liu X, Constantinescu SN. High-throughput gateway bicistronic retroviral vectors for stable expression in mammalian cells: exploring the biologic effects of STAT5 overexpression. *DNA Cell Biol* 2004; **23**(6): 355-65.

294. Pear WS, Nolan GP, Scott ML, Baltimore D. Production of high-titer helper-free retroviruses by transient transfection. *Proc Natl Acad Sci U S A* 1993; **90**(18): 8392-6.
295. Naviaux RK, Costanzi E, Haas M, Verma IM. The pCL vector system: rapid production of helper-free, high-titer, recombinant retroviruses. *J Virol* 1996; **70**(8): 5701-5.
296. Palacios R, Henson G, Steinmetz M, McKearn JP. Interleukin-3 supports growth of mouse pre-B-cell clones in vitro. *Nature* 1984; **309**(5964): 126-31.
297. Kohlhuber F, Rogers NC, Watling D, et al. A JAK1/JAK2 chimera can sustain alpha and gamma interferon responses. *Mol Cell Biol* 1997; **17**(2): 695-706.
298. Lee JC, Hapel AJ, Ihle JN. Constitutive production of a unique lymphokine (IL 3) by the WEHI-3 cell line. *J Immunol* 1982; **128**(6): 2393-8.
299. Brooks AJ, Dai W, O'Mara ML, et al. Mechanism of activation of protein kinase JAK2 by the growth hormone receptor. *Science* 2014; **344**(6185): 1249783.
300. Mattoon D, Gupta K, Doyon J, Loll PJ, DiMaio D. Identification of the transmembrane dimer interface of the bovine papillomavirus E5 protein. *Oncogene* 2001; **20**(29): 3824-34.
301. Heitmann P. A model for sulfhydryl groups in proteins. Hydrophobic interactions of the cystein side chain in micelles. *Eur J Biochem* 1968; **3**(3): 346-50.
302. Sievers F, Wilm A, Dineen D, et al. Fast, scalable generation of high-quality protein multiple sequence alignments using Clustal Omega. *Mol Syst Biol* 2011; **7**: 539.
303. Nugent T, Jones DT. Transmembrane protein topology prediction using support vector machines. *BMC Bioinformatics* 2009; **10**: 159.
304. Defour JP, Itaya M, Gryshkova V, et al. Tryptophan at the transmembrane-cytosolic junction modulates thrombopoietin receptor dimerization and activation. *Proc Natl Acad Sci U S A* 2013; **110**(7): 2540-5.
305. Letunic I, Bork P. Interactive Tree Of Life v2: online annotation and display of phylogenetic trees made easy. *Nucleic Acids Res* 2011; **39**(Web Server issue): W475-8.
306. Jones DT. Improving the accuracy of transmembrane protein topology prediction using evolutionary information. *Bioinformatics* 2007; **23**(5): 538-44.

307. Haines DE, Holmes KR, Brett IJ. The hemogram of the colonized lesser bushbaby (Galago senegalensis). *Folia Primatol (Basel)* 1971; **14**(1): 95-100.
308. O'Shea EK, Klemm JD, Kim PS, Alber T. X-ray structure of the GCN4 leucine zipper, a two-stranded, parallel coiled coil. *Science* 1991; **254**(5031): 539-44.
309. Kaushansky K, Lok S, Holly RD, et al. Promotion of megakaryocyte progenitor expansion and differentiation by the c-Mpl ligand thrombopoietin. *Nature* 1994; **369**(6481): 568-71.
310. Yoshihara H, Arai F, Hosokawa K, et al. Thrombopoietin/mpl signaling regulates hematopoietic stem cell quiescence and interaction with the osteoblastic niche. *Cell Stem Cell* 2007; **1**(6): 685-97.
311. Qian H, Buza-Vidas N, Hyland CD, et al. Critical role of thrombopoietin in maintaining adult quiescent hematopoietic stem cells. *Cell Stem Cell* 2007; **1**(6): 671-84.
312. Constantinescu SN, Keren T, Socolovsky M, Nam HS, Henis YI, Lodish HF. Ligand-independent oligomerization of cell-surface erythropoietin receptor is mediated by the transmembrane domain. *Proc Natl Acad Sci USA* 2001; **98**(8): 4379-84.
313. Qazi AM, Tsai-Morris CH, Dufau ML. Ligand-independent homo- and heterodimerization of human prolactin receptor variants: inhibitory action of the short forms by heterodimerization. *Mol Endocrinol* 2006; **20**(8): 1912-23.
314. Defour J-P, Itaya M, Gryshkova V, et al. Tryptophan at the transmembrane-cytosolic junction modulates thrombopoietin receptor dimerization and activation. *Proc Natl Acad Sci USA* 2013; **110**(7): 2540-5.
315. Ding F, Komatsu H, Wakita A, et al. Familial essential thrombocythemia associated with a dominant-positive activating mutation of the c-MPL gene, which encodes for the receptor for thrombopoietin. *Blood* 2004; **103**(11): 4198-200.
316. Ma W, Zhang X, Wang X, et al. MPL mutation profile in JAK2 mutation-negative patients with myeloproliferative disorders. *Diagnostic Molecular Pathology* 2011; **20**(1): 34-9.
317. Beer PA, Campbell PJ, Scott LM, et al. MPL mutations in myeloproliferative disorders: analysis of the PT-1 cohort. *Blood* 2008; **112**(1): 141-9.

318. Staerk J, Defour JP, Pecquet C, et al. Orientation-specific signalling by thrombopoietin receptor dimers. *EMBO J* 2011; **30**(21): 4398-413.
319. Matthews EE, Thevenin D, Rogers JM, et al. Thrombopoietin receptor activation: transmembrane helix dimerization, rotation, and allosteric modulation. *FASEB J* 2011; **25**(7): 2234-44.
320. Staerk J, Lacout C, Sato T, Smith SO, Vainchenker W, Constantinescu SN. An amphipathic motif at the transmembrane-cytoplasmic junction prevents autonomous activation of the thrombopoietin receptor. *Blood* 2006; **107**(5): 1864-71.
321. Remy I, Michnick SW. A highly sensitive protein-protein interaction assay based on Gaussia luciferase. *Nat Methods* 2006; **3**(12): 977-9.
322. Pecquet C, Diaconu CC, Staerk J, et al. Thrombopoietin receptor down-modulation by JAK2 V617F: restoration of receptor levels by inhibitors of pathologic JAK2 signaling and of proteasomes. *Blood* 2012; **119**(20): 4625-35.
323. Samarajiwa SA, Forster S, Auchettl K, Hertzog PJ. INTERFEROME: the database of interferon regulated genes. *Nucleic Acids Res* 2009; **37**(Database issue): D852-7.
324. Essaghir A, Toffalini F, Knoops L, Kallin A, van Helden J, Demoulin JB. Transcription factor regulation can be accurately predicted from the presence of target gene signatures in microarray gene expression data. *Nucleic Acids Res* 2010; **38**(11): e120.
325. Kim MJ, Park SH, Opella SJ, et al. NMR structural studies of interactions of a small, nonpeptidyl Tpo mimic with the thrombopoietin receptor extracellular juxtamembrane and transmembrane domains. *J Biol Chem* 2007; **282**(19): 14253-61.
326. Chan DI, Prenner EJ, Vogel HJ. Tryptophan- and arginine-rich antimicrobial peptides: structures and mechanisms of action. *Biochim Biophys Acta* 2006; **1758**(9): 1184-202.
327. Jing W, Demcoe AR, Vogel HJ. Conformation of a bactericidal domain of puroindoline a: structure and mechanism of action of a 13-residue antimicrobial peptide. *J Bacteriol* 2003; **185**(16): 4938-47.
328. Lensink MF, Christiaens B, Vandekerckhove J, Prochiantz A, Rosseneu M. Penetratin-membrane association: W48/R52/W56 shield the peptide from the aqueous phase. *Biophys J* 2005; **88**(2): 939-52.

329. Haug BE, Skar ML, Svendsen JS. Bulky aromatic amino acids increase the antibacterial activity of 15-residue bovine lactoferricin derivatives. *J Pept Sci* 2001; **7**(8): 425-32.
330. Moraga I, Wernig G, Wilmes S, et al. Tuning cytokine receptor signaling by re-orienting dimer geometry with surrogate ligands. *Cell* 2015; **160**(6): 1196-208.
331. Arpel A, Sawma P, Spenle C, et al. Transmembrane domain targeting peptide antagonizing ErbB2/Neu inhibits breast tumor growth and metastasis. *Cell Rep* 2014; **8**(6): 1714-21.

IX. TABLE OF FIGURE

Figure 1 - TM protein translocation in the membrane 9
Figure 2 - TM protein classification 10
Figure 3 - Hydropathy profile 11
Figure 4 - Micelle and bicelle and bilayers structures 12
Figure 5 - Aromatic ring electronegativity 15
Figure 6 - Cation π interaction 16
Figure 7 - Calreticulin domains 17
Figure 8 - N glycosylation and chaperones in the ER 18
Figure 9 - Endoplasmic reticulum associated degradation 19
Figure 10 - Degradation pathways in Golgi 20
Figure 11 - Plasma membrane associated degradation and recycling 20
Figure 12 - Left handed coiled coil 22
Figure 13 - Hematopoiesis 23
Figure 14 - Megakaryopoiesis 24
Figure 16 - JAKs structure 28
Figure 17 - JAK/STATs pathway for TpoR and IFNaR 29
Figure 18 TpoR intracellular domain 32
Figure 19 - Structural features of TpoR and comparison to other receptors 33
Figure 20 - RWQFP motif 34
Figure 21 - Tpo physiology and production 34
Figure 22 - Eltrombopag structure 36
Figure 23 - Tilt, rotation and translation for dimeric transmembrane domains 37
Figure 24 - TpoR signaling adapted from Judith Staerk thesis 39
Figure 25 - Negative regulators of cytokine signalisation 43
Figure 26 - Tpo dual role in hematopoiesis 44
Figure 27 - Comparative blood cytology of chicken 47
Figure 28 - Bone marrow of an ET patient 50
Figure 29 - Driver mutations in MPNs 51
Figure 30 - Epigenetic regulators of DNA methylation 55
Figure 31 - Toxcat assay 58
Figure 32 - Deuterium MAS NMR 59
Figure 33 - DARR NMR 60
Figure 34 – ATR-FTIR spectroscopy 61
Figure 35 - Analytical ultracentrifugation 62
Figure 36 - Gaussia Protein-fragment complementation assay 63
Figure 37 - Dual luciferase assay 64
Figure 38 - Growth assay 65
Figure 39 - Bone marrow transplantation protocol 66
Figure 40 - Coiled coils inducing dimerization 67

Figure 41 - Luciferase assay of TYK2V678F via coiled coils 90
Figure 42 - Luciferase assay of JAK2V617F via coiled coils 90
Figure 43 - Luciferase assay competition of TYK2 with JAK2KD 91
Figure 44 - Luciferase assay: TYK2 does not compete with JAK2 91
Figure 45 - Luciferase assay: TYK2 does not compete with JAK2 on a full-length receptor 92
Figure 46 - Luciferase assay: TYK2KD does not compete with JAK on a full-length receptor 92
Figure 47 – Amino acids frequency at the edge of single span type I transmembrane domain 106
Figure 48 - Luciferase assay: tryptophan at the fourth position in the motif 108
Figure 49 - Western blots results for reversal mutants 109
Figure 50 - Luciferase assay of Trp reversal mutants in pMegix 110
Figure 51 - Luciferase assay: attempt to inhibit W515K via an intermolecular mechanism 110
Figure 52 - Luciferase assay: one side Trp reversal of W515A 111
Figure 53 - Cell viability assay: one side Trp reversal of W515A 111
Figure 54 - Deuterium MAS spectra 112
Figure 55 - Luciferase assay: Trp after small residues 113
Figure 56 - Luciferase assay of deletions in the motif 119
Figure 57 - Luciferase assay of EpoR with Asn and KWQFP motif insertion 121
Figure 58 - Luciferase assay of the cystein containing motifs 121
Figure 59 - Luciferase assay of alanine mutation at first, second and third position in the motif 122
Figure 60 - Luciferase assay of mutations at Q516 122
Figure 61 - Luciferase assay of active W515H and Q516H and the requirement of two Trp for efficient control 122
Figure 62 - Cell viability assay showing activity of Q516H 123
Figure 63 - Luciferase assay via pGGR5: Q516F controls W515R or W515K active mutants 123
Figure 64 - Luciferase assay via spi-luc: Q516F controls W515R or W515K active mutants 124
Figure 65 – Cell viability assay: Q516F controls W515K active mutant 124
Figure 66 – Evolutionary clusters based on full lenght TpoR sequence 125
Figure 68 - big apes alignments 145
Figure 69 - Asn activity is increased when going closer to the cytosolic border. 165
Figure 70 - Luciferase assay: PI3 kinase activity of Asn mutants 166
Figure 71 - Luciferase assay: Asn activity of 2 clones of L500N compared to S498N or A499N 166
Figure 72 - Cell viability and pictures of Baf3 stably transfected with WT and L500N TpoR 167
Figure 73 - Cell surface localization of L500N 167

Figure 74 - Luciferase assay via jAK2 and TYK2 of L500N 168
Figure 75 Cell surface localization of TpoR + alanines 168
Figure 76 - Luciferase assay: alanines insertions before the KWQFP motif 169
Figure 77- LHCC tilt angle 169
Figure 78 - Luciferase assay: double S505N W515K oncogenic activity 170
Figure 79 - Luciferase assay: cytosolic W529A 171
Figure 80 - Crosslinking of tr-mTpoR L505C with Tpo agonist 171
Figure 81 - Crosslinking of tr-mTpoR L505C with Asn mutants. 172
Figure 82 - Crosslinking of tr-mTpoR L505C and L506C with Tpo agonist. 172
Figure 83 - Tpo induced phosphorylation of STAT2 176
Figure 84 - Tpo induced phosphorylation of STAT2 in platelets of patient 177
Figure 85 - Activation of STAT2 Is a direct TpoR Induced Effect 177
Figure 86 - Tpo induce IFN type I transcriptional activity 178
Figure 87 - RT PCR for IFN stimulated gene 178
Figure 88 - SiRNA targeting STAT2 prevent the antiproliferative effect of Tpo. 179
Figure 89 - STAT2 phosphorylation and transcriptional activity is induced by strong cc-TpoR-IV 179
Figure 90- Type-I interferon like transcriptional activity of TpoR and TpoR mutants 180
Figure 91 - Coiled coil VI interface 184
Figure 92 - Coiled coil II interface 184
Figure 93 - Coiled coil V interface 186
Figure 94 - Coiled coil I interface 187
Figure 95 - Coiled coil IV interface 187
Figure 96 - Model for TpoR and JAK2 activation. 188
Figure 97 – hypothesis for crosslinked dimers with tr-mTpoR L500N - L505C 189
Figure 99 - Our general model of TpoR activation 190

X. TABLE of TABLE

Table 1 - Concomitant mutations in MPN 49
Table 2 - Mutations in MPL 54
Table 3 - FTIR data W515K and RAWFP 112
Table 4 - Alignment of RWQFP analogs 128
Table 5 - Human and murine inactive interface 183
Table 6 - Human active interfaces 185
Table 7 - Murine active interfaces 186

ACKNOWLEDGMENTS

I am really grateful to my promoter **Prof. Stefan Constantinescu**. You have been my 6 cylinders follow-me-car and brought me constantly to the next level. Your way of going about it was to place me in an office with your highest-level scientists, multiple burning issues and let the pressure go up. I would like to thank also your wife **Dr Anca Boeras** who introduced me to you and that kept everything smooth and friendly.

I would like to specially thank **Prof. Steven O Smith** for his unique expertise in structural biology and for bringing us biophysics approaches and ingenious thoughts to unravel the mechanism of TpoR activation and for being an external members of my Jury. A huge thank to **Professor Iris Behrmann** for coming to Brussels and for reading the thesis.

I deeply acknowledge **Professor Bernard Chatelain** and **Professor Augustin Ferrant** for teaching me principles of laboratory and clinical Hematology and for being internal members of my Jury.
I amm extremely thankful to the other internal members of my Jury: **Professor Thomas Michiels**, **Professor Miikka Vikkula and Professor Pierre Van der Bruggen**.

I want to acknowledge **members of the Stefan N. Constantinescu lab** and friends present and past Christian Pecquet, Celine Mouton, Judith Staerk, Emilie Leroy, Ilyas Chachoua, Leila Varghese, Joanne van Hees, Michael Girardot, Roxana Albu, Thomas Balligand, Xavier Cahu, Yasmine Ould amer, Alexandra Dusa, Jean-Michel Heine, Vitalina Gryshkova, Nancy Caceres, Jhansi Kota, Florian Perrin, Yohan Royer, Carmen Diaconu, Lidvine Genet, Gaelle Vertenoeil, Zulrahman Erlangga (Zul), Salwa Najjar, Myat Marlar Shwe.
I would like to thank also people from the Clinical laboratory (**Prof. Dominique Latinne, Prof. Pascale Saussoy, Prof. Stephane Eeckhoudt**), technicians (Tam, Laurence, Fabienne, Hilde, Patricia, Daphne, Anne-Marie, Christiane, Sabrina) and assistants (Laurence and Madeleine) that help me for the routine.

I have received funds from the **FRIA (FNRS)** Belgium that allow me to start this thesis and from **Cliniques Universitaires St Luc** that brings me support to finish this thesis.

Je remercie mes parents Thierry et Monique, mes beaux parents Cécile et Etienne, mes grand-parents à qui je pense beaucoup, mon frère jumeau Paul-Antoine et mon petit frère Florent et enfin mes amis dont mon vieux Gus pour leur soutien.

Je réserve une attention particulière pour ma brillante moitié Anne, qui m'a supporté et réconforté. Merci aussi à mon fils Edouard (ma plus grande découverte) qui est en train d'applaudir en imitant un dimère et de faire « ainsi font, font, font…» comme pour me montrer la bonne interface au moment où j'écris ces dernières lignes.